Computational & Multiscale Mechanics of Materials

CM3

www.ltas-cm3.ulg.ac.be

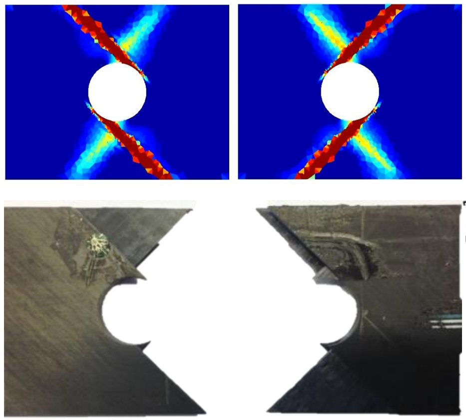

Non-local damage mean-field-homogenization

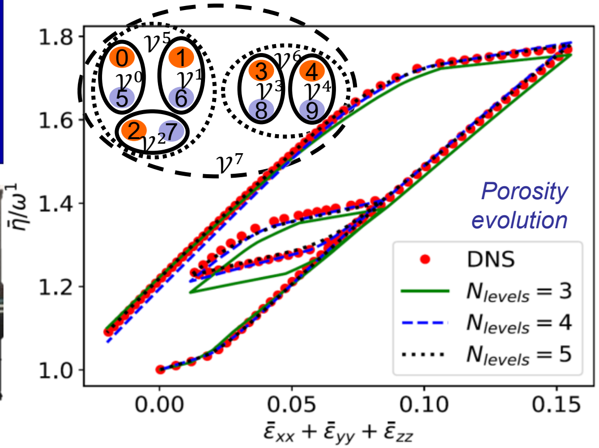

Deep-Material-Networks

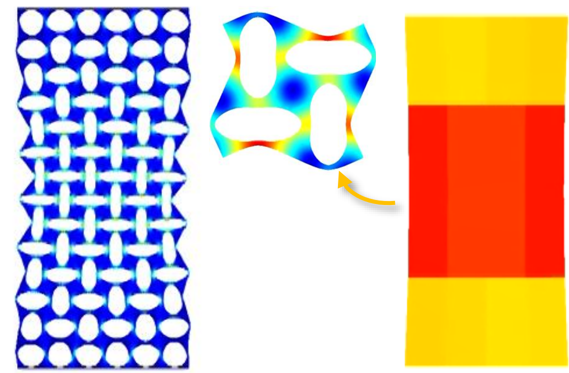

FE2 homogenization of metamaterials

Stochastic multi-scale methods

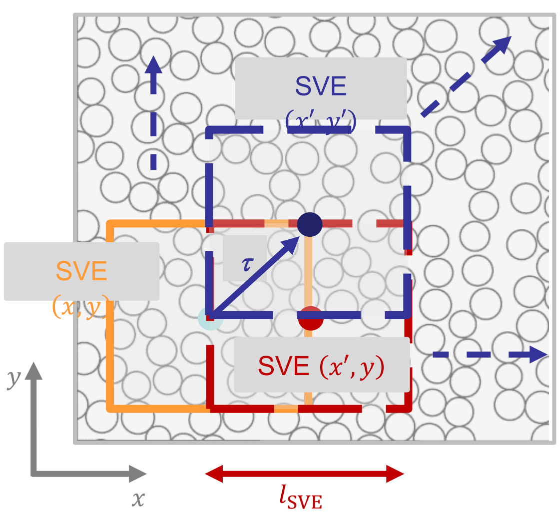

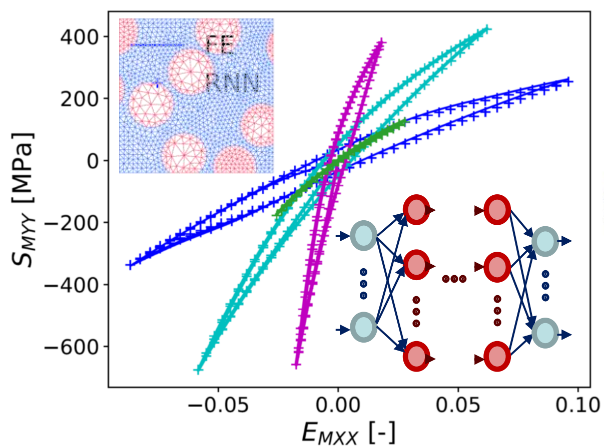

Data-driven multi-scale simulations

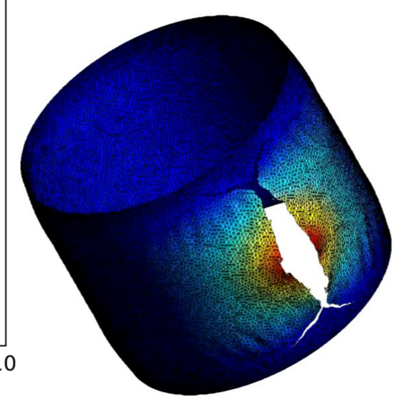

DG-based fracture

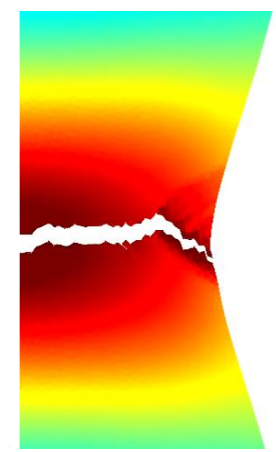

Nonlocal Gurson to crack transition

Direct links

- Hybrid quantum annealer-classical computer variational framework for elasto-plastic materials
- Data-driven approaches
  - Deep Material Networks from the interaction viewpoint ;
  - Mean-Field-Based Deep Material Networks for woven composites ;
  - Stochastic Interaction-Based Deep Material Network ;
  - Recurrent Neural Network-accelerated multi-scale simulations in elasto-plasticity ;
  - Self-Consistent Recurrent Neural Network for multi-scale simulations with irreversible behaviours ;
  - Recurrent Neural Network with dimensionality reduction and break down ;
  - Multi-Scale optimisation of meta-materials ;
  - Sequential Bayesian Inference of complex model parameters ;
  - Bayesian identification of stochastic MFH model parameters ;
- Complex constitutive models for failure prediction under complex loading states
  - Shear and necking coalescence model for porous materials ;
  - Ductile failure of High-Entropy Alloys (HEA) ;
  - Damage-enhanced viscoelastic-viscoplastic finite strain model for crosslinked resin ;
  - Finite-strain thermomechanical quasi-nonlinear-viscoelastic viscoplastic model for thermoplastics ;
  - One-Way and Two-Way Shape Memory Polymers ;
- Homogenization & Multi-Scale methods
  - Second order Computational Homogenization for Honeycombs ;
  - Second order homogenization without RVE size effect for cellular and metamaterials ;
  - Mean-Field-Homogenization for Elasto-Visco-Plastic Composites ;
  - Micro-structural simulation of fiber-reinforced highly crosslinked epoxy ;
  - Non-Local Damage Mean-Field-Homogenization ;
  - Non-Local Damage & Phase-Field-Enhanced Mean-Field-Homogenization ;
  - Stochastic Homogenization of Composite Materials ;
  - Stochastic 3-Scale Models for Polycrystalline Materials ;
  - Boundary conditions and tangent operator in multi-physics FE^2;
- Fracture Mechanics
  - DG-Based Multi-Scale Fracture, DG-Based Dynamic Fracture ;
  - DG-Based Damage elastic damage to crack transition ;
  - Non-local Gurson damage model to crack transition ;

Hybrid quantum annealer-classical computer variational framework for elasto-plastic materials

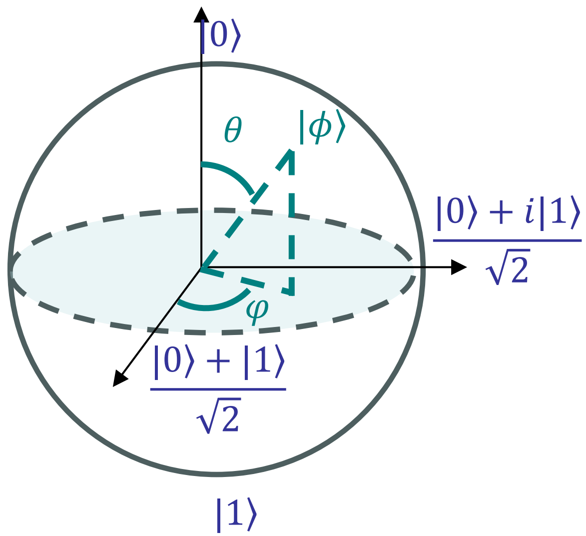

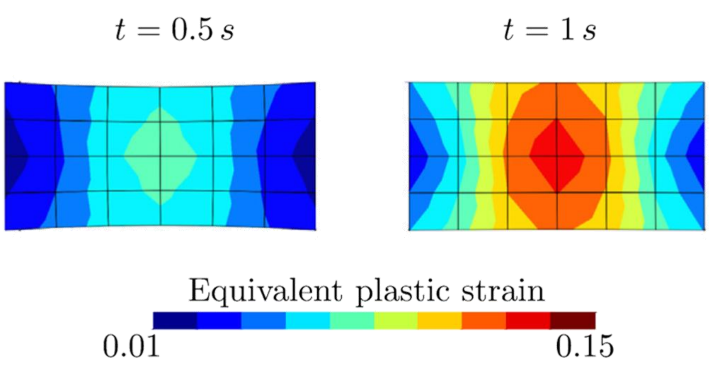

This work is partially supported by a “Strategic Opportunity” grant from the University of Liege

- Bits vs. Qubits:
  - Superposition of states:
    - A quantum bit can be 0 or 1 at the same time

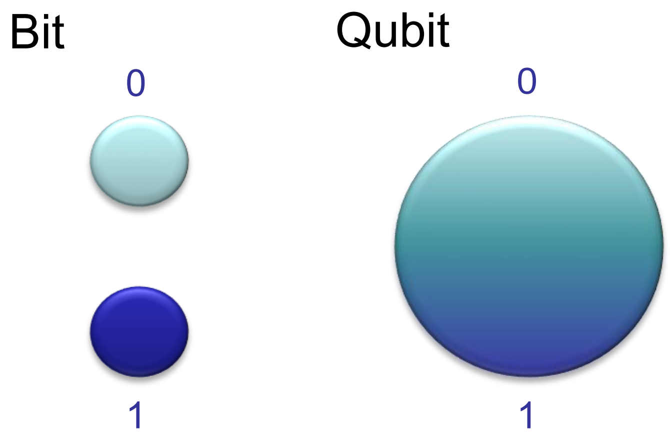

  - State vector of a qubit
    - Computational basis $|0\rangle = \begin{pmatrix}1\\0\end{pmatrix}$ & $|1\rangle = \begin{pmatrix}0\\1\end{pmatrix}$
    - Notations: $\begin{cases} |\phi\rangle = \begin{pmatrix}\alpha\\ \beta\end{pmatrix} = \alpha|0\rangle + \beta|1\rangle \\ \langle\phi| = (\alpha^* \quad \beta^*) \end{cases}$ $|\alpha|^2 + |\beta|^2 = 1$
    - Qubit represented on the surface of the Bloch Sphere

$$|\phi\rangle = e^{i\delta}\left(\cos\left(\frac{\theta}{2}\right)|0\rangle + e^{i\varphi}\sin\left(\frac{\theta}{2}\right)|1\rangle\right)$$

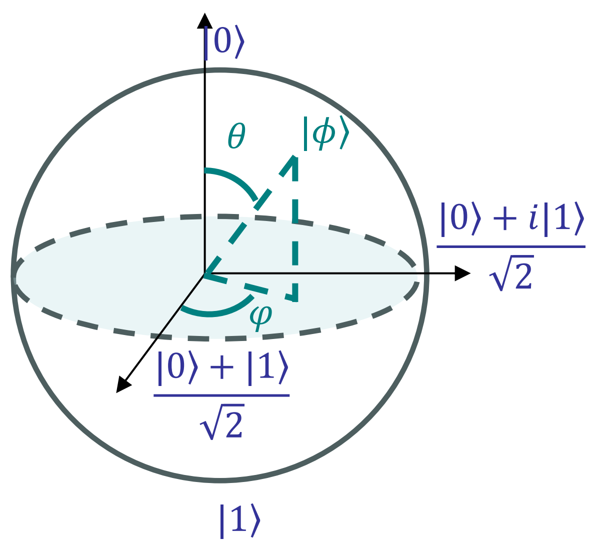

    - Global phase $e^{i\delta}$ has no observable consequence

      (NB relative phase has consequence)
  - At measurement (in the computational basis)
    - Either $|0\rangle$ or $|1\rangle$ with respective probability $|\alpha|^2$ and $|\beta|^2$

- Multiple (connected) qubits:
  - Product state of 2 1-qubit states: $\begin{cases} |\phi_0\rangle = \alpha_0|0\rangle + \beta_0|1\rangle \\ |\phi_1\rangle = \alpha_1|0\rangle + \beta_1|1\rangle \end{cases}$

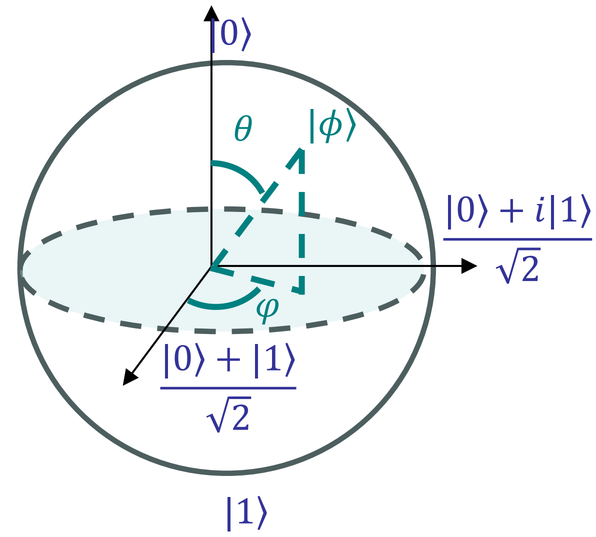

⇒ $|\boldsymbol{\phi}\rangle = |\phi_0\rangle \otimes |\phi_1\rangle = \alpha_0\alpha_1|00\rangle + \alpha_0\beta_1|01\rangle + \alpha_1\beta_0|10\rangle + \beta_0\beta_1|11\rangle$

  - Most general 2-qubit state

$$|\boldsymbol{\phi}\rangle = \alpha_{00}|00\rangle + \alpha_{01}|01\rangle + \alpha_{10}|10\rangle + \alpha_{11}|11\rangle$$

⇒ Because of entanglement, a K-qubit state is more general (it cannot always be written as the product of K 1-qubit states)

⇒ There is not always K equivalent 1-qubit states to a K-qubit state, e.g.

$$|\boldsymbol{\phi}\rangle = \frac{1}{\sqrt{2}}|00\rangle + 0|01\rangle + 0|10\rangle + \frac{1}{\sqrt{2}}|11\rangle$$

  - A system of K coupled qubits
    - Is a 2^K -state quantum-mechanical system
    - Whose state can be represented by any normalised linear combination of 2^K basis states:

$$|\boldsymbol{\phi}\rangle = \phi_0|0\rangle \otimes |0\rangle \ldots \otimes |0\rangle + \phi_1|0\rangle \otimes |0\rangle \ldots \otimes |1\rangle + \cdots + \phi_{2^K-1}|1\rangle \ldots \otimes |1\rangle \otimes |1\rangle$$

with $\sum_{i=0}^{2^K-1} |\phi_i|^2 = 1$ ⇒ Because of superposition, potentially, a quantum computer with K qubits can take 2^K bitstrings of size K in parallel at the same time. A classical computer can only take 1 bitstring of size K

- Quantum annealer
  - Goal: finding the ground state of a Hamiltonian $\mathbf{H}$

$$|\boldsymbol{\phi}_0\rangle = \arg\min_{|\boldsymbol{\phi}\rangle} \langle \boldsymbol{\phi}|\mathbf{H}\,|\boldsymbol{\phi}\rangle$$

  - Based on quantum adiabatic theorem:
    - Considering a time-varying Hamiltonian $\mathbf{H}_{\mathbf{QA}}(t)$ initially at ground state, if its time evolution is slow enough, it is likely to remain at the ground state
  - Adiabatic quantum computing:
    - Starts from the ground state of an easy to prepare Hamiltonian $\mathbf{H}_i$
    - Evolves to the ground state of the Hamiltonian $\mathbf{H}$ which encodes the sought solution

$$\mathbf{H}_{\mathbf{QA}}(t) = \frac{(t_a - t)}{t_a}\,\mathbf{H}_i + \frac{t}{t_a}\,\mathbf{H}$$

  - Quantum annealing
    - Exploits quantum effect such as quantum tunneling
    - Less sensitive to noise than Gate-based QC
    - Less versatile than Gate-based QC

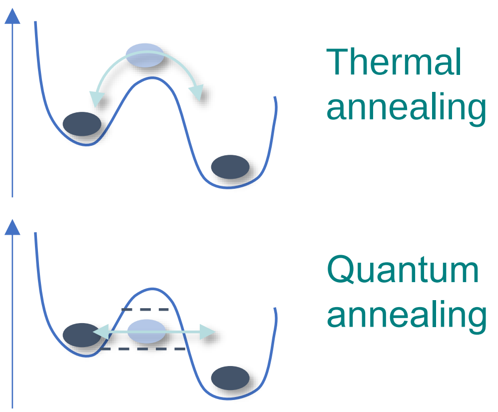

- Ising Hamiltonian
  - Goal: finding the ground state of a Hamiltonian $\mathbf{H}$

$$|\boldsymbol{\phi}_0\rangle = \arg\min_{|\boldsymbol{\phi}\rangle} \langle\boldsymbol{\phi}|\mathbf{H}\,|\boldsymbol{\phi}\rangle$$

  - Some definitions
    - Set of K qubits $V = \{0, \dots K-1\}$
    - Set of interactions between 2 qubits $E \subset \{(i,j) \mid i \in V, j \in V, i < j)\}$
    - Pauli- Z operator $\mathbf{Z} = \begin{bmatrix} 1 & 0 \\ 0 & -1 \end{bmatrix}$ and identity $\mathbf{I} = \begin{bmatrix} 1 & 0 \\ 0 & 1 \end{bmatrix}$
    - Pauli- Z operator applied on qubit i: $\mathbf{Z}_i = \underbrace{\mathbf{I}}_{0} \otimes \cdots \otimes \mathbf{I} \otimes \underbrace{\mathbf{Z}}_{i} \otimes \mathbf{I} \otimes \cdots \otimes \underbrace{\mathbf{I}}_{K-1}$
    - Pauli- Z operator applied on qubits i and j:

$$\mathbf{Z}_{ij} = \underbrace{\mathbf{I}}_{0} \otimes \cdots \otimes \mathbf{I} \otimes \underbrace{\mathbf{Z}}_{i} \otimes \mathbf{I} \otimes \cdots \otimes \mathbf{I} \otimes \underbrace{\mathbf{Z}}_{j} \otimes \mathbf{I} \otimes \cdots \otimes \underbrace{\mathbf{I}}_{K-1}$$

  - Ising Hamiltonian represented by an undirected graph (V, E):
    - $\mathbf{H} = \sum_{i \in V} h_i \mathbf{Z}_i + \sum_{(i,j) \in E} J_{ij} \mathbf{Z}_{ij}$
    - Is a $2^K \times 2^K$ diagonal operator in the computational basis

- Quadratic Unconstrained Binary Optimization (QUBO)
  - Goal: finding the ground state of a Hamiltonian $\mathbf{H}$

$$|\boldsymbol{\phi}_0\rangle = \arg\min_{|\boldsymbol{\phi}\rangle} \langle\boldsymbol{\phi}|\mathbf{H}\,|\boldsymbol{\phi}\rangle \qquad \text{with} \quad \mathbf{H} = \sum_{i\in V} h_i \mathbf{Z}_i + \sum_{(i,j)\in E} J_{ij}\mathbf{Z}_{ij}$$

  - In terms of spin variables
    - Computational basis of $\mathbf{H}$ $\quad |\boldsymbol{\phi}\rangle = |b_0\, b_1\, \dots b_{K-1}\rangle$ with $b_i \in \{0,1\}$
    - We have successively

$$\mathbf{Z} = \begin{bmatrix}1 & 0\\ 0 & -1\end{bmatrix} \Rightarrow \mathbf{Z}|b_i\rangle = (-1)^{b_i}|b_i\rangle \qquad |0\rangle = \begin{pmatrix}1\\0\end{pmatrix} \qquad |1\rangle = \begin{pmatrix}0\\1\end{pmatrix}$$

$$\mathbf{Z}_i = \underbrace{\mathbf{I}}_{0} \otimes \cdots \otimes \mathbf{I} \otimes \underbrace{\mathbf{Z}}_{i} \otimes \mathbf{I} \otimes \cdots \otimes \underbrace{\mathbf{I}}_{K-1} \Rightarrow \mathbf{Z}_i|\boldsymbol{\phi}\rangle = (-1)^{b_i}|\boldsymbol{\phi}\rangle$$

$$\mathbf{Z}_{ij} = \underbrace{\mathbf{I}}_{0} \otimes \cdots \otimes \mathbf{I} \otimes \underbrace{\mathbf{Z}}_{i} \otimes \mathbf{I} \otimes \cdots \otimes \mathbf{I} \otimes \underbrace{\mathbf{Z}}_{j} \otimes \mathbf{I} \otimes \cdots \otimes \underbrace{\mathbf{I}}_{K-1} \Rightarrow \mathbf{Z}_{ij}|\boldsymbol{\phi}\rangle = (-1)^{b_i}(-1)^{b_j}|\boldsymbol{\phi}\rangle$$

    - Defining the vector of spin variables: $\mathbf{s} = [(-1)^{b_i}\ \ \forall i \in V]$

$\Rightarrow$ The eigenvalue of $\mathbf{H}$ reads $\mathcal{F}_{\text{Ising}} = \sum_{i\in V} h_i s_i + \sum_{(i,j)\in E} J_{ij} s_i s_j = \mathbf{s}^T\mathbf{h} + \mathbf{s}^T\mathbf{J}\mathbf{s}$

with $\mathbf{h} = [h_i\ \ \forall i \in V]$ & $\mathbf{J} = [J_{ij}\ \ \forall (i,j) \in E]$

User programmable parameters

$$\Rightarrow |\boldsymbol{\phi}_0\rangle = \arg\min_{\boldsymbol{\phi}} \langle\boldsymbol{\phi}|\mathbf{H}\,|\boldsymbol{\phi}\rangle \Leftrightarrow \mathbf{s} = \arg\min_{\mathbf{s}'} \mathcal{F}_{\text{Ising}}(\mathbf{s}';\mathbf{h},\mathbf{J})$$

- Quadratic Unconstrained Binary Optimization (QUBO)
  - Goal: finding the ground state of a Hamiltonian $\mathbf{H}$

$$|\boldsymbol{\phi}_0\rangle = \arg\min_{|\boldsymbol{\phi}\rangle} \langle \boldsymbol{\phi}|\mathbf{H}\,|\boldsymbol{\phi}\rangle \quad \text{with} \quad \mathbf{H} = \sum_{i\in V} h_i \mathbf{Z}_i + \sum_{(i,j)\in E} J_{ij}\mathbf{Z}_{ij}$$

  - In terms of spin variables
    - Computational basis of $\mathbf{H}$ $\quad |\boldsymbol{\phi}\rangle = |b_0\, b_1\, \dots b_{K-1}\rangle$ with $b_i \in \{0,1\}$
    - Vector of spin variables: $\mathbf{s} = [(-1)^{b_i}\ \forall i \in V]$

The eigenvalue of $\mathbf{H}$ reads $\mathcal{F}_{\text{Ising}} = \sum_{i\in V} h_i s_i + \sum_{(i,j)\in E} J_{ij} s_i s_j = \mathbf{s}^T\mathbf{h} + \mathbf{s}^T\mathbf{J}\mathbf{s}$

with $\mathbf{h} = [h_i\ \forall i \in V]$ & $\mathbf{J} = \left[J_{ij}\ \forall (i,j) \in E\right]$

User programmable parameters

$$\Rightarrow |\boldsymbol{\phi}_0\rangle = \arg\min_{\boldsymbol{\phi}} \langle \boldsymbol{\phi}|\mathbf{H}\,|\boldsymbol{\phi}\rangle \Leftrightarrow \mathbf{s} = \arg\min_{\mathbf{s}'} \mathcal{F}_{\text{Ising}}(\mathbf{s}'; \mathbf{h}, \mathbf{J})$$

  - In terms of binary variables
    - Vector of binary variables $\mathbf{b} = [b_i\ \forall i \in V]$
    - Spin-binary variable transformation $s_i = 2b_i - 1 : \{0,1\} \to \{-1,1\}$ & property $b_i^2 = b_i$

$$\Rightarrow \mathcal{F}_{\text{Ising}} = \sum_{i\in V} h_i s_i + \sum_{(i,j)\in E} J_{ij} s_i s_j \Rightarrow \mathcal{F}_{\text{QUBO}} = \sum_{(i,j)\in E\cup\{(i,i)\forall i\in V\}} A_{ij} b_i b_j = \mathbf{b}^T\mathbf{A}\mathbf{b}$$

$$\Rightarrow |\boldsymbol{\phi}_0\rangle = \arg\min_{\boldsymbol{\phi}} \langle \boldsymbol{\phi}|\mathbf{H}\,|\boldsymbol{\phi}\rangle \Leftrightarrow \mathbf{b} = \arg\min_{\mathbf{b}'} \mathcal{F}_{\text{QUBO}}(\mathbf{b}'; \mathbf{A})$$

User programmable parameters

- Summary
  - Goal: finding the ground state of a Hamiltonian $\mathbf{H}$

$$|\boldsymbol{\phi}_0\rangle = \arg\min_{|\boldsymbol{\phi}\rangle} \langle\boldsymbol{\phi}|\mathbf{H}\,|\boldsymbol{\phi}\rangle \qquad \text{with} \quad \mathbf{H} = \sum_{i\in V} h_i \mathbf{Z}_i + \sum_{(i,j)\in E} J_{ij}\mathbf{Z}_{ij}$$

  - Adiabatic annealing
    - Starts from the ground state of an easy to prepare $\mathbf{H}_i$
    - Evolves to the ground state of the Hamiltonian $\mathbf{H}$

$$\mathbf{H}_{\mathbf{QA}}(t) = \frac{(t_a - t)}{t_a}\,\mathbf{H}_i + \frac{t}{t_a}\,\mathbf{H}$$

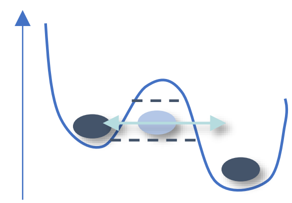

Quantum annealing

  - Problem reformulated in terms of binary variables
    - $\mathbf{b} = [b_i \ \forall i \in V]$ with $b_i \in \{0, 1\}$
    - Eigenvalue $\mathcal{F}_{\text{QUBO}} = \mathbf{b}^T\mathbf{A}\mathbf{b}$
    - QUBO optimization $\mathbf{b} = \arg\min_{\mathbf{b}'} \mathcal{F}_{\text{QUBO}}(\mathbf{b}';\mathbf{A})$

User programmable parameters

  - In practice
    - Provide the QUBO matrix **A**
    - Set the annealing time t_a (typically 20 µs)
    - One annealing returns a sample of $\mathbf{b}$
    - A single run may not provide the global minimum due to environmental noises, hardware imperfections, pre- and post-processing errors requires several reads

- Set of PDEs to be solved
  - Strong form ⇒ Weak form:

$$\nabla \cdot \boldsymbol{\sigma}(\boldsymbol{x}) + \boldsymbol{b}_0(\boldsymbol{x}) = \boldsymbol{0} \quad \Rightarrow \quad \int_V \boldsymbol{\sigma}(\boldsymbol{x}) : \nabla \otimes^s \boldsymbol{\delta u}(\boldsymbol{x}) dV = \int_V \boldsymbol{b}_0 \cdot \boldsymbol{\delta u} dV + \int_{\partial_N V} \boldsymbol{n} \cdot \boldsymbol{\sigma} \cdot \boldsymbol{\delta u} d\partial V$$

  - Constitutive model:

$$\boldsymbol{\sigma}(\boldsymbol{x}, t) = \boldsymbol{\sigma}\left(\boldsymbol{\nabla} \otimes^s \boldsymbol{u}(\boldsymbol{x}, t); \mathbf{q}(\boldsymbol{x}, t)\right) \quad \text{with evolution law} \quad \boldsymbol{Q}\left(\boldsymbol{\sigma}(\boldsymbol{x}, t), \mathbf{q}(\boldsymbol{\nabla} \otimes^s \boldsymbol{u}(\boldsymbol{x}, \tau) : \tau \leq t)\right) = \boldsymbol{0}$$

- Finite element formulation
  - Displacement field at quadrature point Ξ from nodal displacements vector $\mathbf{U}$

$$\boldsymbol{u}(\Xi) = N_a(\Xi) \boldsymbol{U}_a \quad \Rightarrow \quad \boldsymbol{\varepsilon}(\Xi) = \boldsymbol{\nabla} \otimes^s \boldsymbol{u}(\Xi) = \mathbf{B}_a(\Xi) \boldsymbol{U}_a$$

  - Resulting non-linear system of equations on time interval $[t_n \; t_{n+1}]$

$$\int_V \boldsymbol{\sigma}(\boldsymbol{x}) : \nabla \otimes^s \boldsymbol{\delta u}(\boldsymbol{x}, t) dV = \int_V \boldsymbol{b}_0 \cdot \boldsymbol{\delta u} dV + \int_{\partial_N V} \boldsymbol{n} \cdot \boldsymbol{\sigma} \cdot \boldsymbol{\delta u} d\partial V$$

$$\Rightarrow \quad \boldsymbol{\delta U}_{\boldsymbol{b}}^{\mathrm{T}} \cdot \sum_{\Xi} \mathbf{B}_b^{\mathrm{T}}(\Xi) \, \boldsymbol{\sigma}\big((\Xi)\big) \omega^{\Xi} = \boldsymbol{\delta U}_{\boldsymbol{b}}^{\mathrm{T}} \cdot \sum_{\Xi} N_b(\Xi) \, \boldsymbol{b}_0(\Xi) \omega^{\Xi}$$

Omitting surface tractions

$$\Rightarrow \quad \boldsymbol{f}_b^{\mathrm{int}} = \sum_{\Xi} \mathbf{B}_b^{\mathrm{T}}(\Xi) \, \boldsymbol{\sigma}(\Xi) \omega^{\Xi} = \sum_{\Xi} N_b(\Xi) \, \boldsymbol{b}_0(\Xi) \omega^{\Xi} = \boldsymbol{f}_b^{\mathrm{ext}}$$

with

$$\begin{cases} \boldsymbol{\sigma}(\Xi, t_{n+1}) = \boldsymbol{\sigma}\left(\mathbf{B}_a(\Xi) \boldsymbol{U}_{a\, n+1}; \mathbf{q}(\Xi, \boldsymbol{t_{n+1}})\right) \\ \boldsymbol{Q}\left(\boldsymbol{\sigma}(\Xi, t_{n+1}), \mathbf{q}(\Xi, t_{n+1}), \mathbf{q}(\Xi, t_n)\right) = \boldsymbol{0} \end{cases}$$

- Consider classical finite element resolution on Quantum Computers?

FE Newton-Raphson iteration $(i) \leftarrow (i) + 1$

Constitutive NR iteration $(k) \leftarrow (k) + 1$

$$\mathbf{q}^{(k)}(\Xi) \mathrel{-}= \left(\frac{\partial \boldsymbol{Q}}{\partial \mathbf{q}}\right)^{-1} \boldsymbol{Q}\left(\mathbf{q}^{(k)}(\Xi)\right)$$

$$\boldsymbol{\sigma}^{(k)}(\Xi^{\eta}) = \boldsymbol{\sigma}\left(\mathbf{B}_a \boldsymbol{U}_{a\,n+1}^{(i)}; \mathbf{q}^{(k)}(\Xi^{\eta})\right)$$

$$\mathrm{U}_{n+1}^{(i)} \mathrel{-}= \left(\frac{\partial \boldsymbol{f}^{\mathrm{int}}}{\partial \mathbf{U}}\right)^{-1} \left[\boldsymbol{f}^{\mathrm{int}}\left(\boldsymbol{\sigma}\left(\boldsymbol{U}_{a\,n+1}^{(i)}\right)\right) - f^{\mathrm{ext}}\right]$$

  - What can be solved on a Quantum Computer?
    - Optimization problems can be solved (Actually Quantum Annealers look for a ground state)
    - Some operations can be achieved efficiently on classical computers like assembly
  - Do we need the same resolution structure?
    - Do we need intricated NR loops?
    - Do we even need to use the discretized form of the weak form?

$$\int_V \boldsymbol{\sigma}(\boldsymbol{x}) : \nabla \otimes^s \boldsymbol{\delta u}(\boldsymbol{x}) dV = \int_V \boldsymbol{b}_0 \cdot \boldsymbol{\delta u} dV \Rightarrow \boldsymbol{f}_b^{\mathrm{int}} = \sum_{\Xi} \mathbf{B}_b^{\mathrm{T}}(\Xi)\, \boldsymbol{\sigma}(\Xi) \omega^{\Xi} = \boldsymbol{f}_b^{\mathrm{ext}}$$

- Linear finite element resolution on Quantum Computers?
  - Assuming linear elasticity
    - Existence of a free energy $\Psi = \frac{1}{2}\boldsymbol{\varepsilon}(x):\mathbb{C}(x):\boldsymbol{\varepsilon}(x)$ with $\boldsymbol{\varepsilon}(x) = \nabla \otimes^s \boldsymbol{u}(\boldsymbol{x})$
    - Stress results from $\boldsymbol{\sigma}(\boldsymbol{x}) = \frac{\partial \Psi}{\partial \boldsymbol{\varepsilon}} = \mathbb{C}(x):\boldsymbol{\varepsilon}(x) = \mathbb{C}(x):\left(\nabla \otimes^s \boldsymbol{u}(\boldsymbol{x})\right)$
  - Finite element form:
    - At quadrature point using nodal shape function derivatives: $\boldsymbol{\sigma}(\Xi) = \boldsymbol{C}(\Xi)\mathbf{B}_a(\Xi)\boldsymbol{U}_a$
    - FE equations $\boldsymbol{f}_b^{\text{int}} = \sum_{\Xi} \mathbf{B}_b^{\mathrm{T}}(\Xi)\,\boldsymbol{\sigma}(\Xi)\omega^{\Xi} = \boldsymbol{f}_b^{\text{ext}}$

$$\Rightarrow \sum_{\Xi} \mathbf{B}_b^{\mathrm{T}}(\Xi)\boldsymbol{C}(x)\mathbf{B}_a\omega^{\Xi}\boldsymbol{U}_a = \mathbf{K}_{ab}\boldsymbol{U}_a = \boldsymbol{f}_b^{\text{ext}}$$

    - Defining the internal energy and work of external forces

$$\Phi = \frac{1}{2}\boldsymbol{U}_b\mathbf{K}_{ab}\boldsymbol{U}_a - W^{\text{ext}} \quad \text{with} \quad W^{\text{ext}} = \boldsymbol{f}_b^{\text{ext}}\boldsymbol{U}_b$$

$\Rightarrow$ The solution of the FE equations minimizes the energy

$$\mathbf{U} = \arg\min_{\mathbf{U}'}\left(\frac{1}{2}\mathbf{U}'^{\mathrm{T}}\mathbf{K}\mathbf{U}' - \mathbf{f}^{\text{ext}^{\mathrm{T}}}\mathbf{U}'\right)$$

  - We are looking for the ground state of a Hamiltonian

$$\mathbf{H} = \sum_{i\in V} h_i\mathbf{Z}_i + \sum_{(i,j)\in E} J_{ij}\mathbf{Z}_{ij}$$

- Non-linear finite element resolution on Quantum Computers?
  - Weak form: $\int_V \boldsymbol{\sigma}(\boldsymbol{x}) : \nabla \otimes^s \boldsymbol{\delta u}(\boldsymbol{x}) dV = \int_V \boldsymbol{b}_0 \cdot \boldsymbol{\delta u} dV$
  - Assuming non-linear elasticity
    - Existence of a free energy $\Psi(\boldsymbol{\varepsilon}(x))$ with $\boldsymbol{\varepsilon}(x) = \nabla \otimes^s \boldsymbol{u}(\boldsymbol{x})$
    - Stress results from $\boldsymbol{\sigma}(\boldsymbol{x}) = \frac{\partial \Psi}{\partial \boldsymbol{\varepsilon}}$

    ⇒ The weak form becomes $\int_V \frac{\partial \Psi(\boldsymbol{x})}{\partial \boldsymbol{\varepsilon}} : \boldsymbol{\delta\varepsilon}(\boldsymbol{x}) dV = \int_V \boldsymbol{b}_0 \cdot \boldsymbol{\delta u} dV$
  - Introduction of a functional
    - $\Phi(\boldsymbol{u}(V)) = \int_V \Psi(\nabla \otimes^s \boldsymbol{u}(\boldsymbol{x})) dV - W^{\text{ext}}(\boldsymbol{u}(V))$ & $W^{\text{ext}} = \int_V \boldsymbol{b}_0 \cdot \boldsymbol{u}(\boldsymbol{x}) dV$
    - The weak form results from nulling the Gâteaux derivative

    $$\Phi'\left(\boldsymbol{u}(V); \delta\boldsymbol{u}((V))\right) = \int_V \boldsymbol{\sigma}(\boldsymbol{x}) : \nabla \otimes^s \boldsymbol{\delta u}(\boldsymbol{x}) dV - \int_V \boldsymbol{b}_0 \cdot \boldsymbol{\delta u} dV = \boldsymbol{0}$$

    ⇒ The solution of the weak form minimizes the energy: $\boldsymbol{u}(V) = \arg\min_{\boldsymbol{u}'(V)} \Phi(\boldsymbol{u}'(V))$
  - We are looking for the solution of a minimization problem
    - The potential is convex
    - But it is not quadratic
    - Quid inelastic materials?

- Non-linear finite element resolution on Quantum Computers?
  - Inelastic materials
    - Existence of a Helmholtz free energy $\Psi(\boldsymbol{\varepsilon}(x), \mathbf{q}(x))$ with $\begin{cases} \text{internal variables } \mathbf{q}(x) \\ \boldsymbol{\varepsilon}(x) = \nabla \otimes^s \boldsymbol{u}(\boldsymbol{x}) \end{cases}$
  - Dissipation $\mathcal{D}$ and Clausius-Duhem inequality
    - $\mathcal{D} = \boldsymbol{\sigma} : \dot{\boldsymbol{\varepsilon}} - \dot{\Psi} \geq 0$ with $\dot{\Psi} = \frac{\partial \Psi}{\partial \boldsymbol{\varepsilon}} : \dot{\boldsymbol{\varepsilon}} + \frac{\partial \Psi}{\partial \mathbf{q}} \cdot \dot{\mathbf{q}}$
    - Equality holds in case of a reversible transformation

      $\Rightarrow$ $\boldsymbol{\sigma} = \frac{\partial \Psi}{\partial \boldsymbol{\varepsilon}}$ $\Rightarrow$ for an irreversible process: $\mathcal{D} = \mathbf{Y} \cdot \dot{\mathbf{q}} \geq 0$ with $\mathbf{Y} = -\frac{\partial \Psi}{\partial \mathbf{q}}$
  - Postulate the existence of a pseudo-potential $\Theta(\dot{\mathbf{q}})$ and its convex dual $\Theta^*(\mathbf{Y})$
    - $\Theta(\dot{\mathbf{q}}) = \max_{\mathbf{Y}} [\mathbf{Y} \cdot \dot{\mathbf{q}} - \Theta^*(\mathbf{Y})]$ $\Rightarrow$ $\dot{\mathbf{q}} = \frac{\partial \Theta^*(\mathbf{Y})}{\partial \mathbf{Y}}$ & $\mathbf{Y} = \frac{\partial \Theta(\dot{\mathbf{q}})}{\partial \dot{\mathbf{q}}}$
  - Power functional $\mathcal{E}$
    - New independent variables $(\dot{\boldsymbol{\varepsilon}}, \dot{\mathbf{q}})$
    - $\mathcal{E}(\dot{\boldsymbol{\varepsilon}}, \dot{\mathbf{q}}) = \dot{\Psi} + \Theta(\dot{\mathbf{q}}) = \frac{\partial \Psi}{\partial \boldsymbol{\varepsilon}} : \dot{\boldsymbol{\varepsilon}} - \mathbf{Y} \cdot \dot{\mathbf{q}} + \Theta(\dot{\mathbf{q}})$

      $\Rightarrow$ $\frac{\partial \mathcal{E}}{\partial \dot{\mathbf{q}}} = -\mathbf{Y} + \frac{\partial \Theta(\dot{\mathbf{q}})}{\partial \dot{\mathbf{q}}} = \mathbf{0}$ $\Rightarrow$ $\mathcal{E}$ has to be minimized with respect to internal state
    - Effective power functional* $\mathcal{E}^{\text{eff}}(\dot{\boldsymbol{\varepsilon}}) = \min_{\dot{\mathbf{q}}} \mathcal{E}(\dot{\boldsymbol{\varepsilon}}, \dot{\mathbf{q}})$ with $\boldsymbol{\sigma} = \frac{\partial \Psi}{\partial \boldsymbol{\varepsilon}} = \frac{\partial \mathcal{E}^{\text{eff}}}{\partial \dot{\boldsymbol{\varepsilon}}}$
  - The constitutive model is also a minimization problem

*Radovitzky, R. Ortiz M, CMAME 1999
Ortiz, M., Stainier, L., CMAME 1999

- Non-linear finite element resolution on Quantum Computers?
  - In elasticity we had
    - $\boldsymbol{u}(V) = \arg\min_{\boldsymbol{u}'(V)} \Phi\big(\boldsymbol{u}'(V)\big)$ with $\Phi\big(\boldsymbol{u}(V)\big) = \int_V \Psi\big(\nabla \otimes^s \boldsymbol{u}(\boldsymbol{x})\big) dV - W^{\text{ext}}\big(\boldsymbol{u}(\boldsymbol{x})\big)$
  - Double minimization problem in inelasticity
    - Power functional $\mathcal{E}$

$$\mathcal{E}(\dot{\boldsymbol{\varepsilon}}, \dot{\mathbf{q}}) = \frac{\partial \Psi}{\partial \boldsymbol{\varepsilon}} : \dot{\boldsymbol{\varepsilon}} - \mathbf{Y} \cdot \dot{\mathbf{q}} + \Theta(\dot{\mathbf{q}}) \quad \& \quad \mathcal{E}^{\text{eff}}(\dot{\boldsymbol{\varepsilon}}) = \min_{\dot{\mathbf{q}}} \mathcal{E}(\dot{\boldsymbol{\varepsilon}}, \dot{\mathbf{q}}) \quad \Rightarrow \quad \boldsymbol{\sigma} = \frac{\partial \mathcal{E}^{\text{eff}}}{\partial \dot{\boldsymbol{\varepsilon}}}$$

    - Volume power functional

$$\Phi\big(\dot{\boldsymbol{u}}(V), \dot{\mathbf{q}}(V)\big) = \int_V \mathcal{E}(\nabla \otimes^s \dot{\boldsymbol{u}}, \dot{\mathbf{q}}) - \dot{W}^{\text{ext}}\big(\dot{\boldsymbol{u}}(V)\big)$$

    - Incremental volume energy functional on time interval $[t_n \; t_{n+1}]$*

$$\Delta\Phi(\boldsymbol{u}_{n+1}, \mathbf{q}_{n+1}) = \int_V \Delta\mathcal{E}(\nabla \otimes^s \boldsymbol{u}_{n+1}, q_{n+1}) - \Delta W^{\text{ext}}(\boldsymbol{u}_{n+1})$$

with $\Delta\mathcal{E}(\nabla \otimes^s \boldsymbol{u}_{n+1}, \mathbf{q}_{n+1}) = \int_{t_n}^{t_{n+1}} \mathcal{E}(\nabla \otimes^s \dot{\boldsymbol{u}}, \dot{\mathbf{q}})$ & $\Delta\mathcal{E}^{\text{eff}}(\boldsymbol{\varepsilon}) = \min_{\mathbf{q}} \Delta\mathcal{E}(\boldsymbol{\varepsilon}, \mathbf{q})$, $\boldsymbol{\sigma} = \dfrac{\partial \Delta\mathcal{E}^{\text{eff}}}{\partial \boldsymbol{\varepsilon}}$

    - The problem solution reads

$$\begin{cases} \mathbf{q}_{n+1} = \arg\min_{\mathbf{q}'} \Delta\Phi(\boldsymbol{u}_{n+1}, \mathbf{q}') \\ \Delta\Phi^{\text{eff}}(\boldsymbol{u}_{n+1}) = \min_{\mathbf{q}'} \Delta\Phi(\boldsymbol{u}_{n+1}, \mathbf{q}') = \int_V \Delta\mathcal{E}^{\text{eff}}(\nabla \otimes^s \boldsymbol{u}_{n+1}) - \Delta W^{\text{ext}} \\ \boldsymbol{u}_{n+1} = \arg\min_{\mathbf{u}'\,\text{admissible}} \Delta\Phi^{\text{eff}}(\boldsymbol{u}') \end{cases}$$

*Ortiz, M., Stainier, L., CMAME 1999

- Example: J2-elasto-plasticity
  - Helmholtz free energy
    - $\Psi(\boldsymbol{\varepsilon},\mathbf{q}) = \frac{1}{2}\left(\boldsymbol{\varepsilon}-\boldsymbol{\varepsilon}^{\mathrm{pl}}\right):\mathbb{C}^{\mathrm{el}}:\left(\boldsymbol{\varepsilon}-\boldsymbol{\varepsilon}^{\mathrm{pl}}\right)$ with $\boldsymbol{\Delta\varepsilon}^{\mathrm{pl}} = \Delta\gamma\mathbf{N}$

    ⇒ Internal variables $\mathbf{q} = \{\mathbf{N},\Delta\gamma\}$ under constraints $\mathbf{N}:\mathbf{N} = \frac{3}{2}$, $\mathrm{tr}(\mathbf{N}) = 0$ & $\Delta\gamma \geq 0$
  - Dissipation pseudo-potential
    - $\Theta(\dot{\mathbf{q}}) = \begin{cases}\left(\sigma_y^0 + R(\gamma)\right)\dot{\gamma} & \text{if } \dot{\gamma}\geq 0\\ \infty & \text{otherwise}\end{cases}$ ⇒ $\Theta^*(\mathbf{Y}) = \begin{cases}0 & \text{if } \sigma_{\mathrm{eq}} - \sigma_y^0 - R \leq 0\\ \infty & \text{otherwise}\end{cases}$
  - Increment of the energy functional
    - $\mathcal{E}(\dot{\boldsymbol{\varepsilon}},\dot{\mathbf{q}}) = \dot{\Psi} + \Theta(\dot{\mathbf{q}})$

    ⇒ $$\Delta\mathcal{E}(\boldsymbol{\varepsilon}_{n+1},\mathbf{q}) = \frac{1}{2}\left(\boldsymbol{\varepsilon}_{n+1} - \Delta\gamma\mathbf{N} - \boldsymbol{\varepsilon}_n^{\mathrm{pl}}\right):\mathbb{C}^{\mathrm{el}}:\left(\boldsymbol{\varepsilon}_{n+1} - \Delta\gamma\mathbf{N} - \boldsymbol{\varepsilon}_n^{\mathrm{pl}}\right) + \int_{\gamma_n}^{\gamma_{n+1}}\left(\sigma_y^0 + R(\gamma')\right)d\gamma' - \frac{1}{2}\left(\boldsymbol{\varepsilon}_n - \boldsymbol{\varepsilon}_n^{\mathrm{pl}}\right):\mathbb{C}^{\mathrm{el}}:\left(\boldsymbol{\varepsilon}_n - \boldsymbol{\varepsilon}_n^{\mathrm{pl}}\right)$$

    ⇒ $\Delta\mathcal{E}^{\mathrm{eff}}(\boldsymbol{\varepsilon}) = \min_{\mathbf{q}}\Delta\mathcal{E}(\boldsymbol{\varepsilon},\mathbf{q})$ with constraints $\mathbf{N}:\mathbf{N} = \frac{3}{2}$, $\mathrm{tr}(\mathbf{N}) = 0$ & $\Delta\gamma \geq 0$
  - The problem is stated as a double constrained minimization problem

$$\begin{cases}\mathbf{q}_{n+1} = \arg\min\limits_{\mathbf{q}'\text{constrained}}\Delta\Phi(\boldsymbol{u}_{n+1},\mathbf{q}')\\ \Delta\Phi^{\mathrm{eff}}(\boldsymbol{u}_{n+1}) = \min\limits_{\mathbf{q}'\text{constrained}}\Delta\Phi(\boldsymbol{u}_{n+1},\mathbf{q}') = \int_V \Delta\mathcal{E}^{\mathrm{eff}}(\nabla\otimes^s \boldsymbol{u}_{n+1}) - \Delta W^{\mathrm{ext}}\\ \boldsymbol{u}_{n+1} = \arg\min\limits_{\mathbf{u}'\text{admissible}}\Delta\Phi^{\mathrm{eff}}(\boldsymbol{u}')\end{cases}$$

Quantum computing & finite elements

- Classical finite element resolution

FE Newton-Raphson iteration $(i) \leftarrow (i) + 1$

Constitutive NR iteration $(k) \leftarrow (k) + 1$

$$\mathbf{q}^{(k)}(\Xi) \mathrel{-}= \left(\frac{\partial \mathcal{Q}}{\partial \mathbf{q}}\right)^{-1} \mathcal{Q}\left(\mathbf{q}^{(k)}(\Xi)\right)$$

$$\boldsymbol{\sigma}^{(k)}(\Xi^{\eta}) = \boldsymbol{\sigma}\left(\mathbf{B}_a \boldsymbol{U}^{(i)}_{a\,n+1}; \mathbf{q}^{(k)}(\Xi^{\eta})\right)$$

$$\mathrm{U}^{(i)}_{n+1} \mathrel{-}= \left(\frac{\partial \boldsymbol{f}^{\mathrm{int}}}{\partial \mathbf{U}}\right)^{-1} \left[\boldsymbol{f}^{\mathrm{int}}\left(\boldsymbol{\sigma}\left(\boldsymbol{U}^{(i)}_{a\,n+1}\right)\right) - \boldsymbol{f}^{\mathrm{ext}}\right]$$

- Finite element as a double-minimization problem

Loop until convergence

$$\mathbf{q}_{n+1} = \arg \min_{\mathbf{q}' \text{constrained}} \Delta\Phi(\boldsymbol{u}_{n+1}, \mathbf{q}')\,;$$

$$\Delta\Phi^{\mathrm{eff}} = \min_{\mathbf{q}' \text{constrained}} \Delta\Phi(\boldsymbol{u}_{n+1}, \mathbf{q}')$$

$$\boldsymbol{u}_{n+1} = \arg \min_{\mathbf{u}' \text{admissible}} \Delta\Phi^{\mathrm{eff}}(\mathbf{u}')$$

  - Quantum annealers: ground state of an Ising-Hamiltonian
    - No need for Jacobians
    - No problem of convergence
  - But how to make the optimisation problem solvable by quantum annealing?

Double-minimization process solved by Quantum annealing

- Finite element as a double-minimization problem
  - Finite element problem

Loop until convergence

$$\mathbf{q}_{n+1} = \arg \min_{\mathbf{q}'\text{constrained}} \Delta\Phi(\boldsymbol{u}_{n+1}, \mathbf{q}')\,;$$
$$\Delta\Phi^{\text{eff}} = \min_{\mathbf{q}'\text{constrained}} \Delta\Phi(\boldsymbol{u}_{n+1}, \mathbf{q}')$$
$$\boldsymbol{u}_{n+1} = \arg \min_{\mathbf{u}'\text{admissible}} \Delta\Phi^{\text{eff}}(\mathbf{u}')$$

  - Ising Hamiltonian for Quantum annealing
    - Goal: finding the ground state of a Hamiltonian $\mathbf{H}$: $\mathbf{H} = \sum_{i\in V} h_i \mathbf{Z}_i + \sum_{(i,j)\in E} J_{ij}\mathbf{Z}_{ij}$

$$|\boldsymbol{\phi}_0\rangle = \arg\min_{|\boldsymbol{\phi}\rangle} \langle \boldsymbol{\phi}|\mathbf{H}\,|\boldsymbol{\phi}\rangle$$

    - Problem reformulated in terms of binary variables $\mathbf{b} = [b_i\ \forall i \in V]$ with $b_i \in \{0,1\}$
    - QUBO optimisation problem $\mathcal{F}_{\text{QUBO}} = \sum_{(i,j)\in E\cup\{(i,i)\forall i\in V\}} A_{ij} b_i b_j = \mathbf{b}^T\mathbf{A}\mathbf{b}$

$$\mathbf{b} = \arg\min_{\mathbf{b}'} \mathcal{F}_{\text{QUBO}}(\mathbf{b}'; \mathbf{A})$$

User programmable parameters

  - Steps to follow
    - Transform the constrained minimization problem into an unconstrained one
    - Transform the general unconstrained optimization problem into a series of quadratic ones
    - Transform each continuous quadratic optimization problem into a binarized one
    - Apply to the double-minimization framework

Double-minimization process solved by Quantum annealing

- Transform the constrained minimization problem into an unconstrained one
  - Constrained multivariate minimization problem
    - $\min_{\mathbf{w}} f(\mathbf{w})$ with $\mathbf{w}^{\min} \leq \mathbf{w} \leq \mathbf{w}^{\max}$
    - Under constraints $h(\mathbf{w}) = 0$ & $l(\mathbf{w}) \leq 0$
  - Augmented minimization problem
    - $f_{\mathrm{aug}}(\mathbf{v}) = f_{\mathrm{aug}}(\mathbf{w}, \lambda) = f(\mathbf{w}) + c^h\left(h(\mathbf{w})\right)^2 + c^l(l(\mathbf{w}) + \lambda)^2$ with $\mathbf{v} = \{\boldsymbol{w}, \lambda \geq 0\}$
  - Unconstrained minimization problem
    - $\min_{\mathbf{v}} f_{\mathrm{aug}}(\mathbf{v})$ with $\mathbf{v}^{\min} \leq \mathbf{v} \leq \mathbf{v}^{\max}$
    - Bounds will be enforced during the binarization process
  - Definition of the double-unconstrained minimization problem

Loop until convergence

$$\mathbf{q}_{n+1} = \arg \min_{\mathbf{q}' \text{constrained}} \Delta\Phi(\boldsymbol{u}_{n+1}, \mathbf{q}')\,;$$
$$\Delta\Phi^{\mathrm{eff}} = \min_{\mathbf{q}' \text{constrained}} \Delta\Phi(\boldsymbol{u}_{n+1}, \mathbf{q}')$$
$$\boldsymbol{u}_{n+1} = \arg \min_{\mathbf{u}' \text{admissible}} \Delta\Phi^{\mathrm{eff}}(\mathbf{u}')$$

Loop until convergence

$$\mathbf{q}_{n+1}, \lambda = \arg \min_{\{\mathbf{q}', \lambda'\}} \Delta\Phi_{\mathrm{aug}}(\boldsymbol{u}_{n+1}, \mathbf{q}', \lambda')\,;$$
$$\Delta\Phi^{\mathrm{eff}} = \min_{\{\mathbf{q}', \lambda'\}} \Delta\Phi_{\mathrm{aug}}(\boldsymbol{u}_{n+1}, \mathbf{q}', \lambda')$$
$$\boldsymbol{u}_{n+1} = \arg \min_{\mathbf{u}' \text{admissible}} \Delta\Phi^{\mathrm{eff}}(\mathbf{u}')$$

Double-minimization process solved by Quantum annealing

- Transform the constrained minimization problem into an unconstrained one
  - E.g. J2-plasticity
    - $$\Delta\mathcal{E} = \frac{1}{2}\left(\boldsymbol{\varepsilon}_{n+1} - \Delta\gamma\mathbf{N} - \boldsymbol{\varepsilon}_n^{\mathrm{pl}}\right) : \mathbb{C}^{\mathbf{el}} : \left(\boldsymbol{\varepsilon}_{n+1} - \Delta\gamma\mathbf{N} - \boldsymbol{\varepsilon}_n^{\mathrm{pl}}\right) + \int_{\gamma_n}^{\gamma_{n+1}} \left(\sigma_y^0 + R(\gamma')\right) d\gamma' - \frac{1}{2}\left(\boldsymbol{\varepsilon}_n - \boldsymbol{\varepsilon}_n^{\mathrm{pl}}\right) : \mathbb{C}^{\mathbf{el}} : \left(\boldsymbol{\varepsilon}_n - \boldsymbol{\varepsilon}_n^{\mathrm{pl}}\right)$$
    - Under constraints $\mathbf{N} : \mathbf{N} = \frac{3}{2}$, $\mathrm{tr}(\mathbf{N}) = 0$ & $\Delta\gamma \geq 0$
    - Change of variables

$$\begin{cases} \mathbf{N} : \mathbf{N} = \boldsymbol{\alpha}^T \mathbf{M} \boldsymbol{\alpha} = \frac{3}{2} \\ \boldsymbol{\alpha} = [\alpha_0 \ldots \alpha_4]^{\mathrm{T}}, -\sqrt{\frac{3}{2}} \leq \alpha_i \leq -\sqrt{\frac{3}{2}}, \end{cases} \quad \mathbf{N} = \begin{bmatrix} \alpha_0 & \alpha_2/\sqrt{2} & \alpha_2/\sqrt{2} \\ & \alpha_1 & \alpha_4/\sqrt{2} \\ \mathrm{SYM} & & -\alpha_0 - \alpha_1 \end{bmatrix} \quad \& \quad \mathbf{M} = \mathbf{cst}$$

    - Definition of the double unconstrained minimization problem

Loop until convergence

$$\mathbf{q}_{n+1} = \arg \min_{\mathbf{q}' \text{constrained}} \Delta\Phi(\boldsymbol{u}_{n+1}, \mathbf{q}') ;$$

$$\Delta\Phi^{\mathrm{eff}} = \min_{\mathbf{q}' \text{constrained}} \Delta\Phi(\boldsymbol{u}_{n+1}, \mathbf{q}')$$

$$\boldsymbol{u}_{n+1} = \arg \min_{\mathbf{u}' \text{admissible}} \Delta\Phi^{\mathrm{eff}}(\mathbf{u}')$$

Loop until convergence

$$\{\Delta\gamma, \boldsymbol{\alpha}\} = \arg \min_{\{\Delta\gamma', \boldsymbol{\alpha}'\}} \left[\int_V \Delta\mathcal{E}\left(\boldsymbol{u}_{n+1}, \Delta\gamma', \boldsymbol{\alpha}'\right) + c^h \left(\alpha^T \mathrm{M} \alpha - \frac{3}{2}\right)^2 dV\right]$$

$$\Delta\Phi^{\mathrm{eff}} = \min_{\{\Delta\gamma', \boldsymbol{\alpha}'\}} \Delta\Phi_{\mathrm{aug}}(\boldsymbol{u}_{n+1}, \Delta\gamma', \boldsymbol{\alpha}')$$

$$\boldsymbol{u}_{n+1} = \arg \min_{\mathbf{u}' \text{admissible}} \Delta\Phi^{\mathrm{eff}}(\mathbf{u}')$$

Double-minimization process solved by Quantum annealing

- Transform the optimization problem into a series of quadratic ones
  - Unconstrained optimization problem
    - $\min_{\mathbf{v}} f_{\text{aug}}(\mathbf{v})$ with $\mathbf{v}^{\min} \leq \mathbf{v} \leq \mathbf{v}^{\max}$
  - Taylor's expansion
    - $f_{\text{aug}}(\mathbf{v}+\mathbf{z}) \simeq f_{\text{aug}}(\mathbf{v}) + \underbrace{\mathbf{z}^{\mathrm{T}} f_{\text{aug},\mathbf{v}} + \frac{1}{2}\mathbf{z}^{\mathrm{T}} f_{\text{aug},\mathbf{vv}}\,\mathbf{z}}_{\mathrm{QF}(\mathbf{z};\, f_{\text{aug},\mathbf{v}},\, f_{\text{aug},\mathbf{vv}})}$

$$\begin{cases} f_{\text{aug},\mathbf{v}\;i} = \left.\dfrac{\partial f_{\text{aug}}}{\partial v_i}\right|_{\mathbf{v}} \\ f_{\text{aug},\mathbf{vv}\;ij} = \left.\dfrac{\partial^2 f_{\text{aug}}}{\partial v_i \partial v_j}\right|_{\mathbf{v}} \end{cases}$$

  - New series of optimization problems
    - Iterate on $\mathbf{z}$ with: $\mathbf{z} = \arg\min_{\mathbf{z}'} \mathrm{QF}(\mathbf{z}';\, f_{\text{aug},\mathbf{v}},\, f_{\text{aug},\mathbf{vv}})$
  - Application to the double minimisation problem

Loop until convergence

$$\mathbf{q}_{n+1}, \lambda = \arg\min_{\{\mathbf{q}',\lambda'\}} \Delta\Phi_{\text{aug}}(\boldsymbol{u}_{n+1}, \mathbf{q}', \lambda')\,;$$

$$\Delta\Phi^{\text{eff}} = \min_{\{\mathbf{q}',\lambda'\}} \Delta\Phi_{\text{aug}}(\boldsymbol{u}_{n+1}, \mathbf{q}', \lambda')$$

$$\boldsymbol{u}_{n+1} = \arg\min_{\mathbf{u}'\text{admissible}} \Delta\Phi^{\text{eff}}(\mathbf{u}')$$

Loop until convergence

Loop on $\boldsymbol{u}_{n+1} \leftarrow \boldsymbol{u}_{n+1} + \boldsymbol{\Delta}\mathbf{u}$

$$\boldsymbol{\Delta u} = \arg\min_{\boldsymbol{\Delta}\mathbf{u}'\text{admissible}} \boldsymbol{\Delta}\mathbf{u}'^{\mathrm{T}} \Delta\Phi^{\text{eff}}_{,\mathbf{u}} + \frac{1}{2}\boldsymbol{\Delta}\mathbf{u}'^{\mathrm{T}} \Delta\Phi^{\text{eff}}_{,\mathbf{uu}}\;\boldsymbol{\Delta}\mathbf{u}'$$

Loop on $\boldsymbol{q}_{n+1} \leftarrow \boldsymbol{q}_{n+1} + \boldsymbol{\Delta}\mathbf{q},\ \boldsymbol{\lambda} \leftarrow \boldsymbol{\lambda} + \Delta\lambda$

$$\boldsymbol{\Delta}\mathbf{q}, \Delta\lambda = \arg\min_{\{\boldsymbol{\Delta}\mathbf{q}',\Delta\lambda'\}} \left[\boldsymbol{\Delta}\mathbf{q}'^{\mathrm{T}} \Delta\lambda'\right] \Delta\Phi_{\text{aug},\{\mathrm{q}\,\lambda\}} + \frac{1}{2}\left[\boldsymbol{\Delta}\mathbf{q}'^{\mathrm{T}} \Delta\lambda'\right] \Delta\Phi_{\text{aug},\{\mathrm{q}\,\lambda\}\{\mathrm{q}\,\lambda\}} \left[\boldsymbol{\Delta}\mathbf{q}'^{\mathrm{T}} \Delta\lambda'\right]^{\mathrm{T}}$$

$$\Delta\Phi^{\text{eff}} = \Delta\Phi_{\text{aug}}(\boldsymbol{u}_{n+1}, \mathbf{q}_{n+1}, \lambda)$$

Double-minimization process solved by Quantum annealing

- Transform the optimization problem into a series of quadratic ones
  - E.g. J2-plasticity
    - Minimization with respect to the internal variables (at constant displacement field)

$$\Delta\Phi_{\text{aug}}(\boldsymbol{u}_{n+1},\Delta\gamma,\boldsymbol{\alpha}) = \int_V \Delta\mathcal{E}(\boldsymbol{u}_{n+1},\Delta\gamma',\boldsymbol{\alpha}) + c^h\left(\boldsymbol{\alpha}^T\mathrm{M}\boldsymbol{\alpha} - \frac{3}{2}\right)^2 dV - \Delta W^{\text{ext}}(\boldsymbol{u}_{n+1})$$

with $\Delta\mathcal{E} = \frac{1}{2}\left(\boldsymbol{\varepsilon}_{n+1} - \Delta\gamma\mathbf{N} - \boldsymbol{\varepsilon}_n^{\text{pl}}\right):\mathbb{C}^{\text{el}}:\left(\boldsymbol{\varepsilon}_{n+1} - \Delta\gamma\mathbf{N} - \boldsymbol{\varepsilon}_n^{\text{pl}}\right) + \int_{\gamma_n}^{\gamma_{n+1}}\left(\sigma_y^0 + R(\gamma')\right)d\gamma' - \frac{1}{2}\left(\boldsymbol{\varepsilon}_n - \boldsymbol{\varepsilon}_n^{\text{pl}}\right):\mathbb{C}^{\text{el}}:\left(\boldsymbol{\varepsilon}_n - \boldsymbol{\varepsilon}_n^{\text{pl}}\right)$

$$\Rightarrow \Delta\Phi_{\text{aug},\boldsymbol{\alpha}} = \sum_{\Xi}\left(\Delta\mathcal{E}_{,\mathbf{N}}:\frac{\partial\mathbf{N}}{\partial\boldsymbol{\alpha}} + 2c^h\mathbf{M}\boldsymbol{\alpha}\left(\boldsymbol{\alpha}^T\mathrm{M}\boldsymbol{\alpha} - \frac{3}{2}\right)\right)\omega^{\Xi} \quad \& \quad \Delta\Phi_{\text{aug},\Delta\gamma} = \sum_{\Xi}\Delta\mathcal{E}_{,\boldsymbol{\Delta\gamma}}\,\omega^{\Xi}$$

$$\Rightarrow \Delta\Phi_{\text{aug},\boldsymbol{\alpha\alpha}},\ \Delta\Phi_{\text{aug},\boldsymbol{\alpha}\Delta\gamma},\ \Delta\Phi_{\text{aug},\Delta\gamma\boldsymbol{\alpha}},\ \Delta\Phi_{\text{aug},\Delta\gamma\Delta\gamma}$$

- Minimization with respect to $\boldsymbol{u}_{n+1}$ (at constant internal variables)

$$\Delta\Phi^{\text{eff}}(\boldsymbol{u}_{n+1}) = \int_V \Delta\mathcal{E}^{\text{eff}}(\boldsymbol{u}_{n+1})\,dV - \Delta W^{\text{ext}}(\boldsymbol{u}_{n+1}) \qquad \text{with} \quad \boldsymbol{\sigma} = \frac{\partial\Delta\mathcal{E}^{\text{eff}}}{\partial\boldsymbol{\varepsilon}}$$

$$\Rightarrow \begin{cases} \Delta\Phi^{\text{eff}}_{,\mathbf{u}}(\boldsymbol{u}_{n+1}) = \sum_{\Xi}\mathbf{B}^{\mathrm{T}}(\Xi)\,\boldsymbol{\sigma}(\Xi)\omega^{\Xi} - \mathbf{f}^{\text{ext}} \\ \Delta\Phi^{\text{eff}}_{,\mathbf{uu}}(\boldsymbol{u}_{n+1}) = \sum_{\Xi}\mathbf{B}^{\mathrm{T}}(\Xi)\,\mathbb{C}^{\text{el}}(\Xi)\,\mathbf{B}(\Xi)\omega^{\Xi} - \mathbf{f}^{\text{ext}} \end{cases}$$

Constant material tensor

  - Only assembly operations required ⇒ Performed on classical computers

Double-minimization process solved by Quantum annealing

- Transform each continuous quadratic optimization problem into a binarized one
  - Optimization problems to be solved
    - $\mathbf{z} = \arg\min_{\mathbf{z}'} \mathrm{QF}(\mathbf{z}', f_{\mathrm{aug},\mathbf{v}}, f_{\mathrm{aug},\mathbf{vv}})$ & $\mathrm{QF}(\mathbf{z}; f_{\mathrm{aug},\mathbf{v}}, f_{\mathrm{aug},\mathbf{vv}}) = \mathbf{z}^{\mathrm{T}} f_{\mathrm{aug},\mathbf{v}} + \frac{\mathbf{1}}{\mathbf{2}} \mathbf{z}^{\mathrm{T}} f_{\mathrm{aug},\mathbf{vv}} \mathbf{z}$
    - With bounds: $\mathbf{v}_{\mathbf{min}} \leq \mathbf{v} + \mathbf{z} \leq \mathbf{v}_{\mathbf{max}}$
    - These are Ising Hamiltonians to be minimized, but not of the QUBO type
  - QUBO
    - $\mathbf{b} = [b_i \ \forall i \in V]$ with $b_i \in \{0, 1\}$
    - Eigen value $\mathcal{F}_{\mathrm{QUBO}} = \mathbf{b}^T \mathbf{A} \mathbf{b}$
    - QUBO optimization $\mathbf{b} = \arg\min_{\mathbf{b}'} \mathcal{F}_{\mathrm{QUBO}}(\mathbf{b}'; \mathbf{A})$ User programmable parameters
  - Binary-decimal conversion of a scalar field
    - Definition of a L-bit string under the form $\mathbf{b_1} = [b_0 \ \ldots b_{L-1}]^{\mathrm{T}}$ with $b_i \in \{0, 1\}$
    - Conversion $b_{L-1} \ \ldots b_0 \equiv \sum_{j=0}^{L-1} b_j \ 2^j = \boldsymbol{\beta}^{\mathrm{T}} \mathbf{b_1}$ with $\boldsymbol{\beta} = [2^0 \ 2^1 \ \ldots \ 2^{L-1}]^{\mathrm{T}}$
    - Introduce the bounds $z \in [z^{\min}, z^{\max}]$

      $\Rightarrow$ $z = z^{\min} + \epsilon_1 \boldsymbol{\beta}^T \mathbf{b_1}$ with the scaling $\epsilon_1 = \dfrac{z^{\max} - z^{\min}}{2^L - 1}$
    - One scalar is represented (in a discrete way) by L qubits
  - Binary-decimal conversion of a vector field
    - Vector of size N represented by $N \times L$ qubits
    - $\mathbf{z} = \mathbf{z}^{\min} + [\epsilon_i \boldsymbol{\beta}^T \mathbf{b}_i \ \text{ for } \ i = 0..N-1]$ $\Rightarrow$ $\mathbf{z} = \mathbf{a} + \mathbf{D}(\boldsymbol{\epsilon})\mathbf{b}$

- Transform each continuous quadratic optimization problem into a binarized one
  - Optimization problems to be solved
    - $\mathbf{z} = \arg\min_{\mathbf{z}'} \mathrm{QF}(\mathbf{z}', f_{\mathrm{aug},\mathbf{v}}, f_{\mathrm{aug},\mathbf{vv}})$ & $\mathrm{QF}(\mathbf{z}; f_{\mathrm{aug},\mathbf{v}}, f_{\mathrm{aug},\mathbf{vv}}) = \mathbf{z}^{\mathrm{T}} f_{\mathrm{aug},\mathbf{v}} + \frac{1}{2}\mathbf{z}^{\mathrm{T}} f_{\mathrm{aug},\mathbf{vv}}\, \mathbf{z}$
    - With bounds: $\mathbf{v}_{\mathbf{min}} \leq \mathbf{v} + \mathbf{z} \leq \mathbf{v}_{\mathbf{max}}$
  - Binarization of $z \in \mathbb{R}^N$ into $N \times L$ qubits
    - $\mathbf{z} = \mathbf{a} + \mathbf{D}(\boldsymbol{\epsilon})\mathbf{b}$ with the bounds defining $\mathbf{a} = \mathbf{z}^{\min}$ & the scales $\boldsymbol{\epsilon} = \dfrac{\mathbf{z}^{\max} - \mathbf{z}^{\min}}{2^L - 1}$

$$\Rightarrow \mathrm{QF}\left(\mathbf{z}; f_{\mathrm{aug},\mathbf{v}}, f_{\mathrm{aug},\mathbf{vv}}\right) = \underbrace{\frac{1}{2}\mathbf{b}^{\mathrm{T}}\mathbf{D}^{\mathrm{T}} f_{\mathrm{aug},\mathbf{vv}}\, \mathbf{D}\mathbf{b} + \mathbf{b}^{\mathrm{T}}\mathbf{D}^{\mathrm{T}}\left(f_{\mathrm{aug},\mathbf{v}} + f_{\mathrm{aug},\mathbf{vv}}\, \mathbf{a}\right)}_{\mathcal{F}_{\mathrm{QUBO}}(\mathbf{b};\mathbf{A})} + \frac{1}{2}\mathbf{a}^{\mathrm{T}}\left(f_{\mathrm{aug},\mathbf{vv}}\, \mathbf{a} + f_{\mathrm{aug},\mathbf{v}}\right)$$

  - Minimization
    - Bound $\mathbf{a} = \mathbf{z}^{\min}$ and
    - Scale $\boldsymbol{\epsilon} = \dfrac{\mathbf{z}^{\max} - \mathbf{z}^{\min}}{2^L - 1}$
    - Updated when building the QUBO

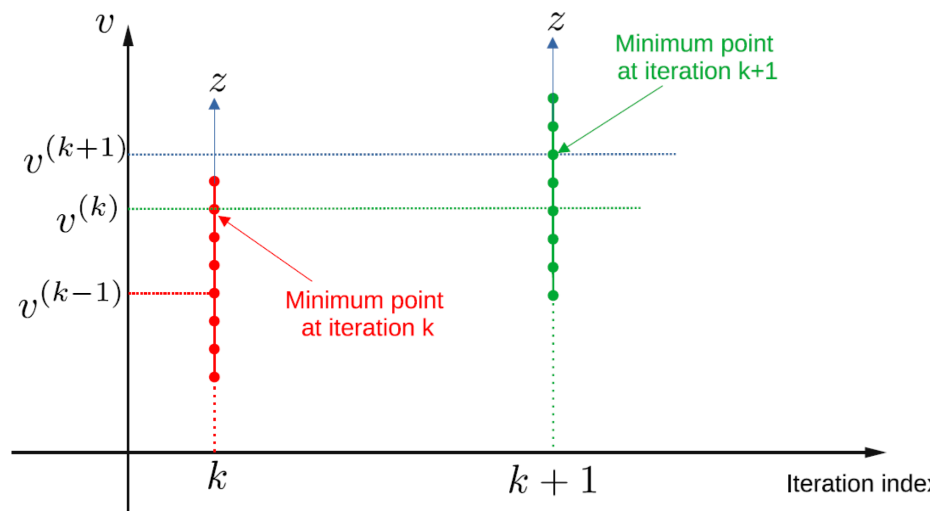

Double-minimization process solved by Quantum annealing

- Application to the double-minimization problem

Loop until convergence

Loop on $\boldsymbol{u}_{n+1} \leftarrow \boldsymbol{u}_{n+1} + \Delta\mathbf{u}$

$$\Delta\boldsymbol{u} = \arg\min_{\Delta\mathbf{u}'\text{admissible}} \Delta\mathbf{u}'^{\mathrm{T}}\Delta\Phi^{\mathrm{eff}}_{,\mathbf{u}} + \frac{1}{2}\Delta\mathbf{u}'^{\mathrm{T}}\Delta\Phi^{\mathrm{eff}}_{,\mathbf{uu}}\ \Delta\mathbf{u}'$$

Loop on $\boldsymbol{q}_{n+1} \leftarrow \boldsymbol{q}_{n+1} + \Delta\mathbf{q}$, $\boldsymbol{\lambda} \leftarrow \boldsymbol{\lambda} + \Delta\lambda$

$$\Delta\mathbf{q}, \Delta\lambda = \arg\min_{\{\Delta\mathbf{q}',\Delta\lambda'\}} [\Delta\mathbf{q}'^{\mathrm{T}}\Delta\lambda']\,\Delta\Phi_{\mathrm{aug},\{q\ \lambda\}} + \frac{1}{2}[\Delta\mathbf{q}'^{\mathrm{T}}\Delta\lambda']\Delta\Phi_{\mathrm{aug},\{q\ \lambda\}\{q\ \lambda\}}\,[\Delta\mathbf{q}'^{\mathrm{T}}\Delta\lambda']^{\mathrm{T}}$$

$$\Delta\Phi^{\mathrm{eff}} = \Delta\Phi_{\mathrm{aug}}(\boldsymbol{u}_{n+1}, \mathbf{q}_{n+1}, \lambda)$$

Loop until convergence

Loop on $\boldsymbol{u}_{n+1} \leftarrow \boldsymbol{u}_{n+1} + \Delta\mathbf{u}$

$$f(\Delta\mathbf{u}) = \Delta\mathbf{u}^{\mathrm{T}}\Delta\Phi^{\mathrm{eff}}_{,\mathbf{u}} + \frac{1}{2}\Delta\mathbf{u}^{\mathrm{T}}\Delta\Phi^{\mathrm{eff}}_{,\mathbf{uu}}\,\Delta\mathbf{u}$$

Update $\mathrm{a_u}, \mathbf{D}(\boldsymbol{\epsilon}_\mathbf{u})$

$$\mathbf{b_u} = \arg\min_{\mathbf{b}'_\mathbf{u}} \left(\frac{1}{2}\mathbf{b}'^{\mathrm{T}}_\mathbf{u}\mathbf{D}^{\mathrm{T}}\Delta\Phi^{\mathrm{eff}}_{,\mathbf{uu}}\mathbf{D}\mathbf{b}'_\mathbf{u} + \mathbf{b}'^{\mathrm{T}}_\mathbf{u}\mathbf{D}^{\mathrm{T}}\left(\Delta\Phi^{\mathrm{eff}}_{,\mathbf{u}} + \Delta\Phi^{\mathrm{eff}}_{,\mathbf{uu}}\mathbf{a_u}\right)\right)$$

Loop on $\boldsymbol{q}_{n+1} \leftarrow \boldsymbol{q}_{n+1} + \Delta\mathbf{q}$, $\boldsymbol{\lambda} \leftarrow \boldsymbol{\lambda} + \Delta\lambda$

$$f(\Delta\mathbf{q}, \Delta\lambda) = [\Delta\mathbf{q}^{\mathrm{T}}\Delta\lambda]\Delta\Phi_{\mathrm{aug},\{q\ \lambda\}} + \frac{1}{2}[\Delta\mathbf{q}^{\mathrm{T}}\Delta\lambda]\Delta\Phi_{\mathrm{aug},\{q\ \lambda\}\{q\ \lambda\}}[\Delta\mathbf{q}^{\mathrm{T}}\Delta\lambda]^{\mathrm{T}}$$

Update $\mathrm{a_q}, \mathbf{D}(\boldsymbol{\epsilon}_\mathbf{q})$

$$\mathbf{b_q} = \arg\min_{\mathbf{b}'_\mathbf{q}} \left(\frac{1}{2}\mathbf{b}'^{\mathrm{T}}_\mathbf{q}\mathbf{D}^{\mathrm{T}}\Delta\Phi_{\mathrm{aug},\{q\ \lambda\}\{q\ \lambda\}}\mathbf{D}\mathbf{b}'_\mathbf{q} + \mathbf{b}'^{\mathrm{T}}_\mathbf{q}\mathbf{D}^{\mathrm{T}}\left(\Phi_{\mathrm{aug},\{q\ \lambda\}} + \Delta\Phi_{\mathrm{aug},\{q\ \lambda\}\{q\ \lambda\}}\mathbf{a_q}\right)\right)$$

$$\Delta\Phi^{\mathrm{eff}} = \Delta\Phi_{\mathrm{aug}}(\boldsymbol{u}_{n+1}, \mathbf{q}_{n+1}, \lambda)$$

Quantum annealing

Quantum annealing

Application on 1D problems

- Uniaxial-strain test

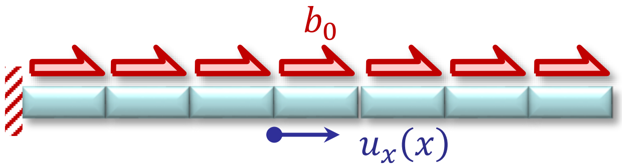

- Elastic case
  - Simple minimization conducted on the displacement field
    - Consider different numbers N of elements
    - Consider different binarizations L of each nodal displacement: $b_{L-1} \dots b_0 \equiv \sum_{j=0}^{L-1} b_j \; 2^j = \boldsymbol{\beta}^{\mathrm{T}}\mathbf{b}_{\boldsymbol{i}}$
  - Resolution by quantum annealing on DWave Advantage QPU

Loop on $\boldsymbol{u}_{n+1} \leftarrow \boldsymbol{u}_{n+1} + \boldsymbol{\Delta}\mathbf{u}$

$$f(\boldsymbol{\Delta}\mathbf{u}) = \boldsymbol{\Delta}\mathbf{u}^{\mathrm{T}}\Delta\Phi^{\mathrm{eff}}_{,\mathbf{u}} + \frac{1}{2}\boldsymbol{\Delta}\mathbf{u}^{\mathrm{T}}\Delta\Phi^{\mathrm{eff}}_{,\mathbf{uu}}\,\boldsymbol{\Delta}\mathbf{u}$$

Update $\mathbf{a}_{\mathrm{u}}, \mathbf{D}(\boldsymbol{\epsilon}_{\mathbf{u}})$

$\mathbf{b}'^{\mathrm{T}}_{u}\mathbf{A}\mathbf{b}'_{u}$

$$\mathbf{b}_{\mathbf{u}} = \arg\min_{\mathbf{b}'_{\mathbf{u}}}\left(\frac{1}{2}\mathbf{b}'_{\mathbf{u}}{}^{\mathrm{T}}\mathbf{D}^{\mathrm{T}}\Delta\Phi^{\mathrm{eff}}_{,\mathbf{uu}}\mathbf{D}\mathbf{b}'_{\mathbf{u}} + \mathbf{b}'_{\mathbf{u}}{}^{\mathrm{T}}\mathbf{D}^{\mathrm{T}}\left(\Delta\Phi^{\mathrm{eff}}_{,\mathbf{u}} + \Delta\Phi^{\mathrm{eff}}_{,\mathbf{uu}}\mathbf{a}_{\mathbf{u}}\right)\right)$$

Quantum annealing

```
from dwave.system import DWaveSampler, EmbeddingComposite
sampler = EmbeddingComposite(DWaveSampler())
sampleset = sampler.sample_qubo(A, num_reads=100, annealing_time=20)
b = sampleset.first.sample
```

Application on 1D problems

- Uniaxial-strain test

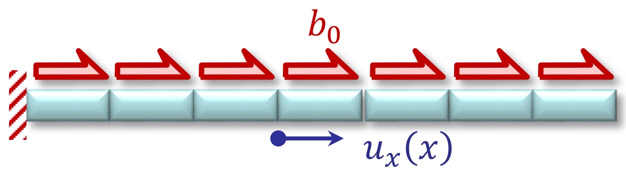

- Elasto-plastic case
  – Double minimization
    - Binarizations L of each nodal displacement and internal variable: $b_{L-1} \ldots b_0 \equiv \sum_{j=0}^{L-1} b_j \; 2^j = \boldsymbol{\beta}^{\mathrm{T}} \mathbf{b}_i$
  – Resolution by quantum annealing on DWave Advantage QPU

Loop until convergence

Loop on $\boldsymbol{u}_{n+1} \leftarrow \boldsymbol{u}_{n+1} + \boldsymbol{\Delta}\mathbf{u}$

$$f(\boldsymbol{\Delta}\mathbf{u}) = \boldsymbol{\Delta}\mathbf{u}^{\mathrm{T}} \Delta\Phi^{\mathrm{eff}}_{,\mathbf{u}} + \frac{1}{2} \boldsymbol{\Delta}\mathbf{u}^{\mathrm{T}} \Delta\Phi^{\mathrm{eff}}_{,\mathbf{uu}} \boldsymbol{\Delta}\mathbf{u}$$

Update $\mathrm{a}_{\mathrm{u}}, \mathbf{D}(\boldsymbol{\epsilon}_{\mathbf{u}})$

$$\mathbf{b}_{\mathbf{u}} = \arg\min_{\mathbf{b}'_{\mathbf{u}}} \left(\frac{1}{2} {\mathbf{b}'_{\mathbf{u}}}^{\mathrm{T}} \mathbf{D}^{\mathrm{T}} \Delta\Phi^{\mathrm{eff}}_{,\mathbf{uu}} \mathbf{D} \mathbf{b}'_{\mathbf{u}} + {\mathbf{b}'_{\mathbf{u}}}^{\mathrm{T}} \mathbf{D}^{\mathrm{T}} \left(\Delta\Phi^{\mathrm{eff}}_{,\mathbf{u}} + \Delta\Phi^{\mathrm{eff}}_{,\mathbf{uu}} \mathbf{a}_{\mathbf{u}} \right) \right)$$

Loop on $\boldsymbol{q}_{n+1} \leftarrow \boldsymbol{q}_{n+1} + \boldsymbol{\Delta}\mathbf{q}$**,** $\boldsymbol{\lambda} \leftarrow \boldsymbol{\lambda} + \boldsymbol{\Delta\lambda}$

$$f(\boldsymbol{\Delta}\mathbf{q}, \Delta\lambda) = [\boldsymbol{\Delta}\mathbf{q}^{\mathrm{T}} \Delta\lambda] \Delta\Phi_{\mathrm{aug},\{\mathrm{q}\,\lambda\}} + \frac{1}{2} [\boldsymbol{\Delta}\mathbf{q}^{\mathrm{T}} \Delta\lambda] \Delta\Phi_{\mathrm{aug},\{\mathrm{q}\,\lambda\}\{\mathrm{q}\,\lambda\}} [\boldsymbol{\Delta}\mathbf{q}^{\mathrm{T}} \Delta\lambda]^{\mathrm{T}}$$

Update $\mathrm{a}_{\mathrm{q}}, \mathbf{D}(\boldsymbol{\epsilon}_{\mathbf{q}})$

$$\mathbf{b}_{\mathbf{q}} = \arg\min_{\mathbf{b}'_{\mathbf{q}}} \left(\frac{1}{2} {\mathbf{b}'_{\mathbf{q}}}^{\mathrm{T}} \mathbf{D}^{\mathrm{T}} \Delta\Phi_{\mathrm{aug},\{\mathrm{q}\,\lambda\}\{\mathrm{q}\,\lambda\}} \mathbf{D} \mathbf{b}'_{\mathbf{q}} + {\mathbf{b}'_{\mathbf{q}}}^{\mathrm{T}} \mathbf{D}^{\mathrm{T}} \left(\Phi_{\mathrm{aug},\{\mathrm{q}\,\lambda\}} + \Delta\Phi_{\mathrm{aug},\{\mathrm{q}\,\lambda\}\{\mathrm{q}\,\lambda\}} \mathbf{a}_{\mathbf{q}} \right) \right)$$

$$\Delta\Phi^{\mathrm{eff}} = \Delta\Phi_{\mathrm{aug}}(\boldsymbol{u}_{n+1}, \mathbf{q}_{n+1}, \lambda)$$

Double minimization iterations

Local iterations

Quantum annealing

Quantum annealing

Application on 1D problems

- Uniaxial-strain test
- Elasto-plastic case
  - Effect of double-minimization & local iterations

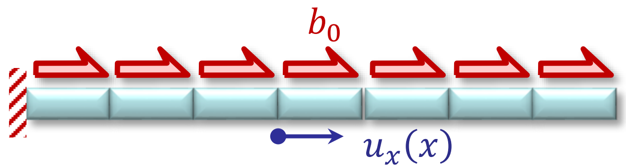

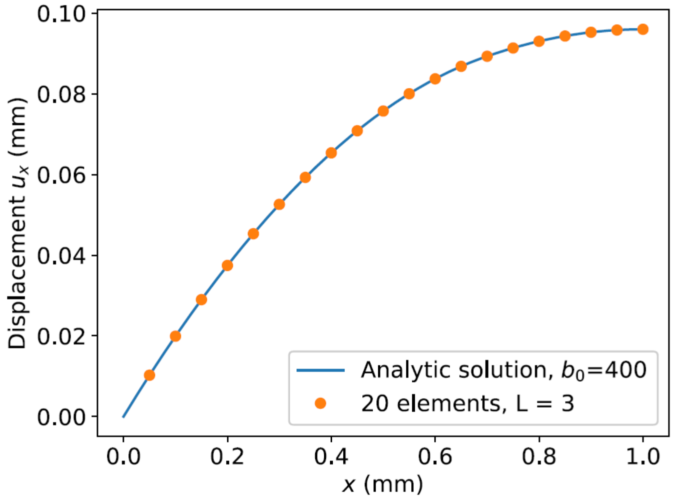

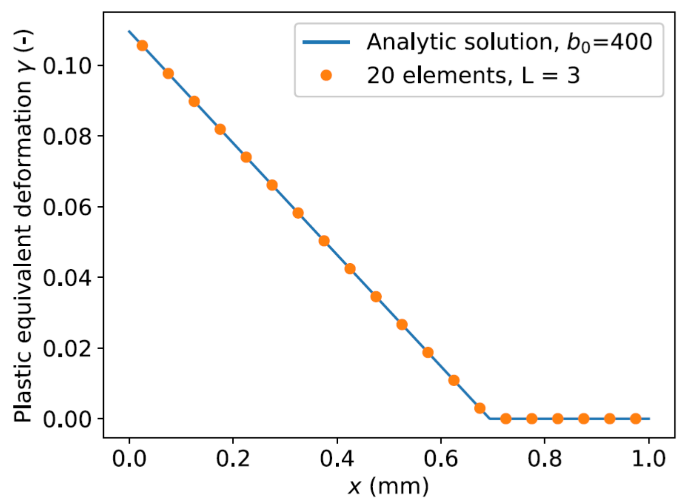

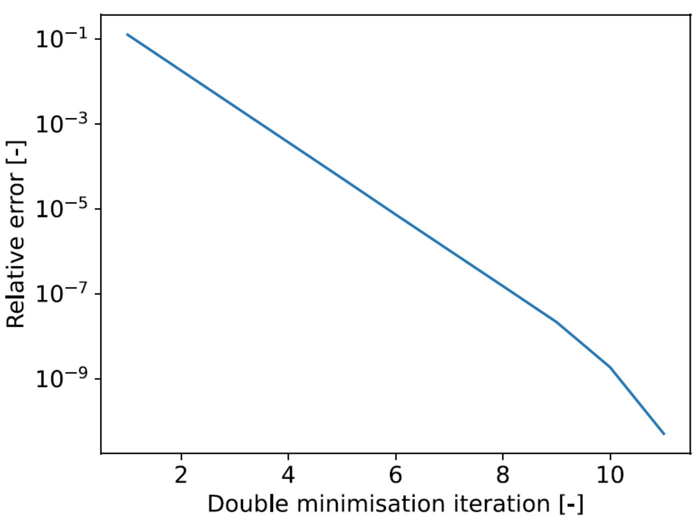

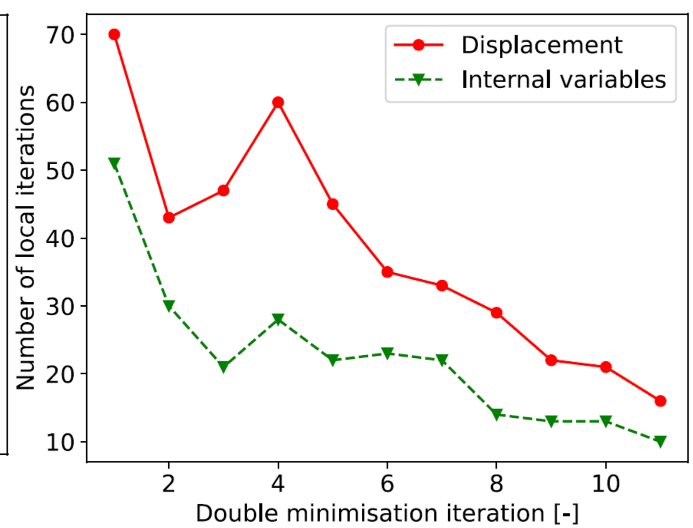

The number of local iterations decreases as the double minimisation iterations proceed

Application on 2D problems

- 2D-elasto-plastic case

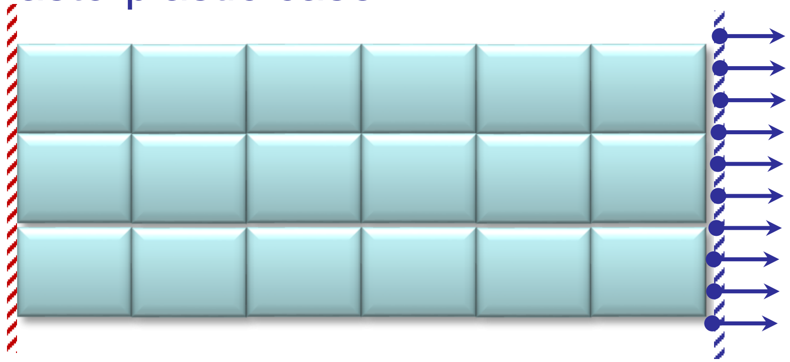

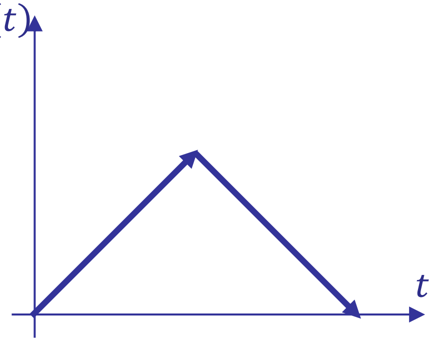

- Double minimization
  - Binarizations L of each nodal displacement and internal variable: $b_{L-1} \ldots b_0 \equiv \sum_{j=0}^{L-1} b_j \; 2^j = \boldsymbol{\beta}^{\mathrm{T}} \mathbf{b}_i$
- Resolution by quantum annealing on DWave Advantage QPU

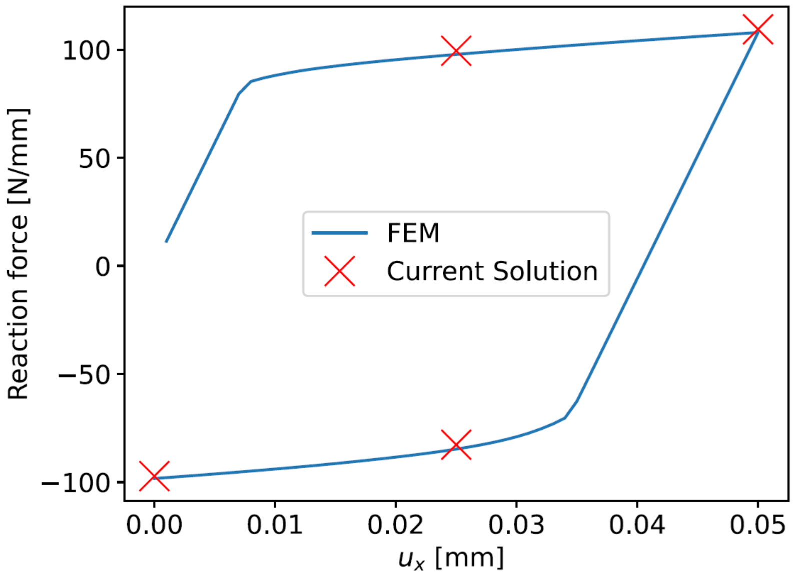

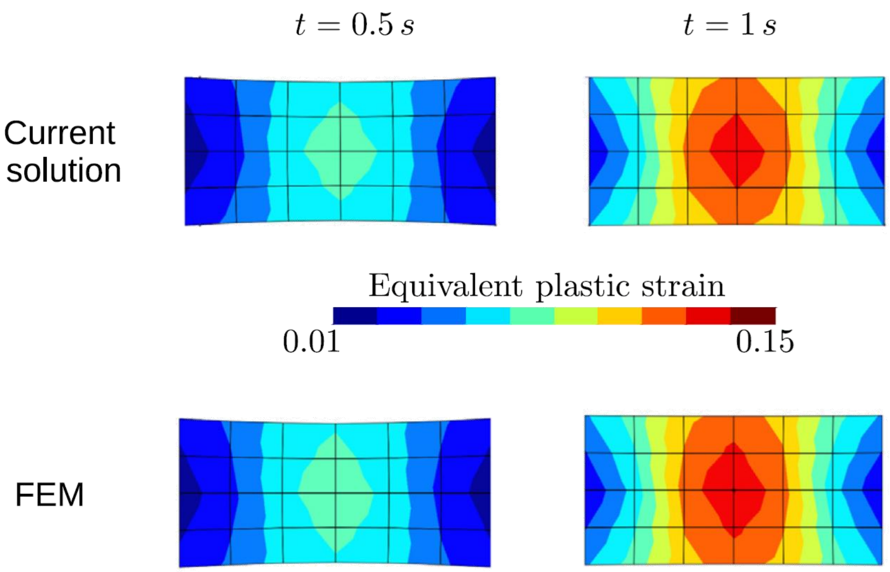

Application on 2D problems

- 2D-elasto-plastic case

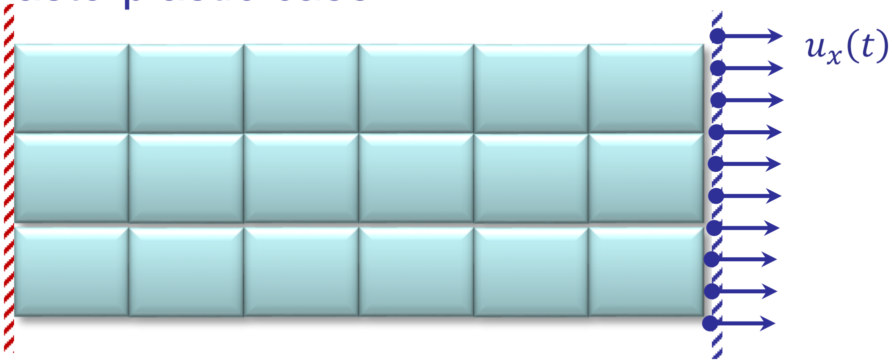

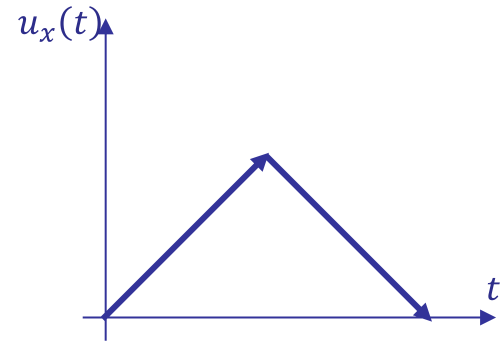

  - Effect of double-minimization & local iterations

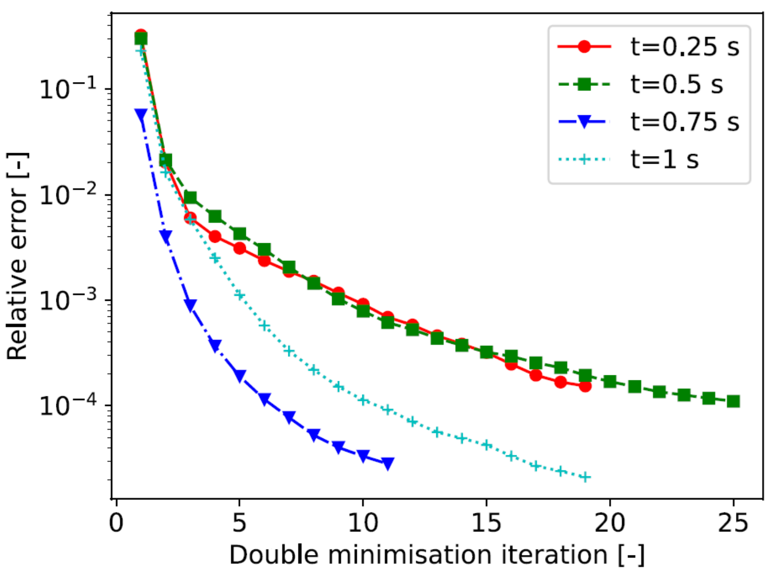

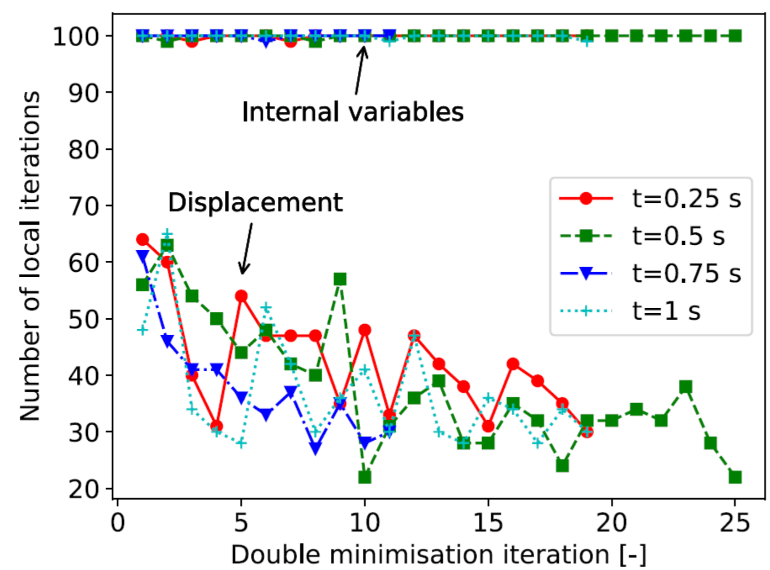

Conclusions

- Application of QC to FEM
  - FE resolution needs to be rethought
  - It will probably stay advantageous to solve part of the problem on classical computers

- Quantum annealing
  - Real annealers can now be used
  - Efficient to solve optimization problem…. FEM is actually a minimization problem
  - Main current limitation is the number of connected qubits

- Publication
  - V. D. Nguyen, F. Remacle, L. Noels. A quantum annealing-sequential quadratic programming assisted finite element simulation for non-linear and history-dependent mechanical problems. *European Journal of Mechanics – A/solids* 105, 105254 10.1016/j.euromechsol.2024.105254
- Data and code on
  - Doi: 10.5281/zenodo.10451584

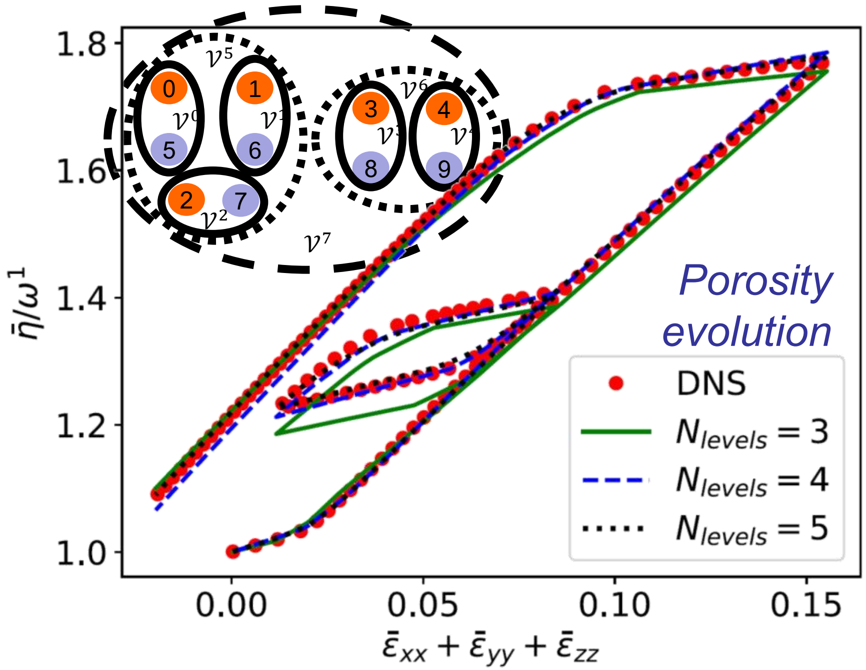

Deep Material Networks from the interaction viewpoint

The authors gratefully acknowledge the financial support from F.R.S-F.N.R.S

Deep Material Networks from the interaction viewpoint

- Architecture of mechanistic building blocks
  - Example for a 2-phase material

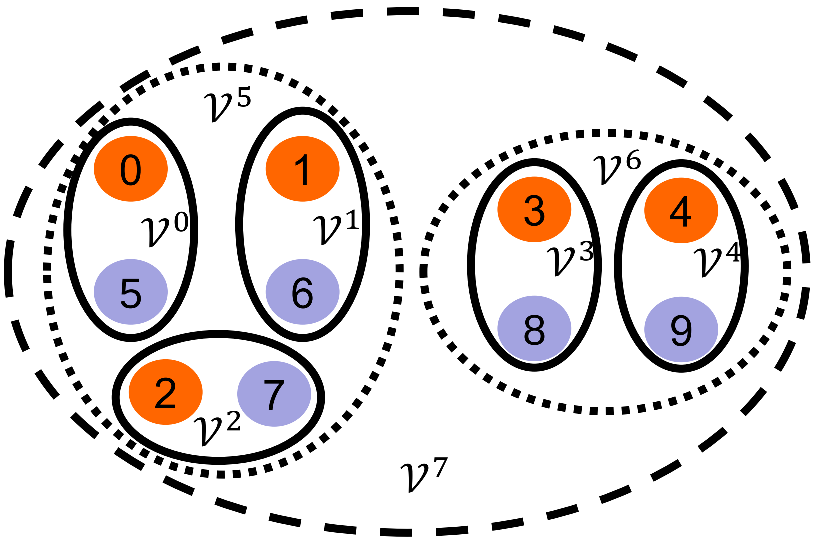

Homogenised behaviour

$$\overline{\boldsymbol{P}}(t) = \overline{\boldsymbol{P}}(\overline{\boldsymbol{F}}(t), z(\tau \leq t))$$

$$\overline{\boldsymbol{P}}(t) = \sum_{i=0}^{9} W^i\, \boldsymbol{P}^i(t)$$

$$\overline{\boldsymbol{F}}(t) = \sum_{i=0}^{9} W^i\, \boldsymbol{F}^i(t)$$

Weight of node i (parameter)

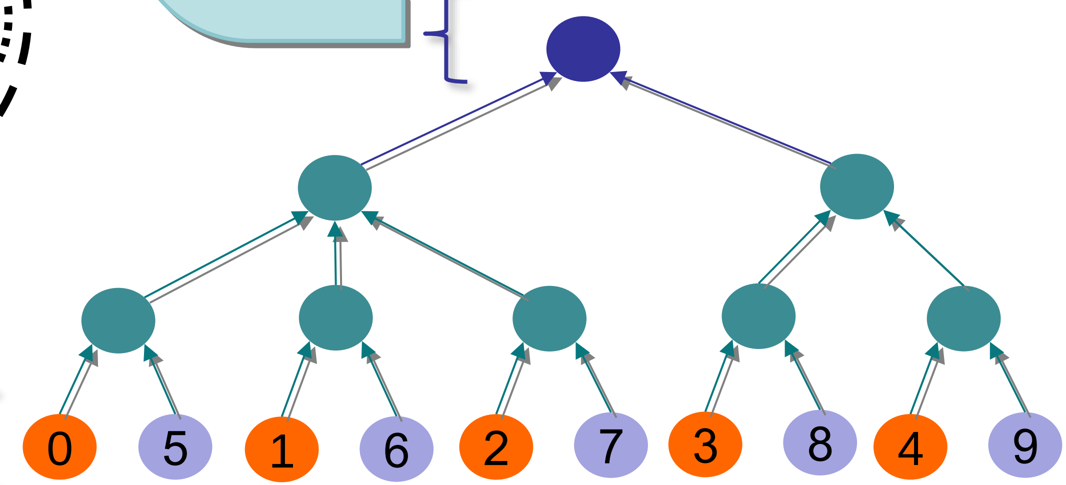

Material node i =0..9, of weight W^i

Constitutive behaviours: $\boldsymbol{P}^p(t) = \boldsymbol{P}^p\left(\boldsymbol{F}^i(t), z(\tau \leq t)\right)$

if node $i \in$ phase p for material p=0 or p=1

Deep Material Networks from the interaction viewpoint

- Mechanism $k = 0..M-1$
  - Link homogenised deformation gradient to node ones
    - Construction of a strain fluctuation field

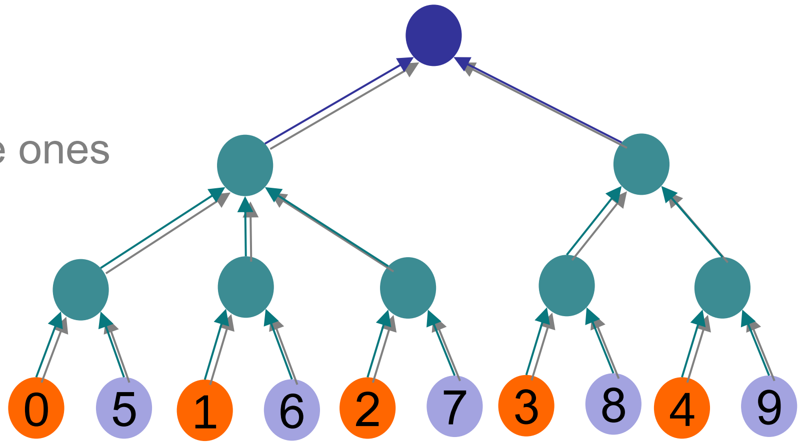

$$\overline{\boldsymbol{F}} + \sum_{k=0}^{M-1} \alpha^{i,k}\, \boldsymbol{a}^k \otimes \boldsymbol{G}^k = \boldsymbol{F}^i\,, \quad i = 0..9$$

Contribution of node i in mechanism k (parameter?)

Degrees of freedom of mechanism k definition the strain fluctuation

Direction of mechanism k (parameter)

Weight of node i (parameter)

  - Constraints from strain averaging
    - $\overline{\boldsymbol{F}} = \sum_i W^i \boldsymbol{F}^i$ ⇨ $\sum_k \left(\sum_i W^i \alpha^{i,k} \right) \boldsymbol{a}^k \otimes \boldsymbol{G}^k = 0$ ⇨ $\sum_i W^i \alpha^{i,k} = 0$
  - Weak form from Hill-Mandel
    - $\overline{\boldsymbol{P}} : \delta\overline{\boldsymbol{F}} = \sum_i W^i\, \boldsymbol{P}^i : \delta\boldsymbol{F}^i$ ⇨ $\left[\sum_k \left(\sum_i W^i \boldsymbol{P}^i \alpha^{i,k} \right) \cdot \boldsymbol{G}^k \right] \cdot\, \delta\boldsymbol{a}^k = 0$

Deep Material Networks from the interaction viewpoint

- Mechanistic building blocks: Laminate
  - Interaction $\mathcal{V}^j$ as a laminate

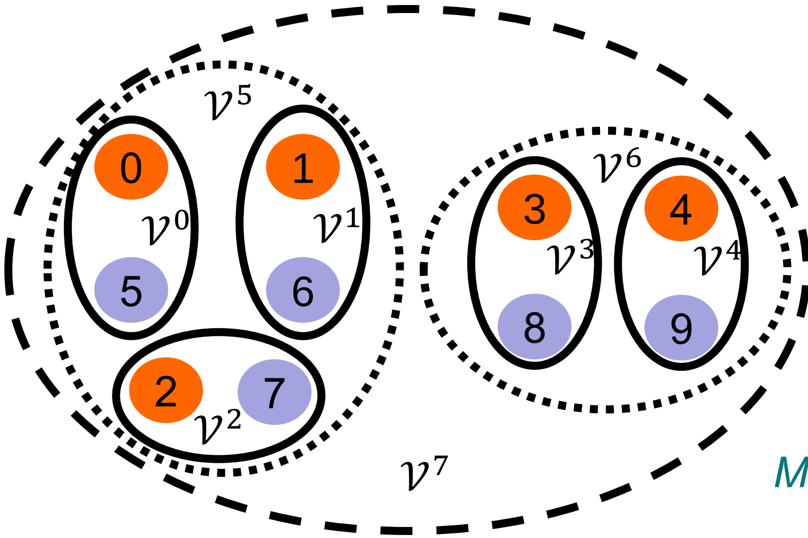

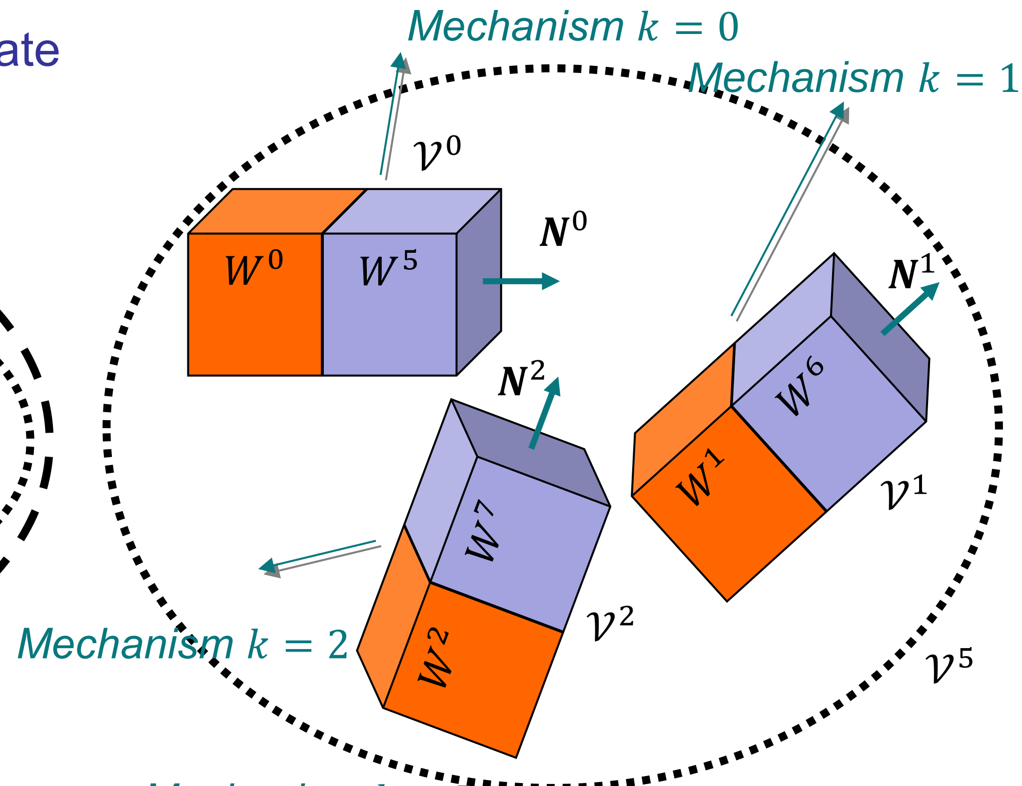

  - Parameters
    - Weight: W^i, $i = 0..9$
    - Unique direction for an interaction $\mathcal{V}^j$:

      $\boldsymbol{G}^k \Rightarrow \boldsymbol{N}^j$, $j = 0..7$
  - Constraint
    - $\sum_i W^i \alpha^{i,k} = 0 \Rightarrow \alpha^{i,k}$ from nodes weight in mechanism k

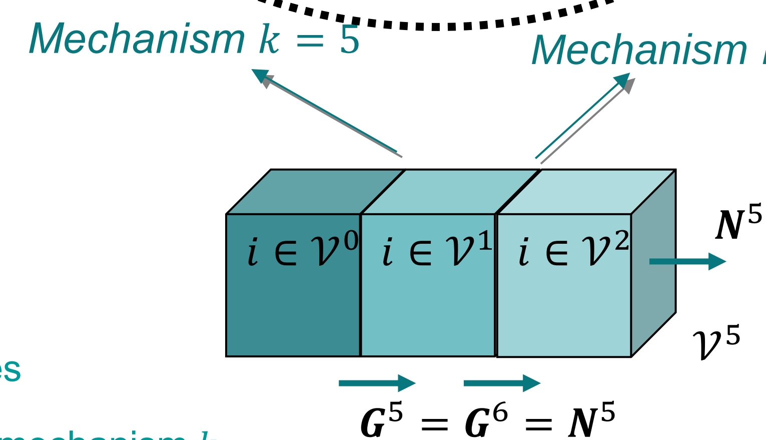

Deep Material Networks from the interaction viewpoint

- Mechanistic building blocks: Laminate
  - Interaction $\mathcal{V}^j$ as a laminate

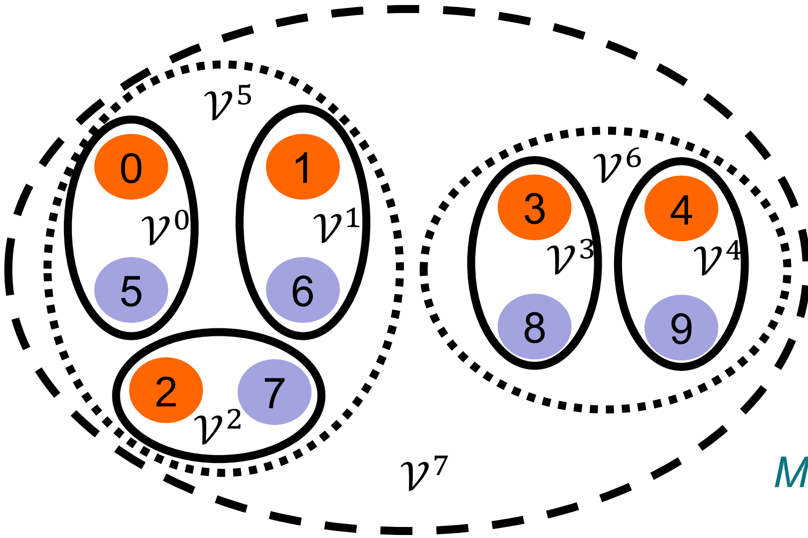

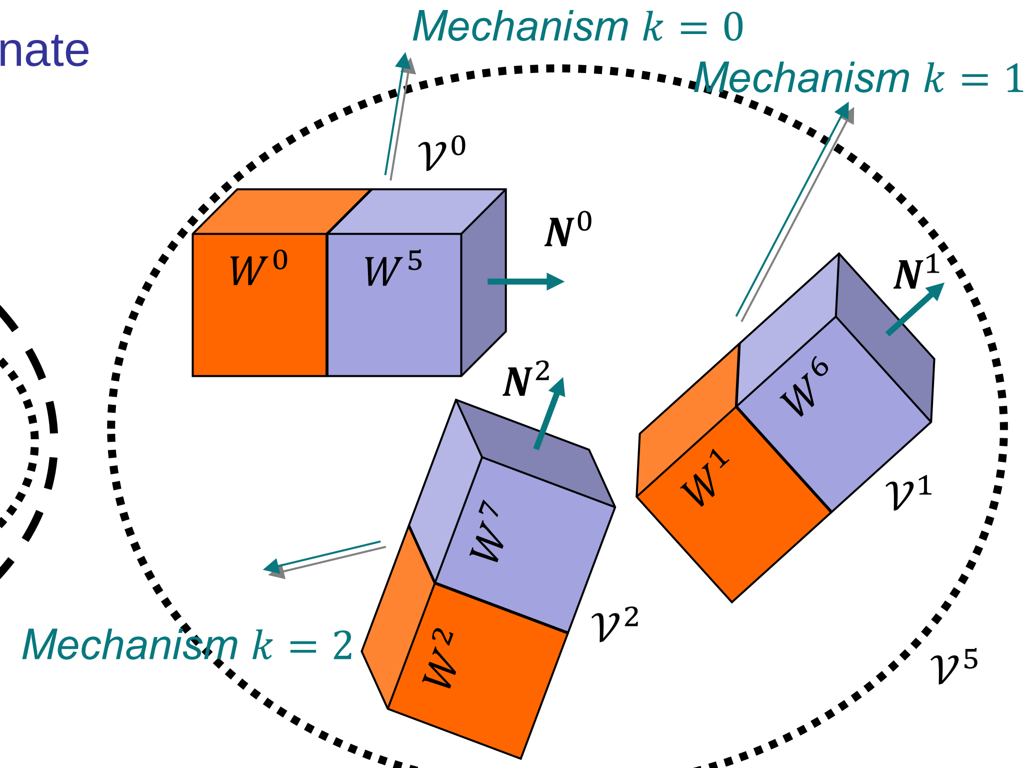

  - Weak form

$$\left[\sum_k \left(\sum_i W^i \boldsymbol{P}^i \alpha^{i,k}\right)\cdot \boldsymbol{G}^k\right]\cdot\ \delta \boldsymbol{a}^k = 0$$

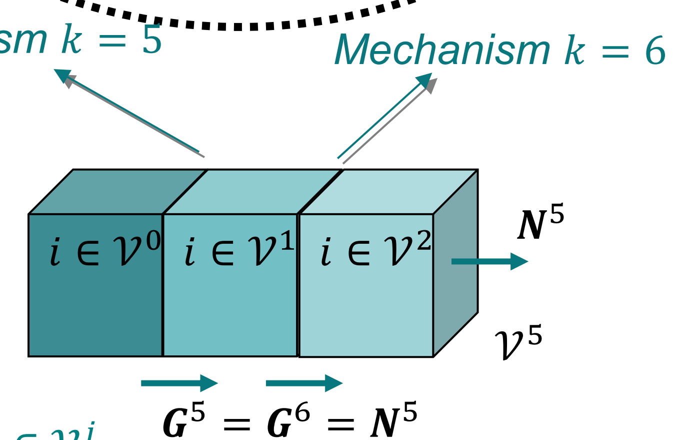

$$\Rightarrow \left(\frac{1}{W(\mathcal{V}^m)}\sum_{i\in\mathcal{V}^m} W^i\boldsymbol{P}^i - \frac{1}{W(\mathcal{V}^{m+1})}\sum_{i\in\mathcal{V}^{m+1}} W^i\boldsymbol{P}^i\right)\cdot \boldsymbol{N}^j = 0$$

$j = 0..7$, $\mathcal{V}^m$ *and* $\mathcal{V}^{m+1}$ *interactions of mechanism* $k\in\mathcal{V}^j$

Deep Material Networks from the interaction viewpoint

- Offline stage on a p-phase RVE
  - Topological parameters χ
    - Weight: $W^i, i = 0..9$
    - Direction of interaction $\mathcal{V}^j$: $\boldsymbol{N}^j, j = 0..7$

      $\chi = [W^0, \dots, W^9, \boldsymbol{N}^0, \dots, \boldsymbol{N}^7]$
  - Using elastic data
    - Random properties on RVE

      $\boldsymbol{\gamma} = [E_0, \nu_0, E_1, \nu_1 \dots E_p, \nu_p,]$

      Direct simulations on RVE $\hat{\mathbb{C}}(\boldsymbol{\gamma})$
    - Cost functions to minimise

$$L(\hat{\mathbb{C}}, \bar{\mathbb{C}}(\boldsymbol{\chi})) = \frac{1}{n}\sum_{s=1}^{n}\frac{\|\hat{\mathbb{C}}(\boldsymbol{\gamma}_s) - \bar{\mathbb{C}}(\boldsymbol{\chi}|\boldsymbol{\gamma}_s)\|}{\|\hat{\mathbb{C}}(\boldsymbol{\gamma}_s)\|}$$

    - « stochastic gradient descent (SGD) » algorithm

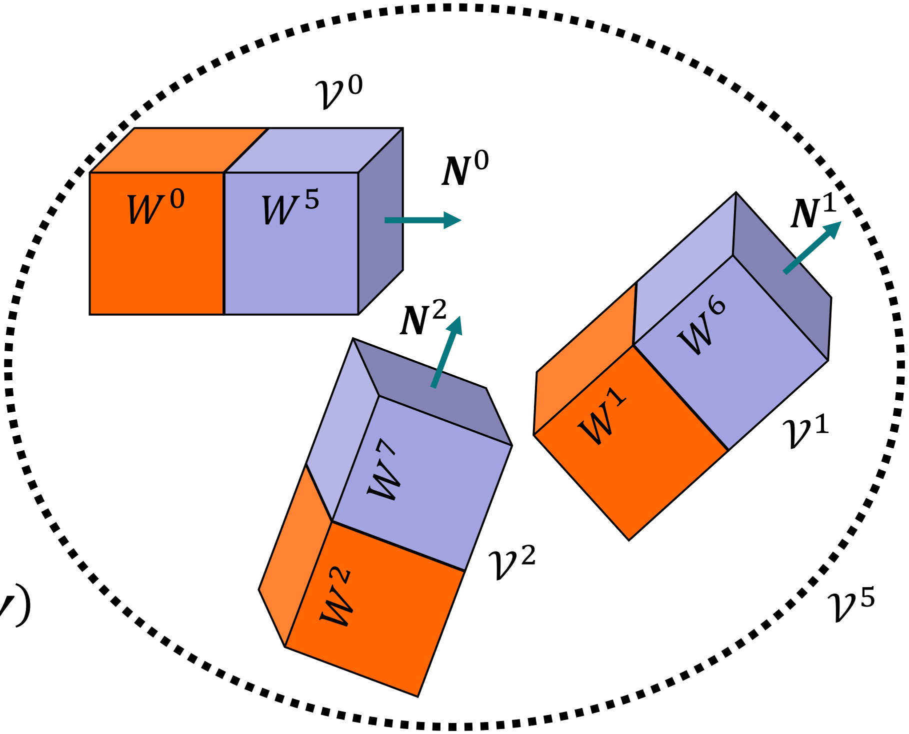

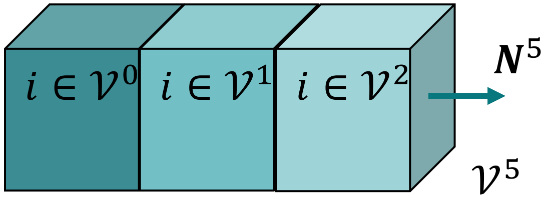

Deep Material Networks from the interaction viewpoint

- Online stage on a particle-reinforced composite
  - Properties
    - Elastic inclusions
    - Elasto-plastic matrix

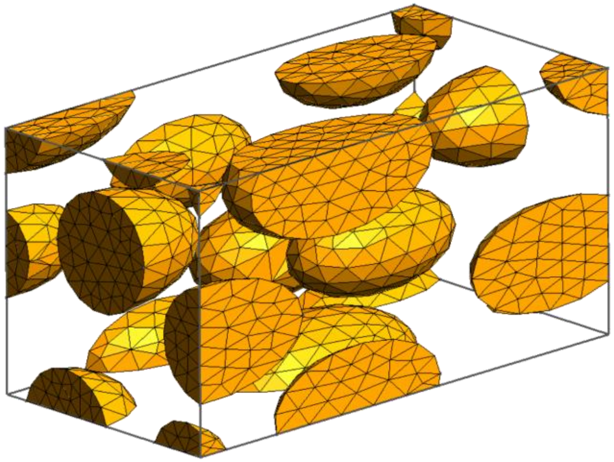

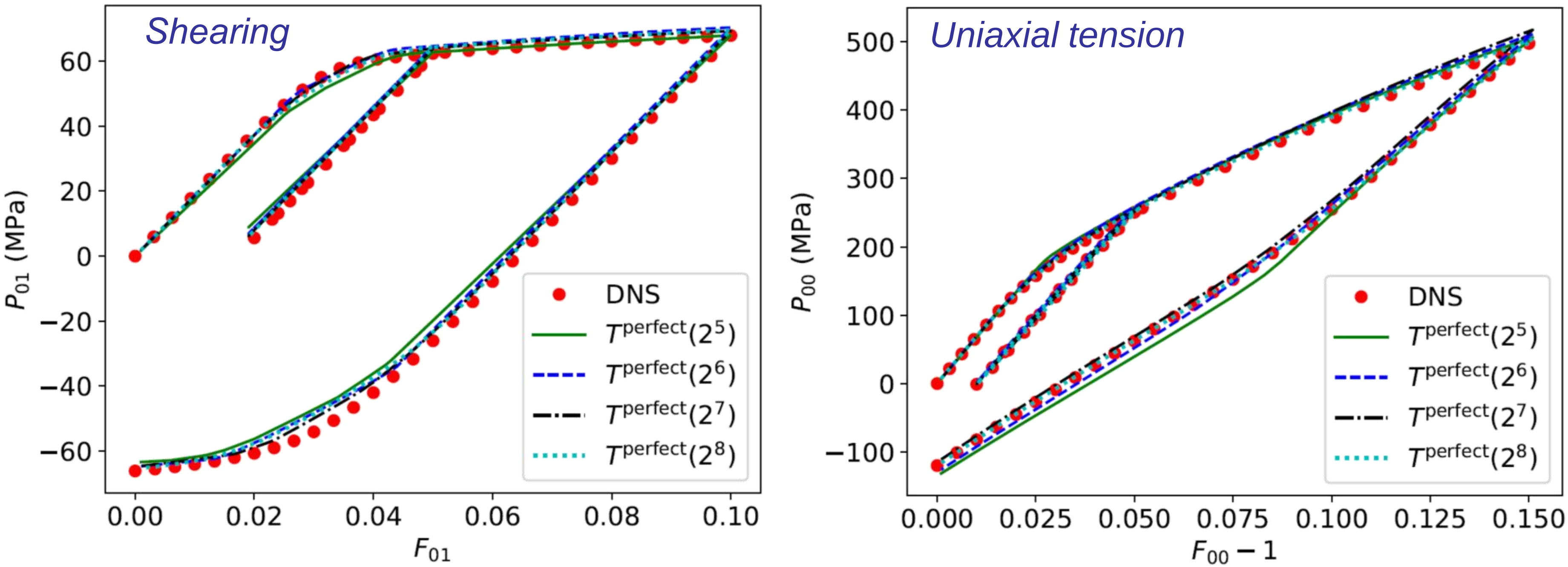

Deep Material Networks from the interaction viewpoint

- Multiscale simulation
  - Elasto-plastic composite RVE
  - Comparison FE^2 vs. DMN-surrogate

Off-line	FE^2	FE-DMN
Data generation	-	10 min.-cpu
Training	-	2 min.-cpu
On-line	**FE^2**	**FE-DMN**
Simulation	18000 h-cpu	½ to 34 h-cpu

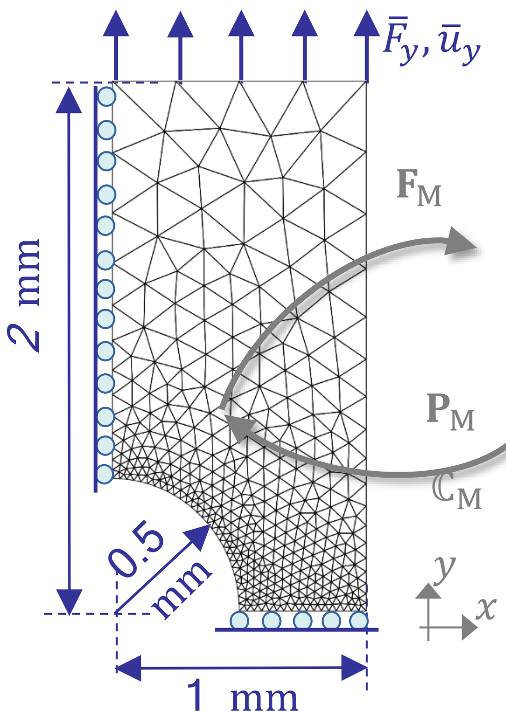

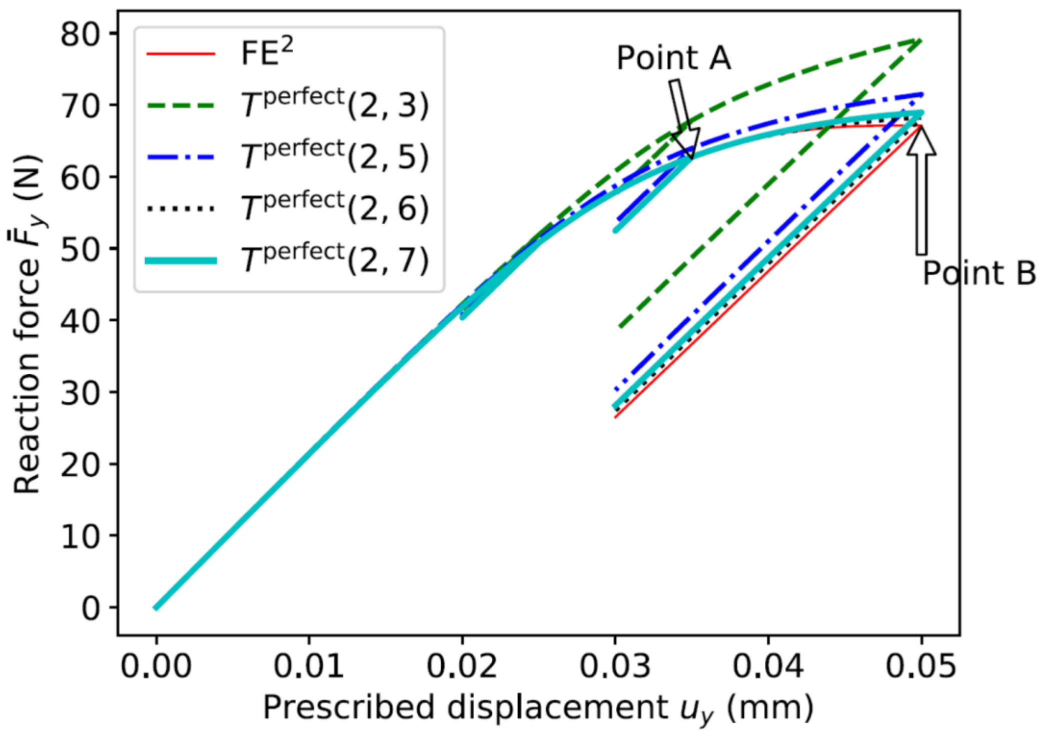

- Multiscale simulation
  - Stress-strain distribution at point A
  - For 2^7 material nodes

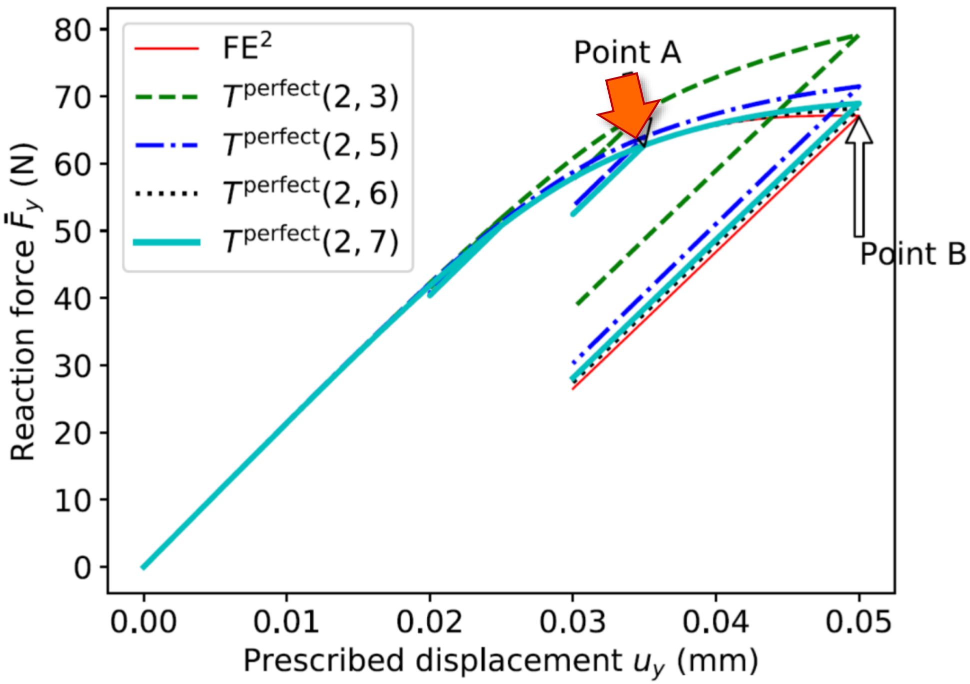

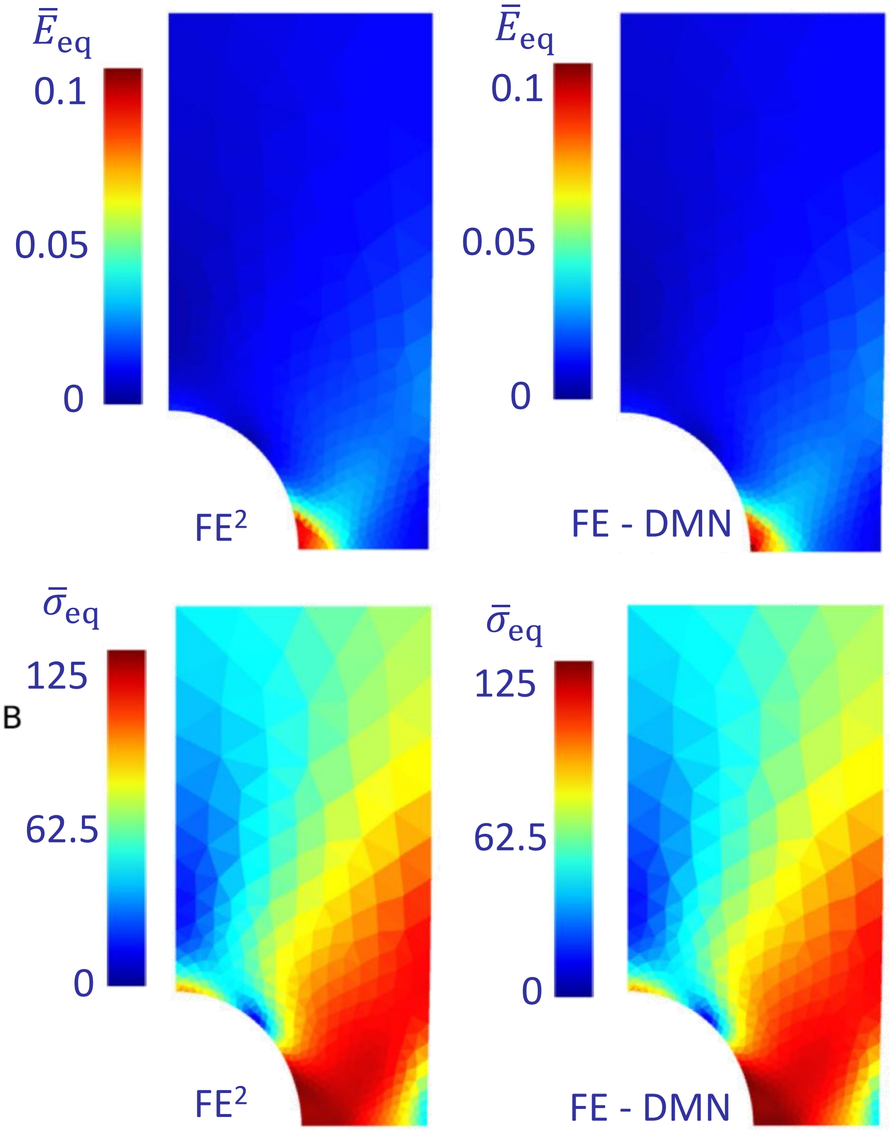

- Multiscale simulation
  - Stress-strain distribution at point B
  - For 2^7 material nodes

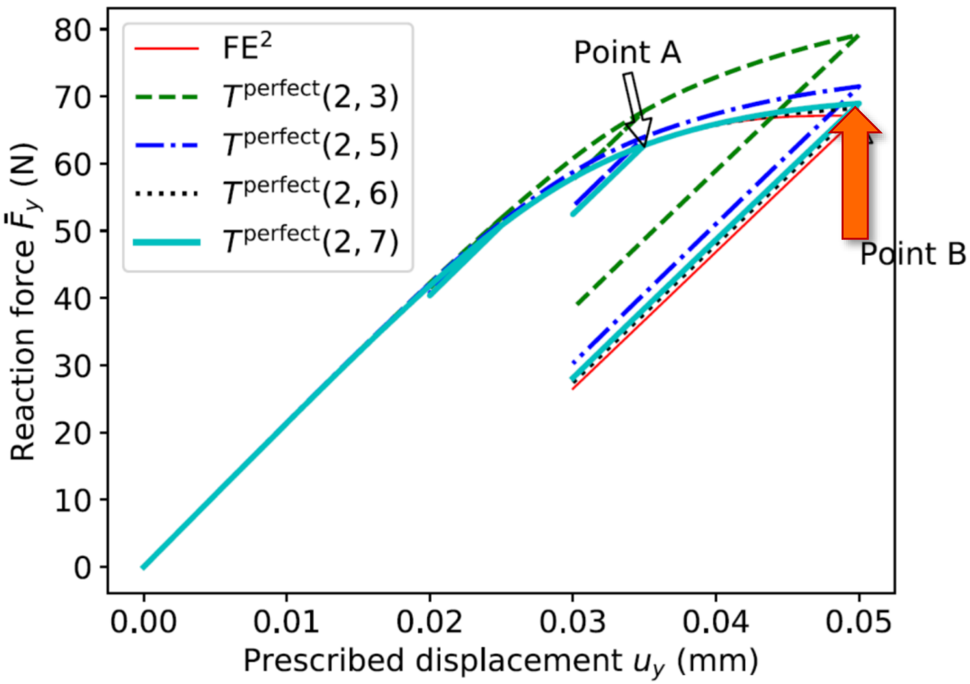

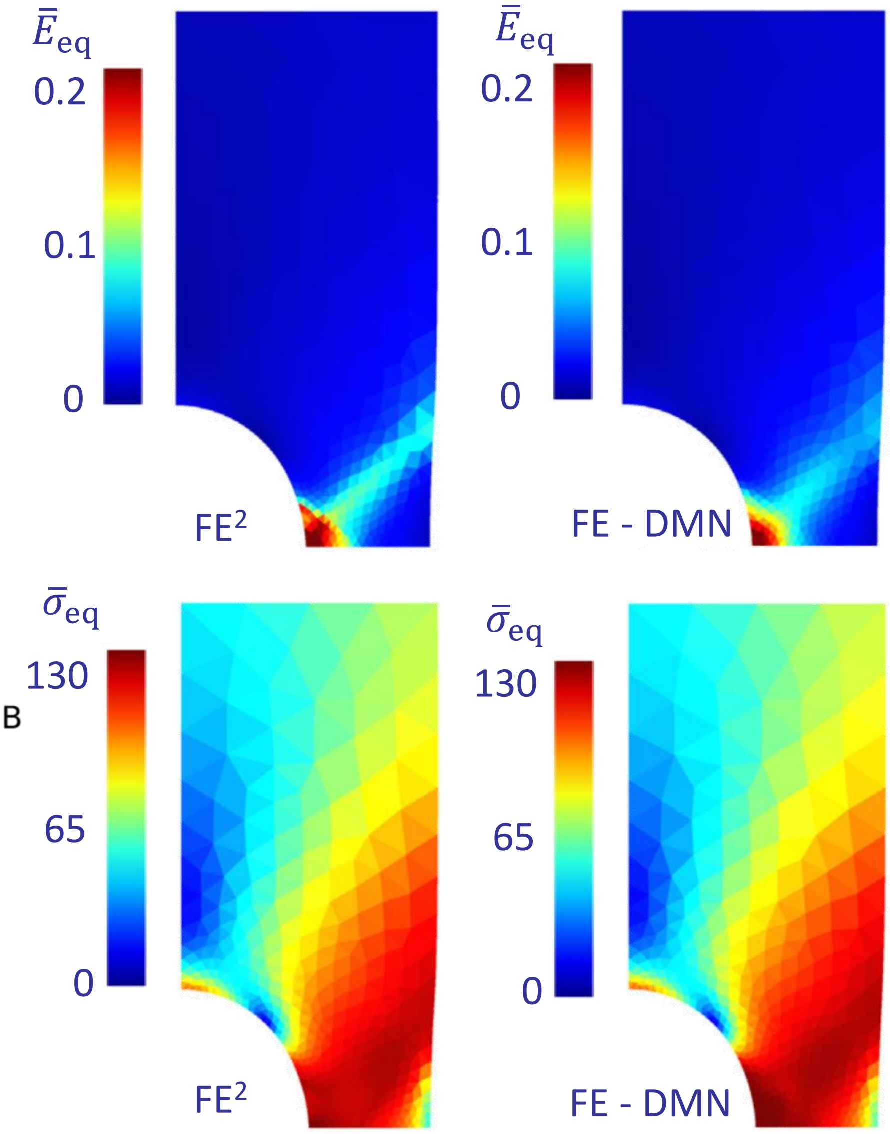

Deep Material Networks from the interaction viewpoint

- Multiscale simulation
  - Localisation step
  - For 2^7 material nodes

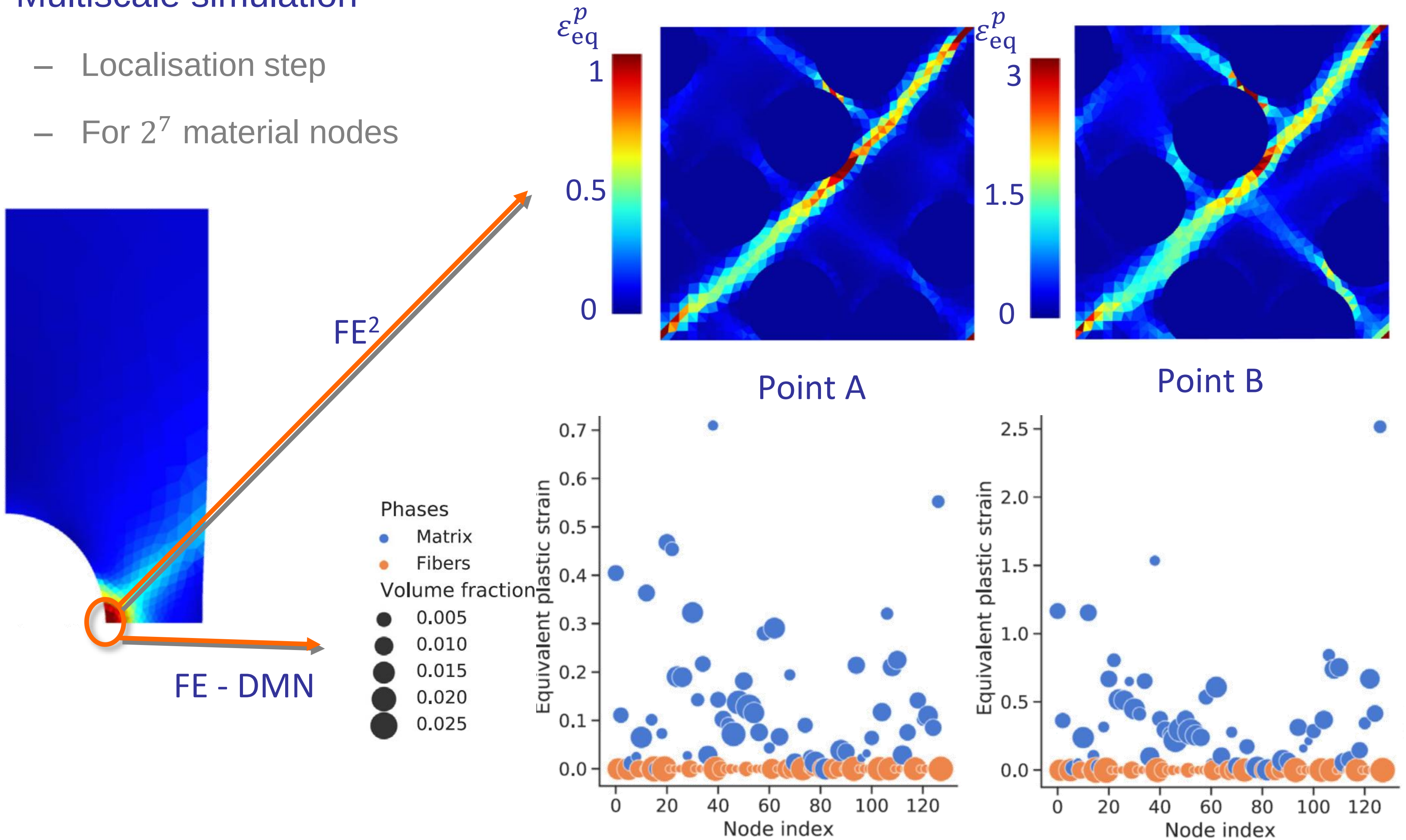

Beginning

Deep Material Networks from the interaction viewpoint

- Alternative to laminate (e.g. for porous material)
- Mechanism $j = 0..M-1$ of interaction $\mathcal{V}^j$
  - Homogenised deformation gradient
    - Construction of a strain fluctuation field

$$\overline{\boldsymbol{F}} + \sum_{j:i\in\mathcal{V}^j} \alpha^{i,j}\, \boldsymbol{a}^j \otimes \boldsymbol{N}^j = \boldsymbol{F}^i\,, \quad j = 0..M-1$$

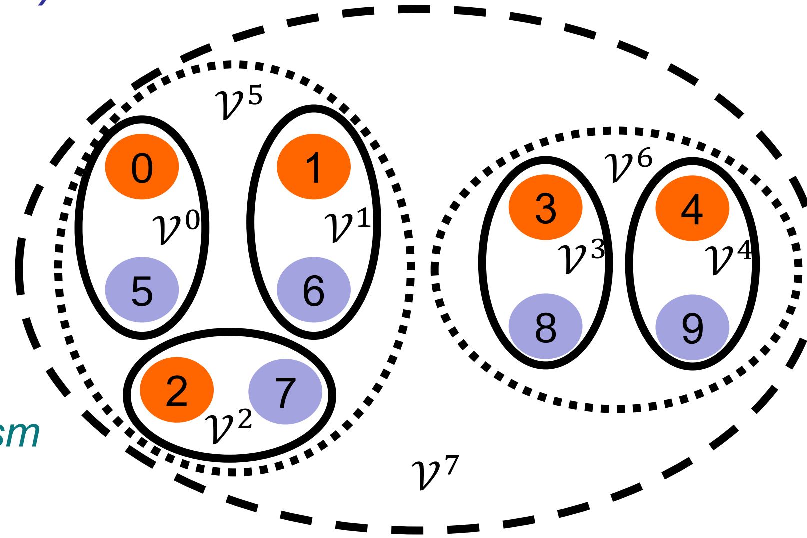

Contribution of node i in mechanism j (parameter?)

Degrees of freedom of mechanism j definition the strain fluctuation

Direction of mechanism j (parameter)

Weight of node i (parameter)

  - Constraints from strain averaging
    - $\overline{\boldsymbol{F}} = \sum_i W^i \boldsymbol{F}^i$ ⇨ $\sum_j \left(\sum_{i\in\mathcal{V}^j} W^i \alpha^{i,j}\right) \boldsymbol{a}^j \otimes \boldsymbol{N}^j = 0$ ⇨ $\sum_{i\in\mathcal{V}^j} W^i \alpha^{i,j} = 0$
  - Weak form from Hill-Mandel
    - $\overline{\boldsymbol{P}} : \delta\overline{\boldsymbol{F}} = \sum_i W^i\, \boldsymbol{P}^i : \delta\boldsymbol{F}^i$ ⇨ $\left[\sum_j \left(\sum_{i\in\mathcal{V}^j} W^i \boldsymbol{P}^i \alpha^{i,j}\right) \cdot \boldsymbol{N}^j\right] \cdot \delta\boldsymbol{a}^j = 0$

Deep Material Networks from the interaction viewpoint

- Mechanistic building blocks: Polyhedra
  - Interaction $\mathcal{V}^j$, $j = 0..M-1$

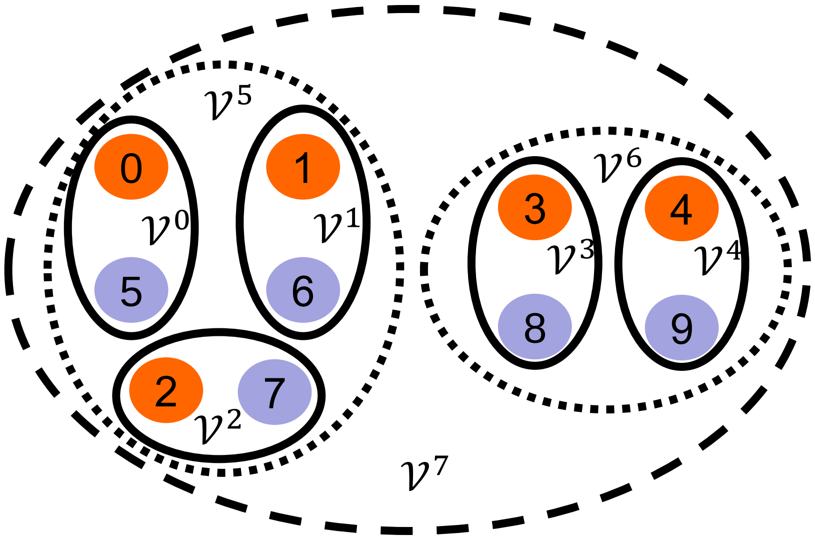

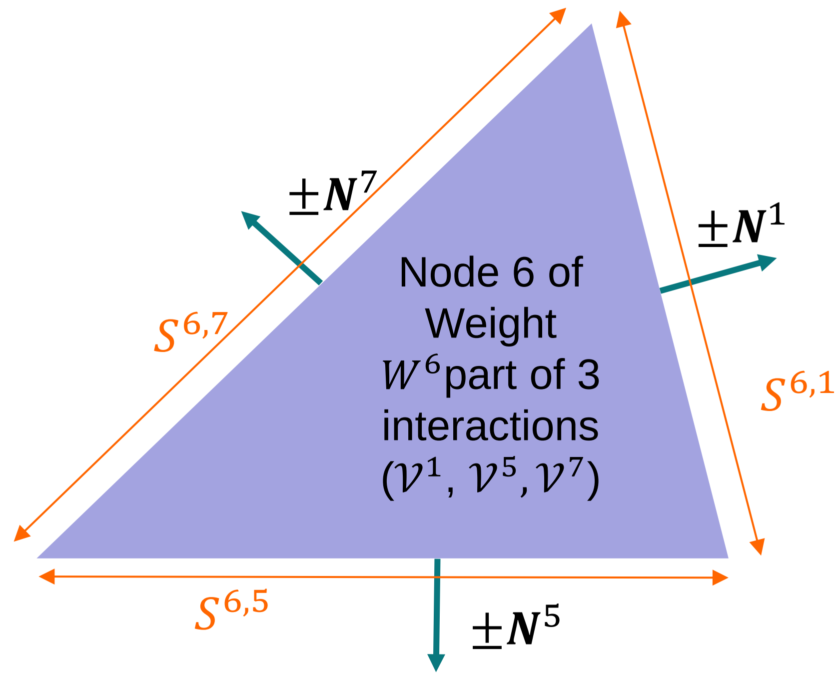

  - Fluctuation field
    - Integration by parts on a polyhedron of volume V^i associated to node i

$$\overline{\boldsymbol{F}} + \frac{1}{V^i}\int_{V^i} \mathbf{w} \otimes \nabla \, dV = \boldsymbol{F}^i \quad \Rightarrow \quad \overline{\boldsymbol{F}} + \sum_{j:i\in\mathcal{V}^j} \frac{S^{i,j}}{V^i} \mathbf{w} \otimes (\pm\mathbf{N}^j) = \boldsymbol{F}^i$$

    - To be compared with the interactions $\overline{\boldsymbol{F}} + \sum_{j:i\in\mathcal{V}^j} \alpha^{i,j} \boldsymbol{a}^j \otimes \boldsymbol{N}^j = \boldsymbol{F}^i$, $j = 0..M-1$

$\Rightarrow$
- $\alpha^{i,j}$ is the weighted surface of a polyhedron face (parameter to be identified)
- $\boldsymbol{N}^j$ is the inward or outward normal of the polyhedron face (parameter to be identified)
- $\boldsymbol{a}^j$ is the fluctuation field (degree of freedom for online simulations)

- Offline stage on a p-phase RVE
  - Topological parameters χ
    - Nodal weight: $W^i,\ i = 0..9$
    - Direction of interaction $\mathcal{V}^j$: $\boldsymbol{N}^j, j = 0..7$
    - Interaction weight: $\alpha^{i,j}$

$$\chi = [W^0, \dots, W^9, \boldsymbol{N}^0, \dots, \boldsymbol{N}^7, \alpha^{0,0}, \dots\ \alpha^{9\,7}]$$

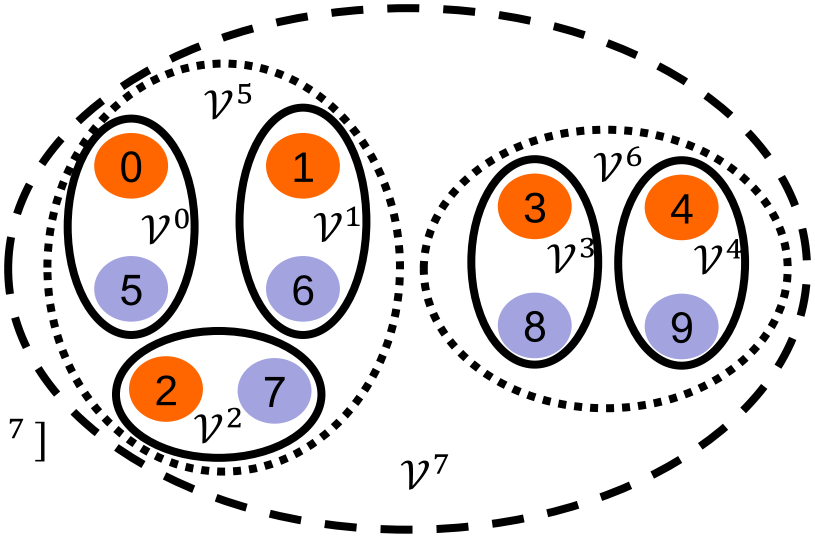

  - Using elastic data
    - Random properties on RVE ⇨ $\hat{\mathbb{C}}(\boldsymbol{\gamma})$

$$\boldsymbol{\gamma} = [E_0,\ \nu_0, E_1,\ \nu_1 \dots E_p,\ \nu_p]$$

    - Cost functions to minimise $L(\hat{\mathbb{C}},\ \mathbb{C}(\boldsymbol{\chi})) = \frac{1}{n}\sum_{s=1}^{n} \frac{\|\hat{\mathbb{C}}(\boldsymbol{\gamma}_s) - \bar{\mathbb{C}}\,(\boldsymbol{\chi}|\boldsymbol{\gamma}_s)\|}{\|\hat{\mathbb{C}}(\boldsymbol{\gamma}_s)\|}$
  - Using non-linear response
    - Random loading on RVE (strain sequence $\bar{\mathbf{F}}_s$)
    - Compare stress history $\mathbf{P}(\bar{\mathbf{F}}_s)$ and quantity of interest $Z(\bar{\mathbf{F}}_s)$ (e.g. porosity)
    - Cost function to minimise $L\left(\hat{\mathbf{P}},\ \mathbf{P}(\boldsymbol{\chi})\right) = \frac{1}{n}\sum_{s=1}^{n} \frac{\|\hat{\mathbf{P}}(\bar{\mathbf{F}}_s) - \bar{\mathbf{P}}(\boldsymbol{\chi}|\bar{\mathbf{F}}_s)\|}{\|\hat{\mathbf{P}}(\bar{\mathbf{F}}_s)\|} + \frac{1}{n}\sum_{s=1}^{n} \frac{\|\hat{Z}(\bar{\mathbf{F}}_s) - \bar{Z}\,(\boldsymbol{\chi}|\bar{\mathbf{F}}_s)\|}{\|\hat{Z}(\bar{\mathbf{F}}_s)\|}$
  - By « stochastic gradient descent (SGD) » algorithm

Deep Material Networks from the interaction viewpoint

- Online stage on a porous material
  - Properties
    - Elasto-plastic matrix
    - Small strain
  - Non-linear training
  - Uniaxial tension

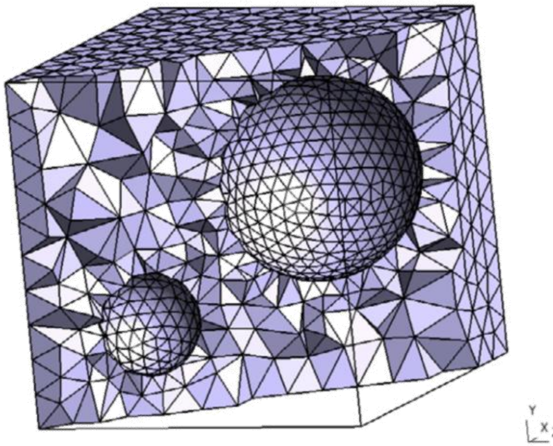

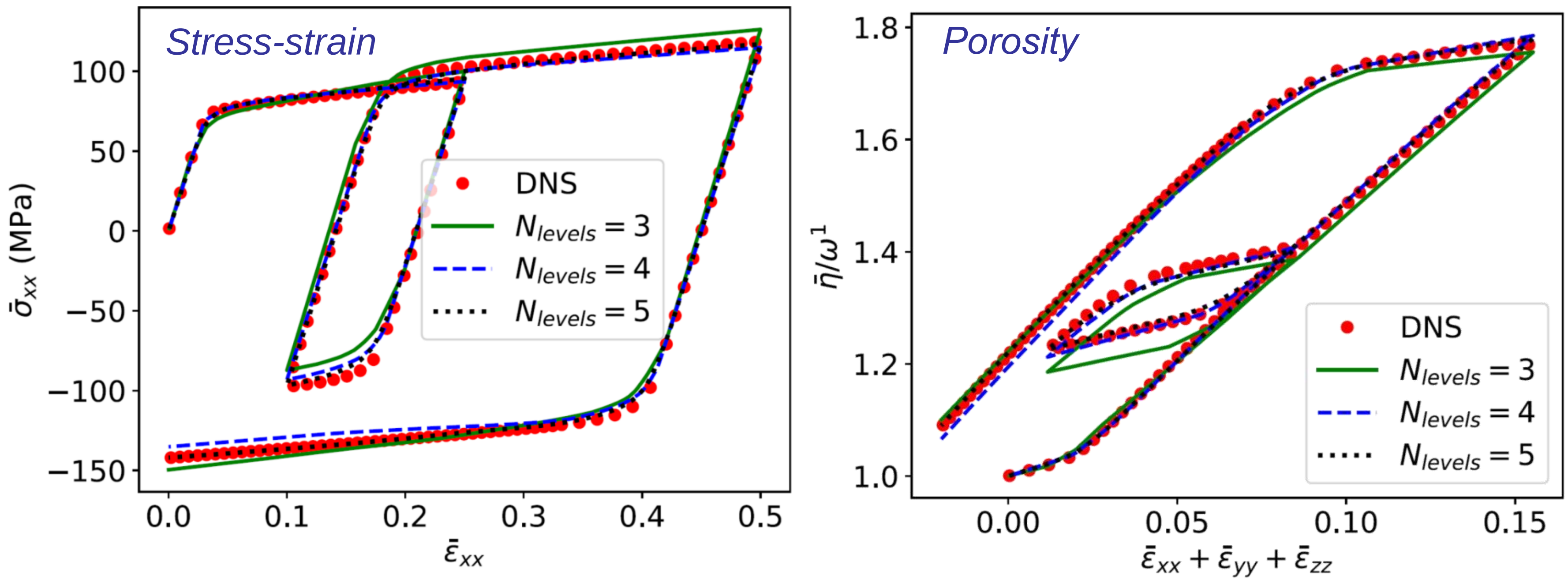

- Online stage on a porous material
  - Properties
    - Elasto-plastic matrix
    - Small strain
  - Non-linear training with Material 1, on-line material 2
  - Random loading

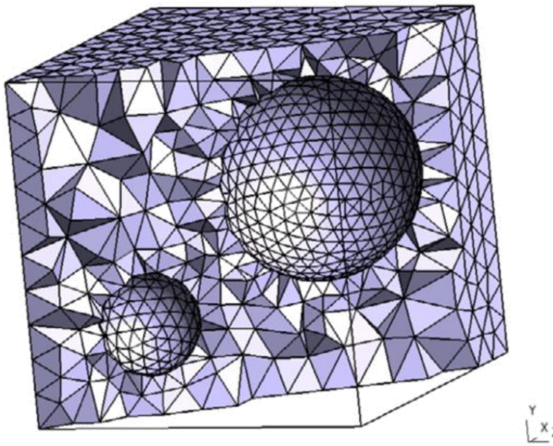

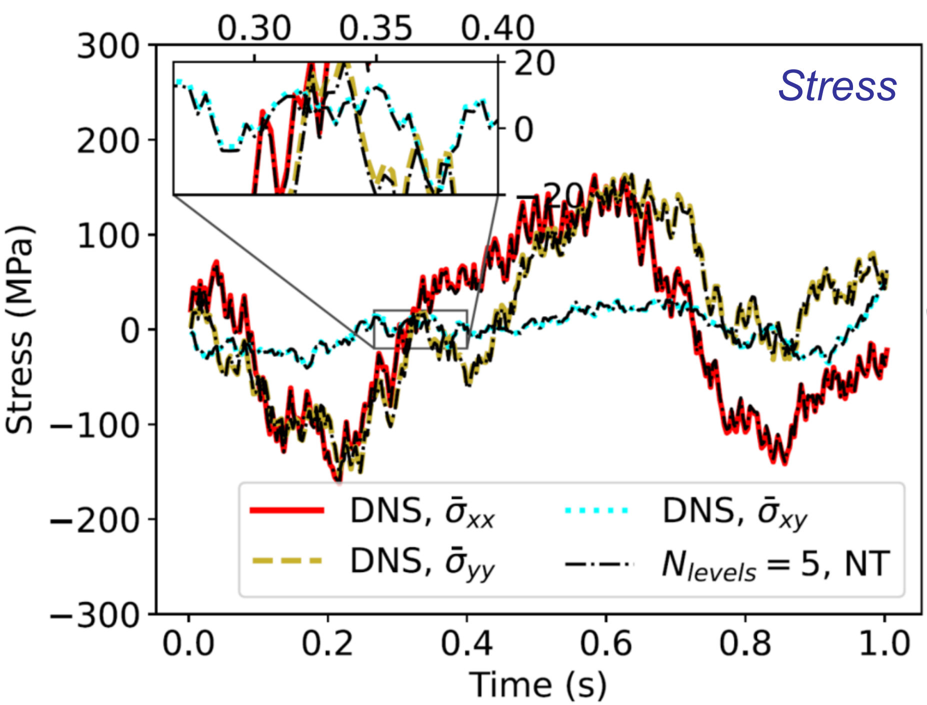

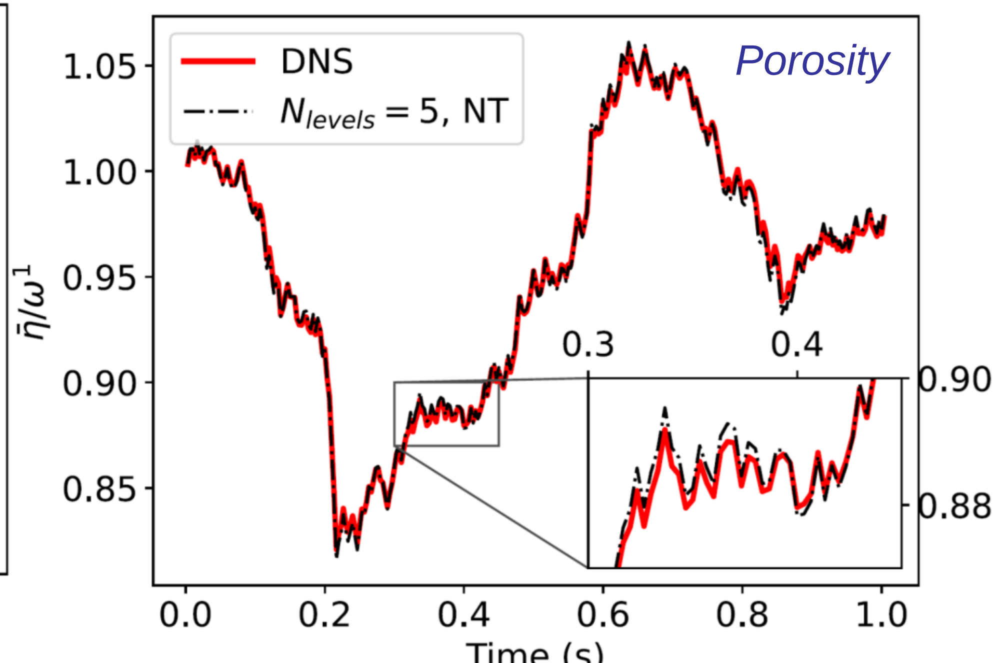

Deep Material Networks from the interaction viewpoint

- Online stage on a porous material
  - Properties
    - Elasto-plastic matrix
    - Small strain
  - Non-linear training
  - Thermodynamically consistent

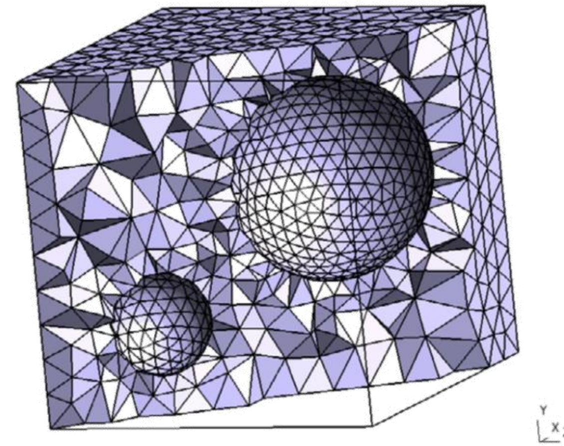

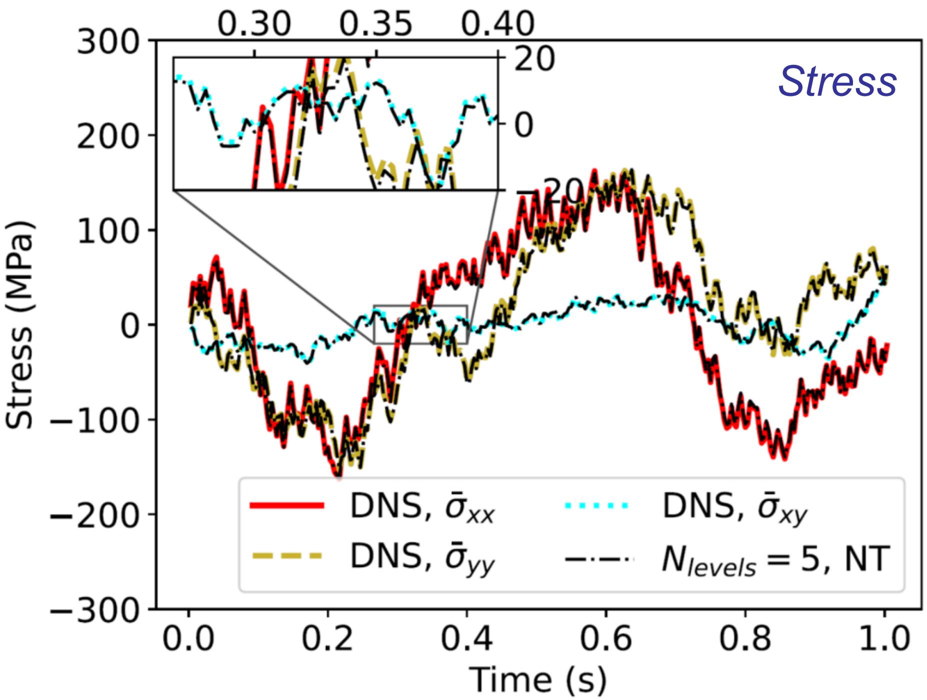

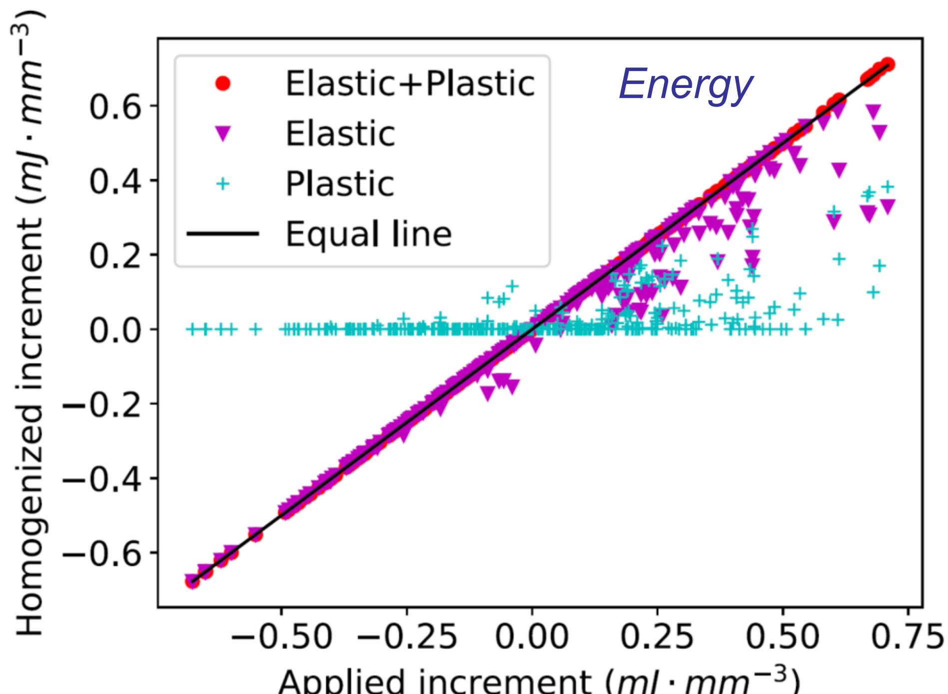

- Multiscale simulation

Off-line	FE²	FE-DMN
Data generation	-	0.04 (linear) – 3.5 (non-linear) hour.-cpu
Training	-	0.16-20 hours.-cpu
On-line	**FE²**	**FE-DMN**
Simulation	7200 h-cpu	0.1 to 1 h-cpu

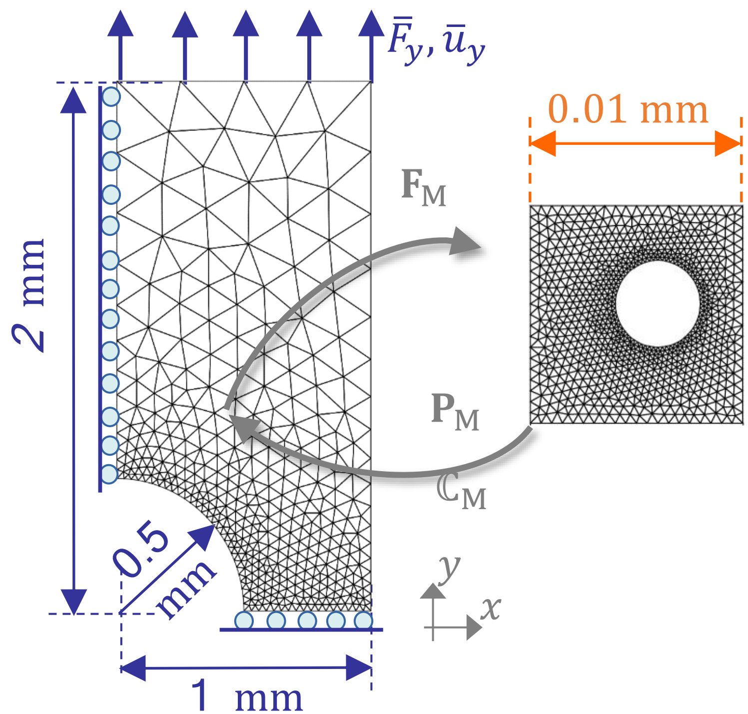

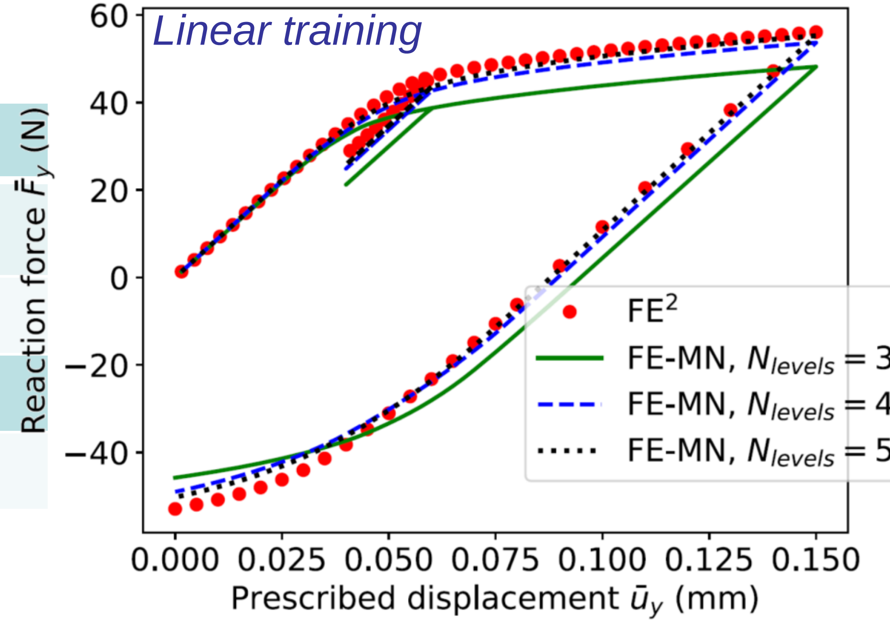

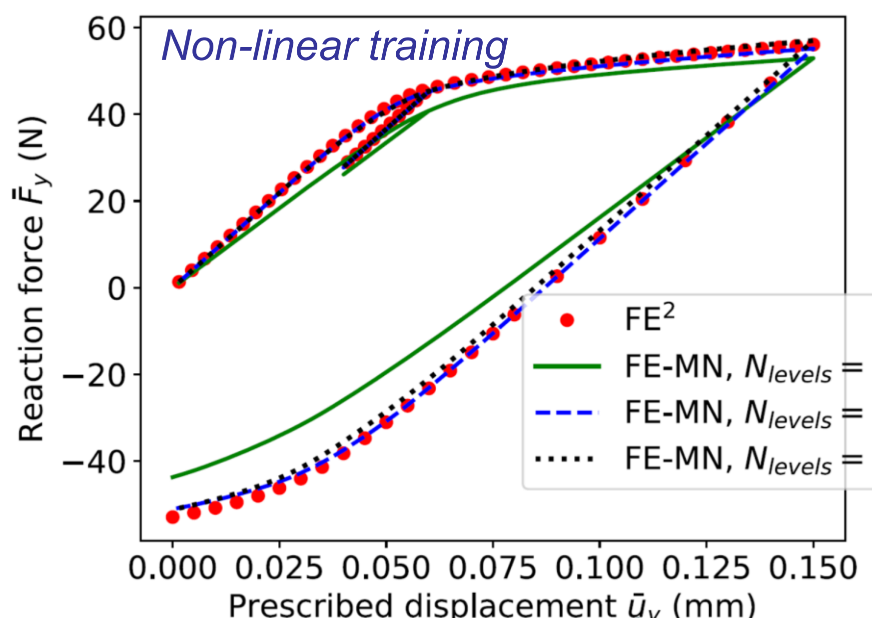

Deep Material Networks from the interaction viewpoint

- Multiscale simulation
  - Stress-strain distribution at point A
  - For 2^5 material nodes
  - Non-linear training

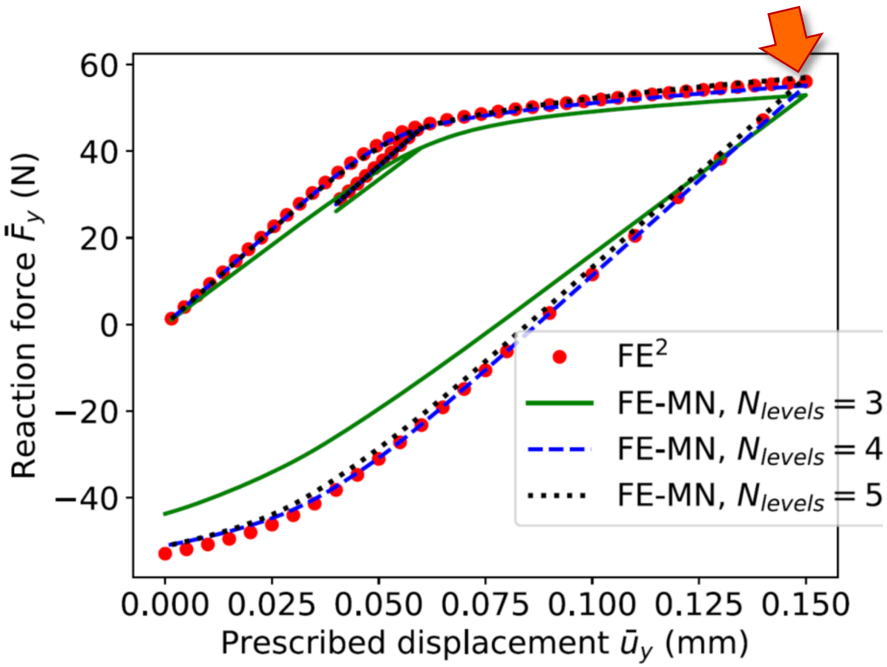

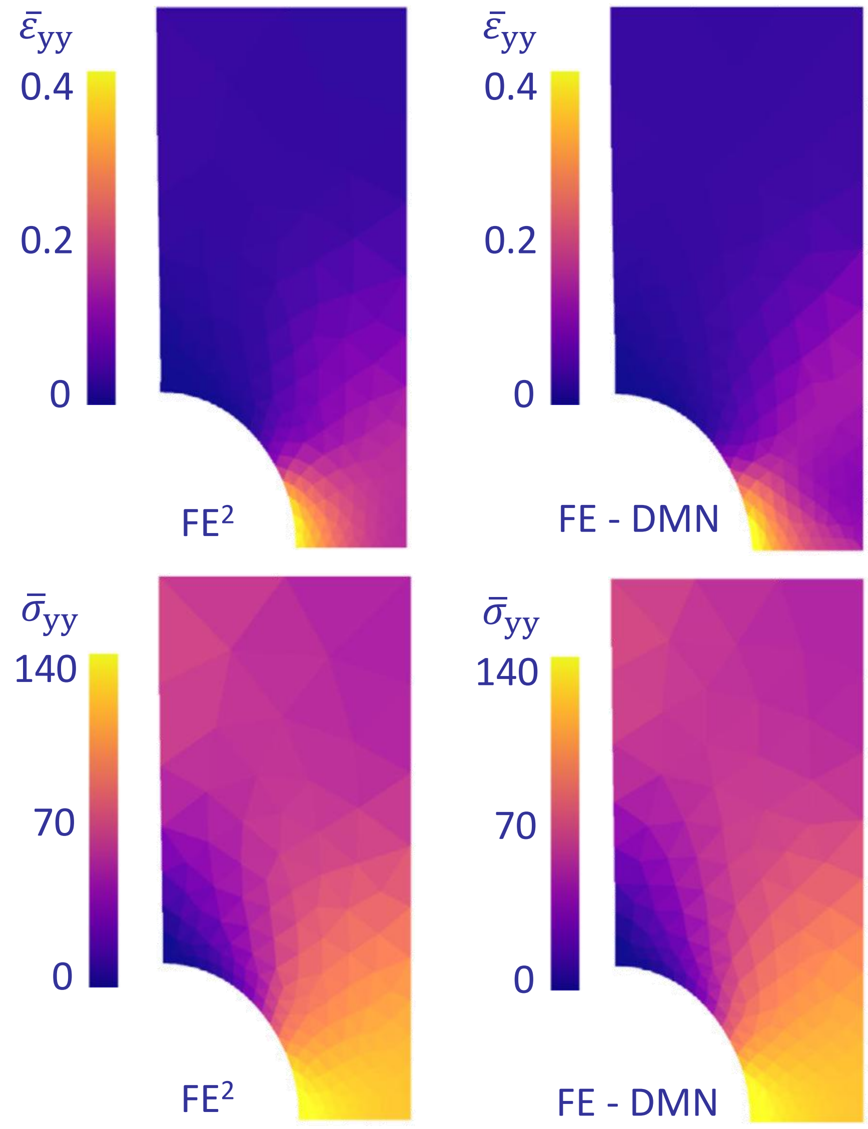

- Multiscale simulation
  - Stress-strain distribution at point B
  - For 2^5 material nodes
  - Non-linear training

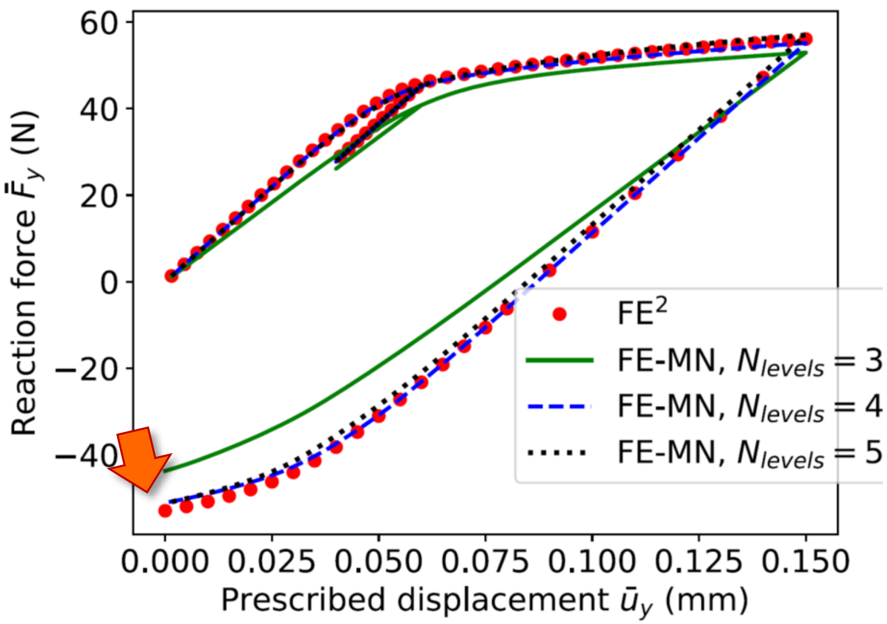

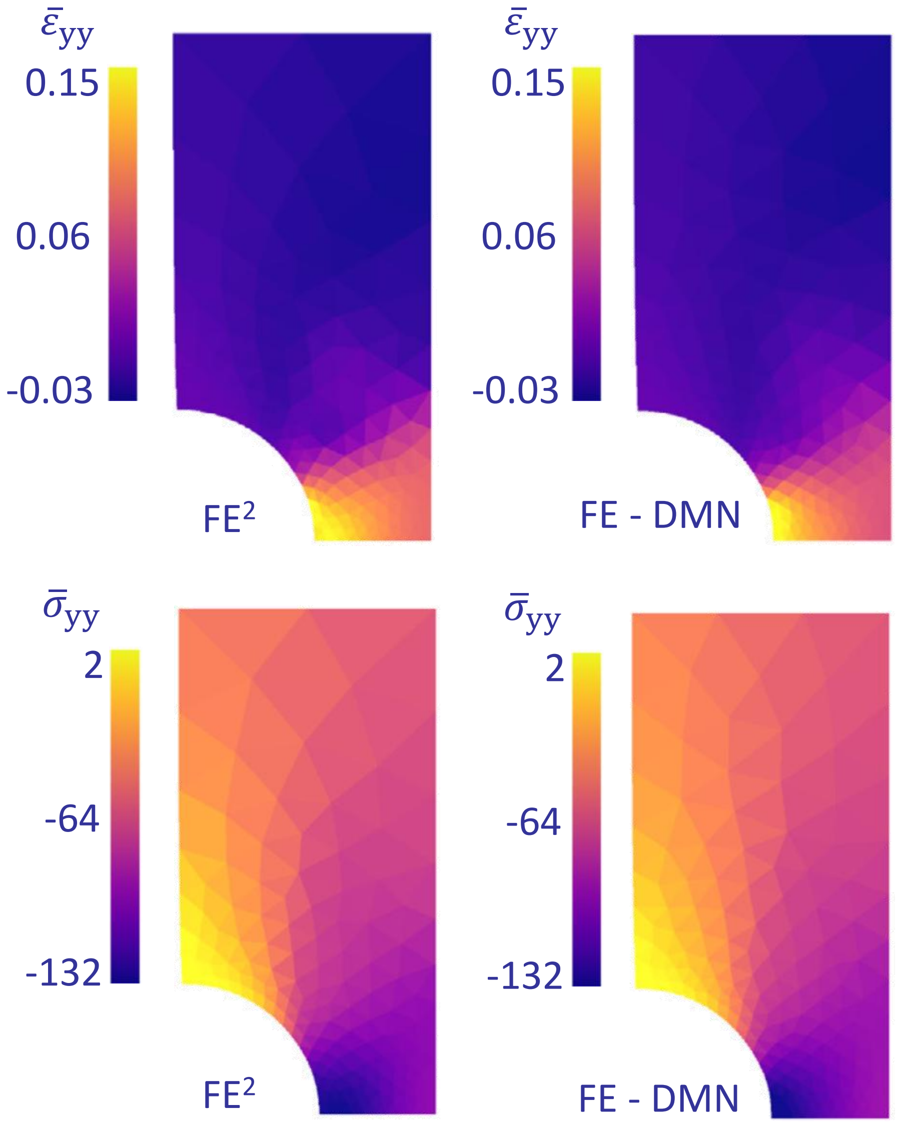

Deep Material Networks from the interaction viewpoint

- Publications (doi)
  - 10.1016/j.cma.2021.114300
    - Open data
  - 10.1016/j.euromechsol.2021.104384
    - Open data

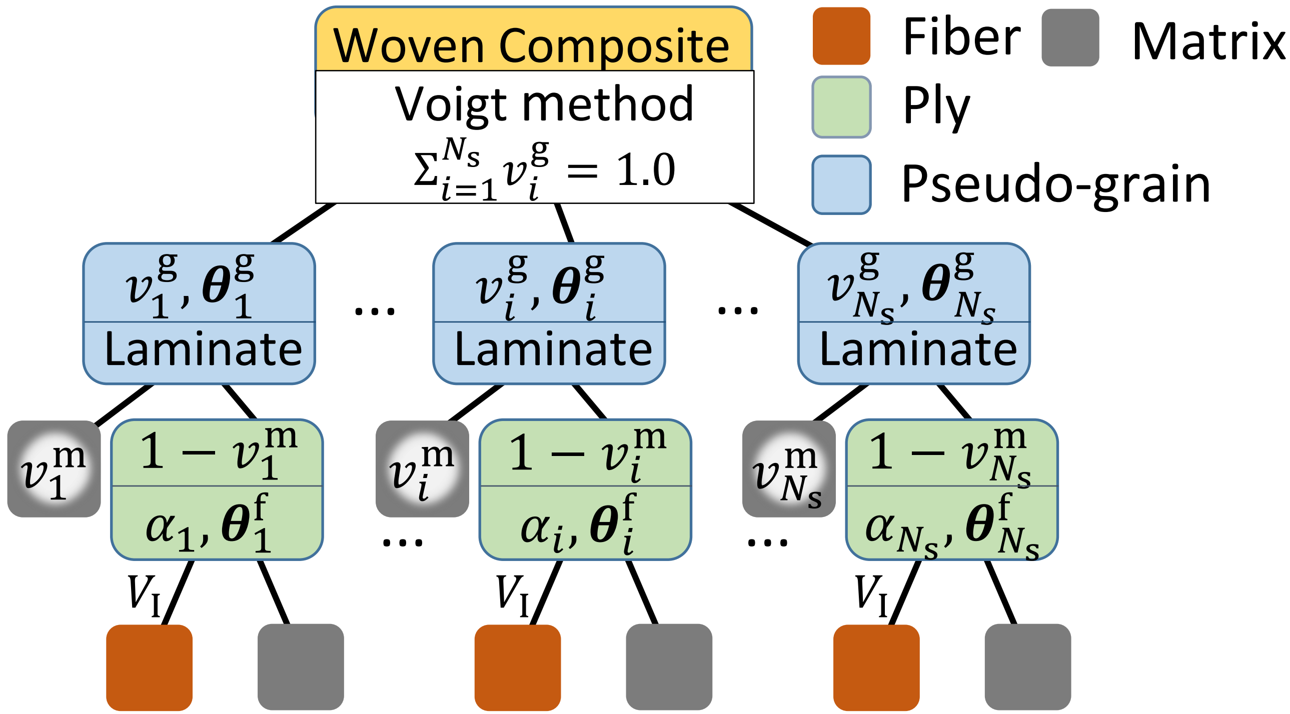

Mean-Field-Based Deep Material Networks for woven composites

The research has been funded by the Walloon Region under the agreement no.7911-VISCOS in the context of the 21st SKYWIN call.

Mean-Field-Based Deep Material Networks for woven composites

- Definition of 3 Reduced-order-models
- Using simple micro-mechanistic grains
  - MFH (short fibre-reinforced matrix)
  - Voigt mixture
  - Laminate theory

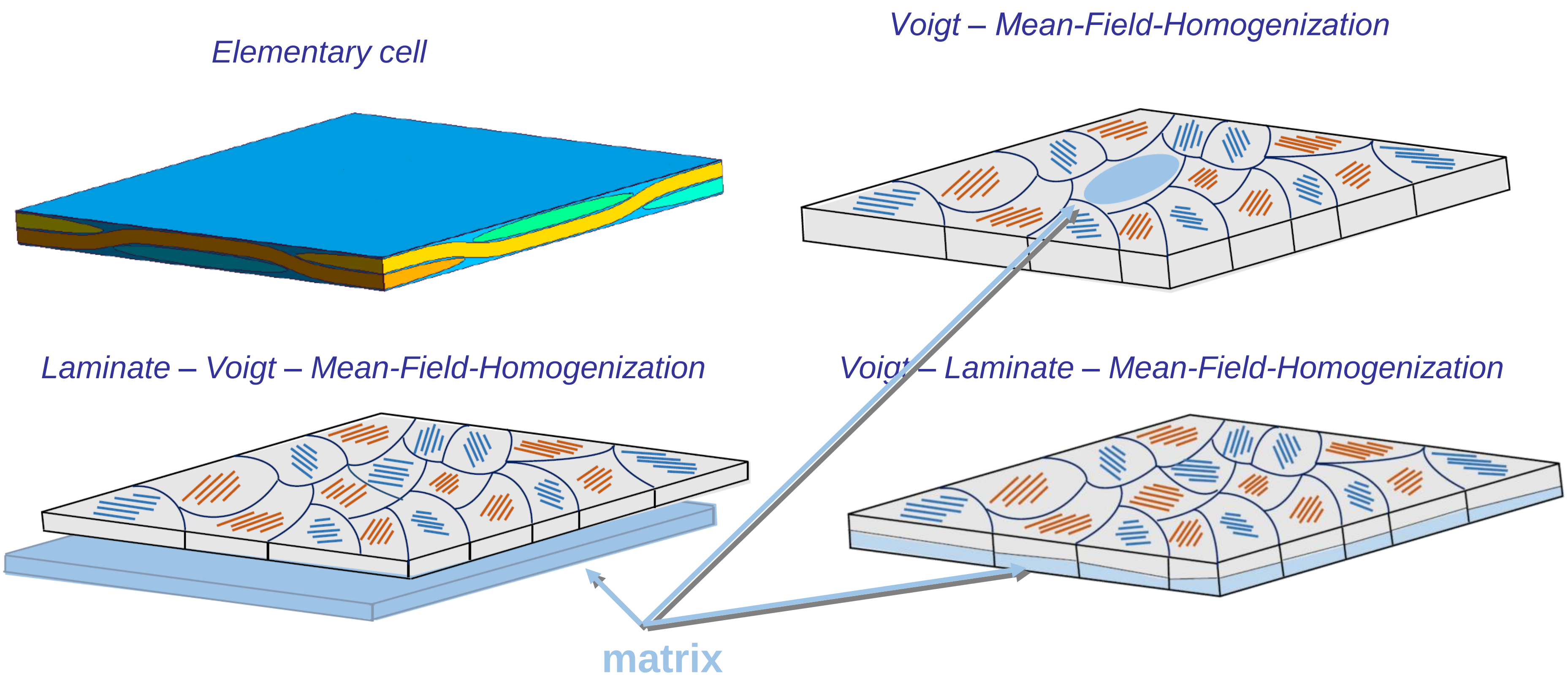

Mean-Field-Based Deep Material Networks for woven composites

- Definition of material networks

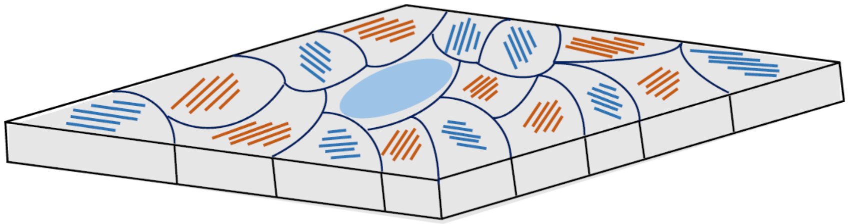

$$\chi^{\mathrm{VM}} = \left\{ v_i,\, \boldsymbol{\theta}_i,\, \alpha_i \mid i = 1, \ldots, N_S;\ \sum_{i=1}^{N_S} v_i = 1.0 - v_0 \right\}$$

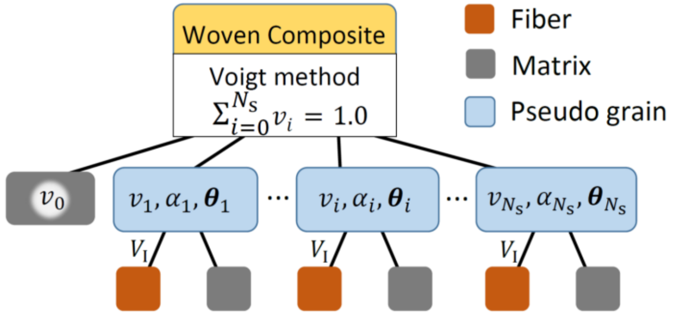

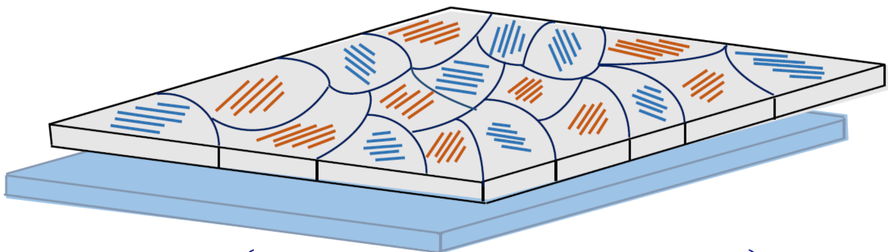

$$\chi^{\mathrm{LVM}} = \left\{ v_i,\, \boldsymbol{\theta}_i,\, \alpha_i \mid i = 1, \ldots, N_S;\ \sum_{i=1}^{N_S} v_i = 1.0 \right\}$$

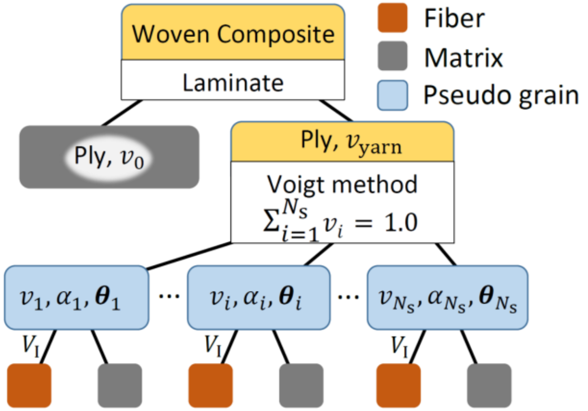

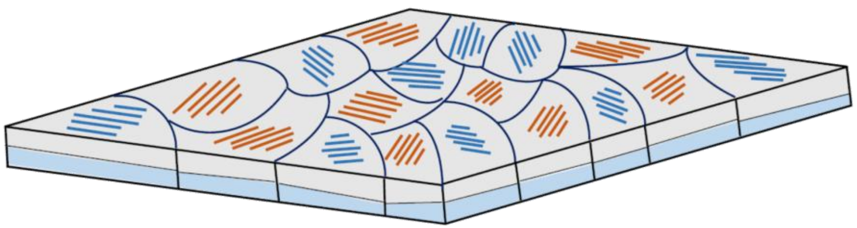

$$\chi^{\mathrm{VLM}} = \left\{ v_i^{\mathrm{g}},\, \boldsymbol{\theta}_i^{\mathrm{g}},\, v_i^{\mathrm{m}},\, \boldsymbol{\theta}_i^{\mathrm{f}},\, \alpha_i \mid i = 1, \ldots, N_S;\ \sum_{i=1}^{N_S} v_i^{\mathrm{g}} = 1.0;\ \sum_{i=1}^{N_S} v_i^{\mathrm{g}} v_i^{\mathrm{m}} = v_0 \right\}$$

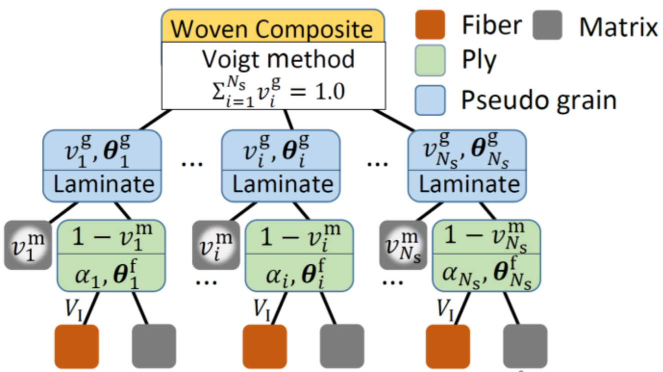

Mean-Field-Based Deep Material Networks for woven composites

- Identification of topological parameters from direct simulations
  - Parameters:

$$\chi^{\mathrm{VM}} = \left\{ v_i,\, \boldsymbol{\theta}_i,\, \alpha_i \mid i = 1, \ldots, N_S;\ \sum_{i=1}^{N_S} v_i = 1.0 - v_0 \right\}$$

$$\chi^{\mathrm{LVM}} = \left\{ v_i,\, \boldsymbol{\theta}_i,\, \alpha_i \mid i = 1, \ldots, N_S;\ \sum_{i=1}^{N_S} v_i = 1.0 \right\}$$

$$\chi^{\mathrm{VLM}} = \left\{ v_i^{\mathrm{g}},\, \boldsymbol{\theta}_i^{\mathrm{g}},\, v_i^{\mathrm{m}},\, \boldsymbol{\theta}_i^{\mathrm{f}},\, \alpha_i \mid i = 1, \ldots, N_S;\ \sum_{i=1}^{N_S} v_i^{\mathrm{g}} = 1.0;\ \sum_{i=1}^{N_S} v_i^{\mathrm{g}} v_i^{\mathrm{m}} = v_0 \right\}$$

Constraints

  - Using elastic data
    - Random properties on RVE

$$\boldsymbol{\gamma} = \left[E_0,\, \nu_0,\, E_{\mathrm{I}}^{\mathrm{T}},\, E_{\mathrm{I}}^{\mathrm{L}},\, \nu_{\mathrm{I}}^{\mathrm{LT}},\, \nu_{\mathrm{I}}^{\mathrm{TT}},\, G_{\mathrm{I}}^{\mathrm{LT}},\, V_{\mathrm{I}}\right]$$

Direct simulations on RVE

    - Cost functions to minimise

$$L(\hat{\mathbb{C}}, \mathbb{C}(\boldsymbol{\chi})) = \frac{1}{n} \sum_{s=1}^{n} \frac{\|\hat{\mathbb{C}}(\boldsymbol{\gamma}_s) - \mathbb{C}(\boldsymbol{\chi}|\boldsymbol{\gamma}_s)\|}{\|\hat{\mathbb{C}}(\boldsymbol{\gamma}_s)\|} + \frac{\lambda}{2} G(\boldsymbol{\chi})$$

    - « stochastic gradient descent (SGD) » algorithm

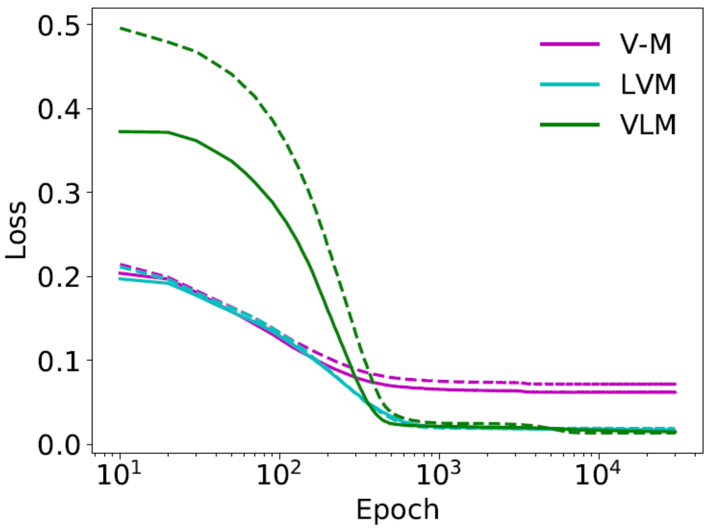

Mean-Field-Based Deep Material Networks for woven composites

- Elasto-plastic matrix case

PBC tension cyclique

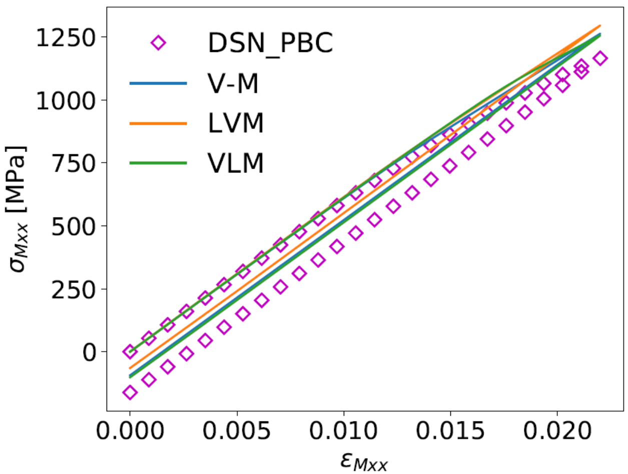

MBC tension cyclique

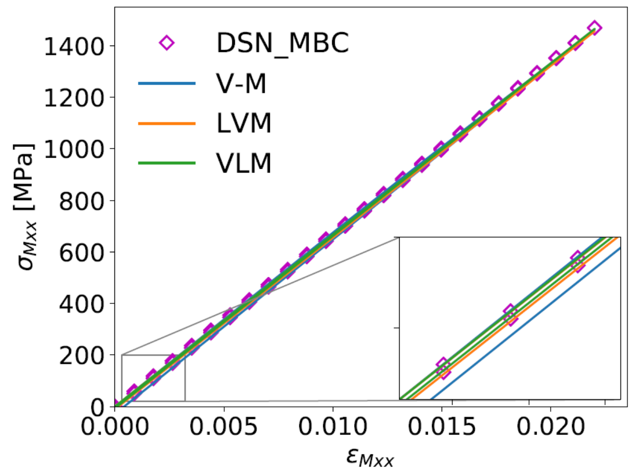

MBC tension

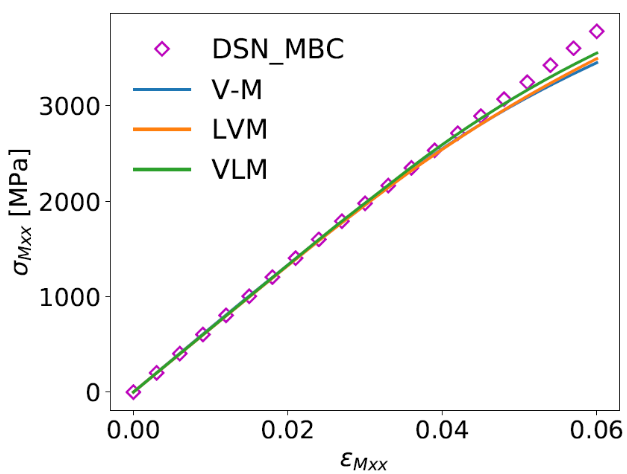

Cisaillement

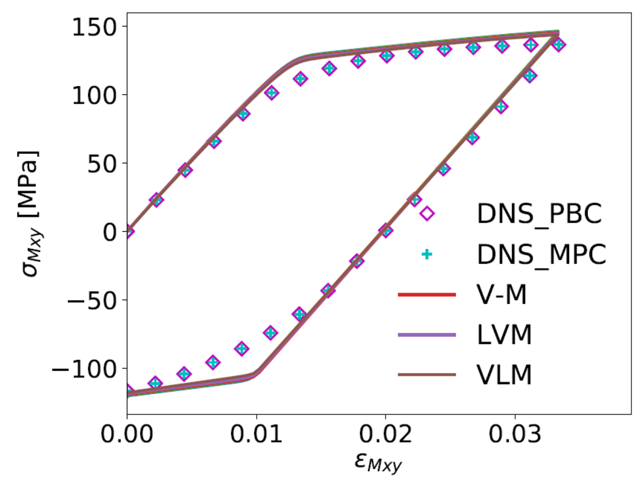

Mean-Field-Based Deep Material Networks for woven composites

- VISCOS project, 21st Call of Skywin
  - SONACA S.A.
  - e-Xstream (Hexagon S.A.)
  - Isomatex S.A.
  - UCL
  - ULiege
- Publications (doi)
  - 10.1016/j.compstruct.2021.114058
    - Open data

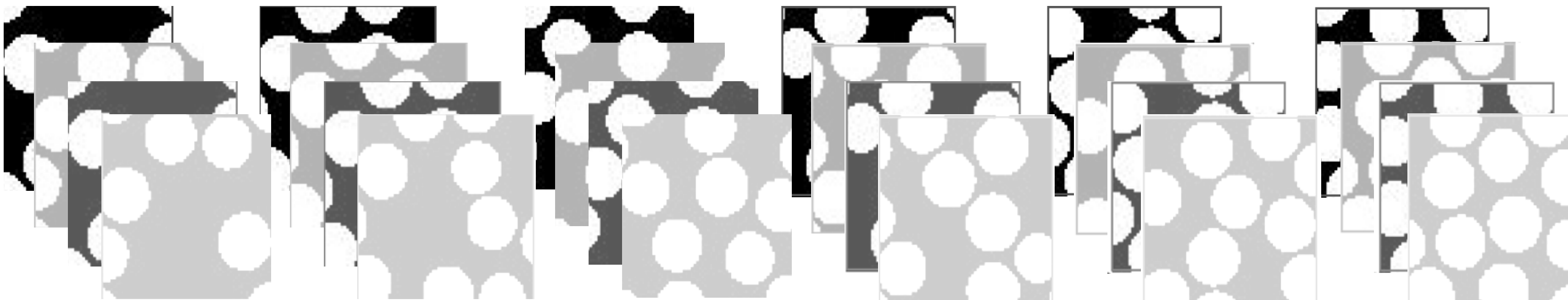

Stochastic Interaction-Based Deep Material Network

This project has received funding from the European Union's Horizon Europe Framework Programme under grant agreement No. 101056682 for the project ''DIgital DEsign strategies to certify and mAnufacture Robust cOmposite sTructures (DIDEAROT)''. The contents of this publication are the sole responsibility of ULiege and do not necessarily reflect the opinion of the European Union. Neither the European Union nor the granting authority can be held responsible for them

- Micro-scale interactions
  - Subdivision in sub-domains Ω_i

$$v_i = \frac{V_i}{V_{\mathrm{M}}}$$

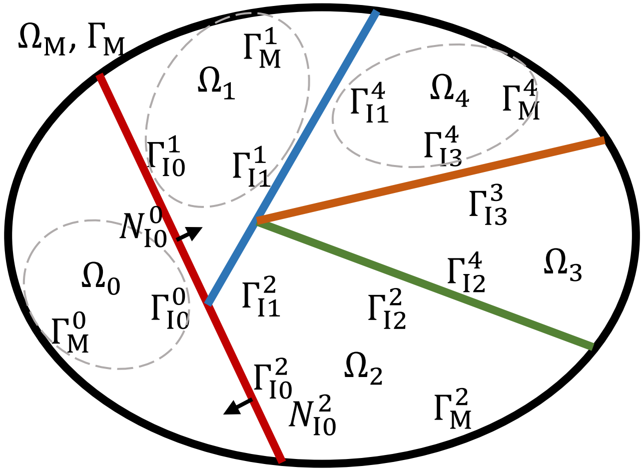

  - Stress-strain averaging

$$\boldsymbol{\varepsilon}_{\mathrm{M}} = \sum_{i=0}^{N_{\mathrm{p}}-1} v_i\, \boldsymbol{\varepsilon}_i\,, \quad \text{and}$$

$$\boldsymbol{\sigma}_{\mathrm{M}} = \sum_{i=0}^{N_{\mathrm{p}}-1} v_i\, \boldsymbol{\sigma}_i$$

  - Introduction of fluctuations

$$\boldsymbol{\varepsilon}_{\mathrm{m}}(\boldsymbol{X}_{\mathrm{m}}) = \boldsymbol{\nabla} \otimes^s \boldsymbol{u}_{\mathrm{m}}(\boldsymbol{X}_{\mathrm{m}}) = \boldsymbol{\varepsilon}_{\mathrm{M}} + \boldsymbol{\nabla} \otimes^s \boldsymbol{u}'(\boldsymbol{X}_{\mathrm{m}}), \quad \boldsymbol{X}_{\mathrm{m}} \in \Omega_{\mathrm{M}}$$

$$\boldsymbol{\varepsilon}_i = \boldsymbol{\varepsilon}_{\mathrm{M}} + \frac{1}{V_i} \sum_{\forall \Gamma_{\mathrm{I}_j}^{i} \neq \emptyset} \int_{\Gamma_{\mathrm{I}_j}^{i}} \boldsymbol{u}'(\boldsymbol{X}_{\mathrm{m}}) \otimes^s \boldsymbol{N}_{\mathrm{I}_j}^{i}\, \mathrm{d}s$$

$$s_j^i = \int_{\Gamma_{\mathrm{I}_j}^{i}} \mathrm{d}\, s$$

$$\boxed{\boldsymbol{\varepsilon}_i \simeq \boldsymbol{\varepsilon}_{\mathrm{M}} + \frac{1}{V_i} \sum_{\forall \Gamma_{\mathrm{I}_j}^{i} \neq \emptyset} s_j^i\, \boldsymbol{u}'_j \otimes^s \boldsymbol{N}_{\mathrm{I}_j}^{i}}$$

- Interactions
  - Introduction of fluctuations

$$\boldsymbol{\varepsilon}_i \simeq \boldsymbol{\varepsilon}_{\mathsf{M}} + \frac{1}{V_i} \sum_{\forall \Gamma_{\mathsf{I}_j}^{\,i} \neq \emptyset} s_j^i \, \boldsymbol{u}'_j \otimes^s \boldsymbol{N}_{\mathsf{I}_j}^{\,i}$$

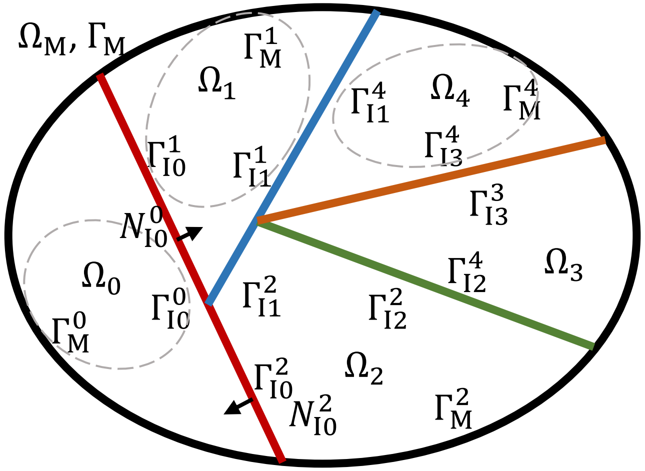

  - Assume constitutive model in each sub-domain

$$\boldsymbol{\sigma}_i = \boldsymbol{\sigma}^p\left(\boldsymbol{\varepsilon}_i(\boldsymbol{u}'_j);\ \boldsymbol{Z}_i\right), \text{ for } i = 0, \ldots, N_{\mathsf{p}} - 1$$

  - Hill-Mandel Condition

$$\boldsymbol{\sigma}_{\mathsf{M}} : \delta\boldsymbol{\varepsilon}_{\mathsf{M}} = \sum_{i=0}^{N_{\mathsf{p}}-1} v_i \, \boldsymbol{\sigma}_i : \delta\boldsymbol{\varepsilon}_i$$

$$\Rightarrow \sum_{i=0}^{N_{\mathsf{p}}-1} \sum_{\forall \Gamma_{\mathsf{I}_j}^{\,i} \neq \emptyset} \frac{v_i s_j^i}{V_i} \boldsymbol{\sigma}_i : \left(\boldsymbol{N}_{\mathsf{I}_j}^{\,i} \otimes^s \delta\boldsymbol{u}'_j\right) = 0$$

  - Weak form is the interface equation

$$\Rightarrow \boxed{\sum_{i=0}^{N_{\mathsf{p}}-1} \int_{\Gamma_{\mathsf{I}_j}^{\,i}} \boldsymbol{\sigma}_i \cdot \boldsymbol{N}_{\mathsf{I}_j}^{\,i} \mathrm{d}s = \sum_{i=0}^{N_{\mathsf{p}}-1} s_j^i \, \boldsymbol{\sigma}_i \cdot \boldsymbol{N}_{\mathsf{I}_j}^{\,i} = \boldsymbol{0}, \text{ for } j = 0, \ldots, N_{\mathsf{I}} - 1}$$

Stochastic Interaction-Based Deep Material Network

- Interactions
  - Weak form $$\sum_{i=0}^{N_\mathrm{p}-1}\int_{\Gamma|_j^i}\boldsymbol{\sigma}_i\cdot\boldsymbol{N}|_j^i\,\mathrm{d}s = \sum_{i=0}^{N_\mathrm{p}-1} s_j^i\,\boldsymbol{\sigma}_i\cdot\boldsymbol{N}|_j^i = \boldsymbol{0}\,,\ \text{for } j = 0,\ldots,N_\mathrm{I}-1$$
  - With $\boldsymbol{\sigma}_i = \boldsymbol{\sigma}^p\left(\boldsymbol{\varepsilon}_i(\boldsymbol{u}'_j);\ \boldsymbol{Z}_i\right)$, for $i = 0,\ldots,N_\mathrm{p}-1$

- One-level two-phase interaction
  - Strain tensors

$$\boldsymbol{\varepsilon}_\mathrm{A} = \boldsymbol{\varepsilon}_\mathrm{M} + \boxed{\frac{1}{v_\mathrm{A}}\frac{s_\mathrm{AB}}{V_\mathrm{M}}\boldsymbol{u}'}\otimes^s \boldsymbol{N}_\mathrm{A} \text{ and } \boldsymbol{\varepsilon}_\mathrm{B} = \boldsymbol{\varepsilon}_\mathrm{M} - \frac{1}{v_\mathrm{B}}\frac{s_\mathrm{AB}}{V_\mathrm{M}}\boldsymbol{u}'\otimes^s \boldsymbol{N}_\mathrm{A}$$

$$\hat{\mathbf{a}} = \frac{s_\mathrm{AB}}{V_\mathrm{M}}\boldsymbol{u}'$$

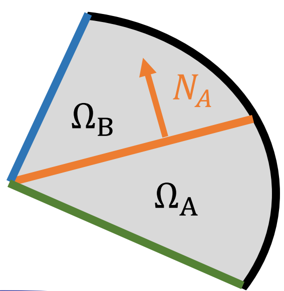

  - In linear elasticity the weak form becomes

$$\mathbb{C}_\mathrm{M} = \boxed{v_\mathrm{A}}\mathbb{C}_\mathrm{A} + (1.0 - \boxed{v_\mathrm{A}})\mathbb{C}_\mathrm{B} + (\mathbb{C}_\mathrm{A} - \mathbb{C}_\mathrm{B})\cdot\boxed{\boldsymbol{N}_\mathrm{A}}\otimes^s [\mathcal{K}^{-1}\boxed{(v_\mathrm{A}, \boldsymbol{N}_\mathrm{A})}\cdot\mathcal{F}\boxed{(v_\mathrm{A}, \boldsymbol{N}_\mathrm{A})}]$$

Topology parameters to be defined $\mathcal{G}^2 = \{v_\mathrm{A}, \boldsymbol{N}_\mathrm{A}\}$

Stochastic Interaction-Based Deep Material Network

- Simple network of material nodes with interactions to Replace volume element

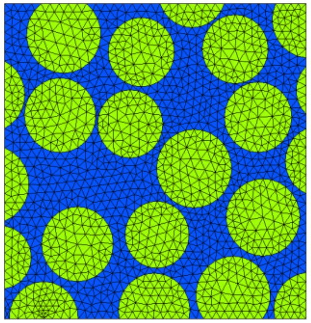

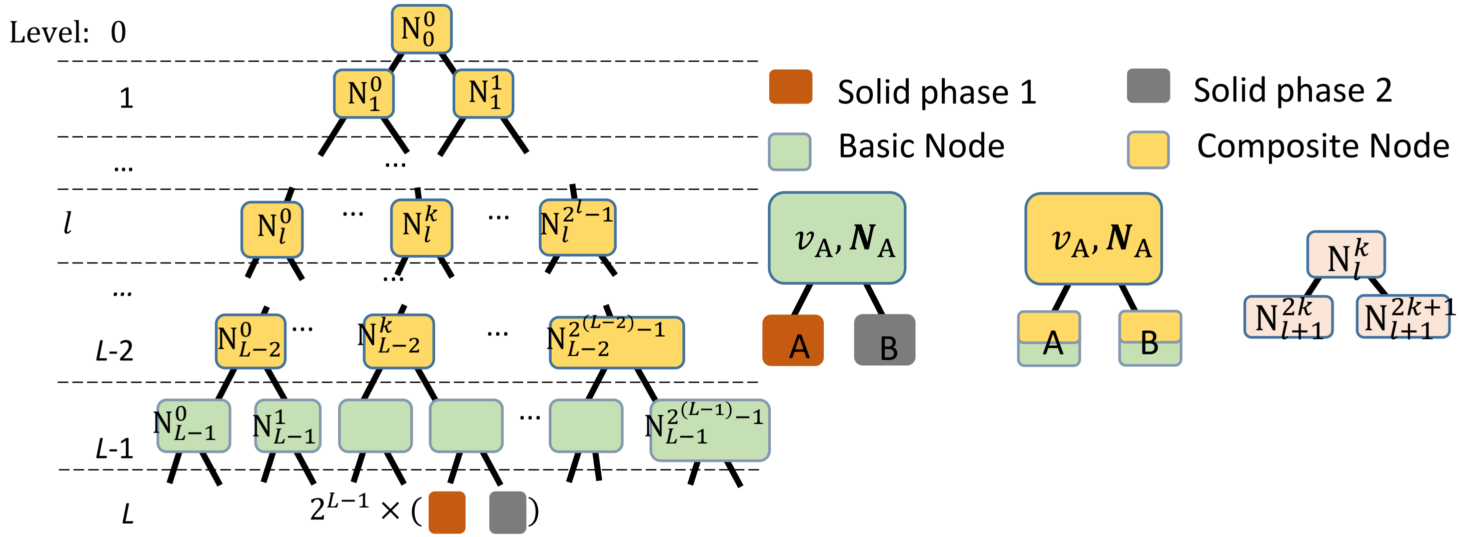

- Elasticity tensor
  - From material tensor evaluation $\mathbb{C}\left(\mathrm{N}_l^k\right) = \mathrm{FUN}\left(l,\, \mathbb{C}_0,\, \mathbb{C}_\mathrm{I},\, \mathcal{G}^2\left(\mathrm{N}_l^k\right)\right)$
    - Requires

$$\begin{cases} \mathbb{C}\left(\mathrm{N}_{l+1}^{2k}\right) = \mathrm{FUN}\left(l+1,\, \mathbb{C}_0,\, \mathbb{C}_\mathrm{I},\, \mathcal{G}^2\left(\mathrm{N}_{l+1}^{2k}\right)\right) \\ \mathbb{C}\left(\mathrm{N}_{l+1}^{2k+1}\right) = \mathrm{FUN}\left(l+1,\, \mathbb{C}_0,\, \mathbb{C}_\mathrm{I},\, \mathcal{G}^2\left(\mathrm{N}_{l+1}^{2k+1}\right)\right) \end{cases}$$

Recursively $\mathbb{C}_\mathrm{M} = \mathrm{FUN}\left(l=0,\, \mathbb{C}_0,\, \mathbb{C}_\mathrm{I},\, \mathcal{G}^2(\mathrm{N}_0^0)\right)$

- Micro-structure topological parameters $\boxed{\mathcal{G}^2(\mathrm{N}_0^0), \mathcal{G}^2(\mathrm{N}_1^0), \mathcal{G}^2(\mathrm{N}_1^1), \ldots, \mathcal{G}^2\left(\mathrm{N}_{L-1}^{2^{(L-1)}-1}\right)}$

- Micro-structure topological parameters

$$\mathcal{G}^2(\mathrm{N}_0^0), \mathcal{G}^2(\mathrm{N}_1^0), \mathcal{G}^2(\mathrm{N}_1^1), \ldots, \mathcal{G}^2\left(\mathrm{N}_{L-1}^{2^{(L-1)}-1}\right)$$

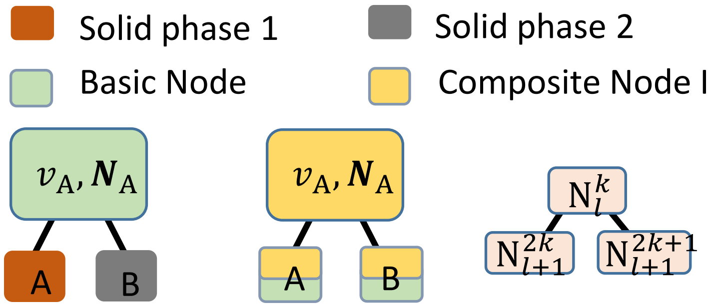

- Elastic training
  - From material tensor evaluation

$$\mathbb{C}_\mathrm{M} = \mathrm{FUN}\left(l = 0,\ \mathbb{C}_0,\ \mathbb{C}_\mathrm{I},\ \mathcal{G}^2(\mathrm{N}_0^0)\right)$$

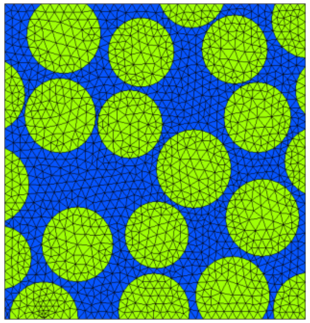

  - Data driven approach:
    - Generate observations $\{\hat{\mathbb{C}}_\mathrm{M}(\mathbb{C}_0^s, \mathbb{C}_\mathrm{I}^s)\}$ by full DNS using random $\mathbb{C}_0^s$, $\mathbb{C}_\mathrm{I}^s$
    - Identify topological parameters from loss function (knowing real volume fraction $\hat{v}_\mathrm{I}$ of phase I)

$$Loss(\hat{\mathbb{C}}_\mathrm{M}, \mathbb{C}_\mathrm{M}) = \frac{1}{n}\sum_{s=0}^{n-1} \frac{\|\hat{\mathbb{C}}_\mathrm{M}(\mathbb{C}_0^s, \mathbb{C}_\mathrm{I}^s) - \mathbb{C}_\mathrm{M}(\mathbb{C}_0^s, \mathbb{C}_\mathrm{I}^s; \mathcal{G}^2)\|}{\|\hat{\mathbb{C}}_\mathrm{M}(\mathbb{C}_0^s, \mathbb{C}_\mathrm{I}^s)\|} + \frac{\lambda}{2}(\hat{v}_\mathrm{I} - v_\mathrm{I})^2$$

Stochastic Interaction-Based Deep Material Network

- Once topological parameters knowns

$$\boxed{\mathcal{G}^2(\mathrm{N}_0^0), \mathcal{G}^2(\mathrm{N}_1^0), \mathcal{G}^2(\mathrm{N}_1^1), \dots, \mathcal{G}^2\left(\mathrm{N}_{L-1}^{2^{(L-1)}-1}\right)}$$

- Online simulations in the non-linear range
  - $\boldsymbol{\varepsilon} \rightarrow \mathbf{F},\ \boldsymbol{\sigma} \rightarrow \mathbf{P},\ \mathbf{P}_i = \mathbf{P}^p\left(\mathbf{F}_i\left(\boldsymbol{u}'_j\right);\ \boldsymbol{Z}_i\right)$
  - Isotropic hardening $f = \tau_{\mathrm{eq}} - \tau_{\mathrm{y}}^0 - h\gamma \leq 0$,
  - Tests on 6 SVEs

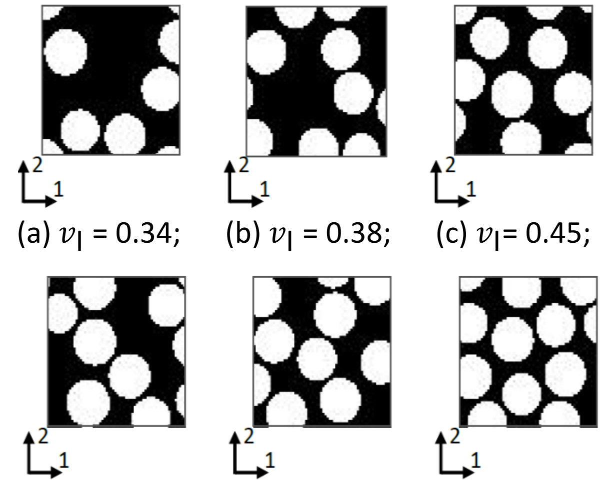

(a) v_I = 0.34; (b) v_I = 0.38; (c) v_I= 0.45;

(d) v_I = 0.47; (e) v_I = 0.52; (f) v_I= 0.58

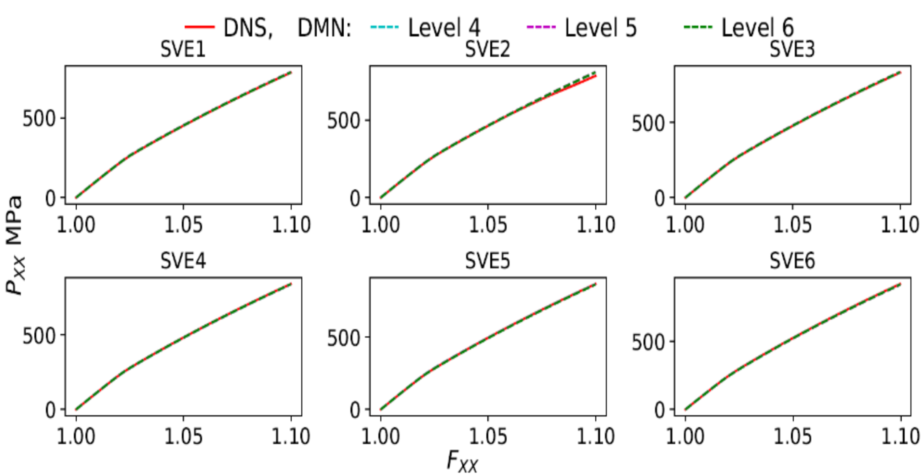

(a) Uni-axial strain

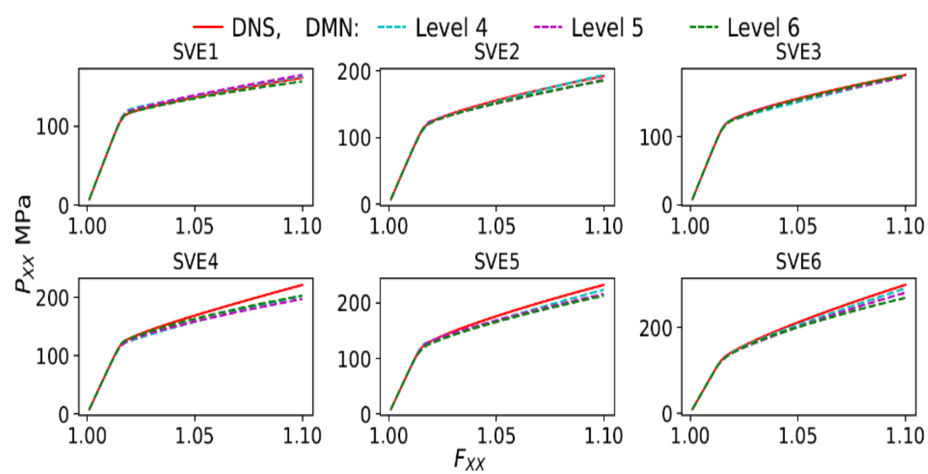

(b) In-plane uni-axial stress

Stochastic Interaction-Based Deep Material Network

- Reformulation of parameters $\mathcal{G}^2 = \{v_\mathrm{A}, \boldsymbol{N}_\mathrm{A}\}$ at node N_l^k
  - Normal $\boldsymbol{N}_\mathrm{A}(\mathrm{N}_l^k)$ from angles $\theta_1(\mathrm{N}_l^k)$ and $\theta_2(\mathrm{N}_l^k)$

$$\theta_1 = 2\pi \mathrm{w}_{\theta_1}(\mathrm{N}_l^k),\ \theta_2 = \pi \mathrm{w}_{\theta_2}(\mathrm{N}_l^k)$$

$$\Rightarrow\ \boxed{\mathrm{w}_{\theta_1}(\mathrm{N}_l^k), \mathrm{w}_{\theta_2}(\mathrm{N}_l^k) \in [0,\ 1)}$$

  - Volume fraction $v_\mathrm{A}(\mathrm{N}_l^k)$

1) "Yellow" Node at level $l = 0$:

$v_\mathrm{I}(\mathrm{N}_0^0) = v_\mathrm{I}$ and $v_0(\mathrm{N}_0^0) = 1 - v_\mathrm{I}$ known

$$\Rightarrow\ \left\{\begin{array}{l} v_\mathrm{A}(\mathrm{N}_0^0) = \mathrm{w}_{\mathrm{v}0}(\mathrm{N}_0^0)\, v_0(\mathrm{N}_0^0) + \mathrm{w}_{\mathrm{vI}}(\mathrm{N}_0^0)\, v_\mathrm{I}(\mathrm{N}_0^0) \\ v_\mathrm{B}(\mathrm{N}_0^0) = 1.0 - v_\mathrm{A}(\mathrm{N}_0^0) \end{array}\right.$$

$\Rightarrow$ { $\mathrm{w}_{\mathrm{v}0}(\mathrm{N}_0^0)$ contribution v_A of N_1^0 and
$\mathrm{w}_{\mathrm{vI}}(\mathrm{N}_0^0)$ contribution v_B of N_1^1 to N_0^0

2) Recursively for "Yellow" Node at level $0 < l < L$

$$\Rightarrow\ \boxed{\mathrm{w}_{\mathrm{v}0}(\mathrm{N}_l^k), \mathrm{w}_{\mathrm{vI}}(\mathrm{N}_l^k) \in [0,\ 1)}$$

3) Basic "Green" Node at level $L - 1$:

$$v_\mathrm{A} = 1.0 - v_\mathrm{I}(\mathrm{N}_{L-1}^k) \text{ and } v_\mathrm{B} = v_\mathrm{I}(\mathrm{N}_{L-1}^k)$$

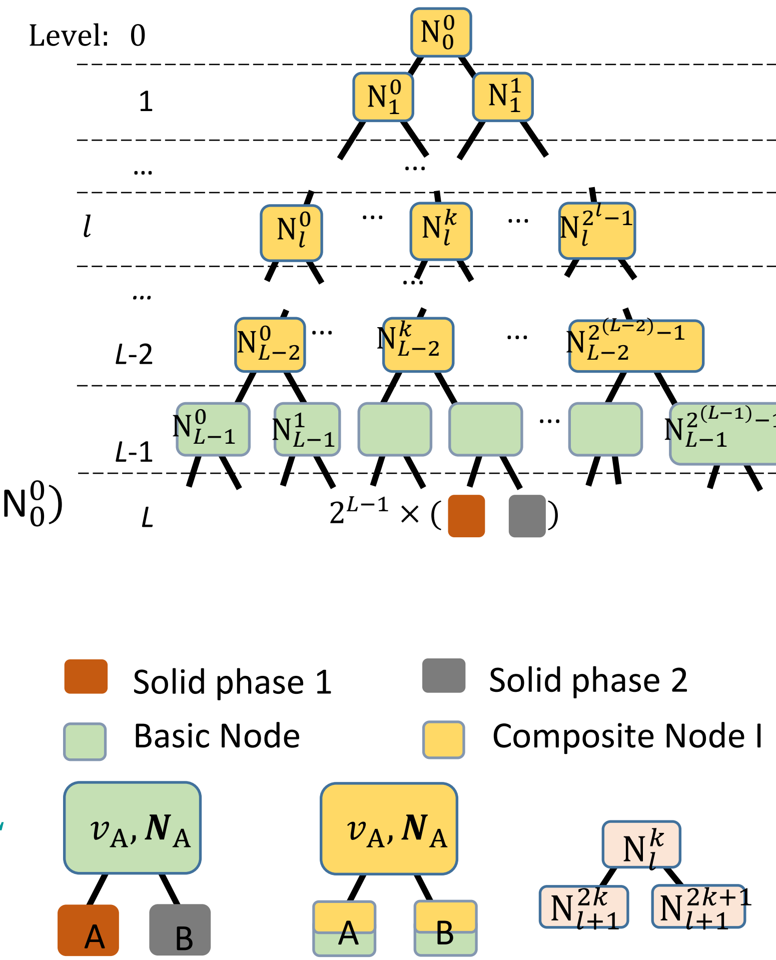

- SVEs batch training
  - New parameters $\tilde{\mathcal{T}}_{\mathrm{n}} = \{\mathrm{w}_{\theta_1}(\mathrm{N}_l^k), \mathrm{w}_{\theta_2}(\mathrm{N}_l^k)\}$ and $\tilde{\mathcal{T}}_{\mathrm{v}} = \{\mathrm{w}_{\mathrm{v0}}(\mathrm{N}_l^k), \mathrm{w}_{\mathrm{vI}}(\mathrm{N}_l^k)\}$
  - Train a generic DMN
    - Random micro-topologies and volume fractions,
    - Random phase properties

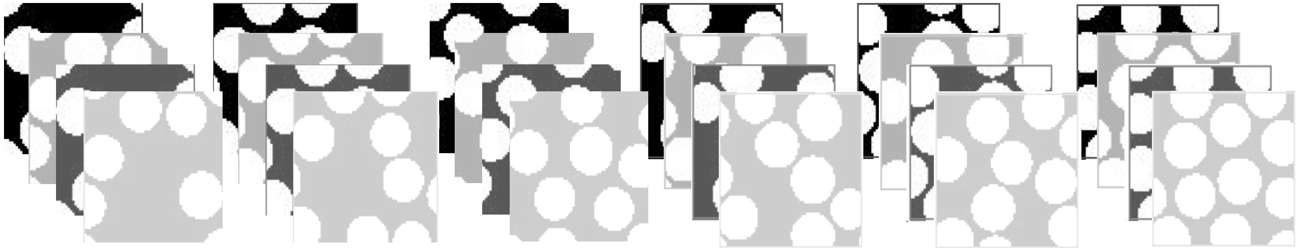

$\{\hat{\mathbb{C}}_{\mathrm{M}}(\mathbb{C}_0^s, \mathbb{C}_{\mathrm{I}}^s)\}$

  - New loss function in which v_{I}^s is known for each SVE

$$Loss(\hat{\mathbb{C}}_{\mathrm{M}}, \mathbb{C}_{\mathrm{M}}) = \frac{1}{n}\sum_{s=1}^{n} \frac{\|\hat{\mathbb{C}}_{\mathrm{M}}(\mathbb{C}_0^s, \mathbb{C}_{\mathrm{I}}^s) - \mathbb{C}_{\mathrm{M}}(\mathbb{C}_0^s, \mathbb{C}_{\mathrm{I}}^s, v_{\mathrm{I}}^s; \tilde{\mathcal{T}}_{\mathrm{n}}, \tilde{\mathcal{T}}_{\mathrm{v}})\|}{\|\hat{\mathbb{C}}_{\mathrm{M}}(\mathbb{C}_0^s, \mathbb{C}_{\mathrm{I}}^s)\|}$$

Identify the generic DMN parameter $\tilde{\mathcal{T}}_{\mathrm{n}}, \tilde{\mathcal{T}}_{\mathrm{v}}$

Stochastic Interaction-Based Deep Material Network

- Perturbate generic DMN
  - $\underline{\tilde{\mathcal{T}}}_{\mathrm{n}}, \underline{\tilde{\mathcal{T}}}_{\mathrm{v}}$ define a generic deterministic DMN with volume fraction v_{I} as input
  - We can perturbate the parameters $\underline{\tilde{\mathcal{T}}}_{\mathrm{n}}, \underline{\tilde{\mathcal{T}}}_{\mathrm{v}}$ to have a stochastic DMN

$$\begin{cases} \underline{\mathcal{T}}_{\mathrm{n}} = (1+\xi) \odot \underline{\tilde{\mathcal{T}}}_{\mathrm{n}} \\ \underline{\mathcal{T}}_{\mathrm{v}} = (1+\xi) \odot \underline{\tilde{\mathcal{T}}}_{\mathrm{v}} \end{cases} \qquad \begin{aligned} \xi &= 2b(\chi - 0.5) \\ \chi &\sim \mathrm{Beta}(\alpha) \end{aligned}$$

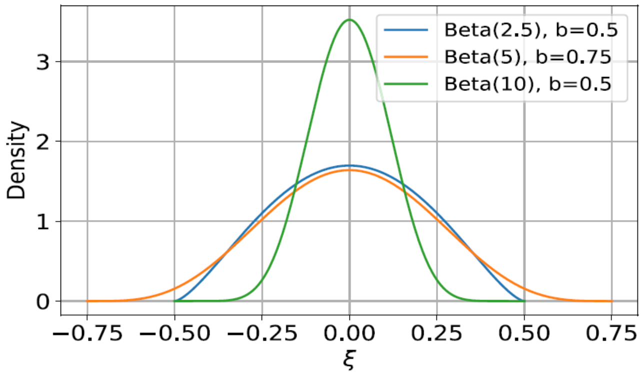

Stochastic Interaction-Based Deep Material Network

- Perturbate generic DMN

$\underline{\mathcal{T}}_{\mathrm{n}} = (1+\xi)\odot\underline{\tilde{\mathcal{T}}}_{\mathrm{n}} \qquad \underline{\mathcal{T}}_{\mathrm{v}} = (1+\xi)\odot\underline{\tilde{\mathcal{T}}}_{\mathrm{v}}$

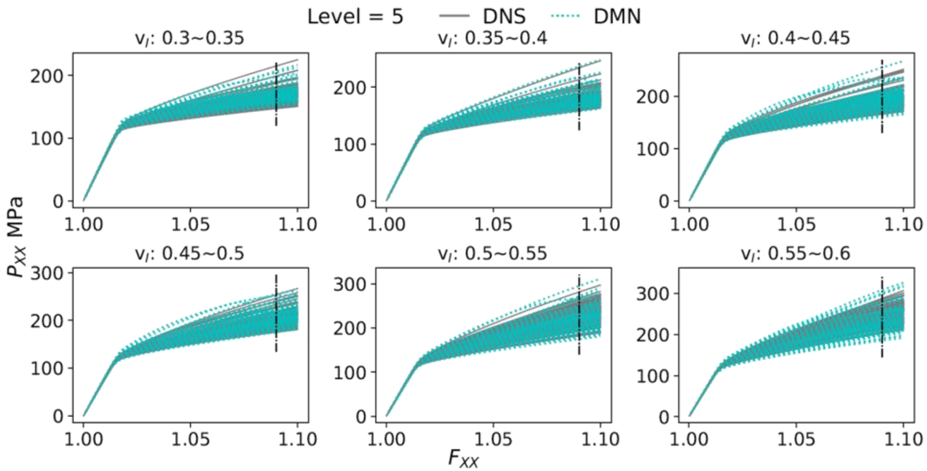

$\xi = (\chi - 0.5) \qquad \chi \sim \mathrm{Beta}(2.5)$

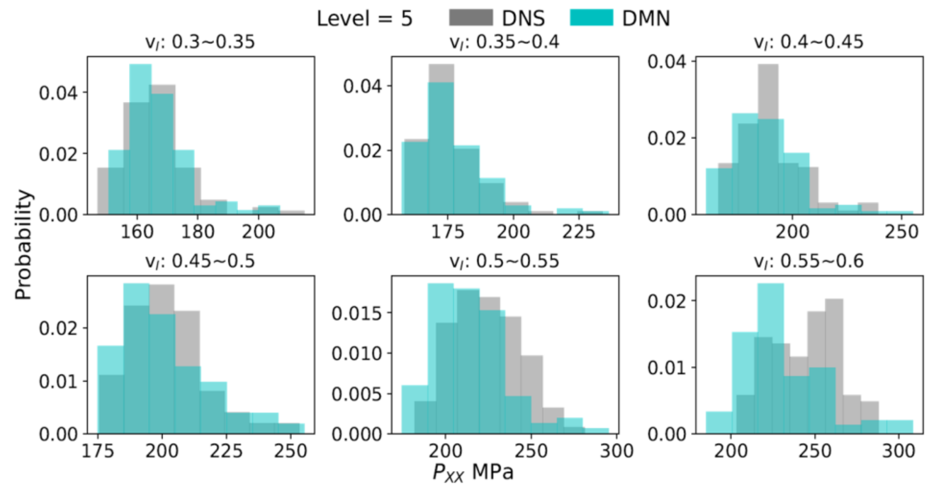

$\xi = 1{,}5(\chi - 0.5) \qquad \chi \sim \mathrm{Beta}(5)$

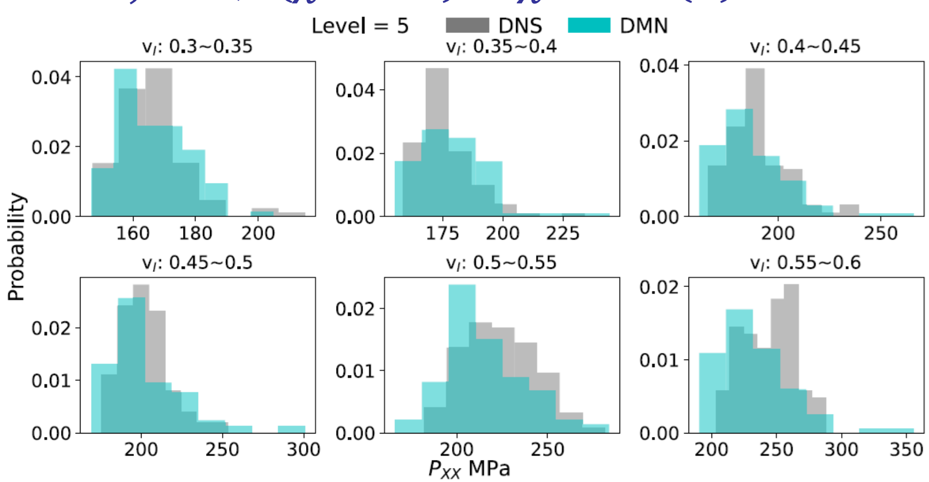

$\xi = (\chi - 0.5) \qquad \chi \sim \mathrm{Beta}(10)$

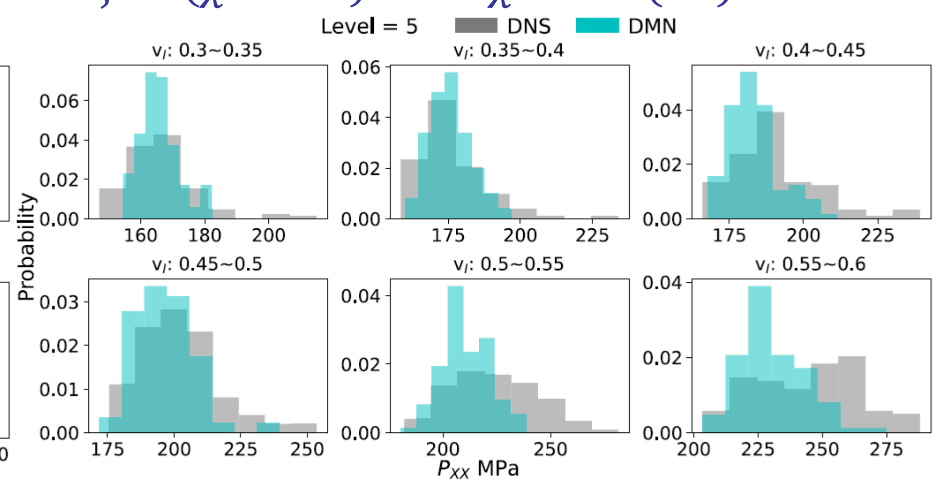

- We still need to find a proper way to infer the perturbation

References

- DIDEAROT project (https://www.didearot-project.eu/)
  - CENAERO, HEXAGON, SONACA, ULiège (Belgium)
  - Tecnalia, Aernnova, Barcelona Supercomputing Center (Spain)
  - Inegi (Portugal)

- Publication
  - L. Wu and L. Noels. "Stochastic deep material networks as efficient surrogates for stochastic homogenisation of non-linear heterogeneous materials." Computer Methods in Applied Mechanics and Engineering, 441 (01 June 2025): 117994. doi: https://doi.org/10.1016/j.cma.2025.117994
- Data and code on
  - Repository: https://gitlab.uliege.be/didearot/didearotPublic/publicationsData/2025_StochasticIBDMN
  - Doi: http://dx.doi.org/10.5281/zenodo.15120313

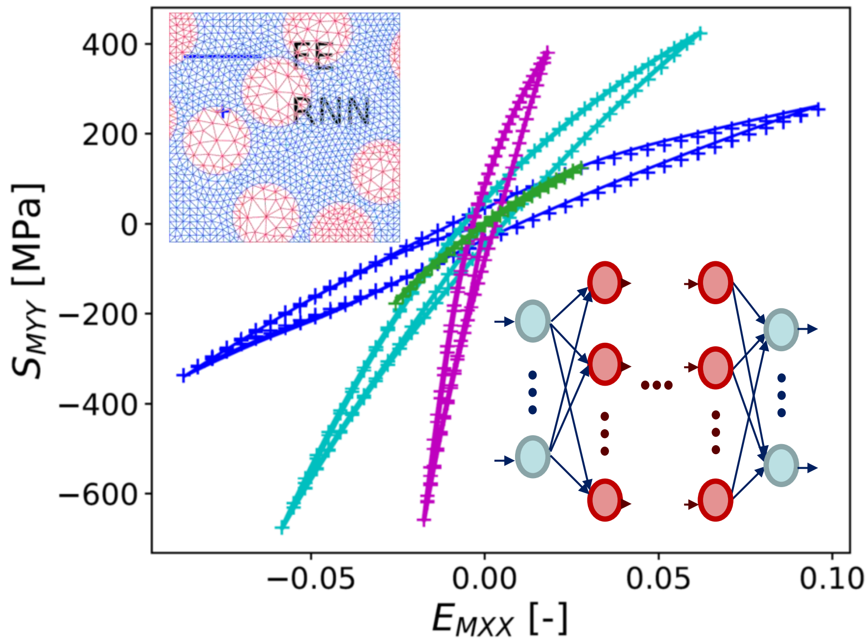

Recurrent Neural Network-accelerated multi-scale simulations in elasto-plasticity

MOAMMM project has received funding from the European Union's Horizon 2020 research and innovation programme under grant agreement No 862015 for the project Multi-scale Optimisation for Additive Manufacturing of fatigue resistant shock-absorbing MetaMaterials (MOAMMM) of the H2020-EU.1.2.1. - FET Open Programme

MOAMMM

LIÈGE université

- Introduction to non-linear multi-scale simulations
  - FE multi-scale simulations
    - Problems to be solved at two scales
    - Requires Newton-Raphson iterations at both scales
  - Use of surrogate models
    - Train a meso-scale surrogate model (off-line)
      - Requires extensive data
      - Obtained from RVE simulations
    - Use the trained surrogate model during analyses (on-line)
      - Surrogate acts as a homogenised constitutive law
      - Expected speed-up of several orders

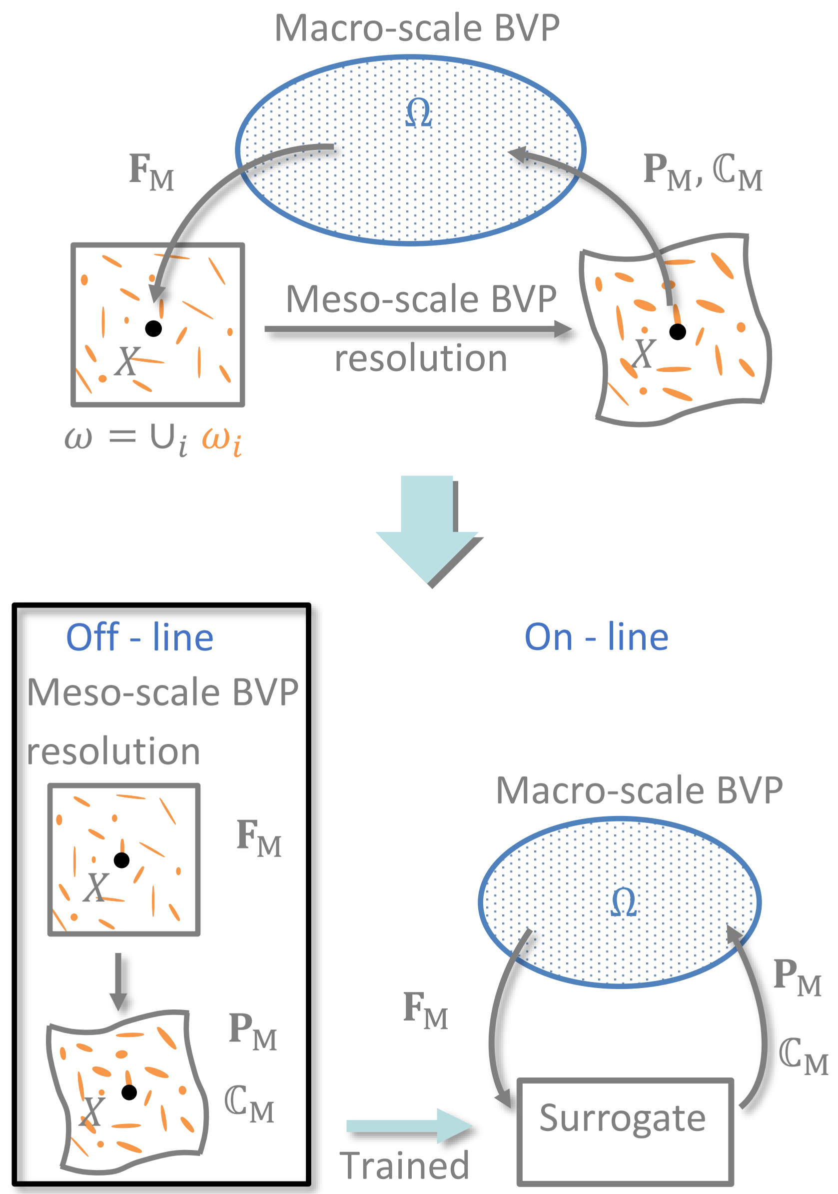

Recurrent Neural Network-accelerated multi-scale simulations

- Definition of the surrogate model
  - Artificial neuron
    - Non-linear function on n_0 inputs u_k
    - Requires evaluation of weights w_k
    - Requires definition of activation function f

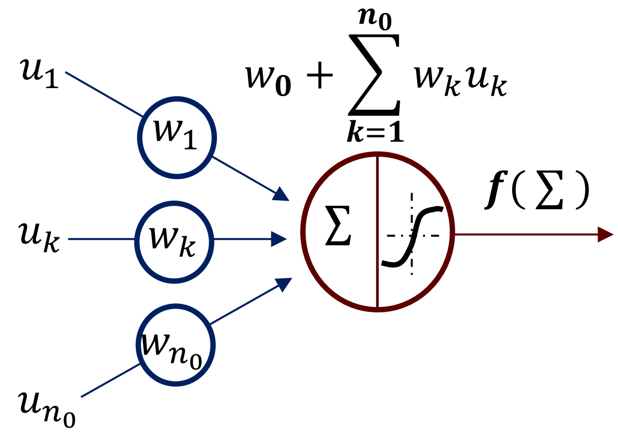

  - Activation functions f

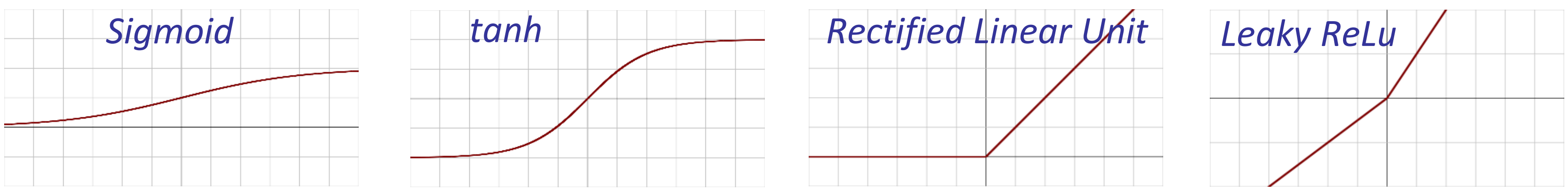

  - Feed-Forward Neuron Network
    - Simplest architecture
    - Layers of neurons
      - Input layer
      - $N-1$ hidden layers
      - Output layers
    - Mapping $\Re^{n_0} \rightarrow \Re^{n_N}: \boldsymbol{v} = \boldsymbol{g}(\boldsymbol{u})$

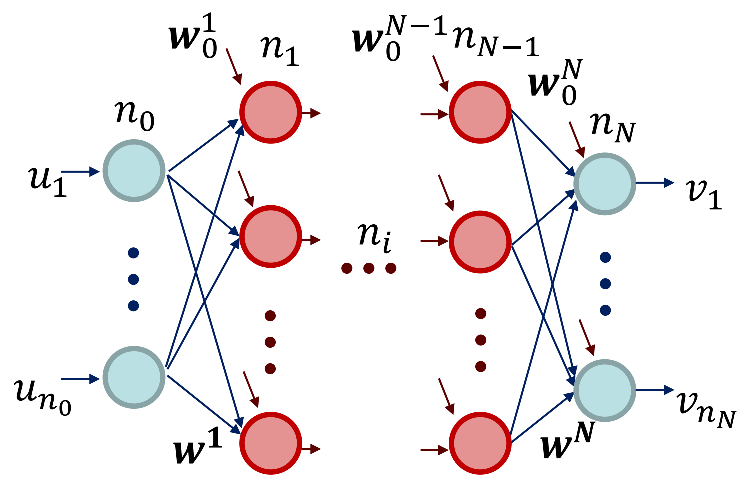

- Training
  - Evaluate
    - The weights w_{kj}^{i}, $k = 1..n_{i-1}, j = 1..n_i$
    - The bias w_0^i
    - Minimise error prediction $\boldsymbol{v}$ vs. real $\boldsymbol{v}^{(p)}$

$$L_{\mathrm{MSE}}\,(\mathbf{W}) = \frac{1}{n}\sum_{i}^{n}\left\|\boldsymbol{v}_i(\mathbf{W}) - \boldsymbol{v}_i^{(p)}\right\|^2$$

    - Requires an optimizer: Stochastic Gradient Descent

$$\boldsymbol{\Delta}\mathbf{W} = -\mathcal{F}\left(\frac{\partial L_i(\mathbf{W})}{\partial \mathbf{W}}, \quad \left(\frac{\partial L_i(\mathbf{W})}{\partial \mathbf{W}}\right)^2, \text{batch size}, \ldots\right)$$

  - Training data
    - Input $\boldsymbol{u}^{(p)}$ & Output $\boldsymbol{v}^{(p)}$
- Testing
  - Use new data
    - Input $\boldsymbol{u}^{(p)}$ & Output $\boldsymbol{v}^{(p)}$
    - Verify prediction $\boldsymbol{v}$ vs. real $\boldsymbol{v}^{(p)}$

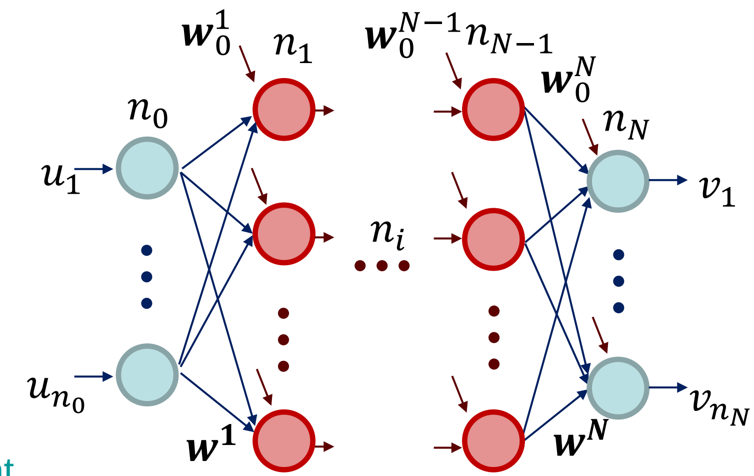

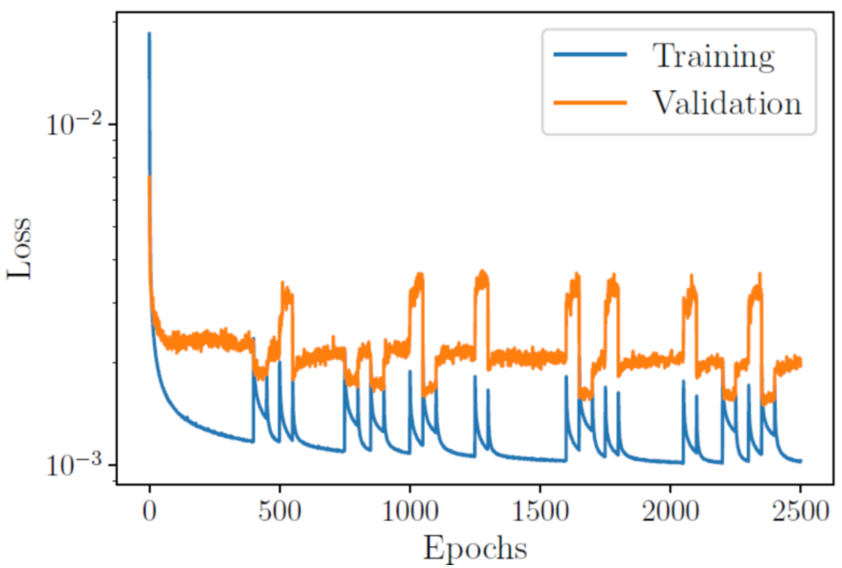

Recurrent Neural Network-accelerated multi-scale simulations

- Input / output definition
  - Input: Strain (history): $\mathbf{F}_{\mathrm{M}}$
  - Output: Stress (history): $\mathbf{P}_{\mathrm{M}}$

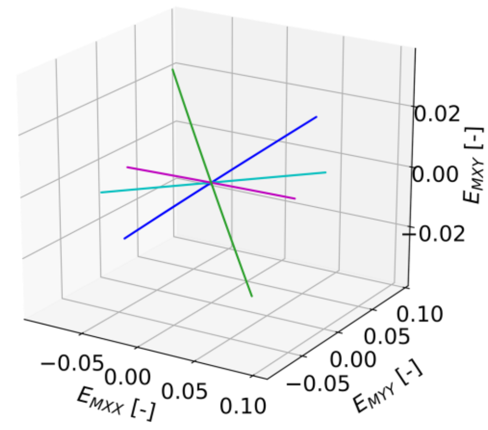

- Elasto-plastic material behaviour
  - No bijective strain-stress relation
    - Feed-forward NNW cannot be used
    - History should be accounted for

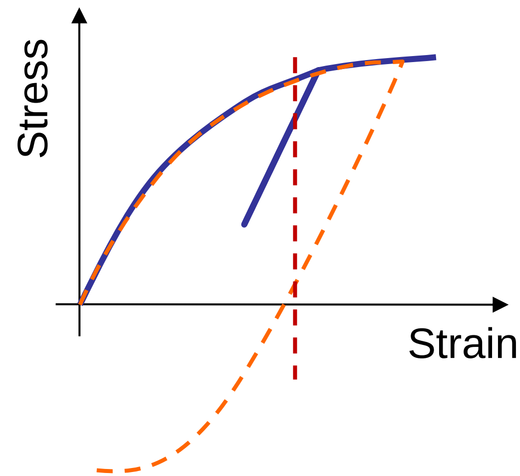

- Recurrent neural network
  - Allows a history dependent relation
    - Input $\boldsymbol{u}_t$
    - Output $\boldsymbol{v}_t = \boldsymbol{g}(\boldsymbol{u}_t, \boldsymbol{h}_{t-1})$
    - Internal variable $\boldsymbol{h}_t = \boldsymbol{g}(\boldsymbol{u}_t, \boldsymbol{h}_{t-1})$
  - Weights matrices $\mathbf{U}, \mathbf{W}, \mathbf{V}$
    - Trained using sequences
      - Inputs $\boldsymbol{u}_{t-n}^{(p)}, \dots, \boldsymbol{u}_t^{(p)}$
      - Output $\boldsymbol{v}_{t-n}^{(p)}, \dots, \boldsymbol{v}_t^{(p)}$

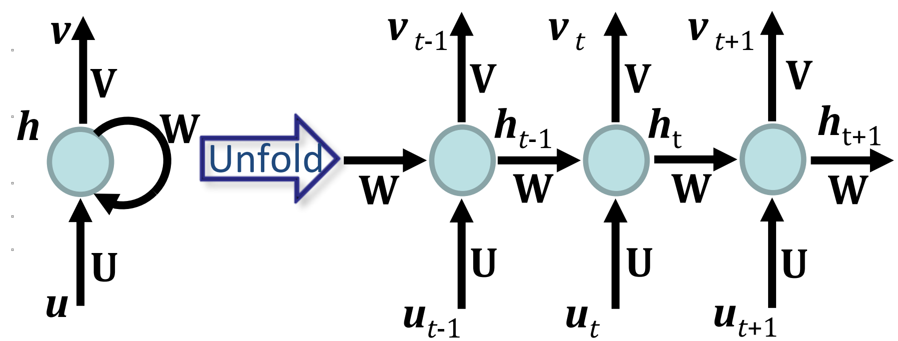

- Gated Recurrent Unit (GRU) at a glance

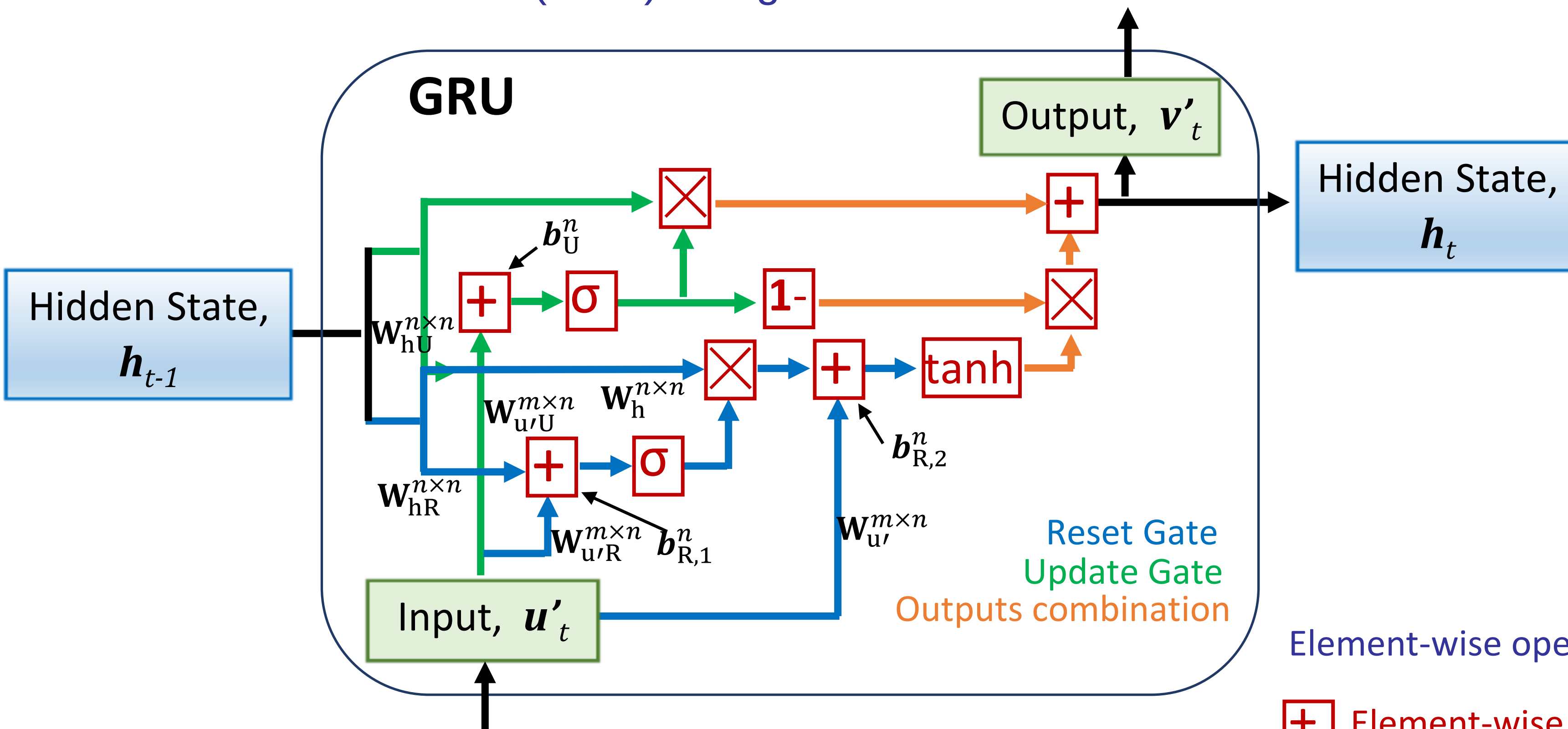

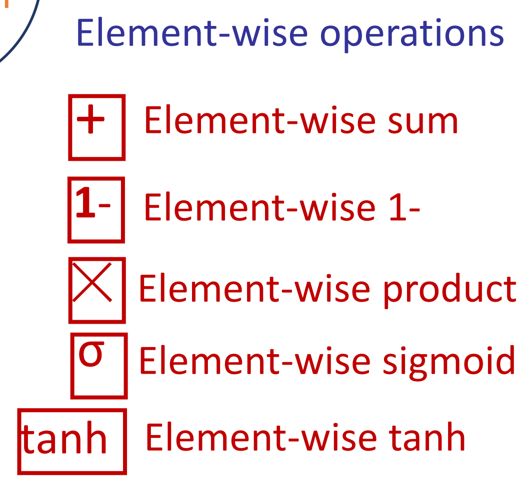

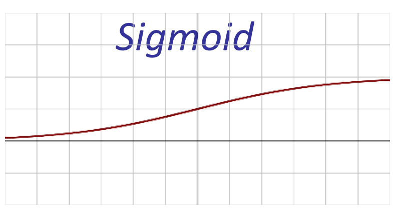

- Recurrent neural network design
  - 1 Gated Recurrent Unit (GRU)
    - Rest gate: select past information to be forgotten
    - Update gate: select past information to be passed along
  - 2 feed-forward NNWs
    - NNW_I to treat inputs $\boldsymbol{u}_t$
    - NNW_O to produce outputs $\boldsymbol{v}_t$
  - Details
    - $\boldsymbol{u}_t$: homogenised GL strain $\mathbf{E}_M$ (symmetric)
    - $\boldsymbol{v}_t$: homogenised 2nd PK stress $\mathbf{S}_M$ (symmetric)
    - 100 hidden variables $\boldsymbol{h}_t$
    - NNW_I one hidden layer of 60 neurons
    - NNW_O two hidden layers of 100 neurons

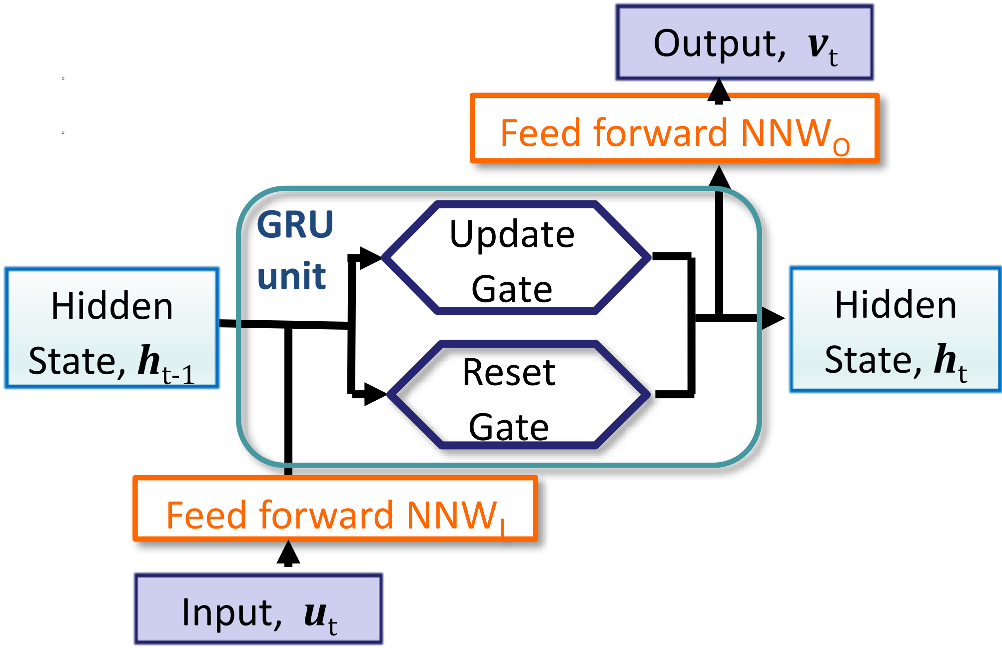

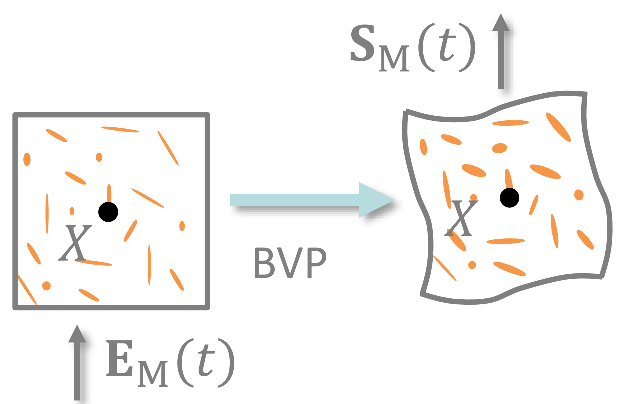

Recurrent Neural Network-accelerated multi-scale simulations

- Data generation
  - Elasto-plastic composite RVE
  - Training stage
    - Should cover full range of possible loading histories
    - Use random walking strategy (thousands)
    - Completes with random cyclic loading (tens)
    - Bounded by a sphere of 10% deformation

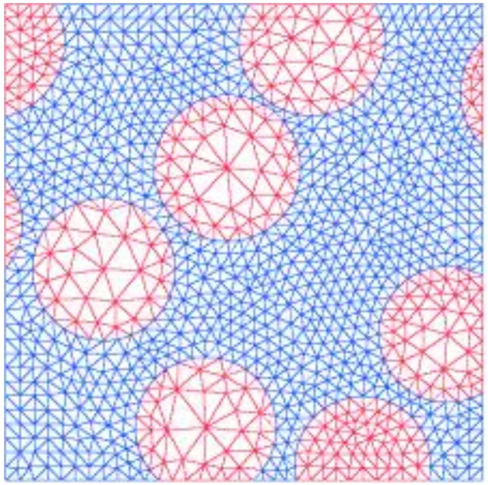

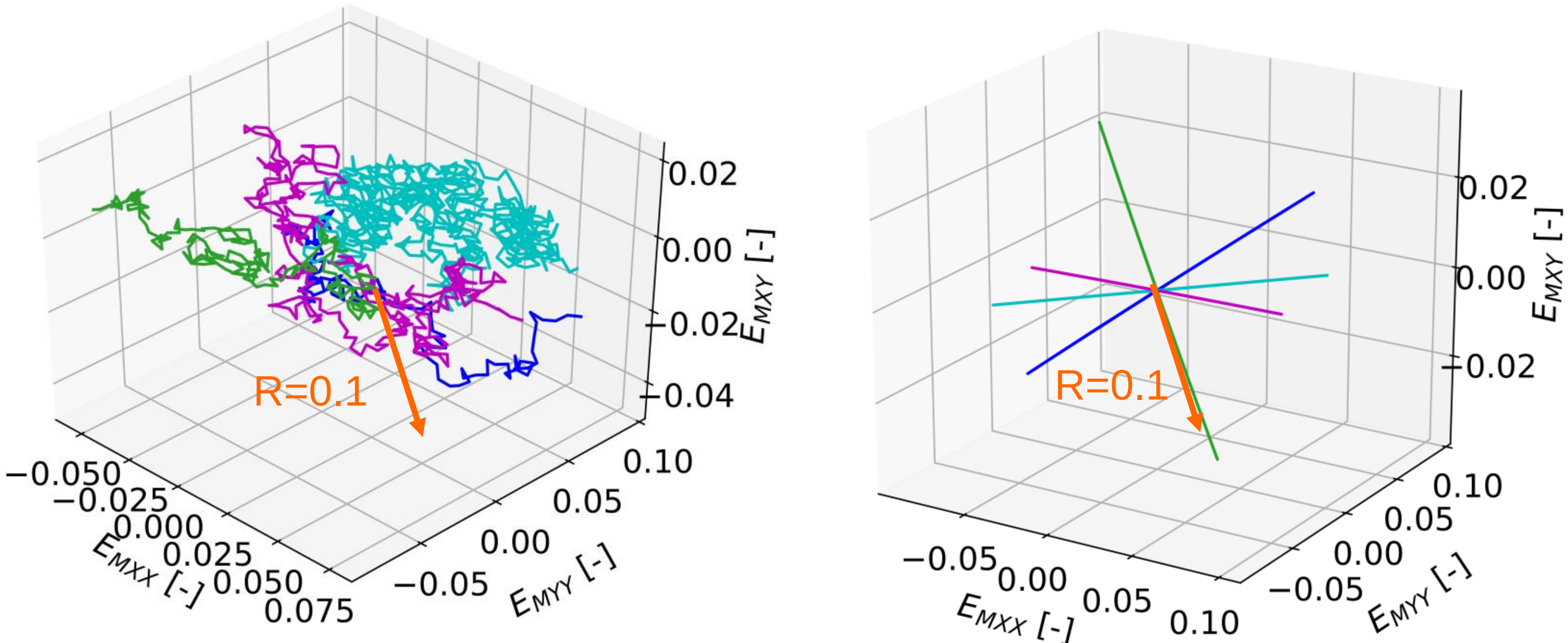

Recurrent Neural Network-accelerated multi-scale simulations

- Testing process (new data)
  - On random walk

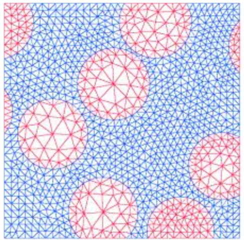

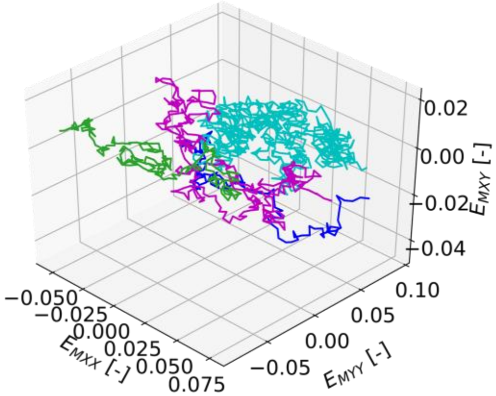

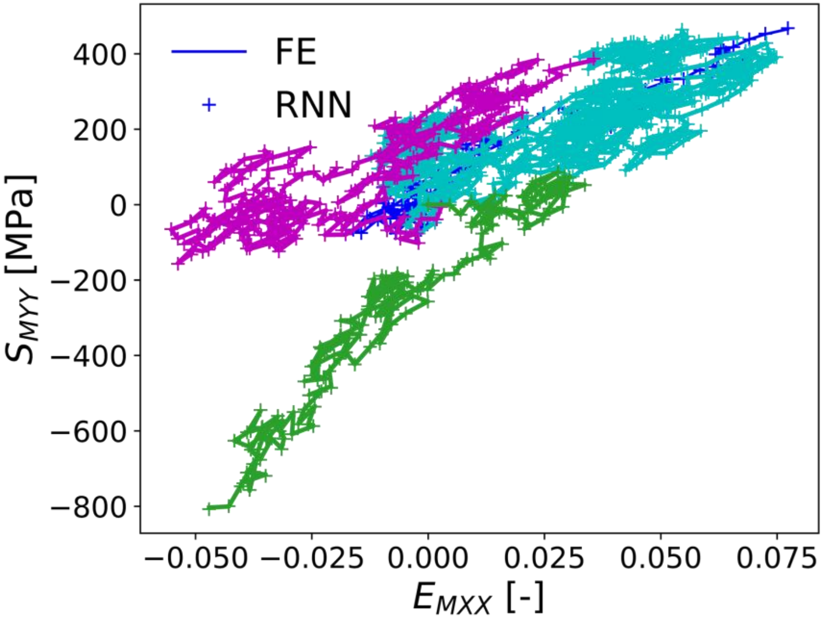

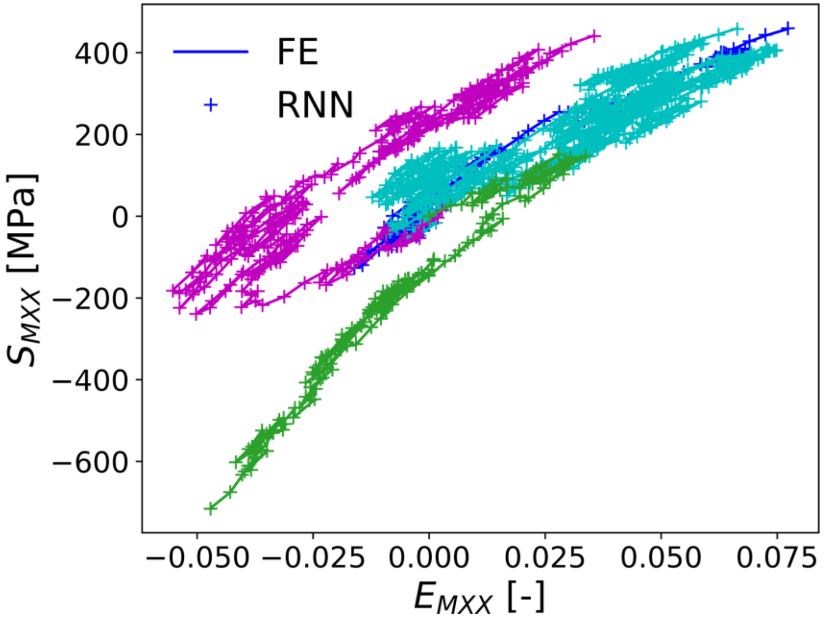

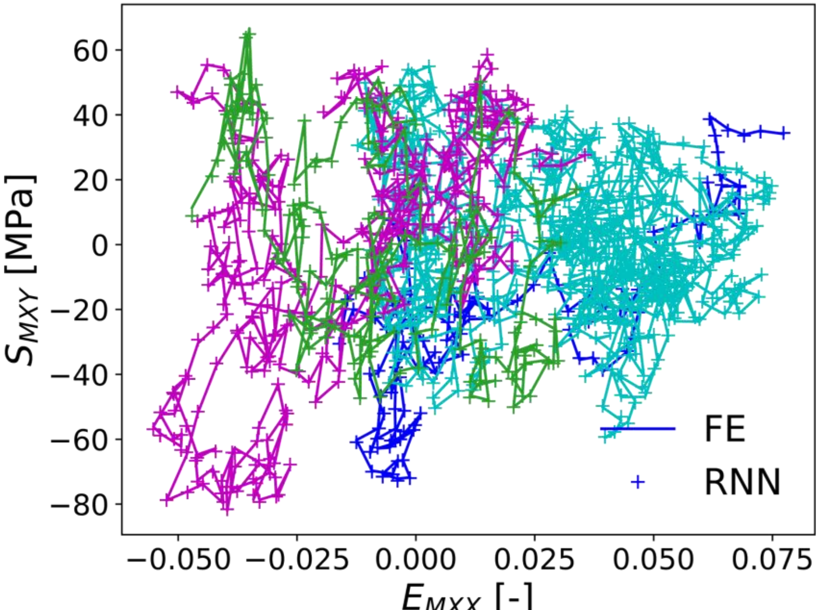

Recurrent Neural Network-accelerated multi-scale simulations

- Testing process (new data)
  - On cyclic loading

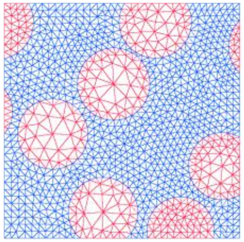

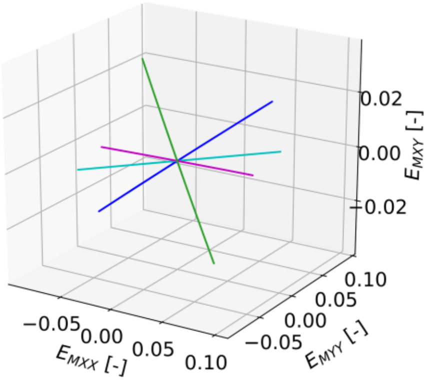

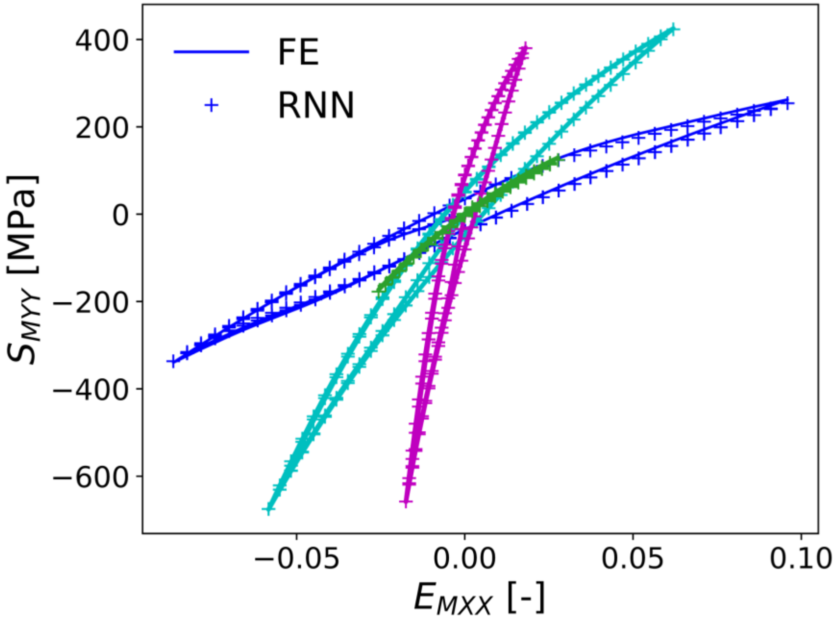

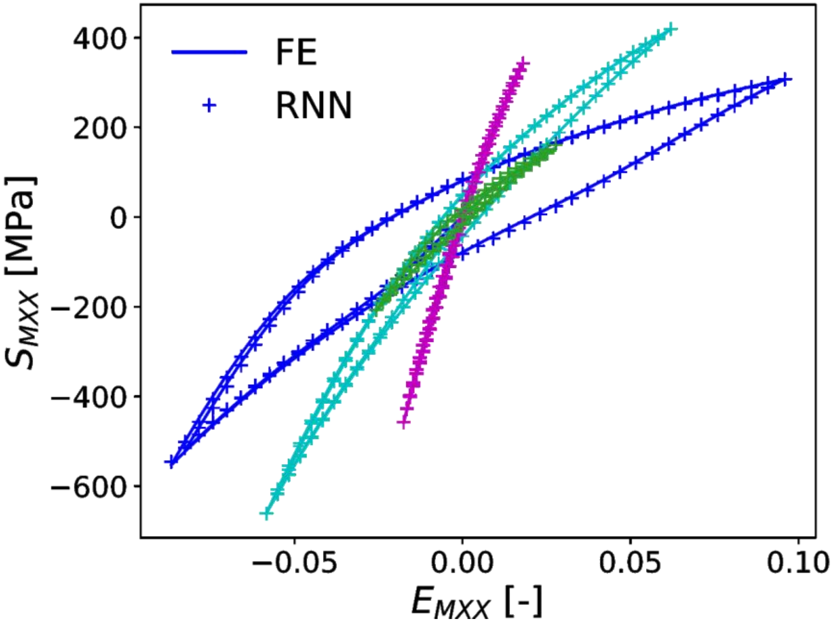

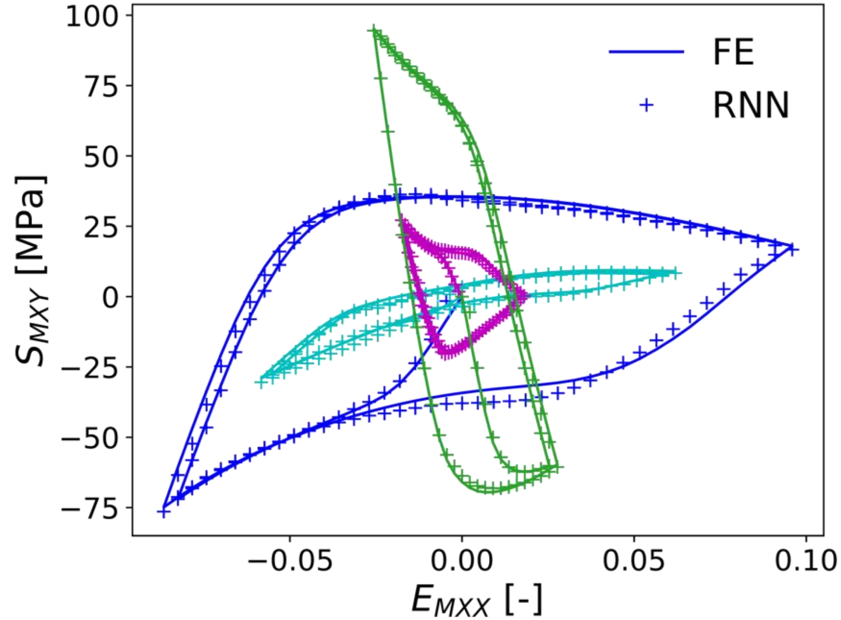

Recurrent Neural Network-accelerated multi-scale simulations

- Multiscale simulation
  - Elasto-plastic composite RVE
  - Comparison FE^2 vs. RNN-surrogate
  - Training data
    - Bounded at 10% deformation

Off-line	FE^2	FE-RNN
Data generation	-	9000 x 2 h-cpu
Training	-	3 day-cpu
On-line	**FE^2**	**FE-RNN**
Simulation	18000 h-cpu	0.5 h-cpu

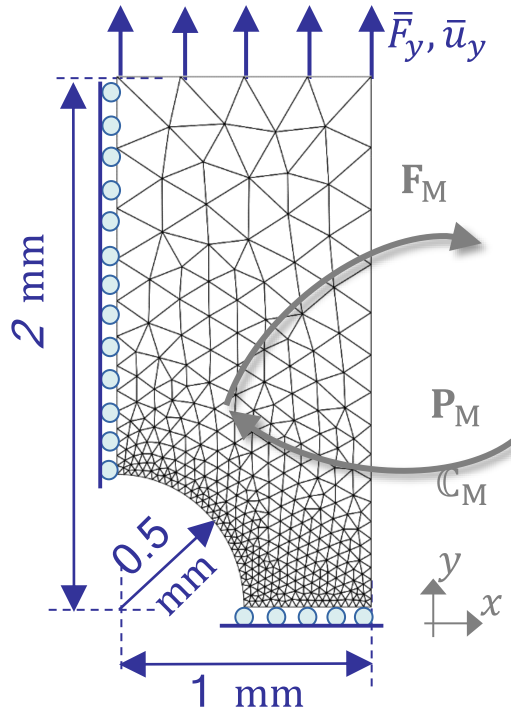

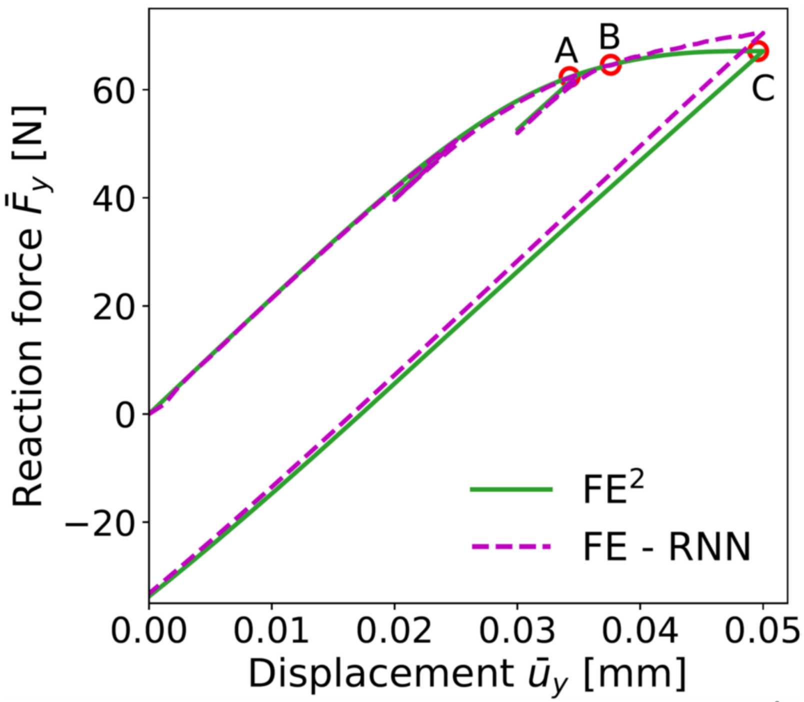

Recurrent Neural Network-accelerated multi-scale simulations

- Multiscale simulation
  - Stress-strain distribution at point A
  - Strain within the 10% training range

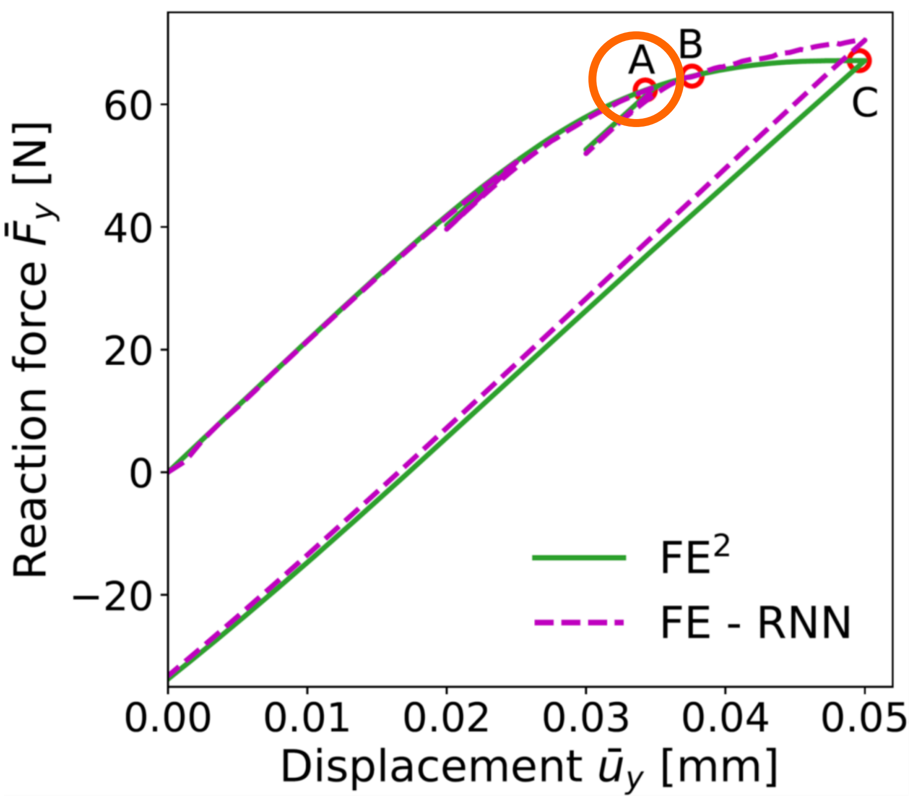

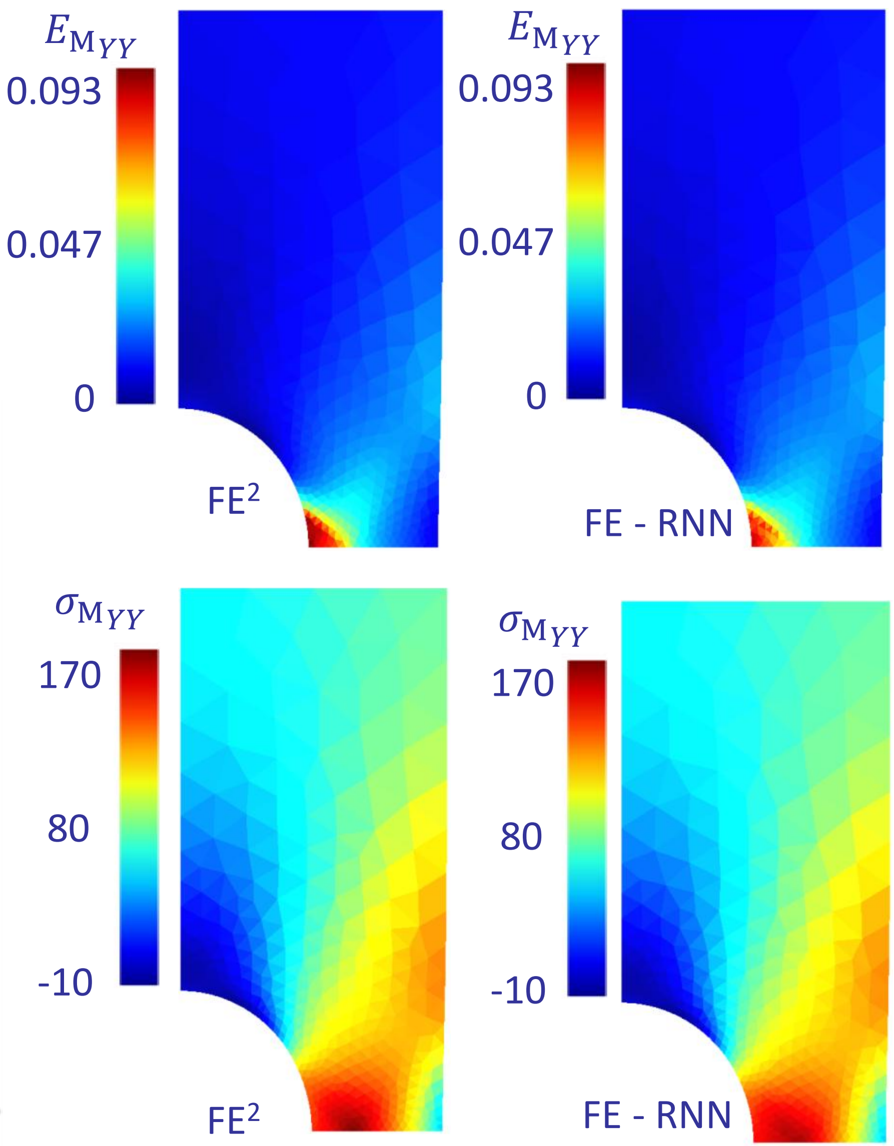

Recurrent Neural Network-accelerated multi-scale simulations

- Multiscale simulation
  - Stress-strain distribution at point B
  - Strain just at 10% training range

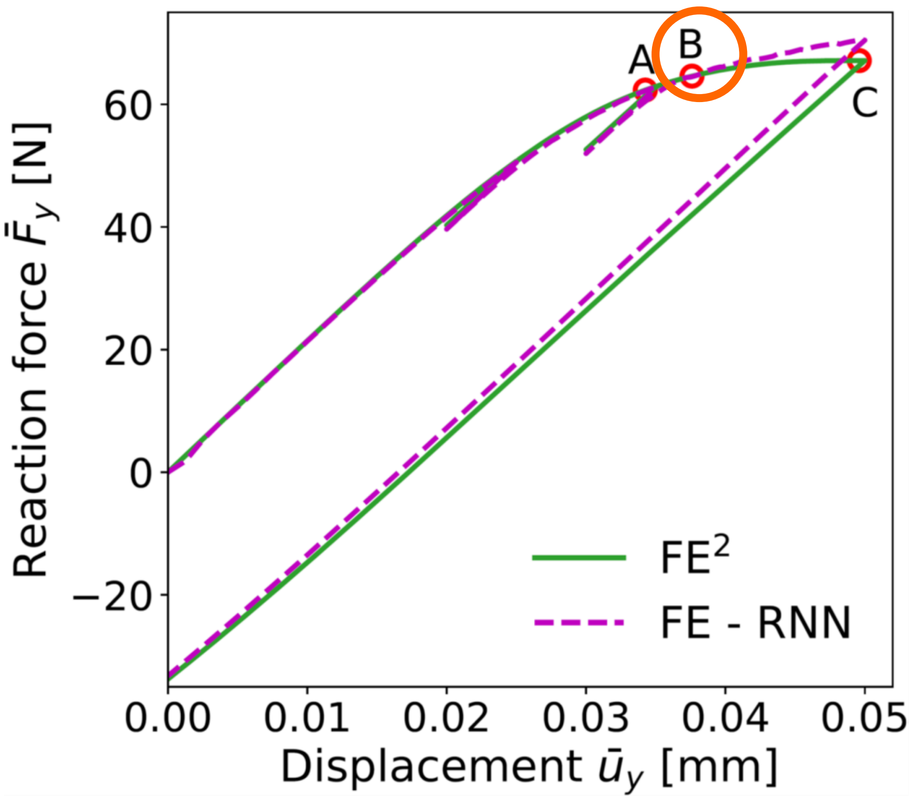

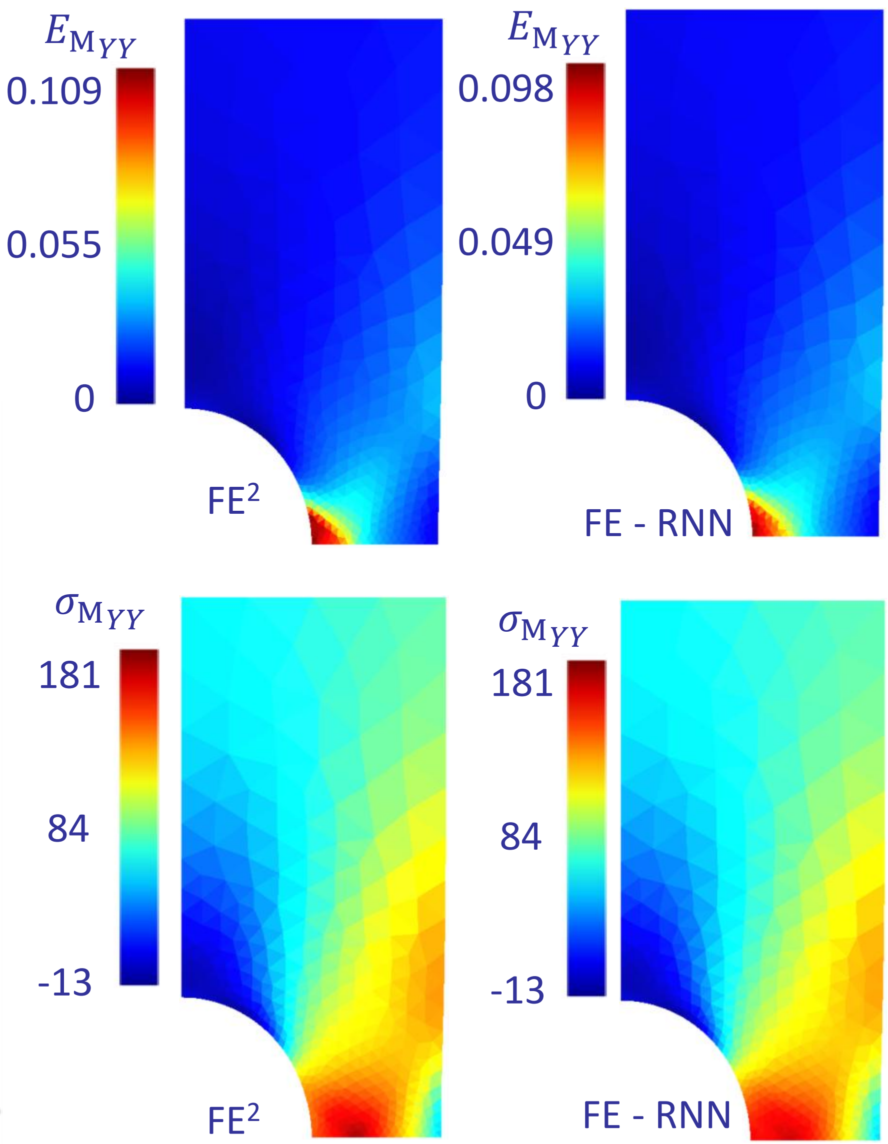

Recurrent Neural Network-accelerated multi-scale simulations

- Multiscale simulation
  - Stress-strain distribution at point C
  - Strain out of 10% training range

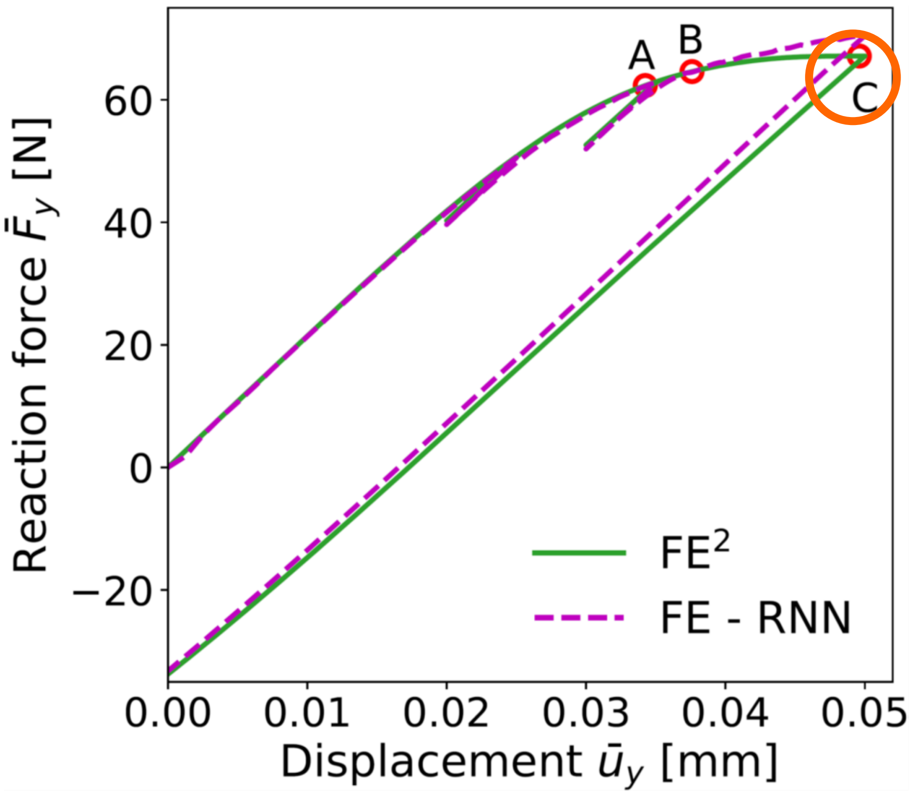

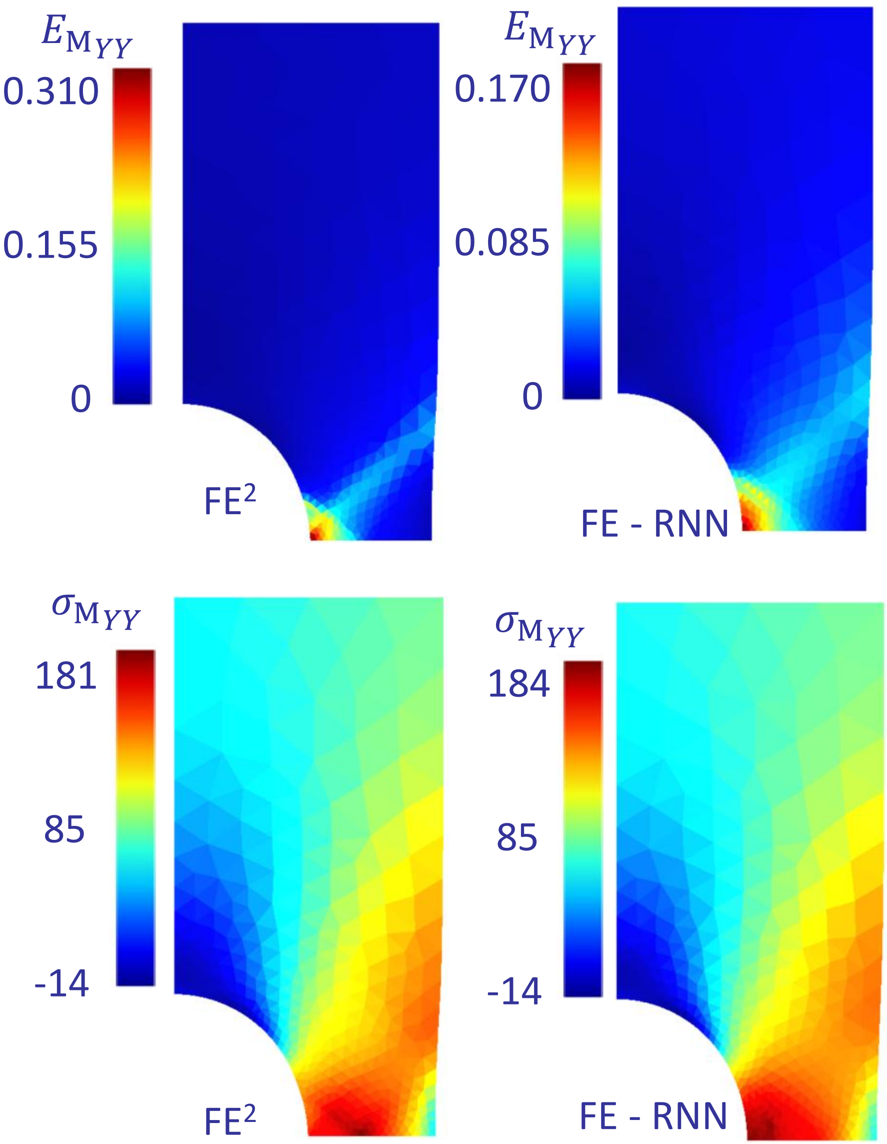

Recurrent Neural Network-accelerated multi-scale simulations

- MOAMMM FET-OPEN project (https://www.moammm.eu/)
  - ULiège, UCL (Belgium)
  - IMDEA Materials (Spain)
  - JKU (Austria)
  - cirp GmbH (Germany)

- Publications (doi)
  - 10.1016/j.cma.2020.113234
    - Open Data: 10.5281/zenodo.3902663
  - 10.1016/j.cma.2021.114476
    - Open Data: 10.5281/zenodo.5668390

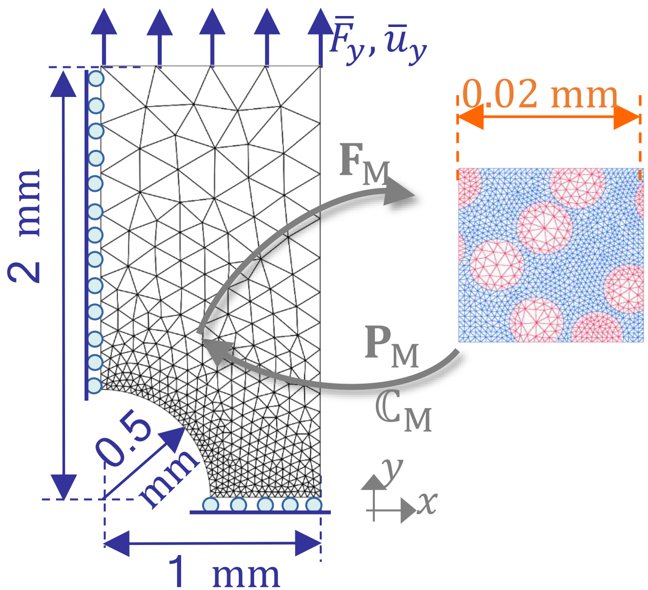

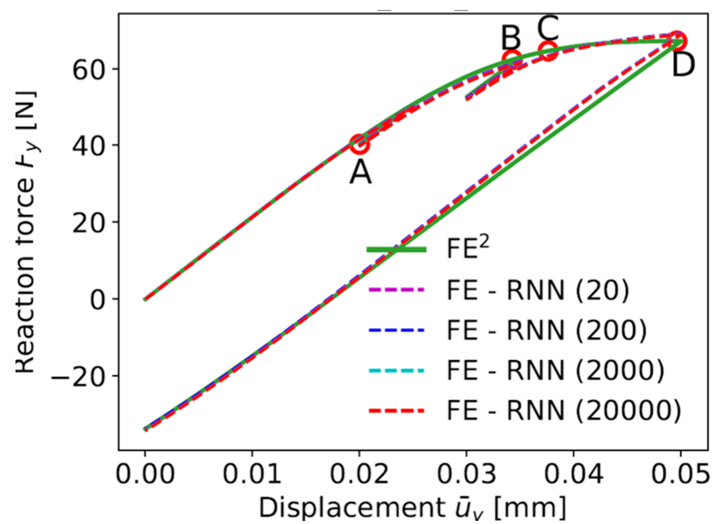

Self-Consistent Recurrent Neural Network for multi-scale simulations with irreversible behaviours

This project has received funding from the European Union’s Horizon Europe Framework Programme under grant agreement No. 101056682 for the project ‘‘DIgital DEsign strategies to certify and mAnufacture Robust cOmposite sTructures (DIDEAROT)’’. The contents of this publication are the sole responsibility of ULiege and do not necessarily reflect the opinion of the European Union. Neither the European Union nor the granting authority can be held responsible for them

Self-Consistent Recurrent Neural Network for multi-scale simulations

- Introduction to non-linear multi-scale simulations
  - FE multi-scale simulations
    - Problems to be solved at two scales
    - Requires Newton-Raphson iterations at both scales
  - Use of surrogate models
    - Train a meso-scale surrogate model (off-line)
      - Requires extensive data
      - Obtained from RVE simulations
    - Use the trained surrogate model during analyses (on-line)
      - Surrogate acts as a homogenised constitutive law
      - Expected speed-up of several orders

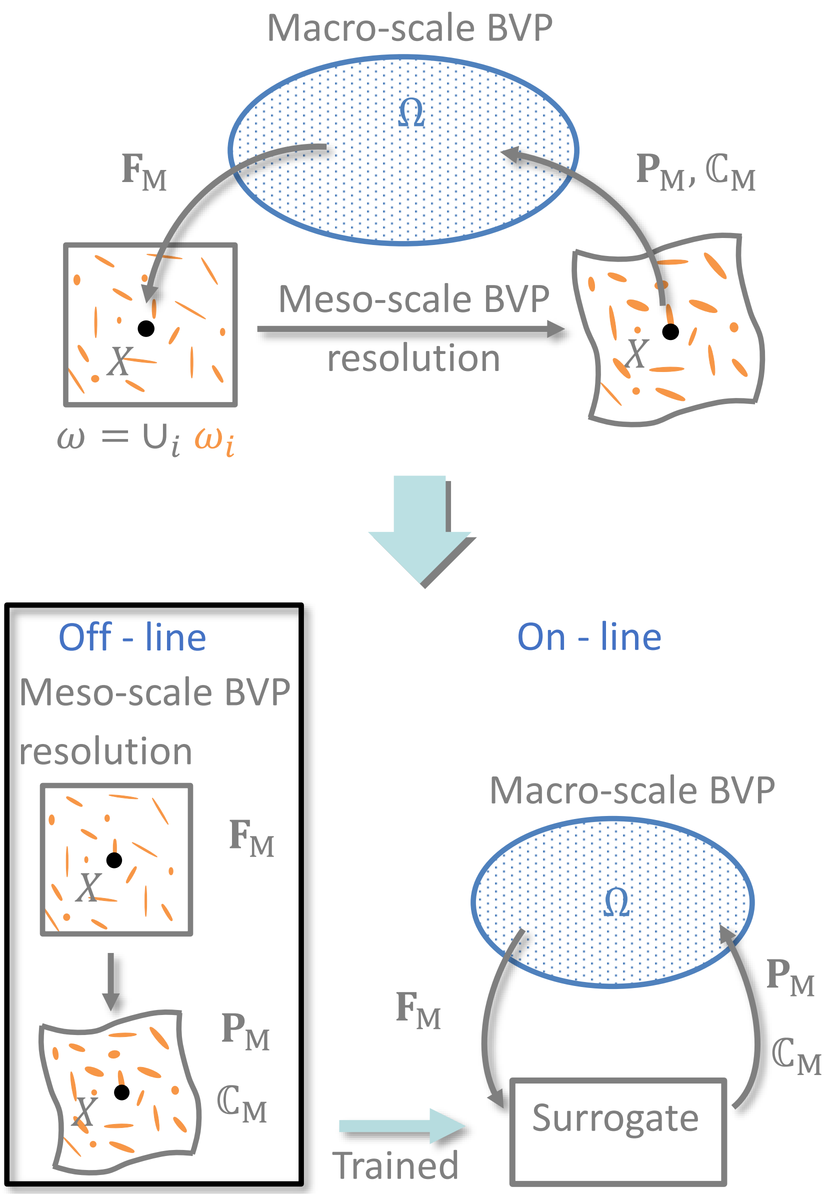

Self-Consistent Recurrent Neural Network for multi-scale simulations

- Input / output definition
  - Input: Strain (history): $\mathbf{F}_{\mathrm{M}}$
  - Output: Stress (history): $\mathbf{P}_{\mathrm{M}}$

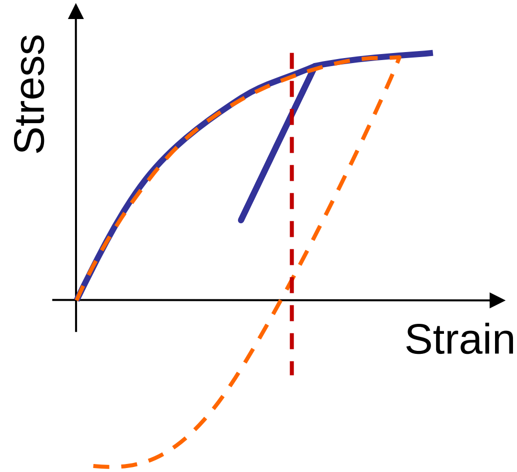

- Elasto-plastic material behaviour
  - No bijective strain-stress relation
    - Feed-forward NNW cannot be used
    - History should be accounted for

- Recurrent neural network
  - Allows a history dependent relation
    - Input: sequence $\boldsymbol{u}_t$
    - Output: sequence $\boldsymbol{v}_t = \boldsymbol{g}(\boldsymbol{u}_t, \boldsymbol{h}_{t-1})$
    - Internal variable $\boldsymbol{h}_t = \boldsymbol{g}(\boldsymbol{u}_t, \boldsymbol{h}_{t-1})$

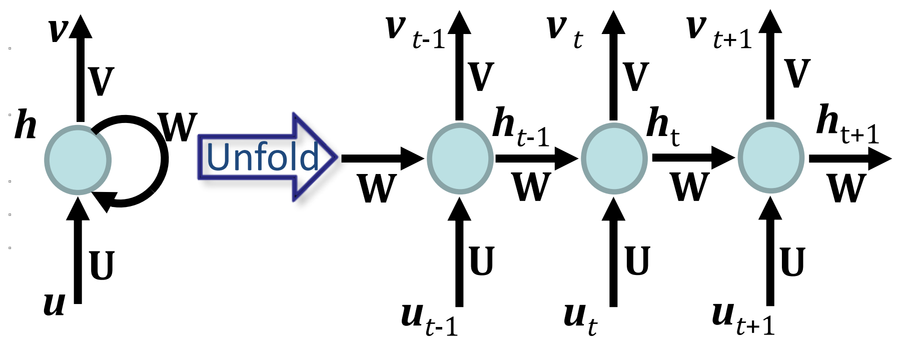

  - Existing recurrent units
    - Oscillations / loss of accuracy can appear with GRU, LSTM* (both developed for Nature Language Processing)
    - One needs to enforce self-consistency*
    - Need to replace the GRU/LSTM unit

*Colin Bonatti, Dirk Mohr, On the importance of self-consistency in recurrent neural network models representing elasto-plastic solids, Journal of the Mechanics and Physics of Solids, 158, 2022, 104697, https://doi.org/10.1016/j.jmps.2021.104697.

Self-Consistent Recurrent Neural Network for multi-scale simulations

- Self-Consistency reinforcement through ad hoc recurrent unit/cell
  - SC-cell originally to surrogate a constitutive model
  - Can we develop easy and fast to train surrogate for RVE responses?

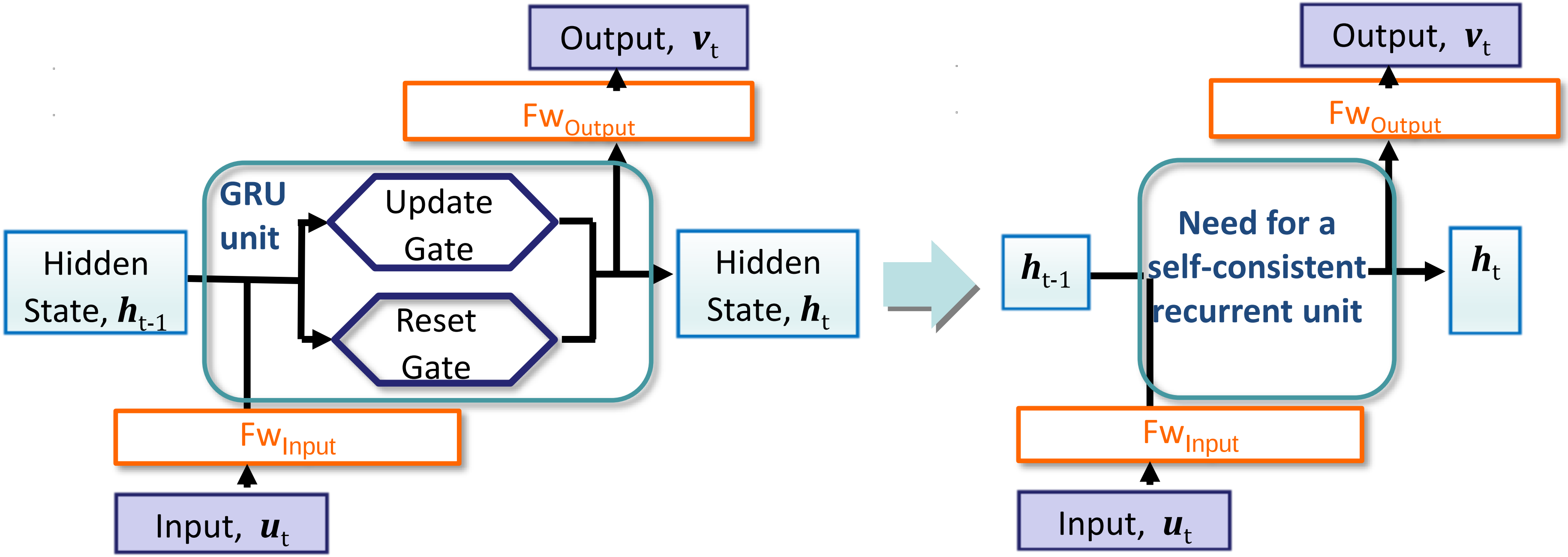

Self-Consistent Recurrent Neural Network for multi-scale simulations

- New cell 1: New simplified recurrent unit: Simplified Minimal Recurrent Unit

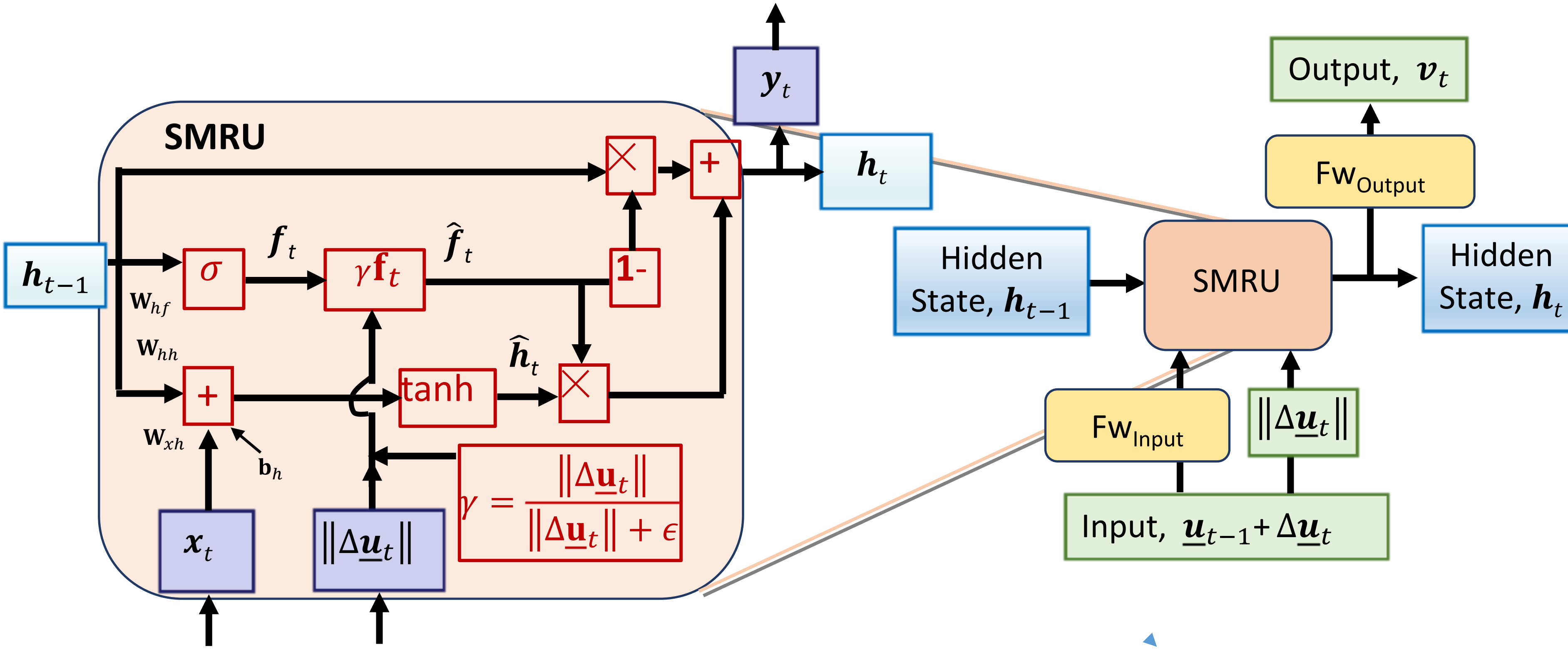

  - The **total form of input variable** as well as **increment norm** $\|\Delta\boldsymbol{u}_t\|$ (like SC-LMSC)
  - **Self-consistency weakly enforced**
    - Using norm of $\|\Delta\boldsymbol{u}_t\|$ and
    - Data augmentation during training (i.e. subdividing randomly increments in training data)

Self-Consistent Recurrent Neural Network for multi-scale simulations

- New cell 2: Self-Consistent Minimal Recurrent Unit with Total form of inputs

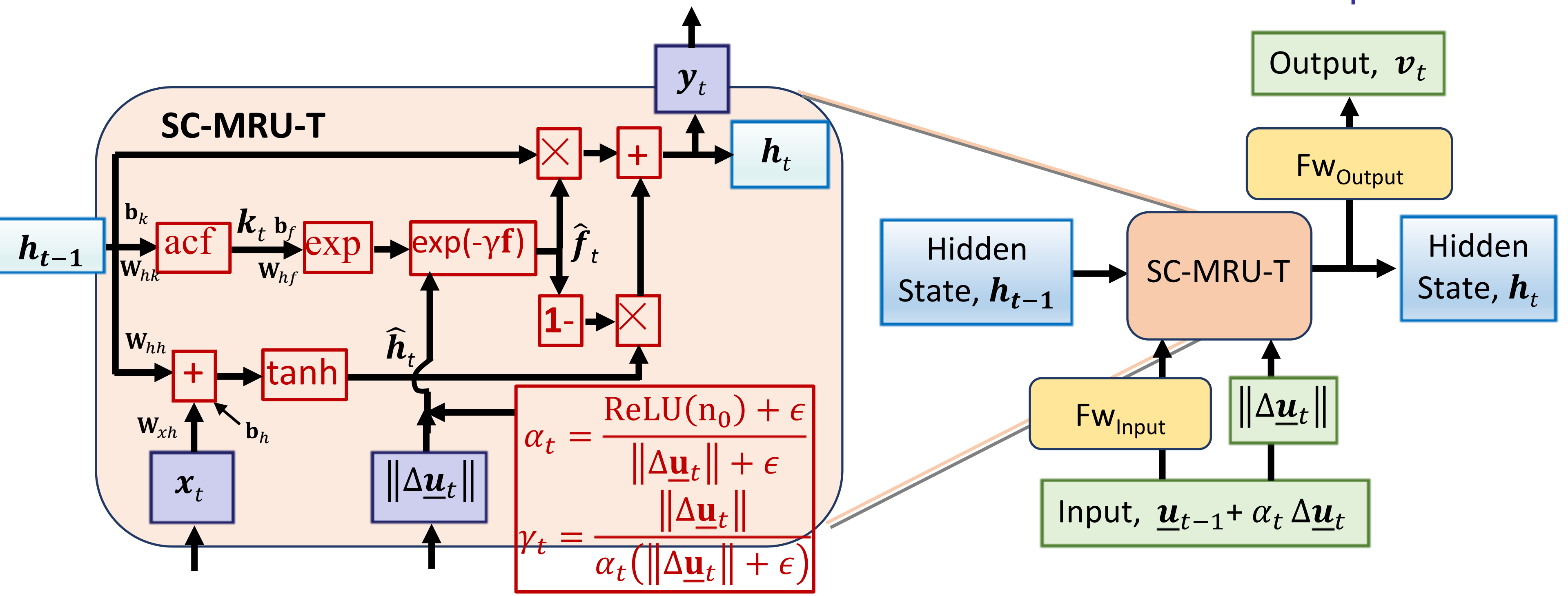

- The **total form of input variable** as well as **increment norm** $\|\Delta \underline{u}_t\|$ (like SC-LMSC)
  - Use as input $\underline{u}_{t-1} + \alpha_t \Delta \underline{u}_t$ (n_0 is a learnable parameter)
  - acf is the same activation function as in $\mathrm{Fw}_{\mathrm{input}}$
- **Self-consistency enforced**
  - Double exponential function $\boldsymbol{f_t} = \mathbf{exp}[\boldsymbol{W_f k_t} + \boldsymbol{b_f}] > \mathbf{0}$ & ratio $\hat{\boldsymbol{f}}_{\boldsymbol{t}} = \mathbf{exp}[-\gamma(\|\Delta \boldsymbol{u}_t\|)\, \boldsymbol{f_t}] \in [\mathbf{0}, \mathbf{1}]$
  - Hidden variables $\boldsymbol{h_t}$ is an element-wise interpolation (ratio $\hat{\boldsymbol{f}}_{\boldsymbol{t}}$ dependent on the norm of $\|\Delta \boldsymbol{u}_t\|$) between previous value $\boldsymbol{h_{t-1}}$ and $\hat{\boldsymbol{h}}_{\boldsymbol{t}}$

Self-Consistent Recurrent Neural Network for multi-scale simulations

- New cell 3: Self-Consistent Minimal Recurrent Unit with Incremental form of inputs

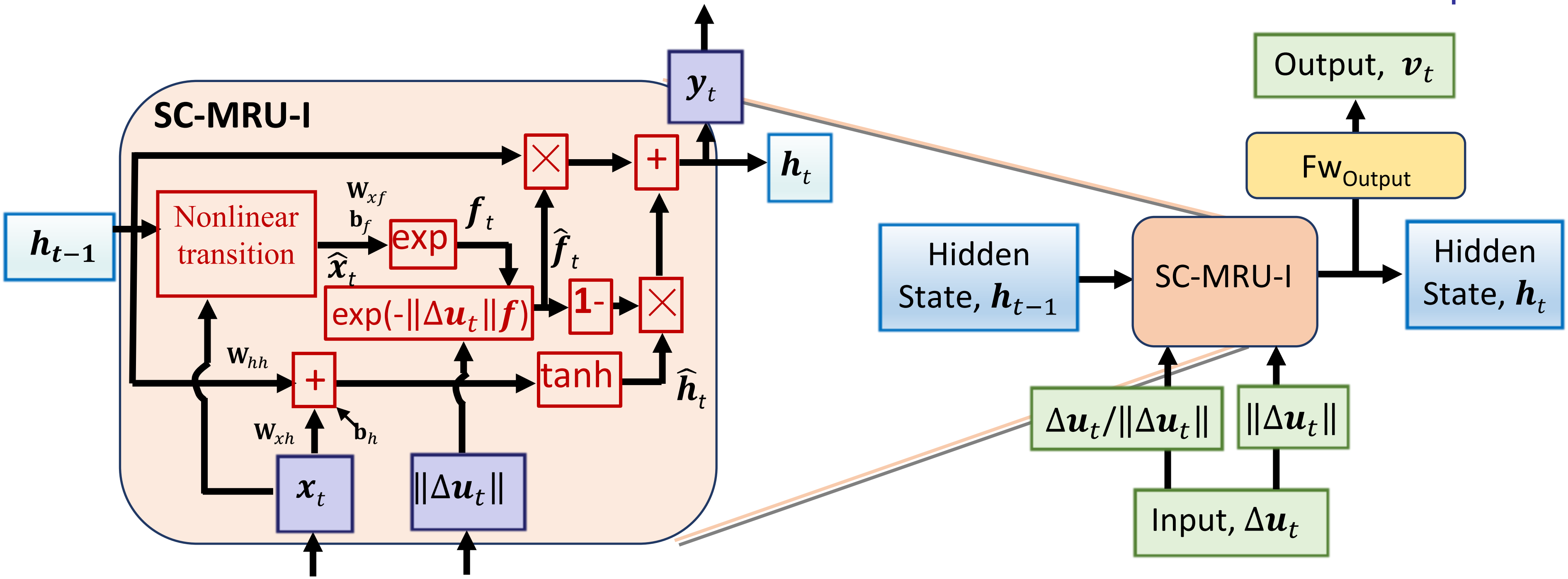

– The **incremental form of input variable** as well as **increment norm** $\|\Delta\boldsymbol{u}_t\|$ (like LMSC)
  - Use as input $\Delta\boldsymbol{u}_t/\|\Delta\boldsymbol{u}_t\|$ and $\|\Delta\boldsymbol{u}_t\|$

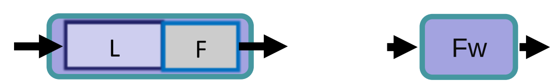

  - Non-linear transition blocks:

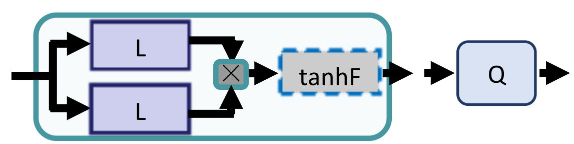

– **Self-consistency enforced**
  - Double exponential function $\boldsymbol{f}_t = \exp\left[\boldsymbol{W}_{xf}\hat{\boldsymbol{x}}_t + \boldsymbol{b}_f\right] > \boldsymbol{0}$ & ratio $\hat{\boldsymbol{f}}_t = \exp[-(\|\Delta\boldsymbol{u}_t\|)\,\boldsymbol{f}_t] \in [\boldsymbol{0}, \boldsymbol{1}]$
  - Hidden variables $\boldsymbol{h}_t$ is an element-wise interpolation (ratio $\hat{\boldsymbol{f}}_t$) between previous value $\boldsymbol{h}_{t-1}$ and $\hat{\boldsymbol{h}}_t$

Self-Consistent Recurrent Neural Network for multi-scale simulations

- Training strategy
  - Elasto-plastic composite RVE

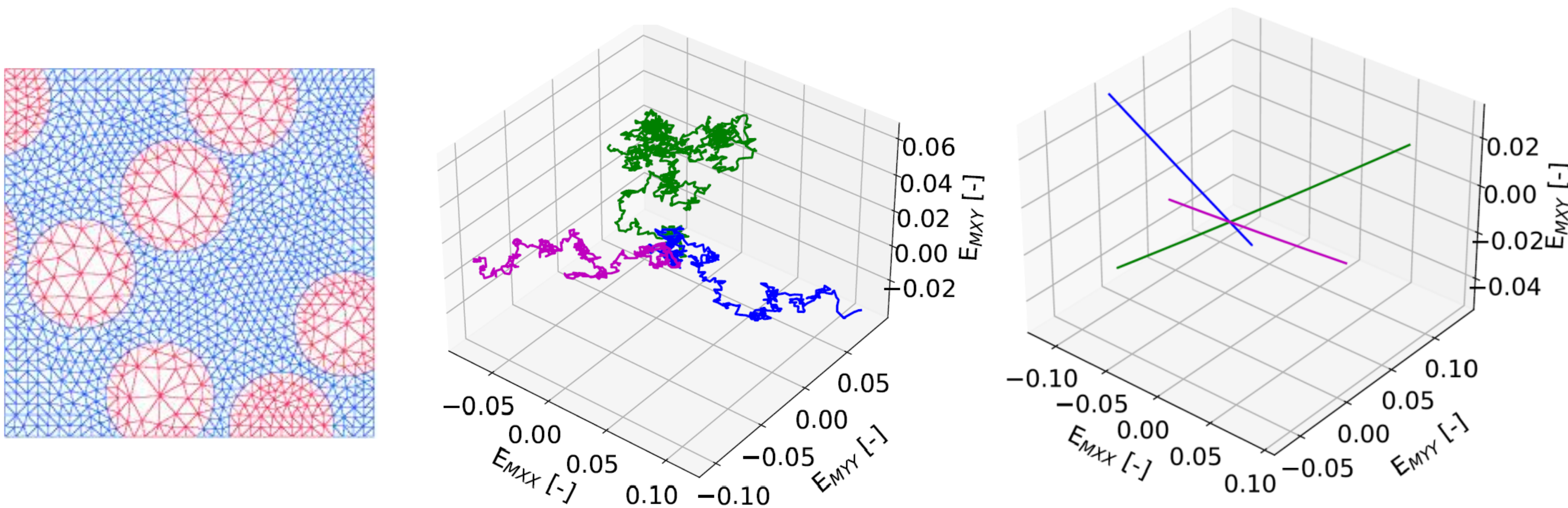

  - Training data
    - Should cover full range of possible loading histories
    - Use random walking strategy
    - Completed with random cyclic loading
    - Bounded by a hypercube of 12% deformation

Self-Consistent Recurrent Neural Network for multi-scale simulations

- Training stage
  - Learnable parameters for 120 hidden variables

Recurrent unit	SMRU	SC-MRU-T	SC-MRU-I		
Transition block	-	-	Q	Fw-Fw	Q-Fw
Learnable parameters	44 284	58 925	59 644	59 284	74 164

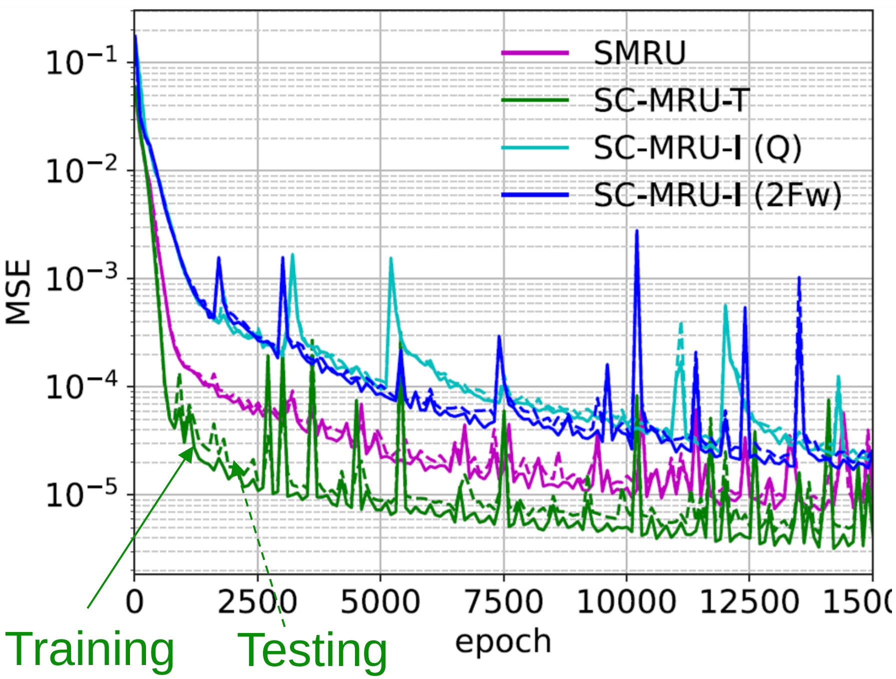

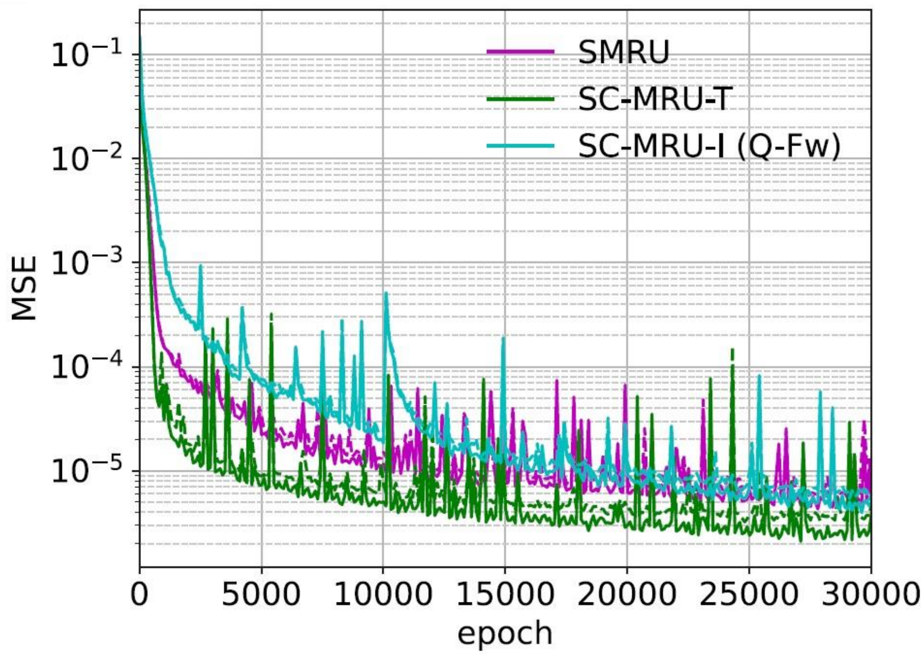

Self-Consistent Recurrent Neural Network for multi-scale simulations

- SC-MRU-T: Testing data with inserted extra-points

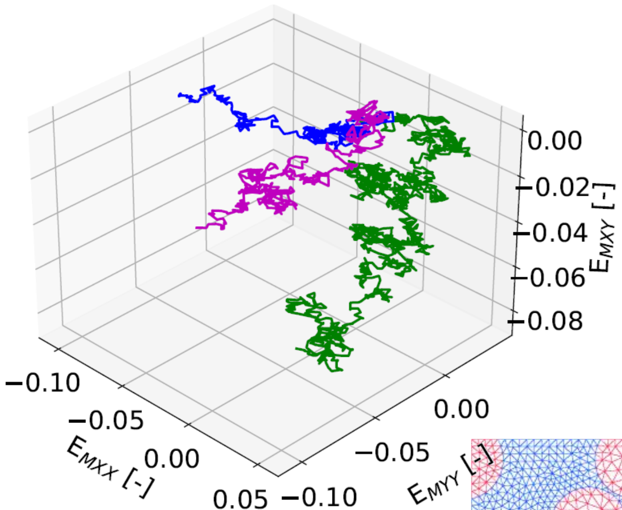

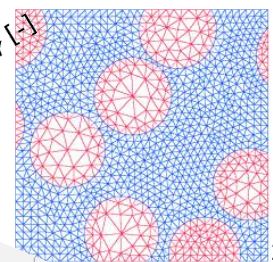

Maximum inserted data points is **5**, **20**, **60** in each loading step

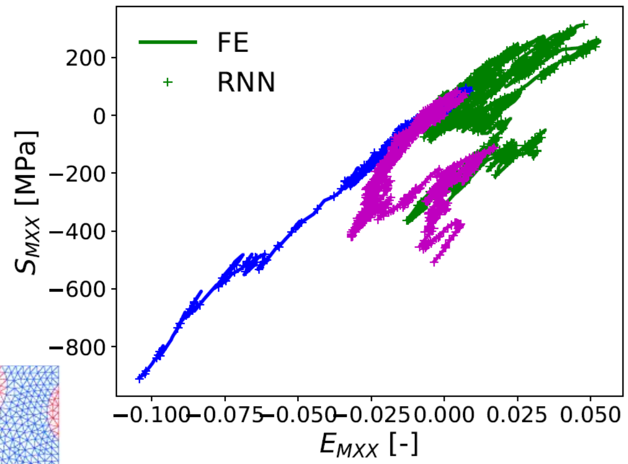

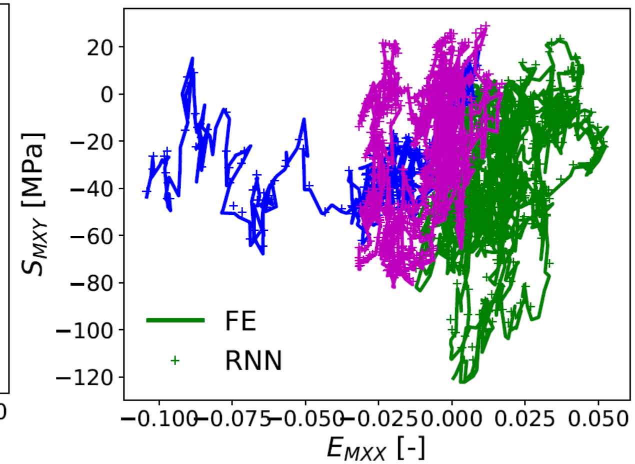

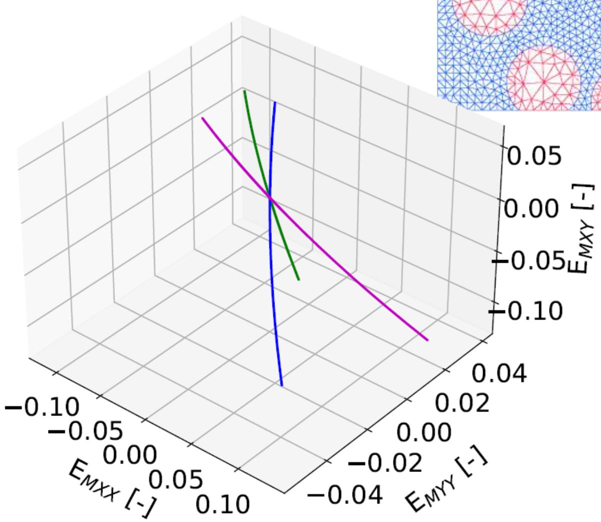

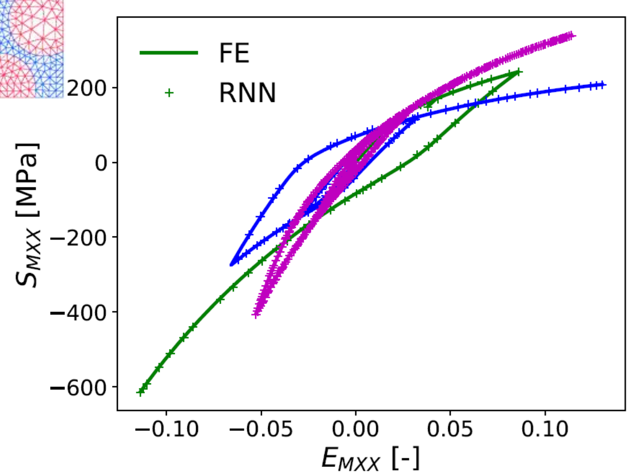

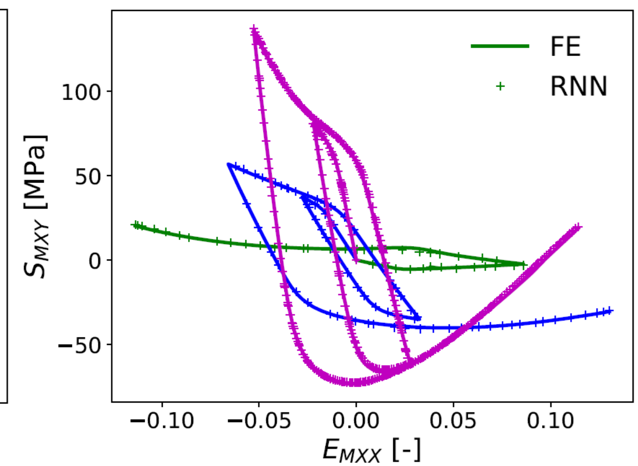

Self-Consistent Recurrent Neural Network for multi-scale simulations

- FE2 vs. FE-RNN: Change in the increment size (between points A&B)

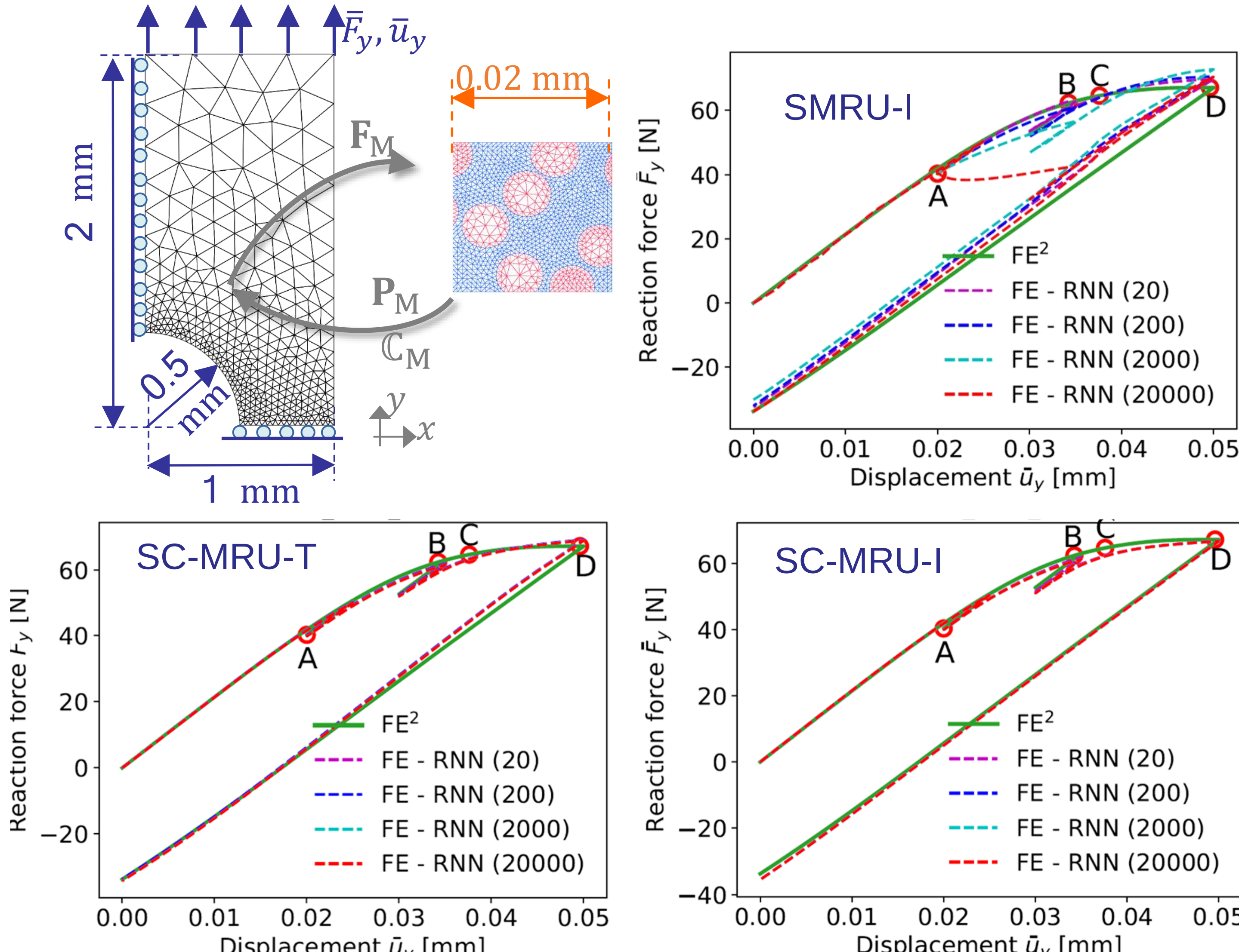

Self-Consistent Recurrent Neural Network for multi-scale simulations

- FE2 vs. FE-RNN: Cost comparison

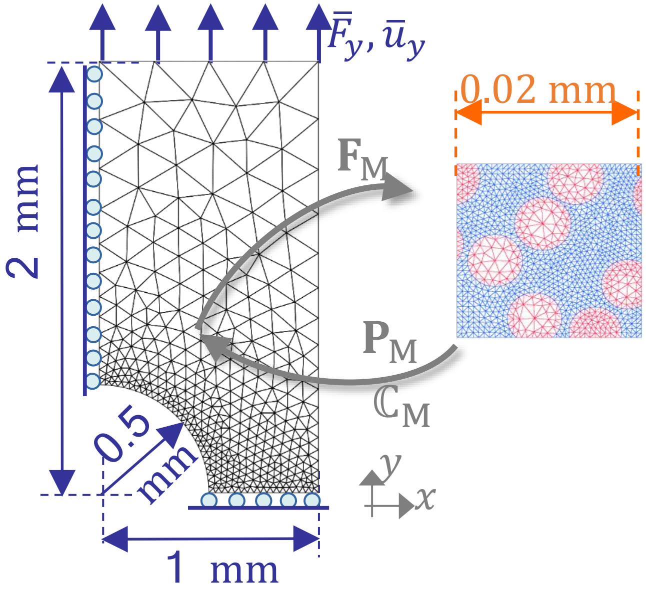

Off-line	FE^2	SMRU	SC-MRU-T	SC-MRU-I
Data generation	-	23500 h-cpu		
Training	-	< 10 h-cpu		
On-line	**FE^2**	**SMRU**	**SC-MRU-T**	**SC-MRU-I**
Simulation	18000 h-cpu	0.27 h-cpu	0.38 h-cpu	0.28 h-cpu

Self-Consistent Recurrent Neural Network for multi-scale simulations

- FE2 vs. FE-RNN: Fields distribution

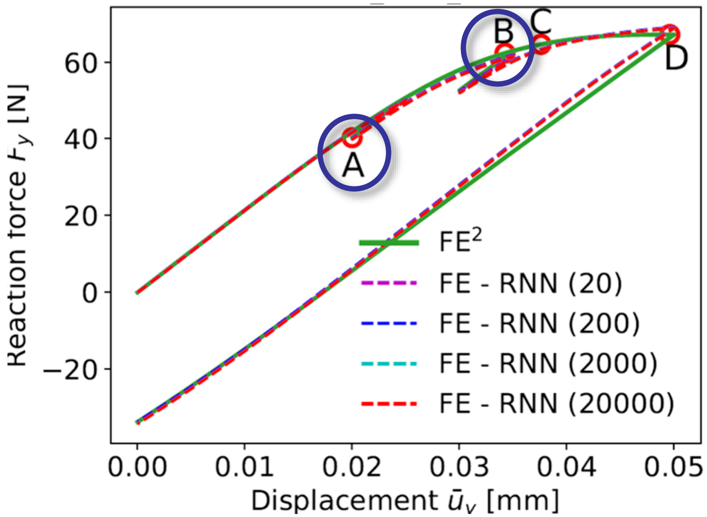

Point A

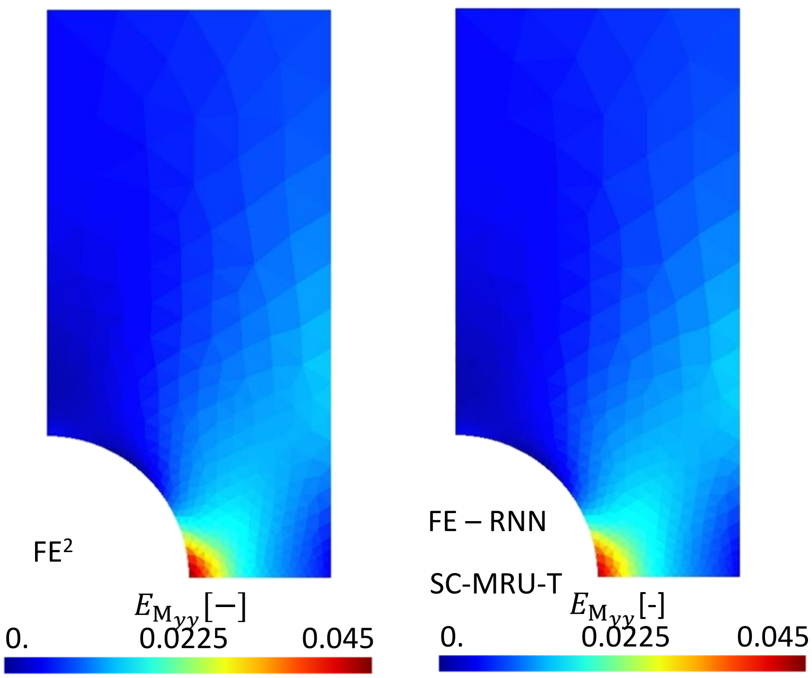

Point B

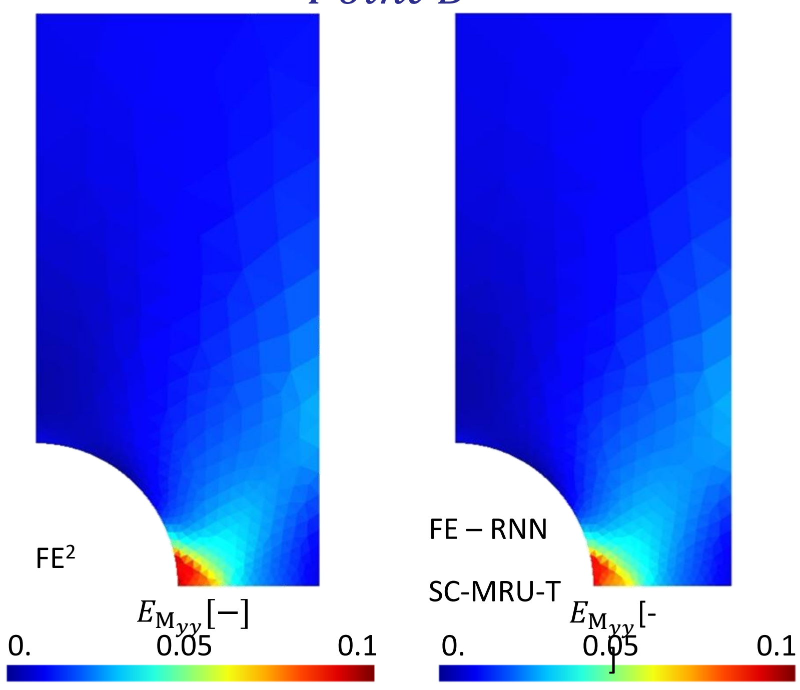

- FE2 vs. FE-RNN: Fields distribution

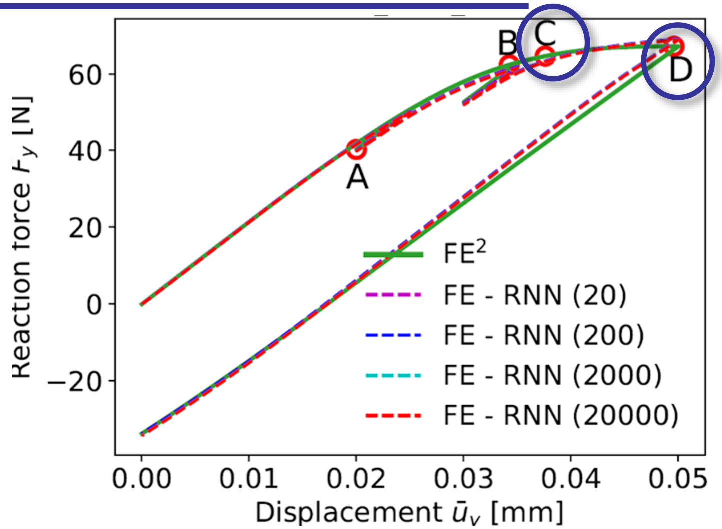

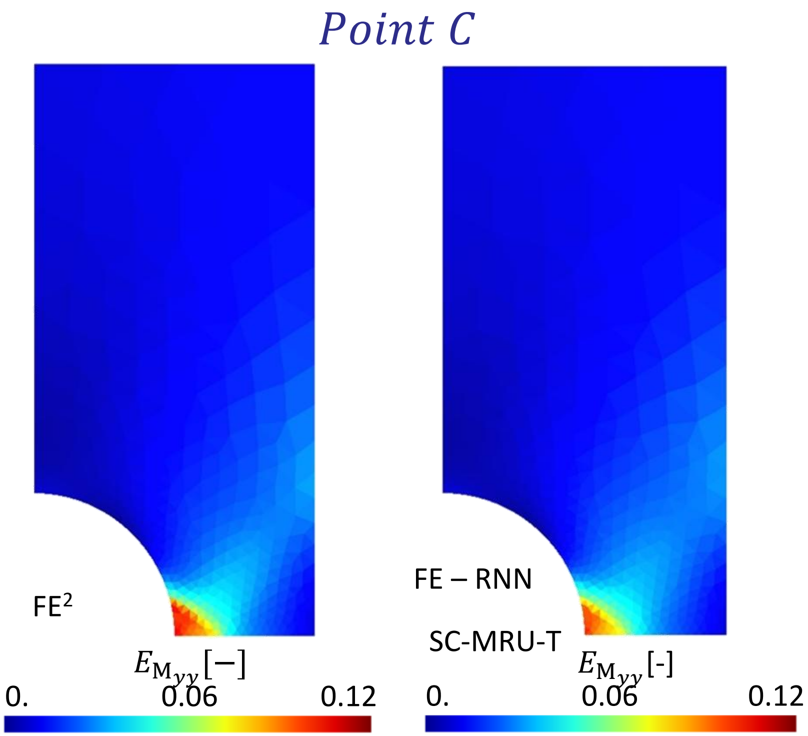

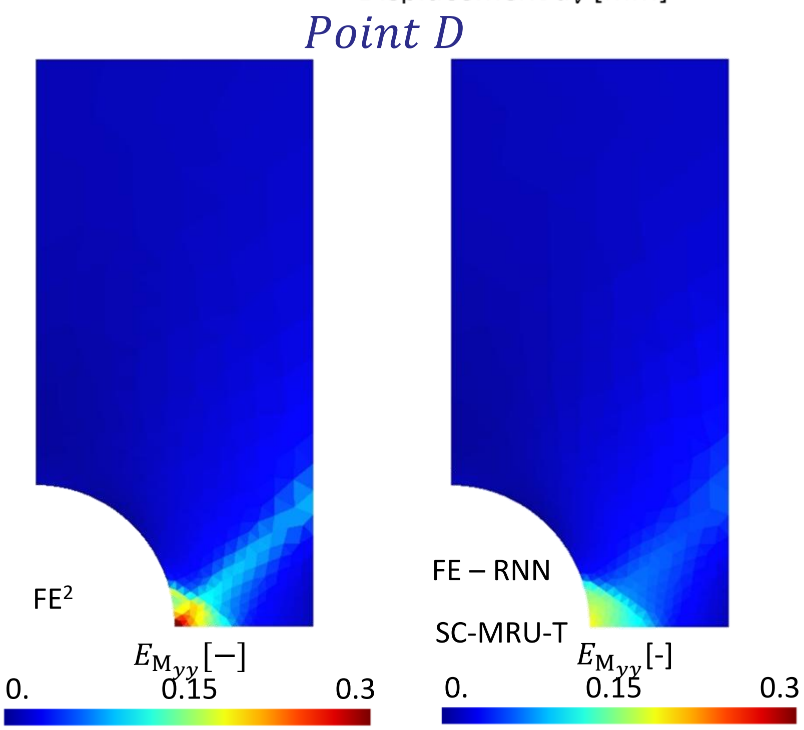

Self-Consistent Recurrent Neural Network for multi-scale simulations

- Self-Consistent model of VE-VP lattice cell response of arbitrary diameter value
  - Objective: Predict response of lattice cell
    - Complex visco-elastic-visco-plastic material response
    - Different strain-rate
    - Arbitrary geometrical parameters $\boldsymbol{\vartheta}_{\text{geo}}$ (e.g. struts diametre)
  - Data
    - Inputs (depend on the surrogate)
      - $\mathbf{E}_{\mathbf{M}_t}$: strain sequence
      - Geometrical parameters $\boldsymbol{\vartheta}_{\text{geo}}$
    - Outputs
    - $\mathbf{S}_{\mathbf{M}_t}$: stress sequence

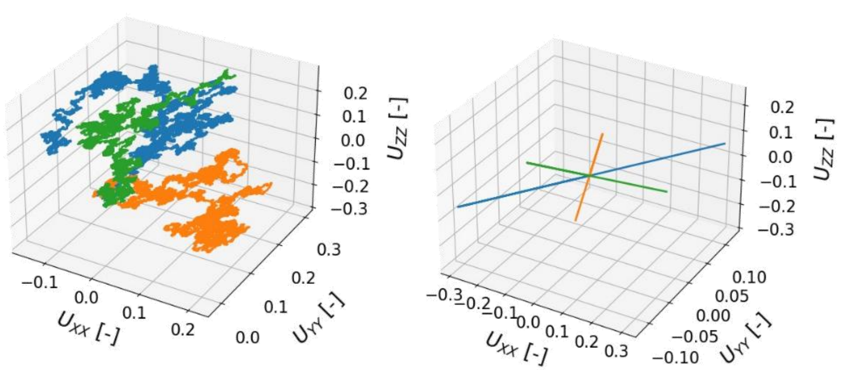

Loading histories at varying strain rate, RW & CC

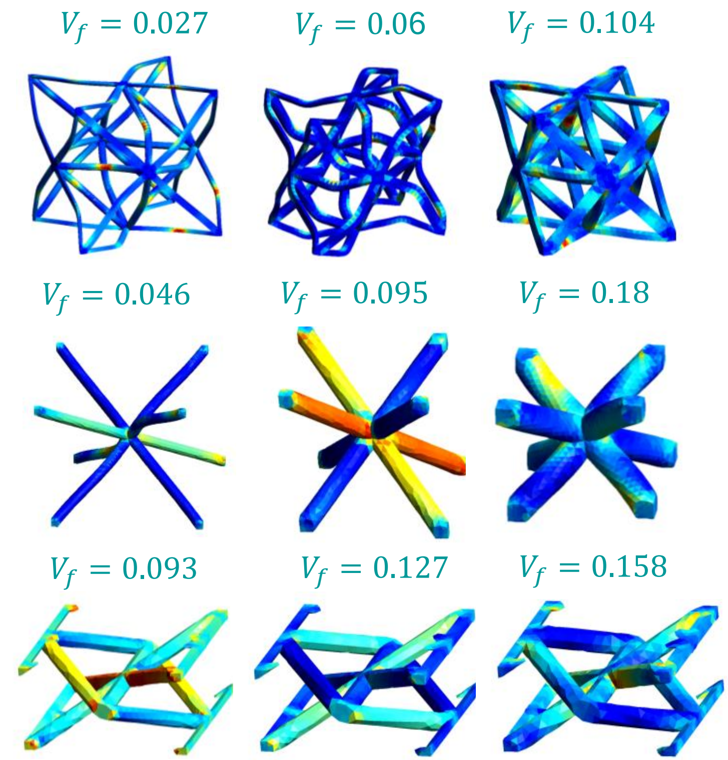

Self-Consistent Recurrent Neural Network for multi-scale simulations

- Self-Consistent model of VE-VP lattice cell response of arbitrary diameter value
  - Key-idea: Use 2 SC units
    - One with time increment alone
    - One with the time increment $\Delta\tau$, one with displacement increment Δu
    - Concatenate first with geometrical parameters $\boldsymbol{\vartheta}_{\text{geo}}$ concatenated

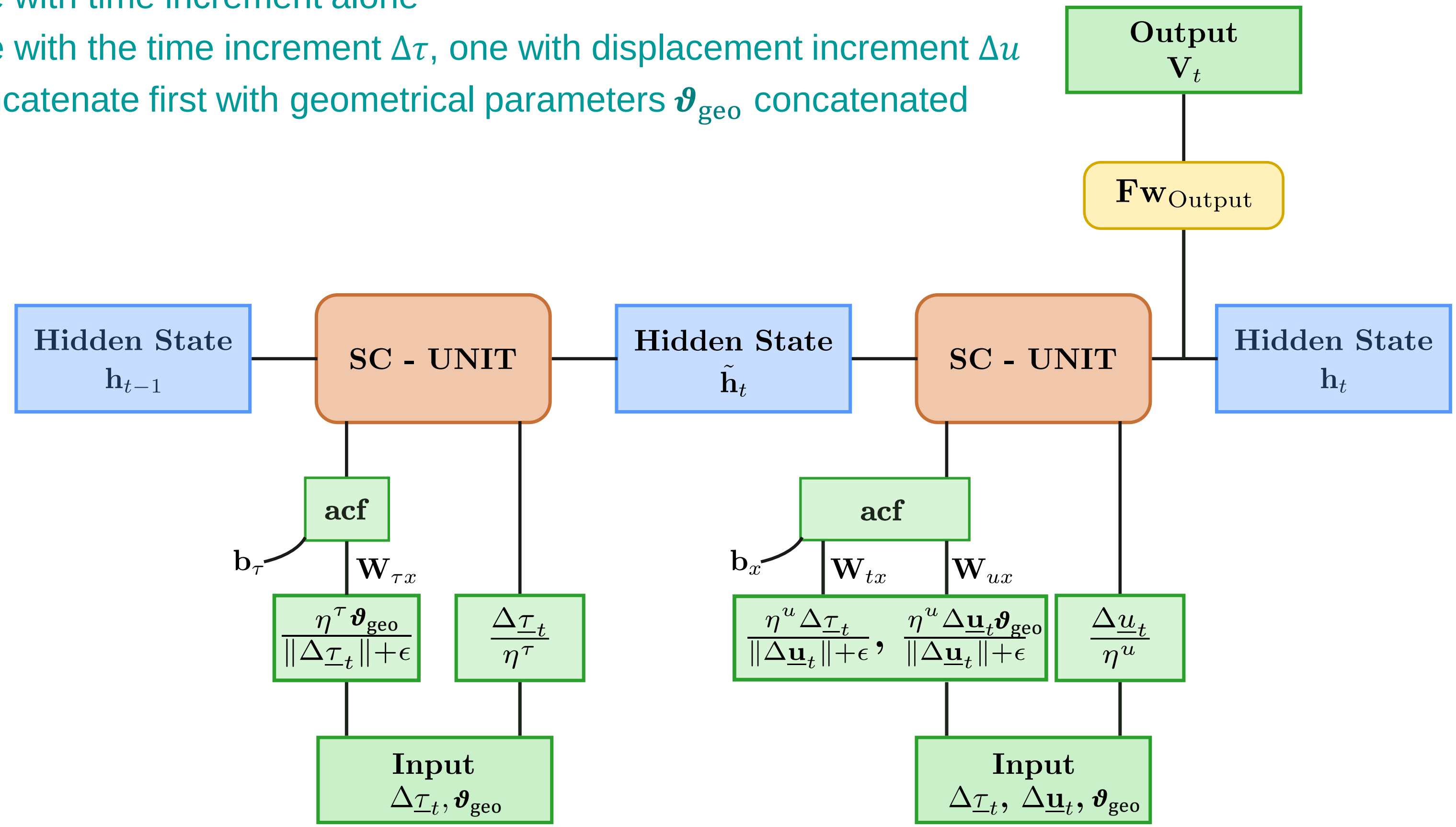

This project has received funding from the European Union's Horizon 2020 research and innovation programme under grant agreement No 862015

MOAMMM

Self-Consistent Recurrent Neural Network for multi-scale simulations

- Testing
  - Inputs (depend on the surrogate)
    - $\mathbf{E}_{\mathbf{M}_t}$: new unseen strain sequence
    - New unseen geometrical parameter realisation $\boldsymbol{\vartheta}_{\mathrm{geo}}$
  - Outputs
    - $\mathbf{S}_{\mathbf{M}_t}$: stress sequence

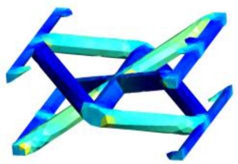

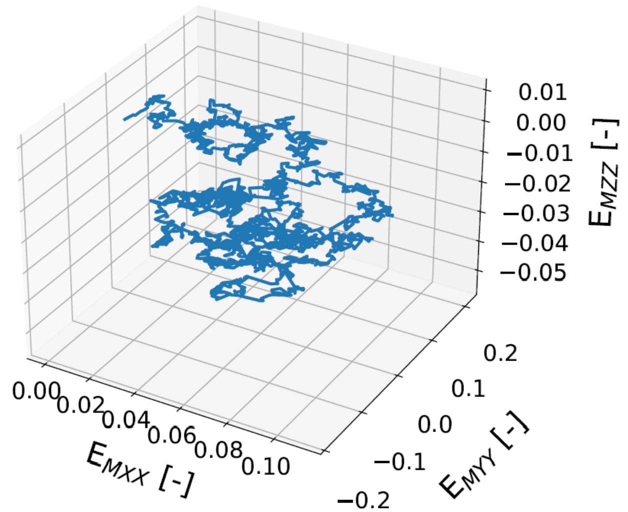

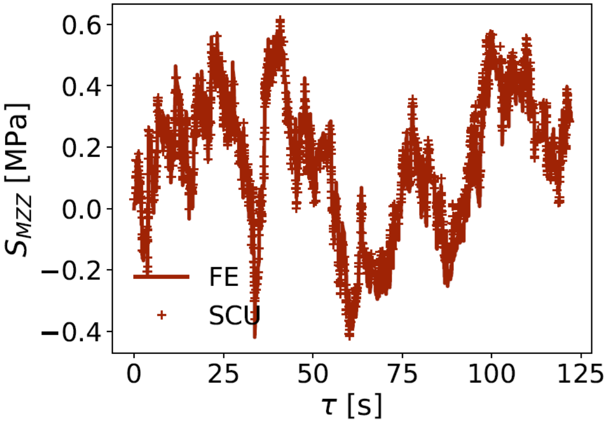

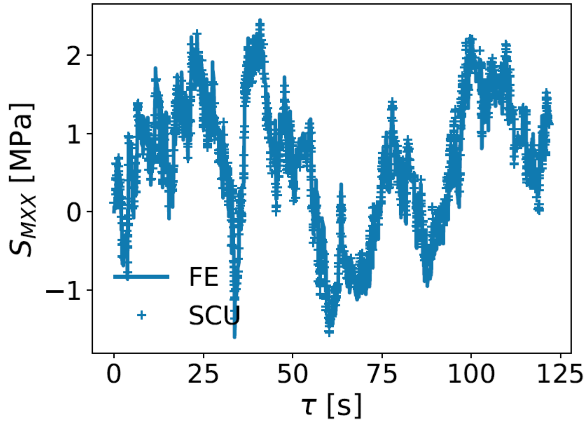

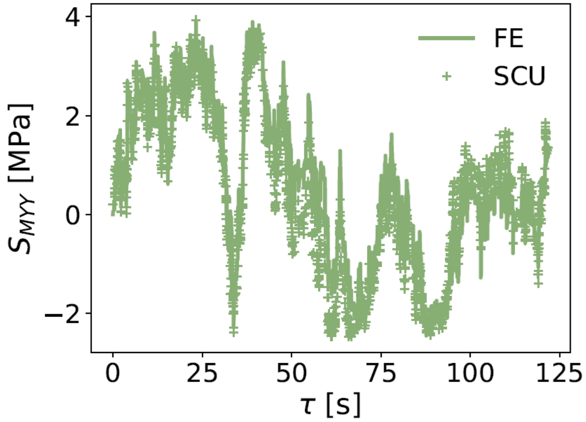

- Validation of meso-scale surrogate model for lattice meta-materials
  - Tension/compression on USF lattice

micro-structure parameter $\boldsymbol{\vartheta}_{\mathrm{geo}}$ not seen in the training stage

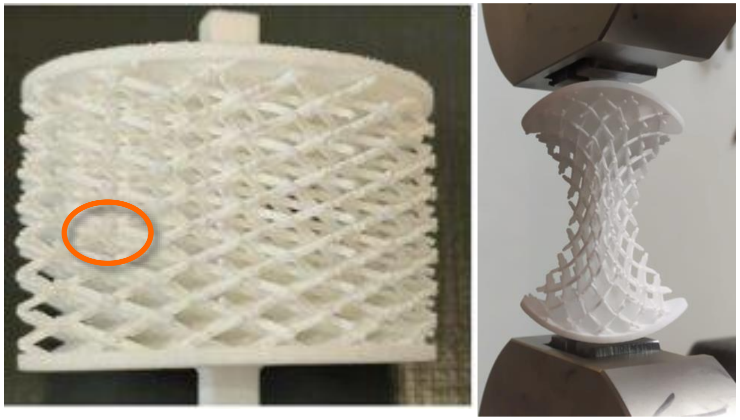

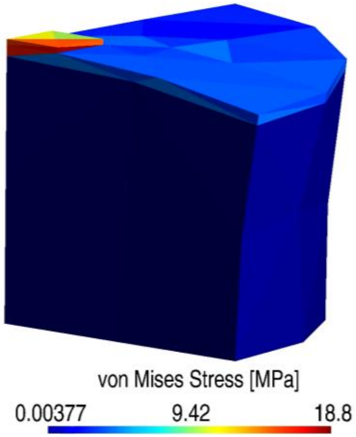

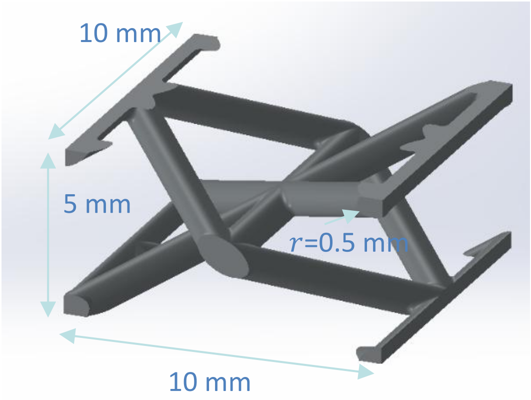

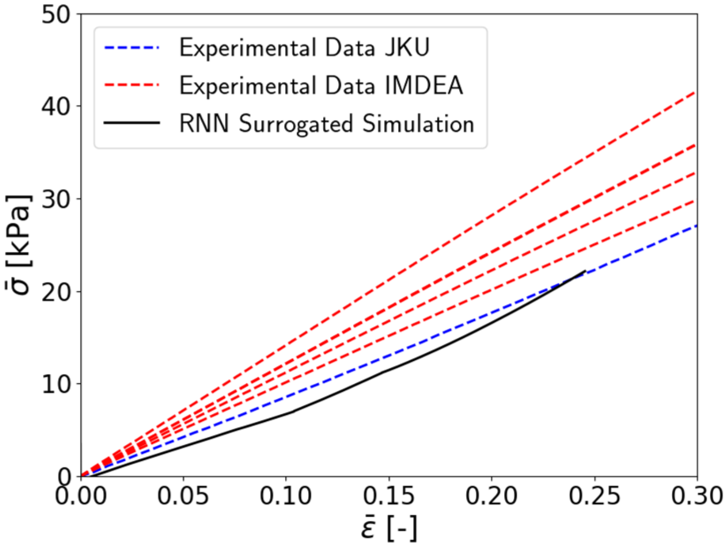

References

- DIDEAROT project (https://www.didearot-project.eu/)
  - CENAERO, HEXAGON, SONACA, ULiège (Belgium)
  - Tecnalia, Aernnova, Barcelona Supercomputing Center (Spain)
  - Inegi (Portugal)

- Publication
  - L. Wu, L. Noels, Self-consistency Reinforced minimal Gated Recurrent Unit for surrogate modelling of history-dependent non-linear problems: Application to history-dependent homogenized response of heterogeneous materials, *Computer Methods in Applied Mechanics and Engineering* 424 (2024) 116881, doi: https://doi.org/10.1016/j.cma.2024.116881

- Data and code on
  - Repository: https://gitlab.uliege.be/didearot/didearotPublic/publicationsData/2024_scmru
  - Doi: http://dx.doi.org/10.5281/zenodo.10551272

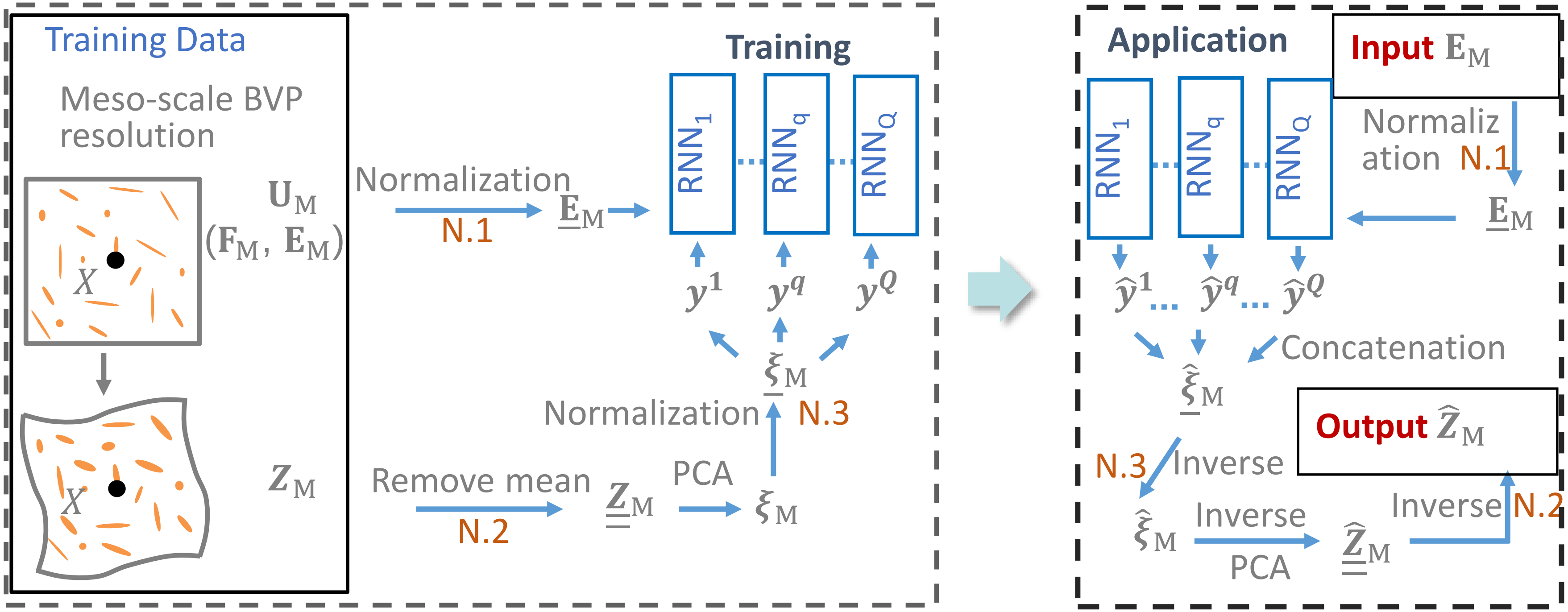

Recurrent Neural Network with dimensionality reduction and break down

MOAMMM project has received funding from the European Union's Horizon 2020 research and innovation programme under grant agreement No 862015 for the project Multi-scale Optimisation for Additive Manufacturing of fatigue resistant shock-absorbing MetaMaterials (MOAMMM) of the H2020-EU.1.2.1. - FET Open Programme

MOAMMM

LIÈGE université

RNN with dimensionality reduction and break down

- Recurrent neural network-accelerated multi-scale simulations
  - FE multi-scale simulations
    - Problems to be solved at two scales
    - Requires Newton-Raphson iterations at both scales
  - Use of surrogate models
    - Train a meso-scale surrogate model (off-line)
      - Requires extensive data
      - Obtained from RVE simulations
    - Use the trained surrogate model during analyses (on-line)
      - Surrogate acts as a homogenised constitutive law
      - Expected speed-up of several orders

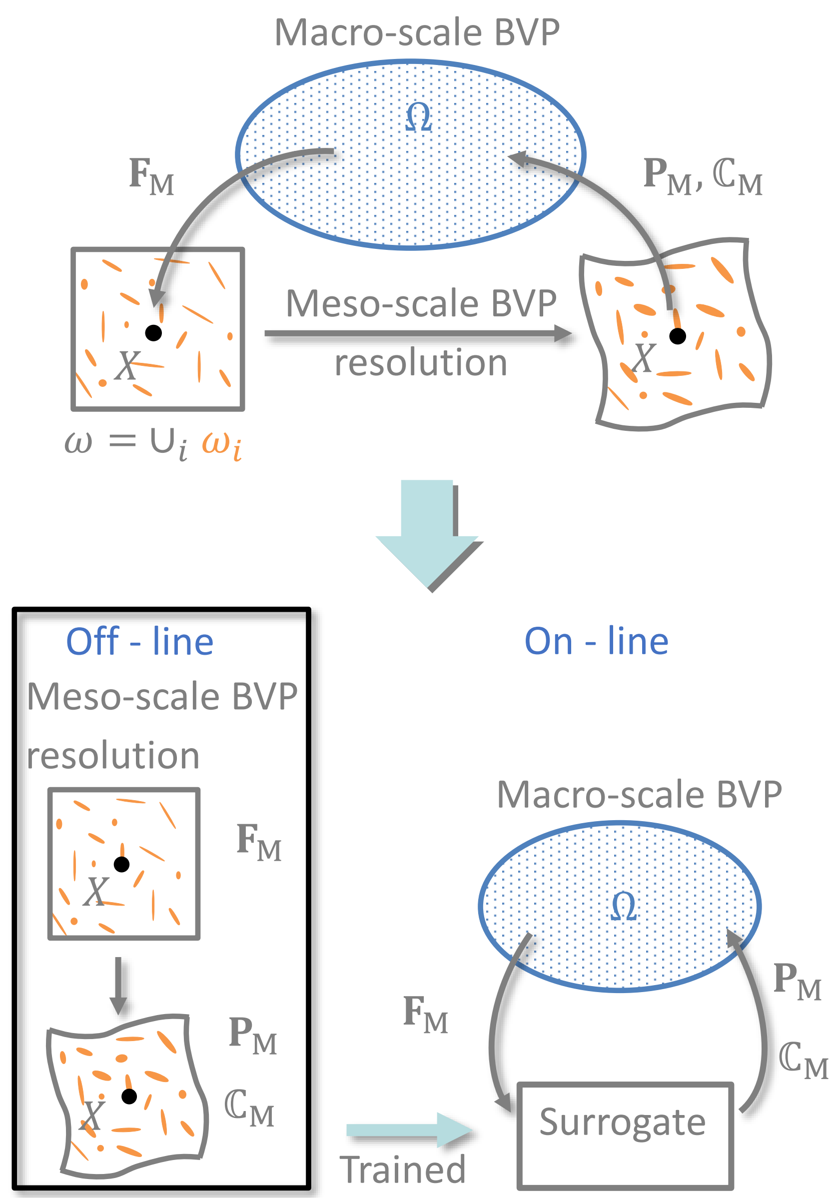

RNN with dimensionality reduction and break down

- Accurate surrogate of homogenised behaviour

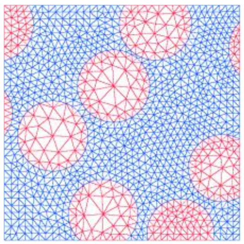

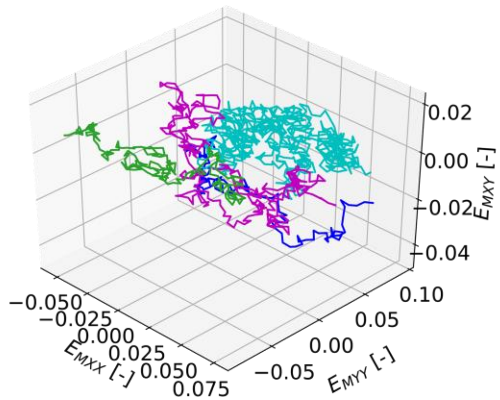

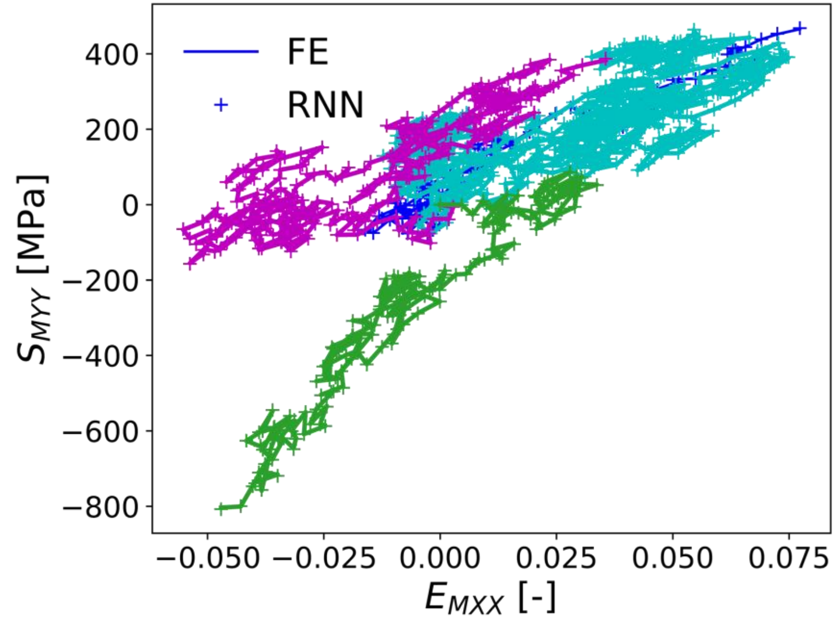

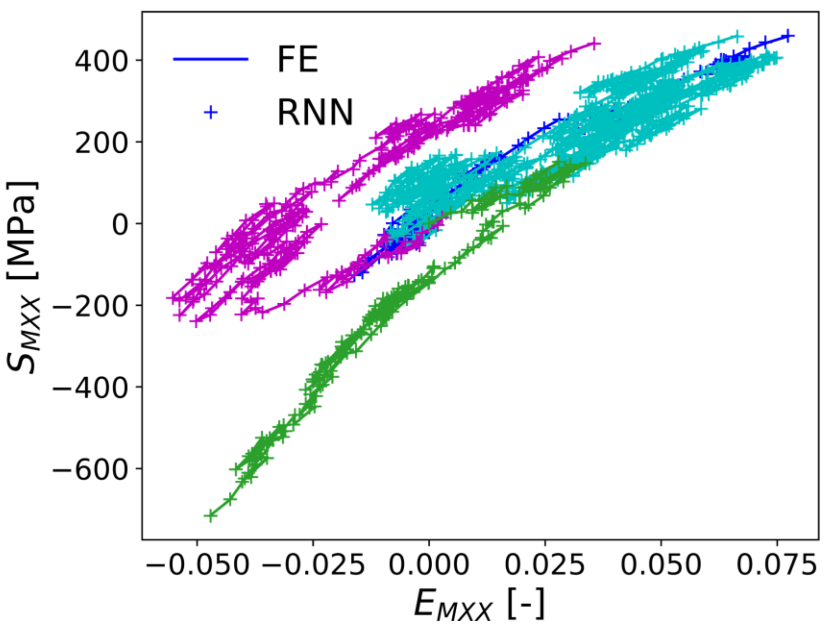

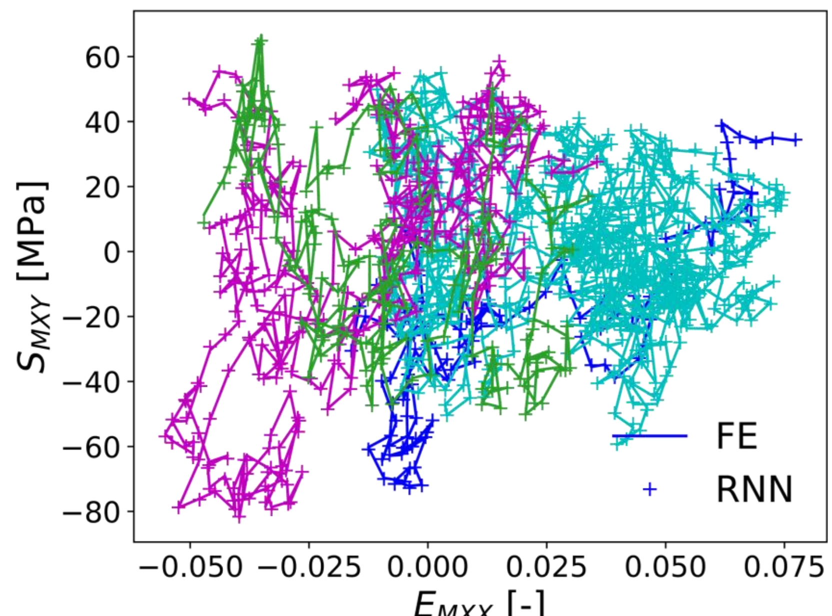

RNN with dimensionality reduction and break down

- Only homogenised output is predicted
  - On random walk

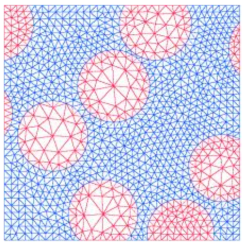

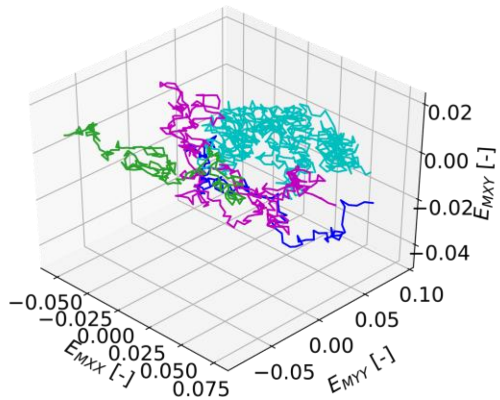

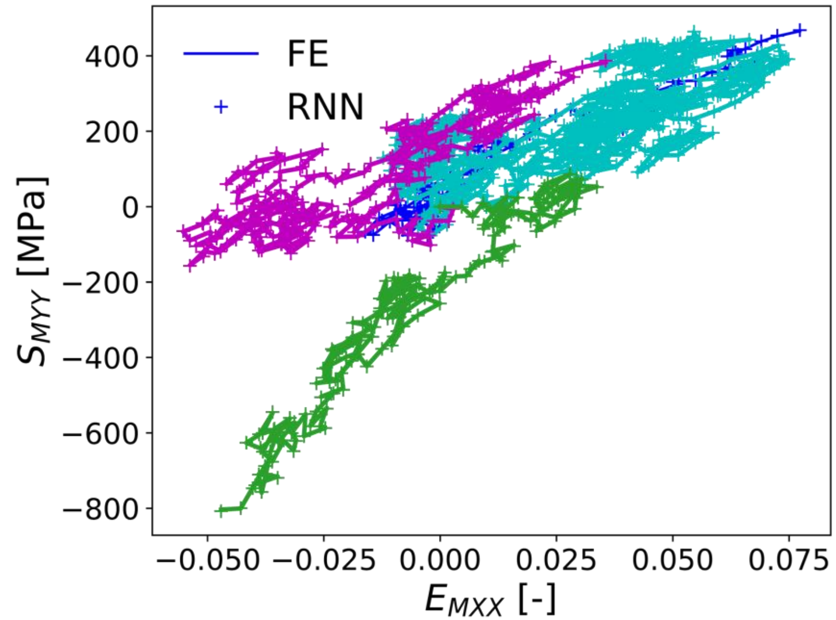

- Quid of local fields?
  - This is an advantage of multiscale methods
  - Useful to predict failure, fatigue etc.
  - Can we get it back at low cost?

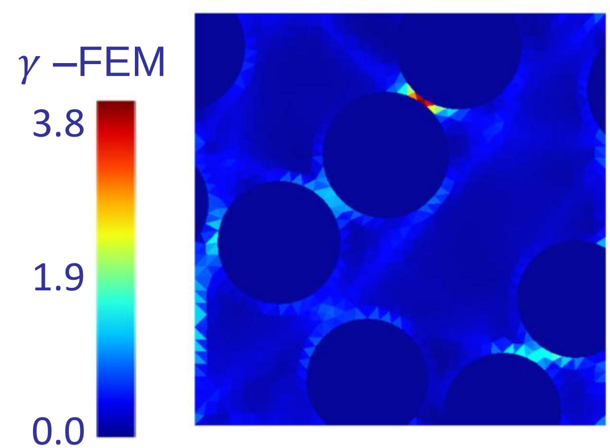

RNN with dimensionality reduction and break down

- Also build a surrogate model of the internal variables

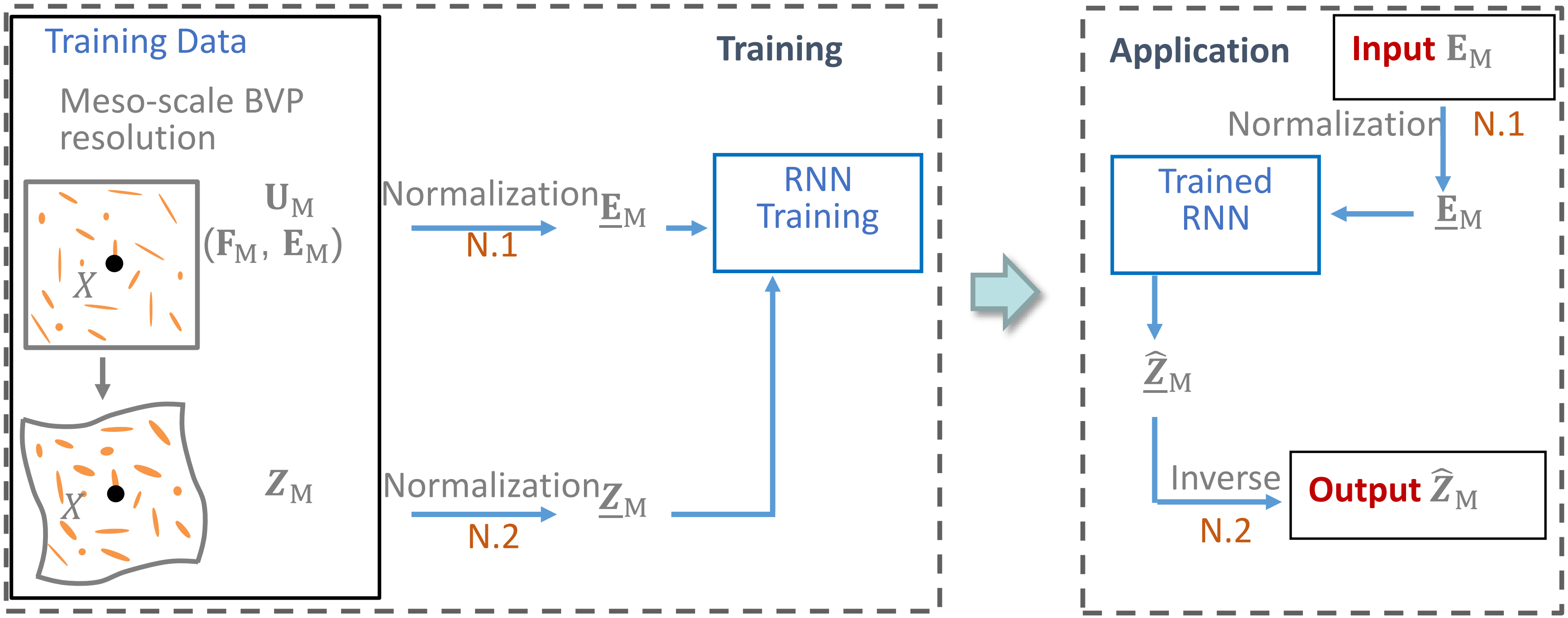

– Problem: The size of $\underline{\boldsymbol{Z}}_\mathrm{M}$ is large

- $\underline{\boldsymbol{Z}}_\mathrm{M}$ of size d the number of Gauss points of the RVE × internal variables by Gauss point

overwhelming cost

RNN with dimensionality reduction and break down

- Optimise the method: reduce the size of the internal variables

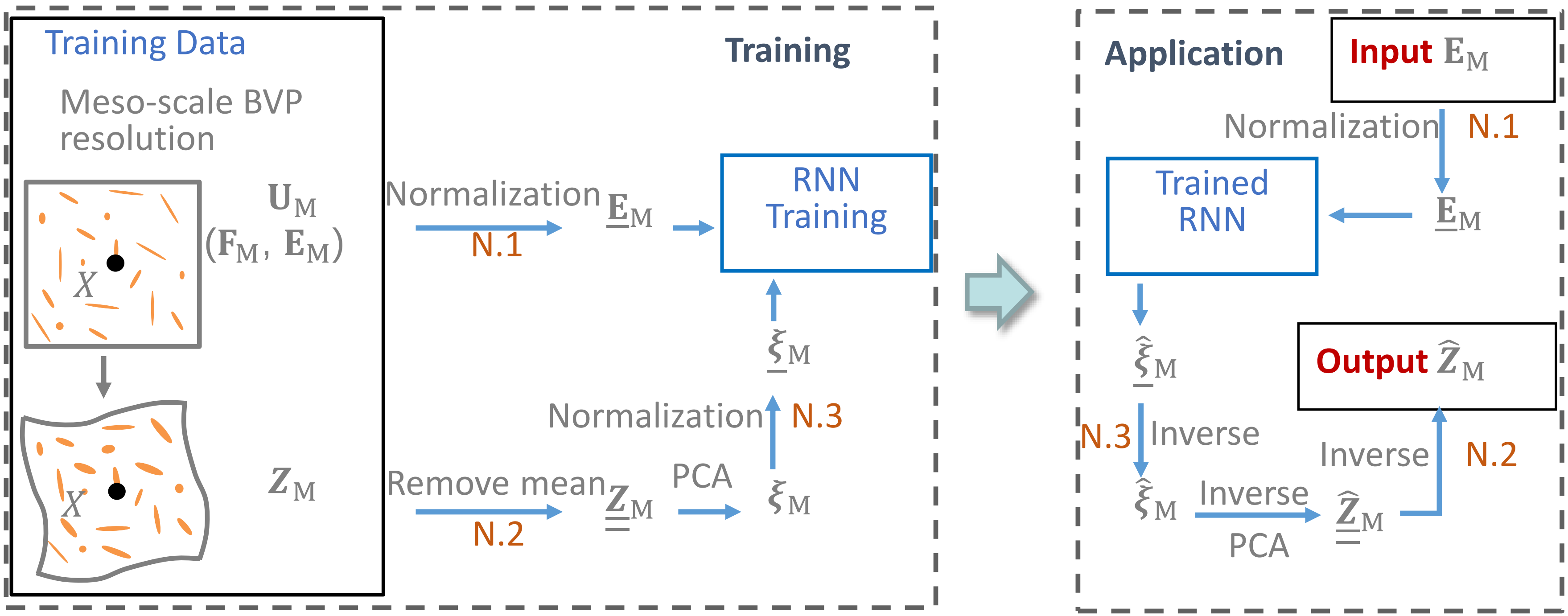

- Principal Component Analysis (PCA) applied on $\boldsymbol{Z}_\mathrm{M}$ to reduce the output of RNN
  - Construct matrix $\mathbf{Z_M} = \left[\underline{\underline{Z}}_{\mathrm{M}_1}\ \underline{\underline{Z}}_{\mathrm{M}_2}\ \dots \underline{\underline{Z}}_{\mathrm{M}_n}\right]_{d\times n}$ from n observations (1% from all data)
  - Extract n ordered eigenvalues Λ_i and eigen vector $\underline{v}_i$ of $\mathbf{Z}_\mathrm{M}^T\mathbf{Z}_\mathrm{M}$
  - Build reduced basis $\mathbf{V} = \left[\ \underline{v}_1\ \underline{v}_2\ \dots \underline{v}_p\ \right]_{d\times p}$ and reduced data $\boldsymbol{\xi}_\mathrm{M} = \mathbf{V}^T \underline{\underline{\boldsymbol{Z}}}_\mathrm{M}$ of size $p < d$
  - Reconstruction $\underline{\underline{\hat{\boldsymbol{Z}}}}_\mathrm{M} = \mathbf{V}\boldsymbol{\xi}_\mathrm{M}$
  - But not enough

RNN with dimensionality reduction and break down

- Dimensionality reduction & break down

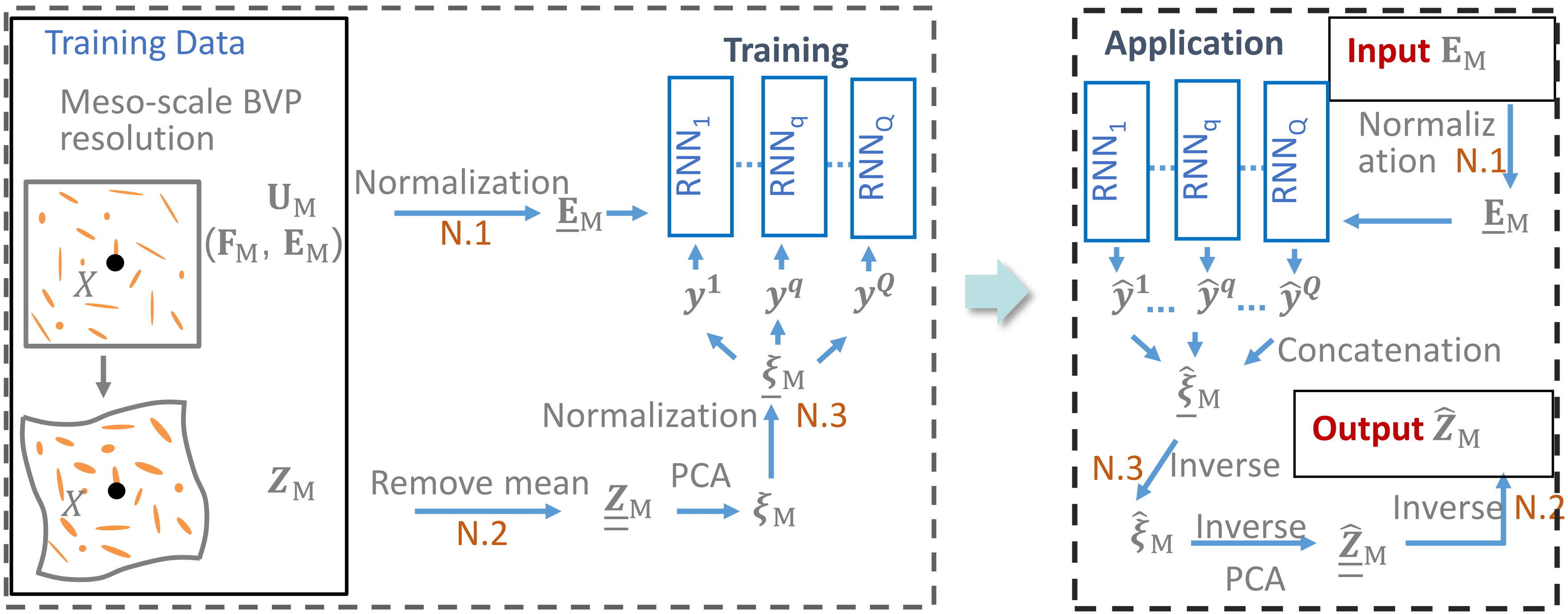

  - To further reduce the output dimension of RNN
    - The surrogate modelling is carried out by a few small RNNs, instead of one big RNN
    - The high dimension output is divided into Q groups, and each RNN is used to reproduce only a part of output
  - PCA reduces $\mathbf{Z}_\mathrm{M}$ to 180 outputs and we use Q=6

RNN with dimensionality reduction and break down

- Effect of dimensionality reduction and number of hidden variables

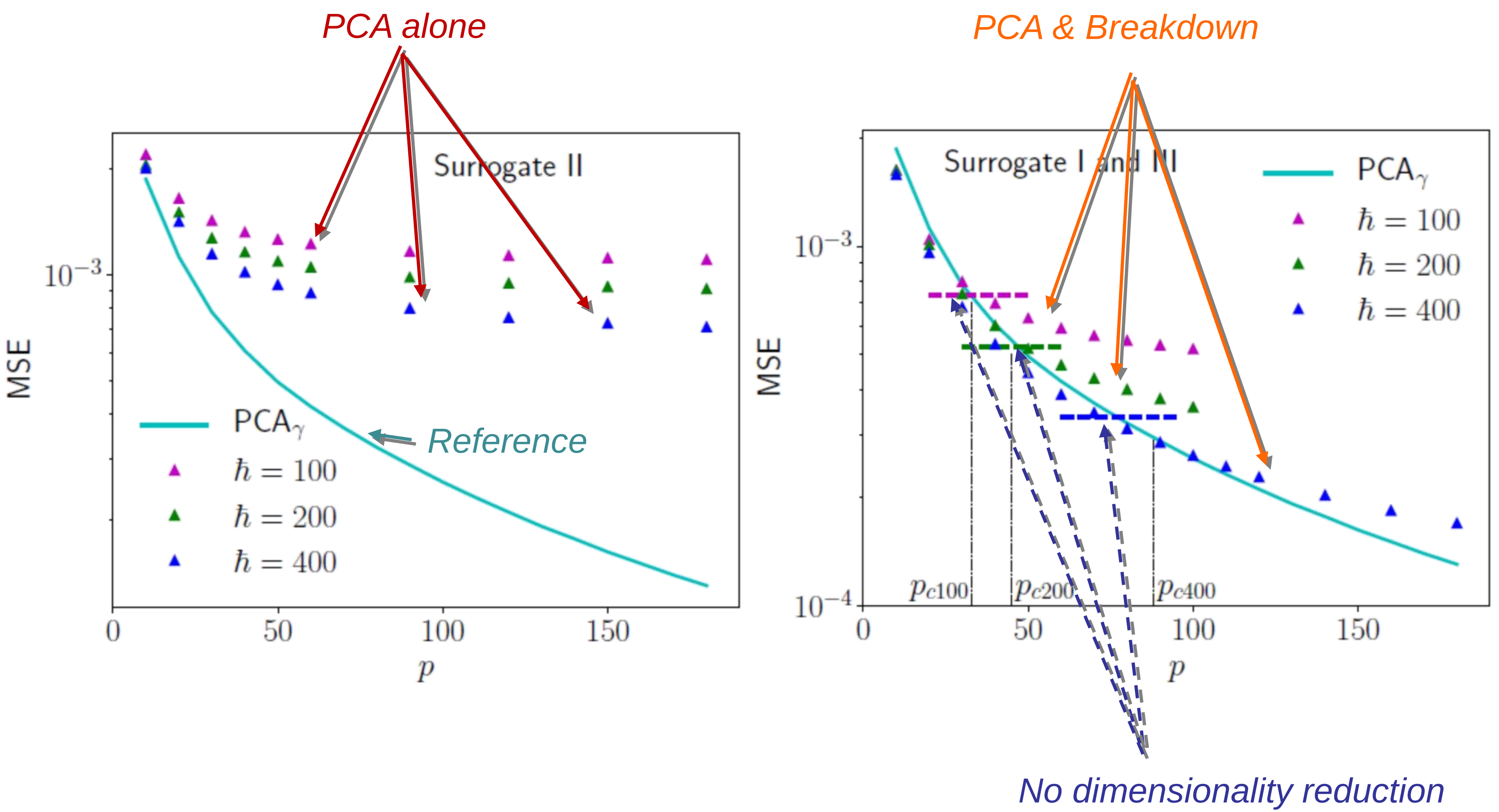

Beginning

RNN with dimensionality reduction and break down

- Evaluation of equivalent plastic strain γ: Random loading (testing data)

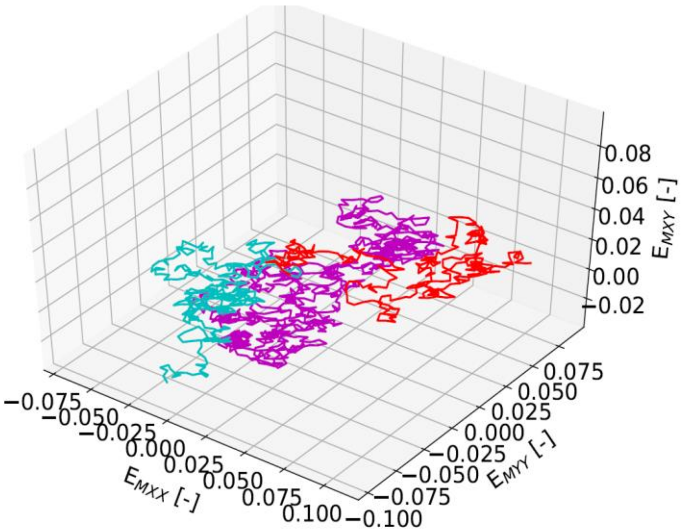

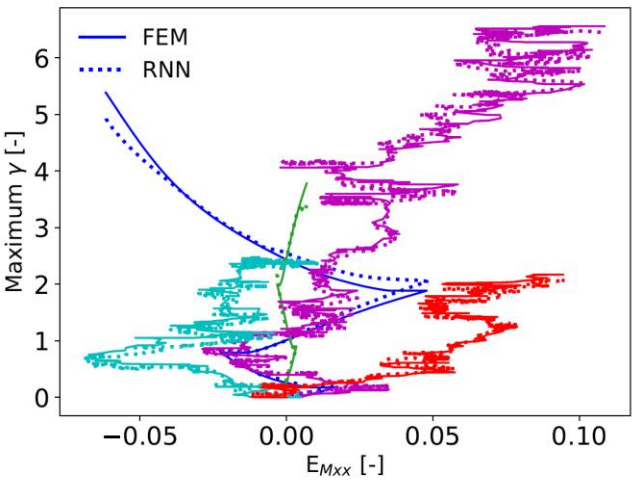

Purple loading – step 500

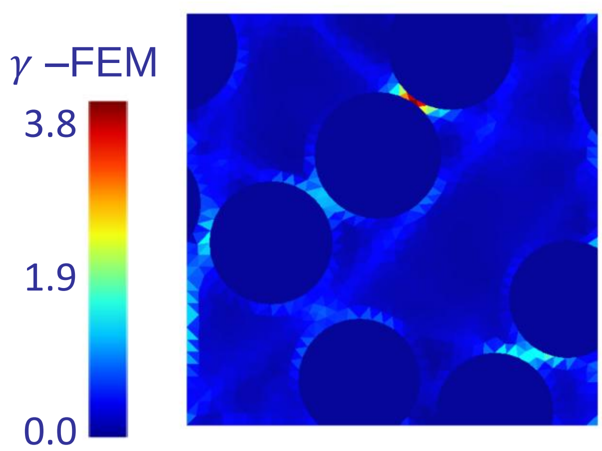

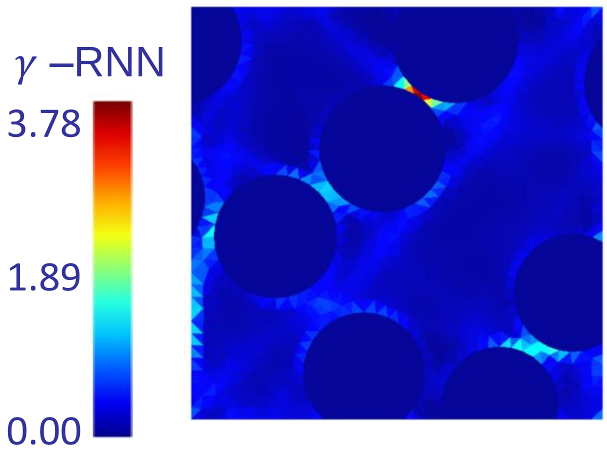

RNN with dimensionality reduction and break down

- Evaluation of equivalent plastic strain γ: Cyclic loading (testing data)

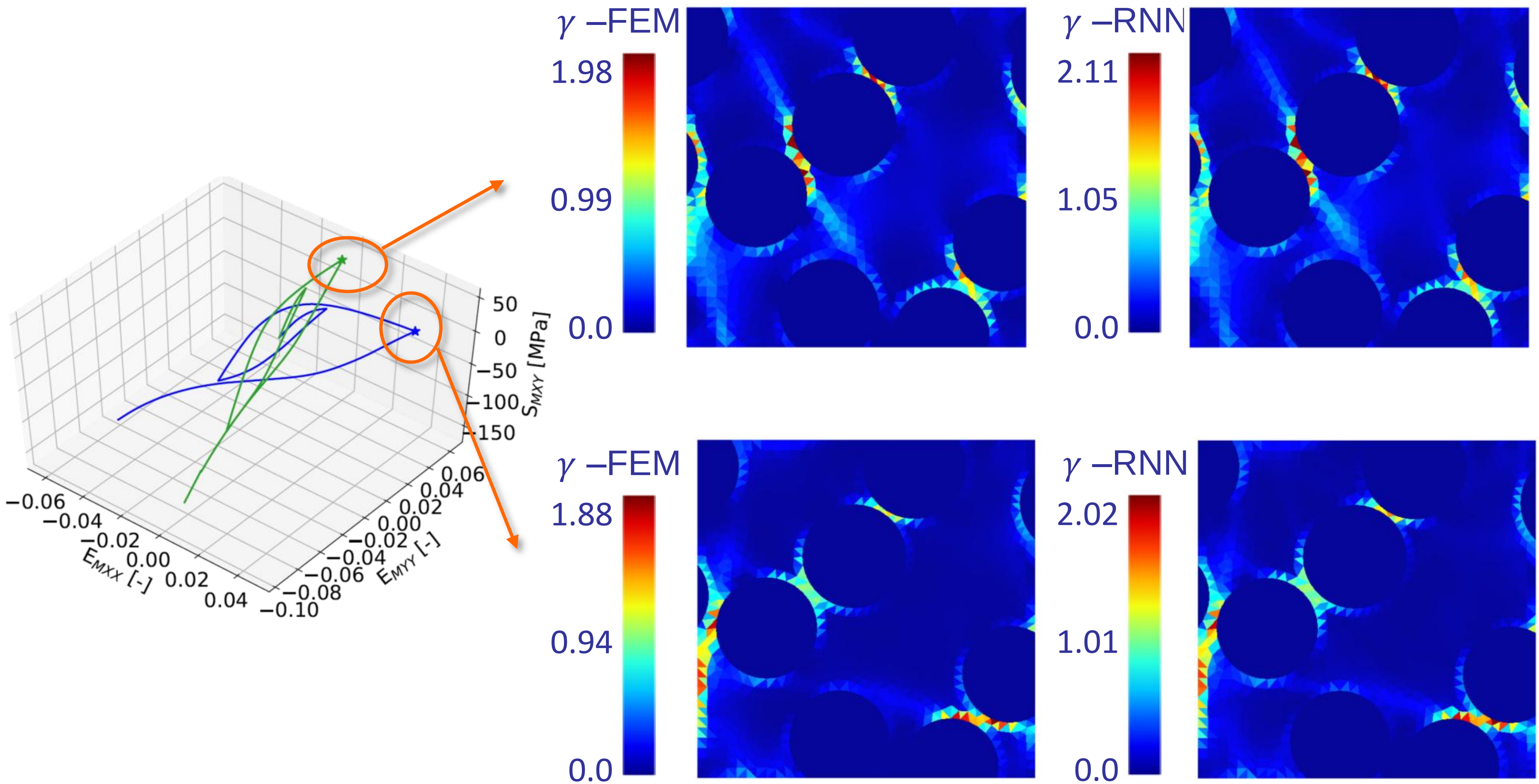

RNN with dimensionality reduction and break down

- MOAMMM FET-OPEN project (https://www.moammm.eu/)
  - ULiège, UCL (Belgium)
  - IMDEA Materials (Spain)
  - JKU (Austria)
  - cirp GmbH (Germany)

- Publications (doi)
  - 10.1016/j.cma.2020.113234
    - Open Data: 10.5281/zenodo.3902663
  - 10.1016/j.cma.2021.114476
    - Open Data: 10.5281/zenodo.5668390

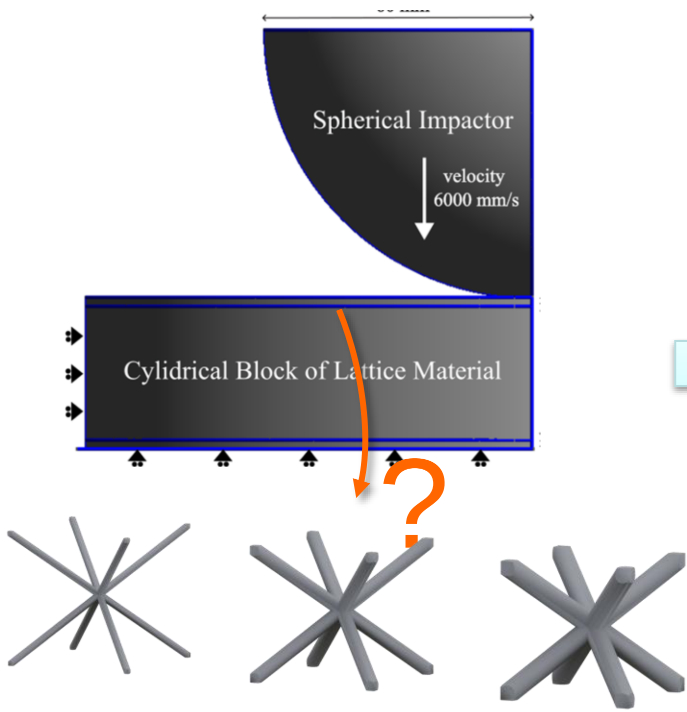

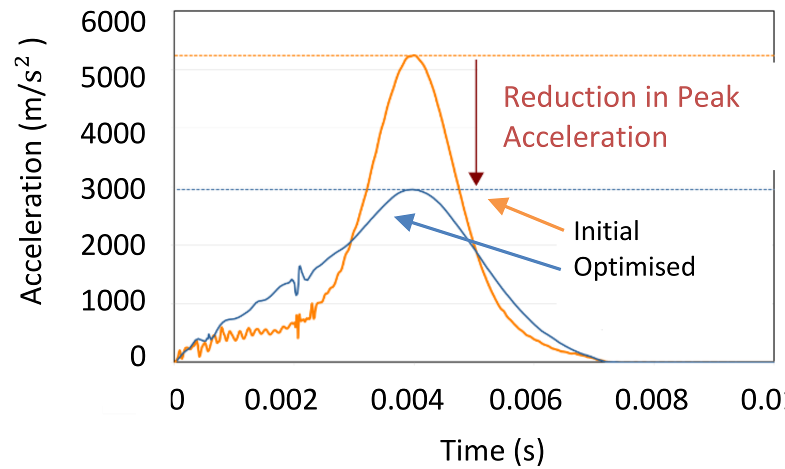

Multi-scale optimization of meta-materials

MOAMMM project has received funding from the European Union's Horizon 2020 research and innovation programme under grant agreement No 862015 for the project Multi-scale Optimisation for Additive Manufacturing of fatigue resistant shock-absorbing MetaMaterials (MOAMMM) of the H2020-EU.1.2.1. - FET Open Programme

MOAMMM

Multi-scale optimization of meta-materials

- Challenge: non-linear multi-scale optimisation with energy dissipation
  - How to conduct an optimisation in the highly non-linear range?

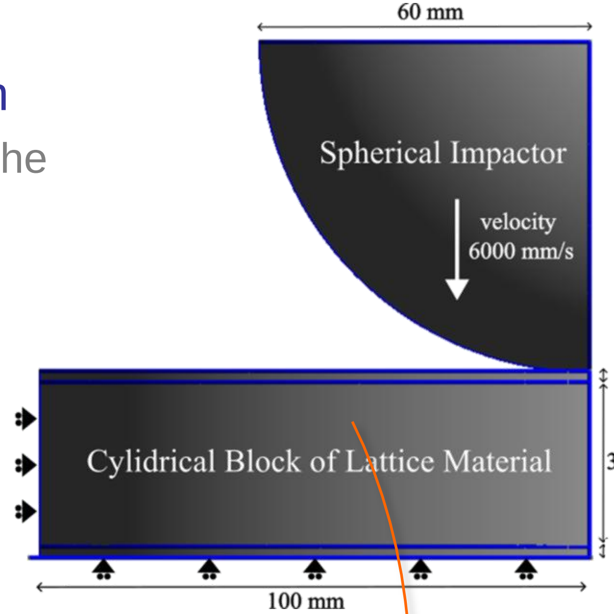

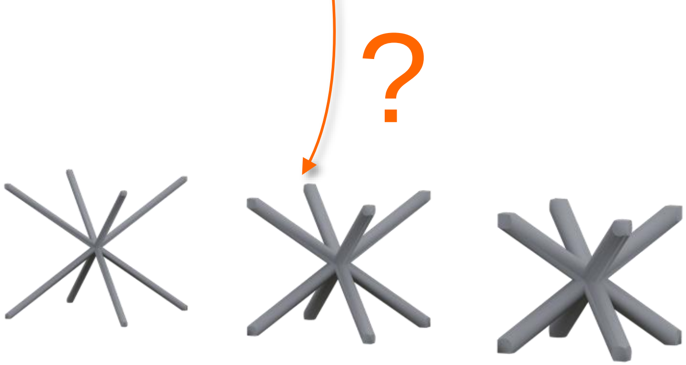

cirp GmbH

Bayesian Optimization

- Objective
  - Exploit AI-accelerated multi-scale model
  - Find lattice geometry distribution to minimise the impactor acceleration

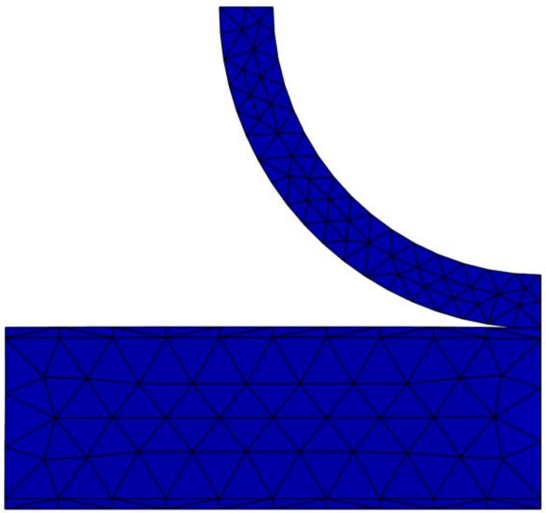

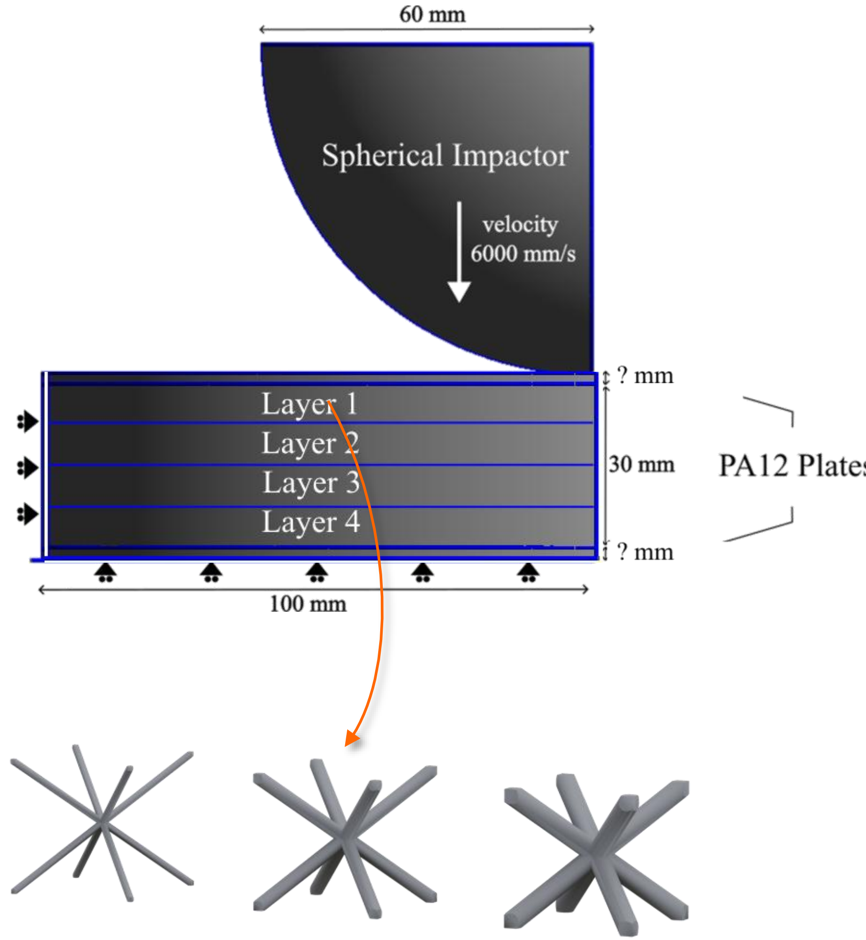

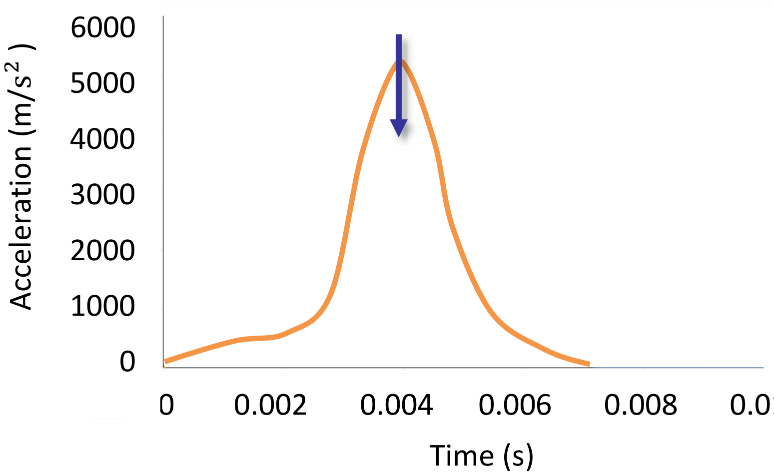

- Gaussian regression as a link between micro and macro-scales
  - Objective function:
    - Computationally expensive to evaluate in the non-linear range
    - Might be contaminated with noise

Regression & Minimisation

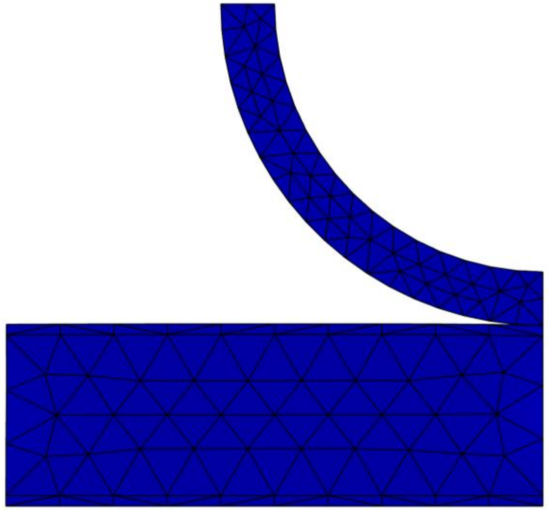

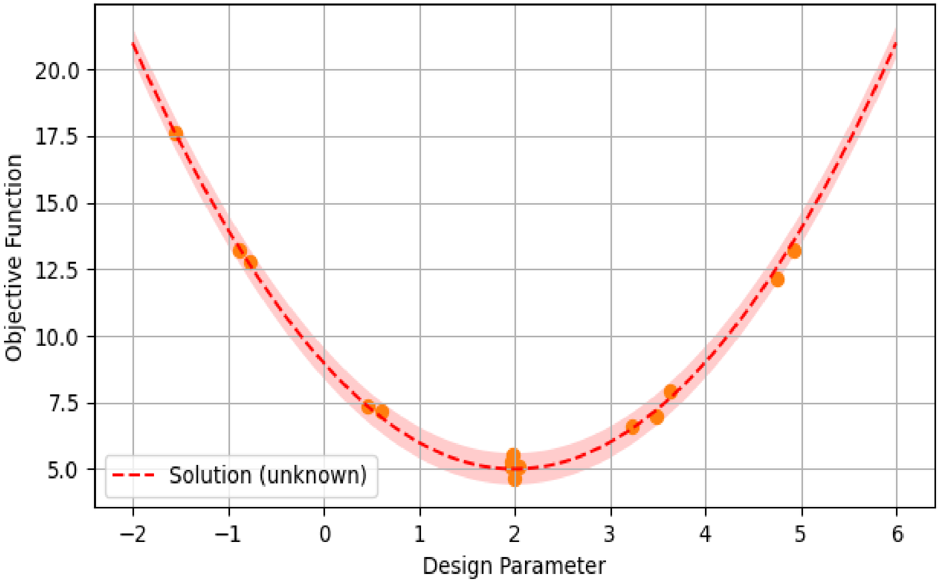

- Gaussian regression as a link between micro and macro-scales
  - Bayesian based approach is adopted:

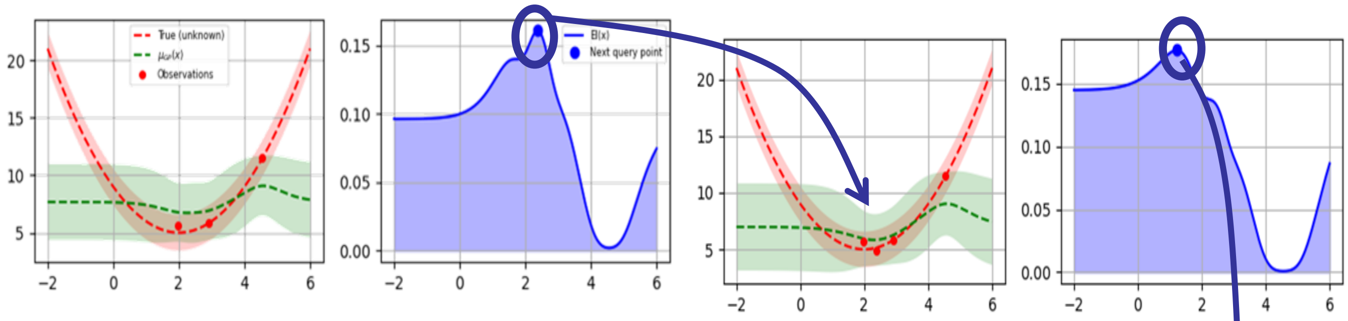

- Surrogate objective function built using Gaussian process regression from data
- Posterior distribution for sampling the next point in design space
- Exploit uncertainty in deciding if more exploration is favourable

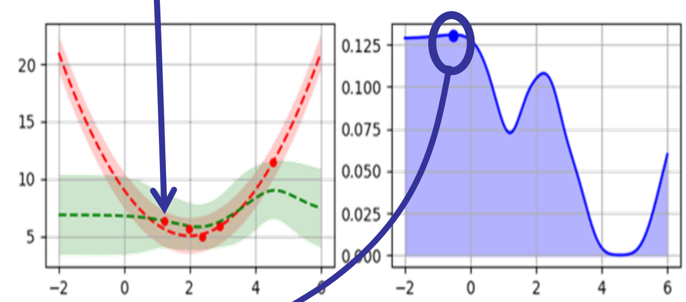

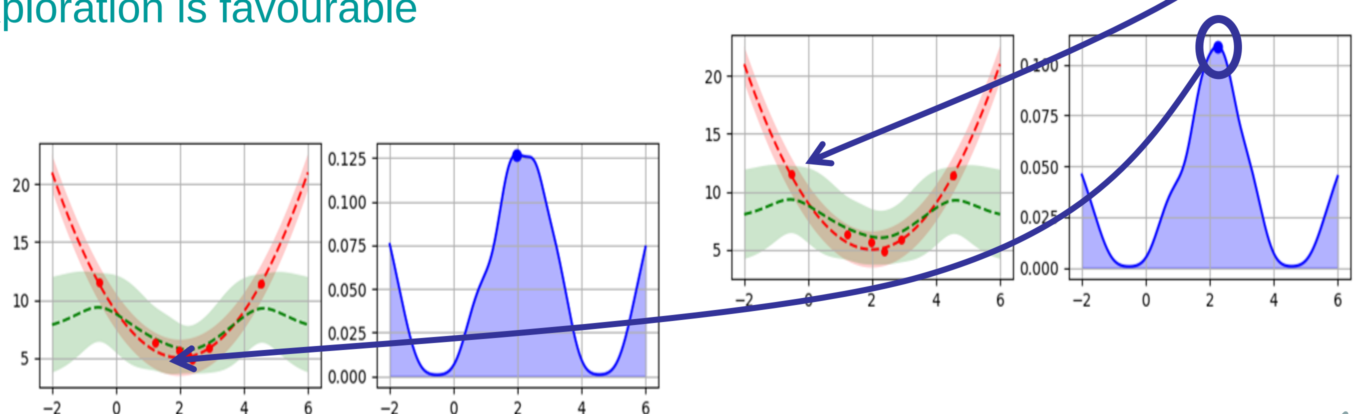

- Optimisation of cell radii distribution to optimise macro-p.o.i.
  - Train a Gaussian Process on random data generated from simulation calls
  - The surrogate is sensitive to the design variables i.e., strut radii distributions

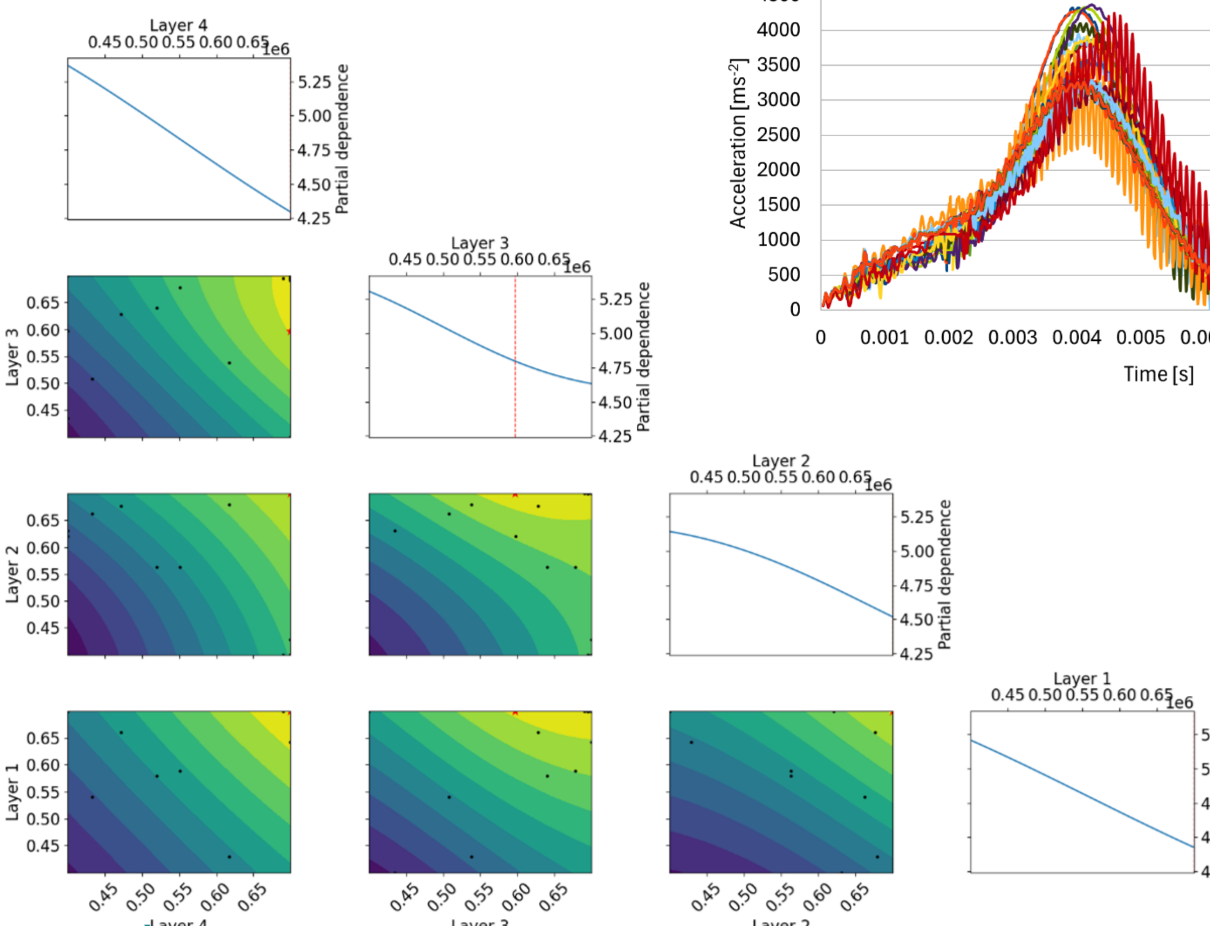

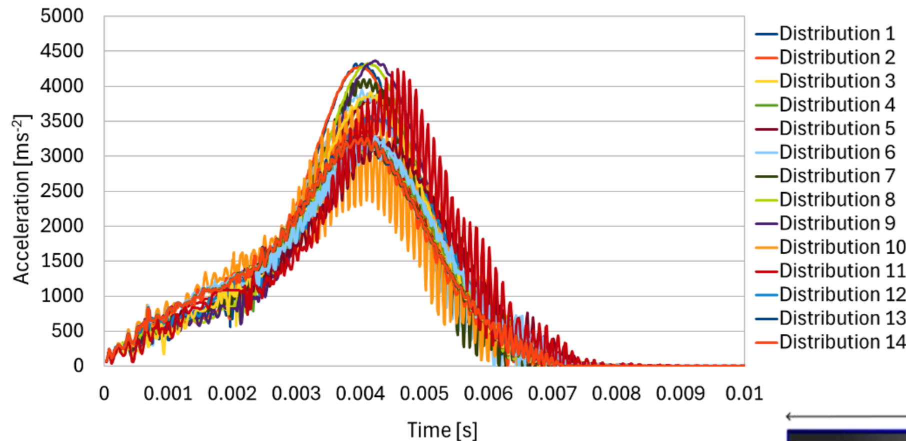

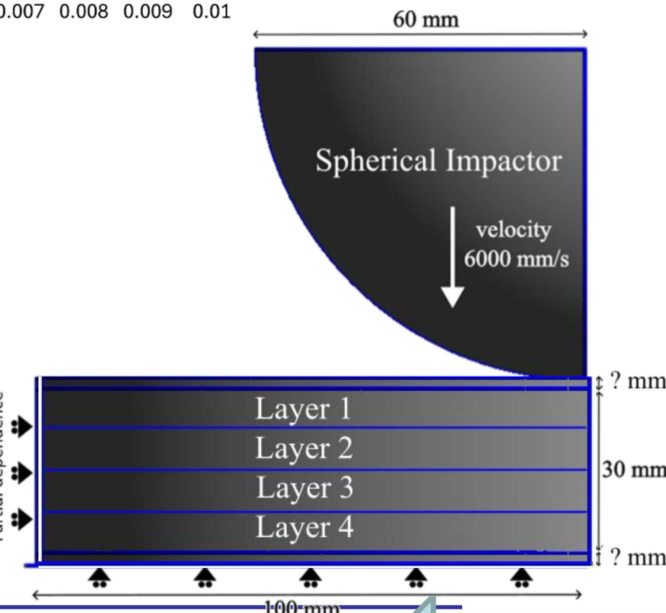

Multi-scale optimization of meta-materials

- Optimisation of cell radii distribution to optimise macro-p.o.i.
  - 2-Scale optimisation of shock absorbent device

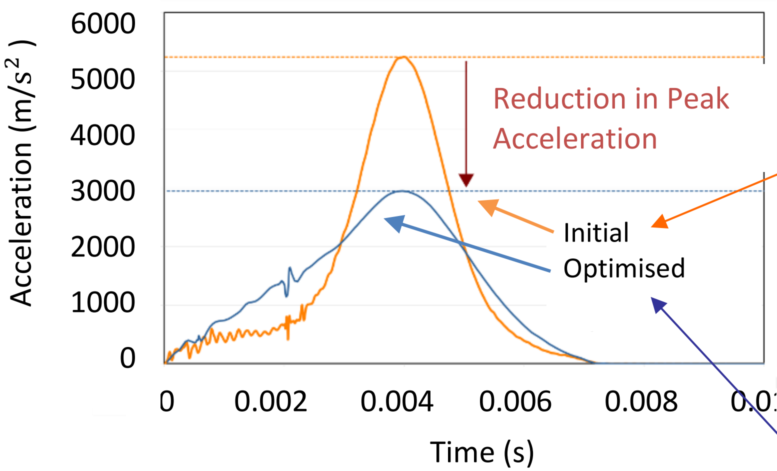

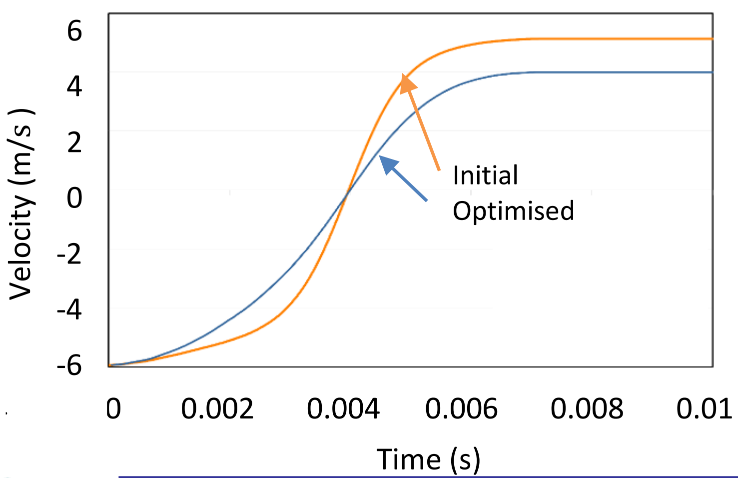

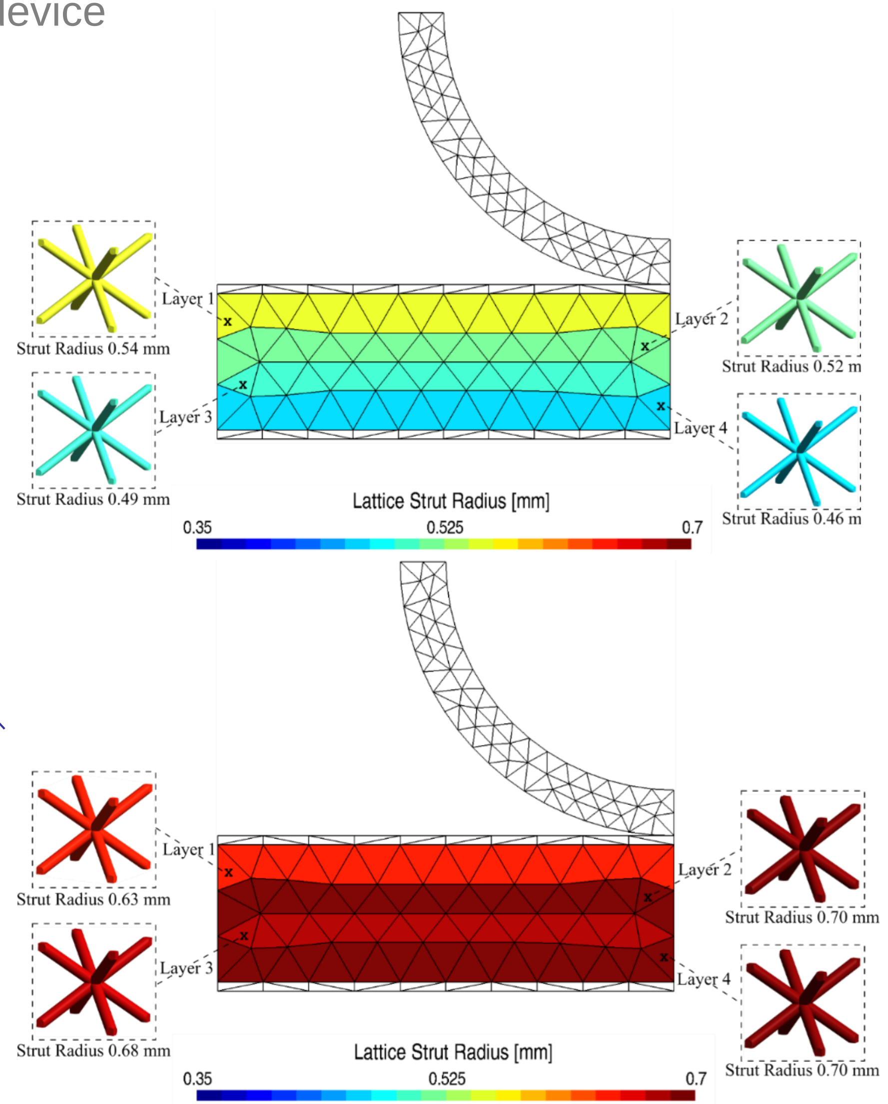

Multi-scale optimization of meta-materials

- Optimisation of cell radii distribution to optimise micro-p.o.i.
  - Fatigue resistant shoe soles
    - Shoe soles should provide support and sustain repeated cyclic loadings
    - Composed of constant cell size but variable strut radii
  - The Properties of Interest (P.O.I) :
    - Fatigue life.
    - Macroscopic deformation
  - Goal of Optimization: Find the optimal distribution of lattice radii such that
    - Fatigue life is maximised
    - Macroscopic deformation is minimised

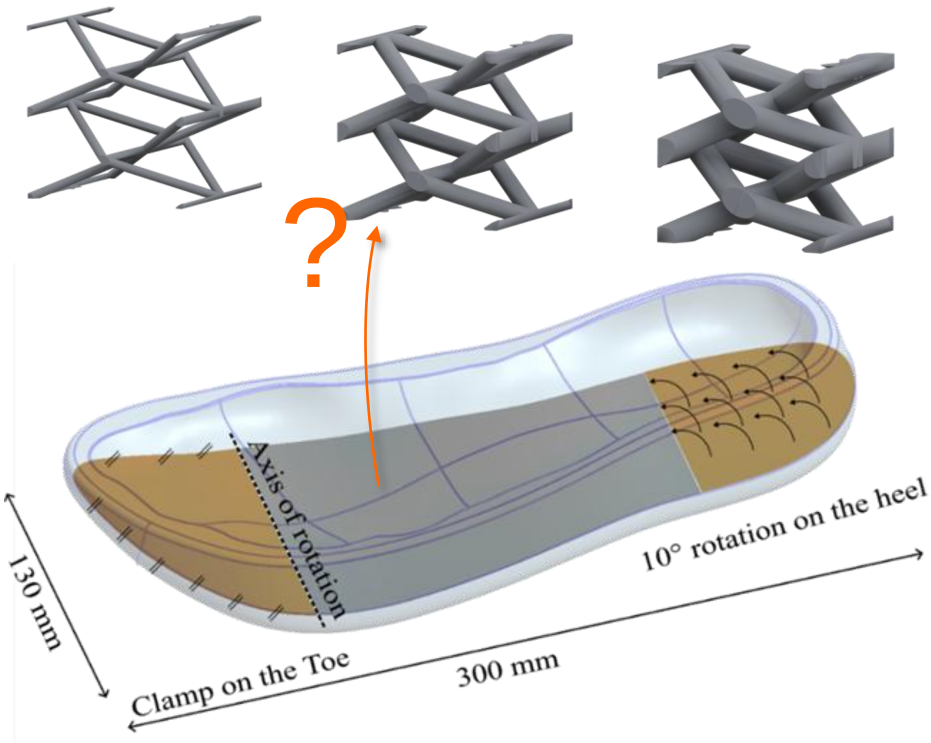

Multi-scale optimization of meta-materials

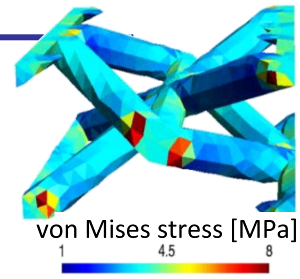

- Optimisation of cell radii distribution to optimise micro-p.o.i.
  - Goal: predict local stress field (e.g. for fatigue)
  - Problem $\boldsymbol{Z}_{\mathrm{M}}$: too many data (a sequence per Gauss Point)

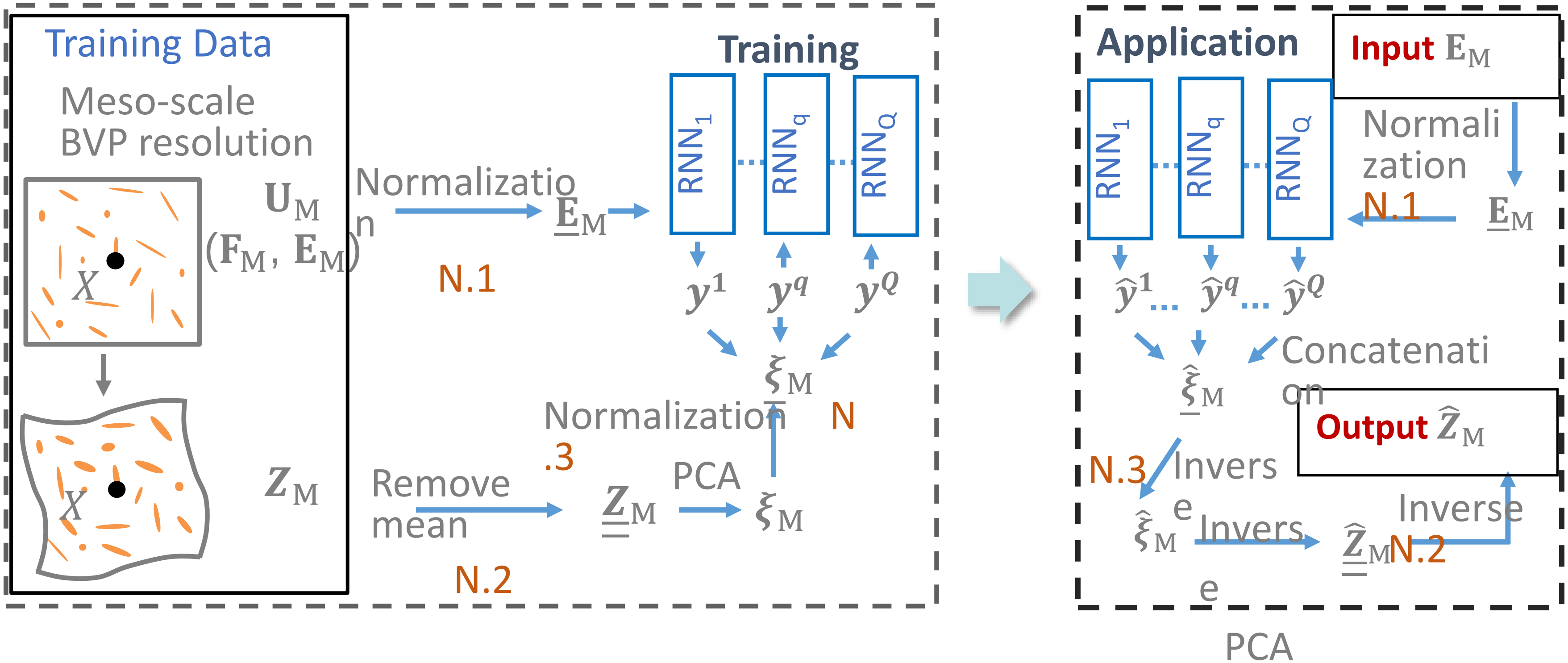

  - Dimensionality and reduction breakdown:
    - Principal Component Analysis (PCA) applied on $\boldsymbol{Z}_{\mathrm{M}}$ to reduce the output of RNN ξ_{M}
    - The high dimension ξ_{M} divided into Q groups, and each RNN is used to reproduce only a part of output

Multi-scale optimization of meta-materials

- Optimisation of cell radii distribution to optimise micro-p.o.i.
  - Goal: predict local stress field (e.g. for fatigue)
  - Problem $\boldsymbol{Z}_{\mathrm{M}}$:
    - $\mathbf{Z}_{\mathrm{M}} = \{\mathbf{z}_{\mathrm{m}}(\boldsymbol{x}), \forall\, \boldsymbol{x} \in \omega\,\}$ size depends on the micro-structure parameters $\boldsymbol{\vartheta}_{\mathrm{geo}}$

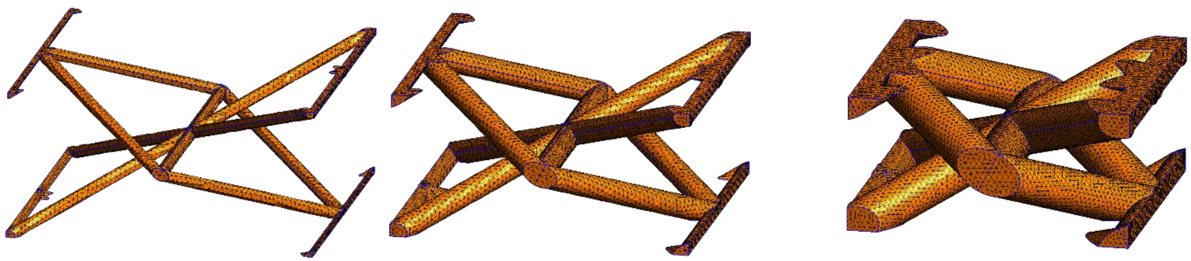

$r = 2\ \mathrm{mm}$ $r = 4\ \mathrm{mm}$ $r = 8\ \mathrm{mm}$

  - Projection on a skeleton of fixed number of elements
    - $\mathbf{Z}_{\mathrm{M}}^{\mathrm{sk}} = \left\{\mathbf{z}_{\mathrm{m}}^{\mathrm{sk}}(\boldsymbol{x}), \forall\, \boldsymbol{x} \in \omega^{\mathrm{sk}}\,\right\}$ $z_{\mathrm{m}_k}^{\mathrm{sk}}\left(\omega_i^{sk}\right) = \dfrac{1}{\sum_{\omega_e \in \{\omega_e\}_i} |\omega_e|} \sum_{\omega_e \in \{\omega_e\}_i} |\omega_e|\, z_{\mathrm{m}_k}(\omega_e)$

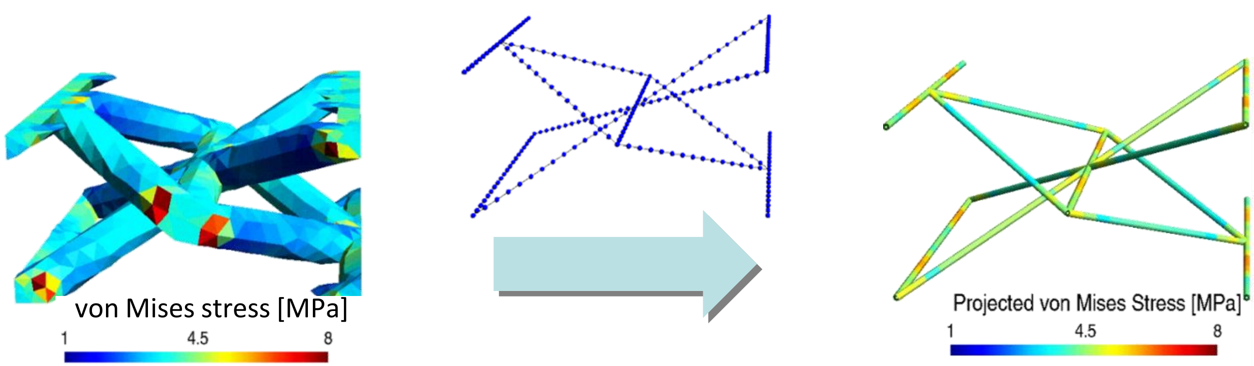

Multi-scale optimization of meta-materials

- Optimisation of cell radii distribution to optimise micro-p.o.i.
  - Numerical Setup
    - Multi-scale simulations
    - Lattice layers response from meso-scale surrogate (Recurrent Neural Network)
    - Local stress field from localisation (RNN with dimensionality reduction)
    - Fatigue criterion from stress field

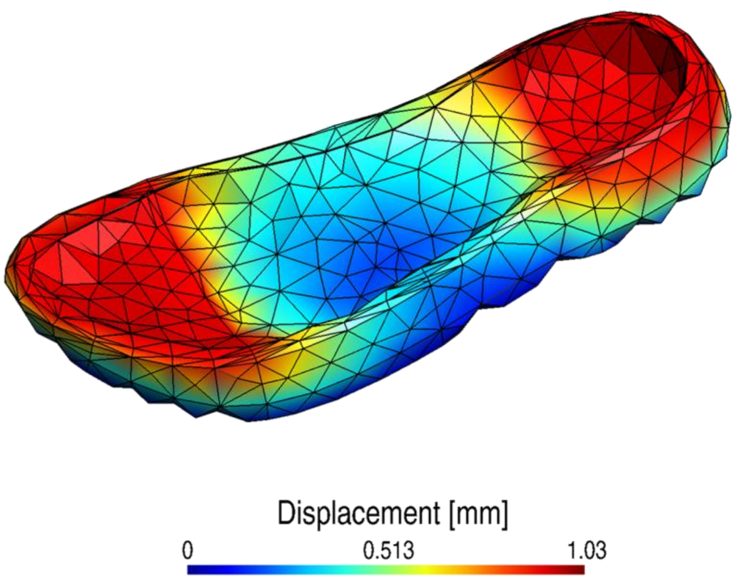

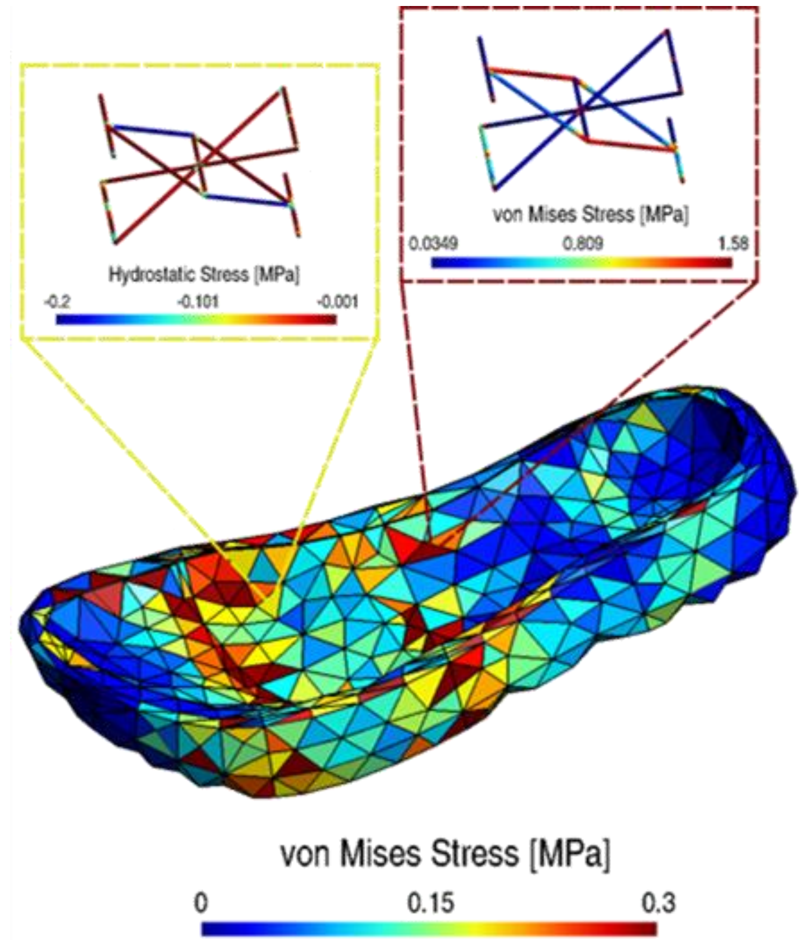

- Optimisation of cell radii distribution to optimise micro-p.o.i.
  - Lattice meta-materials: Large design space
    - Simulation Calls: Computationally expensive to evaluate
  - Substitute by a stochastic surrogate:
    - Train a Gaussian Process on random data generated from simulation calls
    - Surrogate is cheaper to evaluate

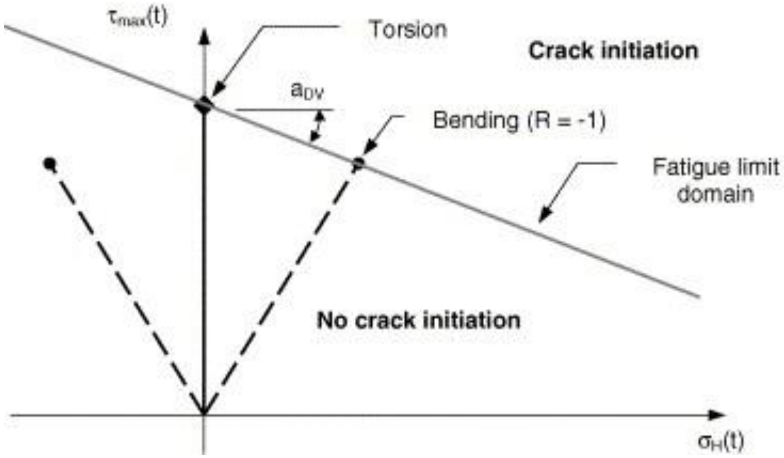

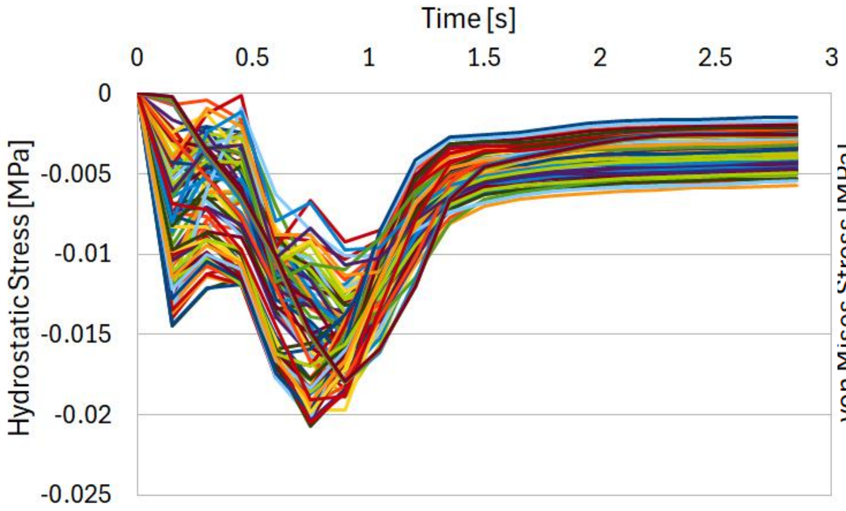

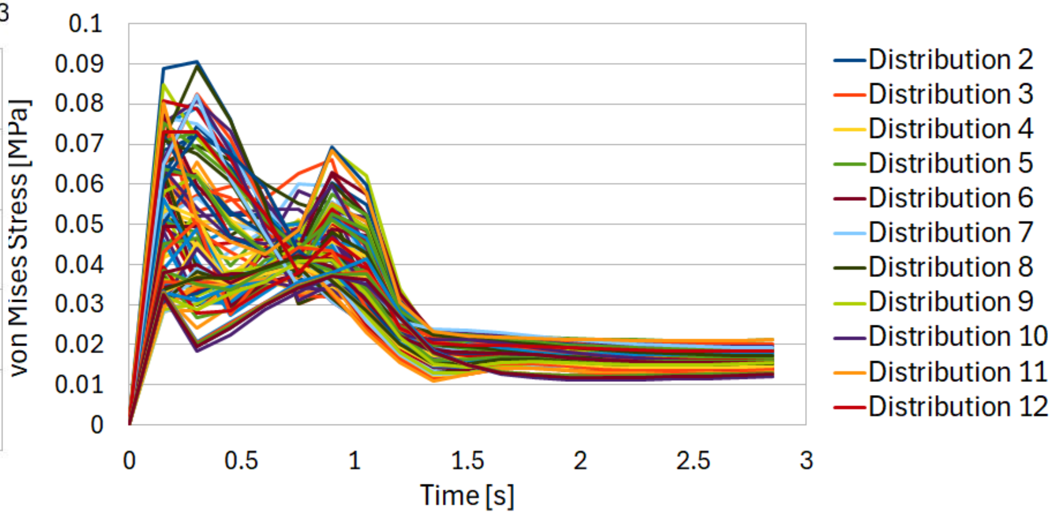

- Optimisation of cell radii distribution to optimise micro-p.o.i.
  - The surrogate is sensitive to the design variables i.e., strut radii distributions
    - Here the layering is for illustration purpose only
    - During optimisation we have full freedom

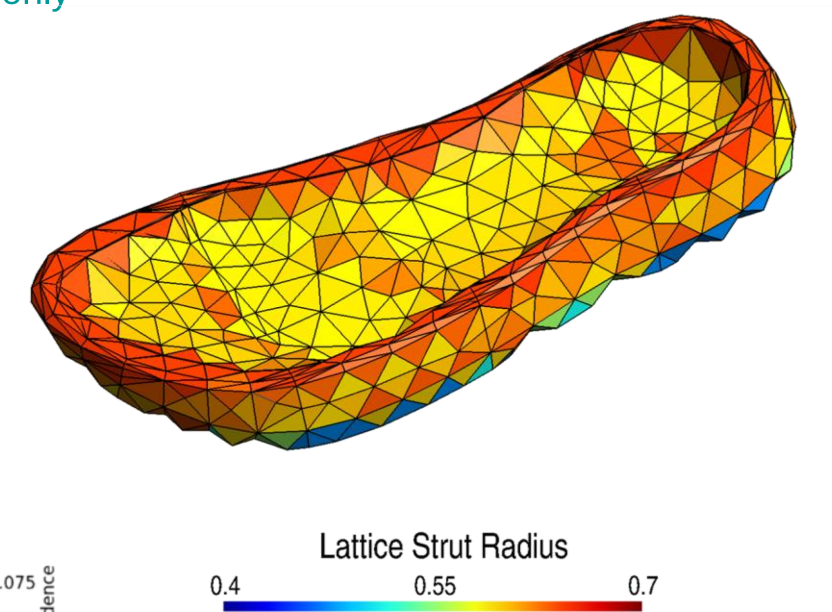

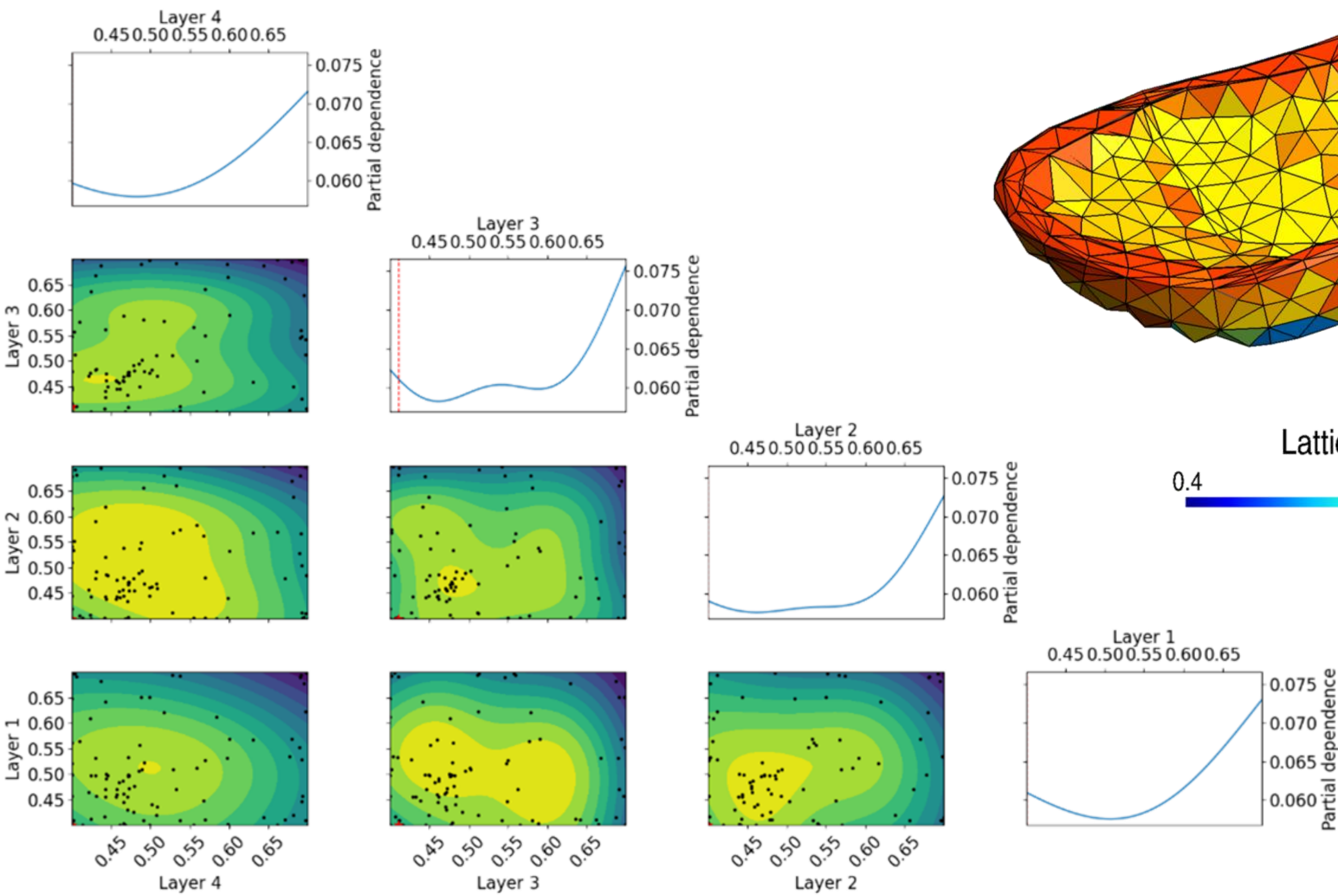

- Optimisation of cell radii distribution to optimise micro-p.o.i.
  - 2-Scale optimisation of shock absorbent device
    - Bayesian Optimisation
    - Using macro-scale p.o.i. surrogate

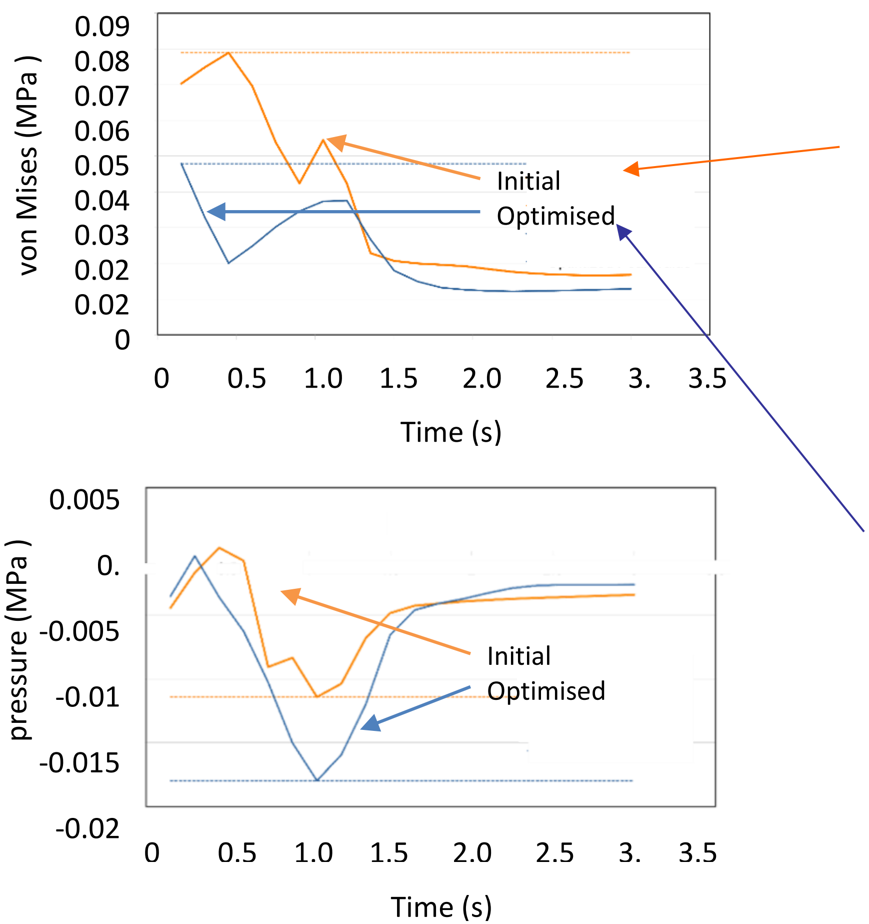

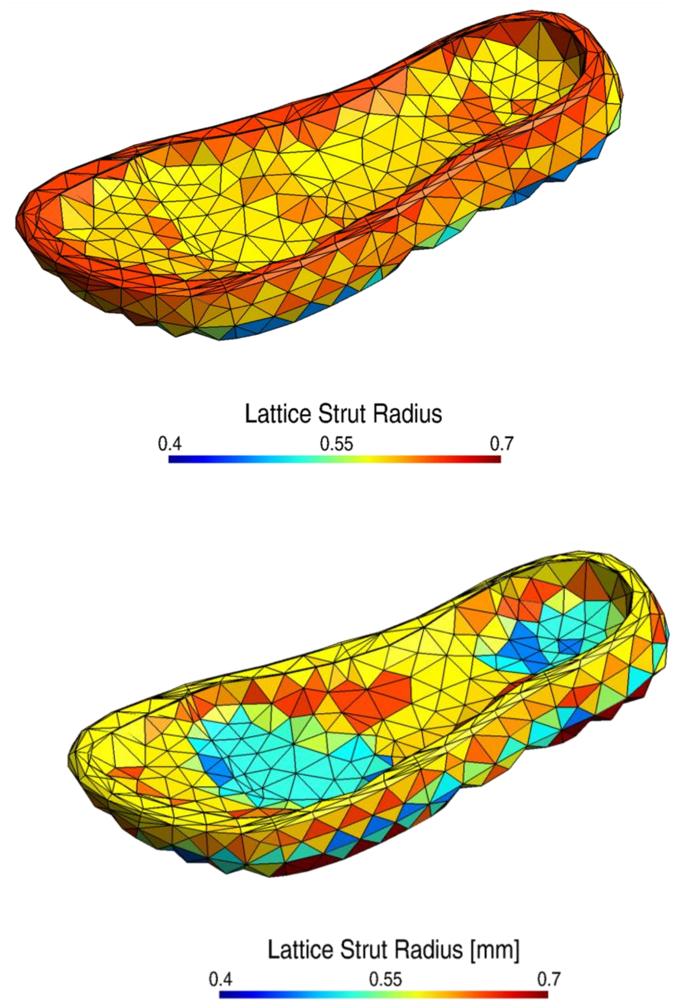

Multi-scale optimization of meta-materials

- MOAMMM FET-OPEN project (https://www.moammm.eu/)
  - ULiège, UCL (Belgium)
  - IMDEA Materials (Spain)
  - JKU (Austria)
  - cirp GmbH (Germany)

- Publications (doi)
  - 10.1016/j.cma.2020.113234
    - Open Data: 10.5281/zenodo.3902663
  - 10.1016/j.cma.2021.114476
    - Open Data: 10.5281/zenodo.5668390

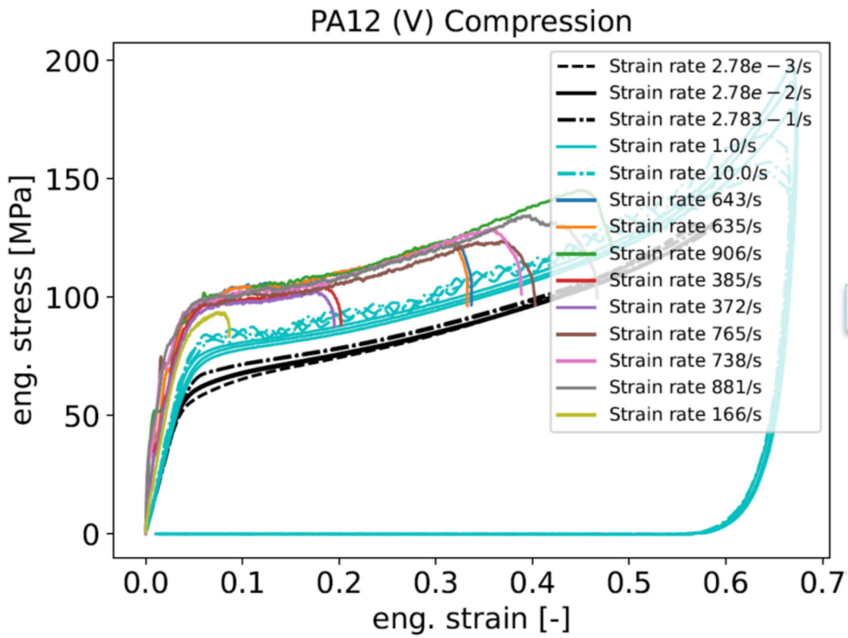

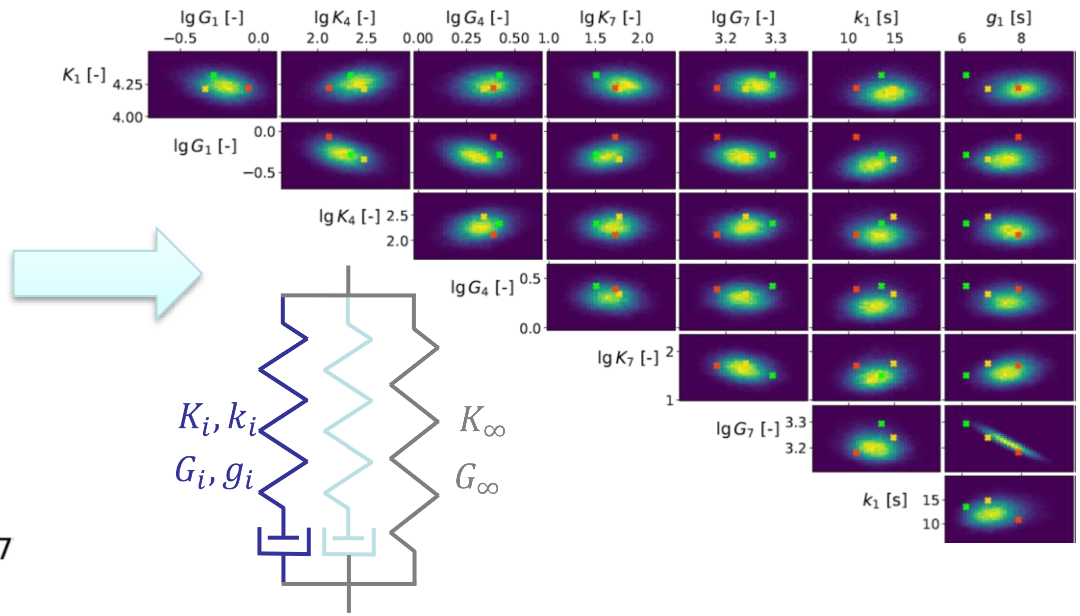

Sequential Bayesian Inference of complex model parameters

MOAMMM project has received funding from the European Union's Horizon 2020 research and innovation programme under grant agreement No 862015 for the project Multi-scale Optimisation for Additive Manufacturing of fatigue resistant shock-absorbing MetaMaterials (MOAMMM) of the H2020-EU.1.2.1. - FET Open Programme

MOAMMM

Sequential Bayesian Inference of complex model parameters

- Difficulties in inferring model parameters
  - On the model side
    - Which model is best suited?
    - Model complexity
      - ⇒ Lot of parameters
      - ⇒ Parameters not univocally linked to a test
    - Model limitation
      - ⇒ Error in predictions
      - ⇒ We cannot reproduce all the tests
    - Example:
      - Visco-elastic-Visco-plastic pressure dependent model
      - Details of the model

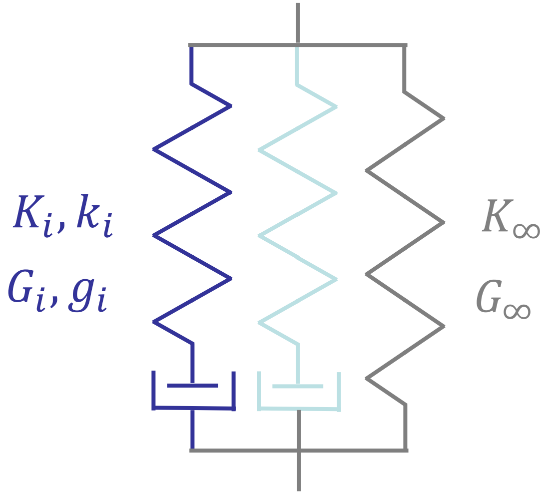

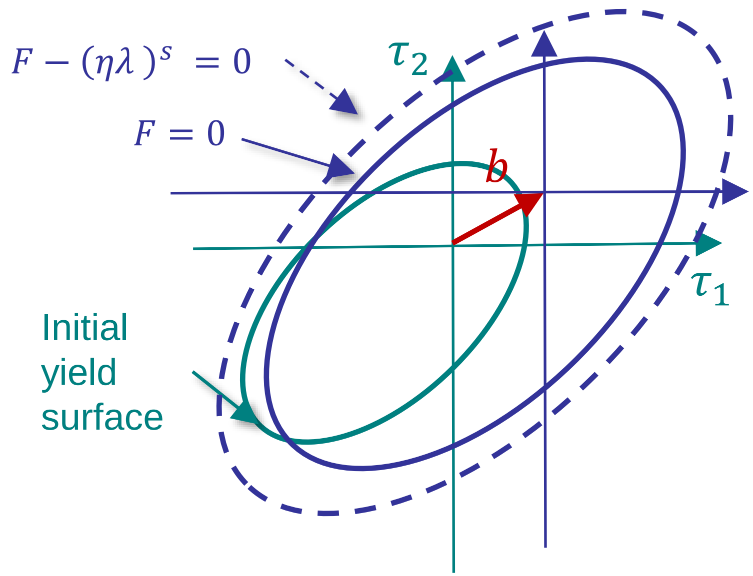

$$F=\left(\frac{(\boldsymbol{\tau}-\boldsymbol{b})^{\mathrm{eq}}}{\sigma_c}\right)^\alpha-\frac{m^\alpha-1}{m+1}\frac{\mathrm{tr}(\boldsymbol{\tau}-\boldsymbol{b})}{\sigma_c}-\frac{m^\alpha+m}{m+1}$$

$$P=(\varphi^{\mathrm{eq}})^2+\beta\left(\frac{\mathrm{tr}\boldsymbol{\varphi}}{3}\right)^2 \qquad m=\frac{\sigma_t}{\sigma_c}$$

Sequential Bayesian Inference of complex model parameters

- Difficulties in inferring model parameters
  - On the experimental side
    - Error during measurements
      - ➔ Which curve to consider?
    - Several tests under several loading conditions
      - ➔ How to use them at once

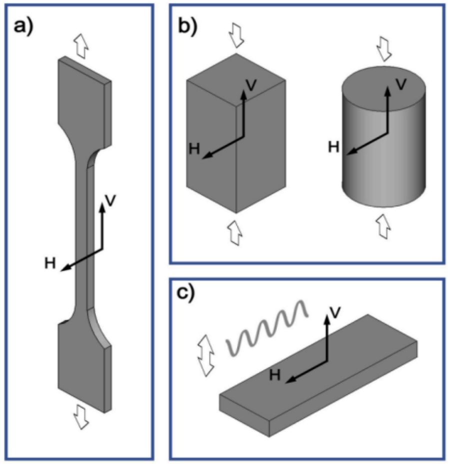

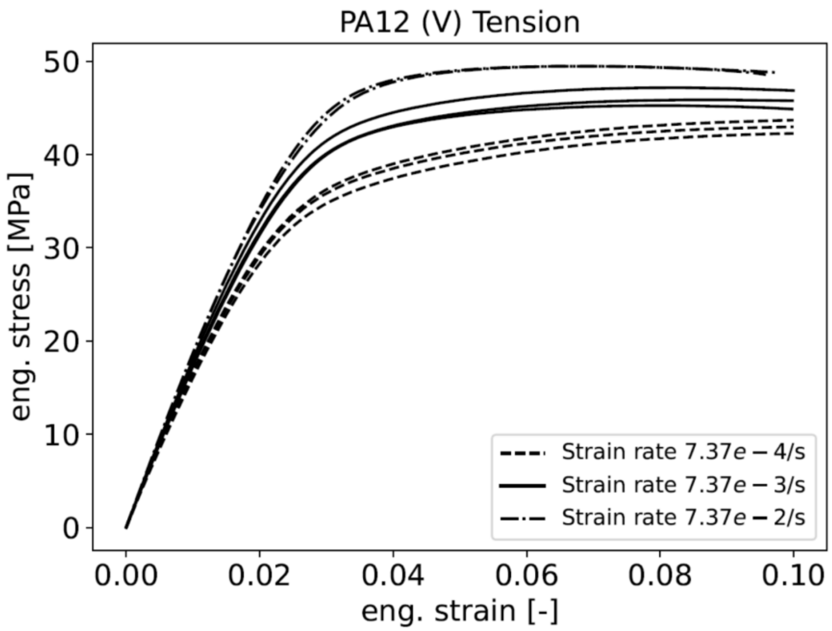

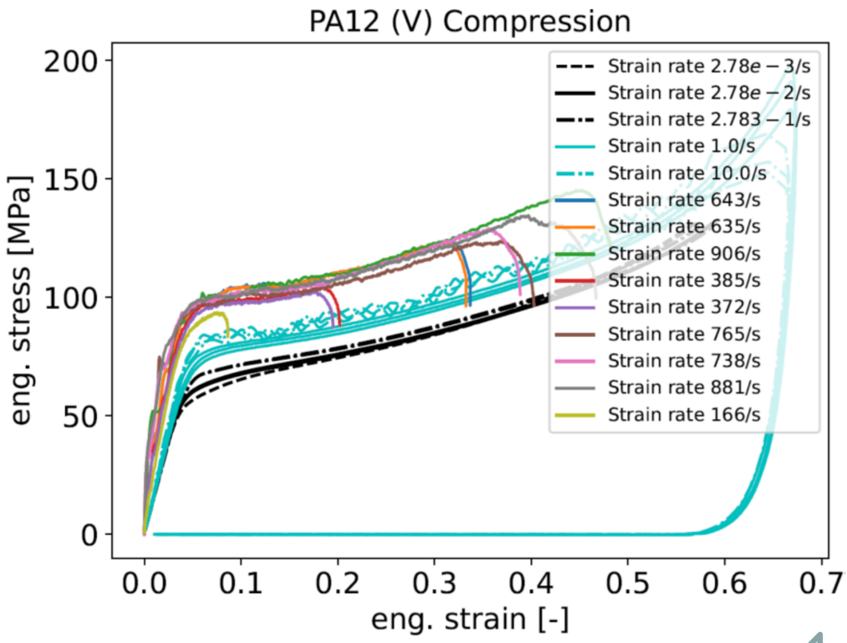

IMDEA-cirp GmbH

Sequential Bayesian Inference of complex model parameters

- Bayesian Inference
  - Identify **distribution** of model/model parameters $\boldsymbol{\vartheta}_{\text{mat}}$
  - Use all experimental observations $\boldsymbol{\sigma}_{\text{exp}} = \left\{\boldsymbol{\sigma}_{\text{exp}}^{(\text{test } j, \text{repetition } k)}\left(\varepsilon^{(i)}\right)\right\}$

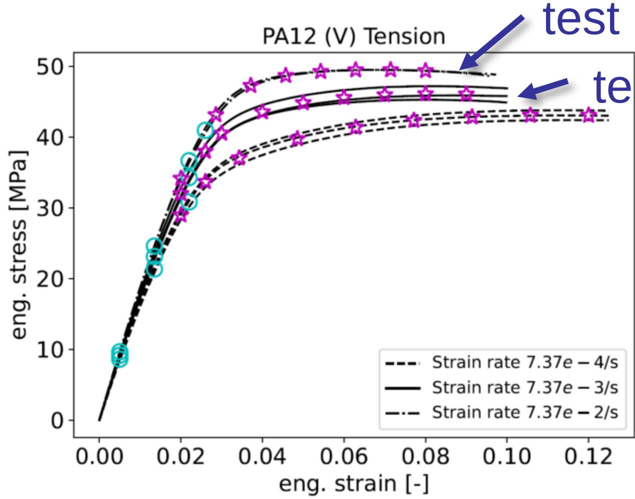

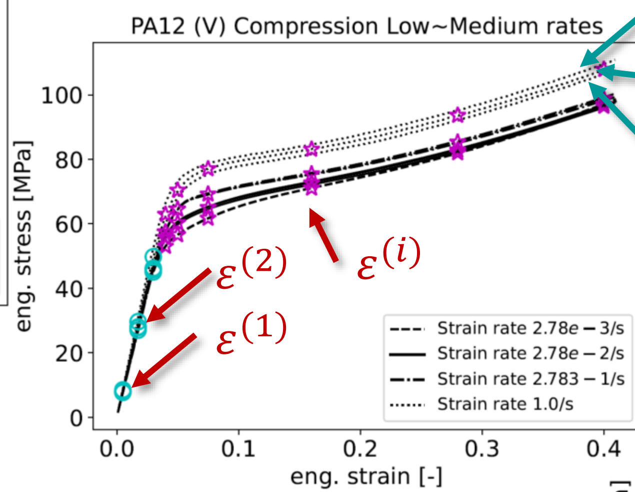

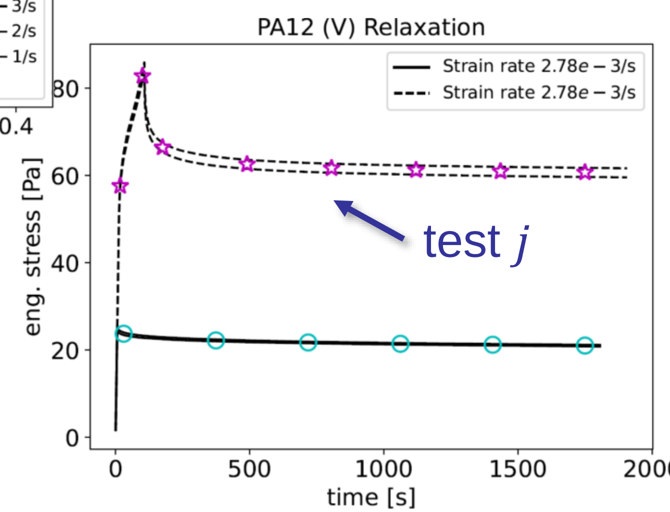

$$\sigma_{\text{exp}}^{(i,j,k)} = \sigma_{\text{model}}^{(i,j)}\left(\boldsymbol{\varepsilon}^{(i)}, \boldsymbol{\vartheta}_{\text{mat}}\right) + \text{noise}^{(i,j)}$$

Follows normal distribution $\mathcal{N}(0, \zeta^2)$

- Bayesian Inference
  - Identify **distribution** of model/model parameters $\boldsymbol{\vartheta}_{\mathrm{mat}}$
  - Use all experimental observations $\boldsymbol{\beta} = (\boldsymbol{\varepsilon}^{(i)}, \boldsymbol{\sigma}_{\mathrm{exp}}^{(\mathrm{test}\ j, \mathrm{repetition}\ k)})$

$$\sigma_{\mathrm{exp}}^{(i,j,k)} = \sigma_{\mathrm{model}}^{(i,j)}\left(\boldsymbol{\varepsilon}^{(i)}, \boldsymbol{\vartheta}_{\mathrm{mat}}\right) + \mathrm{noise}^{(i,j)}$$

Follows normal distribution $\mathcal{N}(0, \zeta^2)$

  - Bayes theorem

What we want

$$\pi_{\mathrm{post}}\left(\boldsymbol{\vartheta}_{\mathrm{mat}} | \boldsymbol{\varepsilon}, \boldsymbol{\sigma}_{\mathrm{exp}}\right) \propto \pi_{\mathrm{likelihood}}\left(\boldsymbol{\sigma}_{\mathrm{exp}} | \boldsymbol{\vartheta}_{\mathrm{mat}}, \boldsymbol{\varepsilon}\right) \pi_{\mathrm{prior}}\left(\boldsymbol{\vartheta}_{\mathrm{mat}}\right)$$

To be evaluated from $\boldsymbol{\sigma}_{\mathrm{model}}^{(i,j)}$ and $\mathrm{noise}^{(i,j)}$

What we know (physical bounds)

$$\pi_{\mathrm{likelihood}}\left(\boldsymbol{\sigma}_{\mathrm{exp}} | \boldsymbol{\vartheta}_{\mathrm{mat}}, \boldsymbol{\varepsilon}\right) = \int \prod_j \prod_i \prod_k \mathcal{N}\left(\left(\boldsymbol{\sigma}_{\mathrm{exp}}^{(j,k)}\left(\varepsilon^{(i)}\right) - \sigma_{\mathrm{model}}^{(i,j)}\left(\boldsymbol{\varepsilon}^{(i)}, \boldsymbol{\vartheta}_{\mathrm{mat}}\right)\right), \zeta^2\right) d\zeta$$

- Material to be inferred:
  - Viscoelastic parameters $\boldsymbol{\vartheta}_{\mathbf{mat}}^{\mathrm{ve}}$: 20 parameters
  - Viscoplastic parameters $\boldsymbol{\vartheta}_{\mathbf{mat}}^{\mathrm{vp}}$: 12 parameters

Posterior remains difficult to be evaluated when the size of $\boldsymbol{\vartheta}_{\mathrm{mat}}$ increases

- Bayes theorem

$$\pi_{\mathrm{post}}(\boldsymbol{\vartheta}_1, \boldsymbol{\vartheta}_2 | \boldsymbol{\beta}_1, \boldsymbol{\beta}_2) \propto \pi_{\mathrm{likelihood}}(\boldsymbol{\beta}_1, \boldsymbol{\beta}_2 | \boldsymbol{\vartheta}_1, \boldsymbol{\vartheta}_2)\, \pi_{\mathrm{prior}}(\boldsymbol{\vartheta}_1, \boldsymbol{\vartheta}_2)$$

$\boldsymbol{\beta}_1, \boldsymbol{\beta}_2$ independent observations

$$\propto \pi_{\mathrm{likelihood}}(\boldsymbol{\beta}_2 | \boldsymbol{\vartheta}_1, \boldsymbol{\vartheta}_2)\, \pi_{\mathrm{likelihood}}(\boldsymbol{\beta}_1 | \boldsymbol{\vartheta}_1, \boldsymbol{\vartheta}_2) \pi_{\mathrm{prior}}(\boldsymbol{\vartheta}_1, \boldsymbol{\vartheta}_2)$$

$\boldsymbol{\vartheta}_1, \boldsymbol{\vartheta}_2$ independent prior distribution

$$\propto \pi_{\mathrm{likelihood}}(\boldsymbol{\beta}_2 | \boldsymbol{\vartheta}_1, \boldsymbol{\vartheta}_2) \pi_{\mathrm{prior}}(\boldsymbol{\vartheta}_2) \pi_{\mathrm{likelihood}}(\boldsymbol{\beta}_1 | \boldsymbol{\vartheta}_1, \boldsymbol{\vartheta}_2) \pi_{\mathrm{prior}}(\boldsymbol{\vartheta}_1)$$

$\boldsymbol{\beta}_1, \boldsymbol{\vartheta}_2$ independent distribution

$$\propto \pi_{\mathrm{likelihood}}(\boldsymbol{\beta}_2 | \boldsymbol{\vartheta}_1, \boldsymbol{\vartheta}_2) \pi_{\mathrm{prior}}(\boldsymbol{\vartheta}_2) \pi_{\mathrm{likelihood}}(\boldsymbol{\beta}_1 | \boldsymbol{\vartheta}_1) \pi_{\mathrm{prior}}(\boldsymbol{\vartheta}_1)$$

$$\pi_{\mathrm{post}}(\boldsymbol{\vartheta}_1 | \boldsymbol{\beta}_1) \propto$$

- Observations $\boldsymbol{\beta} = (\boldsymbol{\varepsilon}, \boldsymbol{\sigma}_{\mathrm{exp}})$

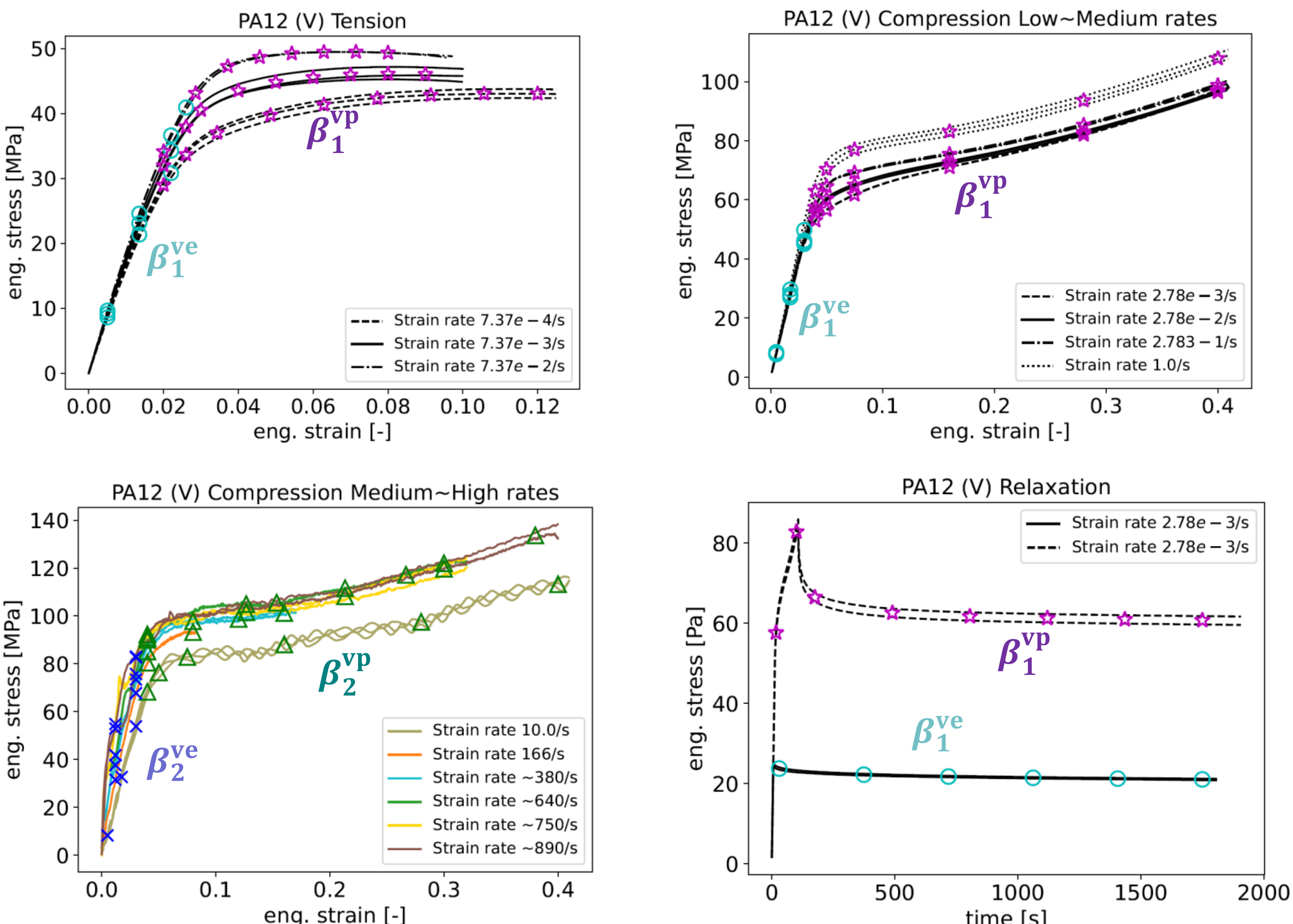

Sequential Bayesian Inference of complex model parameters

- Bayesian inference in sequence
  - $\boldsymbol{\beta} = [\boldsymbol{\beta}^{\mathbf{ve}}, \boldsymbol{\beta}^{\mathrm{vp}}]$, $\boldsymbol{\beta}^{\mathbf{ve}} = [\boldsymbol{\beta}_1^{\mathbf{ve}}, \boldsymbol{\beta}_2^{\mathbf{ve}}]$, $\boldsymbol{\beta}^{\mathrm{vp}} = [\boldsymbol{\beta}_1^{\mathrm{vp}}, \boldsymbol{\beta}_2^{\mathrm{vp}}]$
  - Observations $\boldsymbol{\beta}_1^{\mathbf{ve}}$, $\boldsymbol{\beta}_2^{\mathbf{ve}}$, $\boldsymbol{\beta}_1^{\mathrm{vp}}$, $\boldsymbol{\beta}_2^{\mathrm{vp}}$ are used in sequence

Viscoelastic parameters $\boldsymbol{\vartheta}_{\mathbf{mat}}^{\mathbf{ve}}$		
BI step	I	II
Observation	$\boldsymbol{\beta}_1^{\mathbf{ve}}$, cyan circle	$\boldsymbol{\beta}_2^{\mathbf{ve}}$, blue “x”
Likelihood	$\pi(\boldsymbol{\beta}_1^{\mathbf{ve}} \mid \boldsymbol{\vartheta}^{\mathrm{ve}})$	$\pi(\boldsymbol{\beta}_2^{\mathbf{ve}} \mid \boldsymbol{\vartheta}^{\mathrm{ve}})$
Prior	$\pi_{\mathrm{prior}}(\boldsymbol{\vartheta}^{\mathrm{ve}})$	$\pi_{\mathrm{post}}(\boldsymbol{\vartheta}^{\mathrm{ve}} \mid \boldsymbol{\beta}_1^{\mathbf{ve}})$
Posterior	$\pi_{\mathrm{post}}(\boldsymbol{\vartheta}^{\mathrm{ve}} \mid \boldsymbol{\beta}_1^{\mathbf{ve}})$	$\pi_{\mathrm{post}}(\boldsymbol{\vartheta}^{\mathrm{ve}} \mid \boldsymbol{\beta}^{\mathrm{ve}})$

Viscoplastic parameters $\boldsymbol{\vartheta}_{\mathbf{mat}}^{\mathrm{vp}}$		
BI step	III	IV
Observation	$\boldsymbol{\beta}_1^{\mathbf{vp}}$, magenta star	$\boldsymbol{\beta}_2^{\mathbf{vp}}$, green triangle
Likelihood	$\pi\left(\boldsymbol{\beta}_1^{\mathbf{vp}} \mid \boldsymbol{\vartheta}^{\mathrm{ve}}, \boldsymbol{\vartheta}^{\mathrm{vp}}\right)$	$\pi\left(\boldsymbol{\beta}_2^{\mathbf{vp}} \mid \boldsymbol{\vartheta}^{\mathrm{ve}}, \boldsymbol{\vartheta}^{\mathrm{vp}}\right)$
Prior	$\pi_{\mathrm{prior}}(\boldsymbol{\vartheta}^{\mathrm{vp}})\pi_{\mathrm{post}}(\boldsymbol{\vartheta}^{\mathrm{ve}} \mid \boldsymbol{\beta}^{\mathrm{ve}})$	$\pi_{\mathrm{post}}\left(\boldsymbol{\vartheta}^{\mathrm{ve}}, \boldsymbol{\vartheta}^{\mathrm{vp}} \mid \boldsymbol{\beta}^{\mathrm{ve}}, \boldsymbol{\beta}_1^{\mathbf{vp}}\right)$
Posterior	$\pi_{\mathrm{post}}\left(\boldsymbol{\vartheta}^{\mathrm{ve}}, \boldsymbol{\vartheta}^{\mathrm{vp}} \mid \boldsymbol{\beta}^{\mathrm{ve}}, \boldsymbol{\beta}_1^{\mathbf{vp}}\right)$	$\pi_{\mathrm{post}}(\boldsymbol{\vartheta}^{\mathrm{ve}}, \boldsymbol{\vartheta}^{\mathrm{vp}} \mid \boldsymbol{\beta}^{\mathrm{ve}}, \boldsymbol{\beta}^{\mathrm{vp}})$

Sequential Bayesian Inference of complex model parameters

- Markov-Chain process

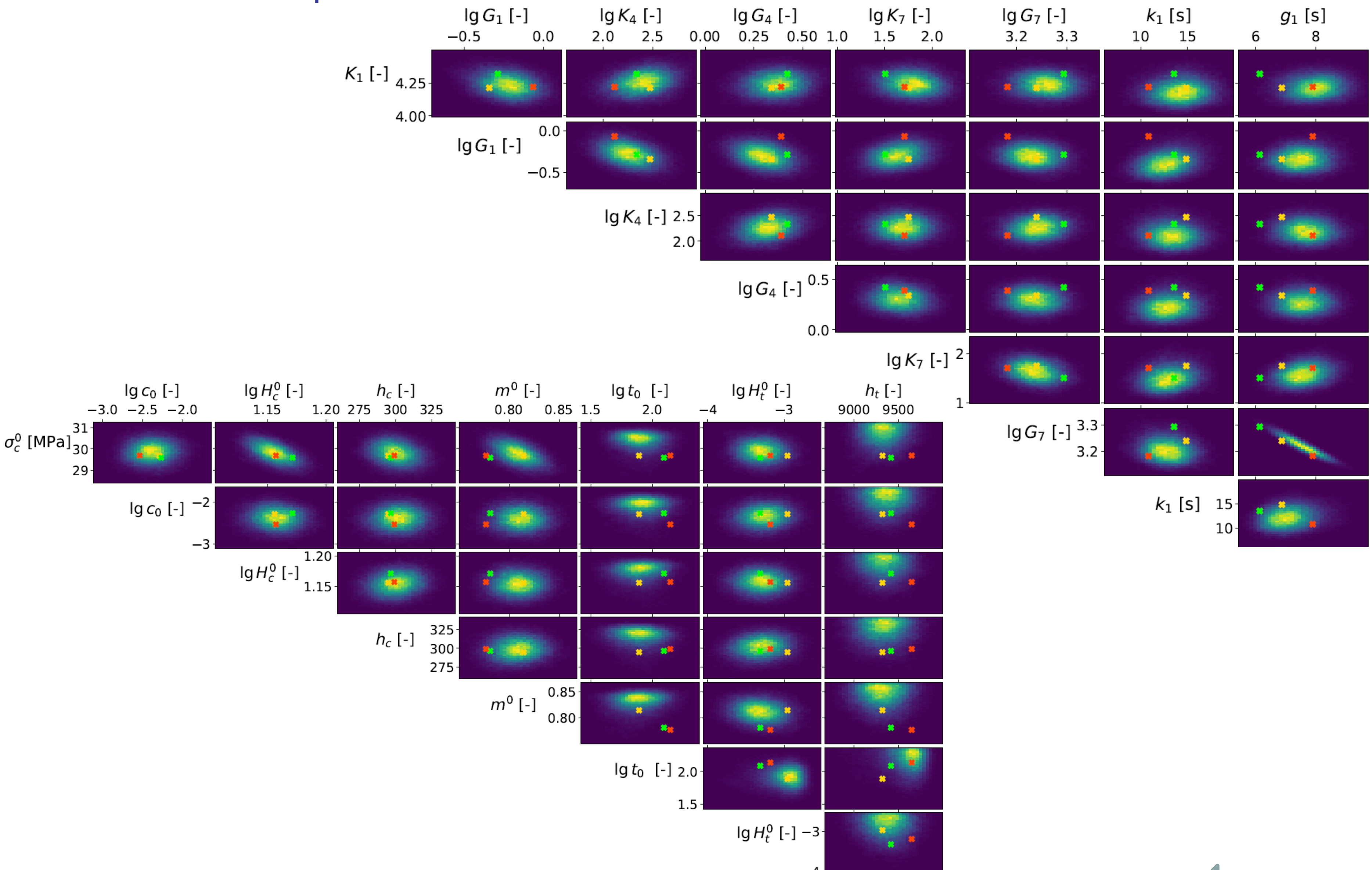

Beginning

Sequential Bayesian Inference of complex model parameters

- Validation for different parameter $\boldsymbol{\vartheta}_{\mathrm{mat}}$ realisations

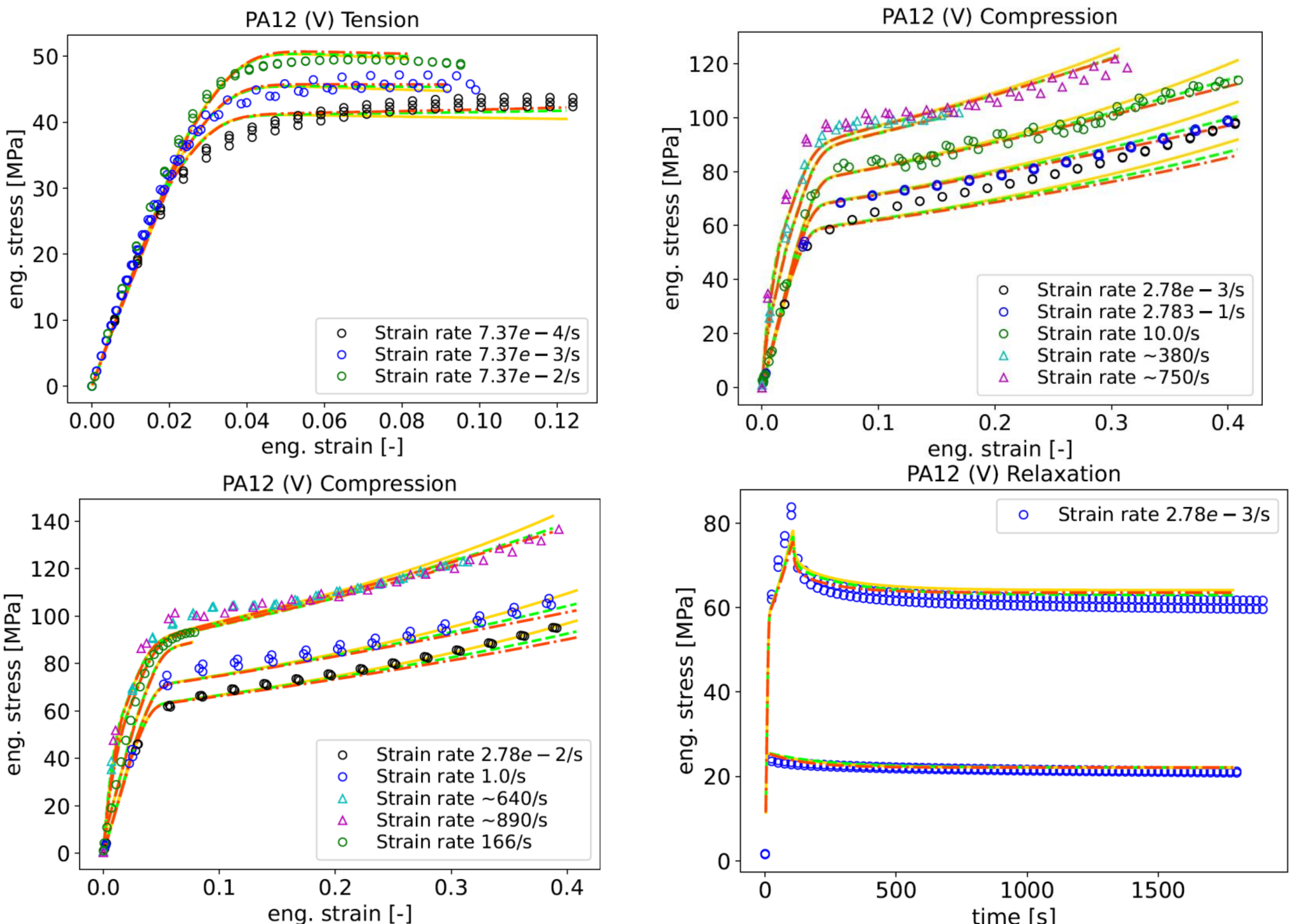

Sequential Bayesian Inference of complex model parameters

- Validation for a given material parameter $\boldsymbol{\vartheta}_{\mathrm{mat}}$ realisation

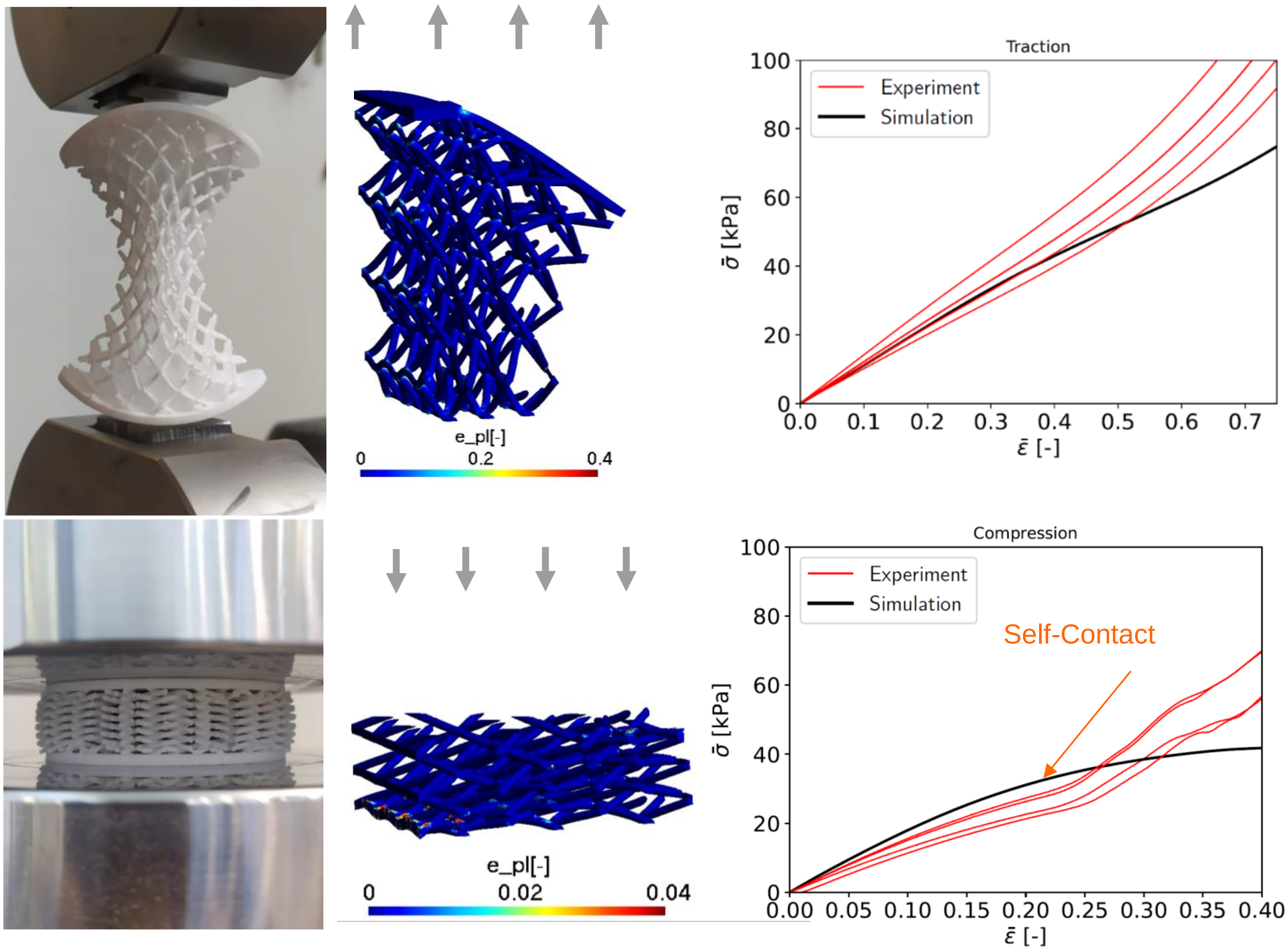

IMDEA-
cirp GmbH

Sequential Bayesian Inference of complex model parameters

- MOAMMM FET-OPEN project (https://www.moammm.eu/)
  - ULiège, UCL (Belgium)
  - IMDEA Materials (Spain)
  - JKU (Austria)
  - cirp GmbH (Germany)

- Publication (doi)
  - 10.2139/ssrn.4457392
    - Open Data: 10.5281/zenodo.7998798

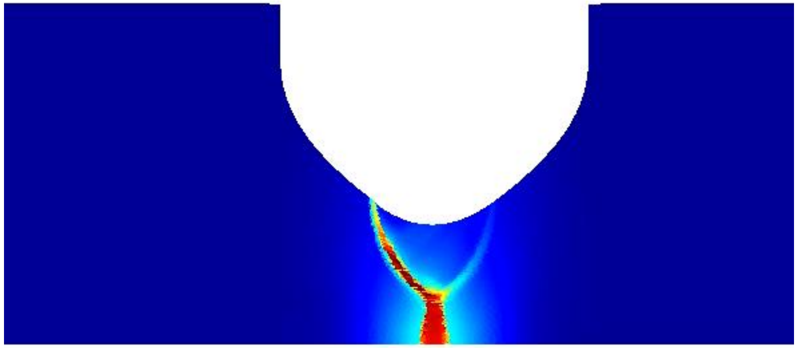

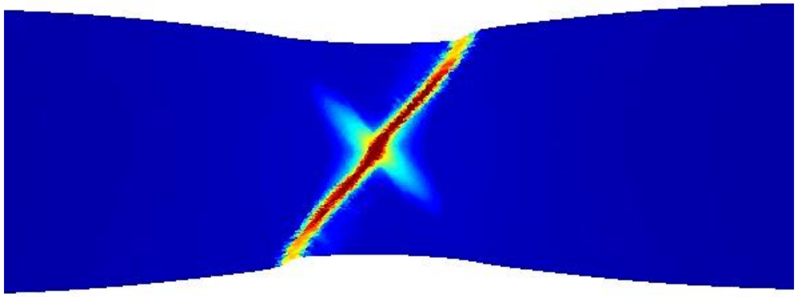

Shear and necking coalescence mechanisms for porous materials

The research has been funded by the Walloon Region under the agreement no. 1610154- EntroTough in the context of the 2016 WalInnov call

Shear and necking coalescence mechanisms for porous materials

- Objective:
  - To develop a non-local ductile failure model accounting for complex loading stress states
- Porous plasticity

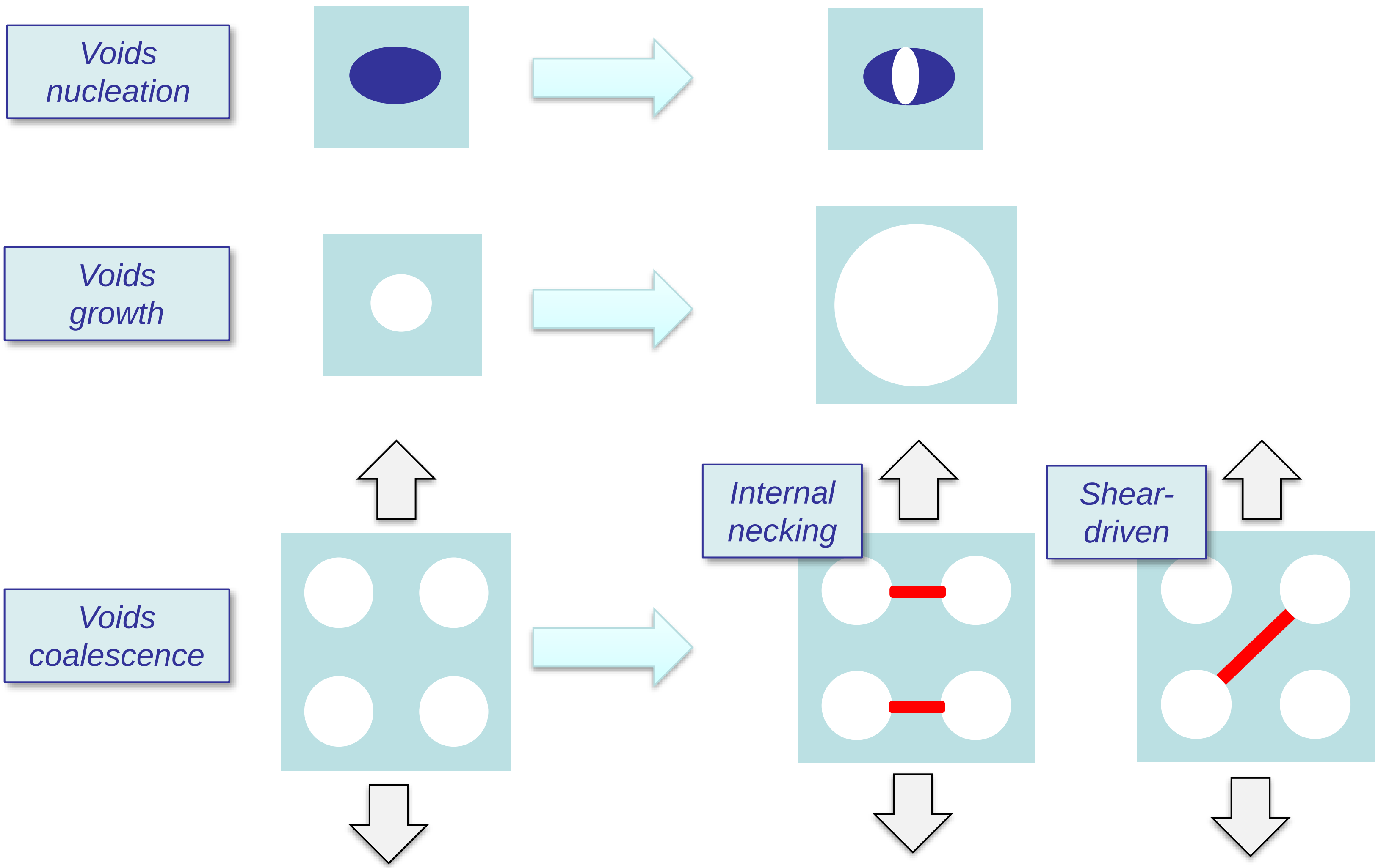

Shear and necking coalescence mechanisms for porous materials

- Ductile failure: stress-state dependent fracture strain
  - Stress triaxiality dependent

$$\eta = \frac{p'}{\sigma_{eq}} \in]-\infty\ \infty[\qquad p = \frac{\mathrm{tr}\,(\boldsymbol{\sigma})}{3} \qquad \sigma_{eq} = \sqrt{\frac{3}{2}\mathrm{dev}(\boldsymbol{\sigma}):\mathrm{dev}(\boldsymbol{\sigma})}$$

  - Lode dependent

$$\theta = \frac{1}{3}\arccos\left(\frac{27 J_3}{2{\sigma_{eq}}^3}\right) \qquad J_3 = \det(\mathrm{dev}(\boldsymbol{\sigma})\,)$$

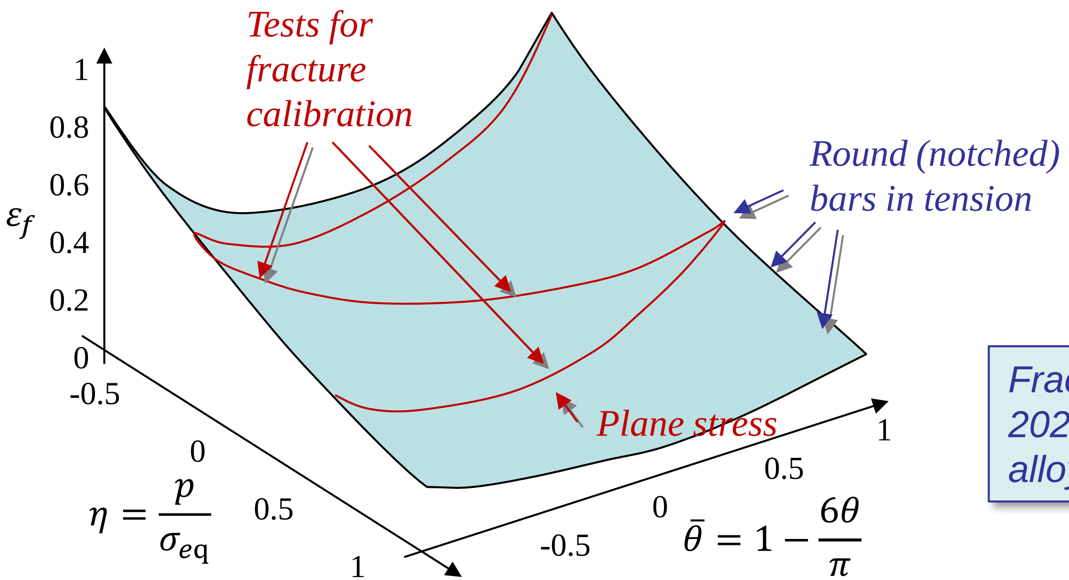

Fracture locus for 2024-T351 aluminum alloy

(Bai & Wierzbicki 2010)

Shear and necking coalescence mechanisms for porous materials

- Hyperelastic-based formulation
  - Multiplicative decomposition
    $\mathbf{F} = \mathbf{F}^{\mathrm{e}} \cdot \mathbf{F}^{\mathrm{p}}, \quad \mathbf{C}^{\mathrm{e}} = \mathbf{F}^{\mathrm{e}^T} \cdot \mathbf{F}^{\mathrm{e}}, \quad J^{e} = \det(\mathbf{F}^{\mathrm{e}})$
  - Stress tensor definition
    - Elastic potential $\psi(\mathbf{C}^{\mathrm{e}})$
    - First Piola-Kirchhoff stress tensor
      $$\mathbf{P} = 2\mathbf{F}^{\mathrm{e}} \cdot \frac{\partial \psi(\mathbf{C}^{\mathrm{e}})}{\partial \mathbf{C}^{\mathrm{e}}} \cdot \mathbf{F}^{\mathrm{p}^{-T}}$$
    - Kirchhoff stress tensors
      - In current configuration
        $$\boldsymbol{\kappa} = \mathbf{P} \cdot \mathbf{F}^{T} = 2\mathbf{F}^{\mathrm{e}} \cdot \frac{\partial \psi(\mathbf{C}^{\mathrm{e}})}{\partial \mathbf{C}^{\mathrm{e}}} \cdot \mathbf{F}^{\mathrm{e}^T}$$
      - In co-rotational space
        $$\boldsymbol{\tau} = \mathbf{C}^{\mathrm{e}} \cdot \mathbf{F}^{\mathrm{e}^{-1}} \cdot \boldsymbol{\kappa} \cdot \mathbf{F}^{\mathrm{e}^{-T}} = 2\mathbf{C}^{\mathrm{e}} \cdot \frac{\partial \psi(\mathbf{C}^{\mathrm{e}})}{\partial \mathbf{C}^{\mathrm{e}}}$$
- Logarithmic deformation
  - Elastic potential ψ:
    $$\psi(\mathbf{C}^{\mathrm{e}}) = \frac{K}{2}\ln^2(J^{e}) + \frac{G}{4}(\ln(\mathbf{C}^{\mathrm{e}}))^{\mathrm{dev}} : (\ln(\mathbf{C}^{\mathrm{e}}))^{\mathrm{dev}}$$
  - Stress tensor in co-rotational space
    $$\boldsymbol{\tau} = \underbrace{K\ln(J^{e})}_{p}\,\mathbf{I} + G(\ln(\mathbf{C}^{\mathrm{e}}))^{\mathrm{dev}}$$

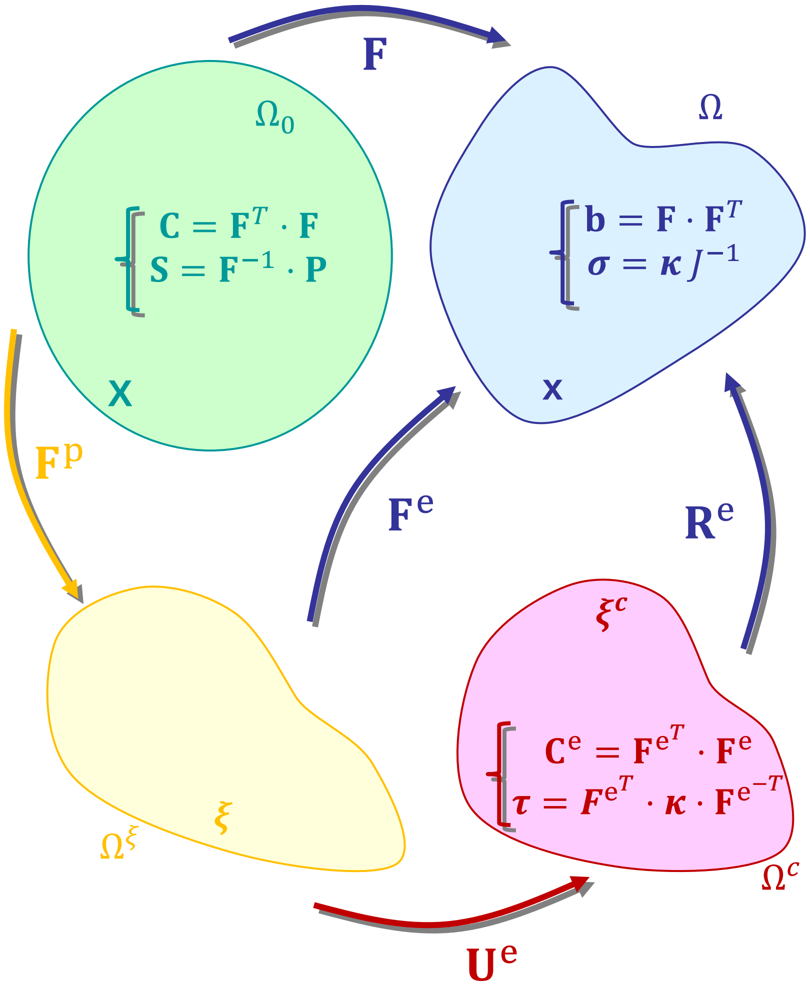

Shear and necking coalescence mechanisms for porous materials

- Material changes represented via internal variables
  - Constitutive law $\boldsymbol{\sigma}\left(\boldsymbol{\varepsilon}; \boldsymbol{Z}(t')\right)$
  - Internal variables $\boldsymbol{Z}(t')$
    - Plastic flow normal to yield surface Φ

$$\mathbf{D}^{\mathrm{p}} = \dot{\mathbf{F}}^{\mathrm{p}}\mathbf{F}^{\mathrm{p}-1} = \dot{\mu}\frac{\partial\Phi}{\partial\boldsymbol{\sigma}}$$

    - Matrix plastic strain rate $\dot{\varepsilon}_m = \dfrac{\boldsymbol{\sigma}:\mathbf{D}^{\mathrm{p}}}{(1-f)\sigma_Y}$
    - Volumetric plastic deformation $\dot{\varepsilon}_v = \mathrm{tr}\left(\mathbf{D}^{\mathrm{p}}\right)$
    - Deviatoric plastic deformation $\dot{\varepsilon}_d = \sqrt{\dfrac{2}{3}\mathrm{dev}(\mathbf{D}^{\mathrm{p}}):\mathrm{dev}(\mathbf{D}^{\mathrm{p}})}$
  - Voids characteristics **Y**
    - Porosity : f
    - Void ligament ratio: χ
    - Void aspect ratio: W
    - Void spacing ratio: λ

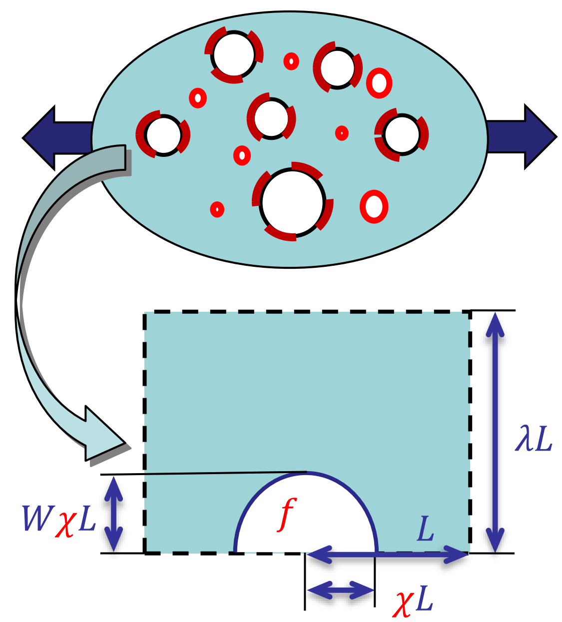

Shear and necking coalescence mechanisms for porous materials

- Non-local formalism
  - Local form
    - Mesh dependency
  - Requires non-local form [Bažant 1988]
    - Introduction of characteristic length l_c
    - Weighted average: $\tilde{Z}_k(\boldsymbol{x}) = \int_{V_C} W(\boldsymbol{y};\boldsymbol{x},l_c)\; Z_k(\mathbf{y})d\boldsymbol{y}$
  - Implicit form [Peerlings et al. 1998]
    - New degrees of freedom: $\tilde{Z}_k$
    - New Helmholtz-type equations: $\tilde{Z}_k - l_c^2\,\Delta\tilde{Z}_k = Z_k$
  - Constitutive law $\boldsymbol{\sigma}\left(\boldsymbol{\varepsilon},\widetilde{\boldsymbol{Z}}(t');\boldsymbol{Z}(t')\right)$

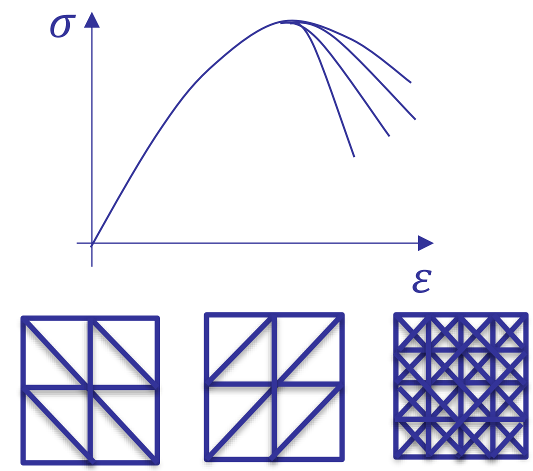

The numerical results change without convergence

- Non-local multi-mechanisms

$$\begin{cases} \dot{\varepsilon}_m = \dfrac{\boldsymbol{\sigma}:\mathbf{D}^{\mathrm{p}}}{(1-f)\sigma_Y} \\ \dot{\varepsilon}_v = \mathrm{tr}\,(\mathbf{D}^{\mathrm{p}}) \\ \dot{\varepsilon}_d = \sqrt{\dfrac{2}{3}\mathrm{dev}(\mathbf{D}^{\mathrm{p}}):\mathrm{dev}(\mathbf{D}^{\mathrm{p}})} \end{cases} \Rightarrow \begin{cases} \tilde{\varepsilon}_m - l_c^2\,\Delta\tilde{\varepsilon}_m = \varepsilon_m \\ \tilde{\varepsilon}_v - l_c^2\,\Delta\tilde{\varepsilon}_v = \varepsilon_v \\ \tilde{\varepsilon}_d - l_c^2\,\Delta\tilde{\varepsilon}_d = \varepsilon_d \end{cases}$$

Shear and necking coalescence mechanisms for porous materials

- Different yield surfaces: void growth
  - Classical GTN model
    - Non-local porosity evolution

$$\dot{f} = \dot{f}_{\text{gr}} + \dot{f}_{\text{nu}} + \dot{f}_{\text{sh}}$$

$$\begin{cases} \dot{f}_{\text{gr}} = (1-f)\dot{\tilde{\varepsilon}}_v \\ \dot{f}_{\text{nu}} = A_n(\tilde{\varepsilon}_m)\dot{\tilde{\varepsilon}}_m \\ \dot{f}_{\text{sh}} = k_w \phi_\eta\left(\dfrac{p}{\sigma_{\text{eq}}}\right)\phi_\omega(\cos 3\theta) f \dot{\tilde{\varepsilon}}_d \end{cases}$$

    - Yield surface

$$\phi_{\text{G}} = \frac{\sigma_{\text{eq}}^2}{\sigma_{\text{Y}}^2} + 2q_1 f \cosh\left(\frac{q_2 p}{2\sigma_{\text{Y}}}\right) - 1 - q_3^2 f^2 \leq 0$$

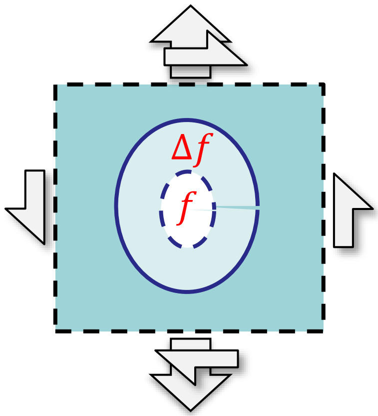

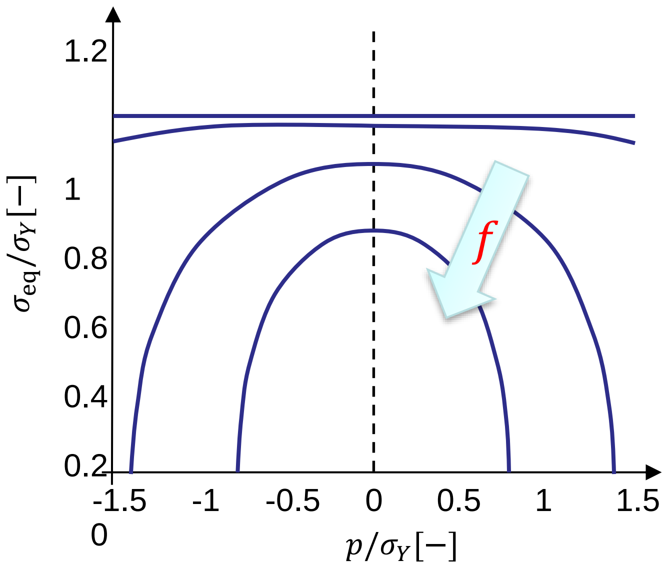

Shear and necking coalescence mechanisms for porous materials

- Different yield surfaces: coalescence
  - Coalescence by necking
    - Yield surface

$$\phi_{\mathrm{T}} = \frac{2}{3}\sigma_{\mathrm{eq}}\cos\theta + |p| - C_{\mathrm{T}}^{f}(\chi, \mathrm{W})\sigma_{\mathrm{Y}} \leq 0$$

Max Principal Stress

    - Limit load factor

$$C_{\mathrm{T}}^{f}(\chi, W) = (1-\chi^2)\left[h\left(\frac{1-\chi}{W\chi}\right)^2 + g\sqrt{\frac{1}{\chi}}\right]$$

    - Cavities evolution

$$\begin{cases} \dot{\lambda} = \kappa\lambda\dot{\hat{\varepsilon}}_d \\ \dot{\chi} = \dfrac{3\lambda}{4W}\left(\dfrac{3}{2\chi^2} - 1\right)\dot{\hat{\varepsilon}}_d \\ \dot{W} = \dfrac{9\lambda}{4\chi}\left(1 - \dfrac{1}{2\chi^2}\right)\dot{\hat{\varepsilon}}_d \\ \dot{f} = f\left(\dfrac{3\dot{\chi}}{\chi} + \dfrac{\dot{W}}{W} - \dfrac{\dot{\lambda}}{\lambda}\right) \end{cases}$$

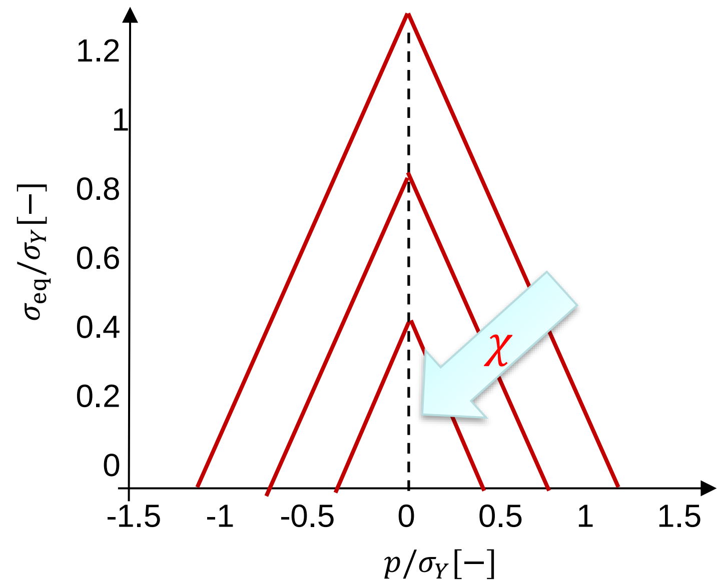

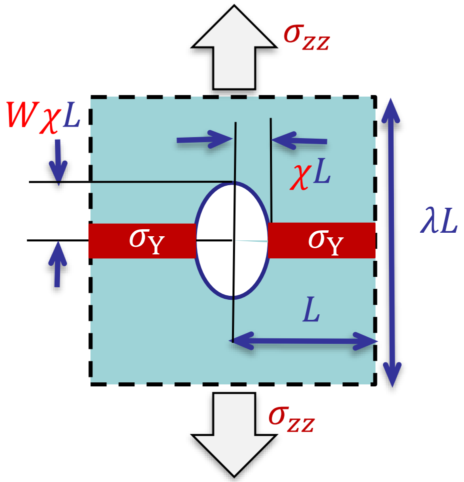

Shear and necking coalescence mechanisms for porous materials

- Different yield surfaces: coalescence
  - Coalescence by shearing
    - Yield surface

$$\phi_{\mathrm{T}} = \frac{2}{3}\sigma_{\mathrm{eq}}\cos\theta + |p| - C_{\mathrm{T}}^{f}(\chi, \mathrm{W})\sigma_{\mathrm{Y}} \leq 0$$

Max Principal Stress

    - Limit load factor

$$C_{\mathrm{T}}^{f}(\chi, W) = (1-\chi^2)\left[h\left(\frac{1-\chi}{W\chi}\right)^2 + g\sqrt{\frac{1}{\chi}}\right]$$

    - Cavities evolution

$$\begin{cases} \dot{\chi} = K_{\chi}\dot{\bar{\varepsilon}}_d \\ \dot{\lambda} = 3\lambda\dfrac{\dot{\chi}}{\chi} \\ \dot{W} = 0 \\ \dot{f} = 0 \end{cases}$$

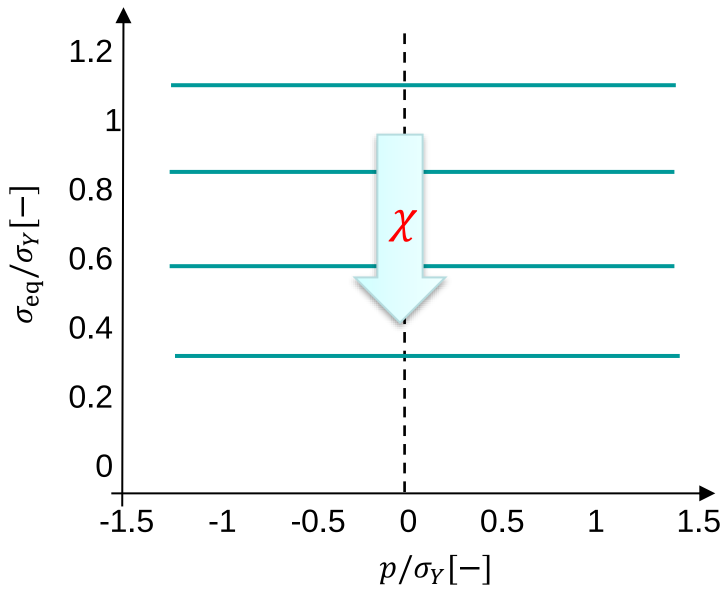

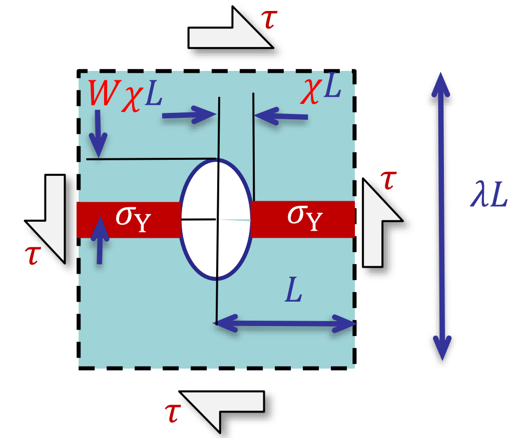

Shear and necking coalescence mechanisms for porous materials

- Multi-surface model
  - Effective yield surface

$$\phi_{\mathrm{e}} = \begin{pmatrix} (\phi_{\mathrm{G}}+1)^m + \\ (\phi_{\mathrm{T}}+1)^m + \\ (\phi_{\mathrm{S}}+1)^m \end{pmatrix}^{1/m}$$

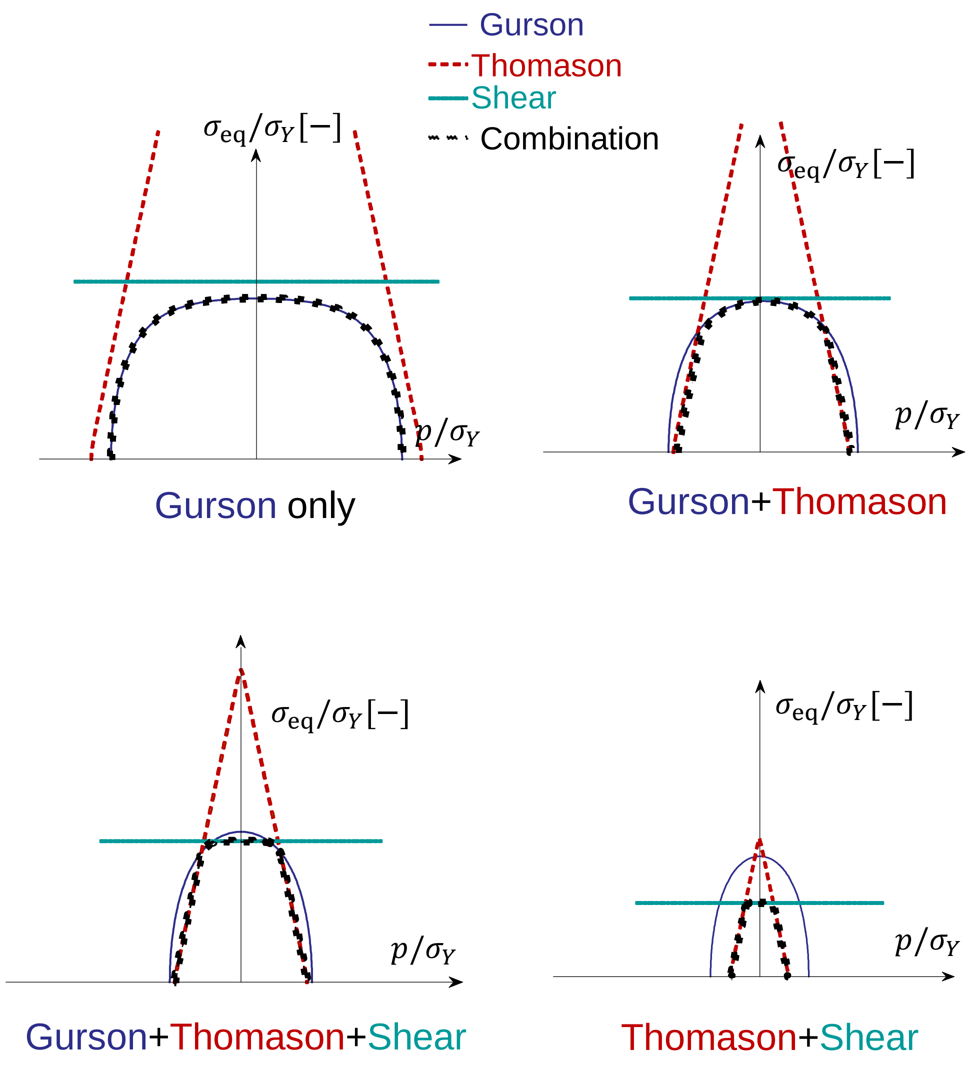

Shear and necking coalescence mechanisms for porous materials

- Solution under proportional loadings
  - Constant
    - Stress triaxiality ($\frac{p}{\sigma_{\text{eq}}}$); and
    - Normalized Lode angle ($\bar{\theta} = 1 - \frac{6\theta}{\pi}$)
  - ε_{dc}- ductility = plastic deformation at coalescence onset

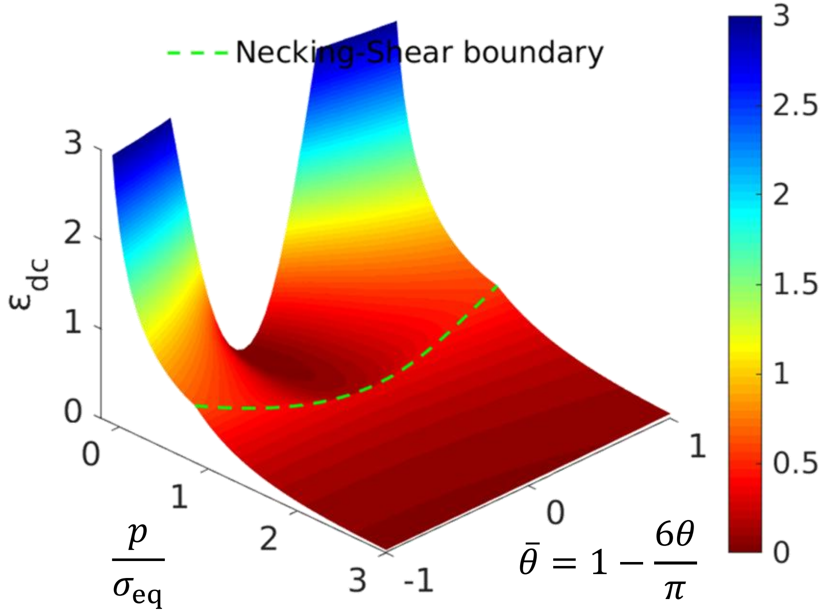

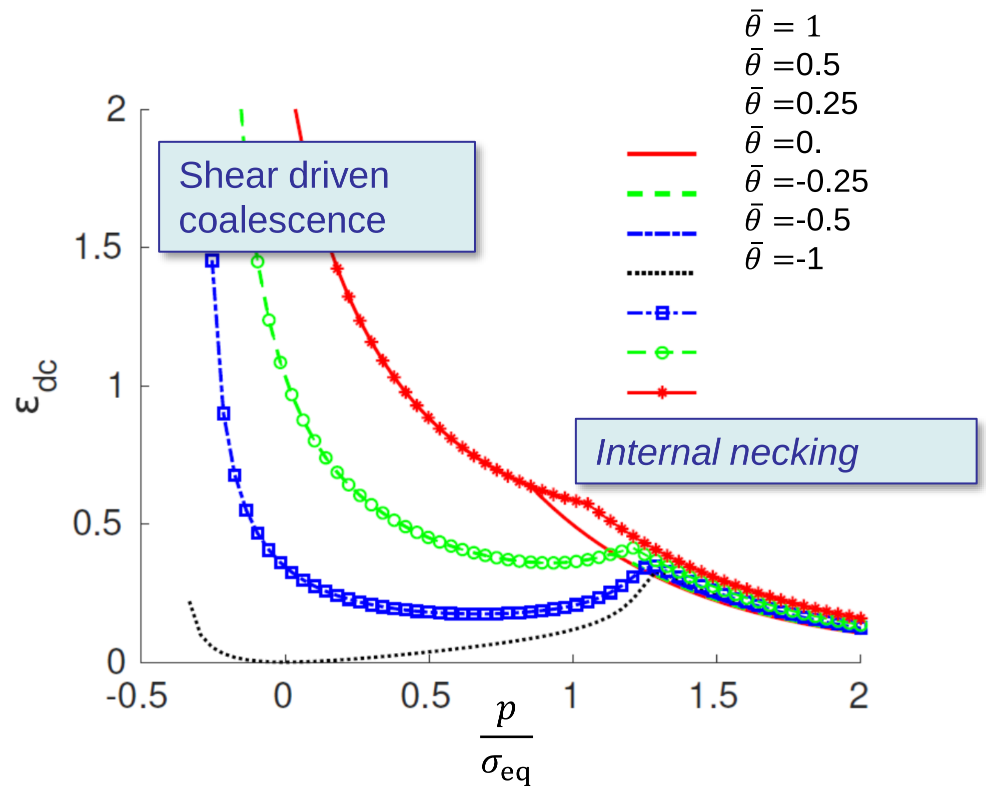

Shear and necking coalescence mechanisms for porous materials

- Plane strain smooth specimen under tensile loading
  - Verification of the nonlocal model: mesh convergence

$L = 12.5$ mm
$e_0 = 3$ mm
$\xi = 1.015$ ($\varepsilon_{ds} = 0.95$)

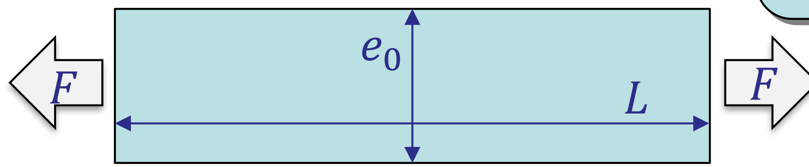

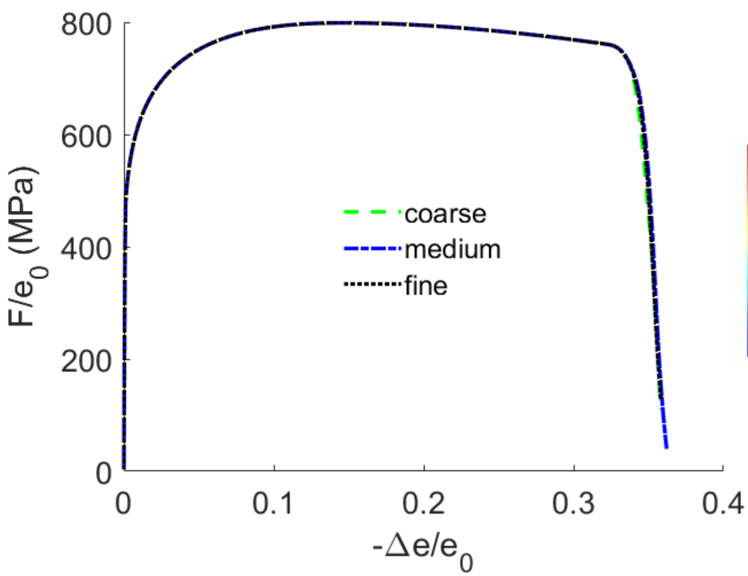

Distribution of void ligament ratio χ

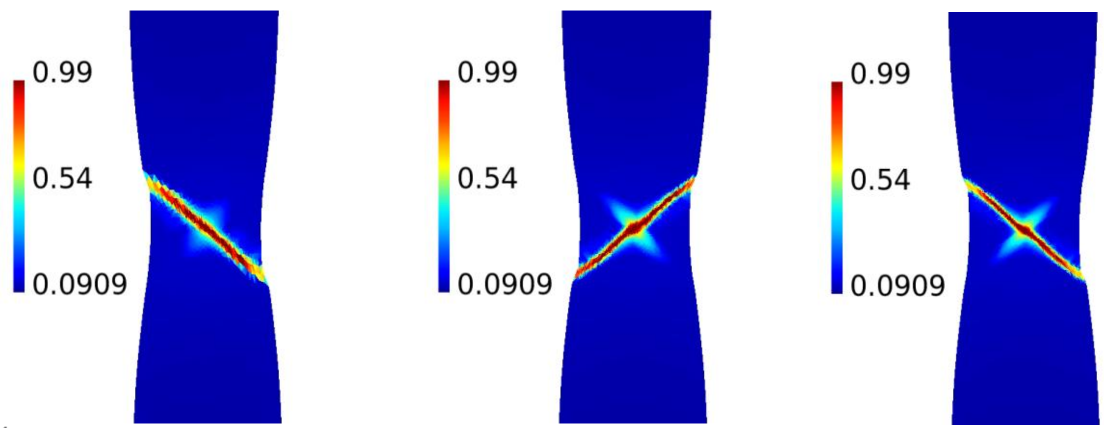

Coarse　Medium　Fine

Capture slant fracture

Shear and necking coalescence mechanisms for porous materials

- Plane strain smooth specimen under tensile loading
  - Effect of ξ

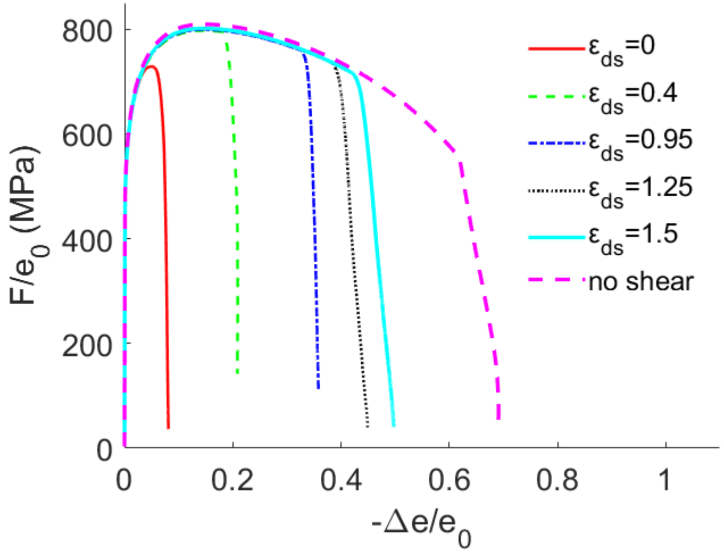

$L = 12.5$ mm
$e_0 = 3$ mm

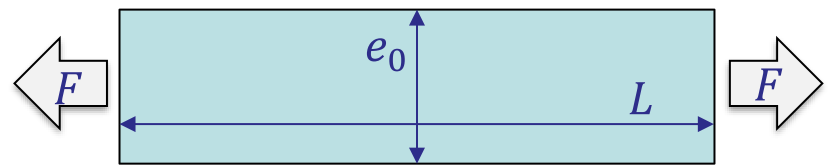

Distribution of void ligament ratio χ

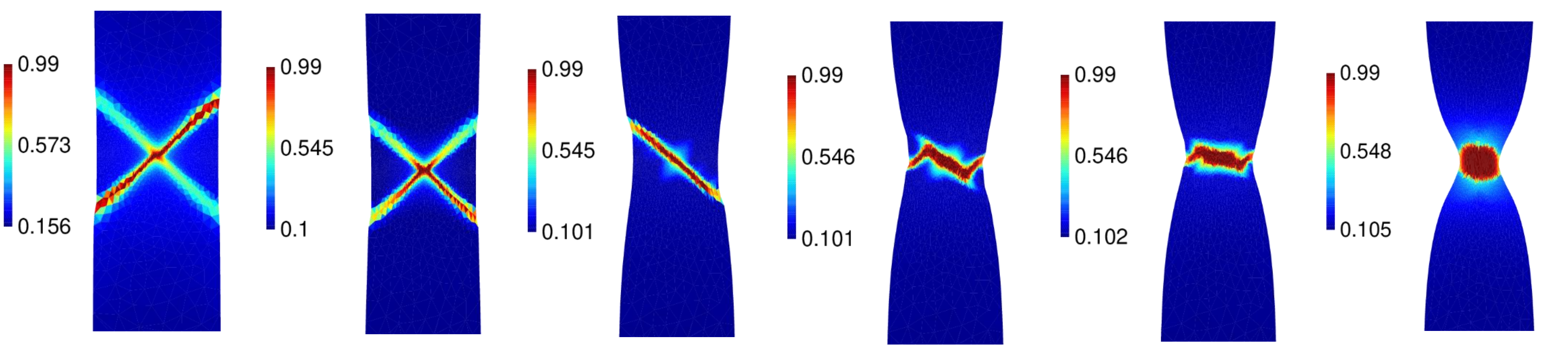

$\varepsilon_{ds} = 0$ | $\varepsilon_{ds} = 0.4$ | $\varepsilon_{ds} = 0.95$ | $\varepsilon_{ds} = 1.25$ | $\varepsilon_{ds} = 1.5$ | no shear

Shear and necking coalescence mechanisms for porous materials

- Axisymmetric (notched) specimens under tensile loading
  - Different notch radii: $R_0/R_n = 0, 0.2, 0.6, 1, 1.5$

$R_0 = 3$ mm
$R_1 = 6$ mm
$L = 25$ mm
$\xi = 1.015$ ($\varepsilon_{ds} = 0.95$)

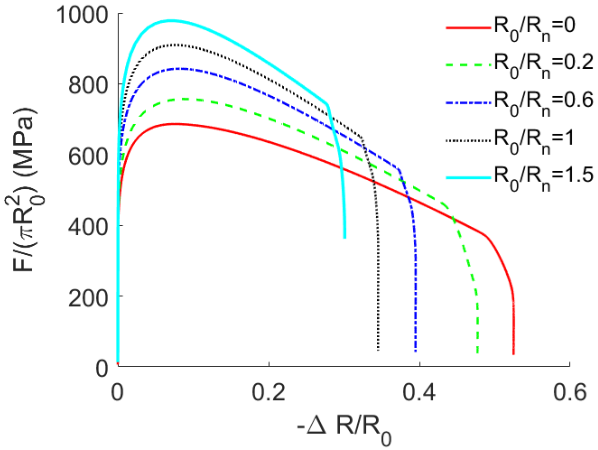

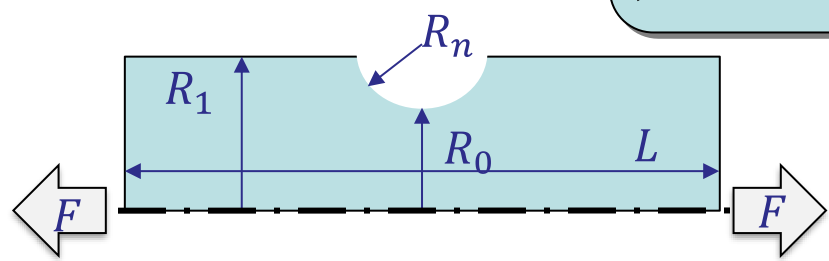

Distribution of void ligament ratio χ

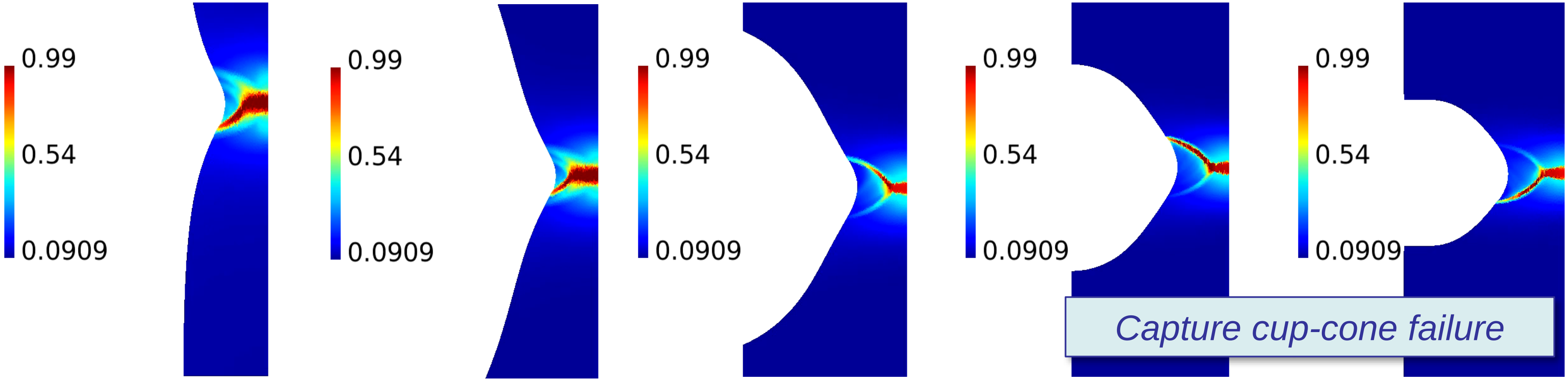

Shear and necking coalescence mechanisms for porous materials

- EntroTough WalInnov project
  - UCL, ULB, ULiege (Belgium)
- Publication (doi)
  - 10.1016/j.jmps.2020.103891
  - 10.1016/j.engfracmech.2022.108844

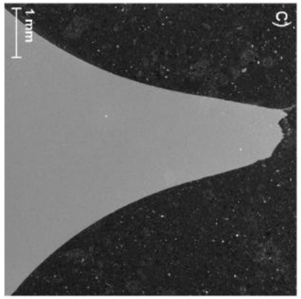

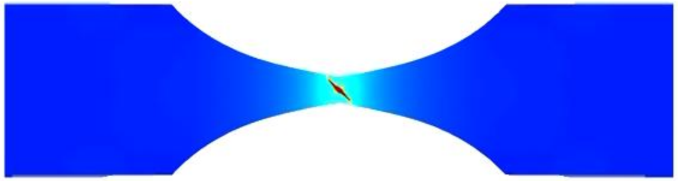

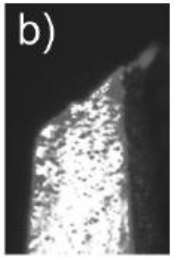

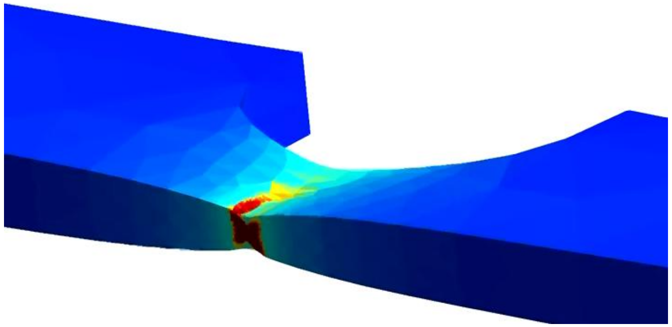

Ductile failure of High-Entropy Alloys (HEA)

The research has been funded by the Walloon Region under the agreement no. 1610154- EntroTough in the context of the 2016 WalInnov call

- Design of experimental campaign on CoCrNi ternary HEA
  - Cover wide range of stress states
    - Triaxiality $\eta = \frac{p}{\sigma_{eq}}$
    - Lode angle: $\theta = \frac{1}{3}\arccos\left(\frac{27\det(\mathrm{dev}(\boldsymbol{\sigma}))}{2{\sigma_{eq}}^3}\right)$

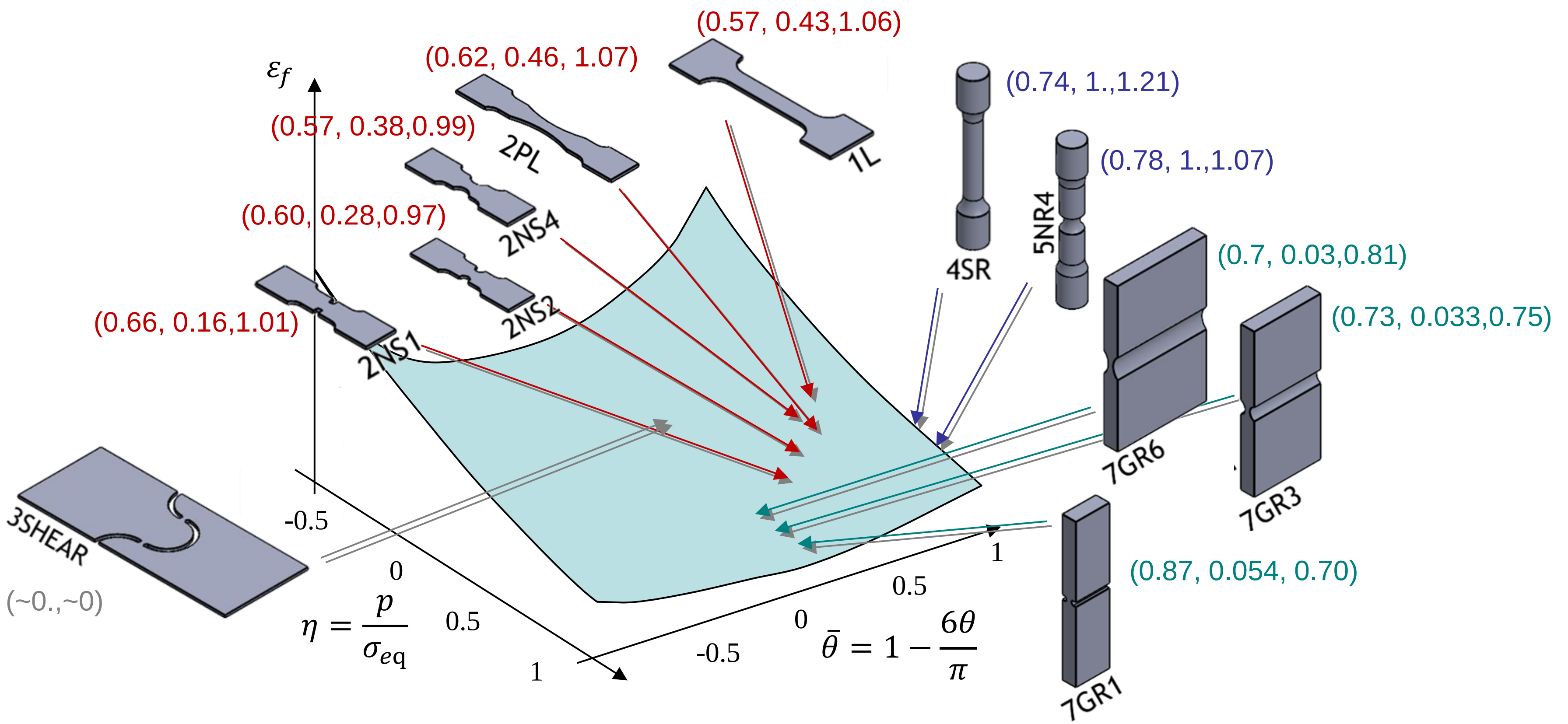

Beginning

- Identification methodology
  - Porosity evolution
    - No initial porosity
    - Fast nucleation from defects

      ⇒ assume initial f_0
    - Evolution from 2PL

      ⇒ $f_0 = 0.002$
  - Non-local lengths
    - From intervoid spacing

$$\begin{cases} \tilde{\varepsilon}_m - l_c^2\, \Delta\tilde{\varepsilon}_m = \varepsilon_m \\ \tilde{\varepsilon}_v - l_c^2\, \Delta\tilde{\varepsilon}_v = \varepsilon_v \\ \tilde{\varepsilon}_d - l_c^2\, \Delta\tilde{\varepsilon}_d = \varepsilon_d \end{cases}$$

⇒ $l_c = 40\ \mu\text{m}$

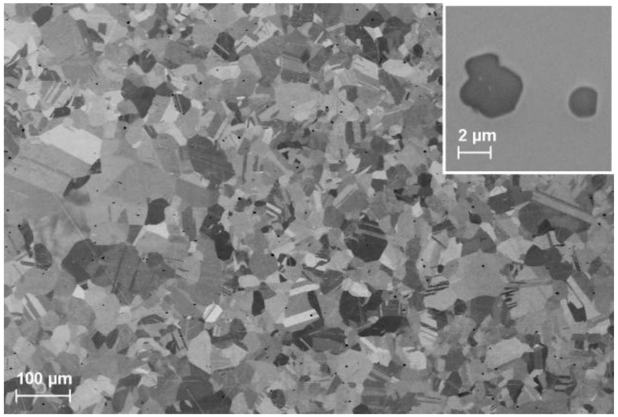

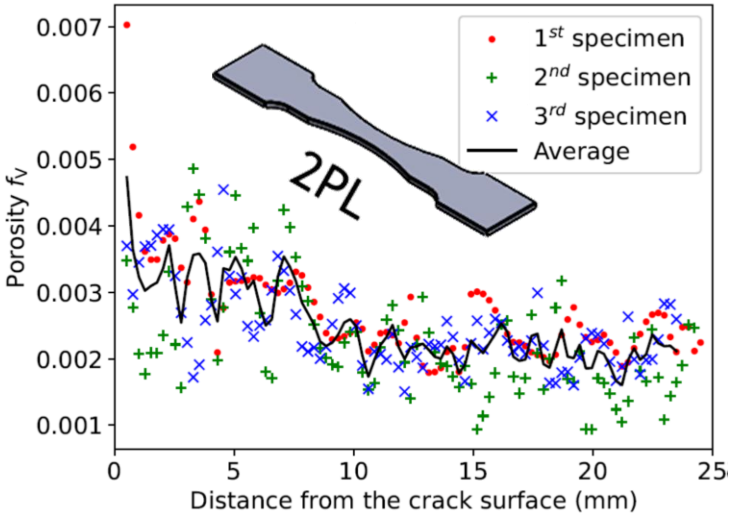

SEM images by A. Hillhorst, UCL

Ductile failure of High-Entropy Alloys (HEA)

- Identification methodology
  - Elasto-plastic matrix
    - Yield surface
      $$\phi_G = \frac{\sigma_{eq}^2}{\sigma_Y^2} + 2q_1 f \cosh\left(\frac{q_2 p}{2\sigma_Y}\right) - 1 - q_3^2 f^2 \leq 0$$
    - Do not consider porosity evolution $f \sim f_0 \sim 0$
    - Hardening law from 1L and 5NR4 samples :

$$\sigma_Y = \begin{cases} \sigma_Y^0 + h_1\varepsilon_m + h_2\left[1 - \exp\left(-\frac{\varepsilon_m}{h_{exp}}\right)\right] & \text{if } \varepsilon_m \leq \varepsilon_{mc} \\ \sigma_{Y_c}\left(\frac{\varepsilon_m}{\varepsilon_{mc}}\right)^{n_c} & \text{if } \varepsilon_m > \varepsilon_{mc} \end{cases}$$

  - Porous plasticity parameters of Gurson
    - Classical:

$$\begin{cases} q_1 = 1.5 \\ q_2 = 1 \end{cases}$$

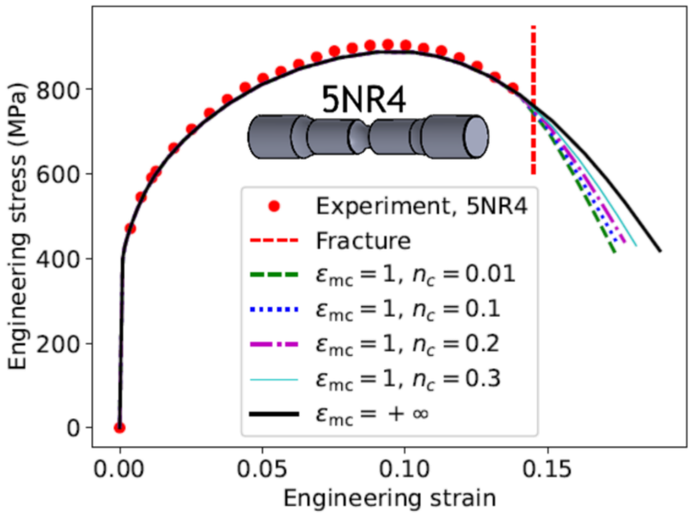

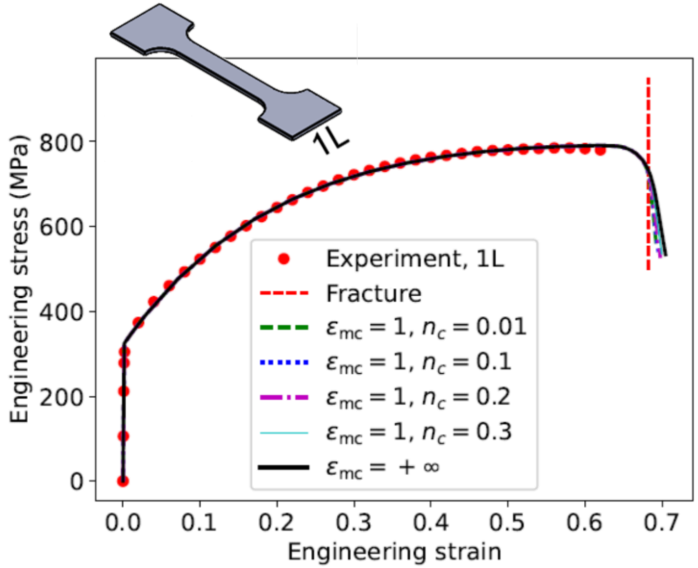

Ductile failure of High-Entropy Alloys (HEA)

- Identification methodology
  - Internal necking
    - Extended Thomason model

$$\phi_{\mathrm{T}} = \frac{2}{3}\sigma_{\mathrm{eq}}\cos\theta \;+ |p| - C_{\mathrm{T}}^{f}(\chi, \mathrm{W})\sigma_{\mathrm{Y}} \leq 0$$

Max Principal Stress

- With

$$C_{\mathrm{T}}^{f}(\chi, W) = (1-\chi^2)\left[h\left(\frac{1-\chi}{W\chi}\right)^2 + g\sqrt{\frac{1}{\chi}}\right]$$

0.1 1.24

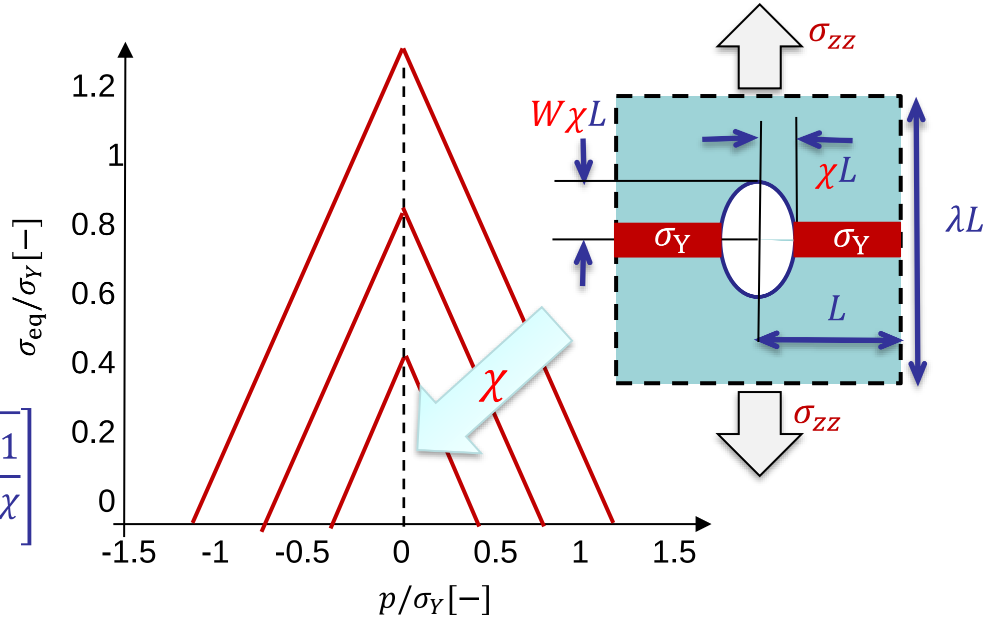

- 5NR4 fails by internal necking

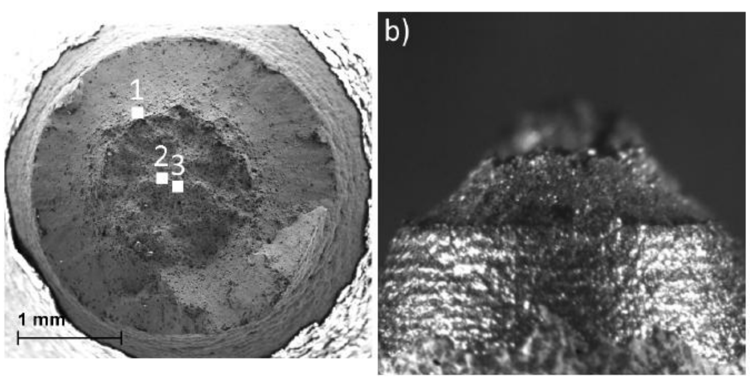

used to calibrate the void spacing factor $\kappa = 1.25$

$$\dot{\lambda} = \kappa\lambda\dot{\bar{\varepsilon}}_d \qquad \dot{\chi} = \frac{3\lambda}{4W}\left(\frac{3}{2\chi^2} - 1\right)\dot{\bar{\varepsilon}}_d$$

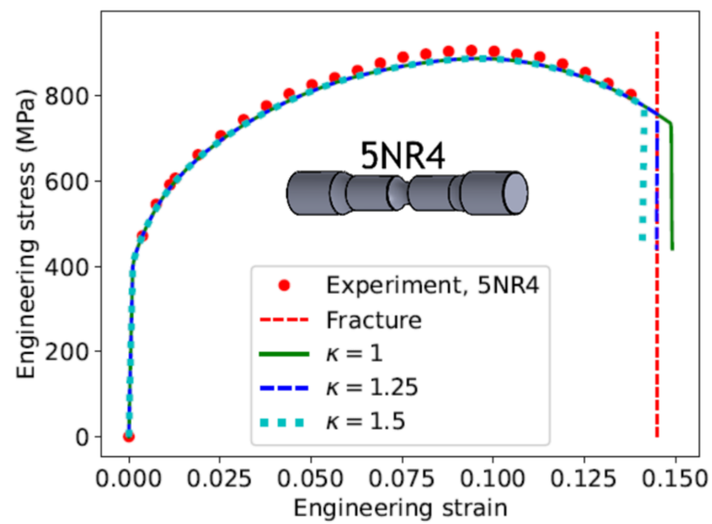

Images by A. Hillhorst, UCL

- Identification methodology
  - Porous plasticity parameters
    - $\dot{f} = \dot{f}_{\mathrm{gr}} + \dot{f}_{\mathrm{nu}} + \dot{f}_{\mathrm{sh}}$ with $\dot{f}_{\mathrm{gr}} = (1-f)\dot{\tilde{\varepsilon}}_v$
    - Assume early nucleation $f_0 = 0.002$

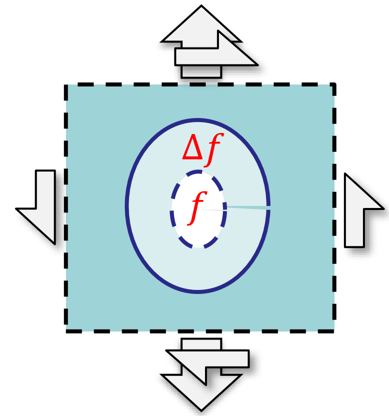

$$\dot{f}_{\mathrm{nu}} = A_n(\tilde{\varepsilon}_m)\dot{\tilde{\varepsilon}}_m = 0$$

- Shear growth

$$\begin{cases} \dot{f}_{\mathrm{sh}} = k_w \phi_\eta\left(\frac{p}{\sigma_{\mathrm{eq}}}\right)\phi_\omega(\cos 3\theta) f \dot{\tilde{\varepsilon}}_d \\ \phi_\eta(\eta) = \exp\left[-\frac{1}{2}\left(\frac{\eta}{\eta_s}\right)^2\right] \\ \phi_\omega(\omega) = 1 - \omega^2 \end{cases}$$

- For $\eta_s = 0.15$: $\phi_\eta(\eta) \simeq 0$ at high triaxiality

For 7GRx $\dot{f}_{\mathrm{sh}} \simeq 0$

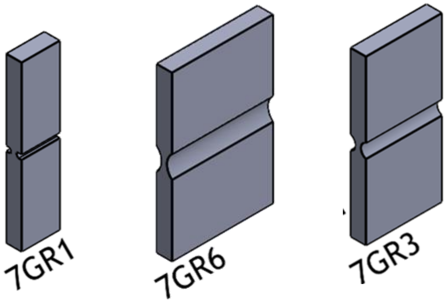

Can be used to characterise remaining parameters

- Identification methodology
  - Coalescence by shearing
    - Shear surface

$$\phi_S = \sqrt{3}\tau - C_S^f(\chi)\sigma_Y$$
$$= \sigma_{eq}\left(\frac{\sin\theta}{2} + \frac{\sqrt{3}\cos\theta}{2}\right) - C_S^f(\chi)\sigma_Y \leq 0$$

Max Shear Stress

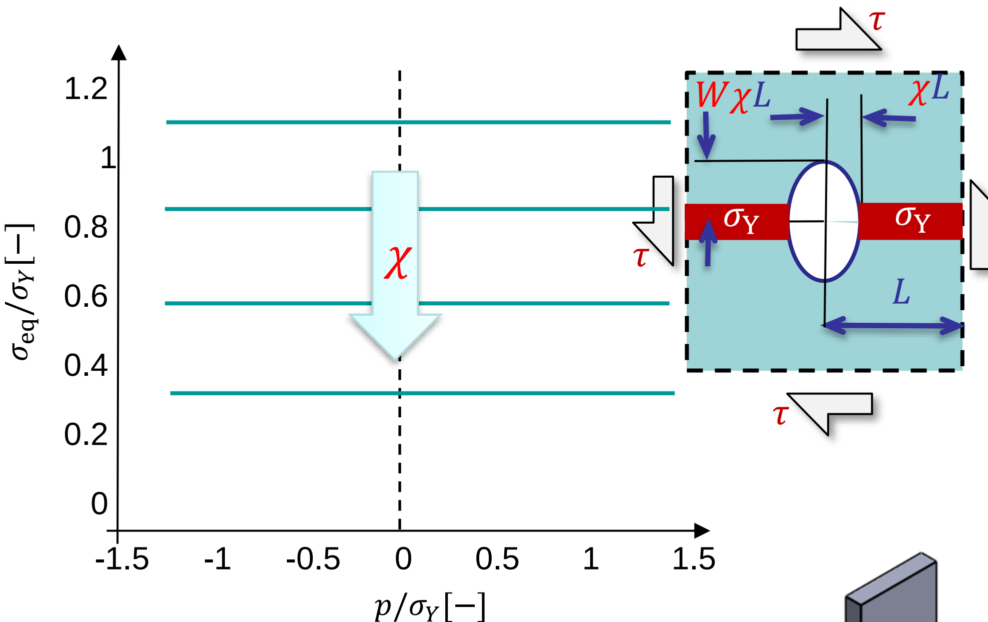

    - With

$$C_S^f(\chi) = \xi(1-\chi^2)$$

    - Ligament evolution

$$\dot{\chi} = K_\chi \dot{\bar{\varepsilon}}_d$$

    - 7GR3 fails by internal necking

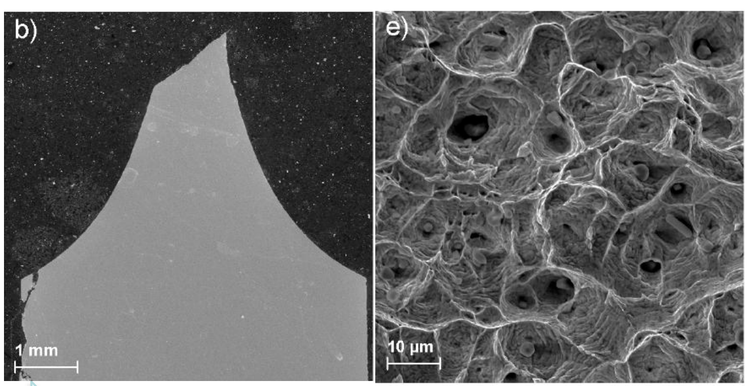

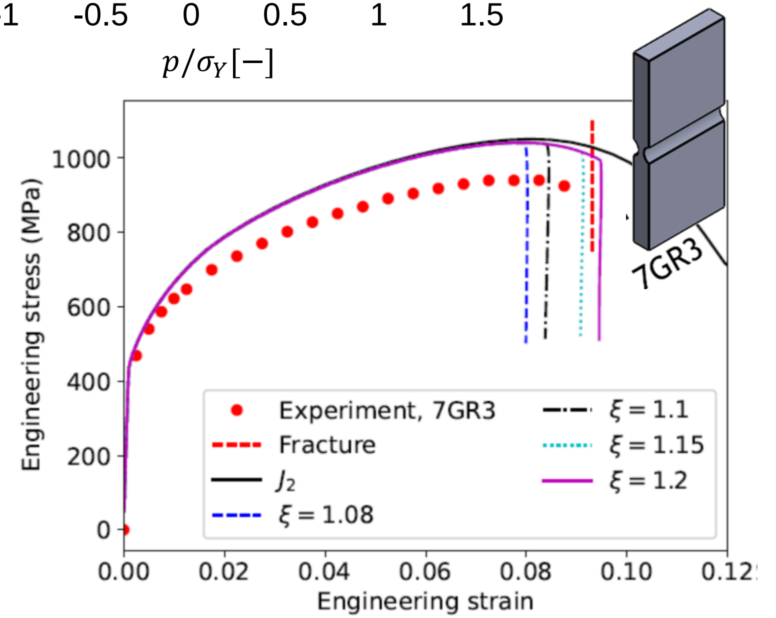

Images by A. Hillhorst, UCL

used to calibrate the shear coalescence parameters $\xi = 1.15$ & $K_\chi = 5$

- Identification methodology
  - Shear-controlled void growth
    - $\dot{f} = \dot{f}_{\text{gr}} + \dot{f}_{\text{nu}} + \dot{f}_{\text{sh}}$ with $\dot{f}_{\text{gr}} = (1-f)\dot{\tilde{\varepsilon}}_v$
    - Assume early nucleation $f_0 = 0.002$

$$\dot{f}_{\text{nu}} = A_n(\tilde{\varepsilon}_m)\dot{\tilde{\varepsilon}}_m = 0$$

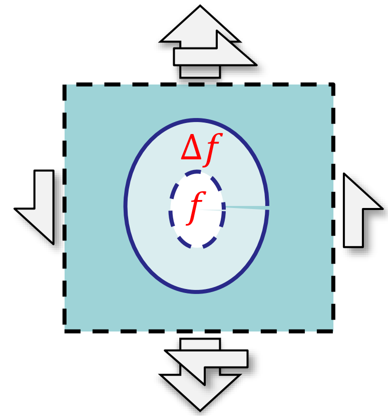

    - Shear growth

$$\begin{cases} \dot{f}_{\text{sh}} = k_w \phi_\eta\left(\frac{p}{\sigma_{\text{eq}}}\right)\phi_\omega(\cos 3\theta) f \dot{\tilde{\varepsilon}}_d \\ \phi_\eta(\eta) = \exp\left[-\frac{1}{2}\left(\frac{\eta}{\eta_s}\right)^2\right] \\ \phi_\omega(\omega) = 1 - \omega^2 \end{cases}$$

    - Last term $k_w = 3.5$ from 3SHEAR

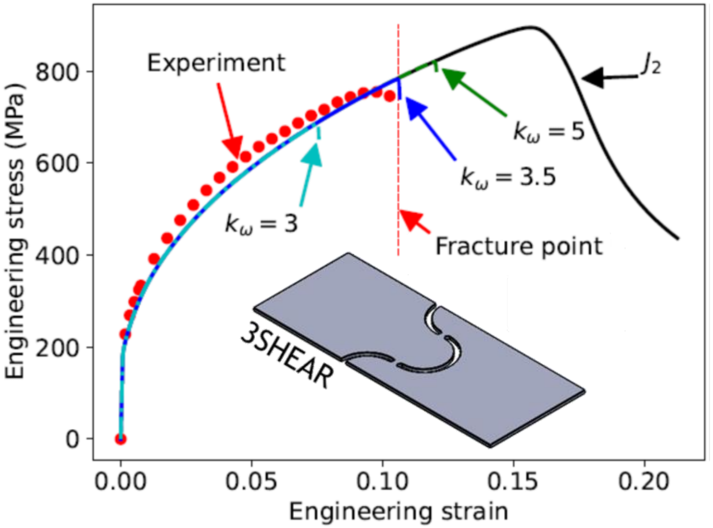

Ductile failure of High-Entropy Alloys (HEA)

- Validation of identified parameters
  - Plates

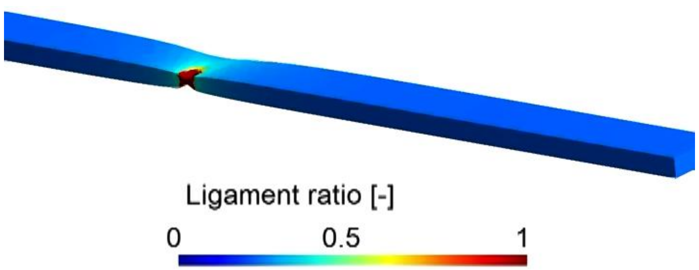

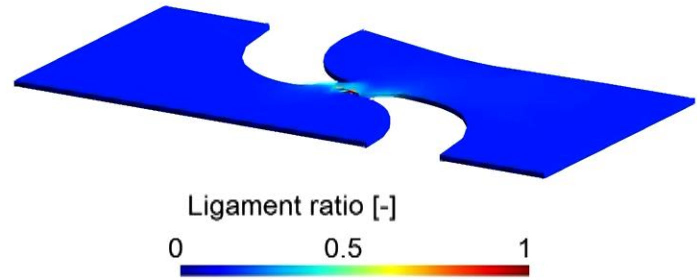

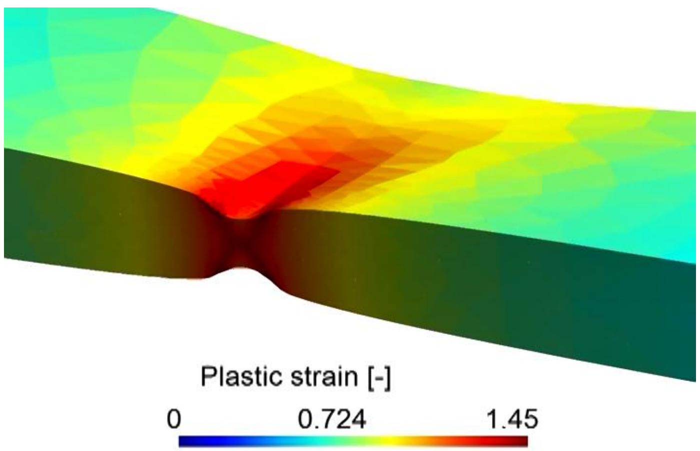

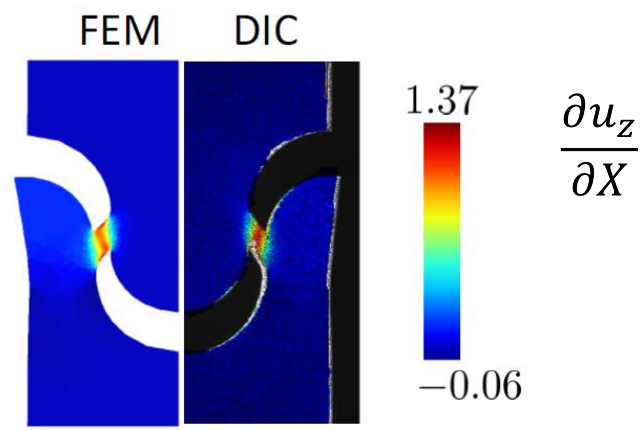

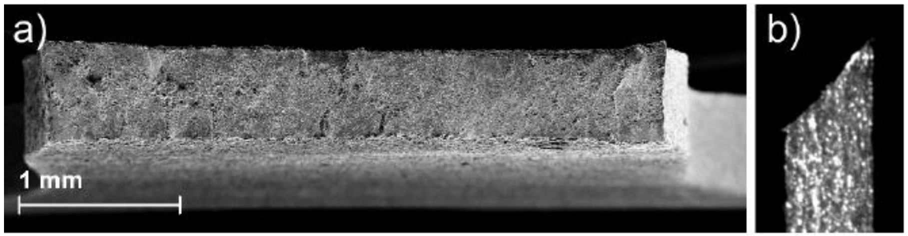

Images by A. Hillhorst, UCL

- Validation of identified parameters
  - Plates (2)

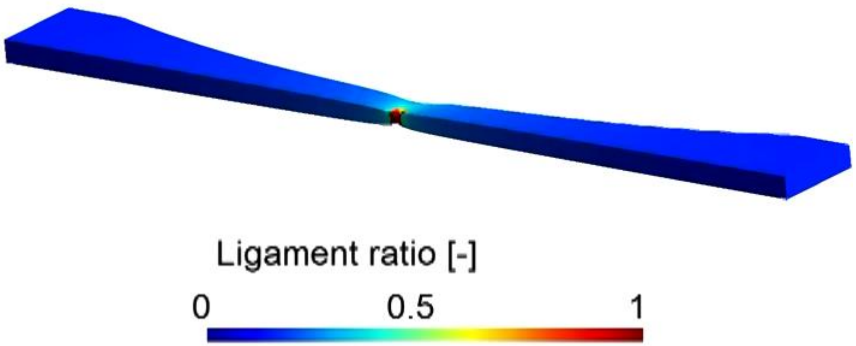

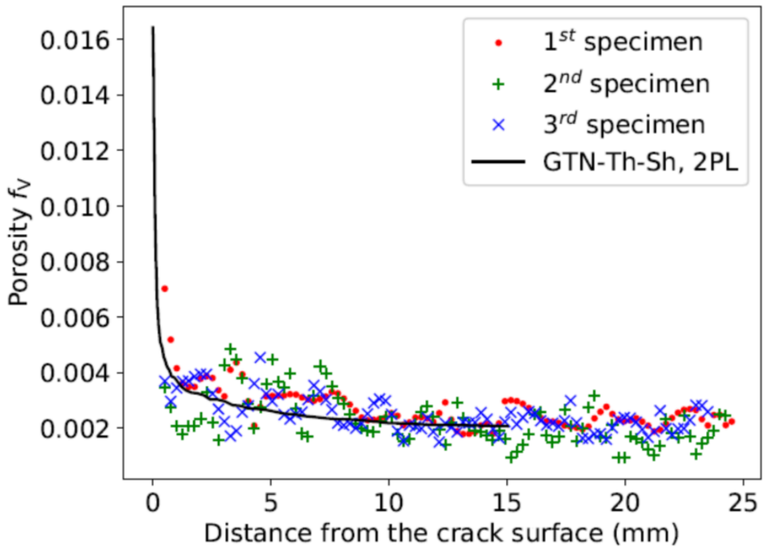

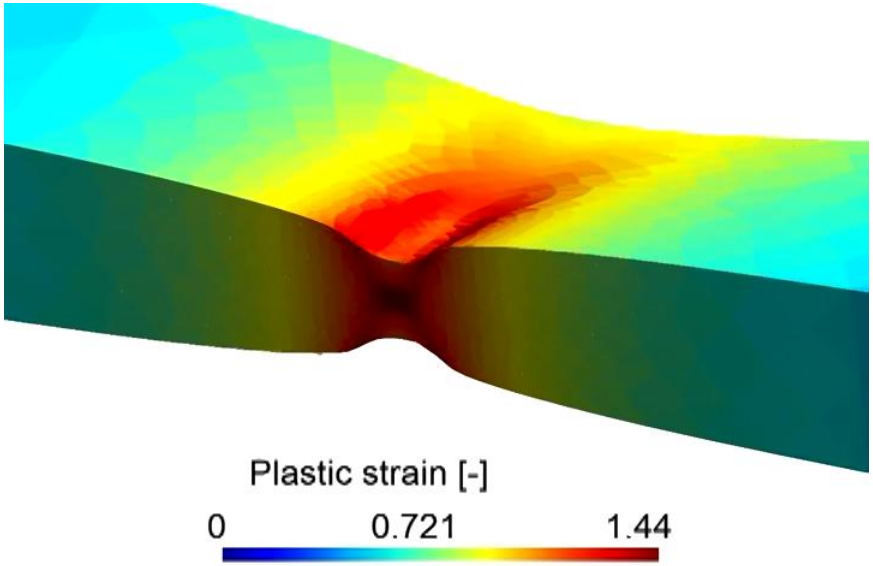

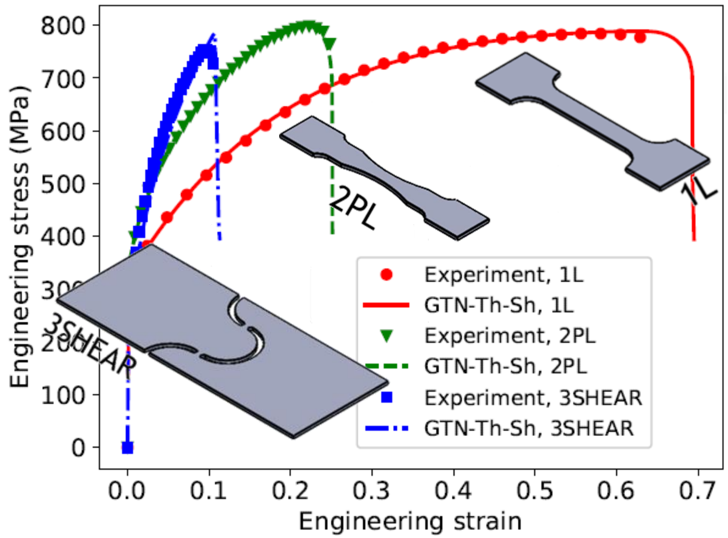

- Validation of identified parameters
  - Notched Plates

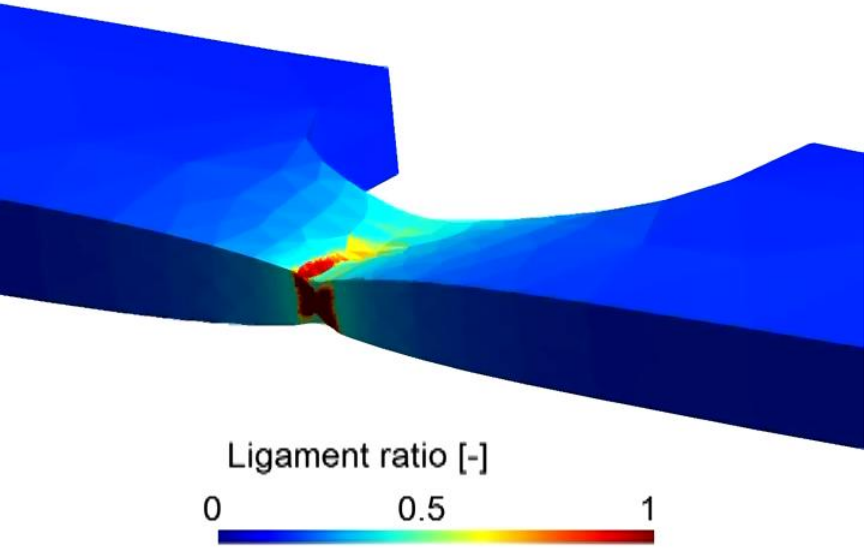

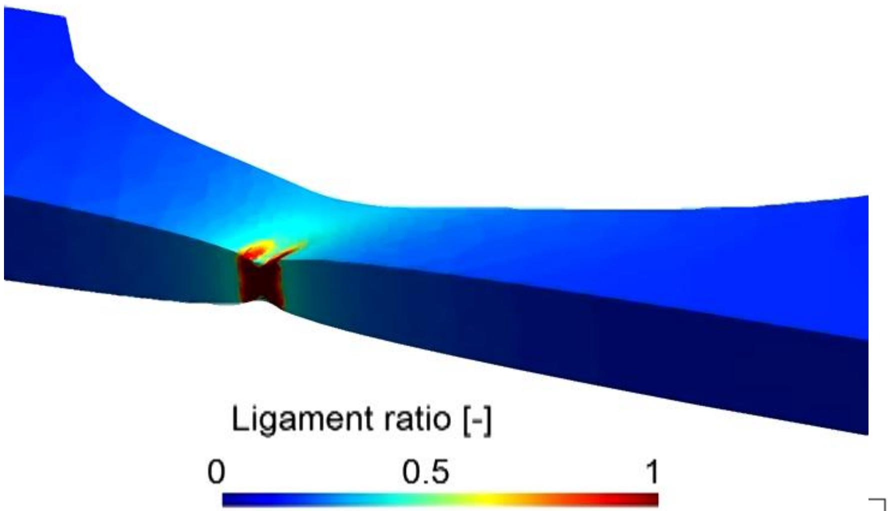

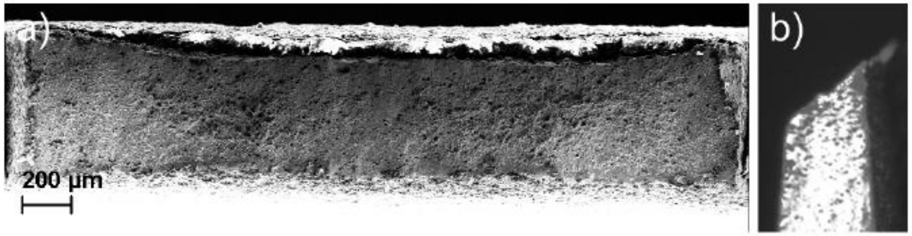

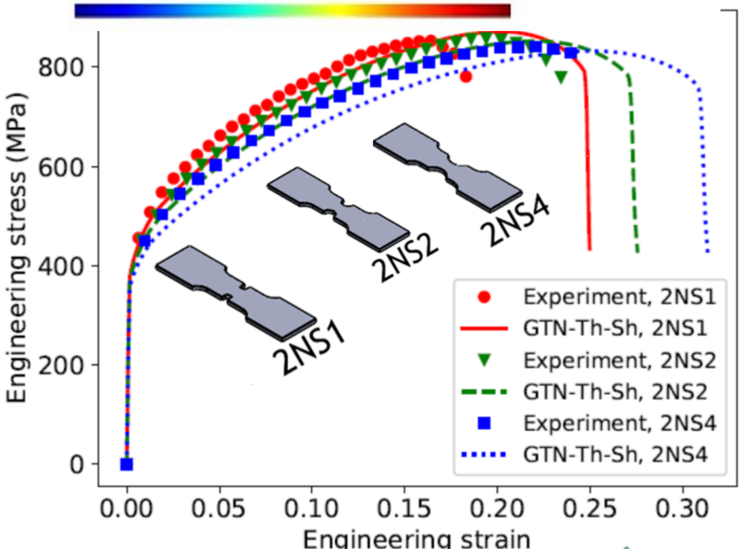

Images by A. Hillhorst, UCL

- Validation of identified parameters
  - Axisymmetric bars

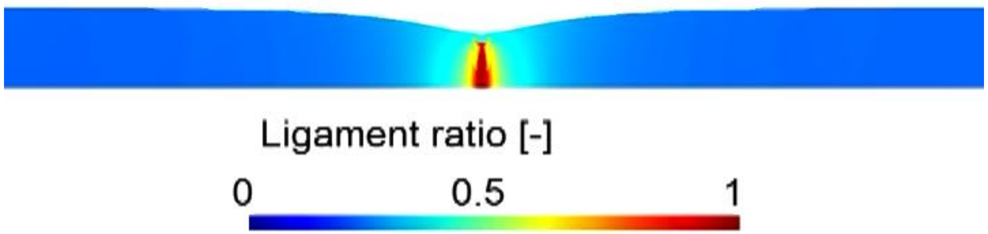

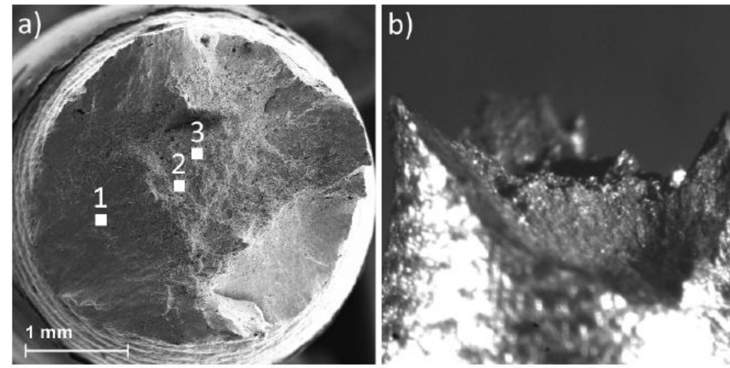

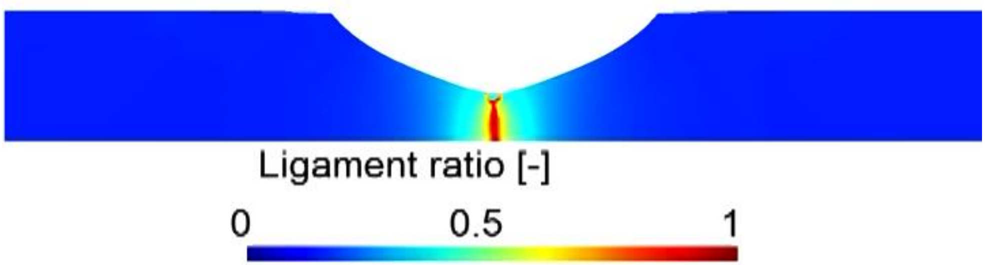

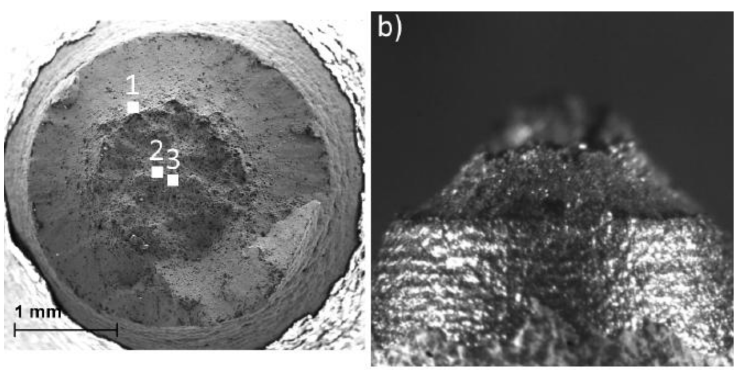

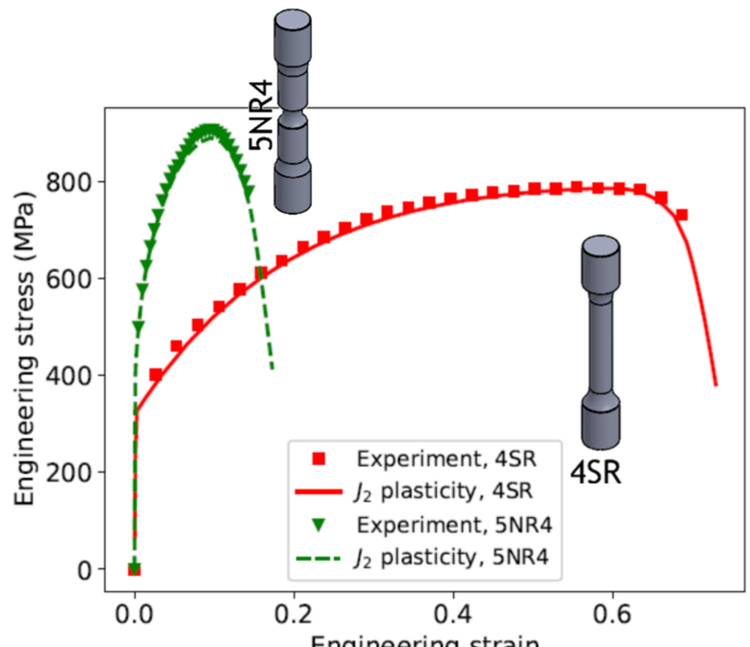

Images by A. Hillhorst, UCL

Ductile failure of High-Entropy Alloys (HEA)

- Validation of identified parameters
  - Grooved plates

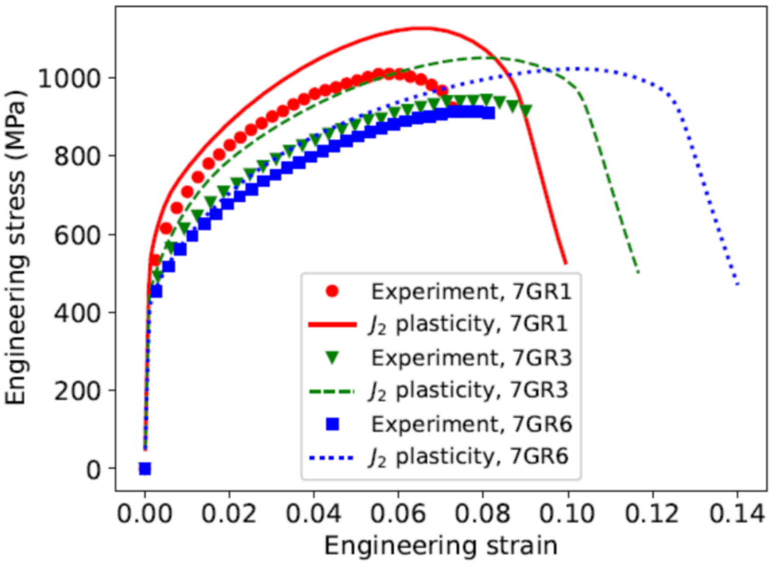

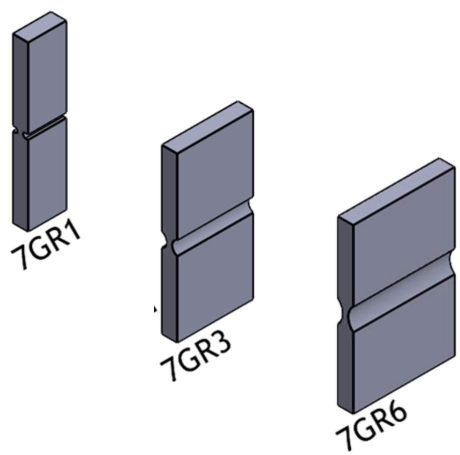

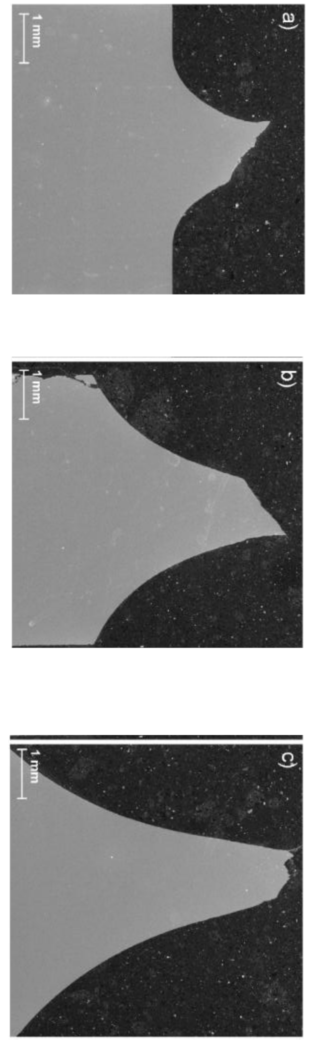

Images by A. Hillhorst, UCL

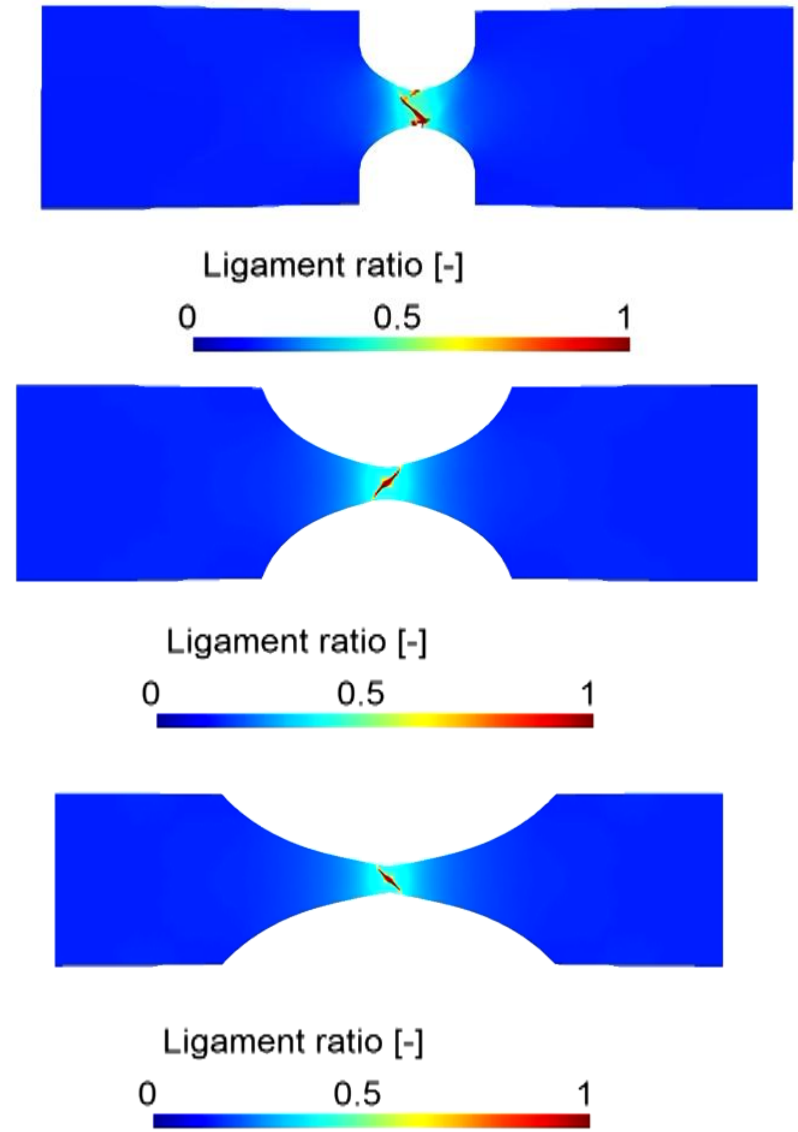

Ductile failure of High-Entropy Alloys (HEA)

- EntroTough WalInnov project
  - UCL, ULB, ULiege (Belgium)
- Publication (doi)
  - 10.1016/j.jmps.2020.103891
  - 10.1016/j.engfracmech.2022.108844

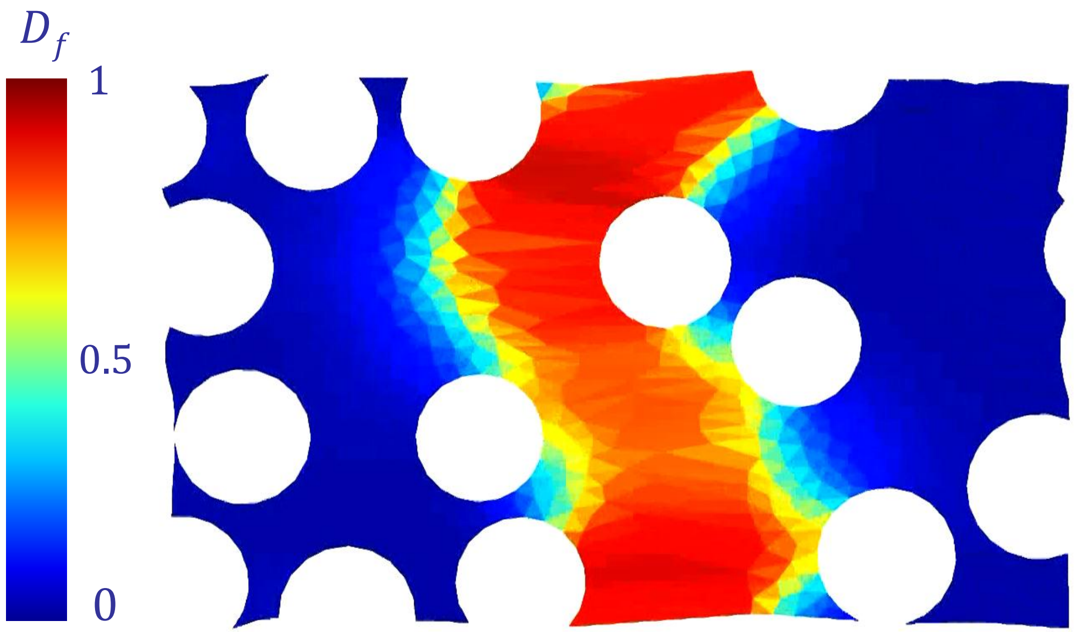

Micro-structural characterization and simulation of fiber-reinforced highly crosslinked epoxy

The authors gratefully acknowledge the financial support from F.R.S-F.N.R.S. under the project number PDR T.1015.14

Micro-structural simulation of fiber-reinforced highly crosslinked epoxy

- Resin behavior (experiments UCL)
  - Viscoelasto-Viscoplaticity
  - Saturated softening
  - Asymmetry tension-compression
  - Pressure-dependent yield
- To used in micro-structural analysis
  - Behavior in composite is different
  - Introduce a length-scale effect

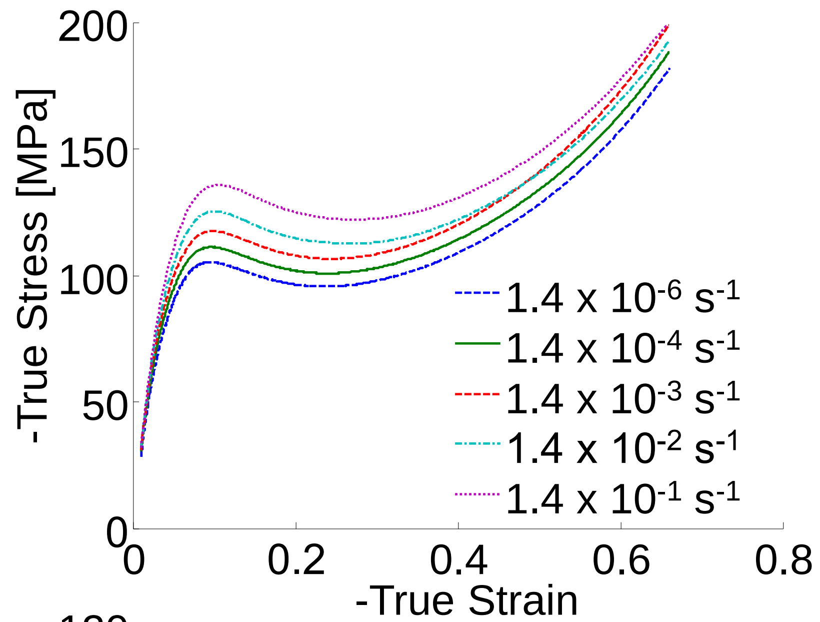

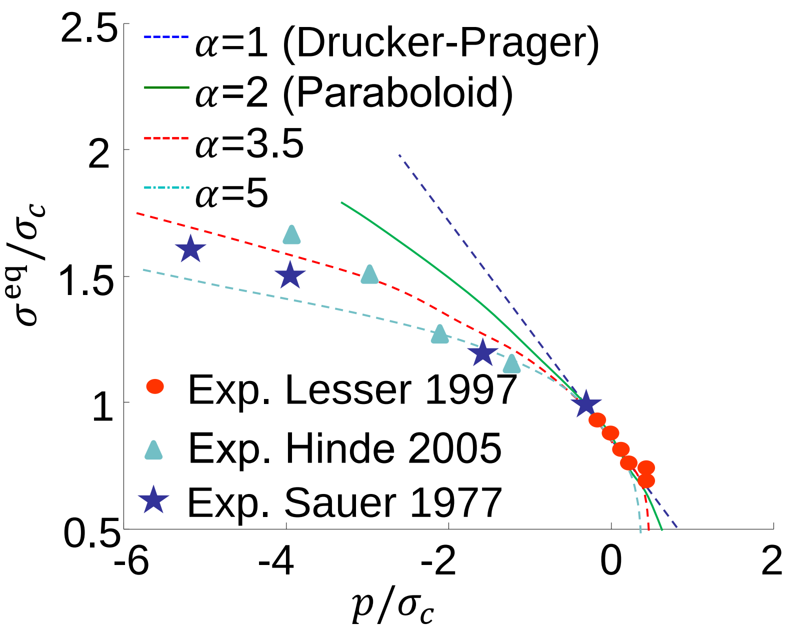

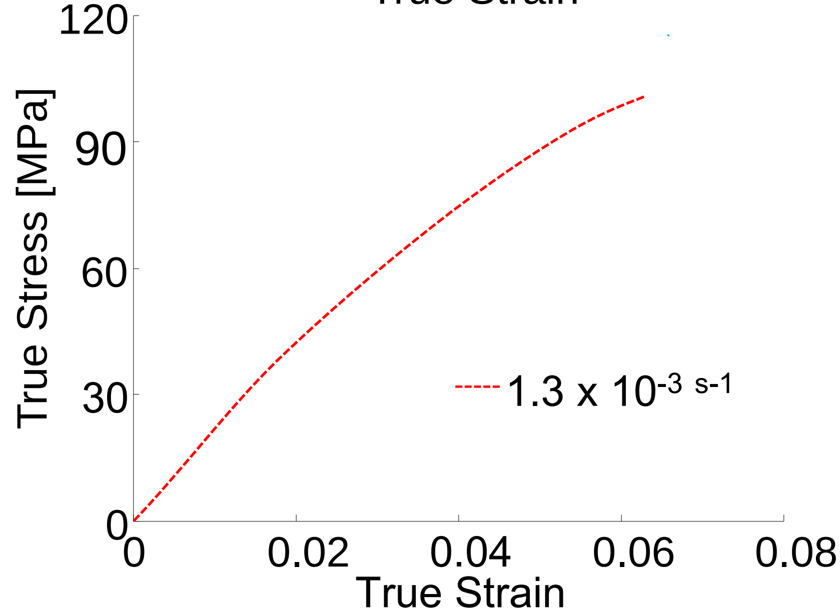

Micro-structural simulation of fiber-reinforced highly crosslinked epoxy

- Material changes represented via internal variables
  - Constitutive law $\mathbf{P}\left(\mathbf{F};\boldsymbol{Z}(t')\right)$
    - Internal variables $\boldsymbol{Z}(t')$
  - Multi-damage strategy
    $$\mathbf{P}=(\mathbf{1}-D_s)(\mathbf{1}-D_f)\widehat{\mathbf{P}}$$
- Resin model implementation:
  - Requires non-local form [Bažant 1988]
    - Introduction of characteristic length l_c
    - Weighted average: $\tilde{Z}(\boldsymbol{x})=\int_{V_C}W(\boldsymbol{y};\boldsymbol{x},l_c)\ Z(\mathbf{y})d\boldsymbol{y}$
  - Implicit form [Peerlings et al. 1998]
    - New degrees of freedom: $\tilde{Z}$
    - New Helmholtz-type equations: $\tilde{Z}-l_c^2\ \Delta\tilde{Z}=Z$
  - Damage evolution laws

$$\begin{cases}\dot{D}_{s/f}=D_{s/f}\left(D_{s/f},\mathbf{F}(t),\chi_{s/f}(t);Z(\tau),\tau\in[0\ t]\right)\dot{\chi}_{s/f}\\ \chi_{s/f}(t)=\max_{\tau}\left(\tilde{\gamma}_{s/f}(\tau)\right)\\ \tilde{\gamma}_{s/f}-l_{s/f}^2\ \Delta\tilde{\gamma}_{s/f}=\gamma_{s/f}\end{cases}$$

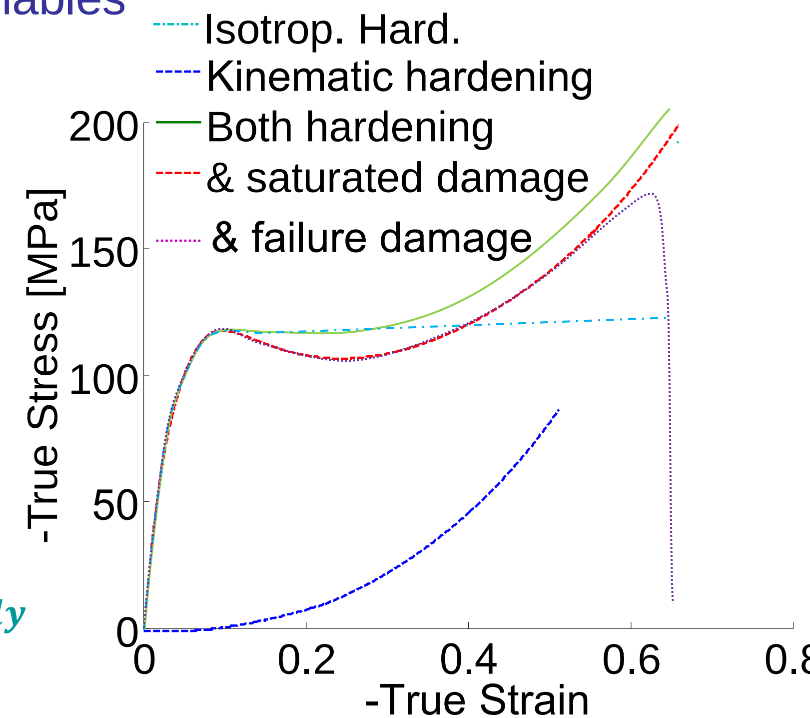

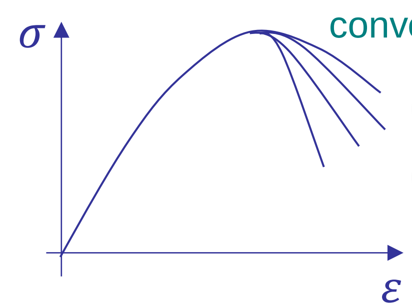

Local: no mesh convergence

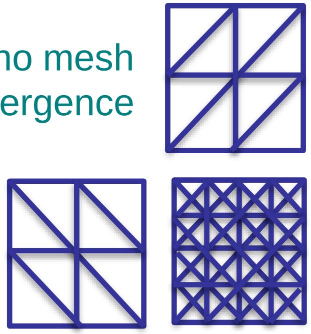

Beginning

Micro-structural simulation of fiber-reinforced highly crosslinked epoxy

- Resin model: hyperelastic-based formulation
  - Multiplicative decomposition

    $\mathbf{F} = \mathbf{F}^{\mathrm{ve}} \cdot \mathbf{F}^{\mathrm{vp}},\quad \mathbf{C}^{\mathrm{ve}} = \mathbf{F}^{\mathrm{ve}^T} \cdot \mathbf{F}^{\mathrm{ve}},\quad J^{\mathrm{ve}} = \det(\mathbf{F}^{\mathrm{ve}})$
  - Undamaged stress tensor definition
    - Elastic potential $\psi(\mathbf{C}^{ve})$
    - Undamaged first Piola-Kirchhoff stress tensor

      $$\widehat{\mathbf{P}} = 2\mathbf{F}^{\mathrm{ve}} \cdot \frac{\partial\psi(\mathbf{C}^{\mathrm{ve}})}{\partial\mathbf{C}^{\mathrm{ve}}} \cdot \mathbf{F}^{\mathrm{vp}^{-T}}$$
    - Undamaged Kirchhoff stress tensors
      - In current configuration

        $$\widehat{\boldsymbol{\kappa}} = \widehat{\mathbf{P}} \cdot \mathbf{F}^T = 2\mathbf{F}^{\mathrm{ve}} \cdot \frac{\partial\psi(\mathbf{C}^{ve})}{\partial\mathbf{C}^{\mathrm{ve}}} \cdot \mathbf{F}^{\mathrm{ve}^T}$$
      - In co-rotational space

        $$\widehat{\boldsymbol{\tau}} = \mathbf{C}^{\mathrm{ve}} \cdot \mathbf{F}^{\mathrm{ve}^{-1}} \cdot \widehat{\boldsymbol{\kappa}} \cdot \mathbf{F}^{\mathrm{ve}^{-T}} = 2\mathbf{C}^{ve} \cdot \frac{\partial\psi(\mathbf{C}^{\mathrm{ve}})}{\partial\mathbf{C}^{\mathrm{ve}}}$$
  - Apparent stress tensor
    - Piola-Kirchhoff stress

      $$\mathbf{P} = (\mathbf{1} - D_s)(\mathbf{1} - D_f)\widehat{\mathbf{P}}$$

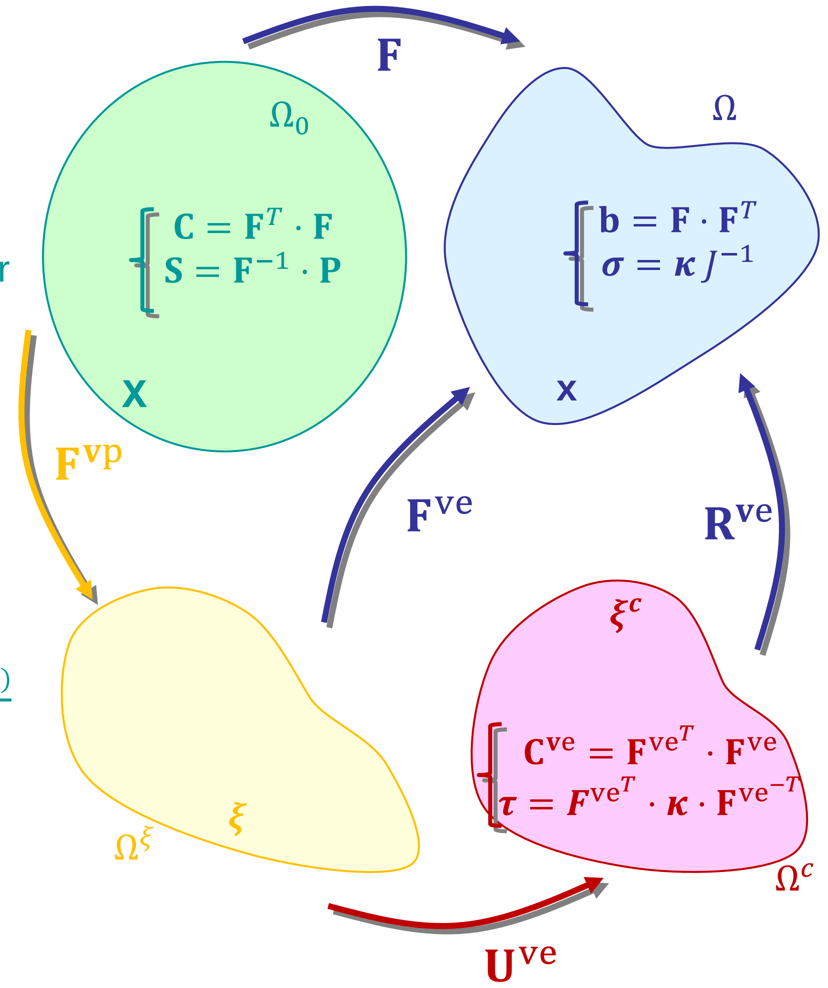

- Resin model: logarithmic visco-elasticity
  - Elastic potentials ψ_i:

$$\psi_i(\mathbf{C}^{\mathrm{ve}}) = \frac{K_i}{2}\ln^2(J^{\mathrm{ve}}) + \frac{G_i}{4}(\ln(\mathbf{C}^{\mathrm{ve}}))^{\mathrm{dev}}:(\ln(\mathbf{C}^{\mathrm{ve}}))^{\mathrm{dev}}$$

  - Dissipative potentials Υ_i

$$\Upsilon_i(\mathbf{C}^{\mathrm{ve}},\mathbf{q}_i) = -\mathbf{q}_i:\ln(\mathbf{C}^{\mathrm{ve}}) + \left[\frac{1}{18K_i}\mathrm{tr}^2(\mathbf{q}_i) + \frac{1}{4G_i}\mathbf{q}_i^{\mathrm{dev}}:\mathbf{q}_i^{\mathrm{dev}}\right]$$

$$\begin{cases} \dot{\mathbf{q}}_i^{\mathrm{dev}} = \dfrac{2G_i}{g_i}\,(\ln(\mathbf{C}^{\mathrm{ve}}))^{\mathrm{dev}} - \dfrac{1}{g_i}\mathbf{q}_i^{\mathrm{dev}} \\ \mathrm{tr}\,(\dot{\mathbf{q}}_i) = \dfrac{3K_i}{k_i}\,\ln^2(J^{\mathrm{ve}}) - \dfrac{1}{k_i}\mathrm{tr}\,(\mathbf{q}_i) \end{cases}$$

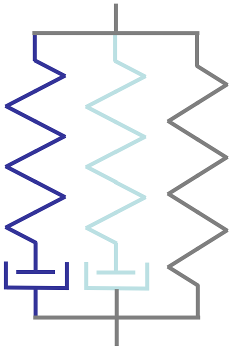

  - Total potential ψ:

$$\begin{cases} \psi(\mathbf{C}^{\mathrm{ve}};\boldsymbol{q}_i) = \psi_\infty(\mathbf{C}^{\mathrm{ve}}) + \sum_i [\psi_i(\mathbf{C}^{\mathrm{ve}}) + \Upsilon_i(\mathbf{C}^{\mathrm{ve}},\mathbf{q}_i)] \\ \widehat{\mathbf{P}} = 2\mathbf{F}^{\mathrm{ve}}\cdot\dfrac{\partial\psi(\mathbf{C}^{\mathrm{ve}})}{\partial\mathbf{C}^{\mathrm{ve}}}\cdot\mathbf{F}^{\mathrm{vp}^{-T}} \end{cases}$$

Micro-structural simulation of fiber-reinforced highly crosslinked epoxy

- Resin model: visco-plasticity
  - Stress, back-stress

    $$\boldsymbol{\varphi} = \hat{\boldsymbol{\tau}} - \hat{\boldsymbol{b}}$$

  - Perzina plastic flow rule

    $$\mathbf{D}^{\mathrm{vp}} = \dot{\mathbf{F}}^{\mathrm{v}p} \cdot \mathbf{F}^{\mathrm{v}p} = \frac{1}{\eta}\langle\phi\rangle^{\frac{1}{p}}\frac{\partial P}{\partial \hat{\boldsymbol{\tau}}}$$

  - Pressure dependent yield surface

    $$\begin{cases} \phi = \left(\dfrac{\varphi^{\mathrm{eq}}}{\sigma_c}\right)^{\alpha} - \dfrac{m^{\alpha}-1}{m+1}\dfrac{\mathrm{tr}\boldsymbol{\varphi}}{\sigma_c} - \dfrac{m^{\alpha}+m}{m+1} \leq 0 \\ m = \dfrac{\sigma_t}{\sigma_c} \end{cases}$$

  - Non-associated flow potential

    $$P = (\varphi^{\mathrm{eq}})^2 + \beta\left(\frac{\mathrm{tr}\boldsymbol{\varphi}}{3}\right)^2$$

  - Equivalent plastic strain rate:

    $$\begin{cases} \dot{\gamma} = \dfrac{\sqrt{\mathbf{D}^{\mathrm{vp}}:\mathbf{D}^{\mathrm{vp}}}}{\sqrt{\mathbf{1}+\mathbf{2}v_p^2}} \\ v_p = \dfrac{9-2\beta}{18+2\beta} \end{cases}$$

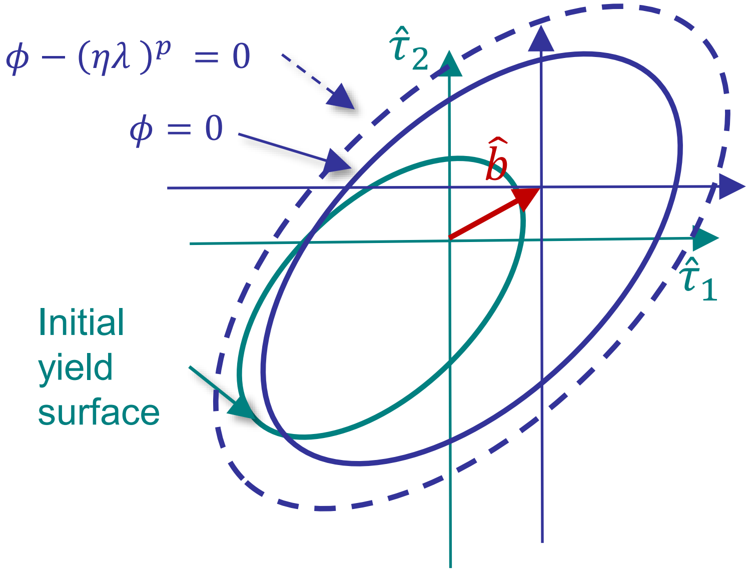

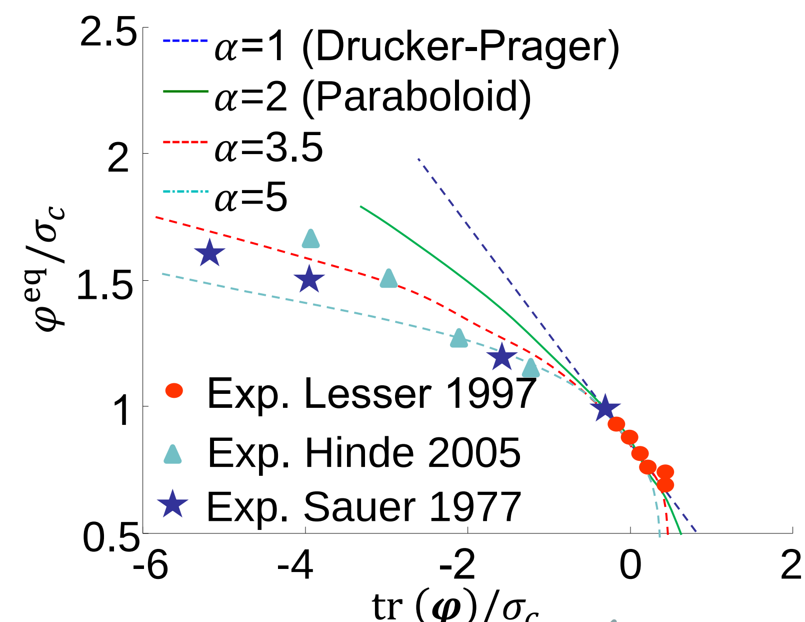

Micro-structural simulation of fiber-reinforced highly crosslinked epoxy

- Resin model: saturated softening
  - Damage evolution

$$\begin{cases} \dot{D}_s = H_s(\chi_s - \chi_{s0})^{\zeta_s}(D_{s\infty} - D_s)\dot{\chi}_s \\ \chi_s = \max_{\tau}\left(\chi_{s0}, \tilde{\gamma}_s(\tau)\right) \\ \tilde{\gamma}_s - l_s^2\,\Delta\tilde{\gamma}_s = \gamma \end{cases}$$

  - Calibration
    - Several hardening/softening combinations
    - Requires composite material tests
      - Length scale effect

$$l_s = 3\mu\text{m}\left(1 - \frac{D_s}{D_{s\infty}}\right)$$

      - Non-local BC at fiber interface $[\![\dot{\tilde{\gamma}}_s]\!] = 0$

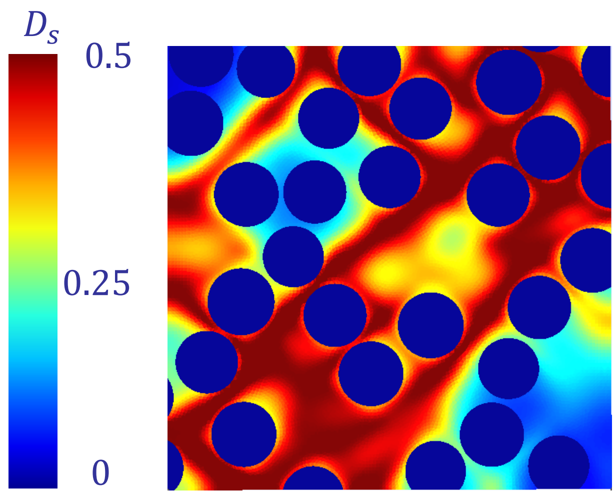

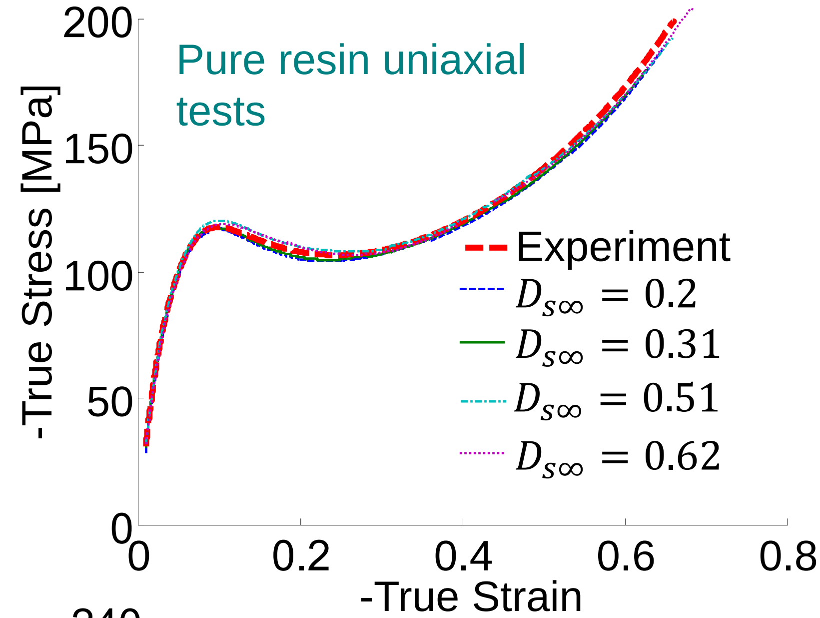

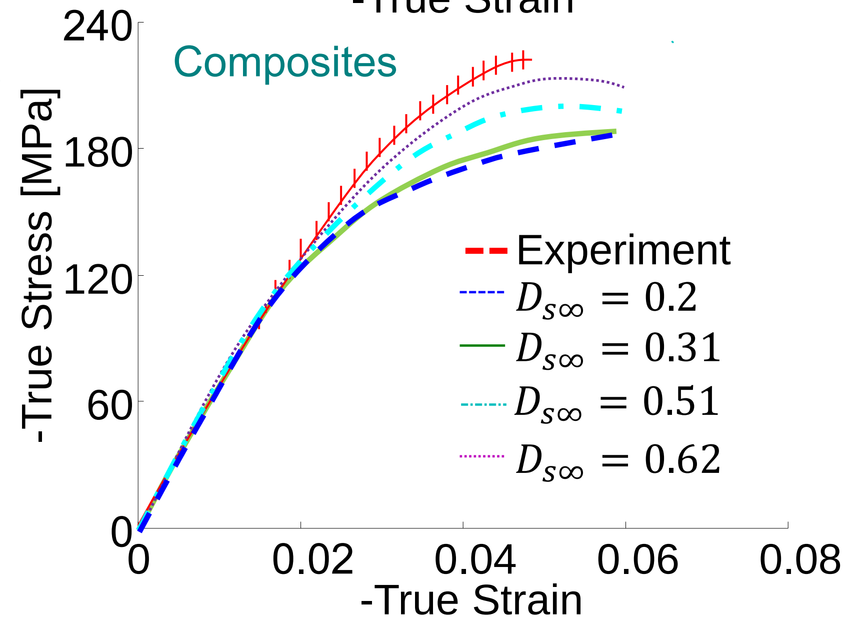

- Resin model: failure softening
  - Failure surface

$$\begin{cases} \phi_f = \gamma - a\exp\left(-b\frac{\mathrm{tr}(\hat{\boldsymbol{\tau}})}{3\hat{\tau}^{eq}}\right) - c \\ \phi_f - r \leq 0;\ \dot{r} \geq 0; \text{and } \dot{r}\left(\phi_f - r\right) = 0 \\ \dot{\gamma}_f = \dot{r} \end{cases}$$

  - Damage evolution

$$\begin{cases} \dot{D}_f = H_f\left(\chi_f\right)^{\zeta_f}\left(1 - D_f\right)^{-\zeta_d}\dot{\chi}_f \\ \chi_f = \max_{\tau}\left(\tilde{\gamma}_f(\tau)\right) \\ \tilde{\gamma}_f - l_f^2\,\Delta\tilde{\gamma}_f = \gamma_f \\ l_f = 3\ \mu\mathrm{m} \qquad \nabla_0\tilde{\gamma}_f \cdot \mathbf{N} = 0 \end{cases}$$

  - Affect ductility

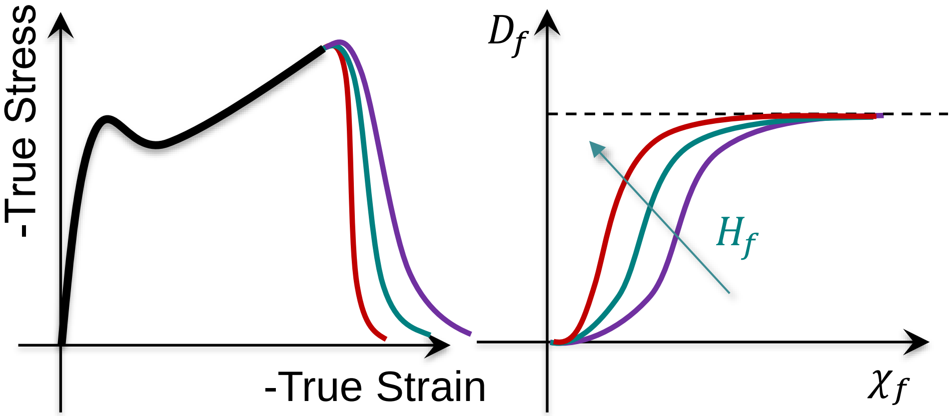

Micro-structural simulation of fiber-reinforced highly crosslinked epoxy

- Resin model: failure softening (2)
  - Damage evolution

    $$\dot{D}_f = H_f(\chi_f)^{\zeta_f}(1 - D_f)^{-\zeta_d}\,\dot{\chi}_f$$

    $$\tilde{\gamma}_f - l_f^2\,\Delta\tilde{\gamma}_f = \gamma_f$$

  - Calibration
    - Recover the epoxy G_c
    - From localization simulation

      $$G_c A = \Upsilon^{\text{end}} - \Upsilon^{\text{loc}}$$

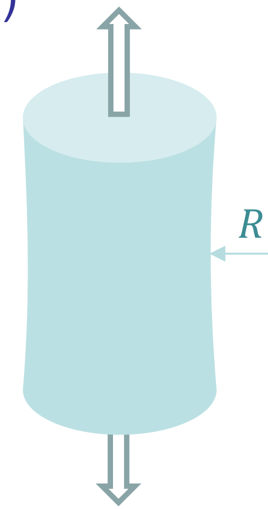

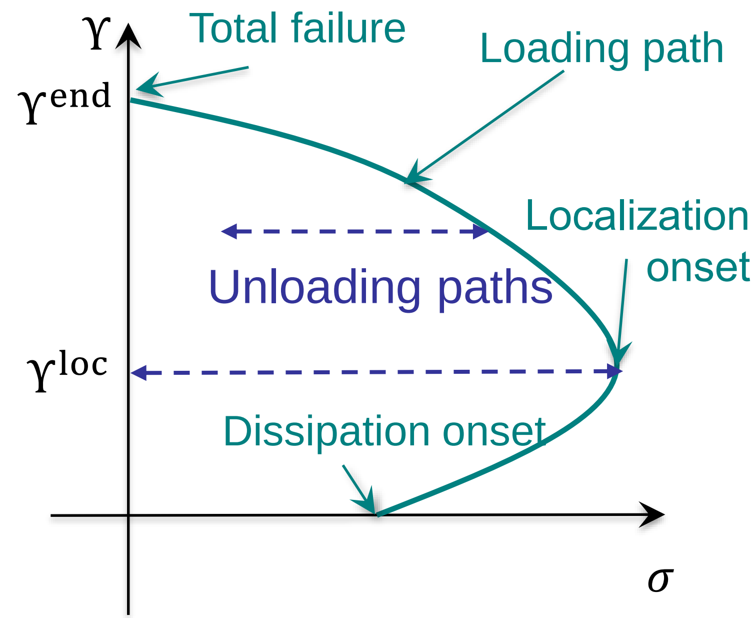

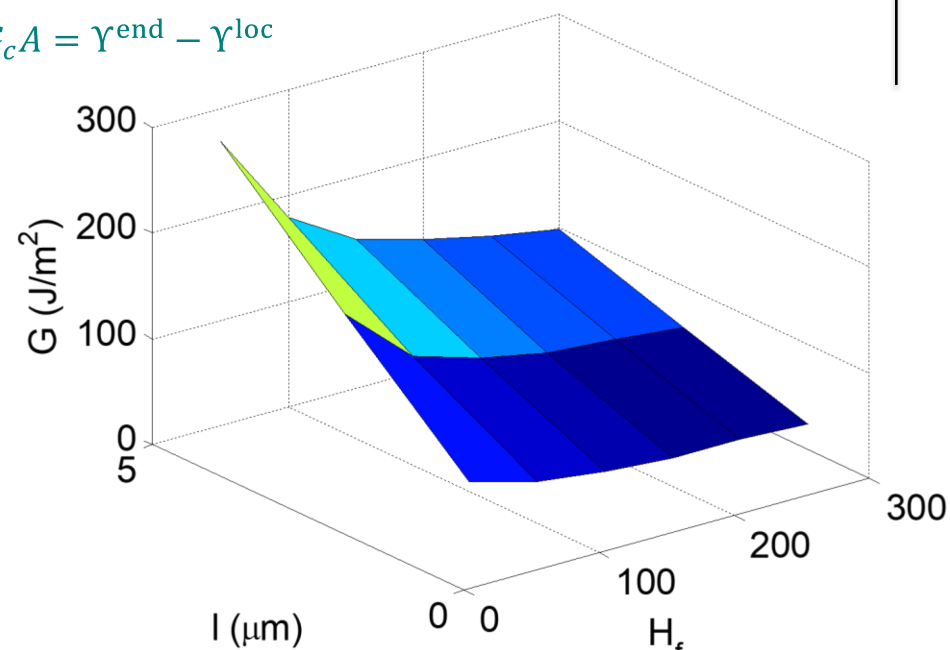

Micro-structural simulation of fiber-reinforced highly crosslinked epoxy

- Resin model: Validation
  - Compression without barrelling effect

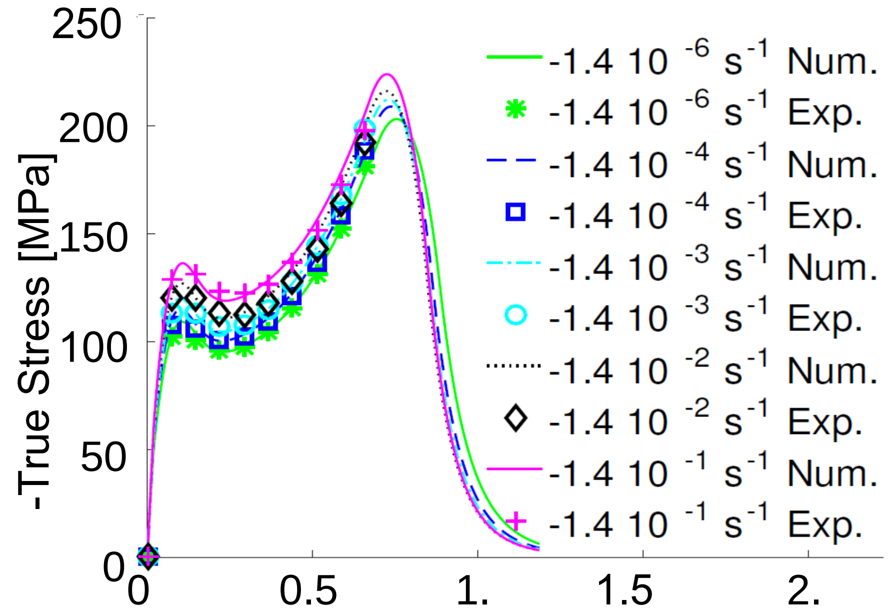

  - With barrelling effect

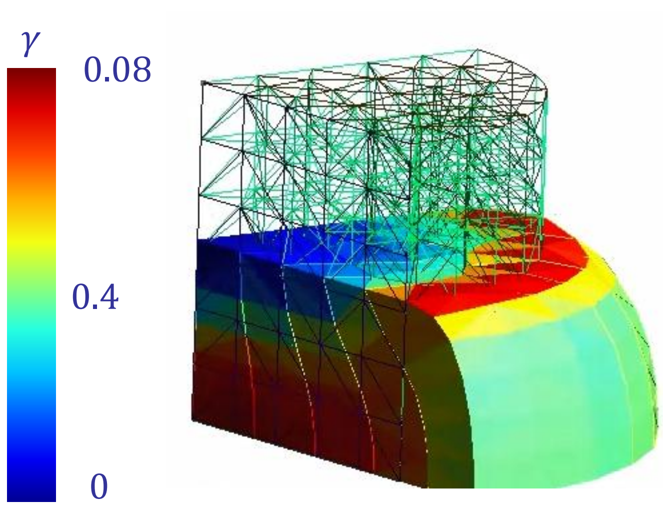

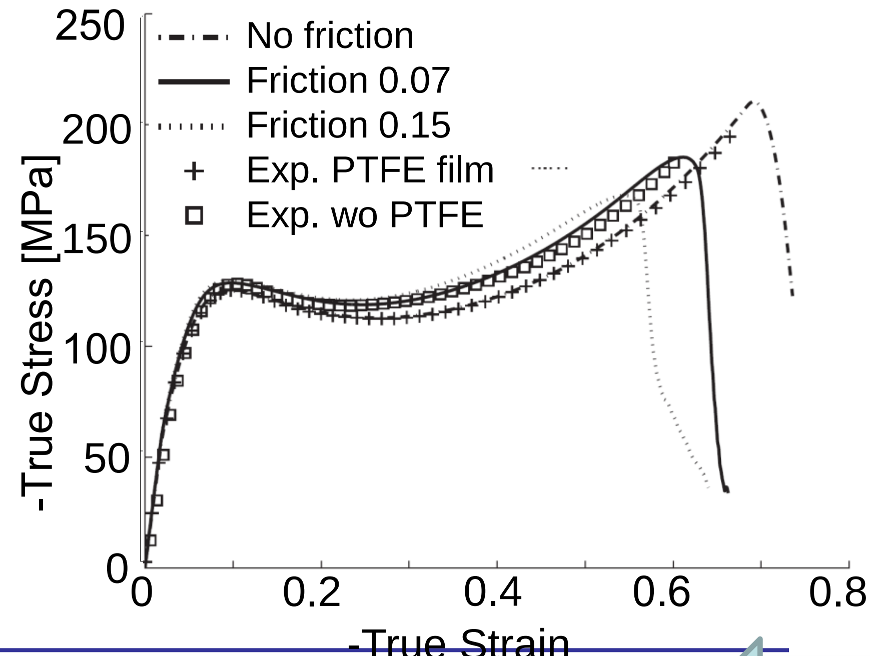

Micro-structural simulation of fiber-reinforced highly crosslinked epoxy

- Composite model: Extraction of G_c

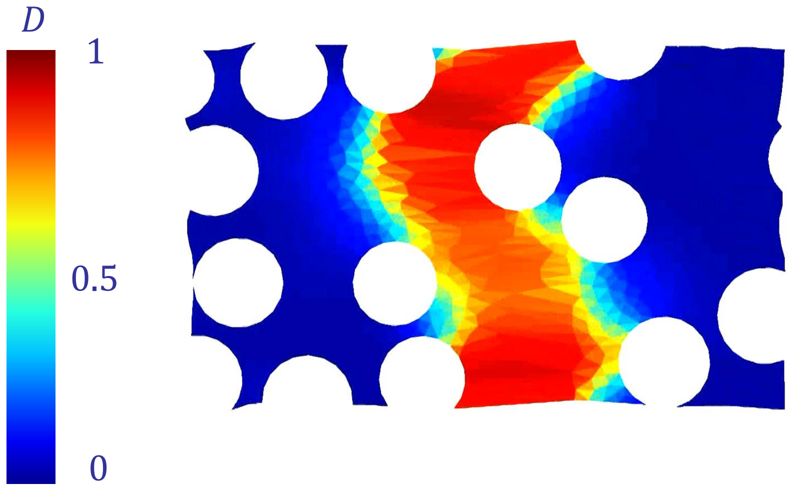

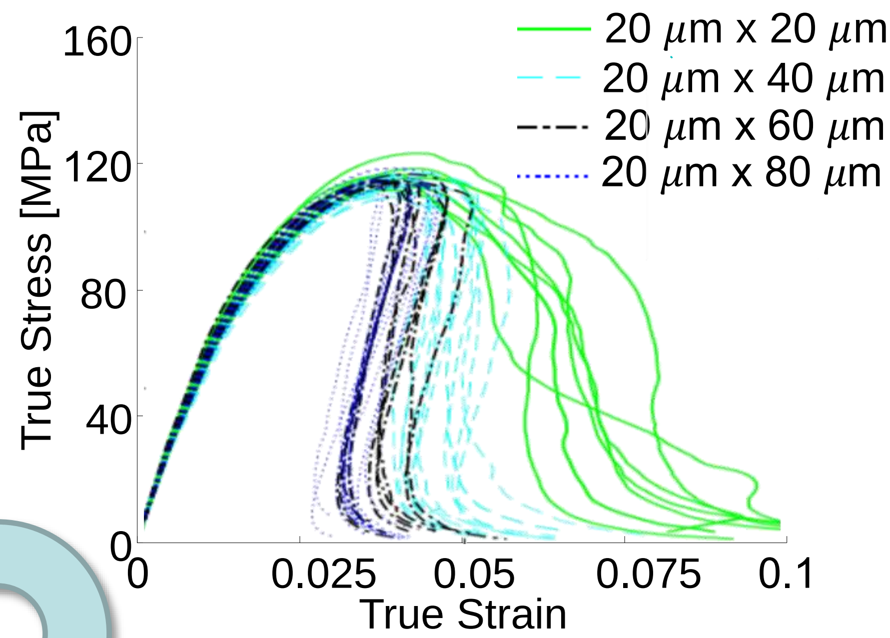

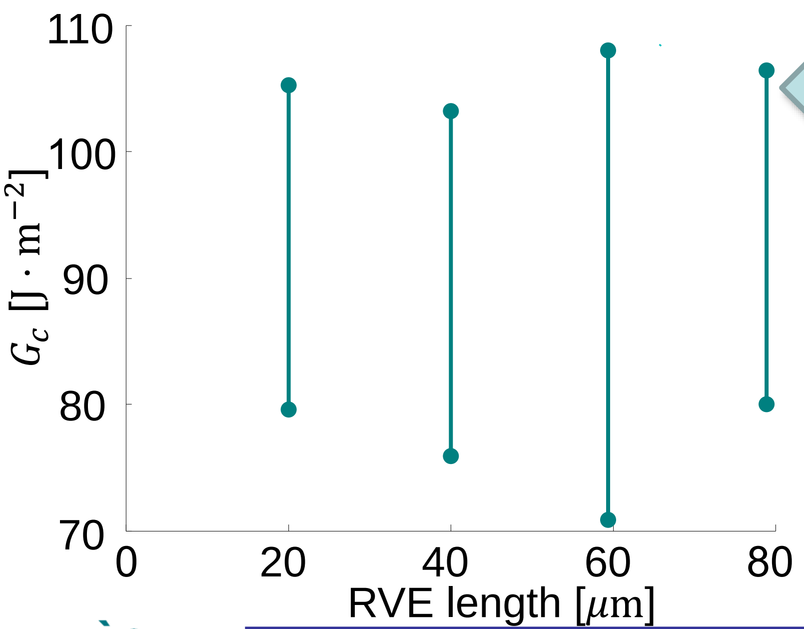

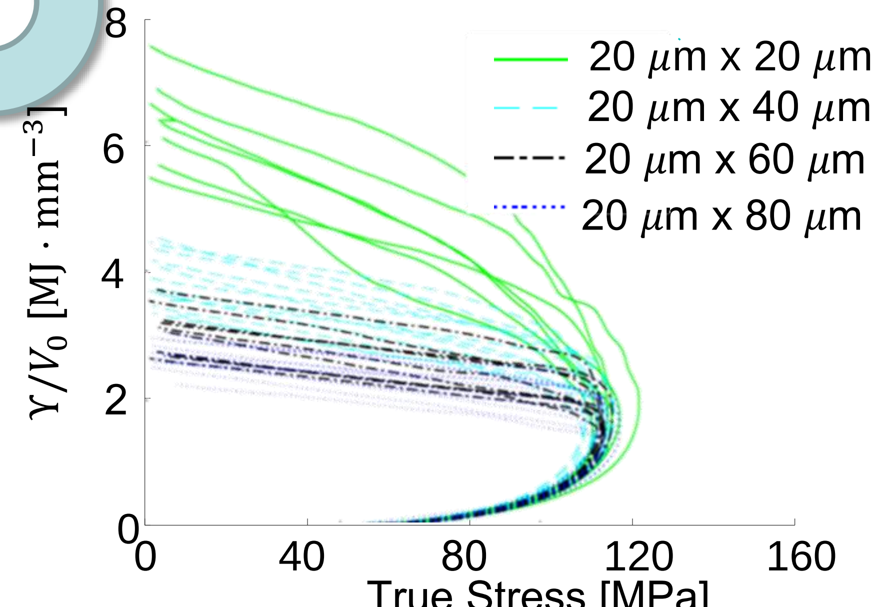

Micro-structural simulation of fiber-reinforced highly crosslinked epoxy

- Composite model: Validation
  - Compression test

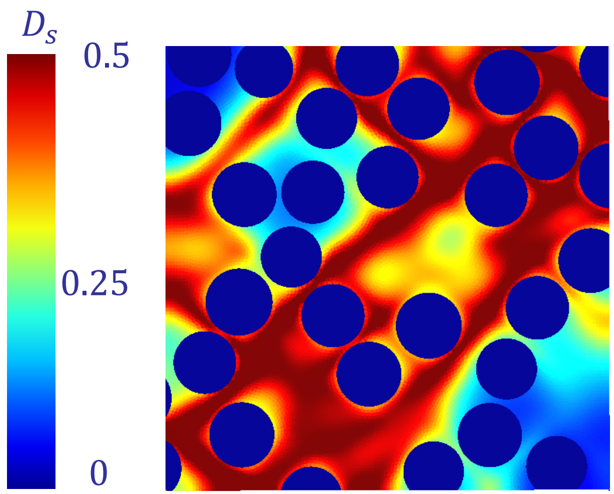

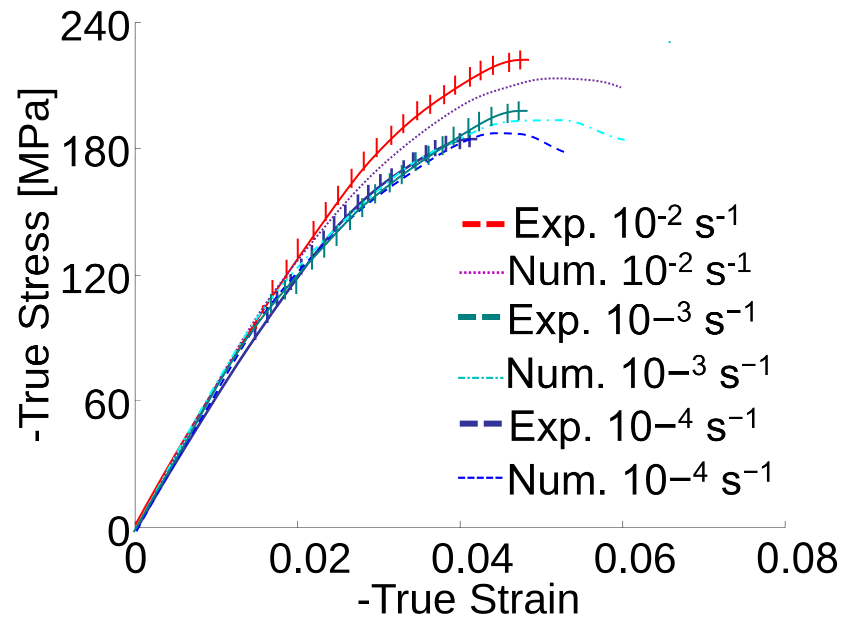

- PDR T.1015.14 project
  - ULiège, UCL (Belgium)

- Publications
  - 10.1016/j.ijsolstr.2016.06.008
  - 10.1016/j.mechmat.2019.02.017

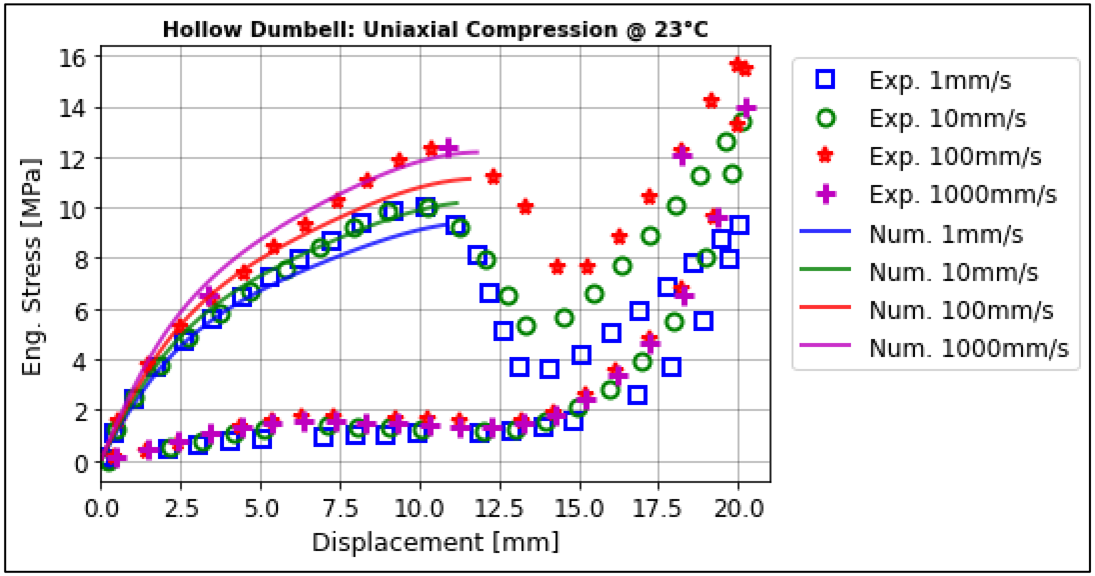

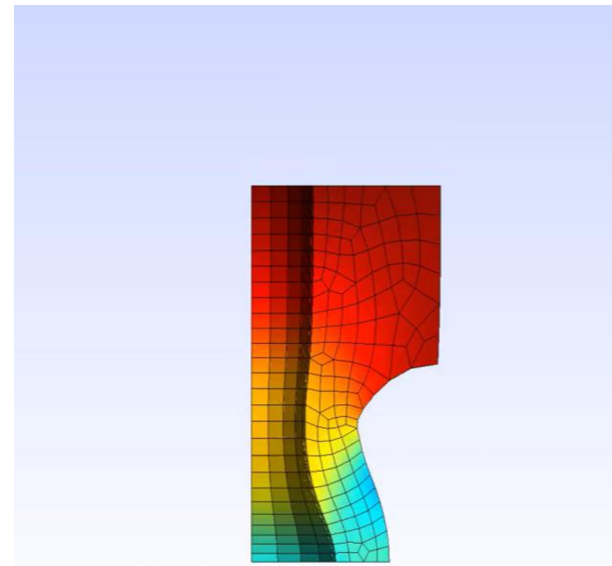

Finite-strain thermomechanical quasi-nonlinear-viscoelastic viscoplastic model for thermoplastics

This research has been funded by the Walloon Region under the agreement no. 2010092-CARBOBRAKE in the context of the M-ERA.Net Join Call 2020 funded by the European Union under the Grant Agreement no. 101102316. TPU experimental results (provided by imdea, JKU) were obtained in MOAMMM project which has received funding from the H2020-EU.1.2.1.-FET Open Programme project MOAMMM under grant No 862015.

Finite-strain thermomechanical quasi-nonlinear-VEVP for thermoplastics

- Basis: Hyperelastic visco-elastic-visco-plastic material model, see VEVP model
  - Strain measure:
    - $\mathbf{F} = \mathbf{F}^{\mathrm{ve}} \cdot \mathbf{F}^{\mathrm{vp}}$, $\mathbf{C}^{\mathrm{ve}} = \mathbf{F}^{\mathrm{veT}} \cdot \mathbf{F}^{\mathrm{ve}}$, $\mathbf{E}^{\mathrm{ve}} = \frac{1}{2}\ln(\mathbf{C}^{\mathrm{ve}})$
    - $\mathbf{L}^{\mathrm{vp}} = \dot{\mathbf{F}}^{\mathrm{vp}} \cdot \mathbf{F}^{\mathrm{vp}-1}$, $\mathbf{D}^{\mathrm{vp}} = \mathbf{L}^{\mathrm{vp}}$
  - Visco-elastic part

$$
\begin{cases}
\boldsymbol{\tau}^{\mathrm{dev}} = \int_{-\infty}^{t} 2G(t-s)\frac{\mathrm{d}}{\mathrm{d}s}\mathrm{dev}(\mathbf{E}^{\mathrm{ve}}(s))\mathrm{d}s \\
p = \frac{1}{3}\boldsymbol{\tau}^{\mathrm{tr}} = \int_{-\infty}^{t} K(t-s)\frac{\mathrm{d}}{\mathrm{d}s}\mathrm{tr}(\mathbf{E}^{\mathrm{ve}}(s))\mathrm{d}s
\end{cases}
$$

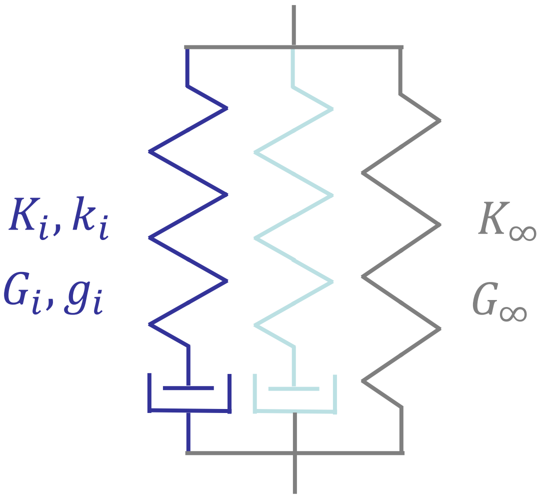

  - Maxwell model
    - $G(t) = G_\infty + \sum_{i=1}^{N} G_i \exp(-\frac{t}{g_i})$
    - $K(t) = K_\infty + \sum_{i=1}^{N} K_i \exp(-\frac{t}{k_i})$
  - Parameters:

$$K_\infty, G_\infty, G_i, g_i \quad K_i, k_i, \qquad i = 1, \dots, N$$

Finite-strain thermomechanical quasi-nonlinear-VEVP for thermoplastics

- Basis: Hyperelastic visco-elastic-visco-plastic material model
  - Visco-plastic part
    - Back-stress
      $\boldsymbol{\varphi} = \boldsymbol{\tau} - \boldsymbol{b}$
    - Perzina plastic flow rule
      $$\mathbf{D}^{\mathrm{vp}} = \dot{\mathbf{F}}^{\mathrm{vp}} \cdot \mathbf{F}^{\mathrm{vp}-1} = \frac{1}{\eta}\langle F\rangle^{\frac{1}{s}}\frac{\partial P}{\partial \boldsymbol{\tau}} = \lambda\frac{\partial P}{\partial \boldsymbol{\tau}}$$
    - Yield surface, flow potential
      $$\begin{cases} F = \left(\frac{\varphi^{\mathrm{eq}}}{Y_c}\right)^{\alpha} - \frac{m^{\alpha}-1}{m+1}\frac{\mathrm{tr}\boldsymbol{\varphi}}{Y_c} - \frac{m^{\alpha}+m}{m+1} \\ m = \frac{\sigma_t}{\sigma_c} \\ P = (\varphi^{\mathrm{eq}})^2 + \beta\left(\frac{\mathrm{tr}\boldsymbol{\varphi}}{3}\right)^2 \end{cases}$$
    - Equivalent plastic strain rate:
      $$\begin{cases} \dot{\gamma} = \frac{\sqrt{\mathbf{D}^{\mathrm{vp}}:\mathbf{D}^{\mathrm{vp}}}}{\sqrt{\mathbf{1}+\mathbf{2}\boldsymbol{v}_{\boldsymbol{p}}^{\mathbf{2}}}} \\ v_p = \frac{9-2\beta}{18+2\beta} \end{cases}$$

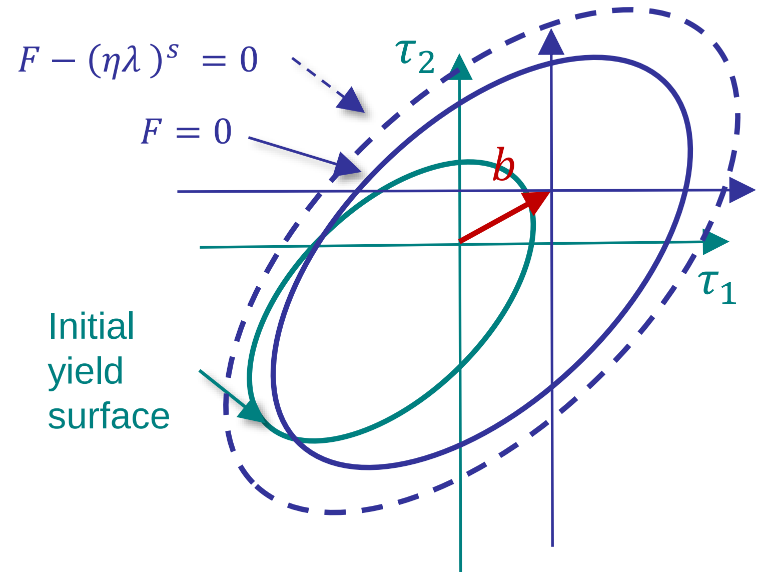

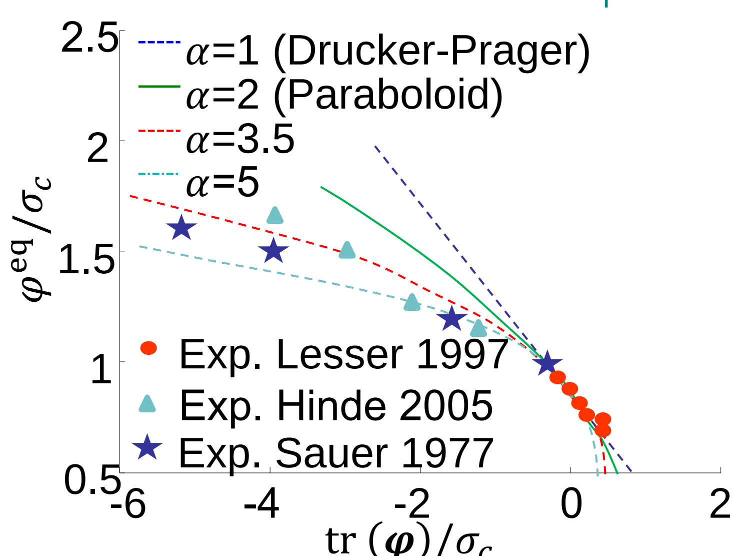

Finite-strain thermomechanical quasi-nonlinear-VEVP for thermoplastics

- Basis: Hyperelastic visco-elastic-visco-plastic material model
  - Visco-plastic part
    - Hardening

$$\begin{cases} \dot{Y}_c = H_c(\gamma)\dot{\gamma} \text{ with } H_c(\gamma) = c_0 + h_c\ H_c^0 \exp(-h_c\ \gamma), \\ \dot{Y}_t = H_t(\gamma)\dot{\gamma} \text{ with } H_t(\gamma) = t_0 + h_t\ H_t^0 \exp(-h_t\ \gamma), \\ \dot{\mathbf{b}} = \frac{H_b(\gamma)}{\sqrt{1+2\nu_p^2}} \mathbf{D}^{vp} \text{ with } H_b(\gamma) = b_0 + h_b\ H_b^0 \exp(-h_b\ \gamma), \end{cases}$$

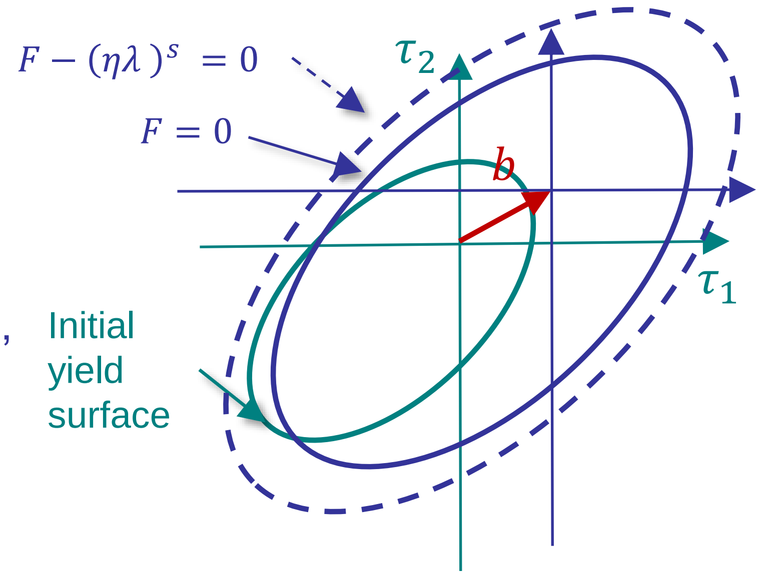

  - Parameters: (back-stress)
    - $\sigma_{c0},\ c_0,\ h_c\ , H_c^0$
    - σ_{t0} or $m_0,\ t_0,\ h_t\ , H_t^0$
    - $\eta,\ s,\ \alpha,\ \beta$

$$\begin{cases} F = \left(\frac{\varphi^{\text{eq}}}{Y_c}\right)^{\alpha} - \frac{m^\alpha - 1}{m+1}\frac{\text{tr}\boldsymbol{\varphi}}{Y_c} - \frac{m^\alpha + m}{m+1} \\ m = \frac{\sigma_t}{\sigma_c} \\ \nu_p = \frac{9-2\beta}{18+2\beta} \end{cases}$$

Finite-strain thermomechanical quasi-nonlinear-VEVP for thermoplastics

- Ingredient for thermoplastics material (model developed in CARBOBRAKE)

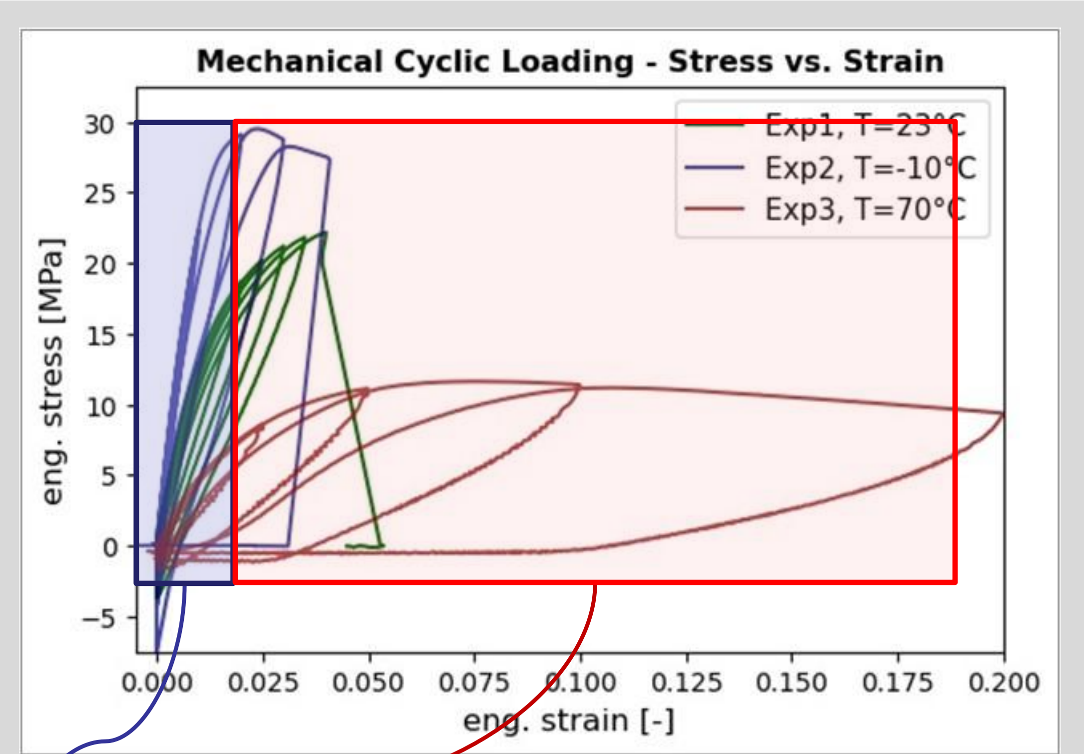

Polypropylene Cyclic Loading

Thermo(Visco)Elasticity – Maxwell Model + TTSP

Thermo(Visco)Plasticity – Power Law YF + Perzyna Flow

Mullins Effect and Self heating

- Ingredient for thermoplastics material
  - Visco-elasticity

$$\begin{cases} \boldsymbol{\tau}^{\mathrm{dev}} = \int_{-\infty}^{t} 2G(t-s)\frac{\mathrm{d}}{\mathrm{d}s}\mathrm{dev}(\mathbf{E}^{\mathrm{ve}}(s))\mathrm{d}s \\ p = \frac{1}{3}\boldsymbol{\tau}^{\mathrm{tr}} = \int_{-\infty}^{t} K(t-s)\frac{\mathrm{d}}{\mathrm{d}s}\mathrm{tr}(\mathbf{E}^{\mathrm{ve}}(s))\mathrm{d}s \end{cases}$$

$$\begin{cases} G(t) = G_\infty + \sum_{i=1}^{N} G_i \exp(-\frac{t}{g_i}) \\ K(t) = K_\infty + \sum_{i=1}^{N} K_i \exp(-\frac{t}{k_i}) \end{cases}$$

$$\Rightarrow \begin{cases} \boldsymbol{\tau}_{\boldsymbol{i}}^{\mathrm{dev}} = 2G_i\left[\exp\left(-\frac{\Delta t}{g_i}\right)\mathrm{dev}(\mathbf{E}^{\mathrm{ve}} - \boldsymbol{\Gamma}_i)_n + \exp\left(-\frac{\Delta t}{2g_i}\right)\mathrm{dev}(\mathbf{E}^{\mathrm{ve}} - \mathbf{E}_{\mathrm{n}}^{\mathrm{ve}})\right] \\ p_{\boldsymbol{i}} = K_i\left[\exp\left(-\frac{\Delta t}{k_i}\right)\mathrm{tr}(\mathbf{E}^{\mathrm{ve}} - \boldsymbol{\Gamma}_i)_n + \exp\left(-\frac{\Delta t}{2k_i}\right)\mathrm{tr}(\mathbf{E}^{\mathrm{ve}} - \mathbf{E}_{\mathrm{n}}^{\mathrm{ve}})\right] \end{cases}$$

  - Thermo-visco-elasticity
    - Introduce a shift factor $\Delta t \rightarrow \int_{t_n}^{t_{n+1}} \frac{1}{a_T(T - T_{\mathrm{ref}})} dT$ from master curve
  - Thermo-visco-elasticity-visco-plasticity
    - Energy consistency demonstrated after turning $\mathbf{E}_{\mathrm{n}}^{\mathrm{ve}}$ and $\boldsymbol{\Gamma}_{in}$ to current unloaded configuration

Finite-strain thermomechanical quasi-nonlinear-VEVP for thermoplastics

- Ingredient for thermoplastics material
  - Visco-elastic part becomes quasi-non-linear

$$
\begin{cases}
K_\infty \rightarrow K_\infty A_{v_\infty}\left(\mathrm{tr}(\mathbf{E}^{\mathrm{ve}})\right) \\
G_\infty \rightarrow G_\infty B_{d_\infty}\left(\mathrm{dev}(\mathbf{E}^{\mathrm{ve}})\right) \\
\\
K_i \rightarrow K_i A_{v_i}\left(\mathrm{tr}(\mathbf{E}^{\mathrm{ve}} - \Gamma_i)\right) \\
G_i \rightarrow G_i B_{d_i}\left(\mathrm{dev}(\mathbf{E}^{\mathrm{ve}} - \Gamma_i)\right)
\end{cases}
$$

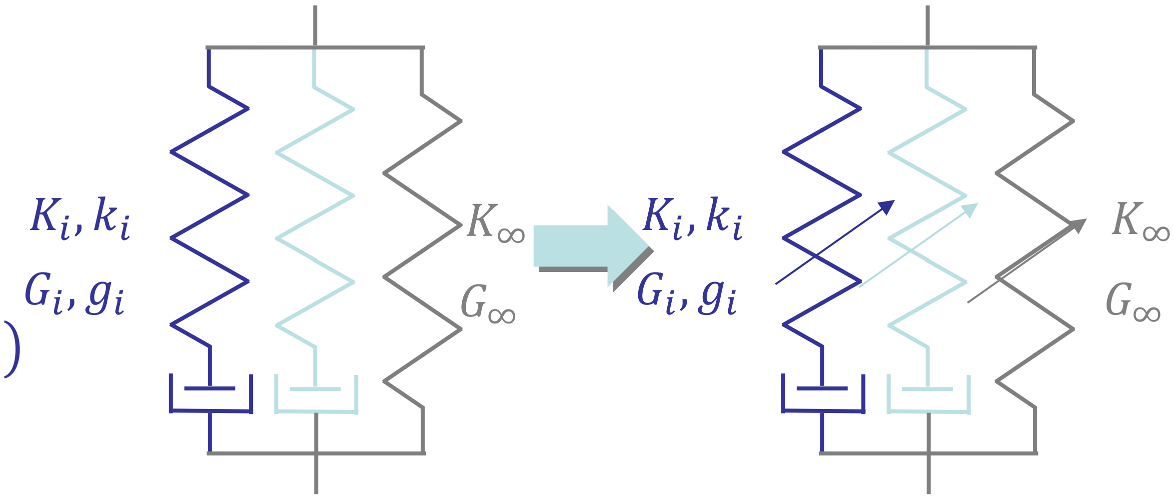

  - Asymmetry tension-compression
    - Logistic function f

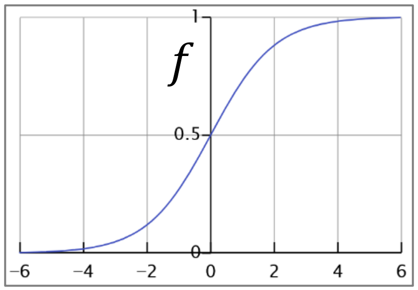

$$
\begin{cases}
A_{v_\infty}\left(\mathrm{tr}(\mathbf{E}^{\mathrm{ve}})\right) \rightarrow f\left(\mathrm{tr}(\mathbf{E}^{\mathrm{ve}})\right) A_{v_1}\left(\mathrm{tr}(\mathbf{E}^{\mathrm{ve}})\right) + C\left(1 - f\left(\mathrm{tr}(\mathbf{E}^{\mathrm{ve}})\right)\right) A_{v_2}\left(\mathrm{tr}(\mathbf{E}^{\mathrm{ve}})\right) \\
B_{d_\infty}\left(\mathrm{dev}(\mathbf{E}^{\mathrm{ve}})\right) \rightarrow f\left(\mathrm{tr}(\mathbf{E}^{\mathrm{ve}})\right) B_{d_1}\left(\mathrm{tr}(\mathbf{E}^{\mathrm{ve}})\right) + C\left(1 - f\left(\mathrm{tr}(\mathbf{E}^{\mathrm{ve}})\right)\right) B_{dv_2}\left(\mathrm{tr}(\mathbf{E}^{\mathrm{ve}})\right) \\
\\
A_{v_i}\left(\mathrm{tr}(\mathbf{E}^{\mathrm{ve}} - \Gamma_i)\right) \rightarrow f\left(\mathrm{tr}(\mathbf{E}^{\mathrm{ve}} - \Gamma_i)\right) A_{v_{i1}}\left(\mathrm{tr}(\mathbf{E}^{\mathrm{ve}} - \Gamma_i)\right) + C\left(1 - f\left(\mathrm{tr}(\mathbf{E}^{\mathrm{ve}} - \Gamma_i)\right)\right) A_{v_{i2}}\left(\mathrm{tr}(\mathbf{E}^{\mathrm{ve}} - \Gamma_i)\right) \\
B_{d_i}\left(\mathrm{dev}(\mathbf{E}^{\mathrm{ve}} - \Gamma_i)\right) \rightarrow f\left(\mathrm{tr}(\mathbf{E}^{\mathrm{ve}} - \Gamma_i)\right) B_{d_{i1}}\left(\mathrm{tr}(\mathbf{E}^{\mathrm{ve}} - \Gamma_i)\right) + C\left(1 - f\left(\mathrm{tr}(\mathbf{E}^{\mathrm{ve}})\right)\right) B_{dv_{i2}}\left(\mathrm{tr}(\mathbf{E}^{\mathrm{ve}} - \Gamma_i)\right)
\end{cases}
$$

Finite-strain thermomechanical quasi-nonlinear-VEVP for thermoplastics

- Ingredient for thermoplastics material
  - Mullin's-like effect
    - Work in an effective space
      - Free visco-elastic energy $\hat{\psi}$
      - Stress $\hat{\boldsymbol{\tau}}$
    - Define a "reversible" damage
      - $\zeta = 1 - z\left(1 - \dfrac{\hat{\psi}}{\hat{\psi}_{\text{max}}}\right)$
      - Dissipate during loading
      - Apparent stress $\boldsymbol{\tau} = \boldsymbol{\zeta}\hat{\boldsymbol{\tau}}$

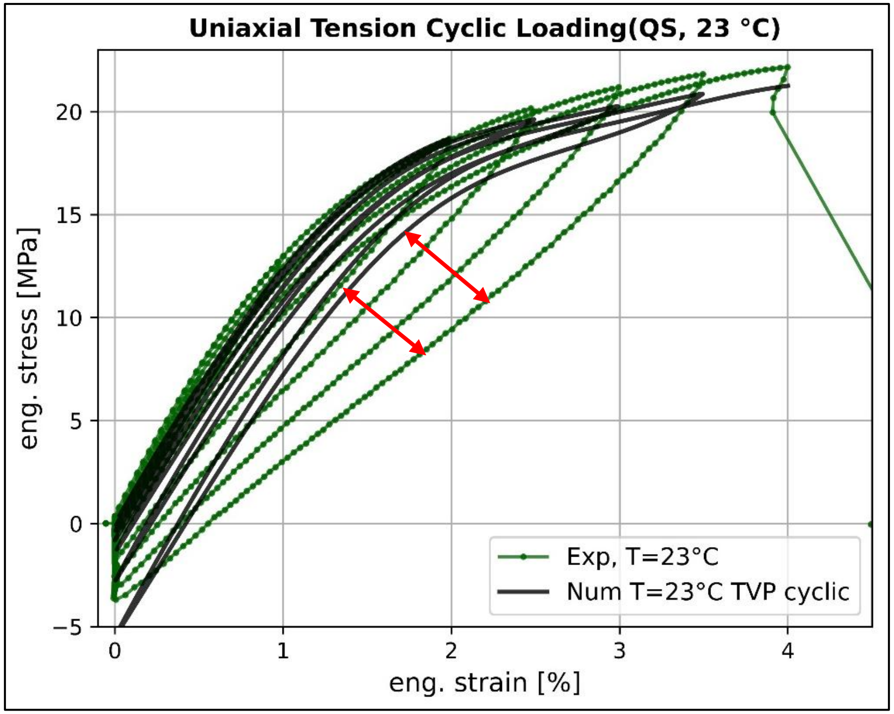

Finite-strain thermomechanical quasi-nonlinear-VEVP for thermoplastics

- Polypropylene BJ380MO (tests from LEARTIKER)

Tension

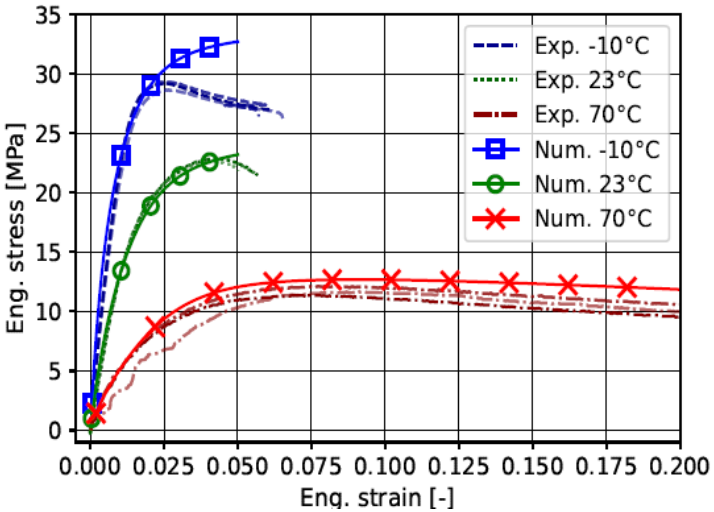

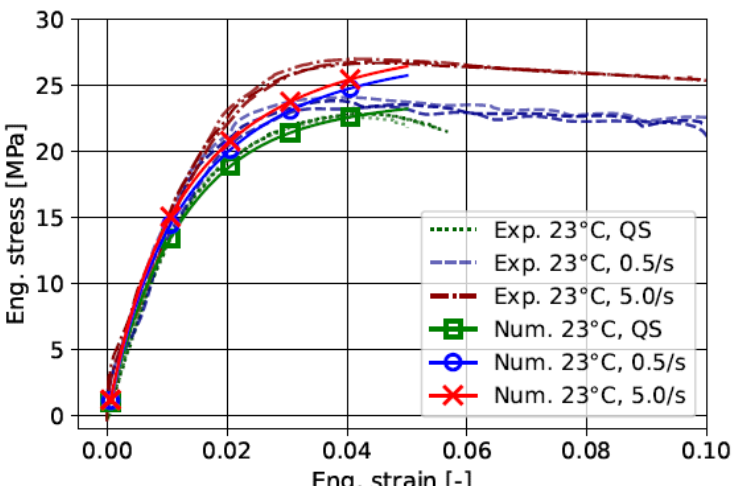

Compression

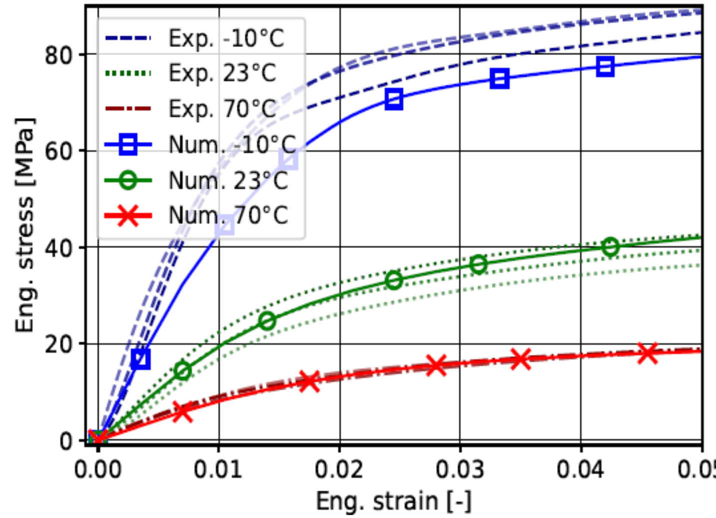

Finite-strain thermomechanical quasi-nonlinear-VEVP for thermoplastics

- Polypropylene BJ380MO (tests from LEARTIKER)

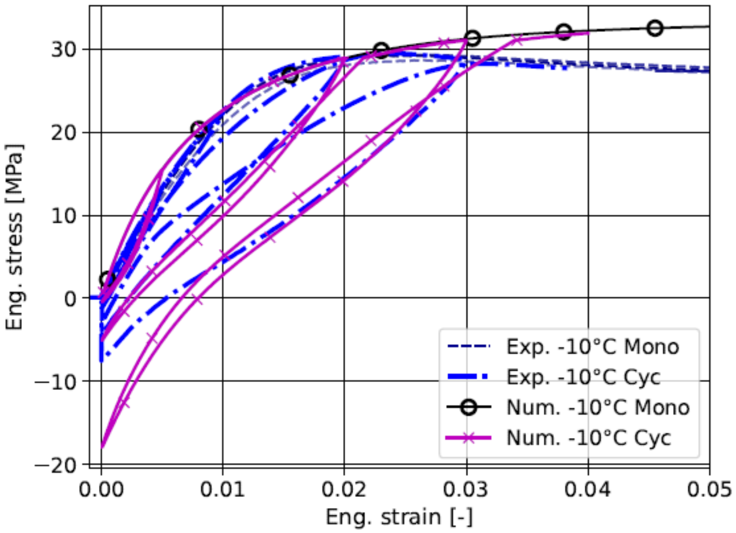

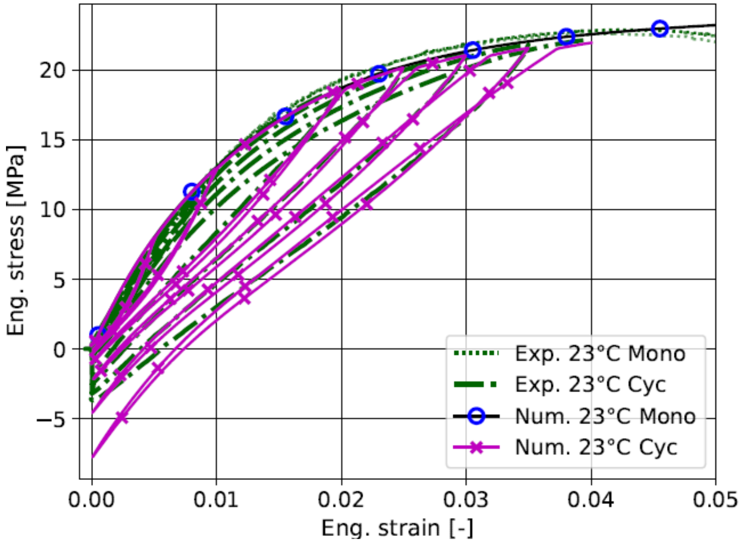

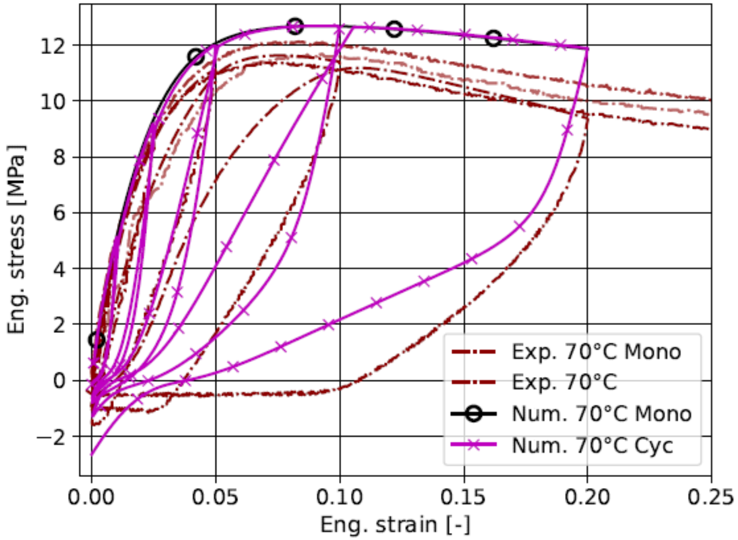

Finite-strain thermomechanical quasi-nonlinear-VEVP for thermoplastics

- Calibration on IMDEA TPU tests: cyclic loading

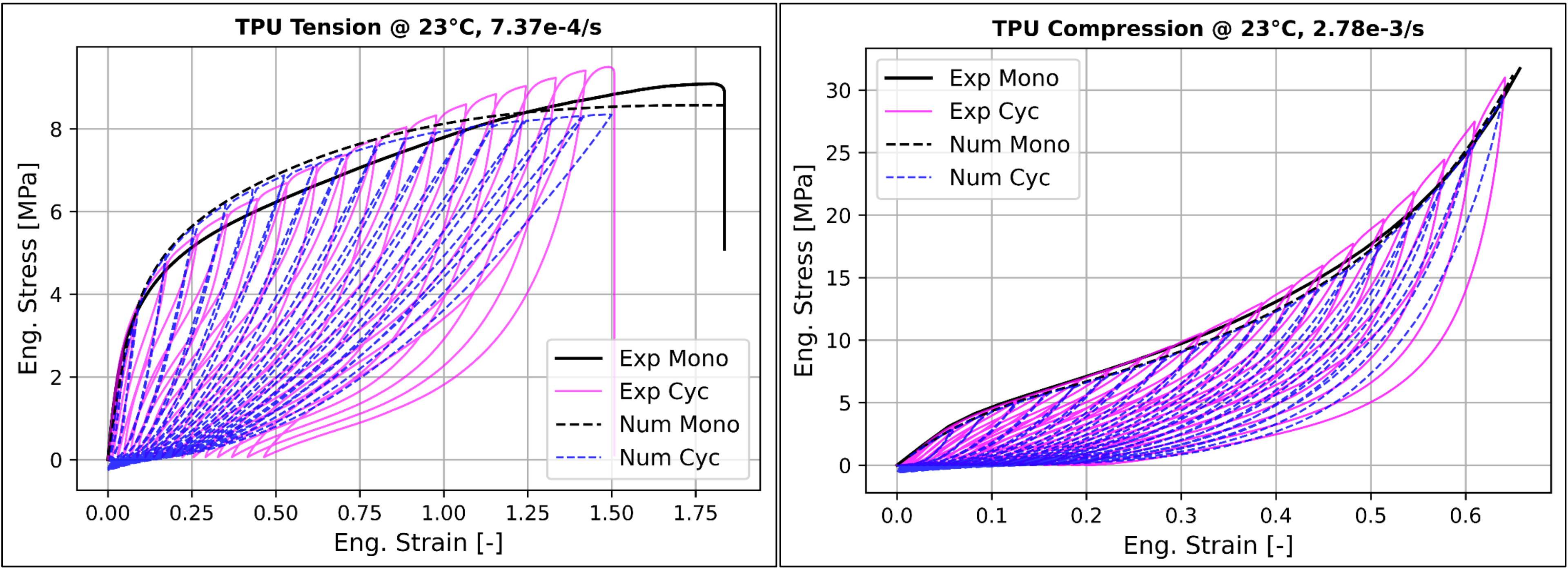

– Numerical Setup - Uniaxial Stress with QNL TVE + linear exponential isotropic hardening + polynomial kinematic hardening TVP + Mullins effect
  - QNL TVE: All TVE branches with equal parameters
  - Good agreement with experimental results in compression, mismatch in tension attributed to less viscoplasticity

Finite-strain thermomechanical quasi-nonlinear-VEVP for thermoplastics

- Calibration on IMDEA TPU tests: strain rate effect

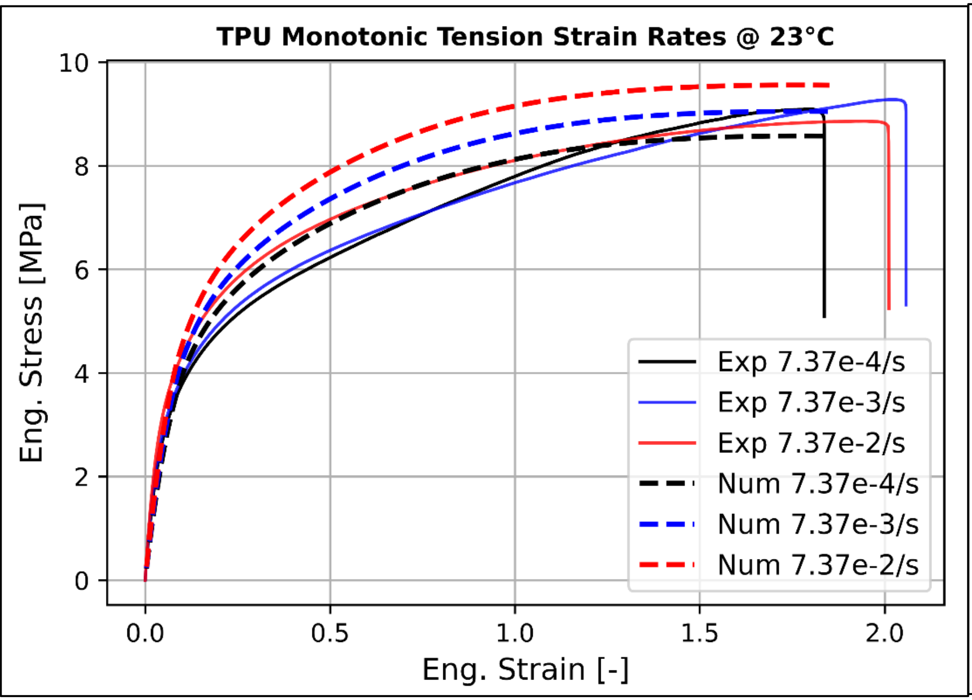

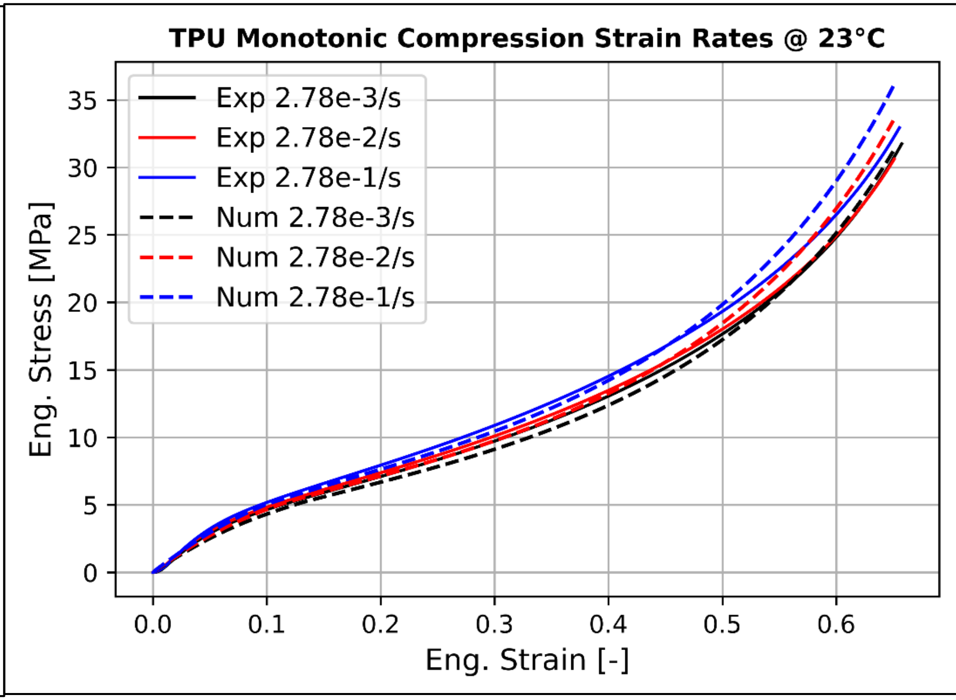

- Numerical Setup - Uniaxial Stress with QNL TVE + linear exponential isotropic + polynomial kinematic hardening TVP
  - QNL TVE: All TVE branches with equal parameters
  - Takeaway: Sensitivity to strain rates is overpredicted by the model

- 3D Axisymmetric Dumbbell – Tension and Compression tests from JKU

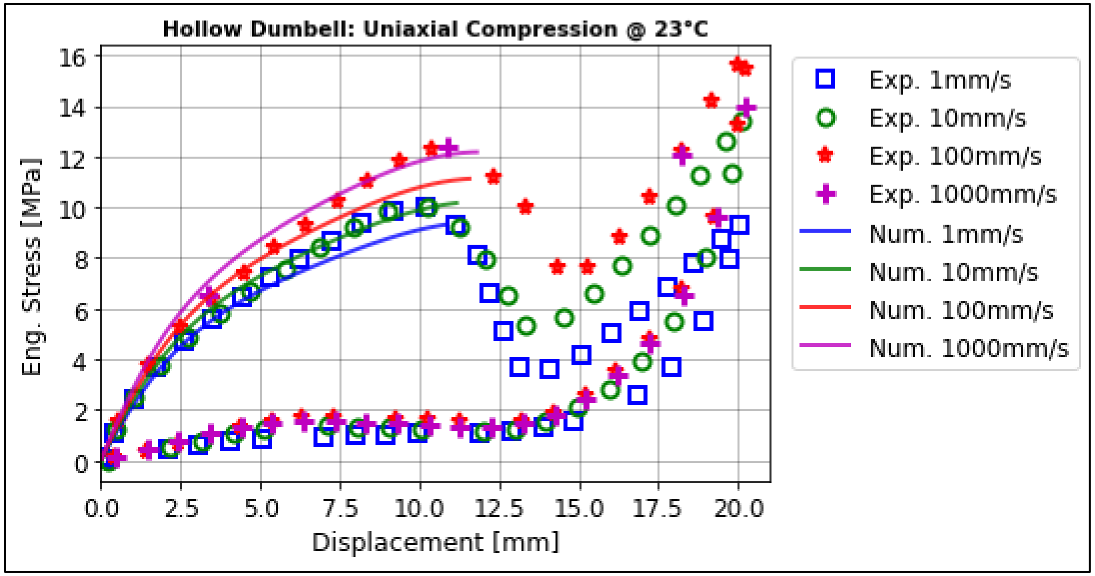

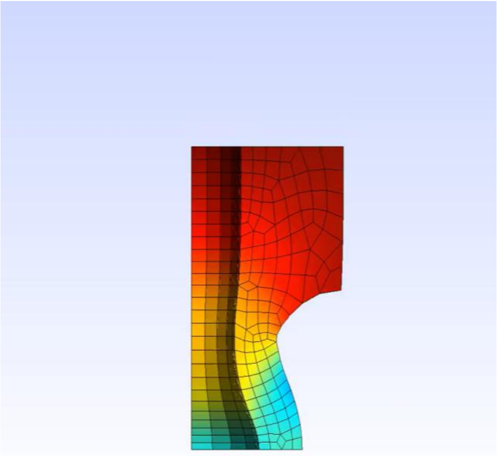

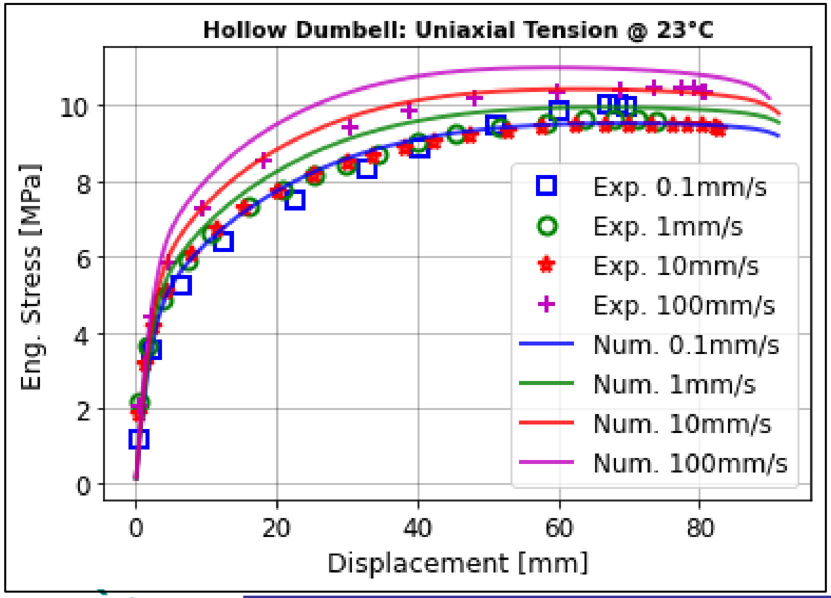

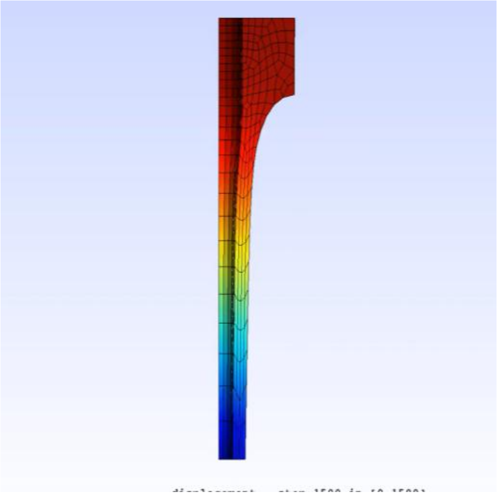

Finite-strain thermomechanical quasi-nonlinear-VEVP for thermoplastics

- 3D Axisymmetric Dumbbell – Torsion test from JKU

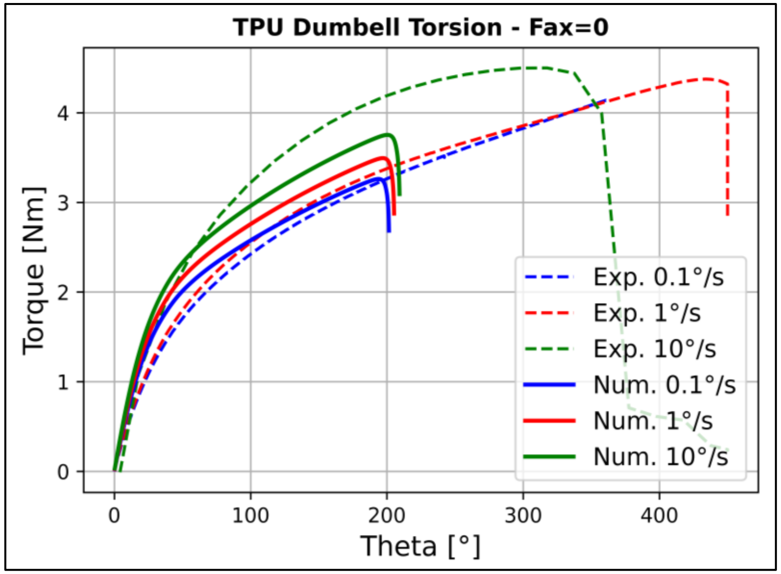

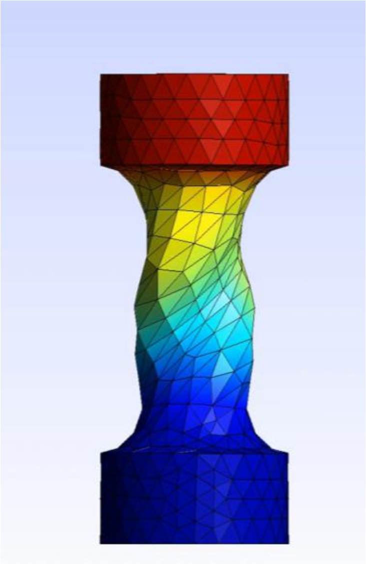

Numerical Setup – Bottom cylindrical surface fixed, Top surface free to move, top cylindrical surface is twisted.

Takeaway: Torsional buckling encountered at lower angles of twist in simulations.

Ductile failure of High-Entropy Alloys (HEA)

- Publication (doi)
  - http://dx.doi.org/10.2139/ssrn.5142306
- Data
  - https://gitlab.onelab.info/cm3/carbobrake

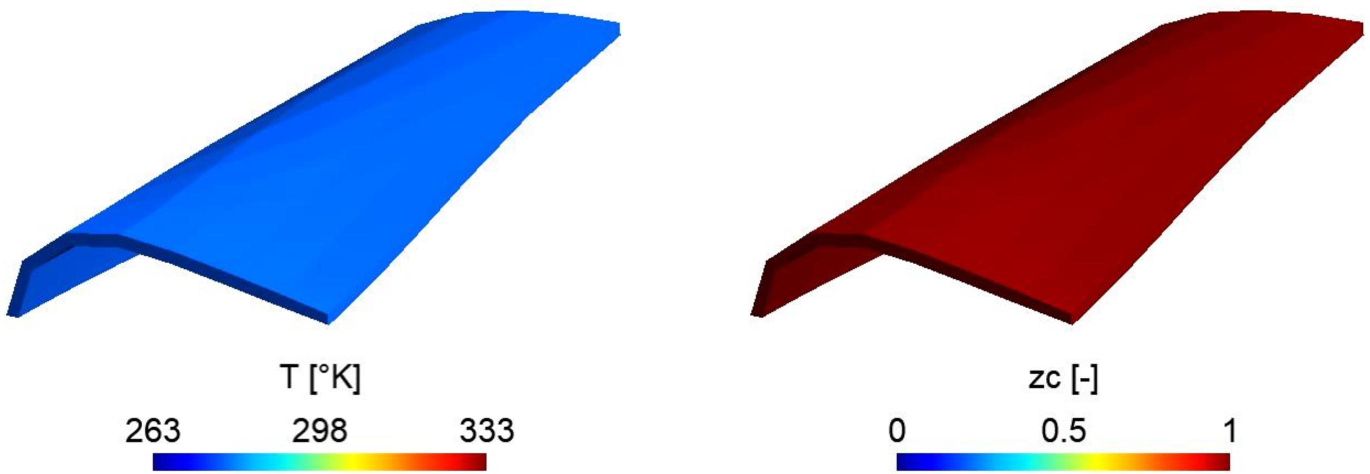

Thermo-Mechanical, Viscoelasto-Plastic Model for Semi-Crystalline Polymers Exhibiting One-Way and Two-Way Shape Memory Effects Under Phase Change

This research was funded through the “Actions de recherche concert´ees 2017-Synthesis, Characterization, and Multiscale Model of Smart Composite Materials (S3CM3) 17/21-07”, financed by the “Direction G´en´erale de l’Enseignement non obligatoire de la Recherche scientifique, Direction de la Recherche scientifique, Communaut´e Fran¸caise de Belgique et octroyées par l’Académie Universitaire Wallonie-Europe”.

One-Way and Two-Way Shape Memory Polymers

- Thermally triggered shape memory effect
  - One-way shape memory effect

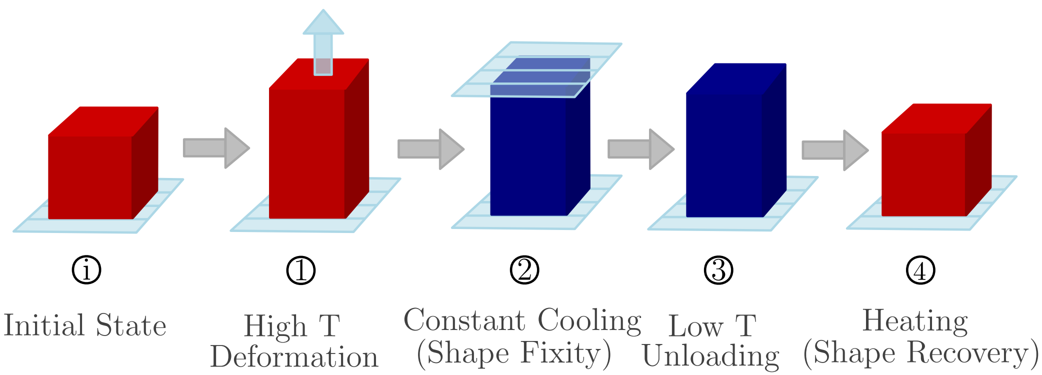

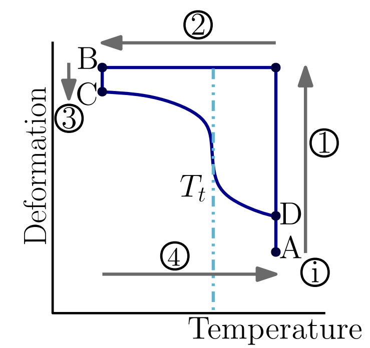

B:perfect shape fixity
C:real shape fixity
A:perfect shape recovery
D:real shape recovery

  - Two-way shape memory effect

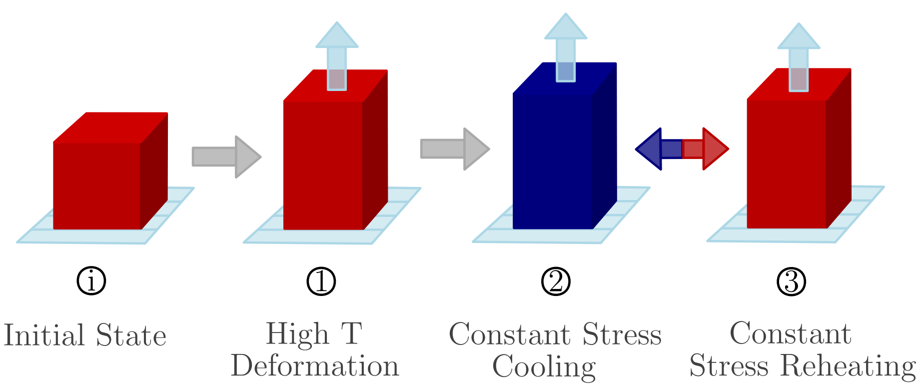

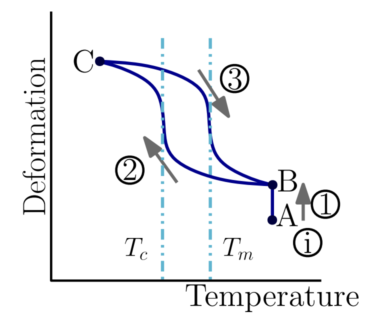

B:1^{st} programmed shape
C:2^{nd} programmed shape
A:zero stress shape

- Model ingredients for Semi-Crystalline Polymers
  - Change of phase in the crystalline region: crystallized vs. melted

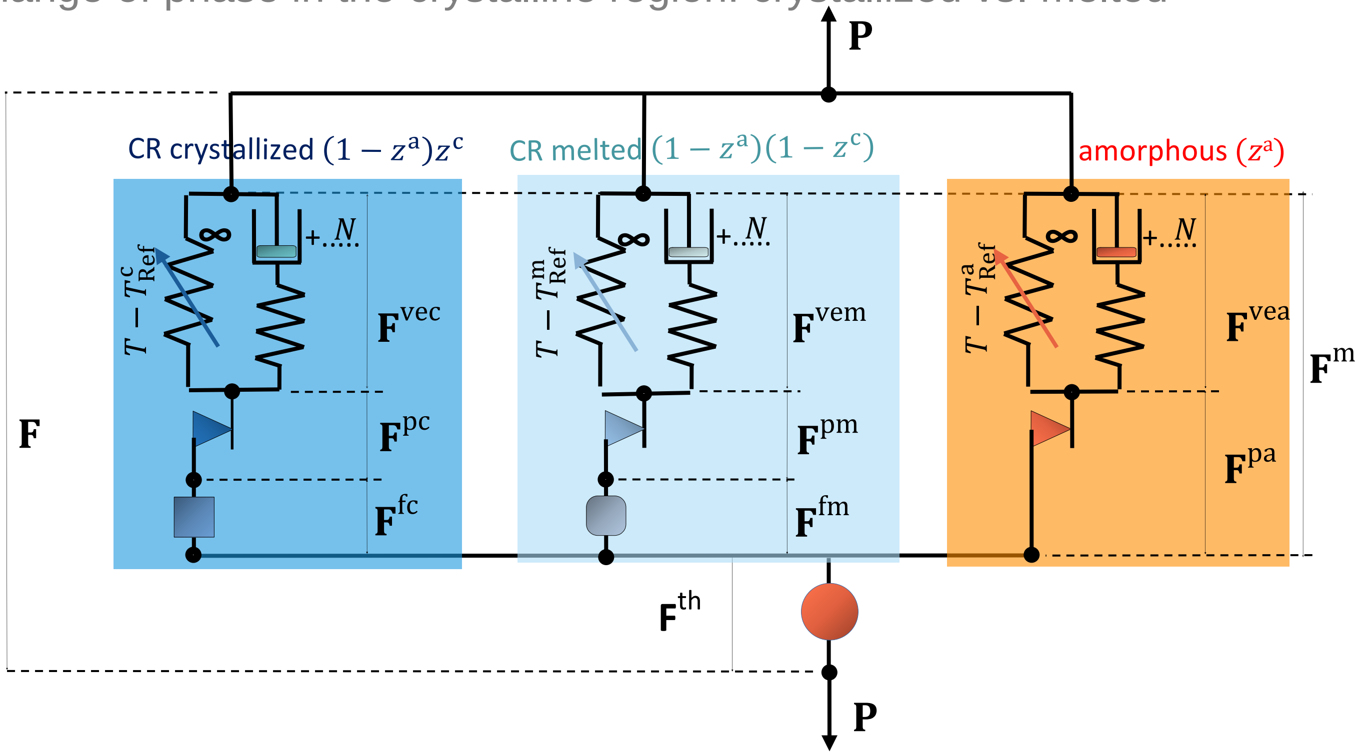

- Crystallinity degree depends on temperature T and on strain measure $\mathbf{E}^{\mathrm{vem}}$

$$\begin{cases} \dot{z}^{c} = -f\left(T, \left|\mathbf{E}^{\mathrm{vem}}\right|\right)\dot{T}\,, \text{ with } z^{c} \in [0{,}1] \\ f\left(T, \left|\mathrm{E}^{\mathrm{vem}}\right|\right) = \dfrac{1}{w_{\mathrm{t}}(|\mathbf{E}^{\mathrm{vem}}|)\sqrt{2\pi}} \exp\left[-\dfrac{1}{2}\left(\dfrac{T-(|\mathbf{E}^{\mathrm{vem}}|)}{w_{\mathrm{t}}(|\mathbf{E}^{\mathrm{vem}}|)}\right)^{2}\right] \end{cases}$$

- Residual strain evaluated at change of phase

$$\mathbf{F}^{\mathrm{fc}} = \begin{cases} \mathbf{F}^{\mathrm{m}} \text{ if melted} \\ \text{constant otherwise} \end{cases} \qquad \mathbf{F}^{\mathrm{fm}} = \mathrm{I}$$

- Model ingredients for Semi-Crystalline Polymers
  - Crystallinity degree depends on temperature T and on strain measure $\mathbf{E}^{\text{vem}}$

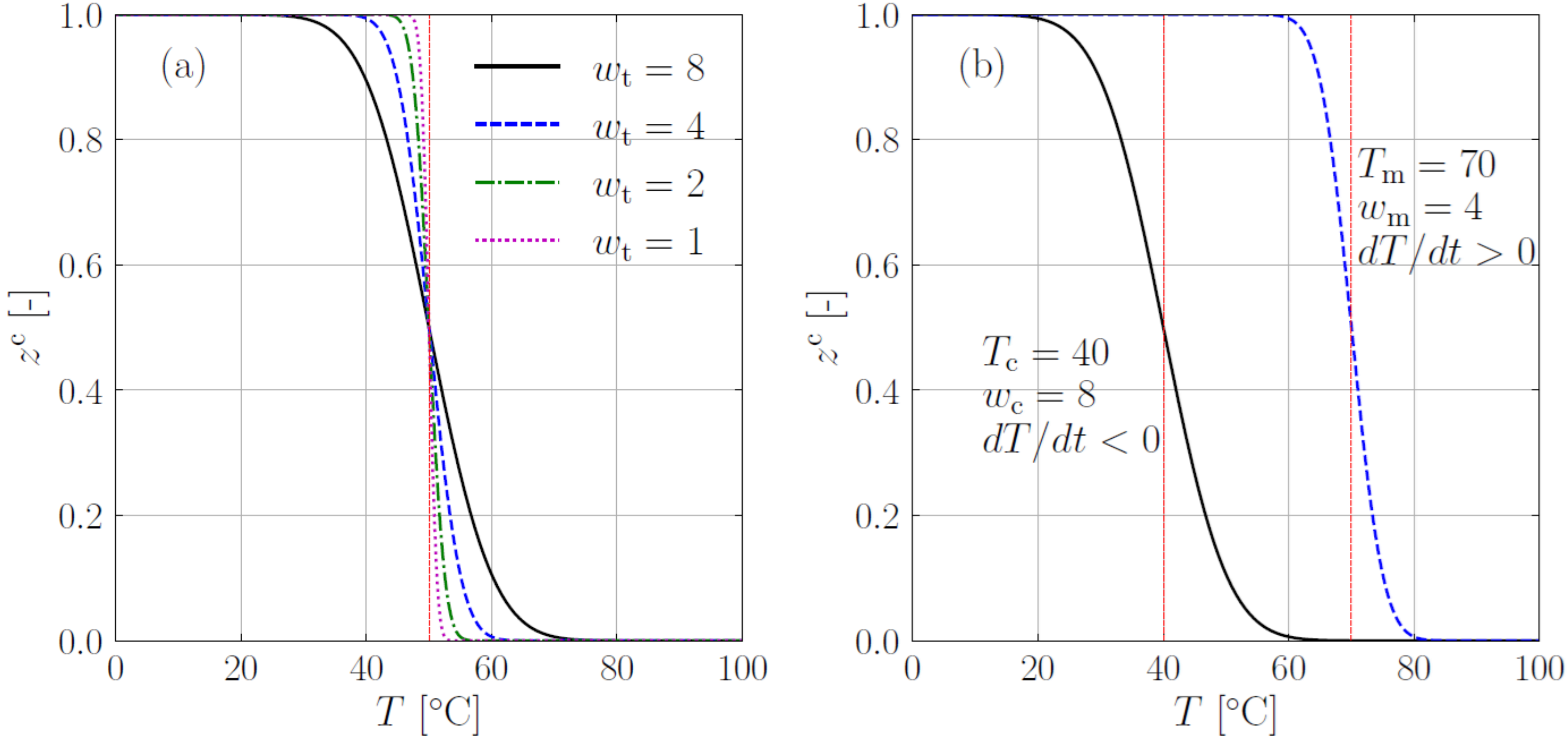

$$\begin{cases} \dot{z}^c = -f\left(T, \left|\mathbf{E}^{\text{vem}}\right|\right)\dot{T}, \text{ with } z^c \in [0,1] \\ f\left(T, \left|\mathbf{E}^{\text{vem}}\right|\right) = \dfrac{1}{w_t\left(\left|\mathbf{E}^{\text{vem}}\right|\right)\sqrt{2\pi}} \exp\left[-\dfrac{1}{2}\left(\dfrac{T - \left(\left|\mathbf{E}^{\text{vem}}\right|\right)}{w_t\left(\left|\mathbf{E}^{\text{vem}}\right|\right)}\right)^2\right] \\ T_t, w_t = \begin{cases} T_c\left(\left|\mathbf{E}^{\text{vem}}\right|\right), w_c\left(\left|\mathbf{E}^{\text{vem}}\right|\right) \text{ if } \dot{T} < 0 \text{ (cooling)} \\ T_m\left(\left|\mathbf{E}^{\text{vem}}\right|\right), w_m\left(\left|\mathbf{E}^{\text{vem}}\right|\right) \text{ if } \dot{T} > 0 \text{ (heating)} \end{cases} \end{cases}$$

- Model ingredients for Semi-Crystalline Polymers
  - Anistropic thermal expansion which depends on the strain measure $\mathbf{E}^{\text{vem}}$

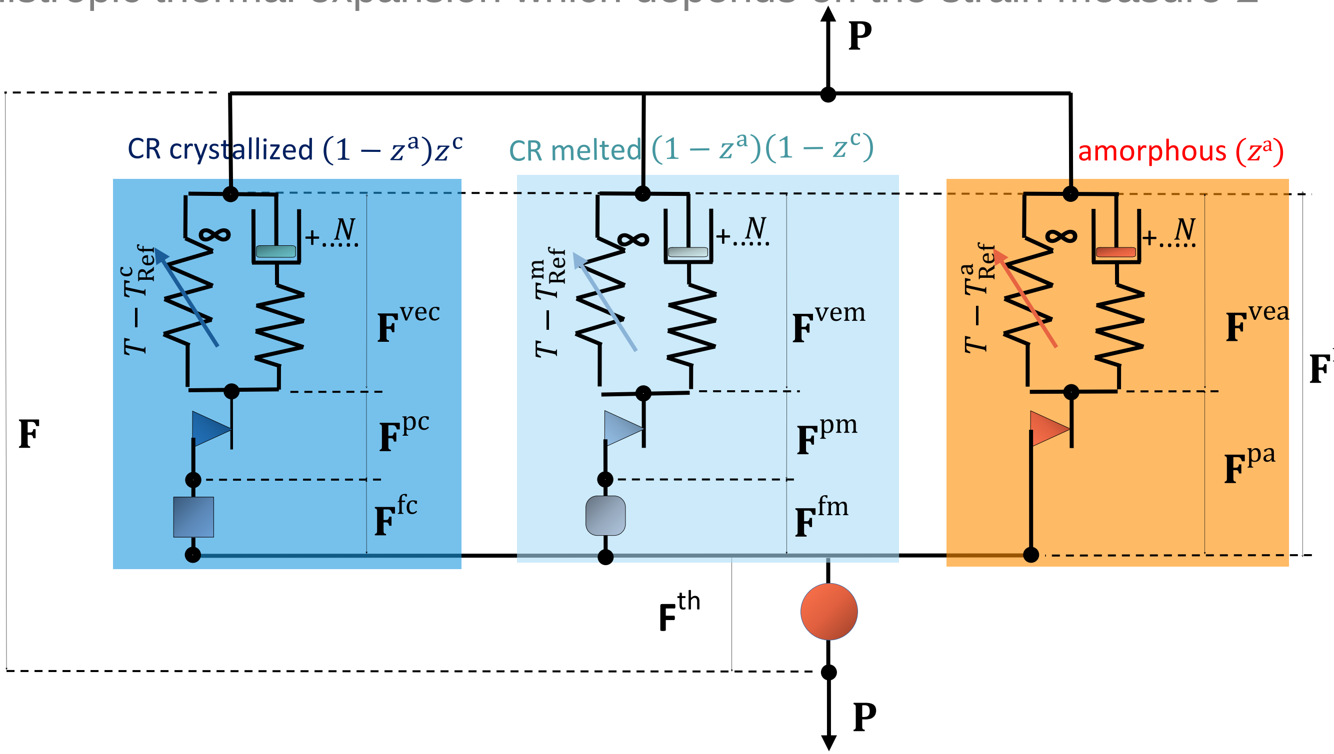

- Model considering spring stiffnesses dependent on a temperature mismatch between phases

$$\hat{G}_\infty^{\text{c/m}}\left(T;\, T^{\text{c/m}}_{\text{Ref}}\right) = \bar{G}_\infty^{\text{c/m}}\left[1 + A_{f_G}^{\text{c/m}}\tanh\left(\alpha_{f_G}^{\text{c/m}}\left(T - T^{\text{c/m}}_{\text{Ref}}\right)\right)\right],$$

$$T^{\text{c}}_{\text{Ref}} = \begin{cases} T \text{ if melted} \\ \text{constant otherwise} \end{cases} \qquad T^{\text{m}}_{\text{Ref}} = \begin{cases} T \text{ if crystallized} \\ \text{constant otherwise} \end{cases}$$

- Model ingredients for Semi-Crystalline Polymers
  - Plastic flow during crystallization when polymer under straining
    - Stress, back-stress $\boldsymbol{\varphi} = \hat{\boldsymbol{\tau}} - \hat{\boldsymbol{b}}$
    - Pressure dependent yield surface

$$\begin{cases} \phi = \left(\dfrac{\varphi^{\mathrm{eq}}}{\sigma_c}\right)^{\alpha} - \dfrac{m^{\alpha}-1}{m+1}\dfrac{\mathrm{tr}\boldsymbol{\varphi}}{\sigma_c} - \dfrac{m^{\alpha}+m}{m+1} \leq 0 \\ m = \dfrac{\sigma_t}{\sigma_c} \end{cases}$$

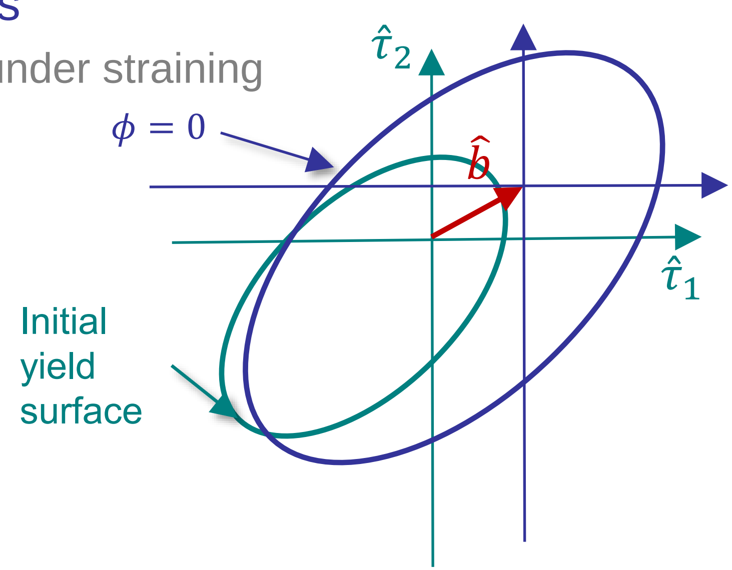

    - Non-associated flow potential

$$P = (\varphi^{\mathrm{eq}})^2 + \beta\left(\frac{\mathrm{tr}\boldsymbol{\varphi}}{3}\right)^2$$

    - Equivalent plastic strain rate:

$$\dot{\boldsymbol{\gamma}} = \frac{\sqrt{\mathbf{D}^{\mathrm{p}}:\mathbf{D}^{\mathrm{p}}}}{\sqrt{\mathbf{1} + \mathbf{2}\boldsymbol{v}_p^2}} \qquad v_p = \frac{9-2\beta}{18+2\beta}$$

    - Yield surface during crystallization

$$\begin{cases} \sigma_{\mathrm{t}}^{\mathrm{c}}(\gamma^i) = h^{\mathrm{c}}(z^{\mathrm{c}})\left[\sigma_{\mathrm{t}}^{0\mathrm{c}} + \int H_{\mathrm{t}}^{\mathrm{c}}(\gamma^{\mathrm{c}})d\gamma^{\mathrm{c}}\right] \\ \sigma_{\mathrm{c}}^{\mathrm{c}}(\gamma^i) = h^{\mathrm{c}}(z^{\mathrm{c}})\left[\sigma_{\mathrm{c}}^{0\mathrm{c}} + \int H_{\mathrm{c}}^{\mathrm{c}}(\gamma^{\mathrm{c}})d\gamma^{\mathrm{c}}\right] \end{cases}$$

$$h^{\mathrm{c}}(z^{\mathrm{c}}) = \begin{cases} h_0^{\mathrm{c}} & \text{if } z^{\mathrm{c}} \leq z_0^{\mathrm{c}} \\ h_0^{\mathrm{c}} + (1-h_0^{\mathrm{c}})\dfrac{z^{\mathrm{c}}-z_0^{\mathrm{c}}}{1-z_0^{\mathrm{c}}} & \text{if } z^{\mathrm{c}} > z_0^{\mathrm{c}} \end{cases}$$

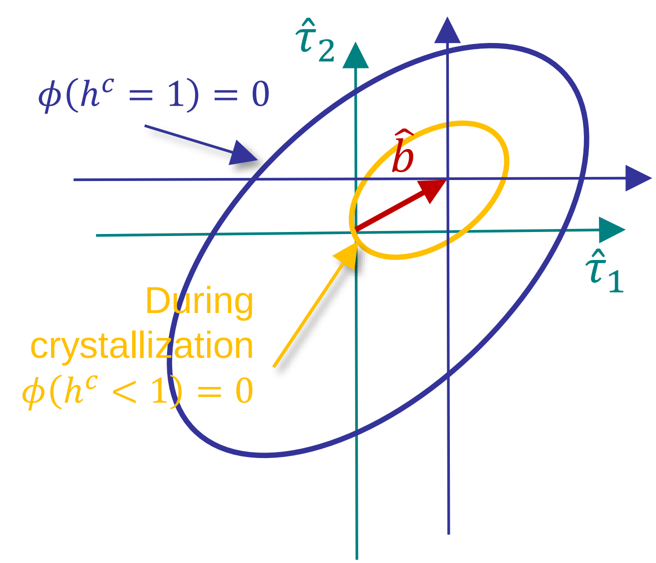

- Validation on PCL76-4MAL/FUR 3 wt% CNT samples: Isothermal loading cases

Temperature T=65°

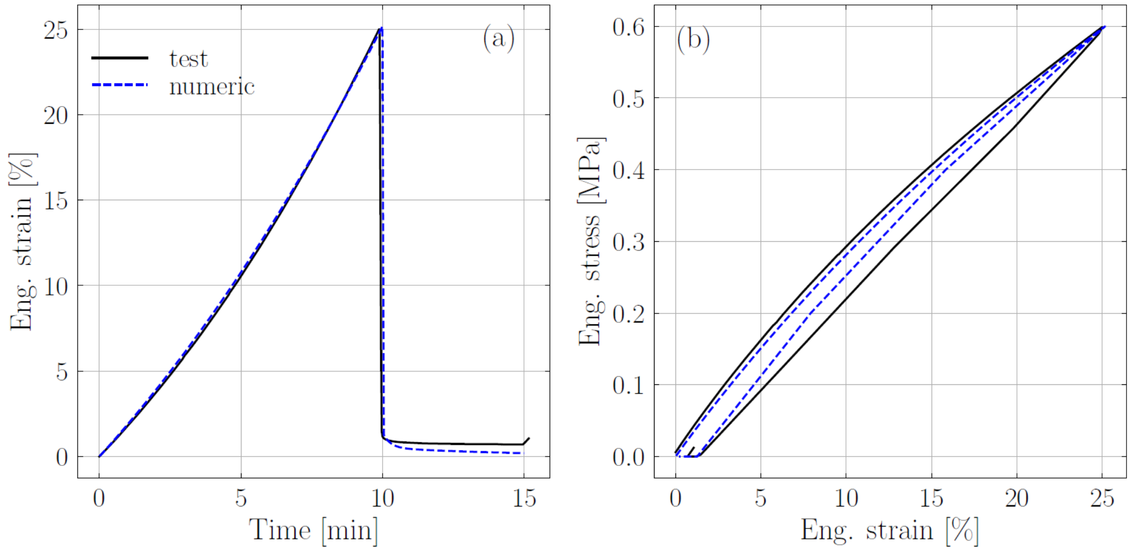

Temperature T=0°

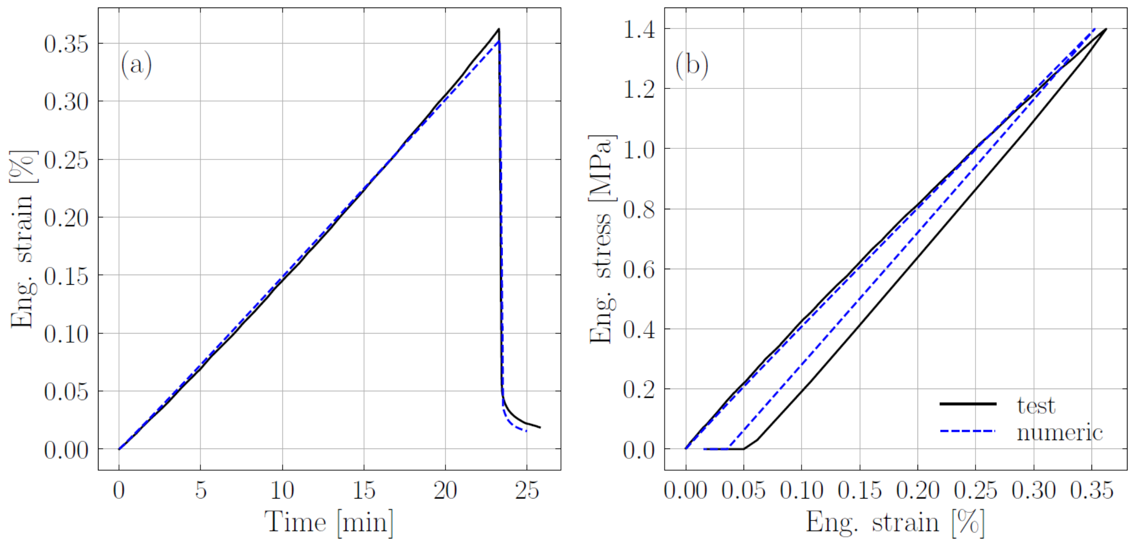

- Validation on PCL76-4MAL/FUR 3 wt% CNT samples: 2-Way SM effect

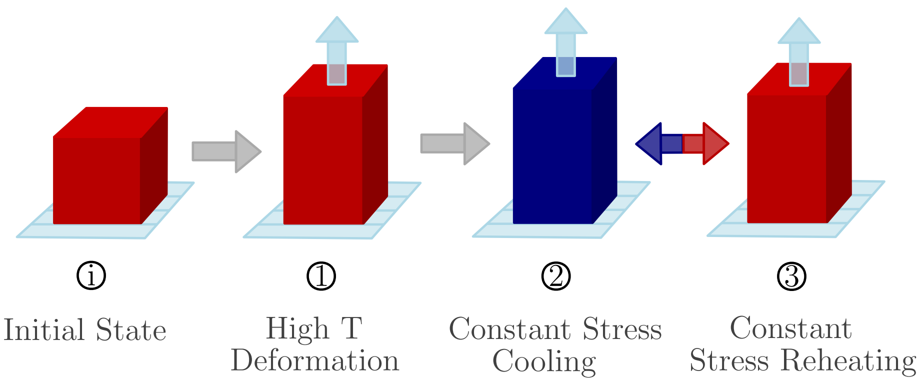

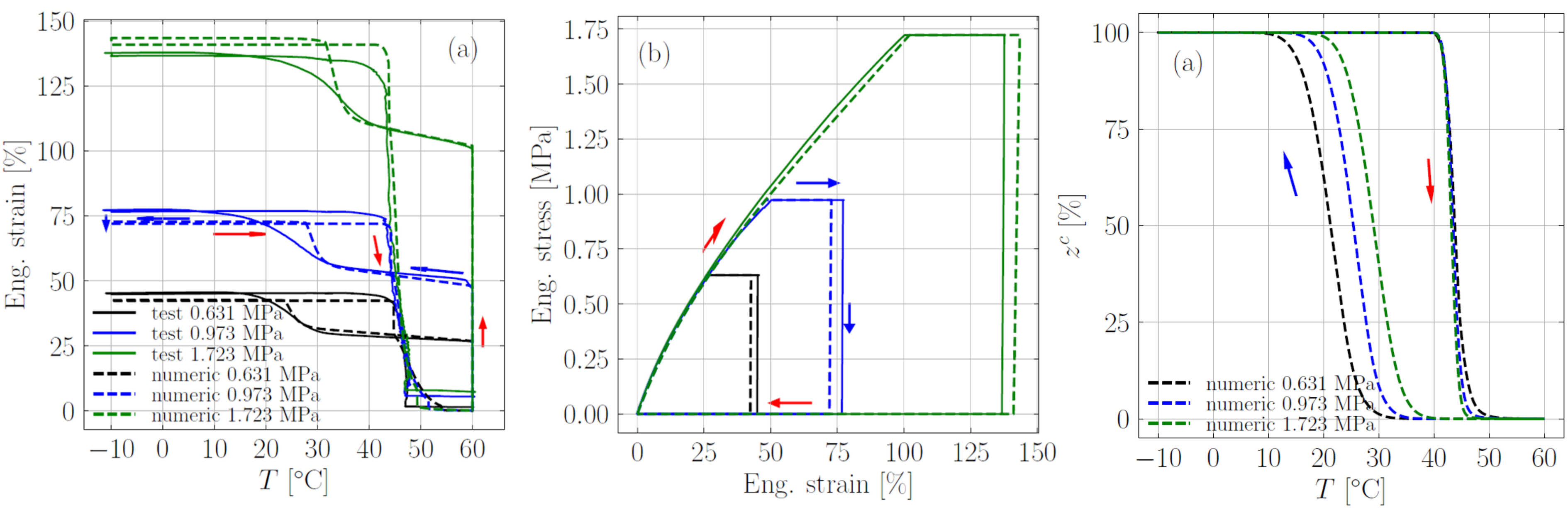

- Validation on PCL76-4MAL/FUR 3 wt% CNT samples: 1-Way SM effect

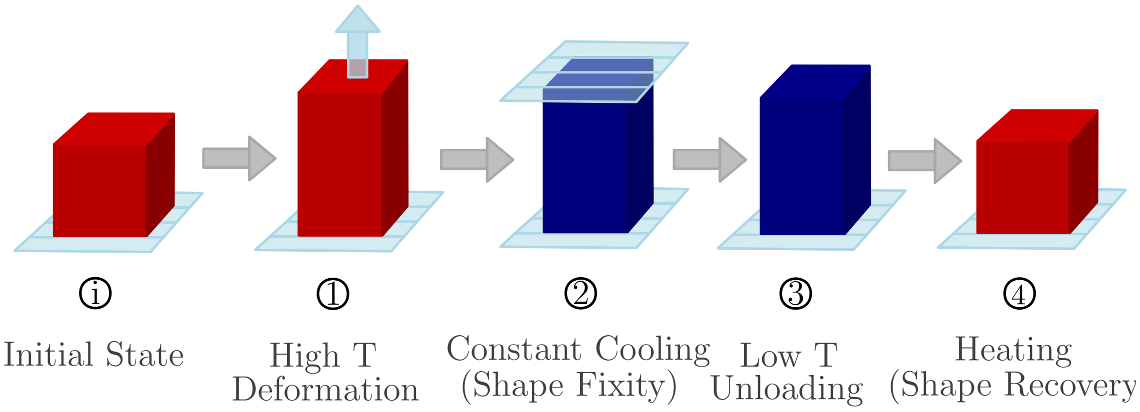

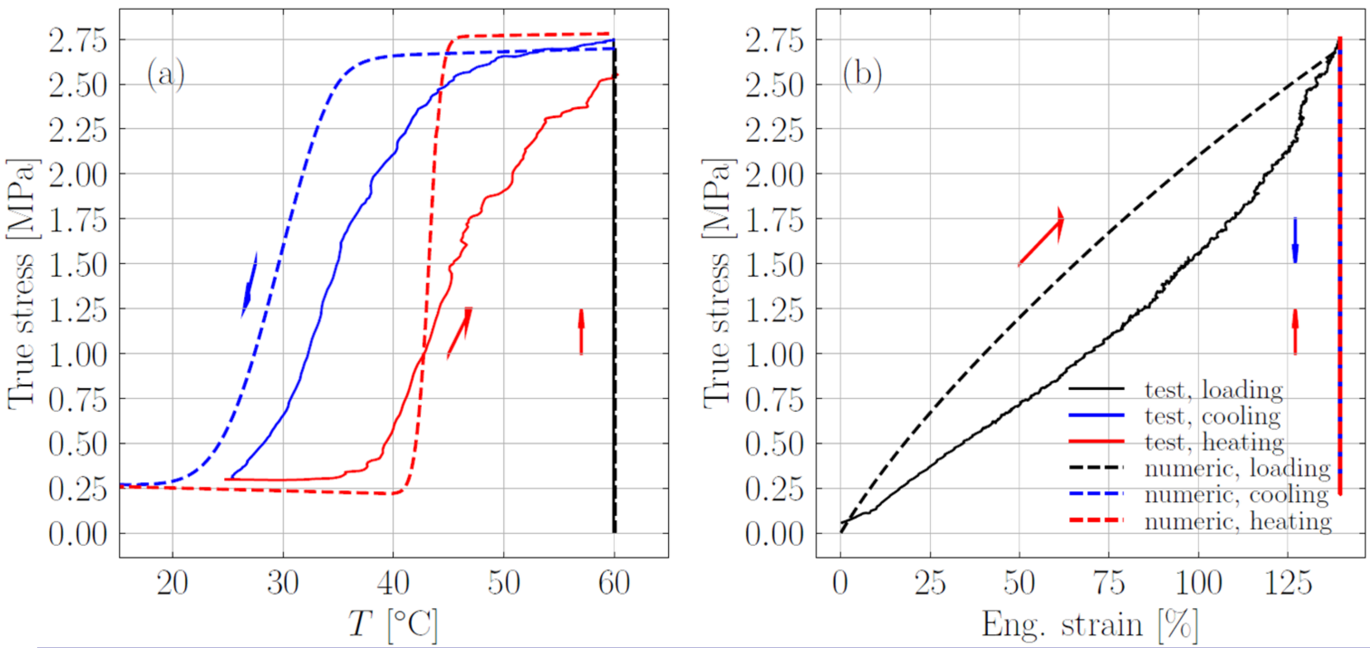

- Validation on PCL76-4MAL/FUR 3 wt% CNT samples: anisotropic expansion

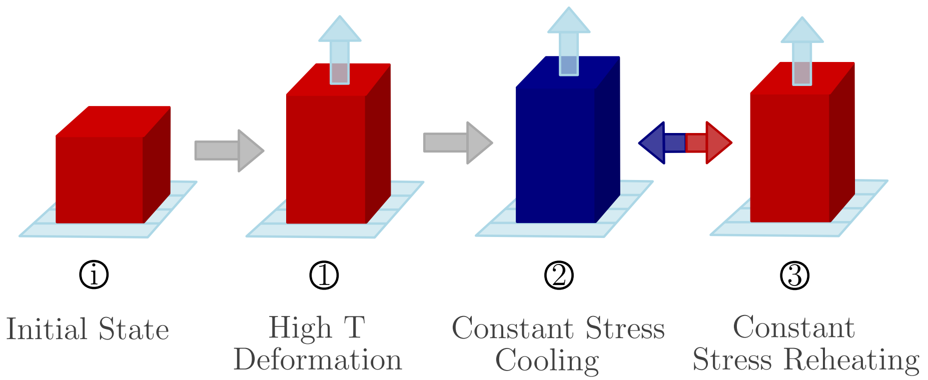

Stress σ = 600 kPa

Stress σ = 0 kPa

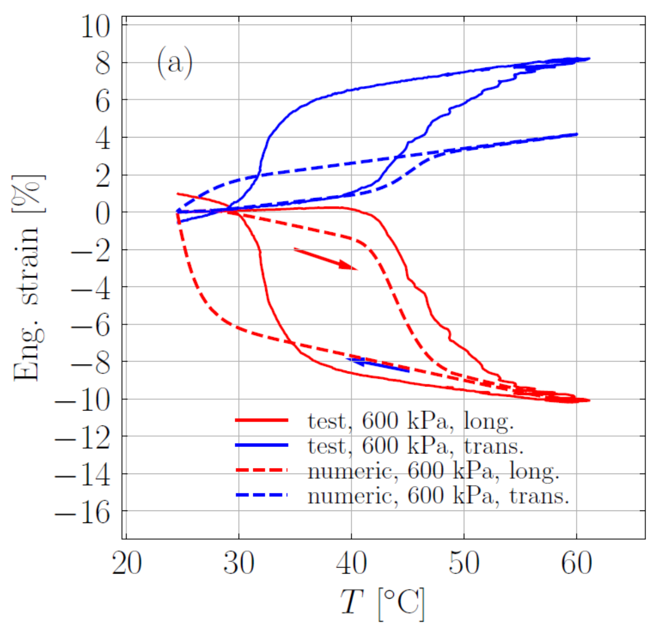

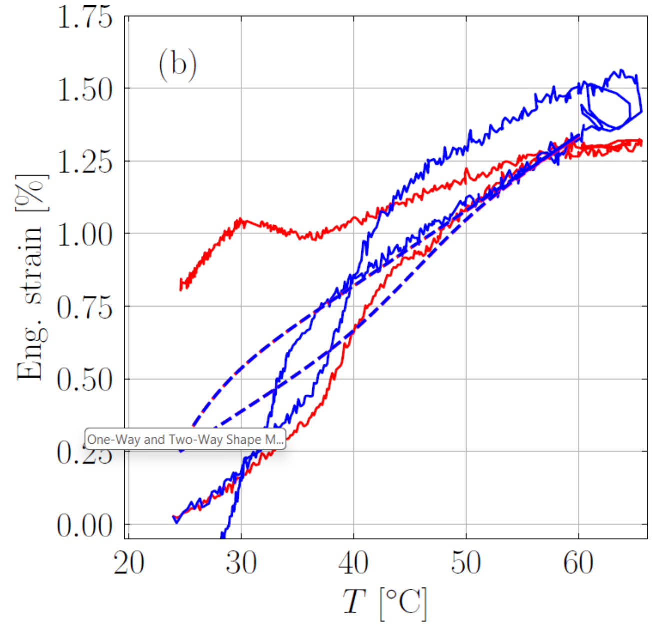

- Validation on PCL76-4MAL/FUR 3 wt% CNT samples: 3D simulation

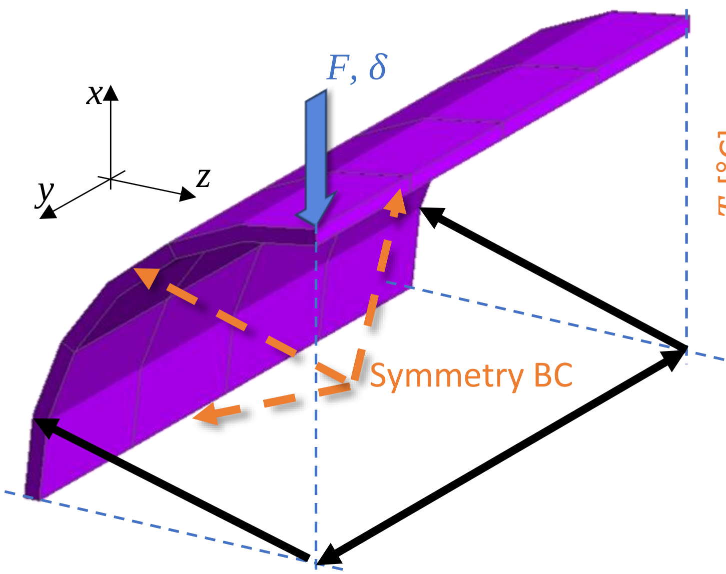

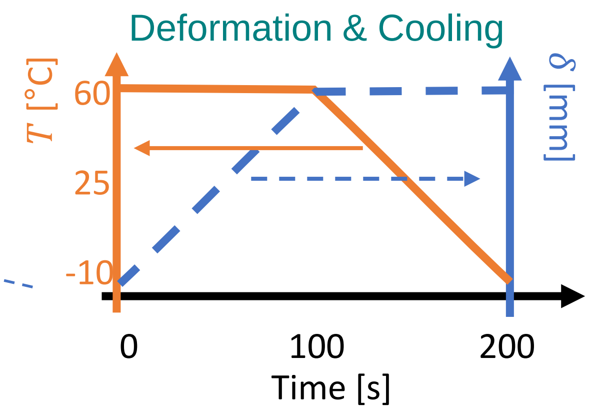

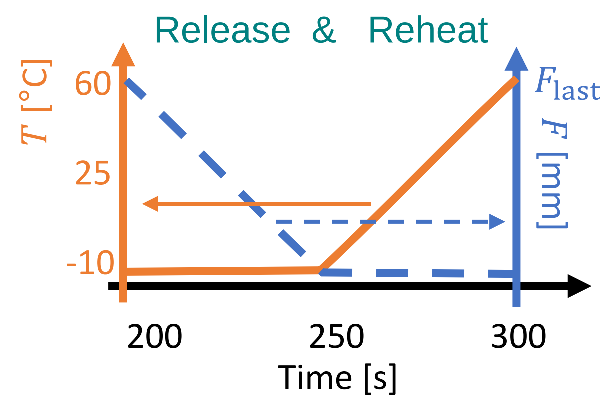

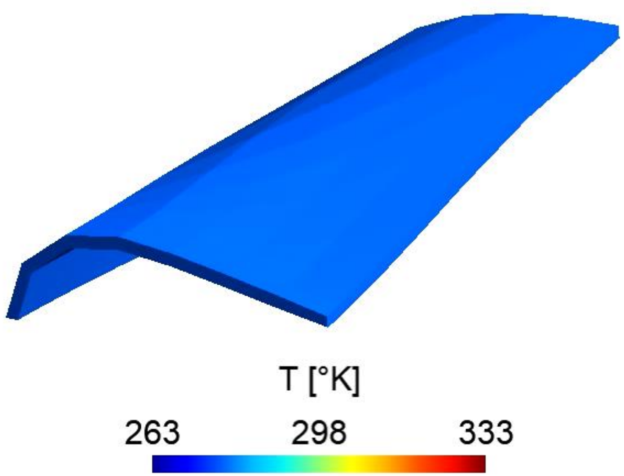

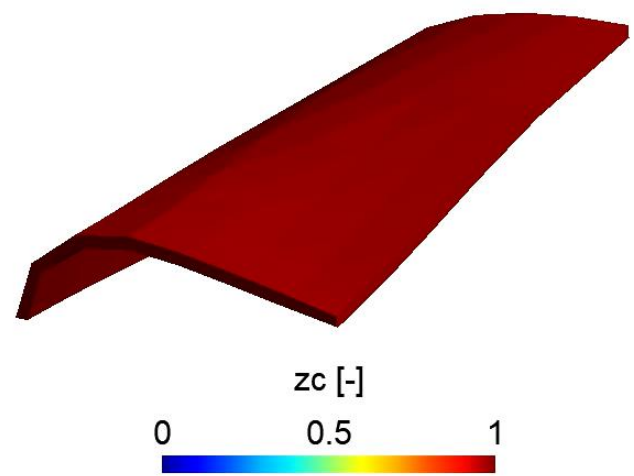

One-Way and Two-Way Shape Memory Polymers

- ARC project
  - Computational & Multiscale Mechanics of Materials (CM3), ULiège
  - Center for Education and Research on Macromolecules (CERM UR CESAM), ULiège
  - Electrical Engineering and Computer Science, ULiège
- Publications
  - 10.1016/j.polymer.2023.125992
  - 10.1088/1361-665X/ac8297
  - 10.1021/acsomega.2c05930
  - 10.1016/j.ijsolstr.2024.112814

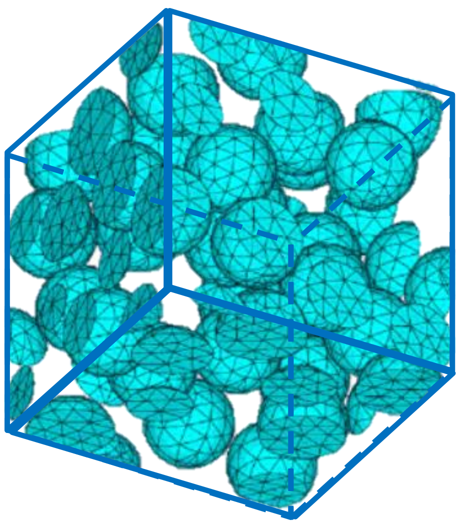

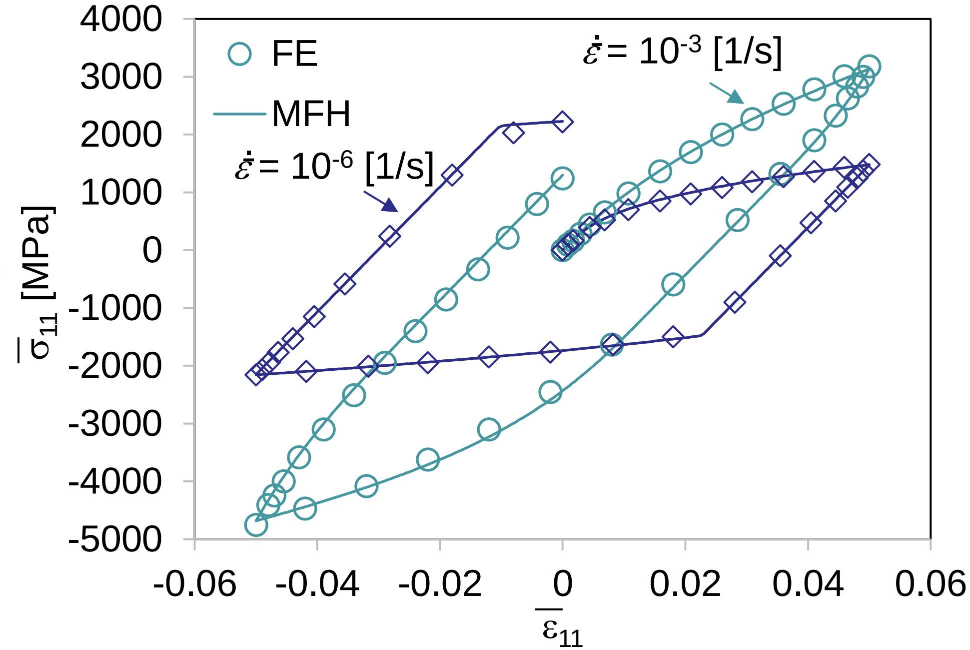

Mean-Field-Homogenization for Elasto-Visco-Plastic Composites

SIMUCOMP The research has been funded by the Walloon Region under the agreement no 1017232 (CT-EUC 2010-10-12) in the context of the ERA-NET +, Matera + framework.
The authors gratefully acknowledge the financial support from F.R.S-F.N.R.S. under the project number PDR T.1015.14
STOMMMAC The research has been funded by the Walloon Region under the agreement no 1410246-STOMMMAC (CT-INT 2013-03-28) in the context of M-ERA.NET Joint Call 2014.

Mean-Field-Homogenization for elasto-visco-plastic composites

- Multi-scale modeling
  - 2 problems are solved concurrently
    - The macro-scale problem
    - The meso-scale problem (on a meso-scale Volume Element)

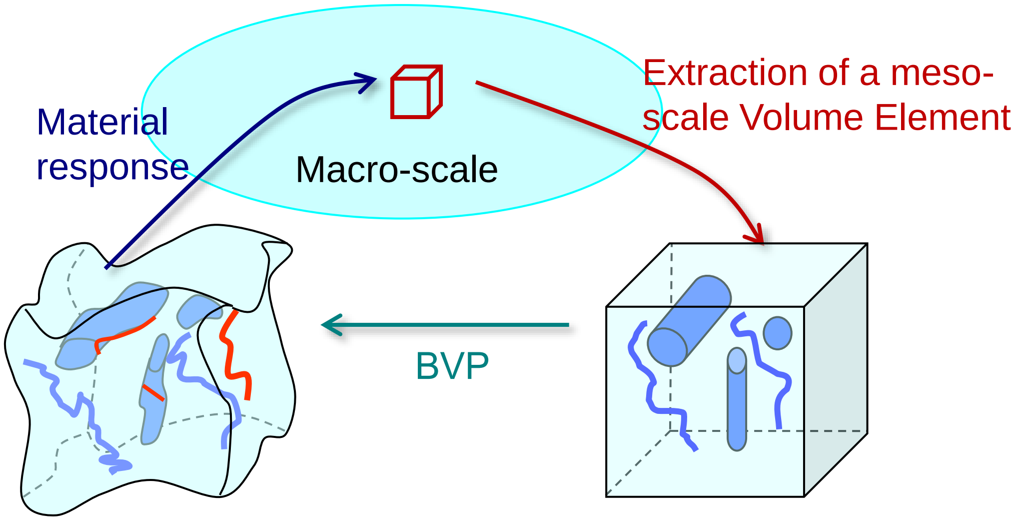

- Length-scales separation

$$L_{macro} >> L_{VE} >> L_{micro}$$

For accuracy: Size of the meso-scale volume element smaller than the characteristic length of the macro-scale loading

To be statistically representative: Size of the meso-scale volume element larger than the characteristic length of the micro-structure

Mean-Field-Homogenization for elasto-visco-plastic composites

- Incremental-secant mean-field-homogenization
  - Linear Comparison Composite material
    - Defined from unloaded state
  - Solve iteratively the system

$$\left\{\begin{array}{l} \Delta\bar{\boldsymbol{\varepsilon}}^{\mathrm{r}} = v_0\Delta\boldsymbol{\varepsilon}_0^{\mathrm{r}} + v_{\mathrm{I}}\Delta\boldsymbol{\varepsilon}_{\mathrm{I}}^{\mathrm{r}} \\ \Delta\boldsymbol{\varepsilon}_{\mathrm{I}}^{\mathrm{r}} = \Delta\boldsymbol{\varepsilon}_{\mathrm{I}} + \Delta\boldsymbol{\varepsilon}_{\mathrm{I}}^{\mathrm{unload}} \\ \Delta\boldsymbol{\varepsilon}_0^{\mathrm{r}} = \Delta\boldsymbol{\varepsilon}_0 + \Delta\boldsymbol{\varepsilon}_0^{\mathrm{unload}} \\ \Delta\boldsymbol{\varepsilon}_{\mathrm{I}}^{\mathrm{r}} = \mathbf{B}^{\varepsilon}\left(\mathrm{I}, \bar{\mathbf{C}}_0^{\mathrm{Sr}}, \bar{\mathbf{C}}_{\mathrm{I}}^{\mathrm{Sr}}\right) : \Delta\boldsymbol{\varepsilon}_0^{\mathrm{r}} \end{array}\right.$$

    - With the stress tensors

$$\left\{\begin{array}{l} \bar{\boldsymbol{\sigma}} = v_0\boldsymbol{\sigma}_0 + v_{\mathrm{I}}\boldsymbol{\sigma}_{\mathrm{I}} \\ \boldsymbol{\sigma}_{\mathrm{I}} = \boldsymbol{\sigma}_{\mathrm{I}}^{\mathrm{res}} + \bar{\mathbf{C}}_{\mathrm{I}}^{\mathrm{Sr}} : \Delta\boldsymbol{\varepsilon}_{\mathrm{I}}^{\mathrm{r}} \\ \boldsymbol{\sigma}_0 = \boldsymbol{\sigma}_0^{\mathrm{res}} + \bar{\mathbf{C}}_0^{\mathrm{Sr}} : \Delta\boldsymbol{\varepsilon}_0^{\mathrm{r}} \end{array}\right.$$

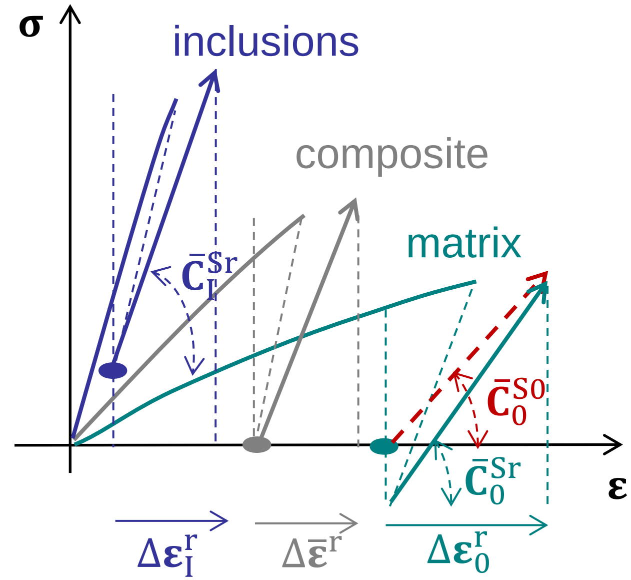

For elasto-plasticity: $f(\sigma^{\mathrm{eq}}, p) = 0$

&

For elasto-visco-plasticity: $\Delta p = g_v(\sigma^{\mathrm{eq}}, p)\Delta t$

  - For soft matrix response
    - Remove residual stress in matrix $\quad \Delta\boldsymbol{\varepsilon}_{\mathrm{I}}^{\mathrm{r}} = \mathbf{B}^{\varepsilon}\left(\mathrm{I}, \bar{\mathbf{C}}_0^{\mathrm{S0}}, \bar{\mathbf{C}}_{\mathrm{I}}^{\mathrm{Sr}}\right) : \Delta\boldsymbol{\varepsilon}_0^{\mathrm{r}}$ & $\boldsymbol{\sigma}_0 = \bar{\mathbf{C}}_0^{\mathrm{S0}} : \Delta\boldsymbol{\varepsilon}_0^{\mathrm{r}}$
    - Or use second moment estimates

- Incremental-secant mean-field-homogenization
  - Stress tensor (2 forms)

$$\begin{cases} \boldsymbol{\sigma}_{\mathrm{I}/0} = \boldsymbol{\sigma}_{\mathrm{I}/0}^{\mathrm{res}} + \bar{\mathbf{C}}_{\mathrm{I}/0}^{\mathrm{Sr}} : \Delta\boldsymbol{\varepsilon}_{\mathrm{I}/0}^{\mathrm{r}} \\ \boldsymbol{\sigma}_{\mathrm{I}/0} = \bar{\mathbf{C}}_{\mathrm{I}/0}^{\mathrm{S0}} : \Delta\boldsymbol{\varepsilon}_{\mathrm{I}/0}^{\mathrm{r}} \end{cases}$$

  - Radial return direction toward residual stress
    - First order approximation in the strain increment (and not in the total strain)
    - Exact for the zero-incremental-secant method
  - The secant operators are naturally isotropic

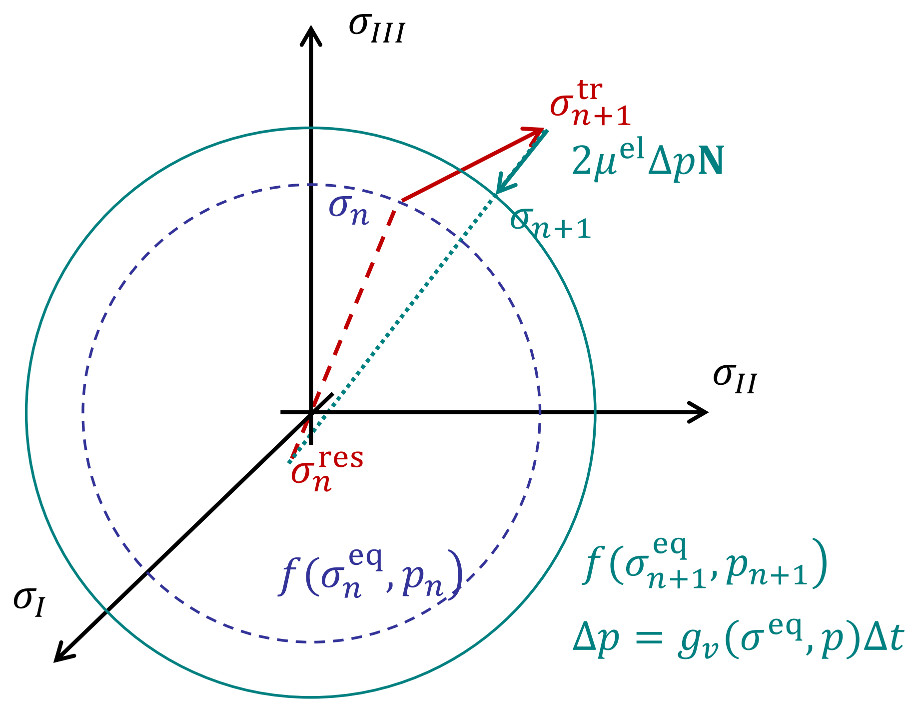

$$\begin{cases} \bar{\mathbf{C}}^{\mathrm{Sr}} = 3\kappa^{\mathrm{el}}\mathbf{I}^{\mathrm{vol}} + 2\left(\mu^{\mathrm{el}} - 3\dfrac{{\mu^{\mathrm{el}}}^2\Delta p}{\left(\boldsymbol{\sigma}_{n+1} - \boldsymbol{\sigma}_n^{\mathrm{res}}\right)^{\mathrm{eq}}}\right)\mathbf{I}^{\mathrm{vol}} \\ \bar{\mathbf{C}}^{\mathrm{S0}} = 3\kappa^{\mathrm{el}}\mathbf{I}^{\mathrm{vol}} + 2\left(\mu^{\mathrm{el}} - 3\dfrac{{\mu^{\mathrm{el}}}^2\Delta p}{\boldsymbol{\sigma}_{n+1}^{\mathrm{eq}}}\right)\mathbf{I}^{\mathrm{vol}} \end{cases}$$

- Incremental-secant mean-field-homogenization
  - Second-statistical moment estimation of the von Mises stress
    - First statistical moment (mean value) not fully representative

$$\bar{\sigma}^{\mathrm{eq}}_{\mathrm{I}/0} = \sqrt{\frac{3}{2}\bar{\boldsymbol{\sigma}}^{\mathrm{dev}}_{\mathrm{I}/0} : \bar{\boldsymbol{\sigma}}^{\mathrm{dev}}_{\mathrm{I}/0}}$$

    - Use second statistical moment estimations to define the yield surface

$$\hat{\hat{\sigma}}^{\mathrm{eq}}_{\mathrm{I}/0} = \sqrt{\frac{3}{2}\mathbf{I}^{\mathrm{dev}} :: \langle \boldsymbol{\sigma}_{\mathrm{I}/0} \otimes \boldsymbol{\sigma}_{\mathrm{I}/0} \rangle_{\omega_{\mathrm{I}/0}}} \geq \bar{\sigma}^{\mathrm{eq}}_{\mathrm{I}/0}$$

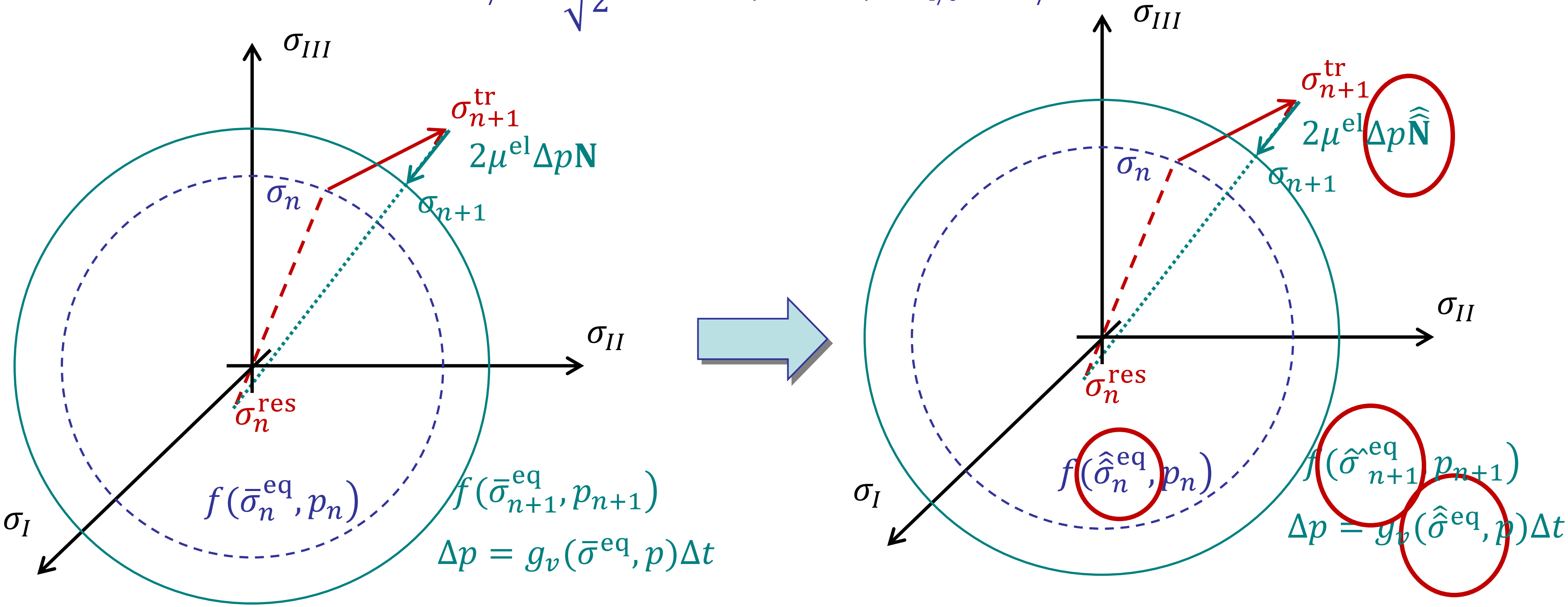

Mean-Field-Homogenization for elasto-visco-plastic composites

- Non-proportional loading
  - Spherical inclusions
    - 17 % volume fraction
    - Elastic
  - Elastic-perfectly-plastic matrix

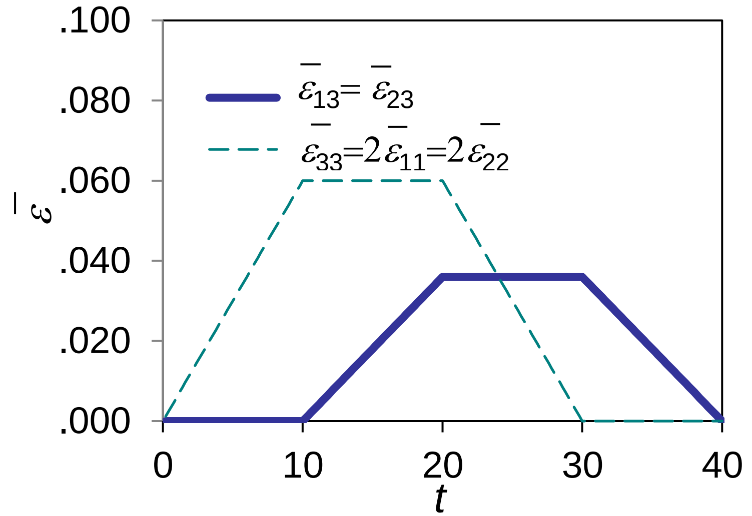

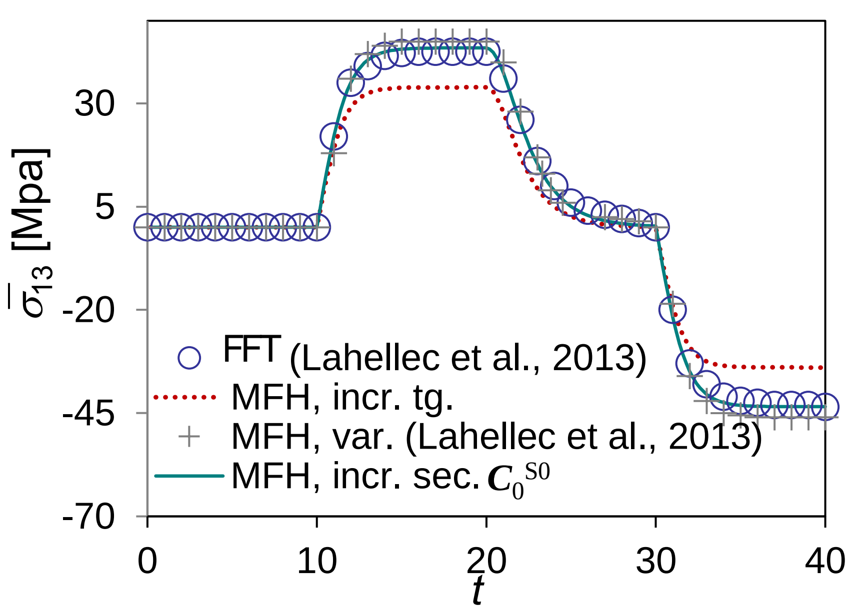

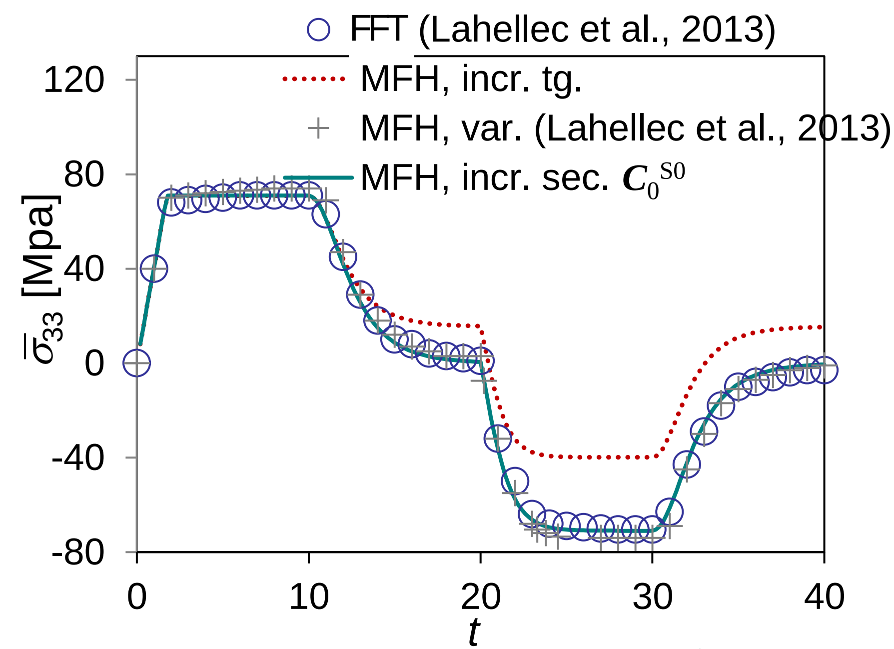

Mean-Field-Homogenization for elasto-visco-plastic composites

- Elasto-visco-plasticity
  - Elasto-visco-plastic short fibres
    - Spherical
    - 30 % volume fraction
  - Elasto-visco-plastic matrix

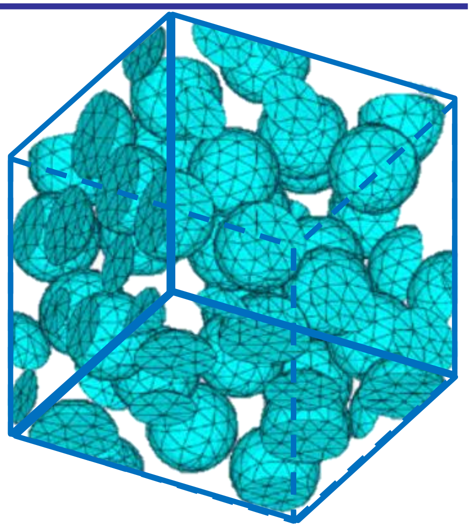

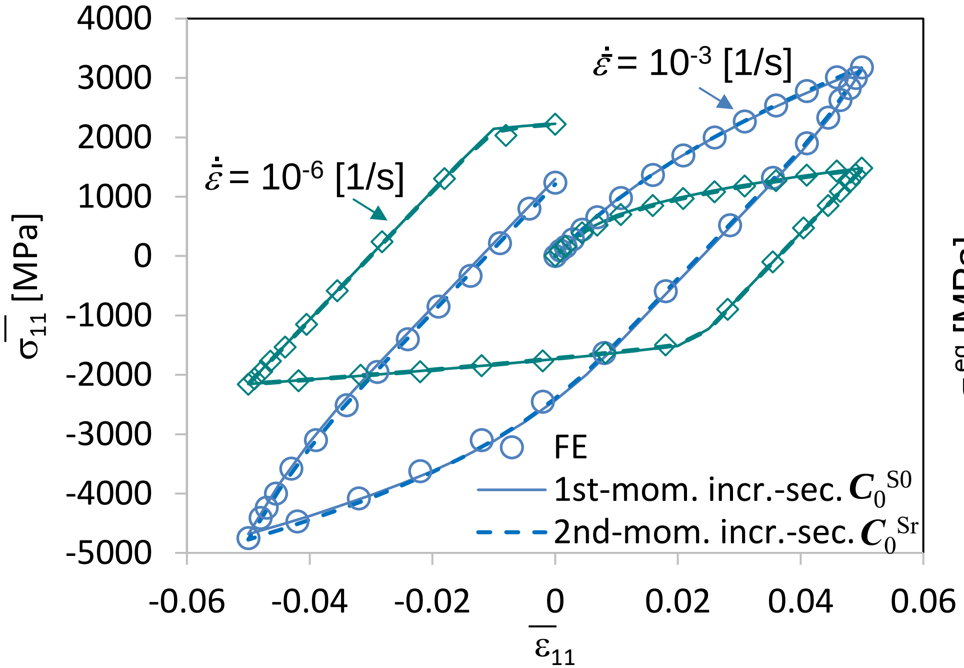

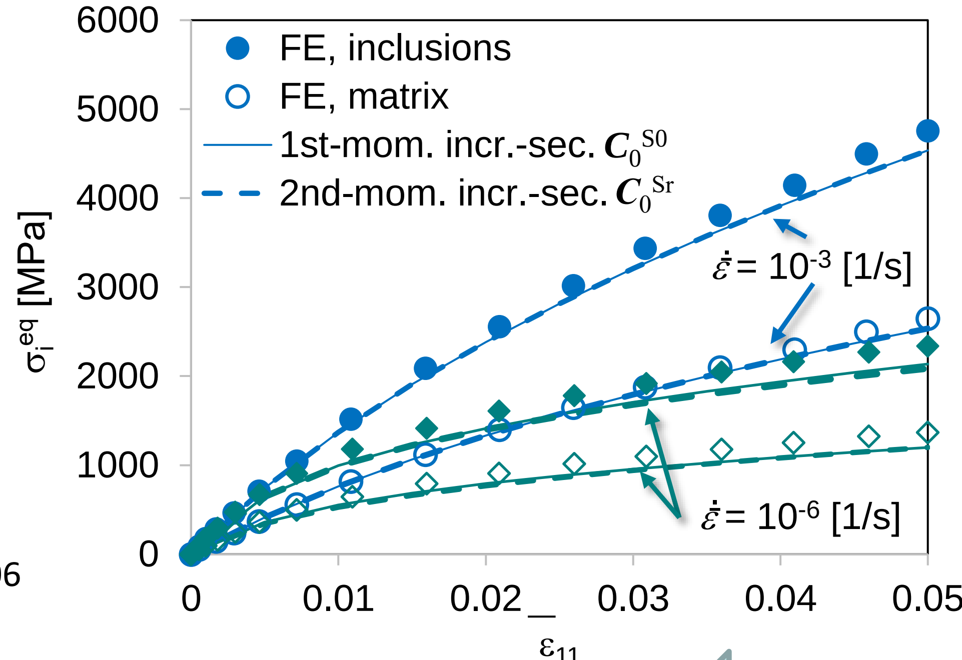

- Extension to finite deformations
  - Formulate everything in terms of elastic left Cauchy-Green tensor

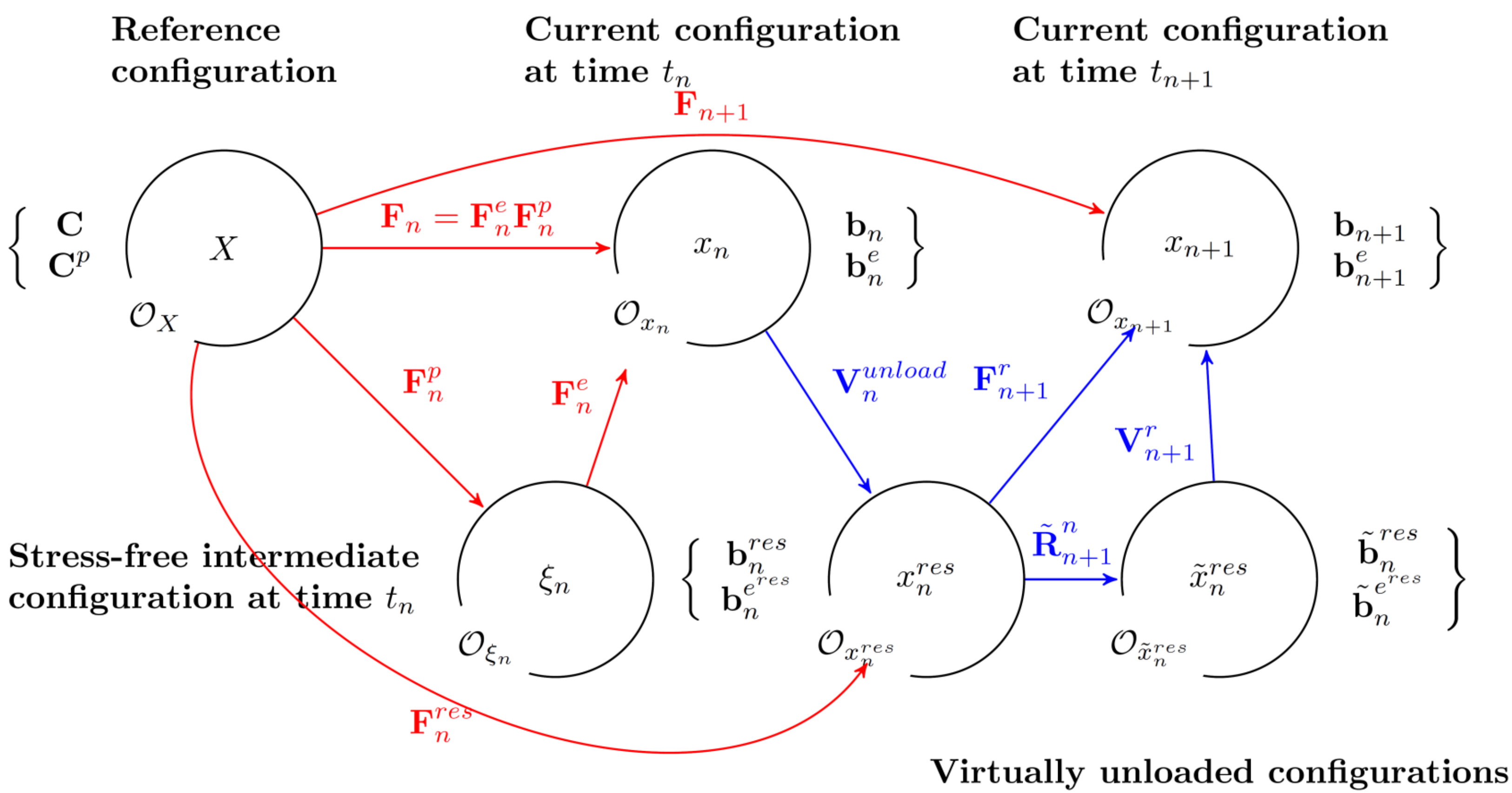

Beginning

Mean-Field-Homogenization for elasto-visco-plastic composites

- Extension to finite deformations
  - Porous material: homogenized response

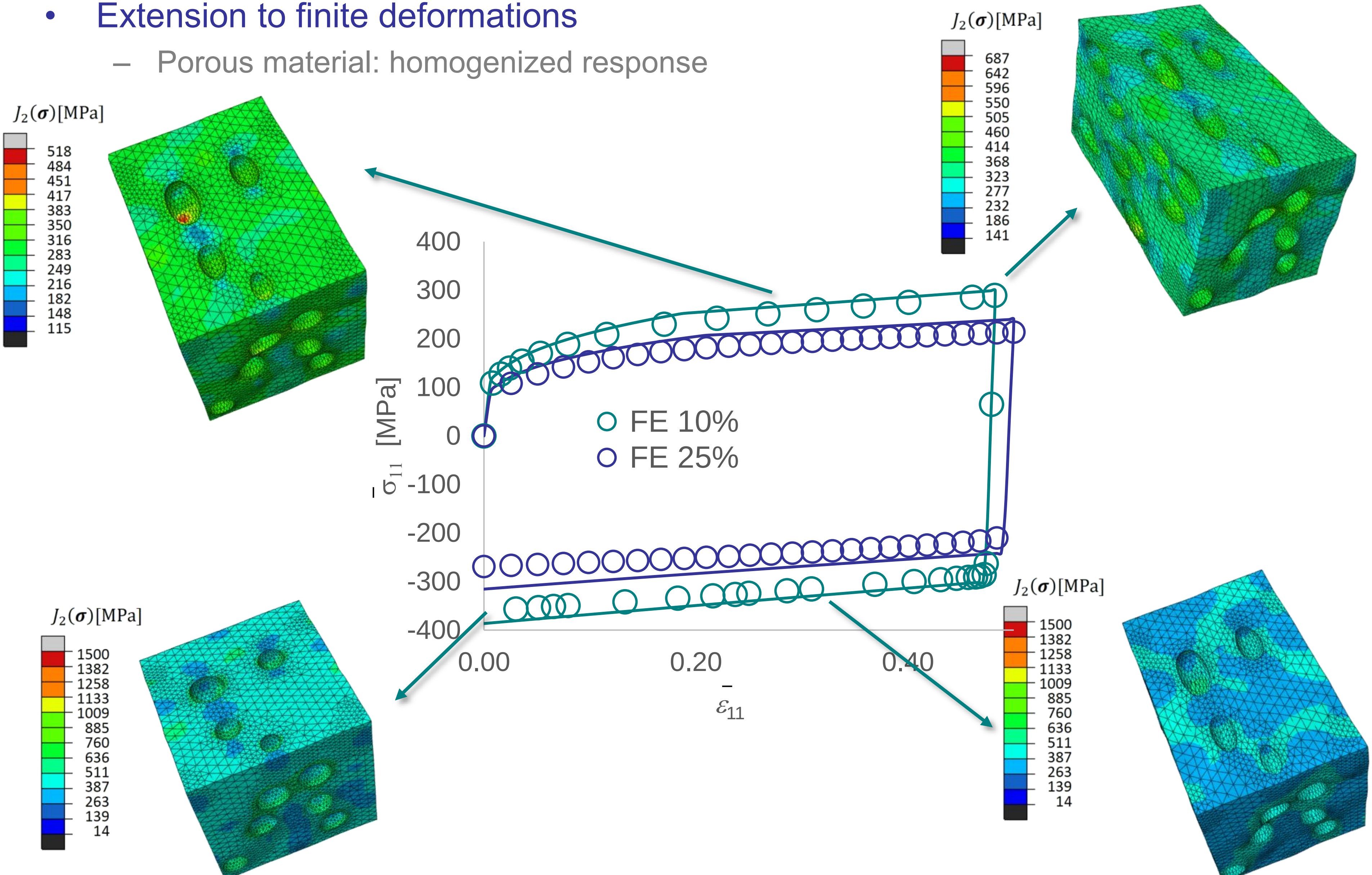

Mean-Field-Homogenization for elasto-visco-plastic composites

- Extension to finite deformations
  - Porous material: micro-structure evolution

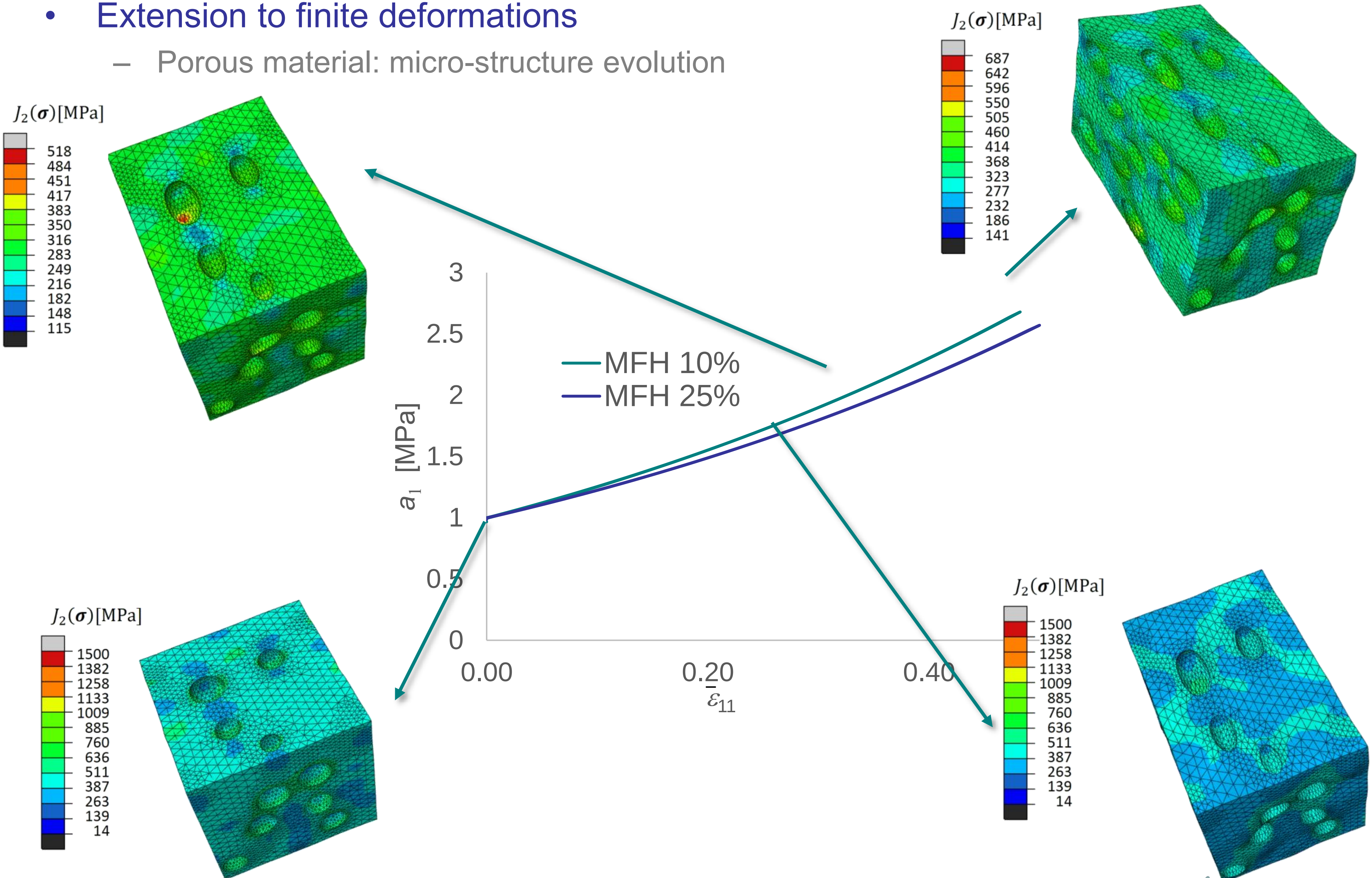

Beginning

Mean-Field-Homogenization for elasto-visco-plastic composites

- SIMUCOMP ERA-NET project (incremental secant MFH)
  - e-Xstream, CENAERO, ULiège (Belgium)
  - IMDEA Materials (Spain)
  - CRP Henri-Tudor (Luxemburg)

- PDR T.1015.14 project (MFH with second-order moments)
  - ULiège, UCL (Belgium)

- STOMMMAC M.ERA-NET project (MFH for elasto-visco-plastic composites)
  - e-Xstream, ULiège (Belgium)
  - BATZ (Spain)
  - JKU, AC (Austria)
  - U Luxembourg (Luxemburg)

- Publications (doi)
  - 10.1016/j.mechmat.2017.08.006
  - 10.1080/14786435.2015.1087653
  - 10.1016/j.ijplas.2013.06.006
  - 10.1016/j.cma.2018.12.007

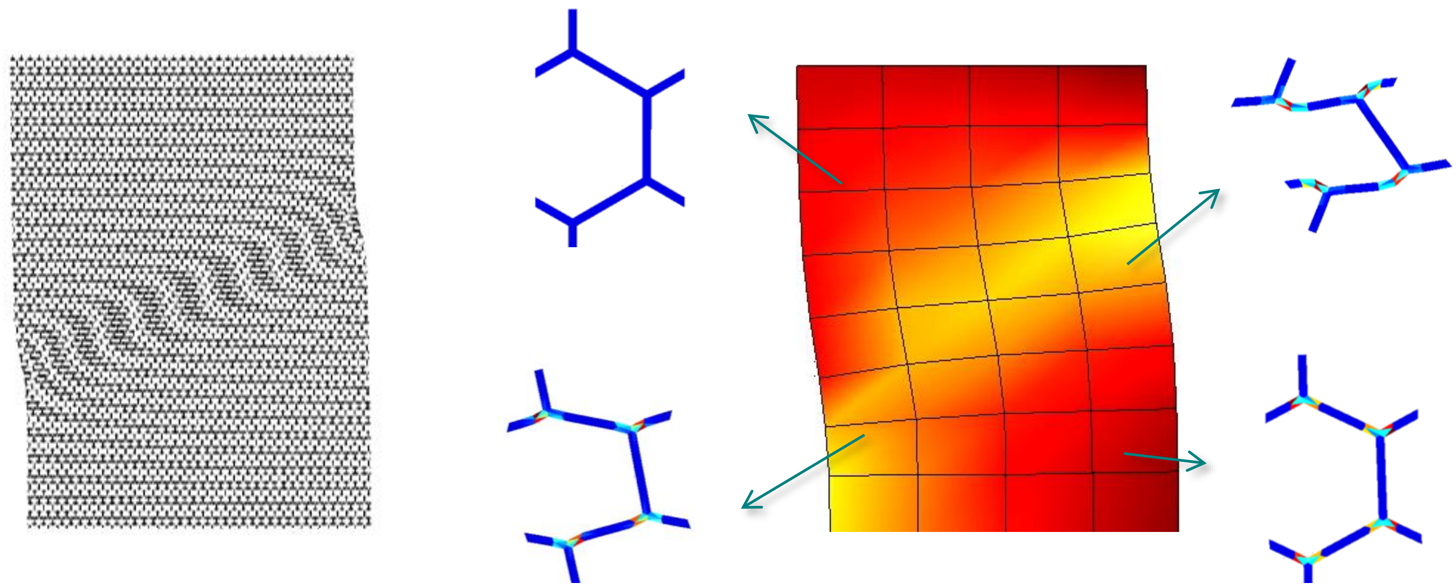

Second order Computational Homogenization for Honeycomb Structures

ARC 09/14-02 BRIDGING - From imaging to geometrical modelling of complex micro structured materials: Bridging computational engineering and material science

Second order Computational Homogenization for Honeycombs

- Multi-scale modeling
  - 2 problems are solved concurrently
    - The macro-scale problem
    - The meso-scale problem (on a meso-scale Volume Element)

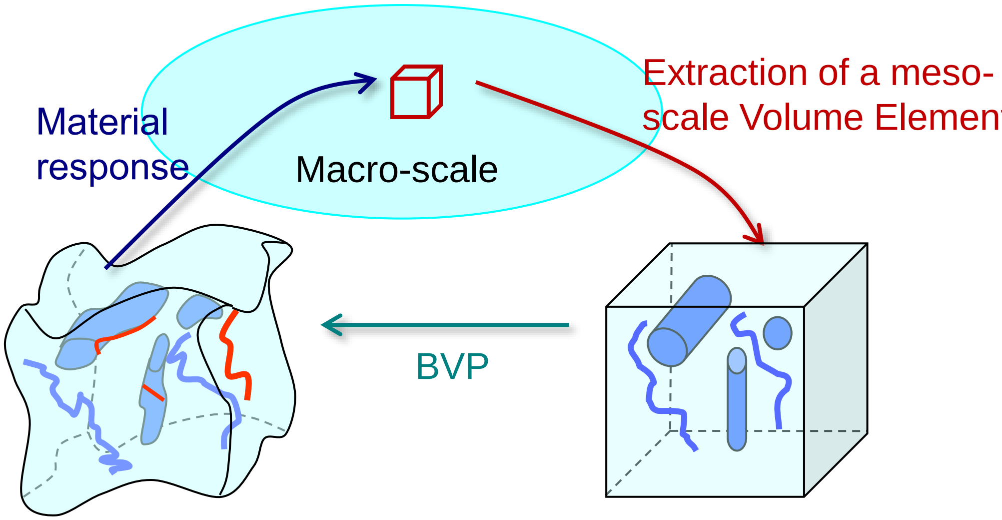

- What if homogenized properties loose ellipticity?
  - Buckling of honeycomb structures

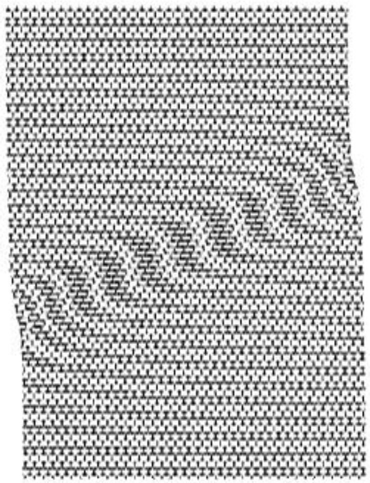

Second order Computational Homogenization for Honeycombs

- DG-based second-order FE^2
  - Macro-scale
    - High-order Strain-Gradient formulation
    - C^1 weakly enforced by DG
    - Partitioned mesh (//)
  - Transition
    - Gauss points on different processors
    - Each Gauss point is associated to one mesh and one solver
  - Micro-scale
    - Usual 3D finite elements
    - High-order periodic boundary conditions
      - Non-conforming mesh
      - Use of interpolant functions

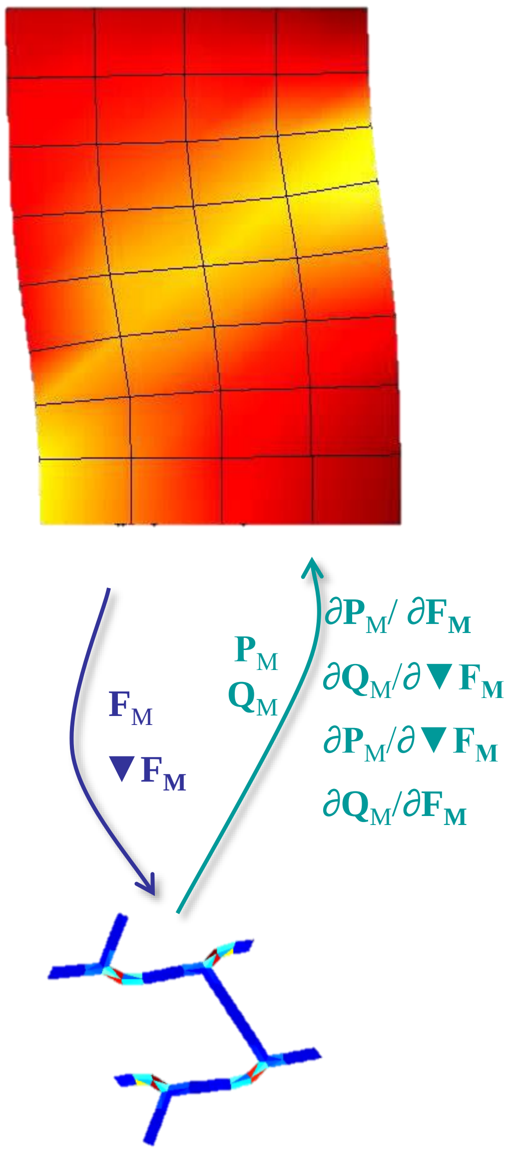

Second order Computational Homogenization for Honeycombs

- Instabilities
  - Micro-scale: buckling
  - Macro-scale: localization bands
  - Captured owing to
    - Second-order homogenization
    - Ad-hoc periodic boundary conditions
    - Path following method

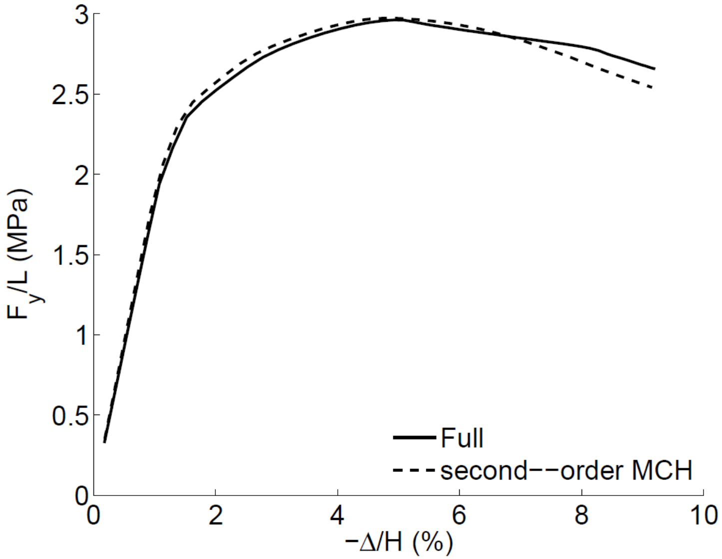

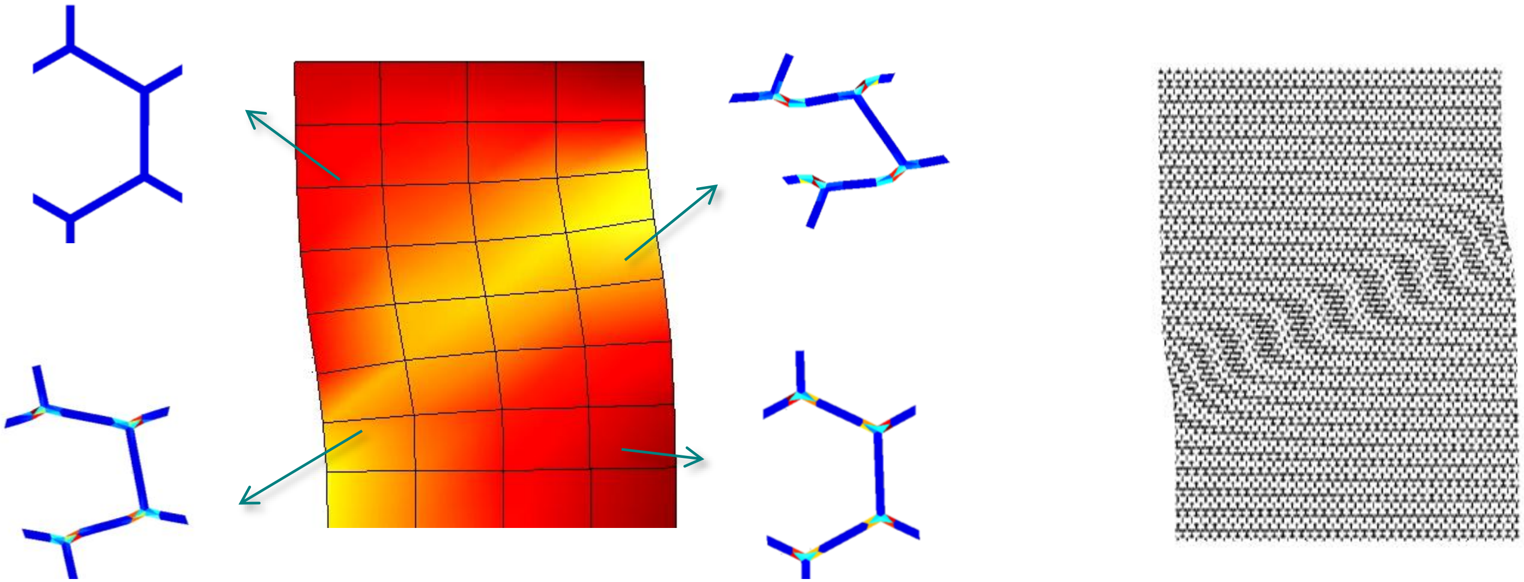

Beginning

Second order Computational Homogenization for Honeycombs

- Open-hole plate

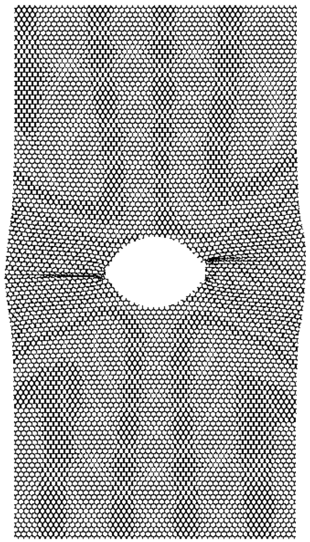

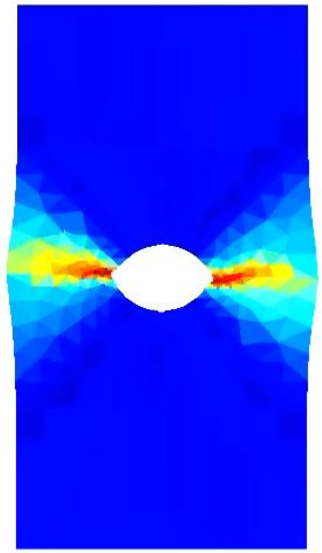

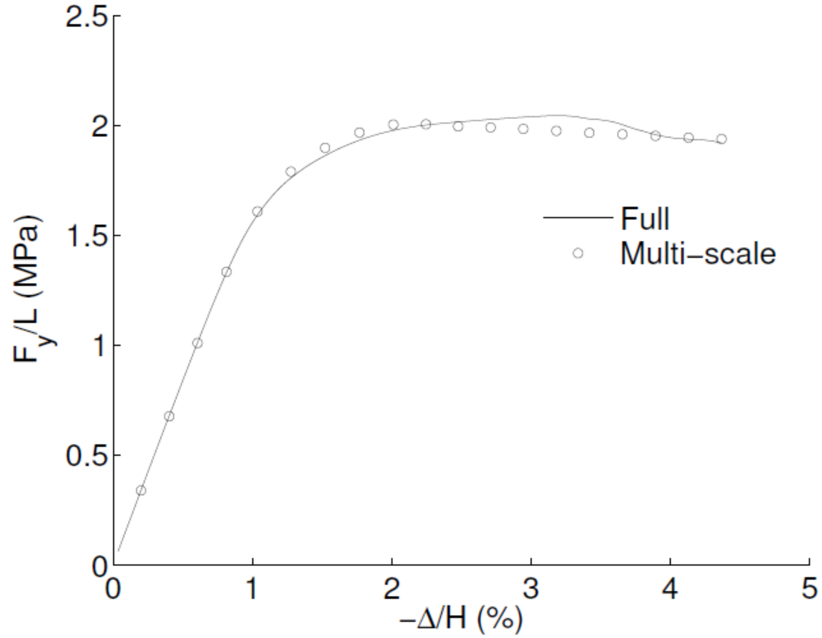

- BRIDGING ARC project
  - ULiège, Applied Sciences (A&M, EEI, ICD)
  - ULiège, Sciences (CERM)
- Publications
  - [10.1016/j.mechmat.2015.07.004]
  - [10.1016/j.ijsolstr.2014.02.029]
  - [10.1016/j.cma.2013.03.024]

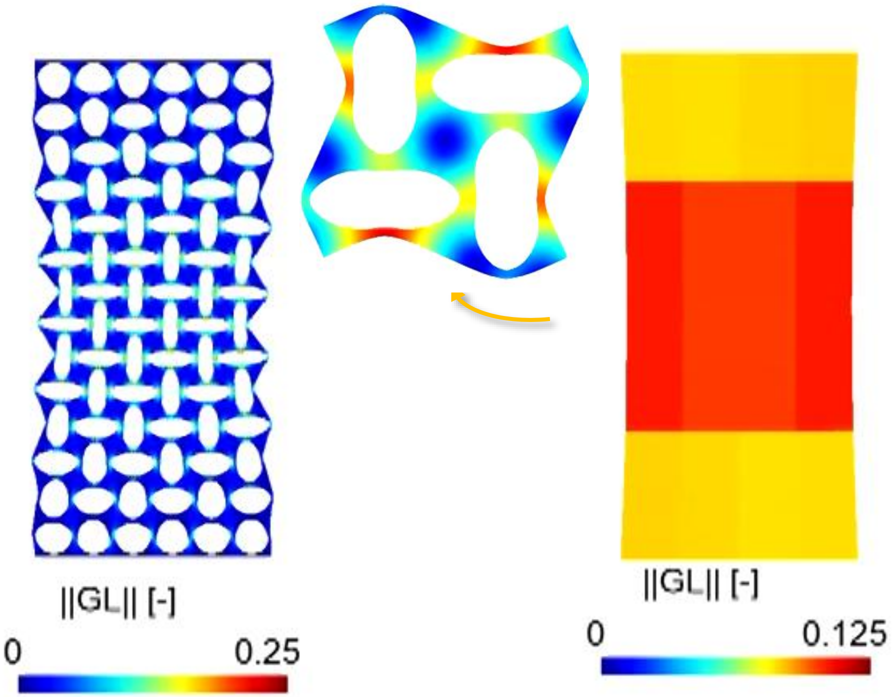

Second order homogenization without RVE size effect for cellular and metamaterials

MOAMMM project has received funding from the European Union's Horizon 2020 research and innovation programme under grant agreement No 862015 for the project Multi-scale Optimisation for Additive Manufacturing of fatigue resistant shock-absorbing MetaMaterials (MOAMMM) of the H2020-EU.1.2.1. - FET Open Programme

MOAMMM

Second order homogenization for cellular and metamaterials

- First vs. second order homogenisation
  - First order homogenisation
    - Does not prevent localisation issue
    - No material length-scale
  - Second-order homogenization
    - High order strain $\mathbf{G}_{\mathrm{M}}$ and stress $\mathbf{Q}_{\mathrm{M}}$ at macro-scale
    - Material length scale related to the RVE length

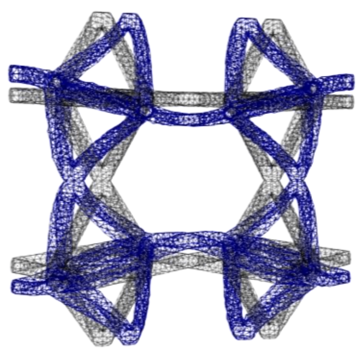

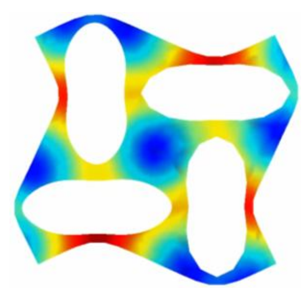

    - Issue for metamaterial: RVE length is larger than unit cell because of patterning change

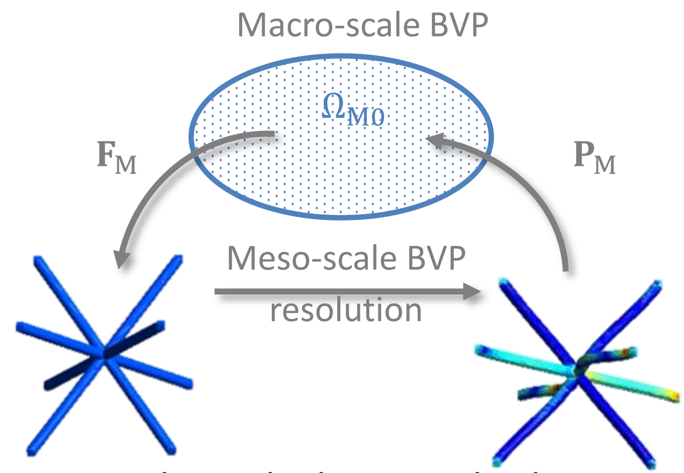

First order homogenisation

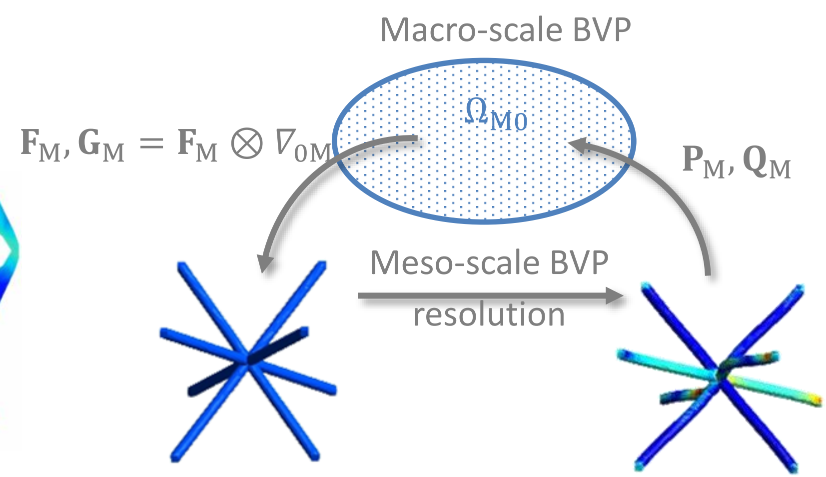

Second order homogenisation

Second order homogenization for cellular and metamaterials

- Account for patterning change
  - Micromorphic approach
    - Constrain change of patterning modes
    - Developed in elasticity (limited number of modes)
  - Enhanced second-order homogenization
    - Remove cell size dependency using a body-force
    - Arises from asymptotic homogenization in linear elasticity
    - How to account for finite strain, elasto-plasticity etc…?

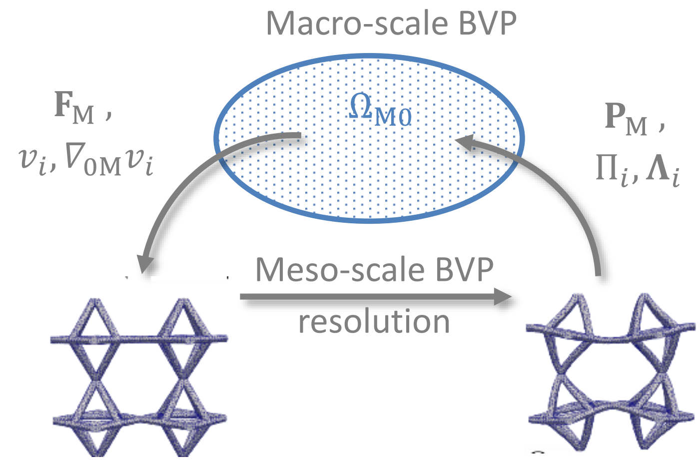

Micromorphic approach

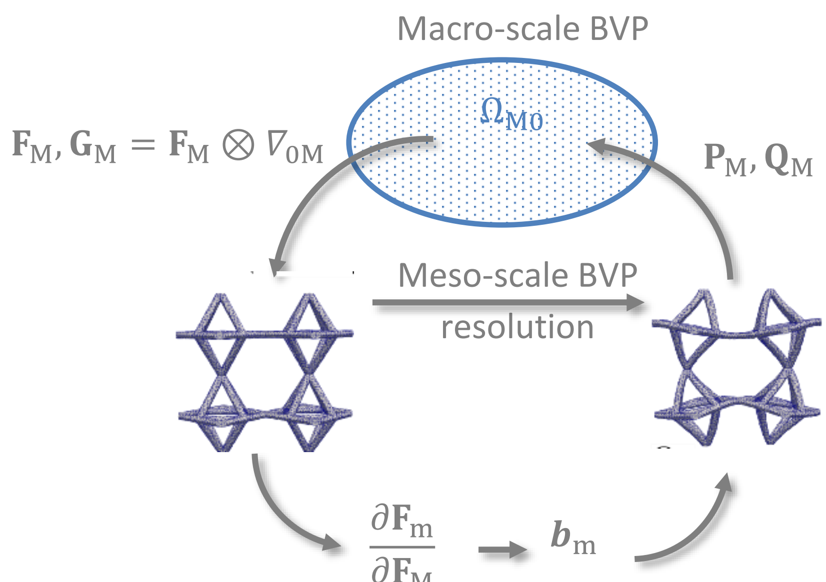

Body-force enhanced second order homogenisation

- Second order homogenization with body force enhancement
  - Consider an equivalent homogeneous volume element
    - Cauchy homogenous — Second order continuum

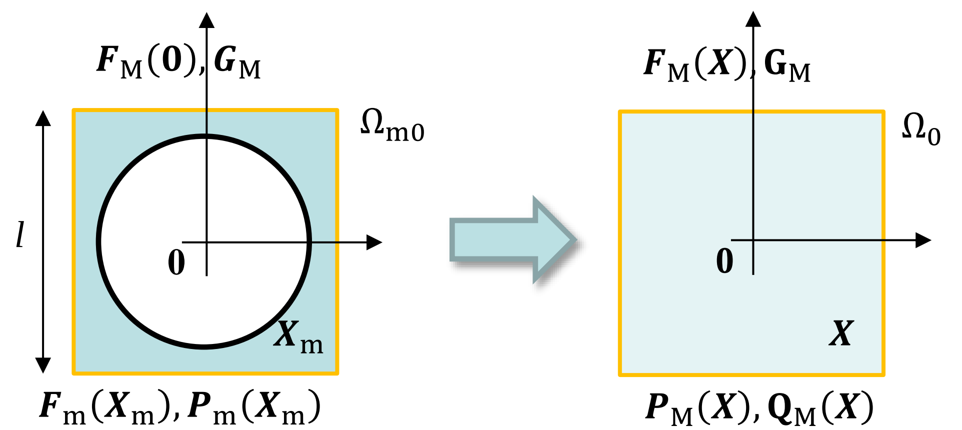

    - Development of the (no-longer) homogeneous field

$$
\begin{cases}
\mathbf{F}_{\mathrm{M}}(\boldsymbol{X}) = \mathbf{F}_{\mathrm{M}}(0) + \mathbf{G}_{\mathrm{M}} \cdot \boldsymbol{X} \\
\mathbf{G}_{\mathrm{M}} = \mathbf{F}_{\mathrm{M}}(\mathbf{0}) \otimes \nabla_{0\mathrm{M}} \\
\mathbf{P}_{\mathrm{M}}(\boldsymbol{X}) = \mathbf{P}_{\mathrm{M}}(0) + \left.\dfrac{\partial \mathbf{P}_{\mathrm{M}}}{\partial \mathbf{F}_{\mathrm{M}}}\right|_{0} : \mathbf{G}_{\mathrm{M}} \cdot \boldsymbol{X} \\
\mathbf{Q}_{\mathrm{M}}(\boldsymbol{X}) = \mathbf{Q}_{\mathrm{M}}(0) + \left.\dfrac{\partial \mathbf{Q}_{\mathrm{M}}}{\partial \mathbf{F}_{\mathrm{M}}}\right|_{0} : \mathbf{G}_{\mathrm{M}} \cdot \boldsymbol{X}
\end{cases}
$$

- Second order homogenization with body force enhancement
  - Consider an equivalent homogeneous volume element
    - The equivalence of energy (Hill-Mandel condition) with introduction of body forces $\boldsymbol{b}_m(\boldsymbol{X}_m)$:

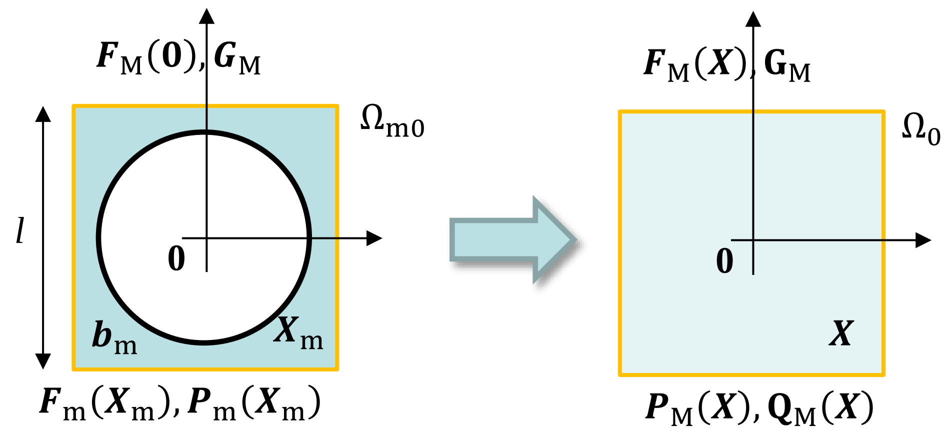

$$\int_{\Omega_{\mathrm{m}0}} [\mathbf{P}_{\mathrm{m}} : \delta\mathbf{F}_{\mathrm{m}} - \mathbf{b}_{\mathrm{m}} \cdot \delta\boldsymbol{u}_{\mathrm{m}}] \mathrm{d}\Omega$$

$$\Leftrightarrow$$

$$\int_{\Omega_0} (\mathbf{P}_{\mathrm{M}} : \delta\mathbf{F}_{\mathrm{M}} + \mathbf{Q}_{\mathrm{M}} \vdots \delta\mathbf{G}_{\mathrm{M}} - \mathbf{B}_{\mathrm{M}} \cdot \delta\boldsymbol{u}_{\mathrm{M}}) \mathrm{d}\Omega$$

- Is satisfied by the following introduction of micro-scale body forces and homogenized stresses

$$\left\{\begin{aligned}
&\mathbf{P}_{\mathrm{M}}(0) = \frac{1}{V_0}\int_{\Omega_{\mathrm{m}0}} (\mathbf{P}_{\mathrm{m}} - \boldsymbol{b}_{\mathrm{m}} \otimes \boldsymbol{X}_{\mathrm{m}})\, \mathrm{d}\Omega \\
&\mathbf{Q}_{\mathrm{M}}(0) = \frac{1}{2V_0}\int_{\Omega_{\mathrm{m}0}} [\mathbf{P}_{\mathrm{m}} \otimes \boldsymbol{X}_{\mathrm{m}} + (\mathbf{P}_{\mathrm{m}} \otimes \boldsymbol{X}_{\mathrm{m}})^T]\, \mathrm{d}\Omega + \frac{1}{2V_0}\int_{\Omega_{\mathrm{m}0}} [\boldsymbol{b}_{\mathrm{m}} \otimes \boldsymbol{X}_{\mathrm{m}} \otimes \boldsymbol{X}_{\mathrm{m}}]\, \mathrm{d}\Omega - \\
&\qquad \frac{1}{2\mathrm{V}_0}\left(\left[\frac{\partial \mathbf{P}_{\mathrm{M}}(0)}{\partial \mathbf{F}_{\mathrm{M}}} : \mathbf{G}_{\mathrm{M}} \cdot \boldsymbol{J}_{\mathrm{M}} + \left(\frac{\partial \mathbf{P}_{\mathrm{M}}(0)}{\partial \mathbf{F}_{\mathrm{M}}} : \mathbf{G}_{\mathrm{M}} \cdot \boldsymbol{J}_{\mathrm{M}}\right)^T\right] - \boldsymbol{B}_{\mathrm{M}} \otimes \boldsymbol{J}_{\mathrm{M}}\right) \\
&\int_{\Omega_{\mathrm{m}0}} \mathbf{b}_{\mathrm{m}} \mathrm{d}\Omega = \int_{\Omega_0} \mathbf{B}_{\mathrm{M}} \mathrm{d}\Omega = -\int_{\Omega_0} \frac{\partial \mathbf{P}_{\mathrm{M}}}{\partial \mathbf{F}_{\mathrm{M}}} : \mathbf{G}_{\mathrm{M}} : \boldsymbol{I} \mathrm{d}\Omega = -\int_{\Omega_{m0}} \frac{\partial \mathbf{P}_{\mathrm{m}}}{\partial \mathbf{F}_{\mathrm{m}}} : \frac{\partial \mathbf{F}_{\mathrm{m}}}{\partial \mathbf{F}_{\mathrm{M}}} : \mathbf{G}_{\mathrm{M}} : \boldsymbol{I} \mathrm{d}\Omega
\end{aligned}\right.$$

- Remove boundary effect
  - Apply $G_{M_{xxx}} = 0.05\ /mm$

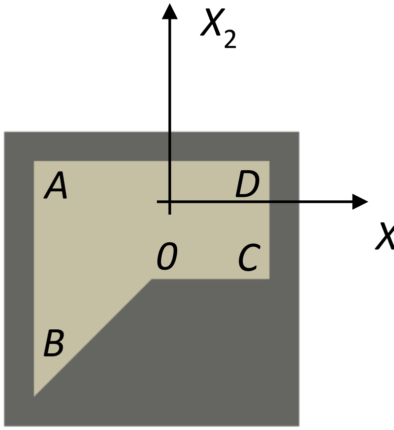

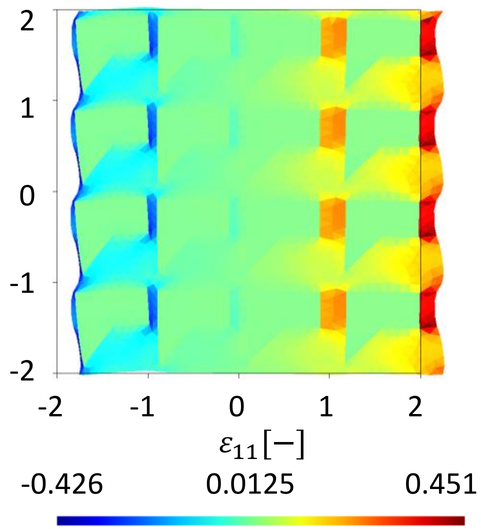

Body-force enhanced second order homogenization

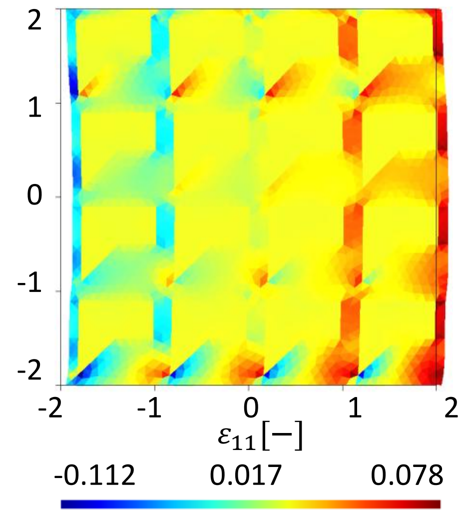

Classical second order homogenization

- Converges toward DNS
  - Linear elasticity: Beam bending

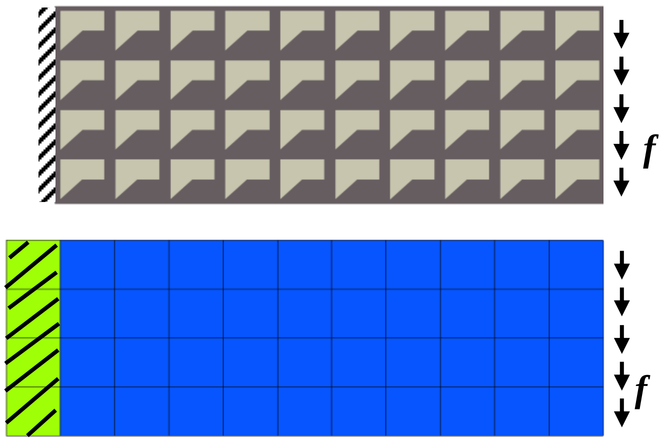

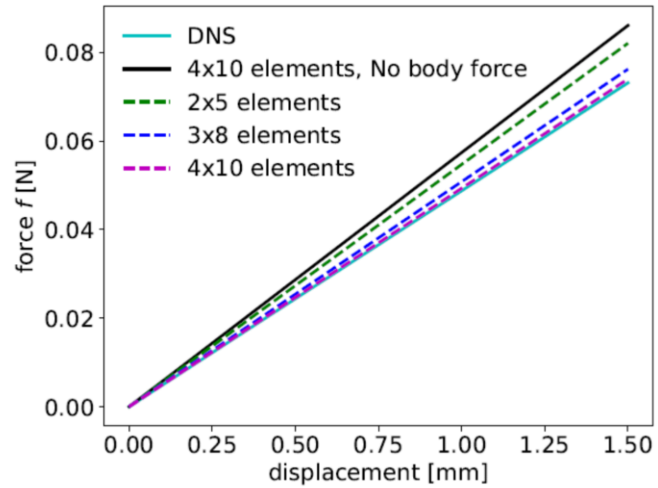

  - Linear elasticity: Beam shearing

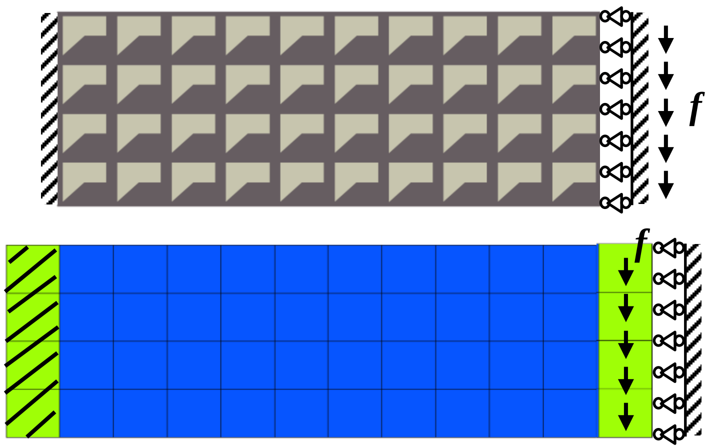

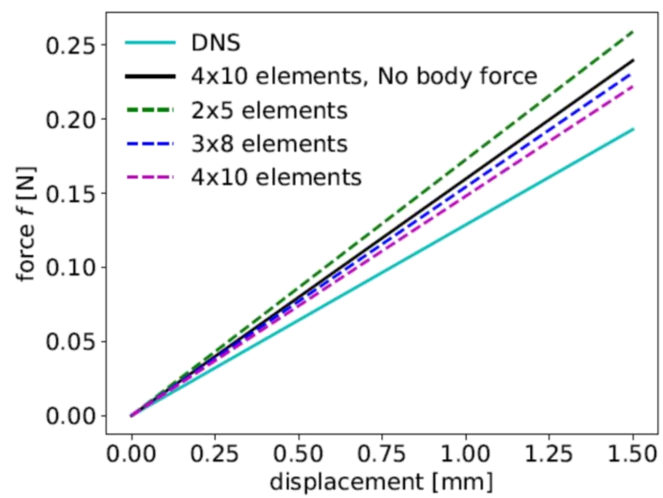

- Multiscale simulation on honeycomb structures
  - Effect of RVE size disappears when considering body forces

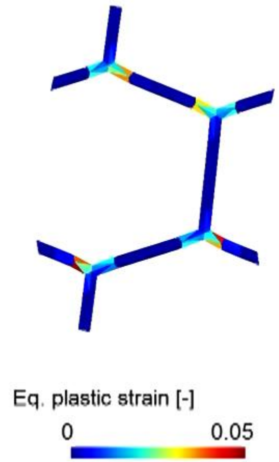

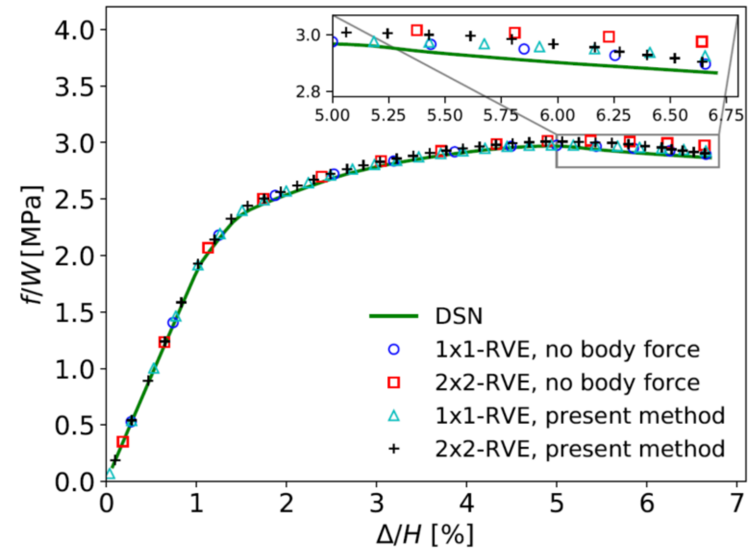

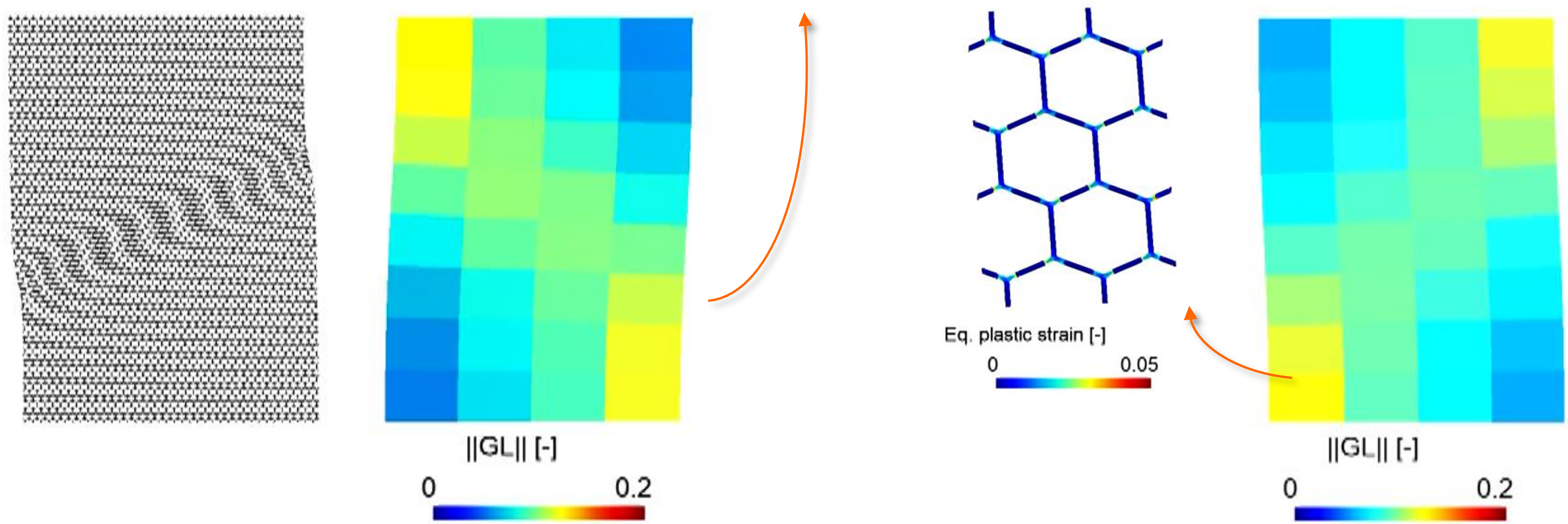

Second order homogenization for cellular and metamaterials

- Multiscale simulation on meta-structures
  - Compression samples of different sizes
    - 6x14 holes ➔ local instability
    - 6x34 holes ➔ global instability

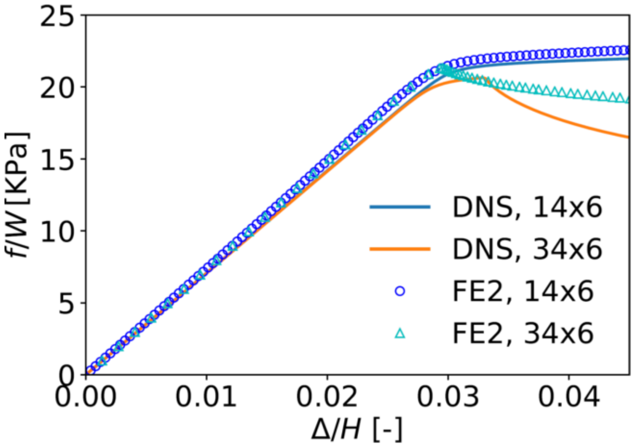

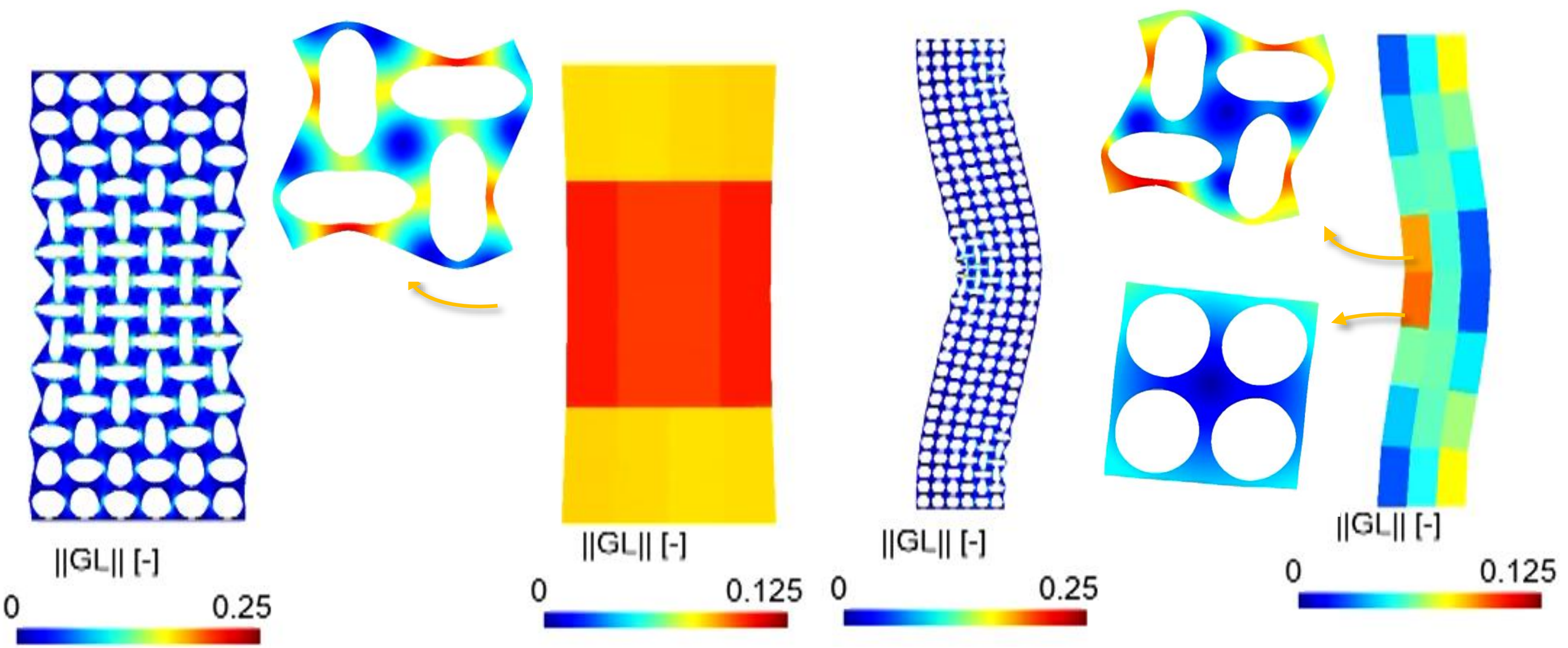

Second order homogenization for cellular and metamaterials

- MOAMMM FET-OPEN project (https://www.moammm.eu/)
  - ULiège, UCL (Belgium)
  - IMDEA Materials (Spain)
  - JKU (Austria)
  - cirp GmbH (Germany)

- Publications (doi)
  - Submitted

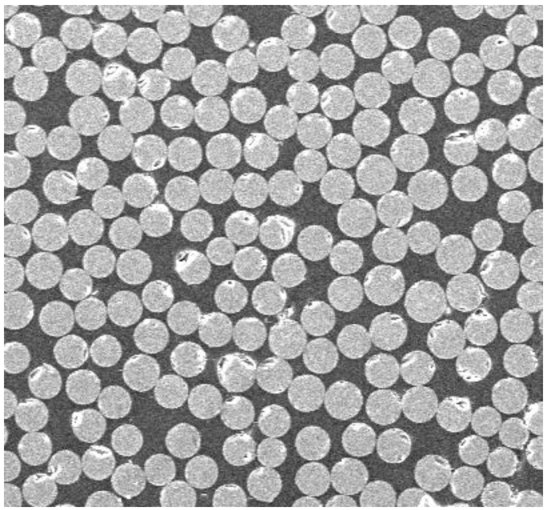

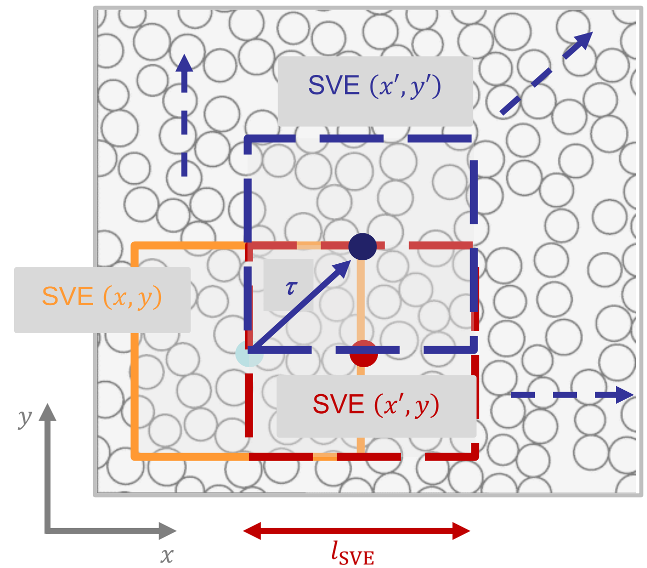

Stochastic Homogenization of Composite Materials

STOMMMAC The research has been funded by the Walloon Region under the agreement no 1410246-STOMMMAC (CT-INT 2013-03-28) in the context of M-ERA.NET Joint Call 2014.

- Multi-scale modeling
  - 2 problems are solved concurrently
    - The macro-scale problem
    - The meso-scale problem (on a meso-scale Volume Element)

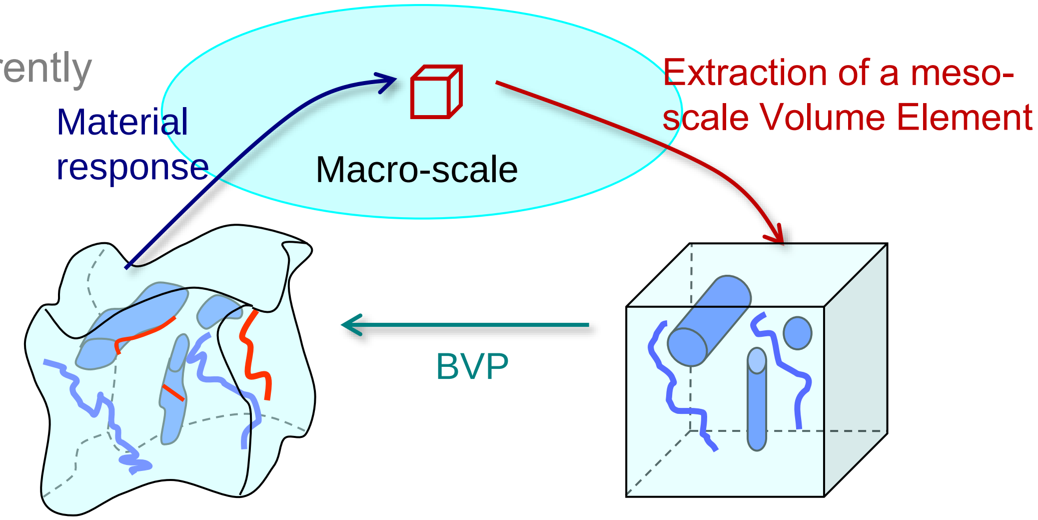

- For structures not several orders larger than the micro-structure size

$$L_{\text{macro}} >> L_{\text{VE}} >\sim L_{\text{micro}}$$

For accuracy: Size of the meso-scale volume element smaller than the characteristic length of the macro-scale loading

Meso-scale volume element no longer statistically representative:
- **Stochastic Volume Elements**

- Material uncertainties affect structural behaviors

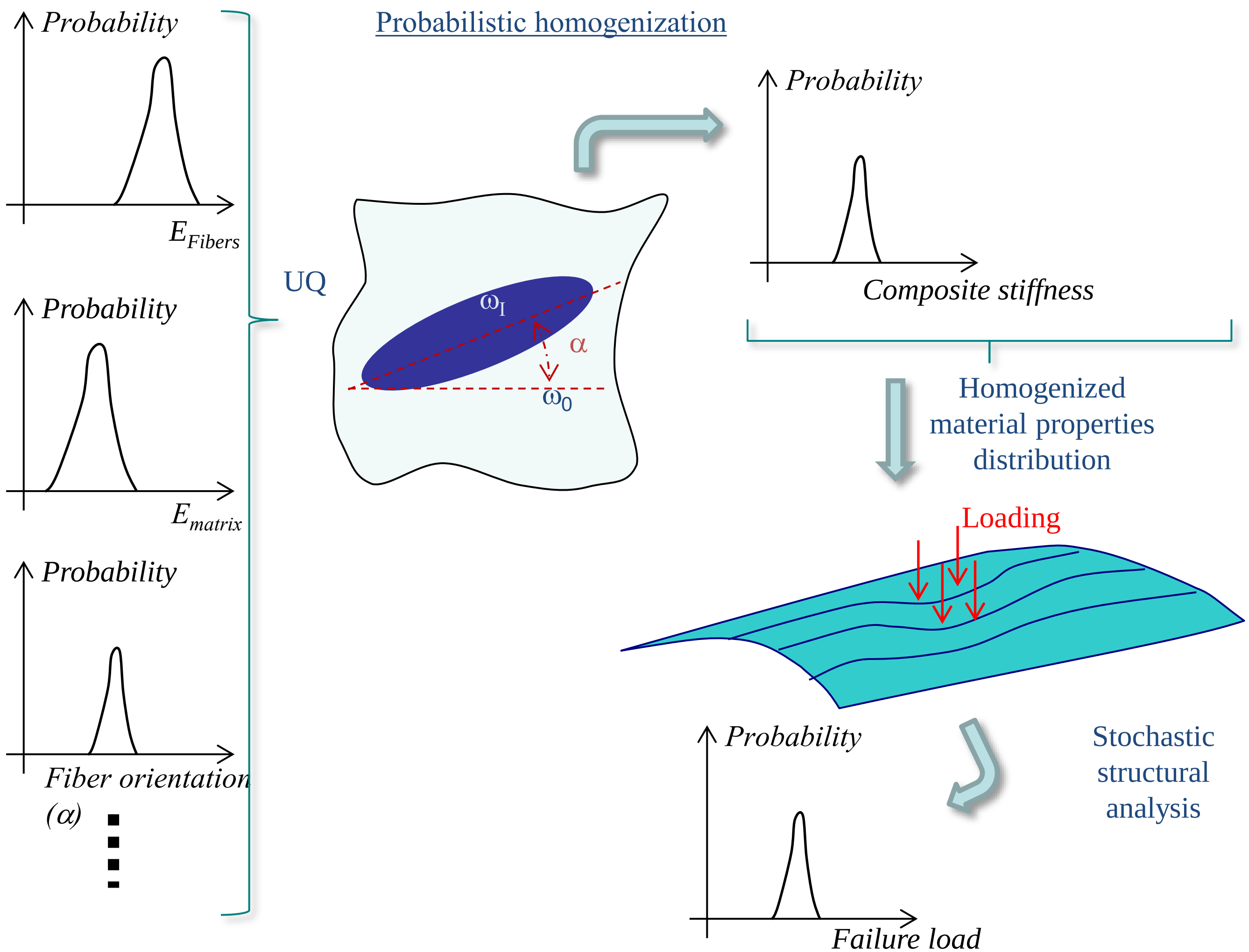

Stochastic Homogenization of Composite Materials

- Proposed methodology for material:
  - To develop a stochastic Mean Field Homogenization method able to predict the probabilistic distribution of material response at an intermediate scale from micro-structural constituents characterization

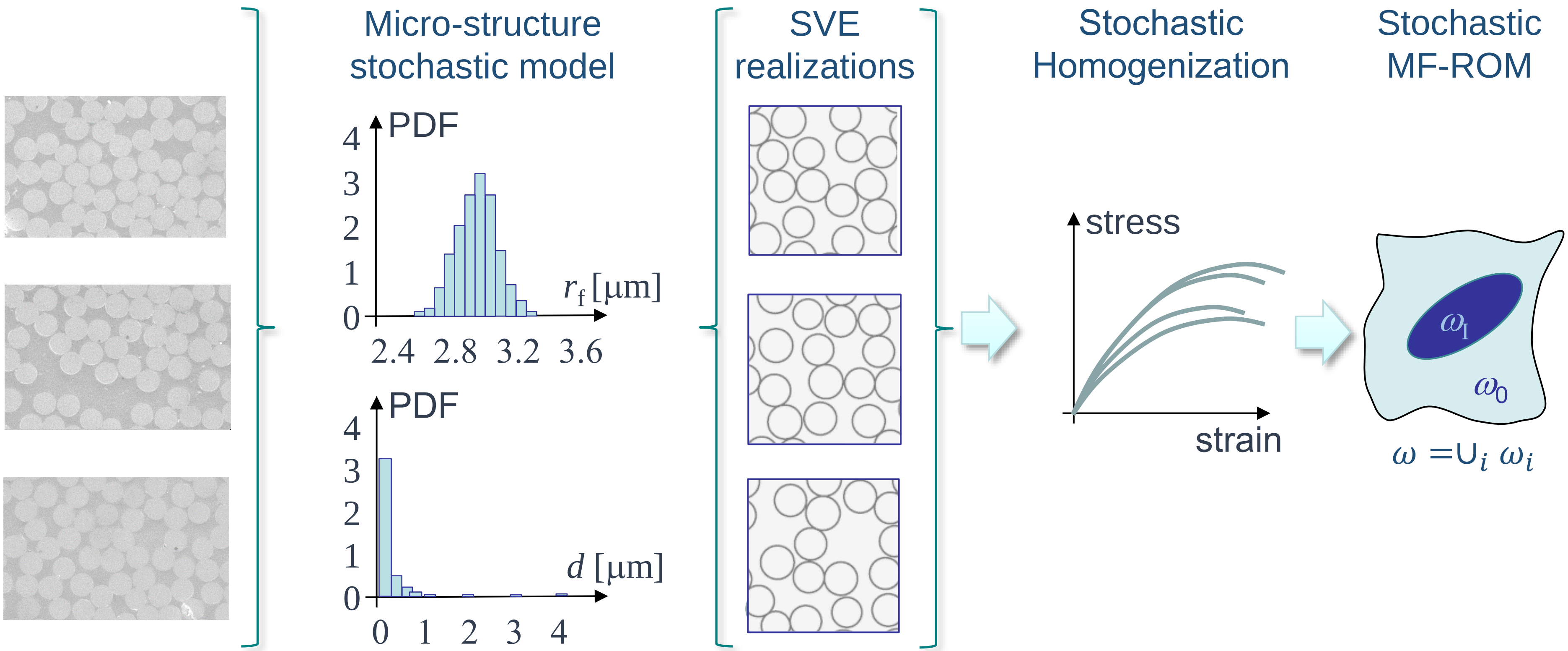

Stochastic Homogenization of Composite Materials

- Micro-structure stochastic model
  - 2000x and 3000x SEM images

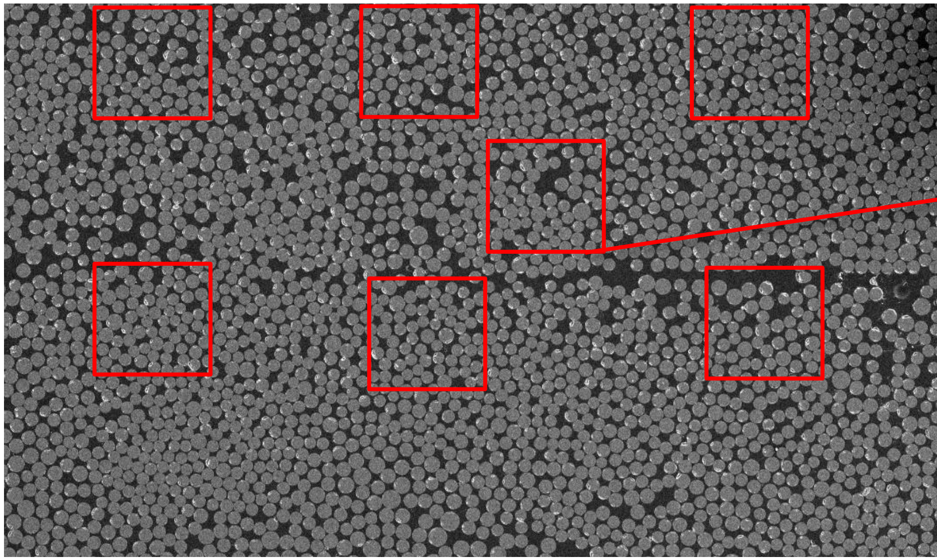

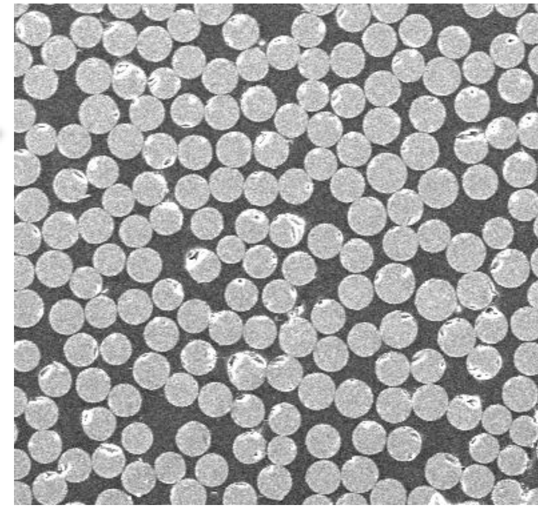

  - Fibers detection

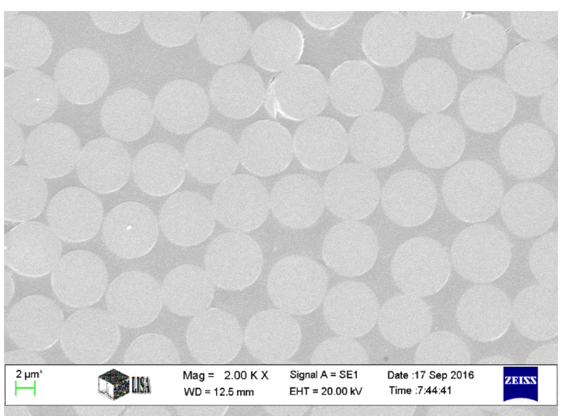

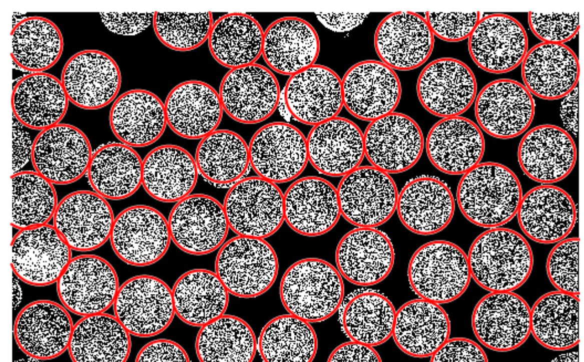

- Micro-structure stochastic model
  - Histograms of random micro-structures' descriptors

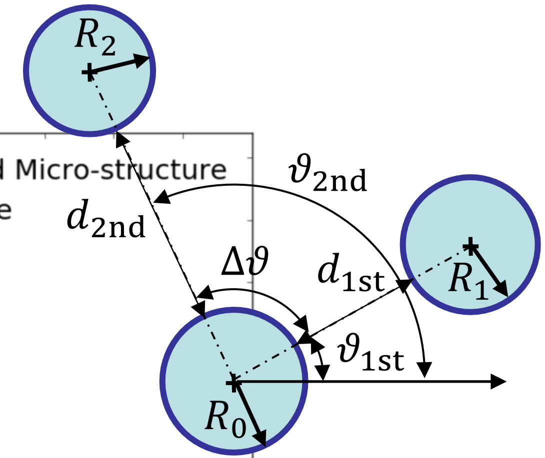

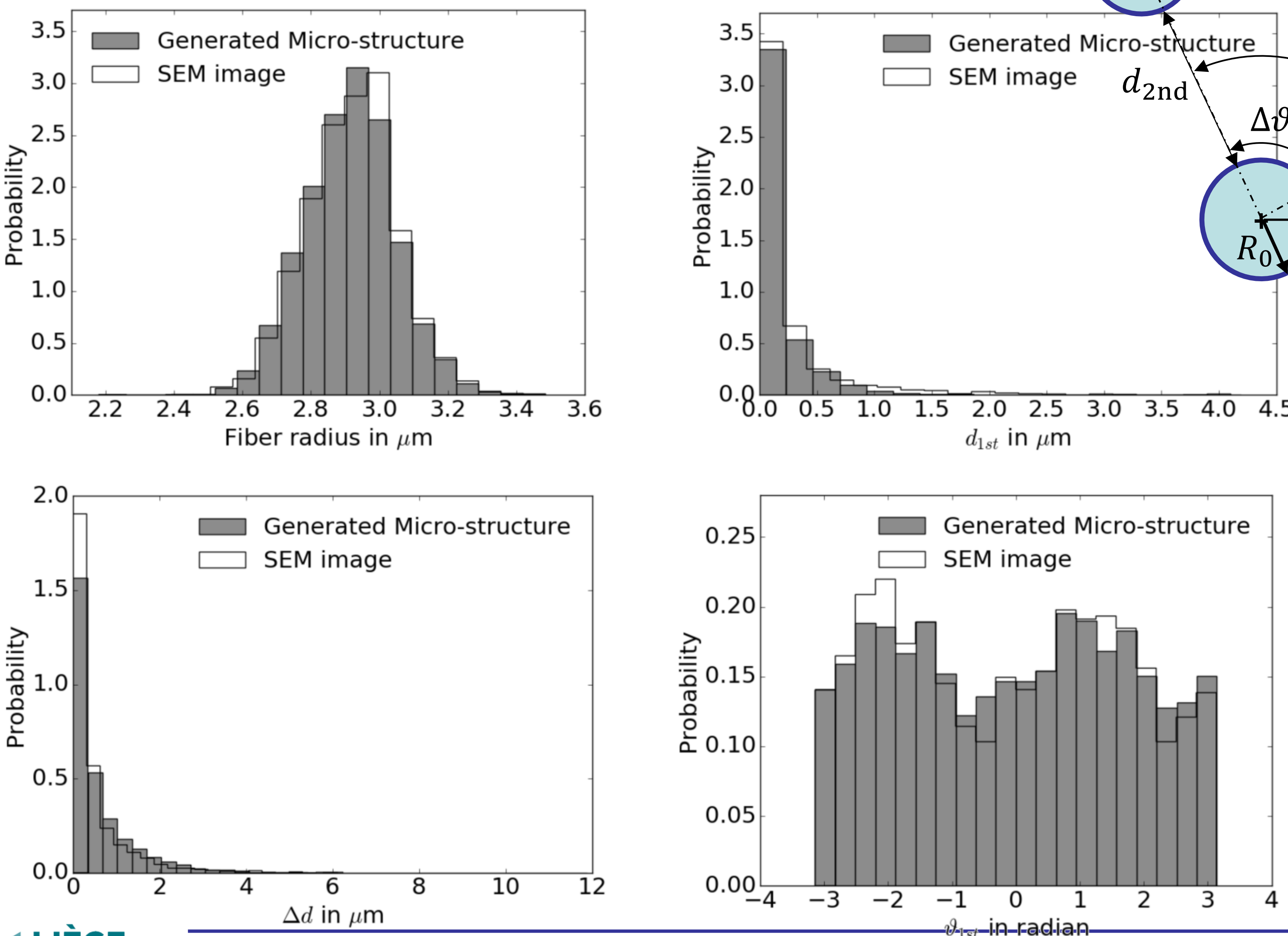

Stochastic Homogenization of Composite Materials

- Micro-structure stochastic model
  - Dependent variables generated using their empirical copula

SEM sample

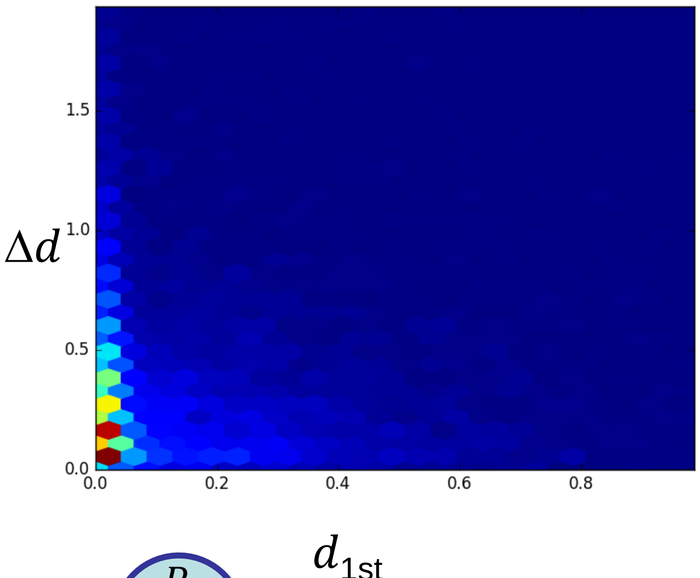

Generated sample

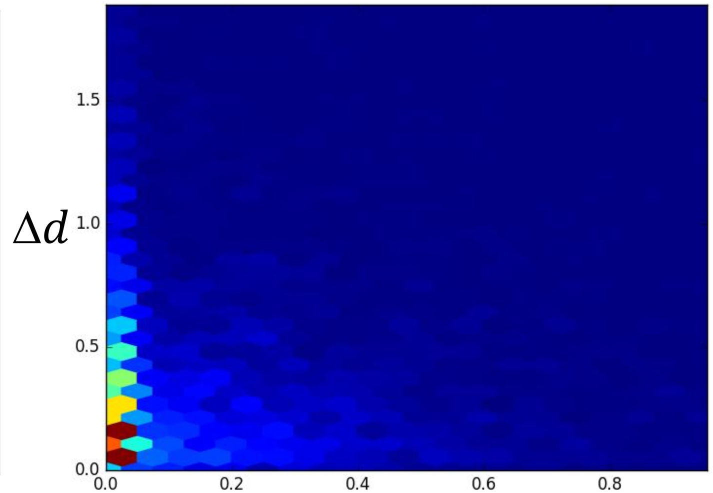

Directly from copula generator

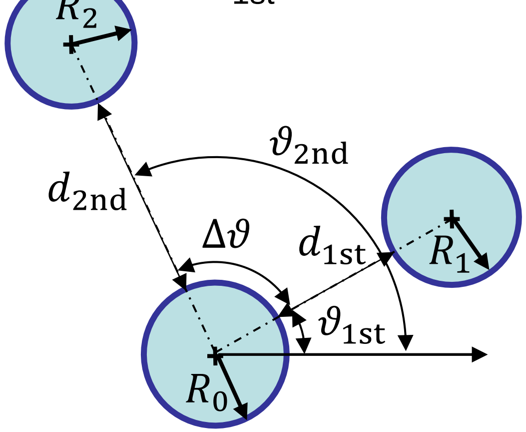

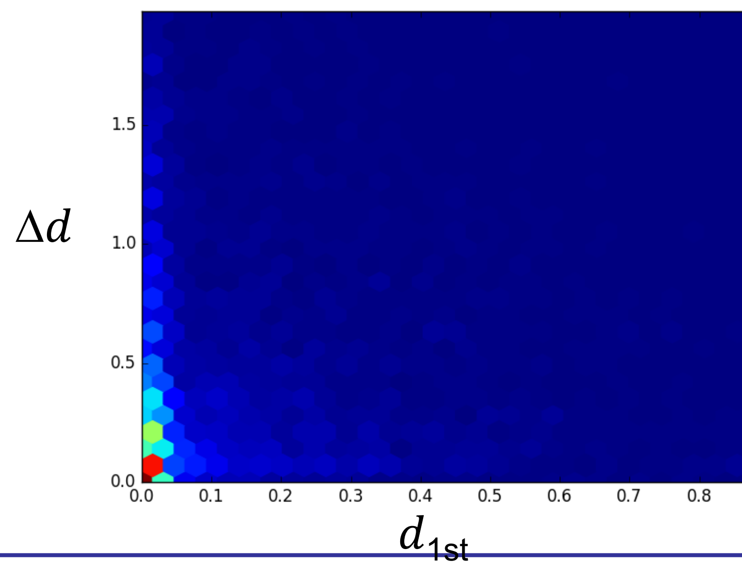

Statistic result from generated SVE

- Micro-structure stochastic model
  - Dependent variables generated using their empirical copula
  - Fiber additive process
    1) Define N seeds with first and second neighbors distances
    2) Generate first neighbor with its own first and second neighbors distances
    3) Generate second neighbor with its own first and second neighbors distances
    4) Change seeds & then change central fiber of the seeds

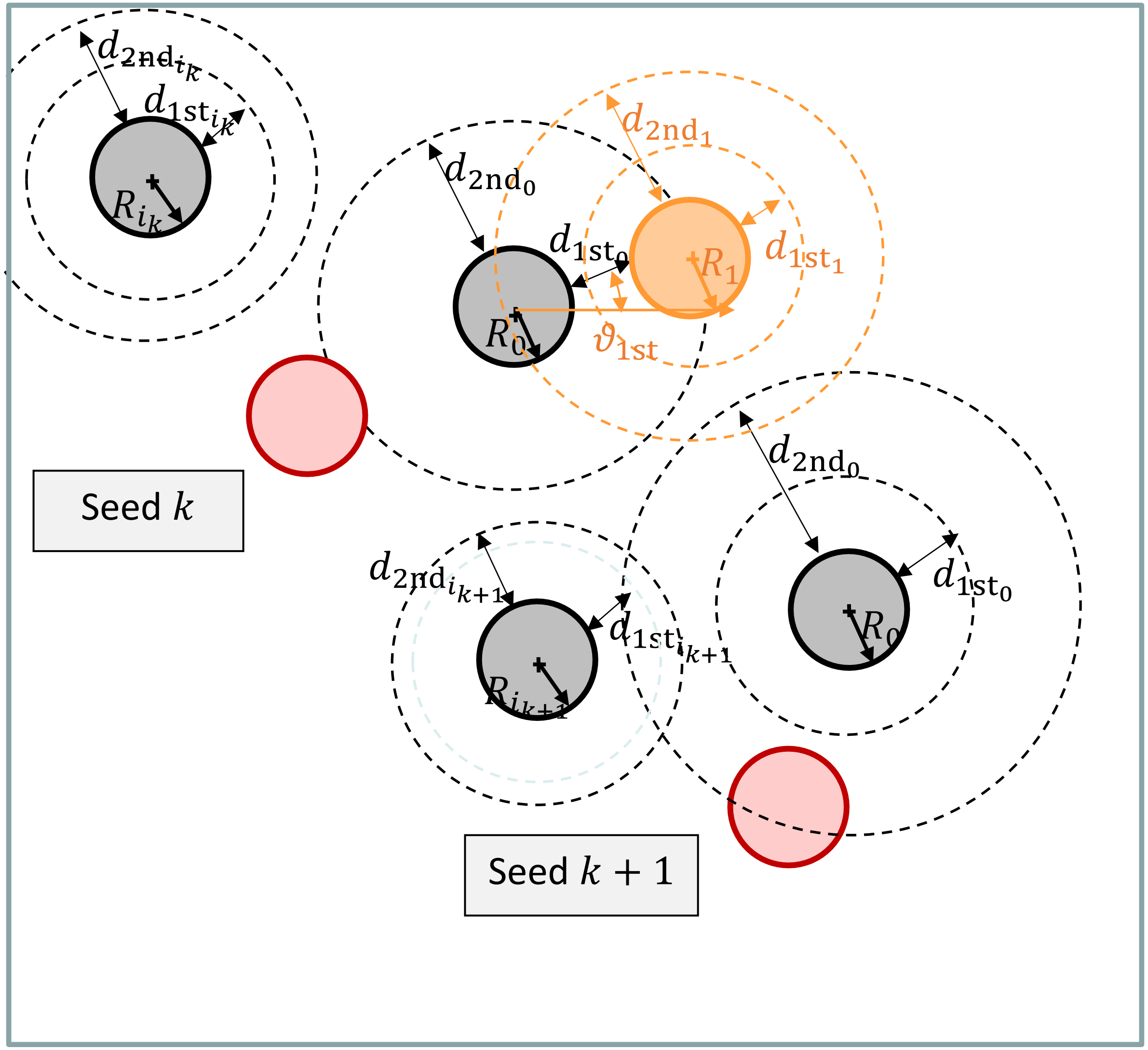

Beginning

- Micro-structure stochastic model
  - Arbitrary size
  - Arbitrary number

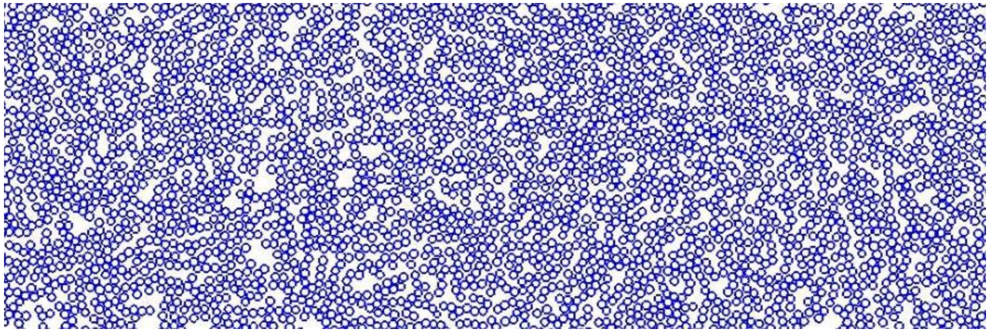

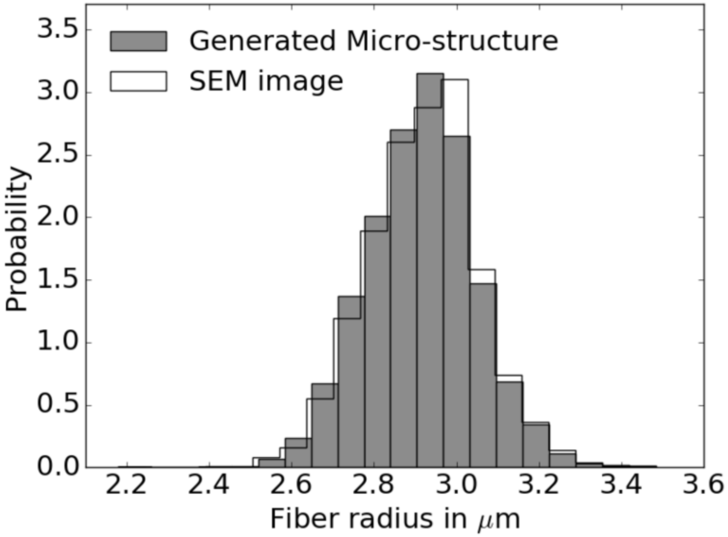

  - Possibility to generate non-homogenous distributions

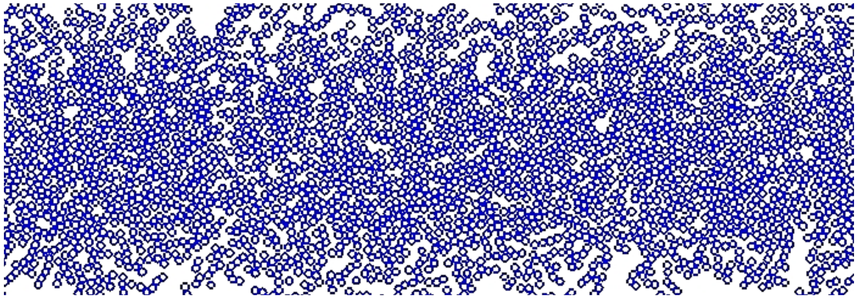

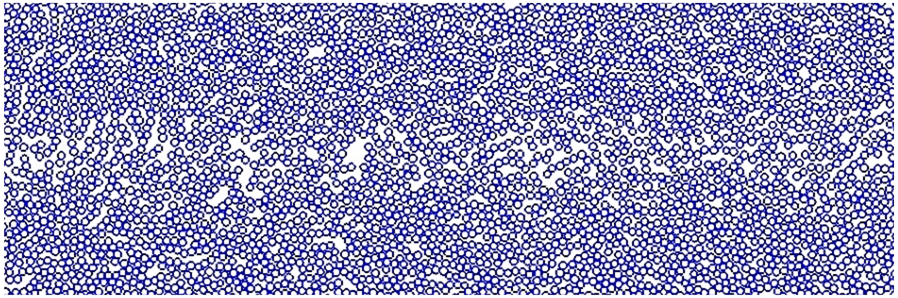

Beginning

- Stochastic homogenization of SVEs
  - Extraction of Stochastic Volume Elements
    - 2 sizes considered: $l_{\text{SVE}} = 10\ \mu m$ & $l_{\text{SVE}} = 25\ \mu m$
    - Window technique to capture correlation

$$R_{\mathbf{rs}}(\boldsymbol{\tau}) = \frac{\mathbb{E}\left[\left(r(\boldsymbol{x}) - \mathbb{E}(r)\right)\left(s(\boldsymbol{x}+\boldsymbol{\tau}) - \mathbb{E}(s)\right)\right]}{\sqrt{\mathbb{E}\left[\left(r - \mathbb{E}(r)\right)^2\right]}\sqrt{\mathbb{E}\left[\left(s - \mathbb{E}(s)\right)^2\right]}}$$

  - For each SVE
    - Extract apparent homogenized material tensor $\mathbb{C}_{\text{M}}$

$$\begin{cases} \boldsymbol{\varepsilon}_{\text{M}} = \dfrac{1}{V(\omega)}\displaystyle\int_{\omega} \boldsymbol{\varepsilon}_{\text{m}} d\omega \\ \boldsymbol{\sigma}_{\text{M}} = \dfrac{1}{V(\omega)}\displaystyle\int_{\omega} \boldsymbol{\sigma}_{\text{m}} d\omega \\ \mathbb{C}_{\text{M}} = \dfrac{\partial \boldsymbol{\sigma}_{\text{M}}}{\partial \boldsymbol{u}_{\text{M}} \otimes \boldsymbol{\nabla}_{\text{M}}} \end{cases}$$

    - Consistent boundary conditions:
      - Periodic (PBC)
      - Minimum kinematics (SUBC)
      - Kinematic (KUBC)

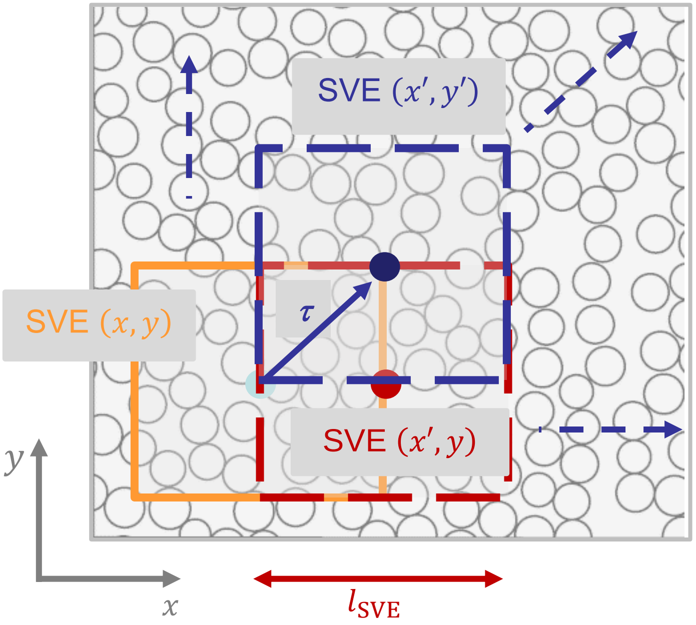

- Stochastic homogenization of SVEs
  - Apparent properties

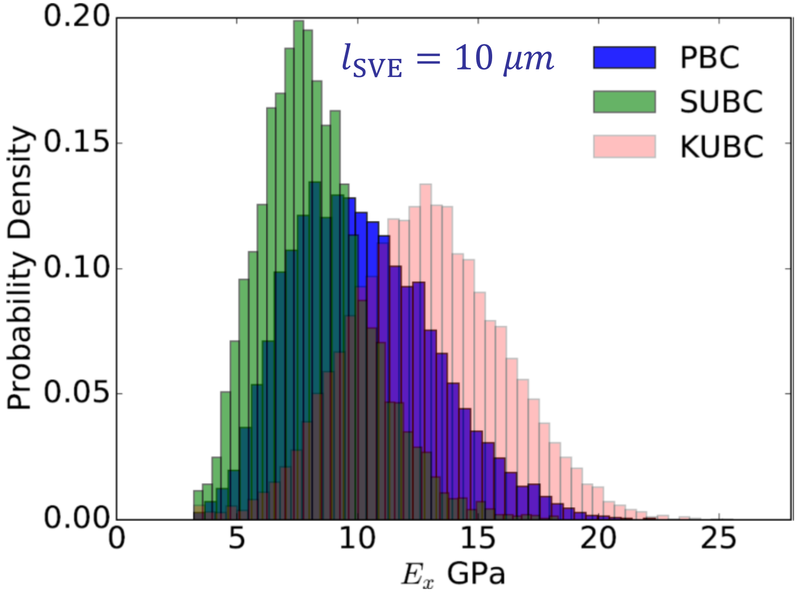

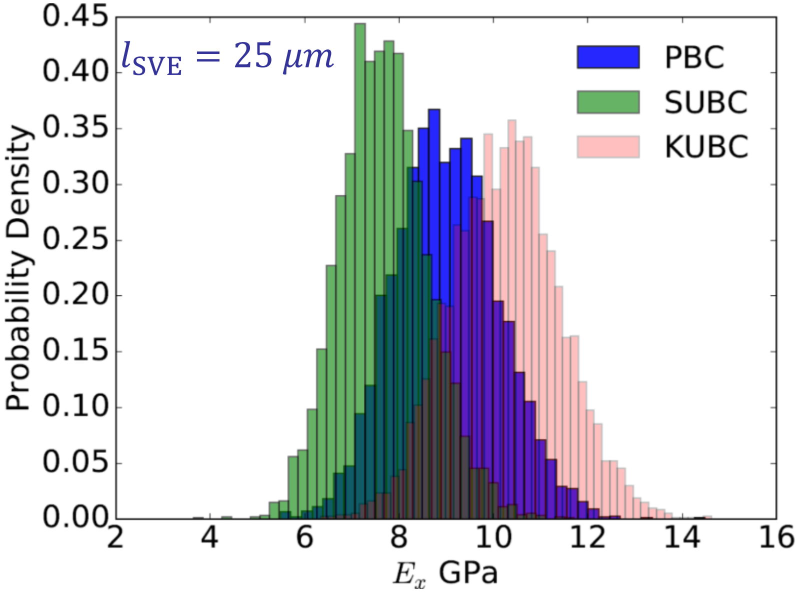

Increasing l_{SVE}

When l_{SVE} increases
- Average values for different BCs get closer (to PBC one)
- Distributions narrow
- Distributions get closer to normal

- Stochastic homogenization of SVEs
  - Correlation study

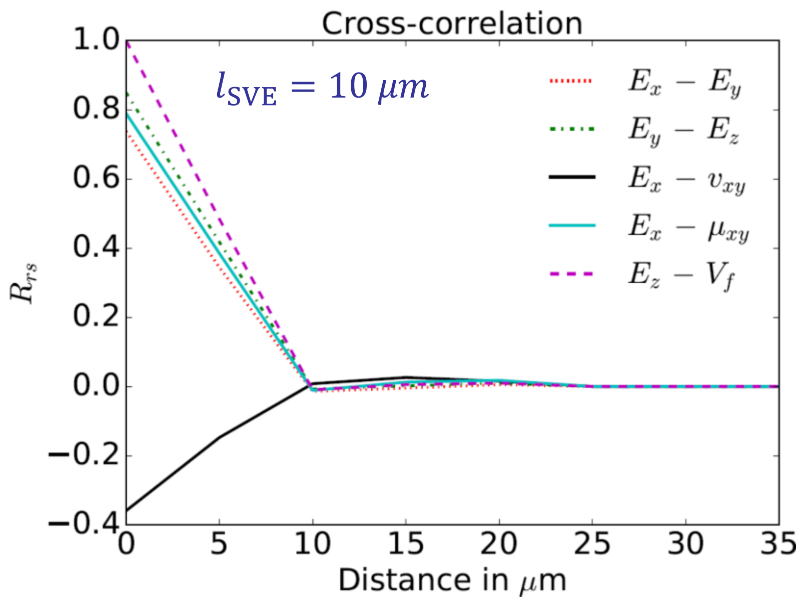

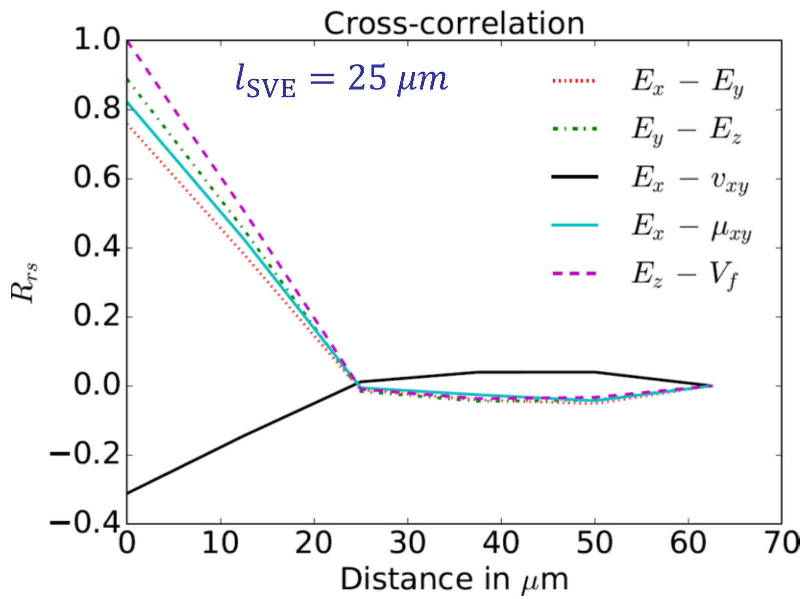

Increasing l_{SVE}

(1) Auto/cross correlation vanishes at $\tau = l_{\text{SVE}}$
(2) When l_{SVE} increases, distributions get closer to normal

(1)+(2) Apparent properties are independent random variables
However the distribution depend on

- l_{SVE}
- The boundary conditions

- Mean-Field-homogenization (MFH)
  - Linear composites

$$\begin{cases} \boldsymbol{\sigma}_{\mathrm{M}} = \bar{\boldsymbol{\sigma}} = v_0 \boldsymbol{\sigma}_0 + v_{\mathrm{I}} \boldsymbol{\sigma}_{\mathrm{I}} \\ \boldsymbol{\varepsilon}_{\mathrm{M}} = \bar{\boldsymbol{\varepsilon}} = v_0 \boldsymbol{\varepsilon}_0 + v_{\mathrm{I}} \boldsymbol{\varepsilon}_{\mathrm{I}} \\ \boldsymbol{\varepsilon}_{\mathrm{I}} = \mathbb{B}^{\varepsilon}(\mathrm{I}, \mathbb{C}_0, \mathbb{C}_{\mathrm{I}}) : \boldsymbol{\varepsilon}_0 \end{cases}$$

$$\Rightarrow \quad \hat{\mathbb{C}}_{\mathrm{M}} = \hat{\mathbb{C}}_{\mathrm{M}}(\mathrm{I}, \mathbb{C}_0, \mathbb{C}_{\mathrm{I}}, v_{\mathrm{I}})$$

Defined as random variables

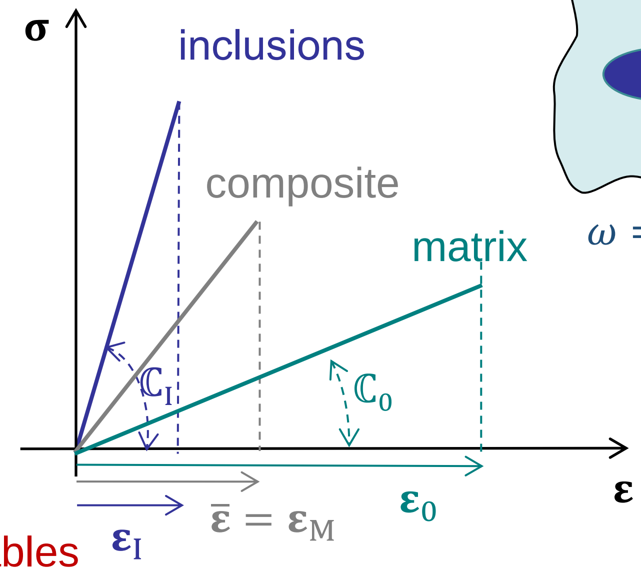

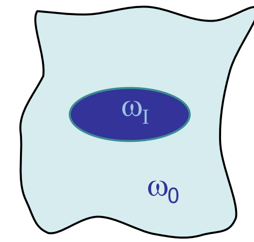

$\omega = \cup_i \, \omega_i$

- Consider an equivalent system
  - For each SVE realization i:
    - $\Rightarrow$ $\mathbb{C}_{\mathrm{M}}$ and v_{I} known
  - Anisotropy from $\mathbb{C}_{\mathrm{M}}^{i}$
    - $\Rightarrow$ θ is evaluated
  - Fiber behavior uniform
    - $\Rightarrow$ $\hat{\mathbb{C}}_{\mathrm{I}}$ for one SVE

$$\mathbb{C}_{\mathrm{M}} \simeq \hat{\mathbb{C}}_{\mathrm{M}}(\hat{\mathrm{I}}, \hat{\mathbb{C}}_0, \hat{\mathbb{C}}_{\mathrm{I}}, v_{\mathrm{I}}, \theta)$$

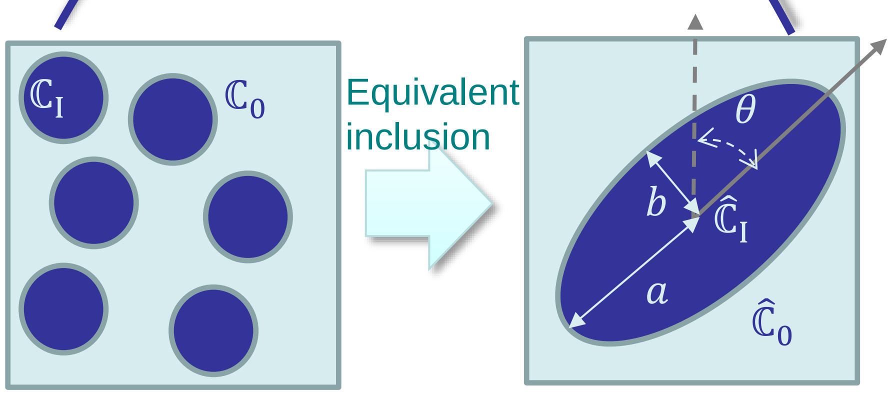

  - Remaining optimization problem:

$$\min_{\frac{a}{b}, \hat{E}_0, \hat{\nu}_0} \left\| \mathbb{C}_{\mathrm{M}} - \hat{\mathbb{C}}_{\mathrm{M}}\left(\frac{a}{b}, \hat{E}_0, \hat{\nu}_0 ; v_{\mathrm{I}}, \theta, \hat{\mathbb{C}}_{\mathrm{I}}\right) \right\|$$

- Inverse stochastic identification
  - Comparison of homogenized properties from SVE realizations and stochastic MFH

$$\mathbb{C}_{\mathrm{M}} \simeq \hat{\mathbb{C}}_{\mathrm{M}}(\hat{\mathrm{I}}, \hat{\mathbb{C}}_0, \hat{\mathbb{C}}_{\mathrm{I}}, v_{\mathrm{I}}, \theta)$$

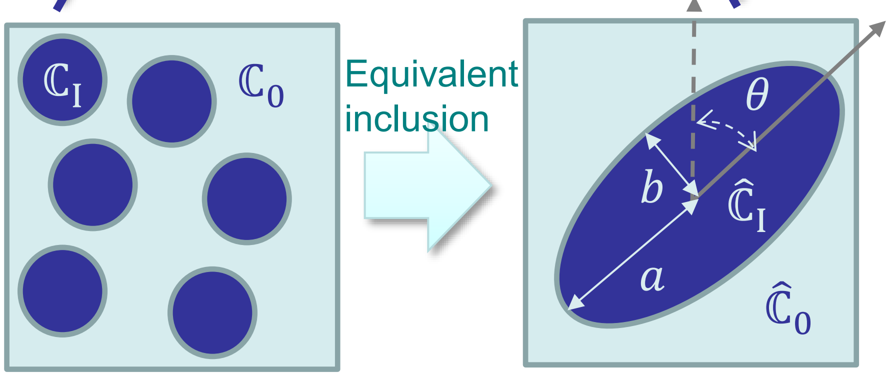

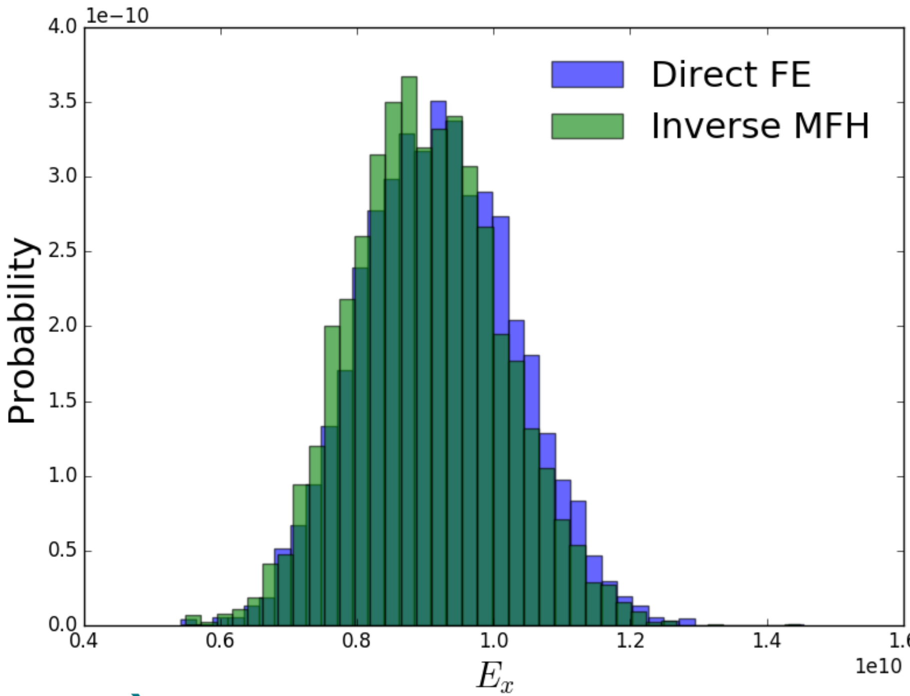

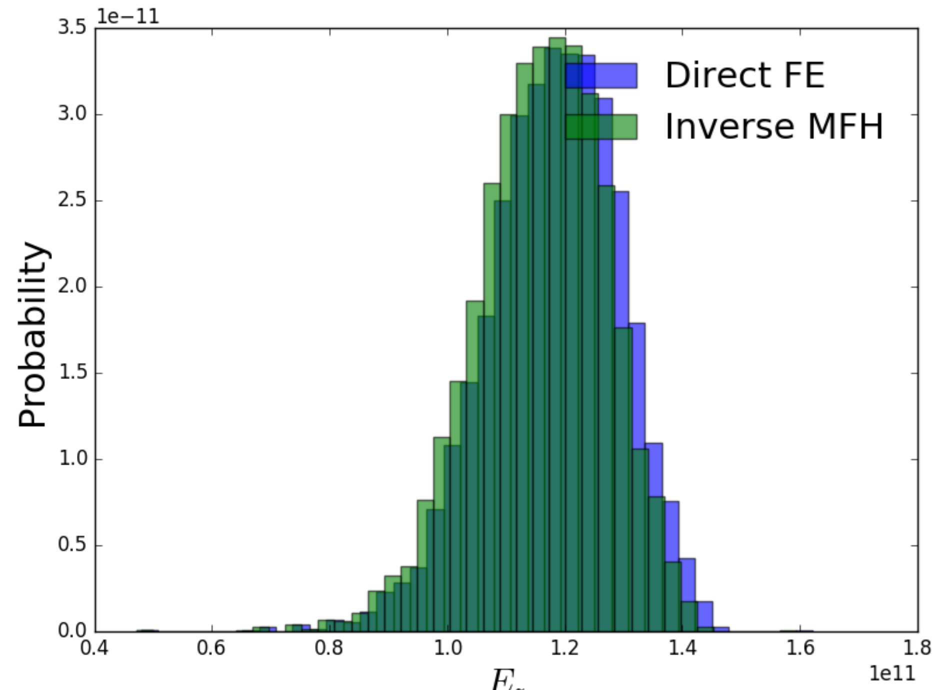

- Incremental-secant Mean-Field-homogenization
  - Virtual elastic unloading from previous state
    - Composite material unloaded to reach the stress-free state
    - Residual stress in components
  - Define Linear Comparison Composite
    - From unloaded state

$$\Delta\boldsymbol{\varepsilon}^{\mathrm{r}}_{\mathrm{I}/0} = \Delta\boldsymbol{\varepsilon}_{\mathrm{I}/0} + \Delta\boldsymbol{\varepsilon}^{\mathrm{unload}}_{\mathrm{I}/0}$$

    - Incremental-secant loading

$$\begin{cases} \boldsymbol{\sigma}_{\mathrm{M}} = \bar{\boldsymbol{\sigma}} = v_0\boldsymbol{\sigma}_0 + v_{\mathrm{I}}\boldsymbol{\sigma}_{\mathrm{I}} \\ \Delta\boldsymbol{\varepsilon}^{\mathrm{r}}_{\mathrm{M}} = \overline{\Delta\boldsymbol{\varepsilon}} = v_0\Delta\boldsymbol{\varepsilon}^{\mathrm{r}}_0 + v_{\mathrm{I}}\Delta\boldsymbol{\varepsilon}^{\mathrm{r}}_{\mathrm{I}} \\ \Delta\boldsymbol{\varepsilon}^{\mathrm{r}}_{\mathrm{I}} = \mathbb{B}^{\varepsilon}\left(\mathrm{I}, \mathbb{C}^{\mathrm{S}}_0, \mathbb{C}^{\mathrm{S}}_{\mathrm{I}}\right) : \Delta\boldsymbol{\varepsilon}^{\mathrm{r}}_0 \end{cases}$$

    - Incremental secant operator

$$\Rightarrow \Delta\boldsymbol{\sigma}_{\mathrm{M}} = \mathbb{C}^{\mathrm{S}}_{\mathrm{M}}\left(\mathrm{I}, \mathbb{C}^{\mathrm{S}}_0, \mathbb{C}^{\mathrm{S}}_{\mathrm{I}}, v_{\mathrm{I}}\right) : \Delta\boldsymbol{\varepsilon}^{\mathrm{r}}_{\mathrm{M}}$$

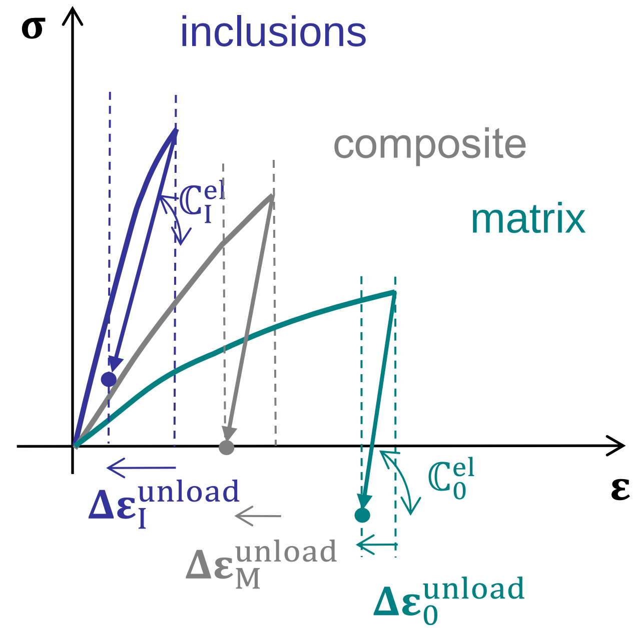

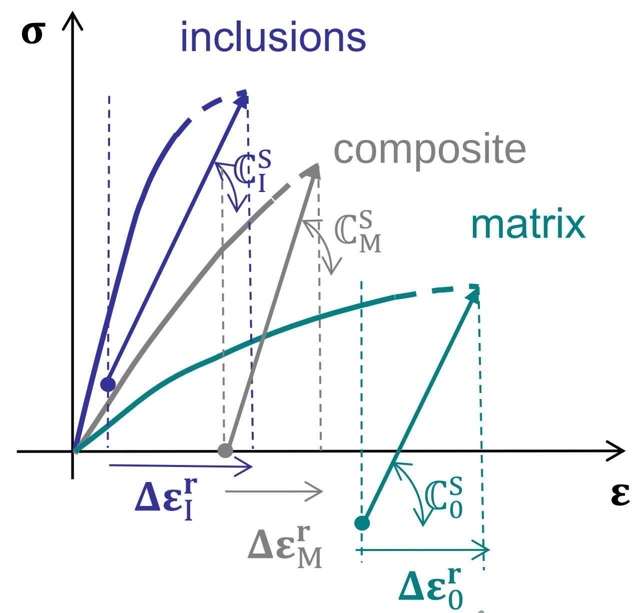

- Non-linear inverse identification
  - First step from elastic response

$$\mathbb{C}_{\mathrm{M}}^{\mathrm{el}} \simeq \hat{\mathbb{C}}_{\mathrm{M}}^{\mathrm{el}}(\hat{\mathrm{I}}, \hat{\mathbb{C}}_{0}^{\mathrm{el}}, \hat{\mathbb{C}}_{\mathrm{I}}^{\mathrm{el}}, v_{\mathrm{I}}, \theta)$$

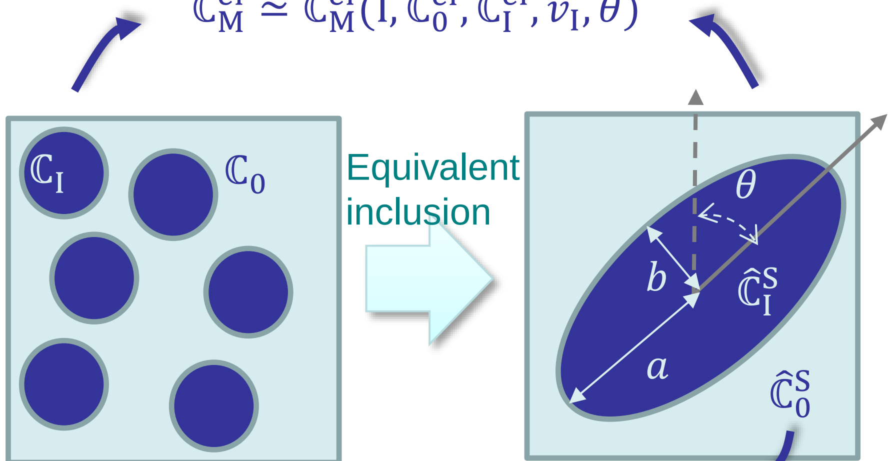

$$\mathbb{C}_{0}^{\mathrm{S}} \simeq \hat{\mathbb{C}}_{0}^{\mathrm{S}}(\hat{R}(\hat{p}_0); \hat{\mathbb{C}}_{0}^{\mathrm{el}})$$

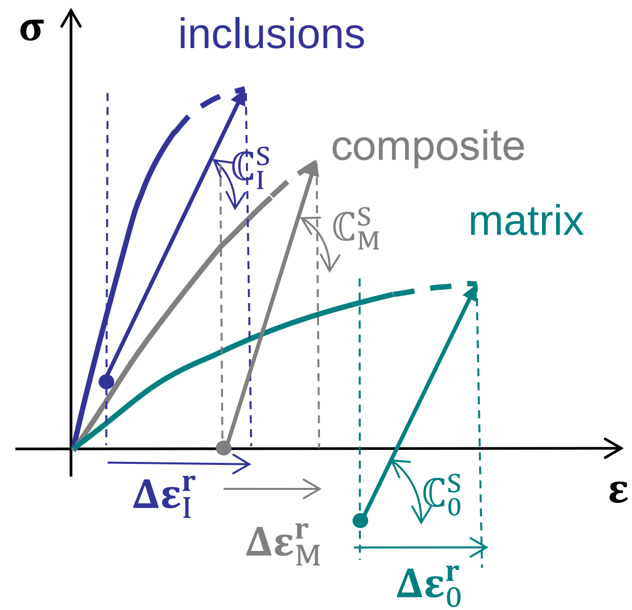

  - Second step from the LCC
    - New optimization problem

$$\boldsymbol{\Delta\sigma}_{\mathrm{M}} \simeq \hat{\mathbb{C}}_{\mathrm{M}}^{\mathrm{S}}\left(\hat{\mathrm{I}}, \hat{\mathbb{C}}_{0}^{\mathrm{S}}, \mathbb{C}_{\mathrm{I}}^{\mathrm{S}}, v_{\mathrm{I}}, \theta\right) : \boldsymbol{\Delta\varepsilon}_{\mathrm{M}}^{\mathbf{r}}$$

    - Extract the equivalent hardening $\hat{R}(\hat{p}_0)$ from the incremental secant tensor

$$\mathbb{C}_{0}^{\mathrm{S}} \simeq \hat{\mathbb{C}}_{0}^{\mathrm{S}}(\hat{R}(\hat{p}_0); \hat{\mathbb{C}}_{0}^{\mathrm{el}})$$

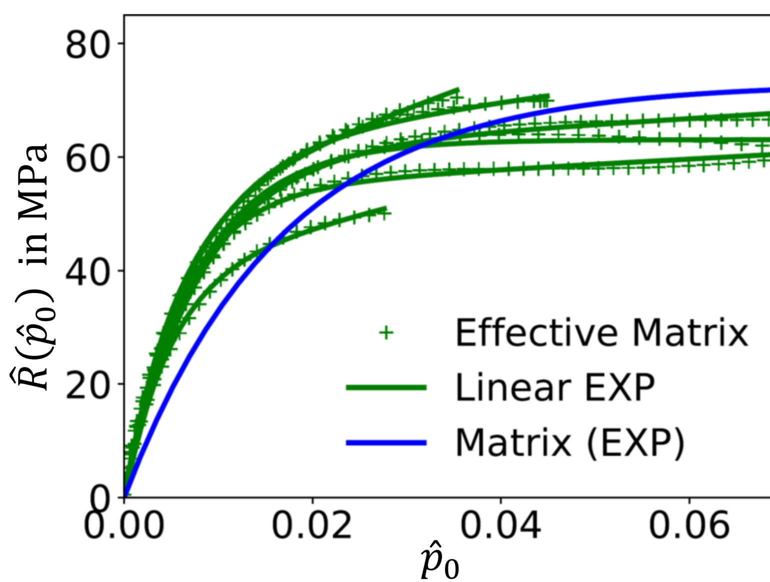

- Non-linear inverse identification
  - Comparison SVE vs. MFH

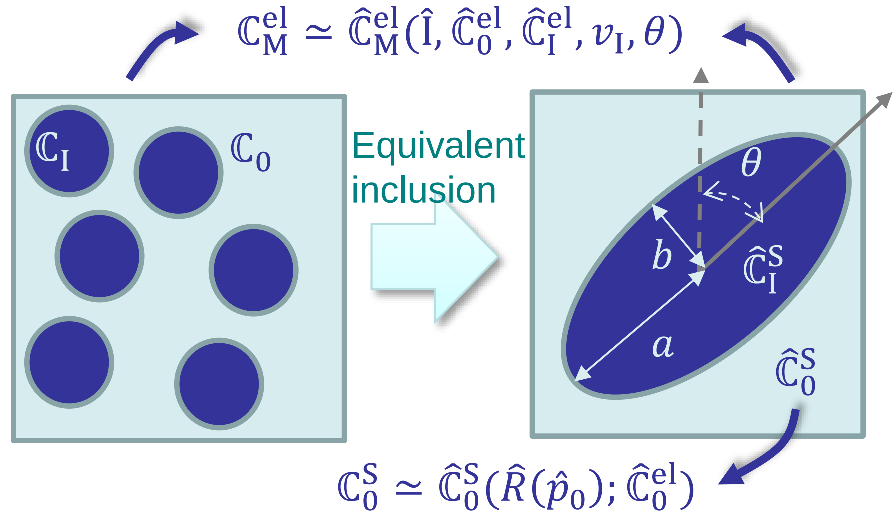

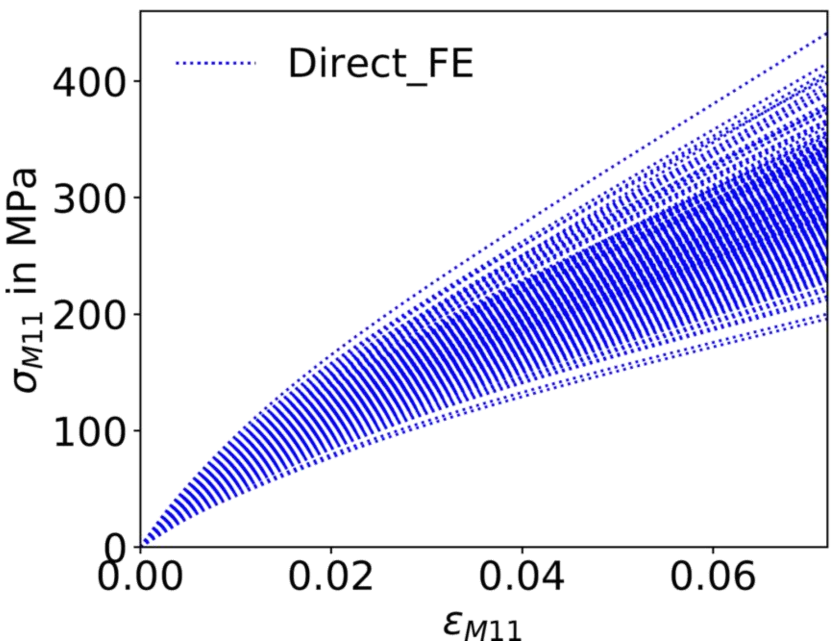

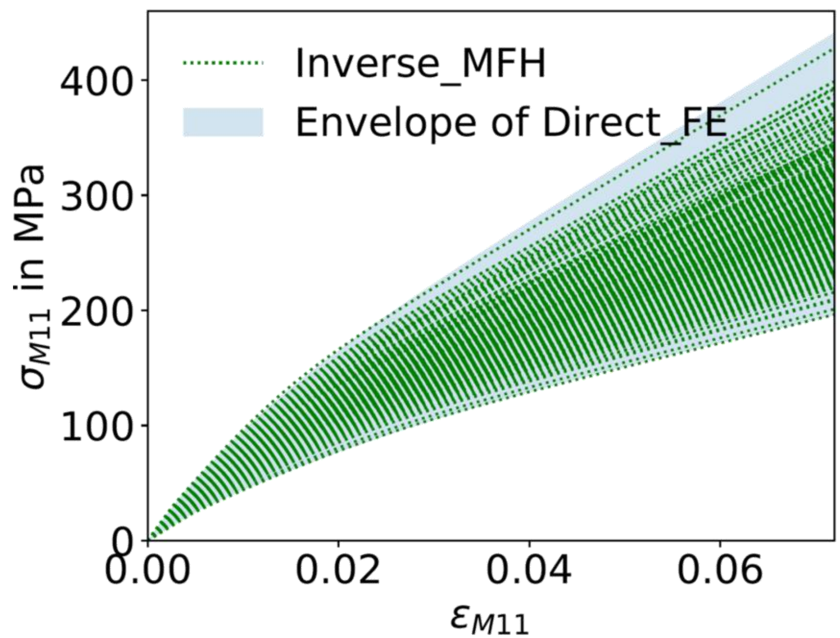

- Damage-enhanced Mean-Field-homogenization
  - Virtual elastic unloading from previous state
    - Composite material unloaded to reach the stress-free state
    - Residual stress in components
  - Define Linear Comparison Composite
    - From elastic state

$$\boldsymbol{\Delta\varepsilon}^{\mathrm{r}}_{\mathrm{I}/0} = \boldsymbol{\Delta\varepsilon}_{\mathrm{I}/0} + \boldsymbol{\Delta\varepsilon}^{\mathrm{unload}}_{\mathrm{I}/0}$$

    - Incremental-secant loading

$$\begin{cases} \boldsymbol{\sigma}_{\mathrm{M}} = \overline{\boldsymbol{\sigma}} = v_0\boldsymbol{\sigma}_0 + v_{\mathrm{I}}\boldsymbol{\sigma}_{\mathrm{I}} \\ \boldsymbol{\Delta\varepsilon}^{\mathrm{r}}_{\mathrm{M}} = \overline{\boldsymbol{\Delta\varepsilon}} = v_0\boldsymbol{\Delta\varepsilon}^{\mathrm{r}}_0 + v_{\mathrm{I}}\boldsymbol{\Delta\varepsilon}^{\mathrm{r}}_{\mathrm{I}} \\ \boldsymbol{\Delta\varepsilon}^{\mathrm{r}}_{\mathrm{I}} = \mathbb{B}^{\varepsilon}\left(\mathrm{I}, (1-D_0)\mathbb{C}^{\mathrm{S}}_0, \mathbb{C}^{\mathrm{S}}_{\mathrm{I}}\right) : \boldsymbol{\Delta\varepsilon}^{\mathrm{r}}_0 \end{cases}$$

    - Incremental secant operator

$$\Rightarrow \quad \boldsymbol{\Delta\sigma}_{\mathrm{M}} = \mathbb{C}^{\mathrm{S}}_{\mathrm{M}}\left(\mathrm{I}, (1-D_0)\mathbb{C}^{\mathrm{S}}_0, \mathbb{C}^{\mathrm{S}}_{\mathrm{I}}, v_{\mathrm{I}}\right) : \boldsymbol{\Delta\varepsilon}^{\mathrm{r}}_{\mathrm{M}}$$

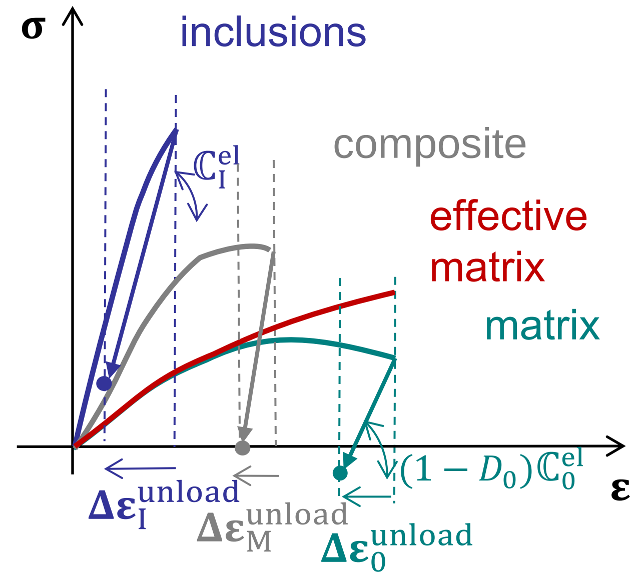

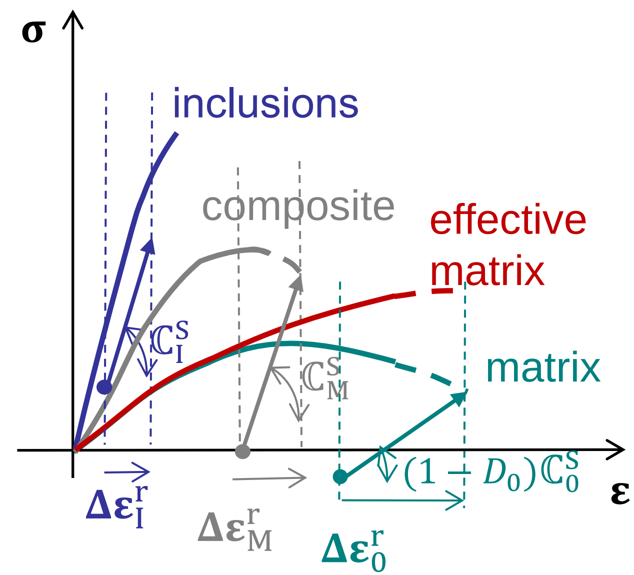

- Damage-enhanced inverse identification
  - Comparison SVE vs. MFH

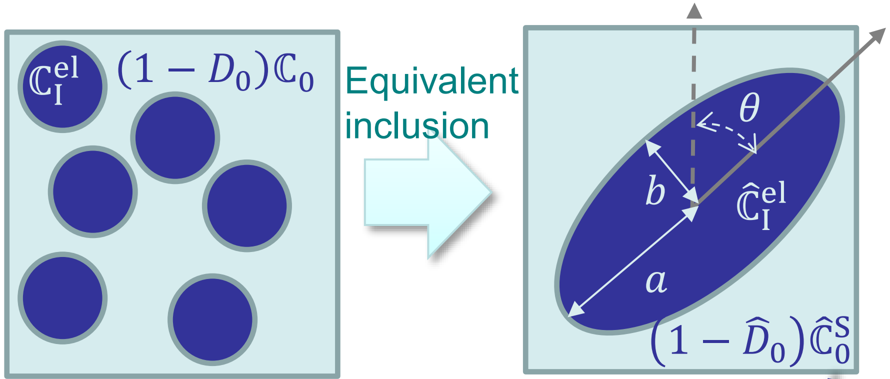

$$(1-\mathrm{D}_0)\mathbb{C}_0^S \simeq \left(1-\hat{\mathrm{D}}_0(\hat{p}_0)\right)\hat{\mathbb{C}}_0^S\left(\hat{R}(\hat{p}_0);\hat{\mathbb{C}}_0^{\mathrm{el}}\right)$$

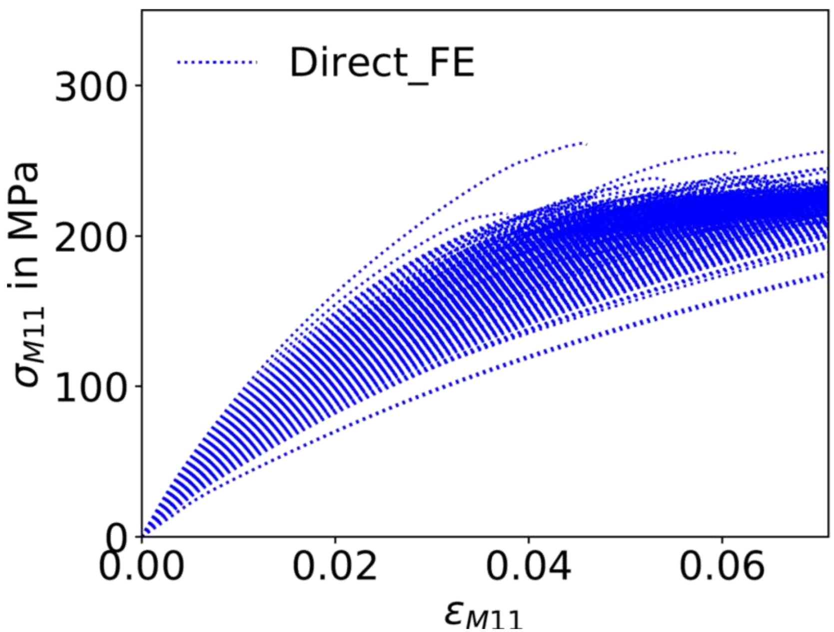

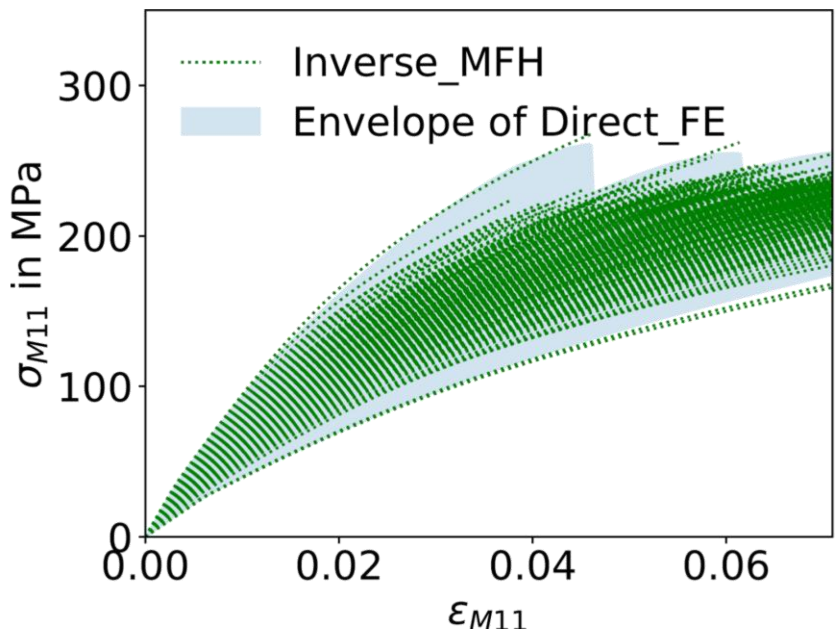

- Generation of random field
  - Comparison inverse identification vs. diffusion map –based generator

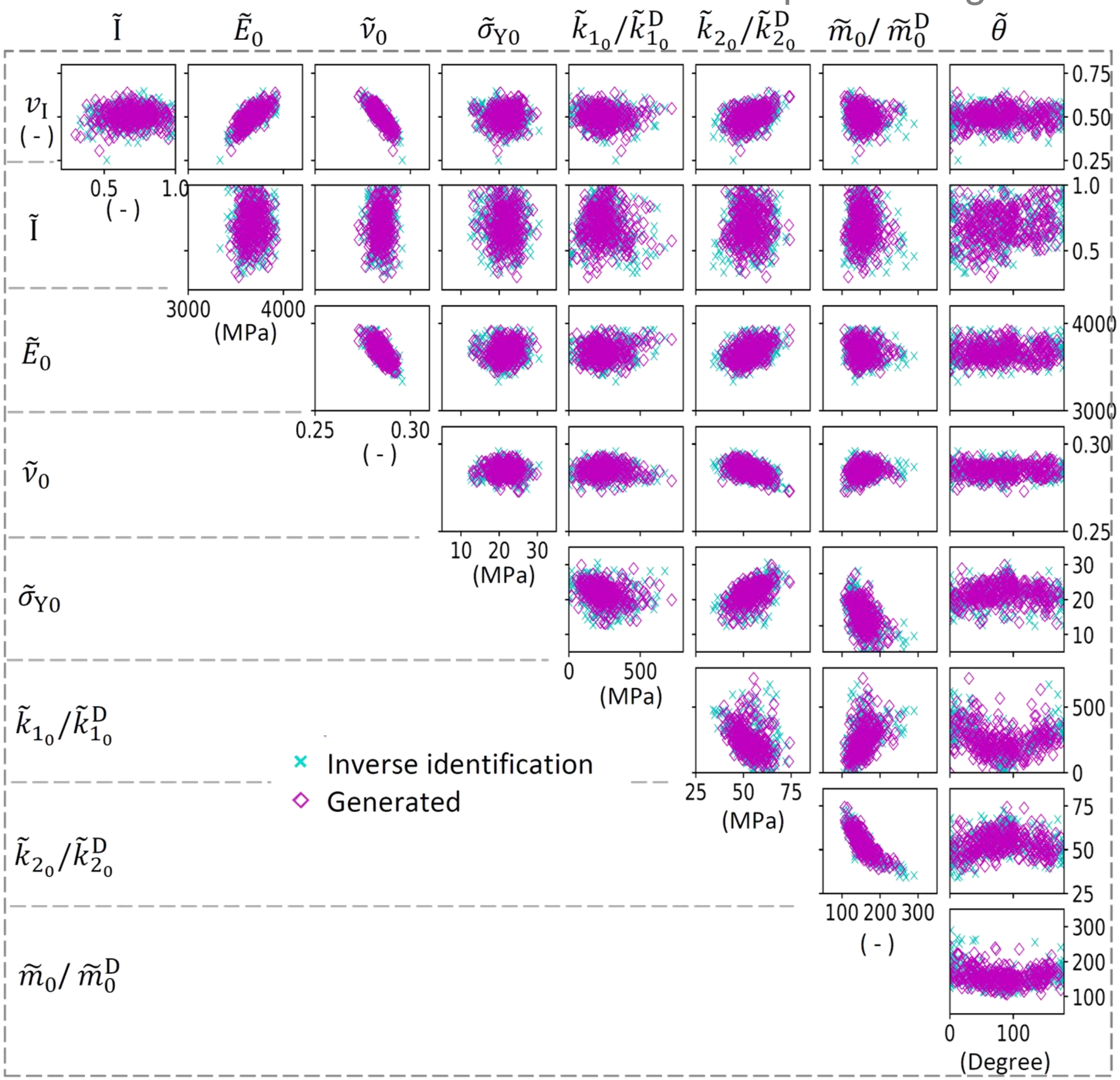

Beginning

Stochastic Homogenization of Composite Materials

- One single ply loading realization
  - Random field and finite elements discretizations
  - Non-uniform homogenized stress distributions
  - Creates damage localization

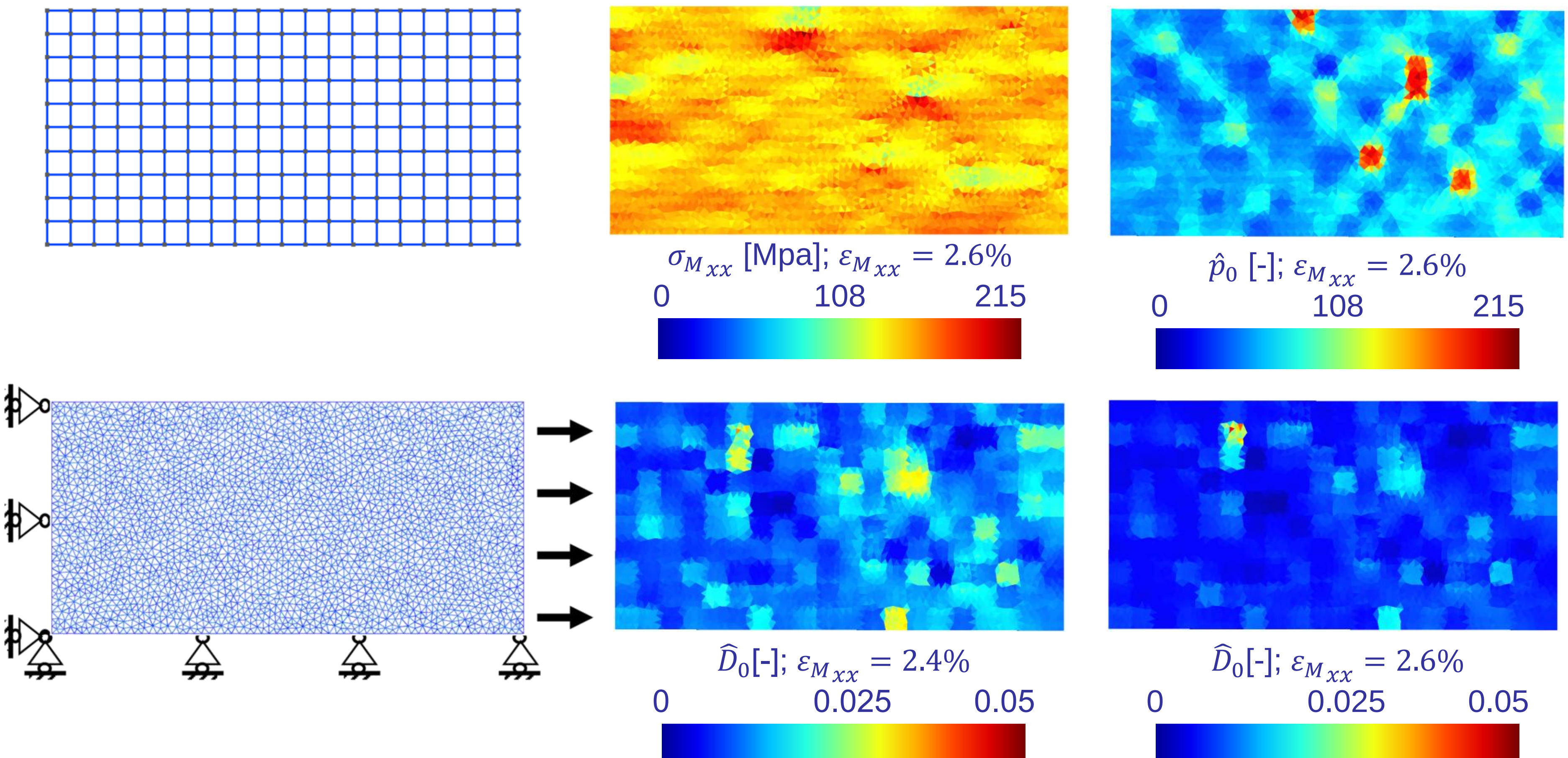

- Ply loading realizations
  - Simple failure criterion at (homogenized stress) loss of ellipticity
  - Discrepancy in failure point

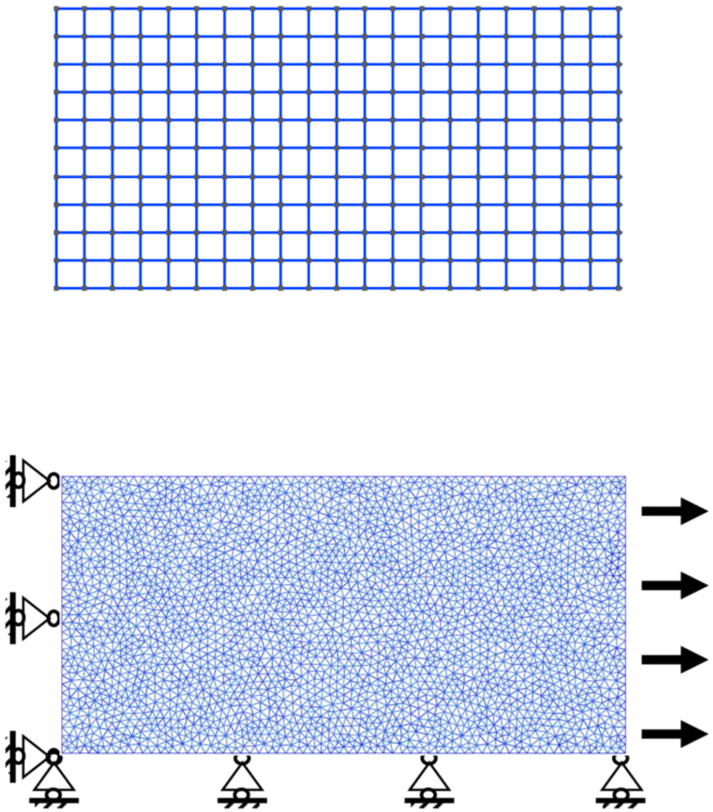

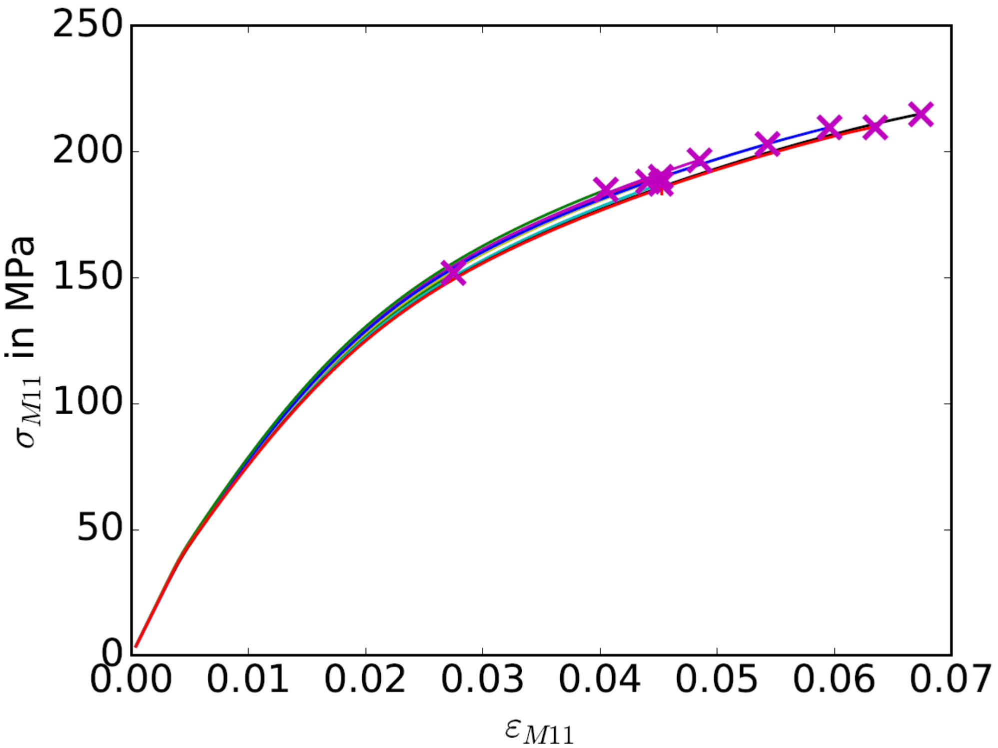

- STOMMMAC M.ERA-NET project (MFH for elasto-visco-plastic composites)
  - e-Xstream, ULiège (Belgium)
  - BATZ (Spain)
  - JKU, AC (Austria)
  - U Luxembourg (Luxemburg)

- Publications (doi)
  - 10.1016/j.compstruct.2018.01.051
  - 10.1002/nme.5903
  - 10.1016/j.cma.2019.01.016

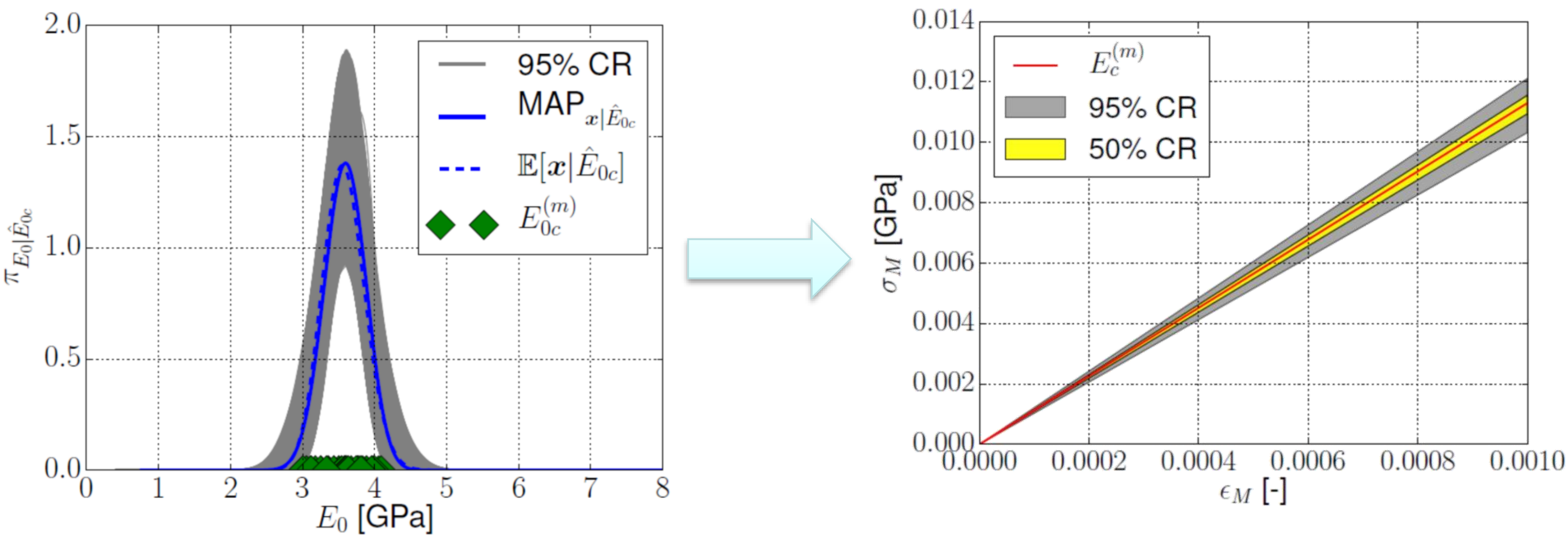

Bayesian identification of stochastic Mean-Field Homogenization model parameters

STOMMMAC The research has been funded by the Walloon Region under the agreement no 1410246-STOMMMAC (CT-INT 2013-03-28) in the context of M-ERA.NET Joint Call 2014.

Bayesian identification of stochastic MFH model parameters

- Multi-scale modeling
  - 2 problems are solved concurrently
    - The macro-scale problem
    - The meso-scale problem (on a meso-scale Volume Element)

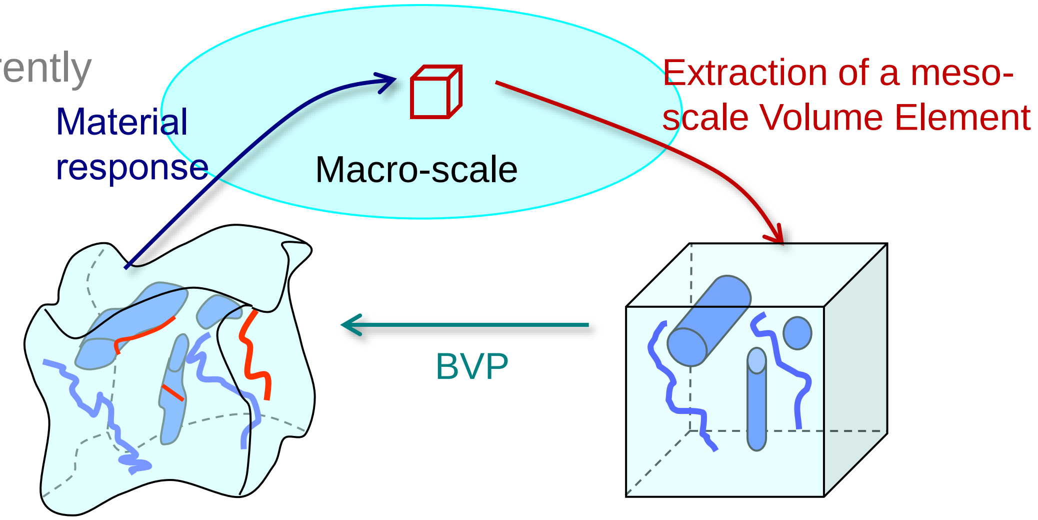

Identification: Requires identification of micro-scale geometrical and material model parameters

Bayesian identification of stochastic MFH model parameters

- Proposed methodology
  - To develop a stochastic Mean Field Homogenization method whose missing micro-constituents properties are inferred from coupons tests

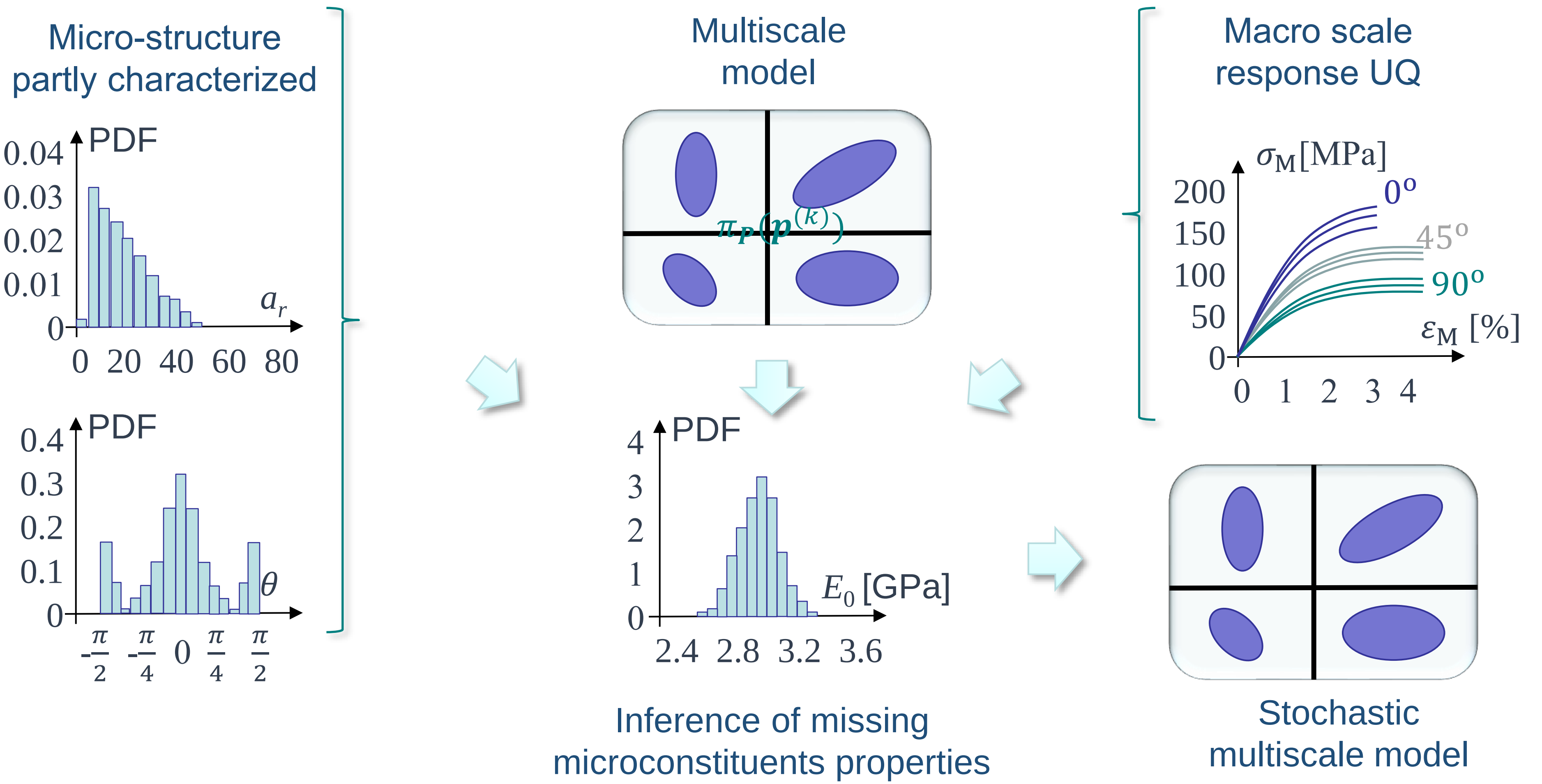

- Fibre distribution effect
  - 2-step homogenization

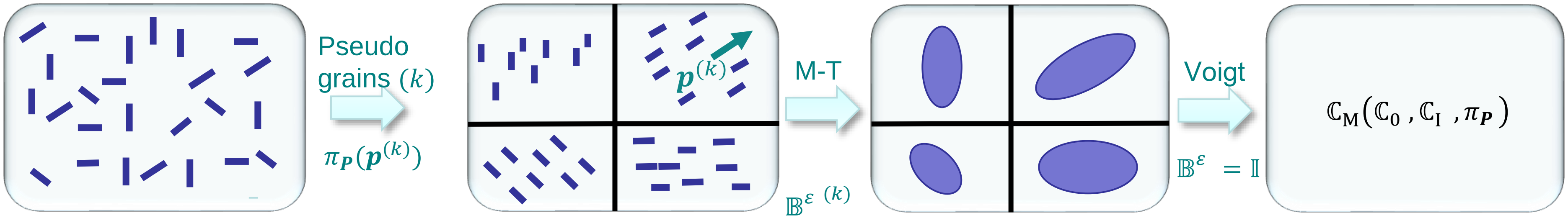

  - For uniaxial tests along direction θ: $\sigma_{\mathrm{M}} = \sigma_{\mathrm{M}}\left(\mathrm{I}(\psi(\boldsymbol{p})), \mathbb{C}_0, \mathbb{C}_{\mathrm{I}}; \theta, \varepsilon_{\mathrm{M}}\right)$

- Fibre distribution effect
  - Skin-core effect

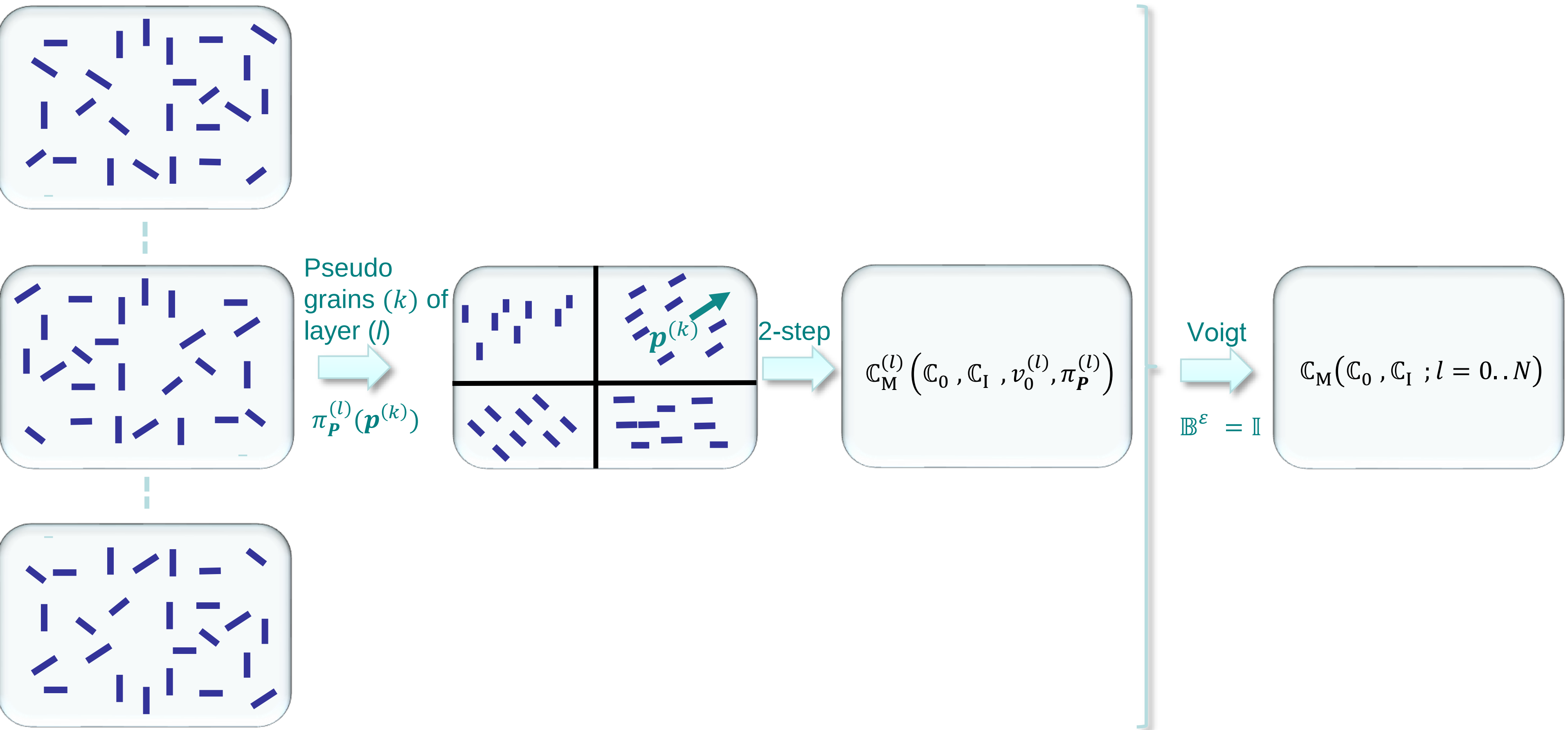

  - For uniaxial tests along direction θ: $\sigma_{\mathrm{M}}\ =\sigma_{\mathrm{M}}\left(\mathrm{I}(\psi(\boldsymbol{p})),\mathbb{C}_0\,,\mathbb{C}_{\mathrm{I}}\;;\theta,\varepsilon_{\mathrm{M}}\right)$

Bayesian identification of stochastic MFH model parameters

- Experimental characterization

Fiber orientation and aspect ratio (JKU)

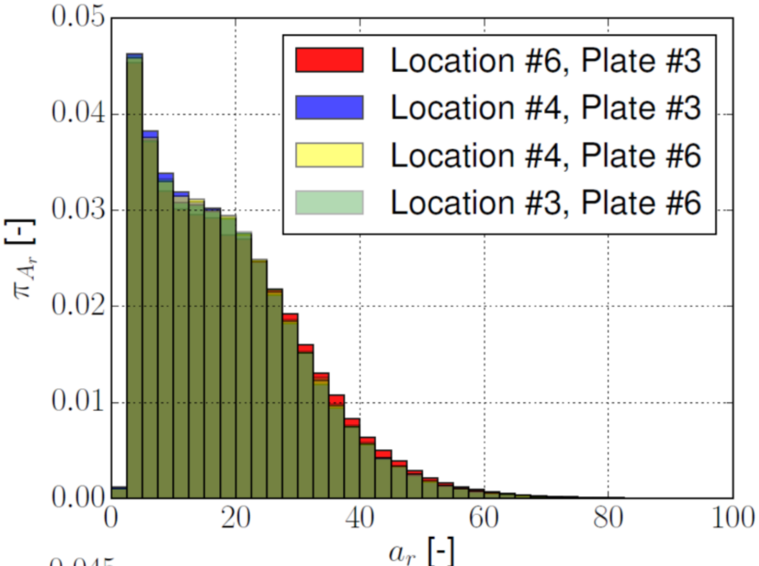

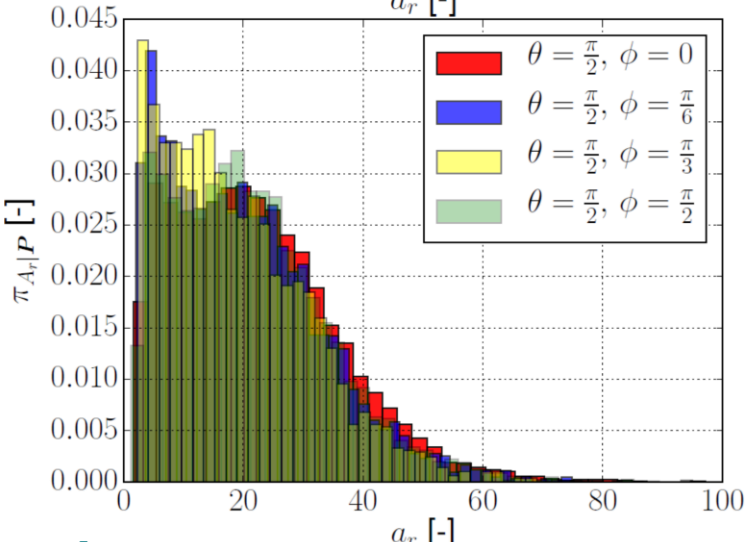

Composite material response (BATZ)

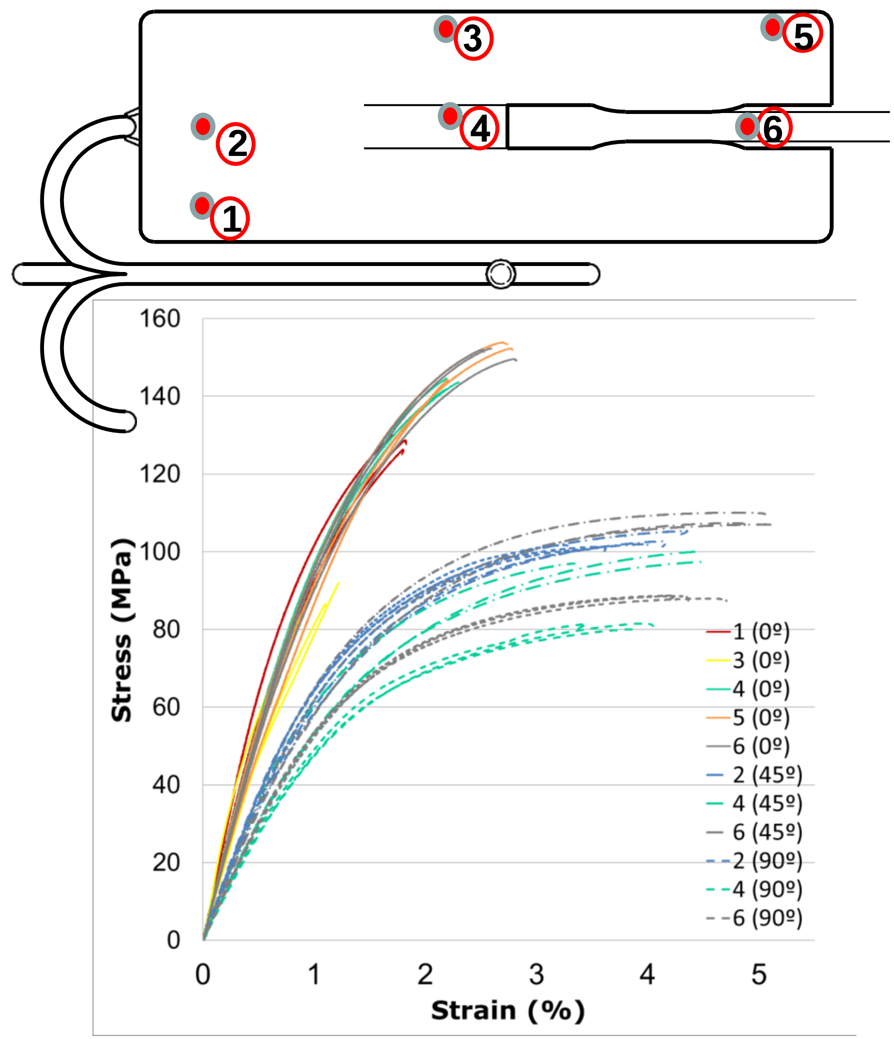

- Assume a distribution of the matrix Young's modulus
  - Beta distribution $E_0 \sim \beta_{\alpha,\beta,a,b}$ with $\beta_{\alpha,\beta,a,b}(y) = \frac{(y-a)^{\alpha-1}(y-b)^{\beta-1}}{(b-a)^{\alpha+\beta+1}B(\alpha,\beta)}$
  - Matrix Young 's modulus corresponding to experimental measurements
    - $E_{0c}^{(n)}$ with $n = 1..n_{\text{total}}$, for all directions and positions
  - Bayes' theorem

$$\pi_{\text{post}}(\alpha,\beta,a,b|\hat{E}_{0c}) \propto \pi(\hat{E}_{0c}|\alpha,\beta,a,b)\pi_{\text{prior}}(\alpha)\pi_{\text{prior}}(\beta)\pi_{\text{prior}}(a)\pi_{\text{prior}}(b)$$

    - Priors: $\pi_{\text{prior}}(x) = \Gamma_{\alpha,\beta,\,a,\,c}$ with $\Gamma_{\alpha,\beta,\,a,\,c}(y) = \frac{\left(\frac{y-a}{c}\right)^{\alpha-1}\beta^{\alpha}e^{-\beta\left(\frac{y-a}{c}\right)}}{c\Gamma(\alpha)}$
    - Likelihood: $\pi(\hat{E}_{\,0c}|\alpha,\beta,a,b) = \prod_{n=1}^{n_{\text{total}}} \beta_{\alpha,\beta,a,b}\left(E_{0c}^{(n)}\right)$

$$\pi_{\text{post}}(\alpha,\beta,a,b|\hat{E}_{0c}) \propto \prod_{n=1}^{n_{\text{total}}} \beta_{\alpha,\beta,a,c}\left(E_{0c}^{(n)}\right)\pi_{\text{prior}}(\alpha)\pi_{\text{prior}}(\beta)\pi_{\text{prior}}(a)\pi_{\text{prior}}(b)$$

Bayesian identification of stochastic MFH model parameters

- Assume a distribution of the matrix Young's modulus
  - Inference: $\pi_{\text{post}}(\alpha, \beta, a, b|\hat{E}_{0c}) \propto \prod_{n=1}^{n_{\text{total}}} \beta_{\alpha,\beta,a,c}\left(E_{0c}^{(n)}\right) \pi_{\text{prior}}(\alpha\,)\pi_{\text{prior}}(\beta)\pi_{\text{prior}}(a)\pi_{\text{prior}}(b)$
    - $i = 1..n_{\text{pos}}$, with n_{pos} the number of positions tested (5, positions #1-#5)

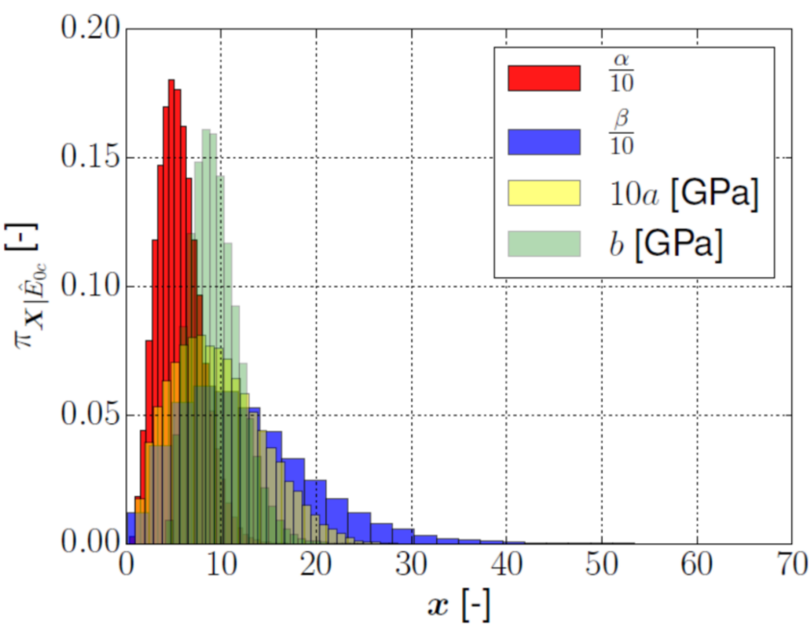

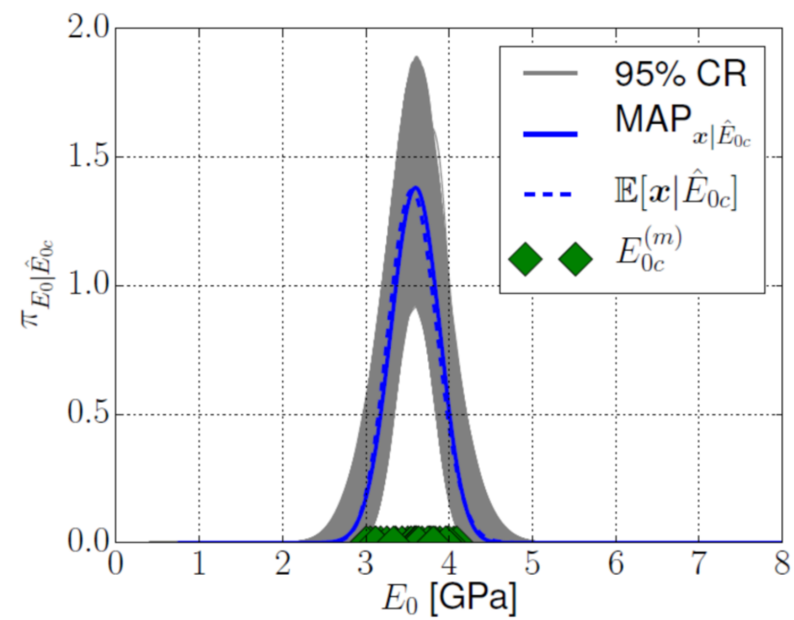

- Validation
  - Evaluate stochastic response at Position 6
    - Perform stochastic homogenization from $\pi_{\text{post}}(\alpha, \beta, a, b|\hat{E}_{0c})$
    - From sampling of $[\alpha, \beta, a, b]$, evaluate $E_0 \sim \beta_{\alpha,\beta,a,b}$
    - From sampling of $[E_0]$, evaluate composite response

$$E_{\text{MFH}} = E_{\text{MFH}}\big(\mathrm{I}(\psi(\boldsymbol{p}), a_r), E_0\ , \mathbb{C}_{\mathrm{I}}\ ; \theta\big)$$

    - Compare with experimental measurements $\hat{E}_c^{(6,j)}$

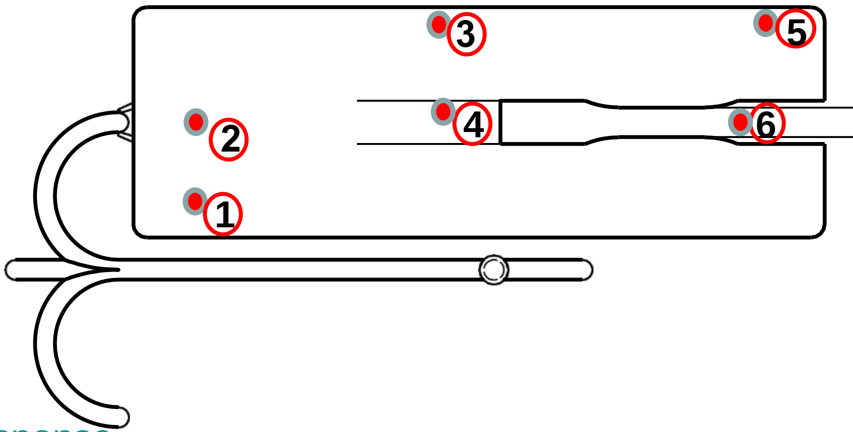

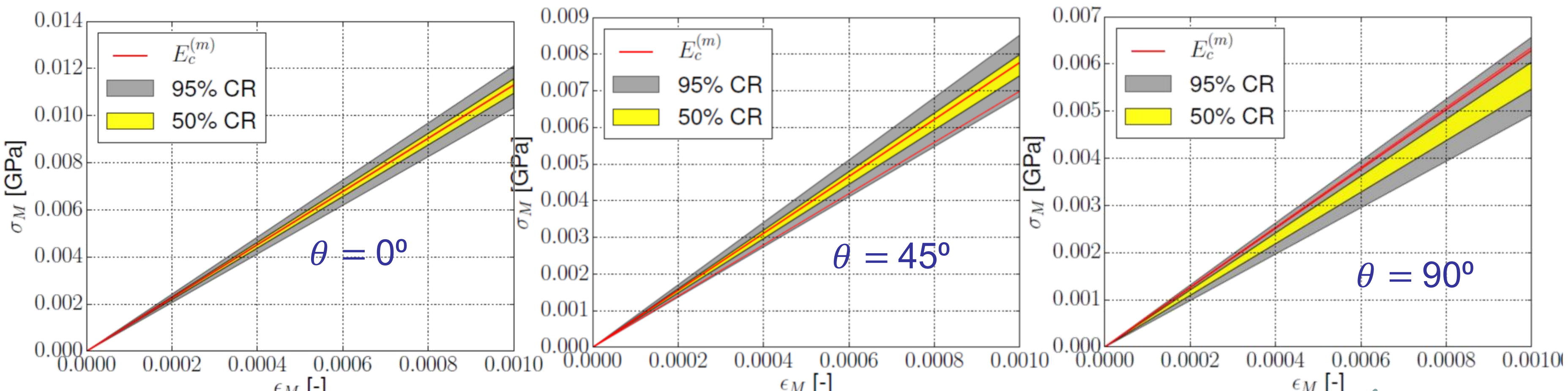

- Extension to non-linear behavior
  - More parameters to infer
    - Matrix Young's modulus E_0
    - Matrix yield stress $\sigma_{Y\,0}$
    - Matrix hardening law
      $R(p_0) = h\, p_0^{m_1}(1 - \exp(-m_2 p_0))$
    - Effective aspect ratio a_r
  - 2-Step MFH model requires many iterations
    - Incremental secant approach

$$\begin{cases} \boldsymbol{\sigma}_{\mathrm{M}} = \overline{\boldsymbol{\sigma}} = v_0\boldsymbol{\sigma}_0 + v_{\mathrm{I}}\boldsymbol{\sigma}_{\mathrm{I}} \\ \Delta\boldsymbol{\varepsilon}^{\mathrm{r}}_{\mathrm{M}} = \overline{\Delta\boldsymbol{\varepsilon}} = v_0\Delta\boldsymbol{\varepsilon}^{\mathrm{r}}_0 + v_{\mathrm{I}}\Delta\boldsymbol{\varepsilon}^{\mathrm{r}}_{\mathrm{I}} \\ \Delta\boldsymbol{\varepsilon}^{\mathrm{r}}_{\mathrm{I}} = \mathbb{B}^{\varepsilon}\left(\mathrm{I}, \mathbb{C}^{\mathrm{S}}_0, \mathbb{C}^{\mathrm{S}}_{\mathrm{I}}\right) : \Delta\boldsymbol{\varepsilon}^{\mathrm{r}}_0 \end{cases}$$

Too expensive for BI

  - Definition of parameters

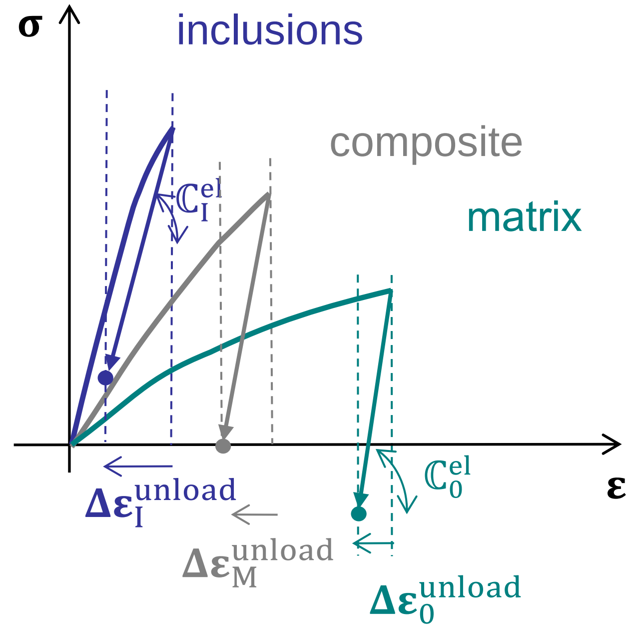

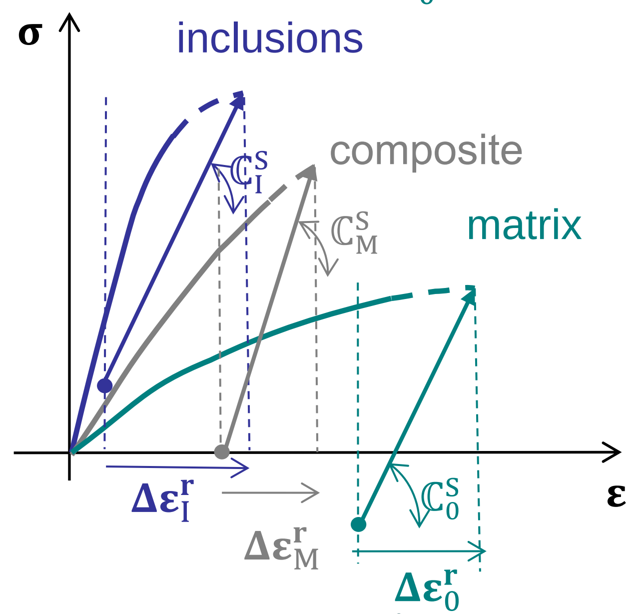

Bayesian identification of stochastic MFH model parameters

- Speed up the evaluation of the likelihood
  - Likelihood
    - $\pi(\hat{\sigma}_{\mathrm{M}}(t)|[\varepsilon_{\mathrm{M}}(t' \leq t), \boldsymbol{\vartheta}])$
    - With $\boldsymbol{\vartheta} = [E_0, \sigma_{Y_0}, h, m_1, m_2, a_r]$
    - 2-Step MFH model

$$\sigma_{\mathrm{MFH}}(t) = \sigma_{\mathrm{MFH}}\big(\mathrm{I}(\psi(\boldsymbol{p}), a_r), E_0\ , \mathbb{C}_{\mathrm{I}}\ , \varepsilon_{\mathrm{M}}(t' \leq t); \theta\big)$$

Too expensive for BI

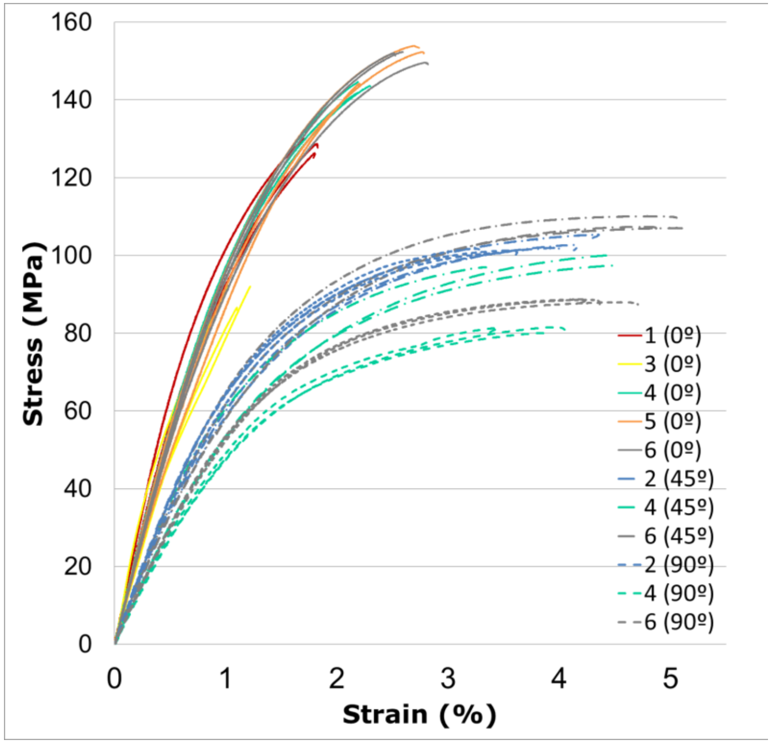

  - Use of a surrogate
    - $\sigma_{\mathrm{NNW}}(t) = \sigma_{\mathrm{NNW}}\big(\boldsymbol{\varepsilon}_{\mathbf{M}}(t), \boldsymbol{\vartheta}, \mathbb{C}_{\mathrm{I}}\ ; \theta\big)$
    - Constructed using artificial Neural Network
    - Trained fusing the 2-Step MFH model

$$\sigma_{\mathrm{MFH}}(t) = \sigma_{\mathrm{MFH}}\big(\mathrm{I}(\psi(\boldsymbol{p}), a_r), E_0\ , \mathbb{C}_{\mathrm{I}}\ , \varepsilon_{\mathrm{M}}(t' \leq t); \theta\big)$$

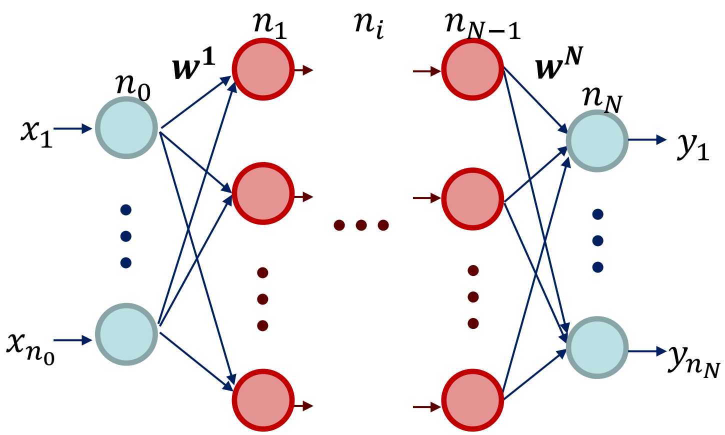

- Assume a noise in the measurements & use surrogate model
  - Measurements at strain i in direction θ_j:

$$\Sigma_c^{(i,j,k)} = \sigma_{\mathrm{NNW}}^{(i,j)}\left(\boldsymbol{\varepsilon}_{\mathbf{M}}^{(\boldsymbol{i},\boldsymbol{j})}, \boldsymbol{\vartheta}, \mathbb{C}_{\mathrm{I}}\ ; \theta_j\right) + \mathrm{noise}^{(i,j)}$$

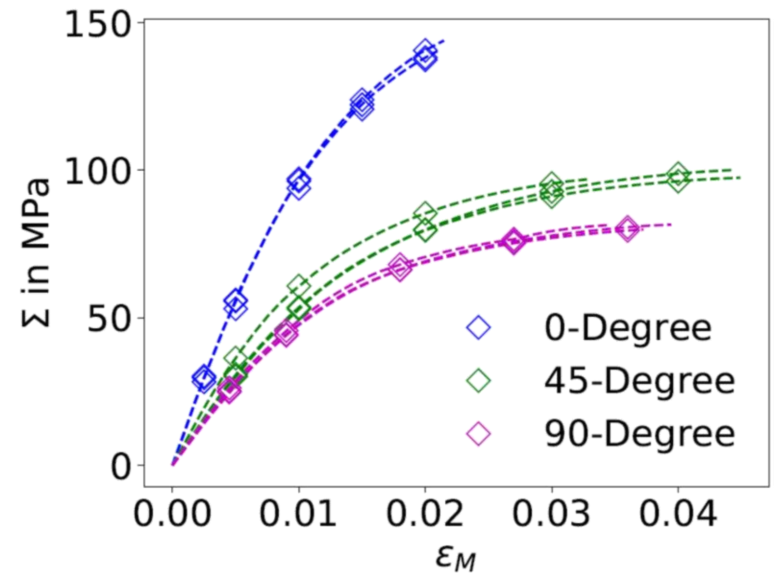

$$\pi\left(\Sigma_c^{(i,j,k)} \middle| \left[\boldsymbol{\varepsilon}_{\mathbf{M}}^{(\boldsymbol{i},\boldsymbol{j})}, \boldsymbol{\vartheta}\right]\right) = \pi_{\mathrm{noise}}^{(i,j)}\left(\Sigma_c^{(i,j,k)} - \sigma_{\mathrm{NNW}}^{(i,j)}\left(\boldsymbol{\varepsilon}_{\mathbf{M}}^{(\boldsymbol{i},\boldsymbol{j})}, \boldsymbol{\vartheta}, \mathbb{C}_{\mathrm{I}}\ ; \theta_j\right)\right)$$

- $j = 1..n_{\mathrm{dir}}$, with
  n_{dir} the number of directions θ_j tested
- $i = 1..n_{\varepsilon}^{(j)}$, with
  n_{ε} the number of stress-strain points
- $k = 1..n_{\mathrm{test}}^{(i,j)}$, with
  $n_{\mathrm{test}}^{(i,j)}$ the number of samples tested at point i along direction θ_j

  - Noise function from $n_{\mathrm{test},i,j}$ measurements at strain i in direction θ_j:

$$\pi_{\mathrm{noise}^{(i,j)}}(y) = \frac{1}{\sqrt{2\pi}\,\sigma_{\Sigma_c^{(i,j)}}} \exp\left(-\frac{y^2}{2\sigma^2_{\Sigma_c^{(i,j)}}}\right)$$

  - Bayes' theory:

$$\pi_{\mathrm{post}}\left(\boldsymbol{\vartheta} \middle| \hat{\boldsymbol{\varepsilon}}_{\mathbf{M}}, \hat{\boldsymbol{\Sigma}}_{\mathrm{c}}\right) \propto \pi_{\mathrm{prior}}(\boldsymbol{\vartheta}) \prod_{j=1}^{n_{\mathrm{dir}}} \prod_{i=1}^{n_{\varepsilon}^{(j)}} \prod_{k=1}^{n_{\mathrm{test}}^{(i,j)}} \pi_{\mathrm{noise}}^{(i,j)}\left(\Sigma_c^{(i,j,k)} - \sigma_{\mathrm{NNW}}^{(i,j)}\left(\boldsymbol{\varepsilon}_{\mathbf{M}}^{(\boldsymbol{i},\boldsymbol{j})}, \boldsymbol{\vartheta}, \mathbb{C}_{\mathrm{I}}\ ; \theta_j\right)\right)$$

Bayesian identification of stochastic MFH model parameters

- Results

$$\pi_{\text{post}}\left(\boldsymbol{\vartheta}|\hat{\boldsymbol{\varepsilon}}_{\mathbf{M}}, \hat{\boldsymbol{\Sigma}}_{\text{c}}\right) \propto \pi_{\text{prior}}(\boldsymbol{\vartheta}) \prod_{j=1}^{n_{\text{dir}}} \prod_{i=1}^{n_{\varepsilon}^{(j)}} \prod_{k=1}^{n_{\text{test}}^{(i,j)}} \pi_{\text{noise}}^{(i,j)}\left(\Sigma_c^{(i,j,k)} - \sigma_{\text{NNW}}^{(i,j)}\left(\boldsymbol{\varepsilon}_{\mathbf{M}}^{(i,j)}, \boldsymbol{\vartheta}, \mathbb{C}_{\text{I}}\ ; \theta_j\right)\right)$$

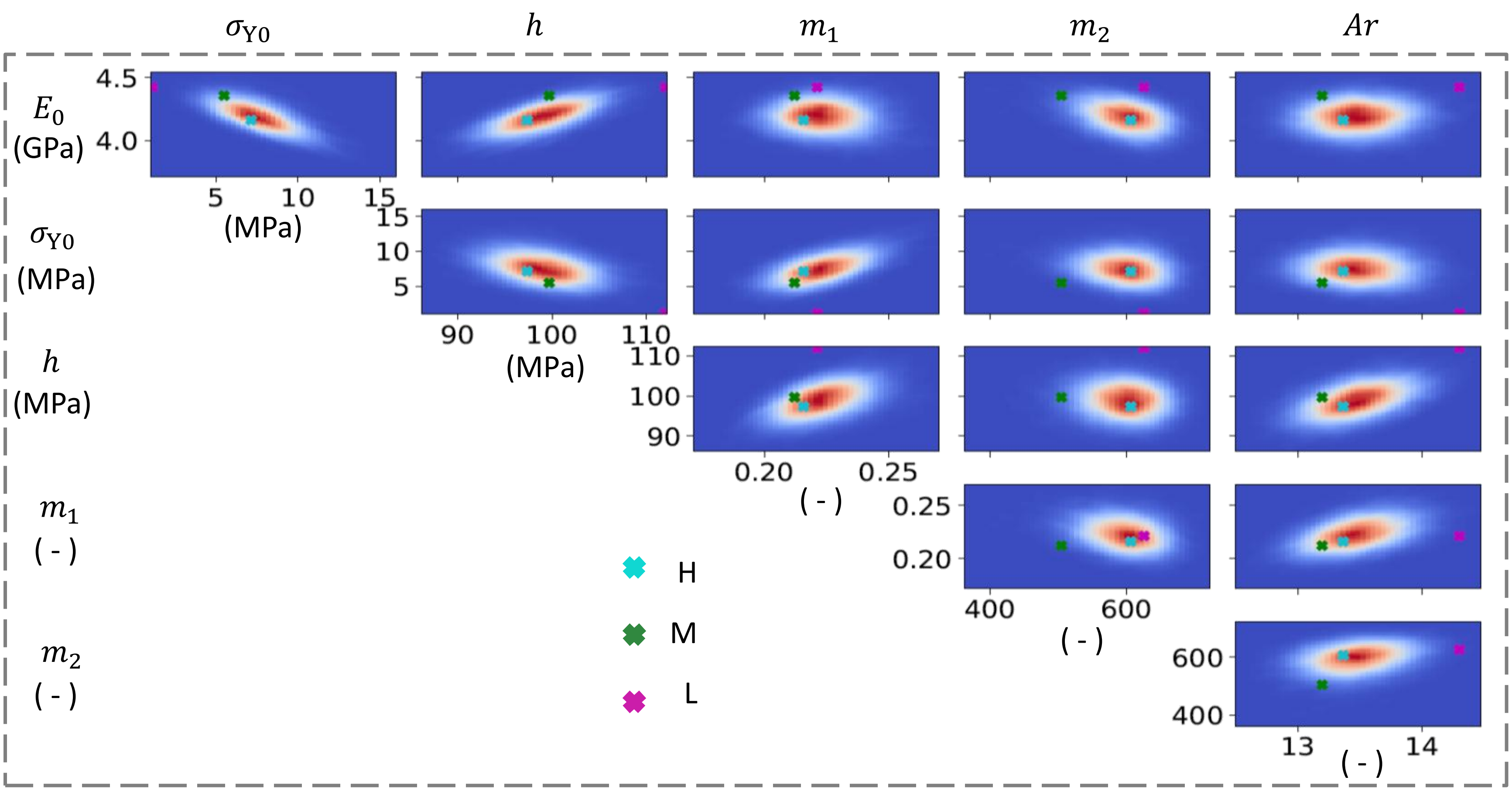

Bayesian identification of stochastic MFH model parameters

- Verification

$$\pi_{\text{post}}\left(\boldsymbol{\vartheta}|\hat{\boldsymbol{\varepsilon}}_{\mathbf{M}}, \hat{\boldsymbol{\Sigma}}_{\mathrm{c}}\right) \propto \pi_{\text{prior}}(\boldsymbol{\vartheta}) \prod_{j=1}^{n_{\text{dir}}} \prod_{i=1}^{n_{\varepsilon}^{(j)}} \prod_{k=1}^{n_{\text{test}}^{(i,j)}} \pi_{\text{noise}}^{(i,j)}\left(\Sigma_c^{(i,j,k)} - \sigma_{\text{NNW}}^{(i,j)}\left(\boldsymbol{\varepsilon}_{\mathbf{M}}^{(\boldsymbol{i},\boldsymbol{j})}, \boldsymbol{\vartheta}, \mathbb{C}_{\mathrm{I}}\ ; \theta_j\right)\right)$$

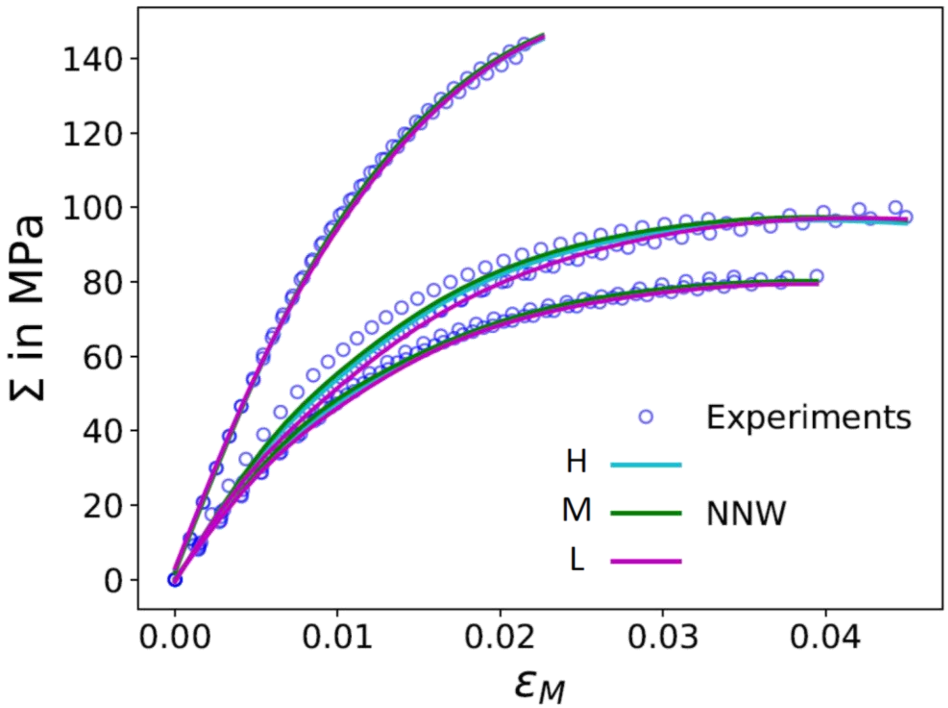

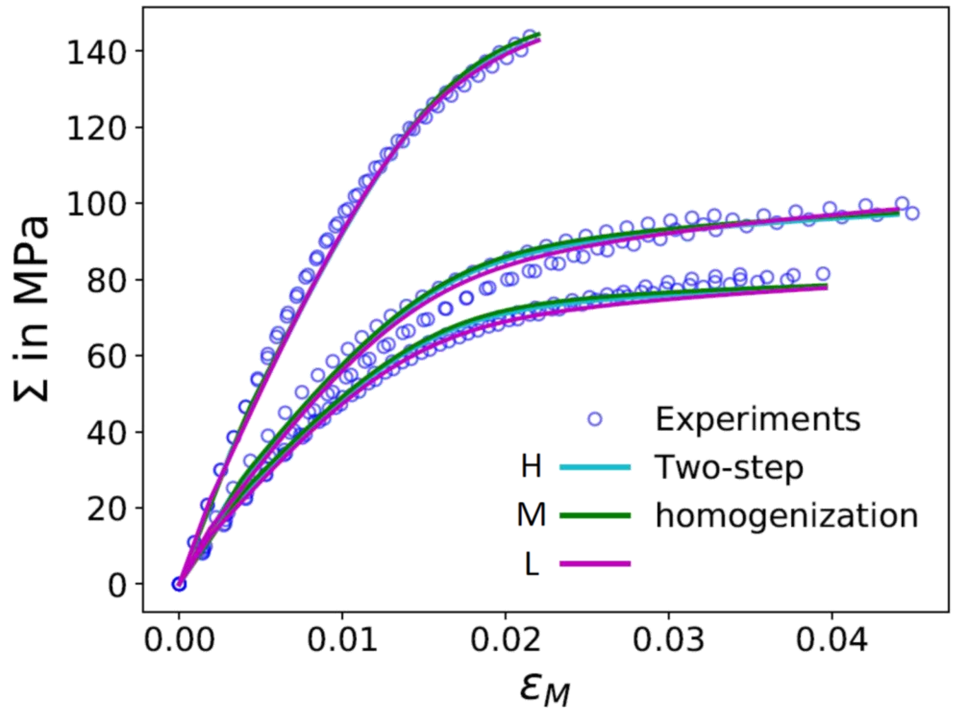

Bayesian identification of stochastic MFH model parameters

- STOMMMAC M.ERA-NET project (MFH for elasto-visco-plastic composites)
  - e-Xstream, ULiège (Belgium)
  - BATZ (Spain)
  - JKU, AC (Austria)
  - U Luxembourg (Luxemburg)

- Publications (doi)
  - 10.1016/j.cma.2019.112693 data on 10.5281/zenodo.3740410
  - 10.1016/j.compstruct.2019.03.066

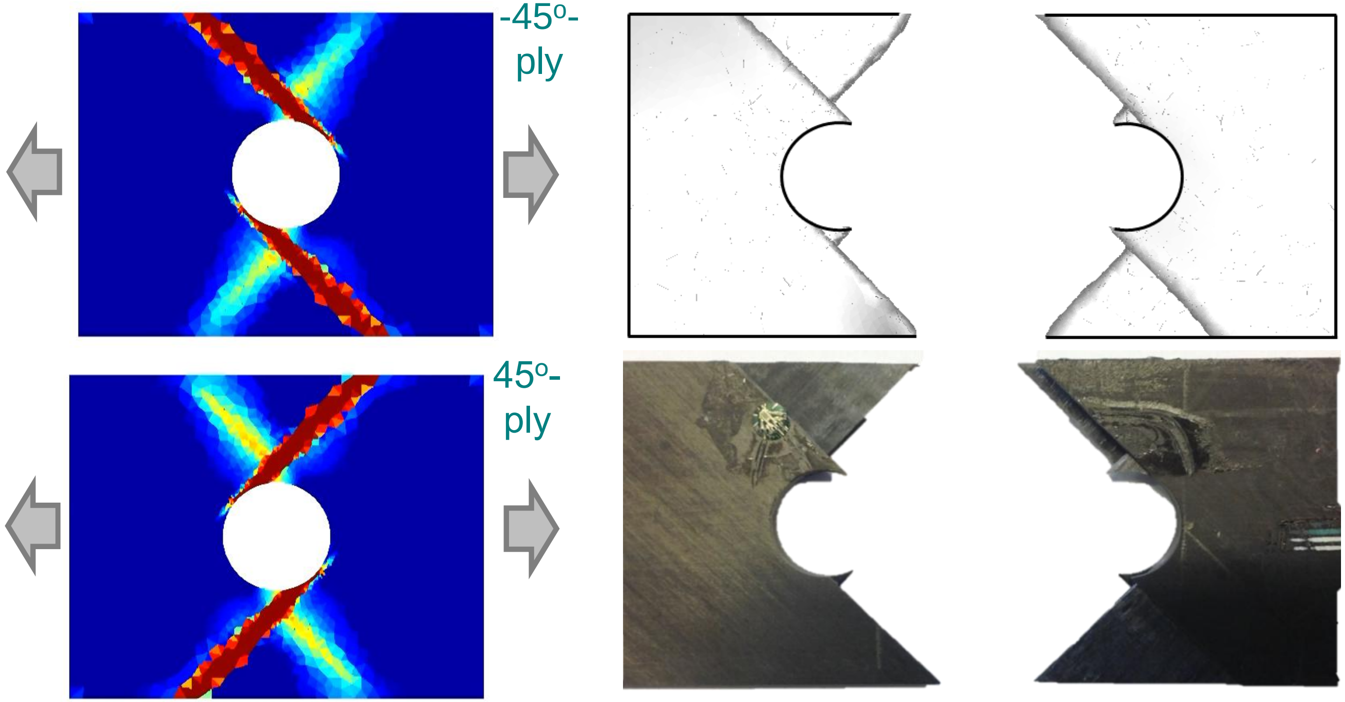

Non-Local Damage & Phase-Field Enhanced Mean-Field-Homogenization

SIMUCOMP The research has been funded by the Walloon Region under the agreement no 1017232 (CT-EUC 2010-10-12) in the context of the ERA-NET +, Matera + framework.

Non-Local Damage Mean-Field-Homogenization

- Multi-scale modeling
  - 2 problems are solved concurrently
    - The macro-scale problem
    - The meso-scale problem (on a meso-scale Volume Element)

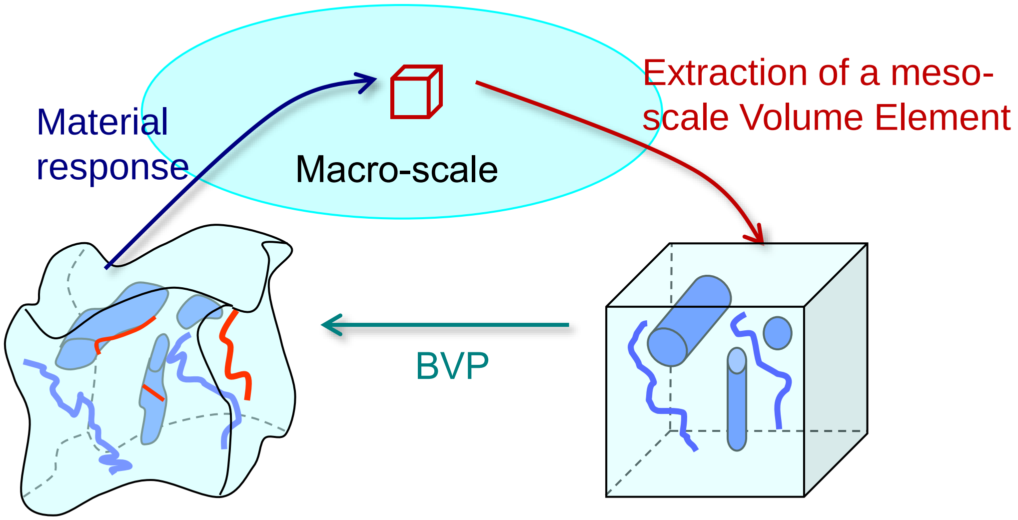

- Length-scales separation

$$L_{macro} >> L_{VE} >> L_{micro}$$

For accuracy: Size of the meso-scale volume element smaller than the characteristic length of the macro-scale loading

To be statistically representative: Size of the meso-scale volume element larger than the characteristic length of the micro-structure

- Materials with strain softening
  - Incremental forms
    - Strain increments in the same direction

$$\Delta\boldsymbol{\varepsilon}_{\mathrm{I}} = \mathbf{B}^{\varepsilon}\left(\mathrm{I}, \bar{\mathbf{C}}_{0}^{\mathrm{alg}}, \bar{\mathbf{C}}_{\mathrm{I}}^{\mathrm{alg}}\right) : \Delta\boldsymbol{\varepsilon}_{0}$$

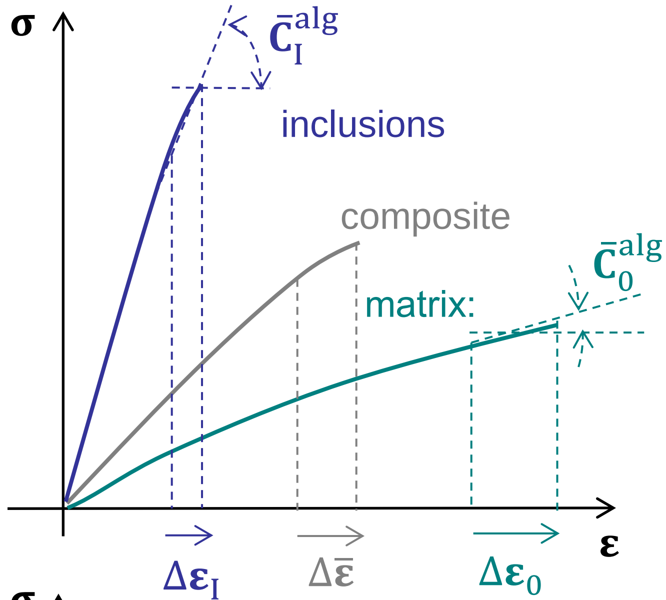

  - Because of the damaging process, the fiber phase is elastically unloaded during matrix softening

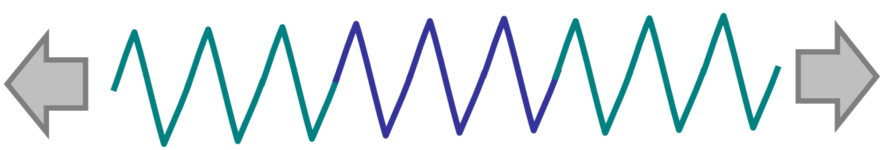

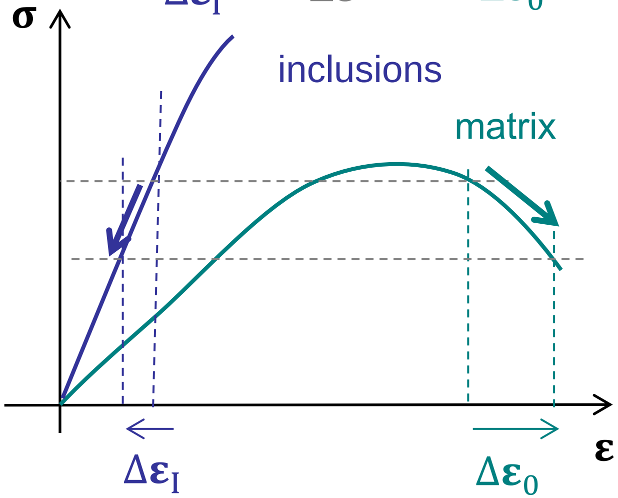

- Solution: new incremental-secant method
  - We need to define the LCC from another stress state

- Based on the incremental-secant approach
  - Perform a virtual elastic unloading from previous solution
    - Composite material unloaded to reach the stress-free state
    - Residual stress in components
  - Apply MFH from unloaded state
    - New strain increments (>0)

$$\Delta\boldsymbol{\varepsilon}^{\mathrm{r}}_{\mathrm{I}/0} = \Delta\boldsymbol{\varepsilon}_{\mathrm{I}/0} + \Delta\boldsymbol{\varepsilon}^{\mathrm{unload}}_{\mathrm{I}/0}$$

    - Use of secant operators

$$\Delta\boldsymbol{\varepsilon}^{\mathrm{r}}_{\mathrm{I}} = \mathbf{B}^{\varepsilon}\left(\mathrm{I}, (1-D)\bar{\mathbf{C}}^{\mathrm{Sr}}_{0}, \bar{\mathbf{C}}^{\mathrm{S0}}_{\mathrm{I}}\right) : \Delta\boldsymbol{\varepsilon}^{\mathrm{r}}_{0}$$

    - Possibility of unloading

$$\begin{cases} \Delta\boldsymbol{\varepsilon}^{\mathrm{r}}_{\mathrm{I}} > \mathbf{0} \\ \Delta\boldsymbol{\varepsilon}_{\mathrm{I}} \ < \mathbf{0} \end{cases}$$

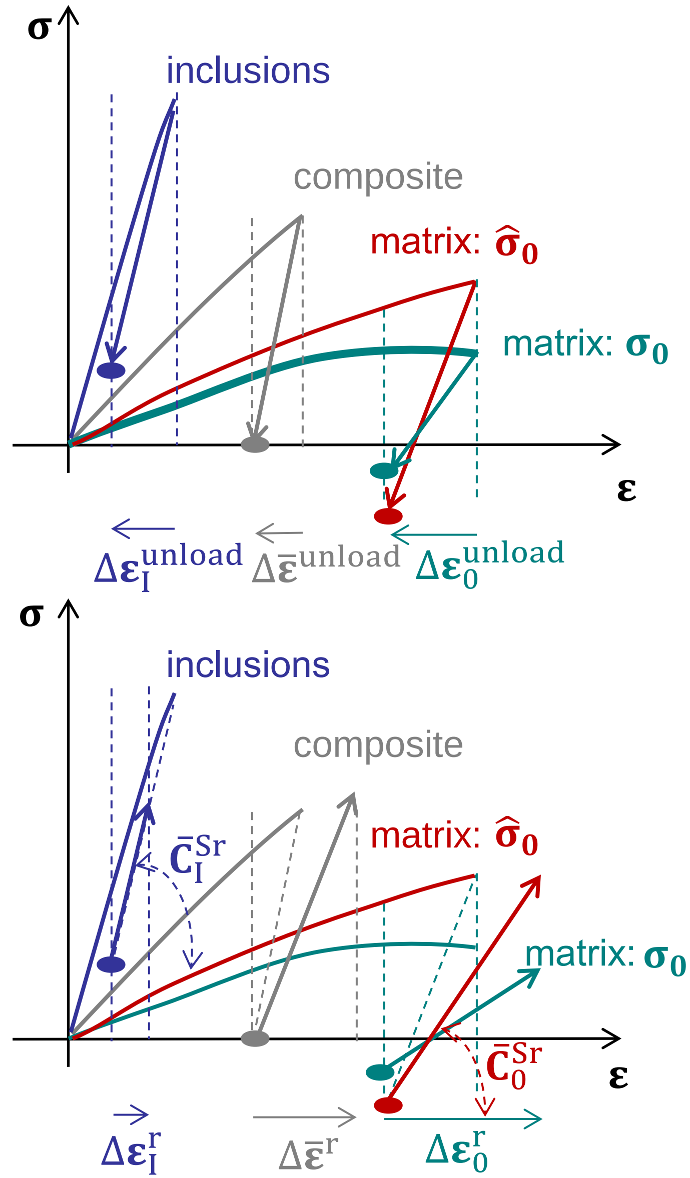

- New results for damage
  - Fictitious composite
    - 50%-UD fibres
  - Elasto-plastic matrix with damage

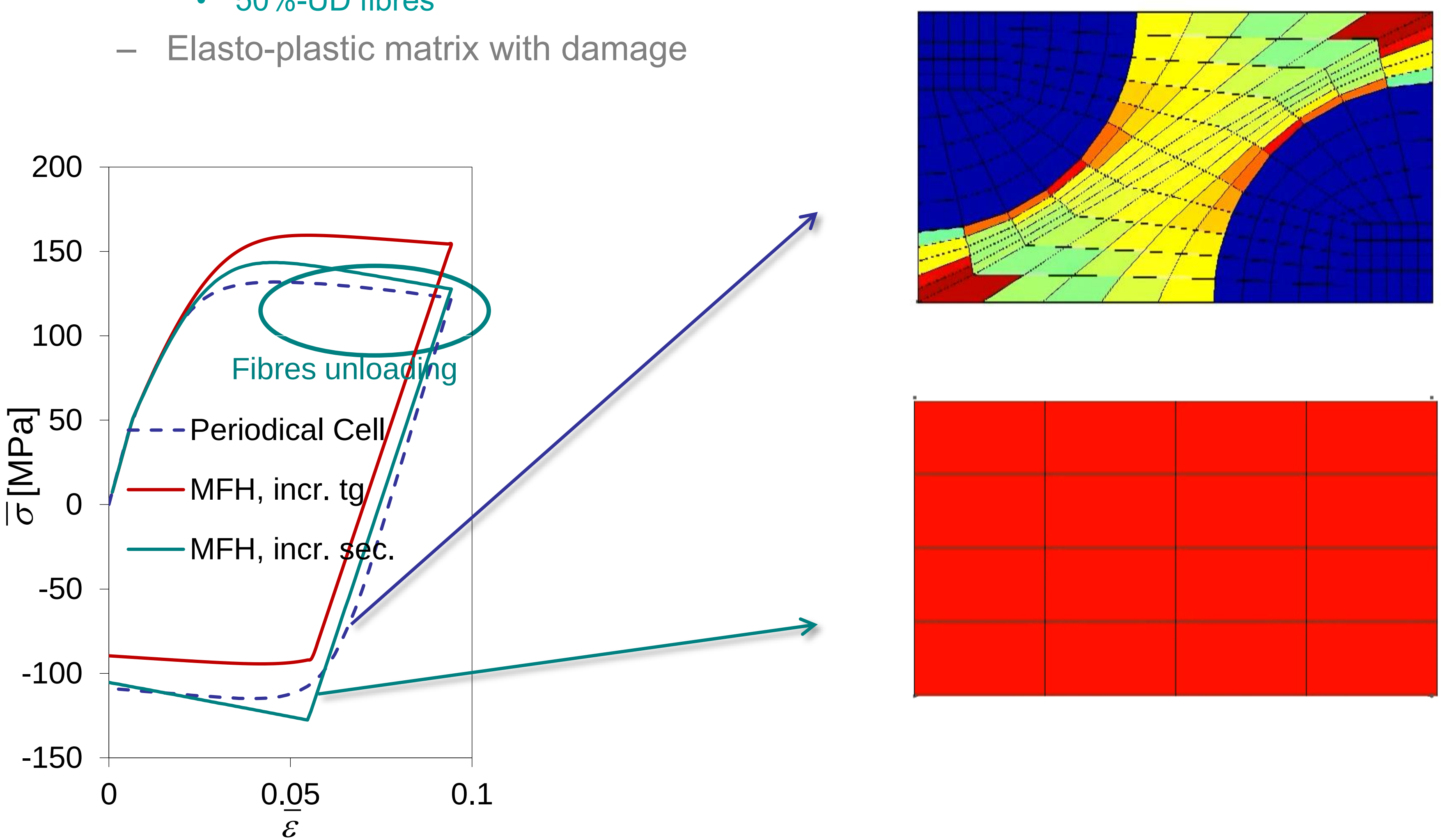

Non-Local Damage Mean-Field-Homogenization

- Material models
  - Elasto-plastic material
    - Stress tensor $\boldsymbol{\sigma} = \mathbf{C}^{\mathrm{el}} : (\boldsymbol{\varepsilon} - \boldsymbol{\varepsilon}^{\mathrm{pl}})$
    - Yield surface $f(\boldsymbol{\sigma}, p) = \boldsymbol{\sigma}^{\mathrm{eq}} - \sigma^{Y} - R(p) \leq 0$
    - Plastic flow $\Delta\boldsymbol{\varepsilon}^{\mathbf{pl}} = \Delta p \mathbf{N}$ & $\mathbf{N} = \dfrac{\partial f}{\partial \boldsymbol{\sigma}}$
  - Local damage model
    - Apparent-effective stress tensors $\boldsymbol{\sigma} = (1 - D)\hat{\boldsymbol{\sigma}}$
    - Plastic flow in the effective stress space
    - Damage evolution $\Delta D = F_D(\boldsymbol{\varepsilon}, \Delta p)$
  - Non-Local damage model [Peerlings et al., 1996]
    - Damage evolution $\Delta D = F_D(\boldsymbol{\varepsilon}, \Delta \tilde{p})$
    - Anisotropic governing equation $\tilde{p} - \nabla \cdot \left(\mathbf{c}_{\mathrm{g}} \cdot \nabla \tilde{p}\right) = p$

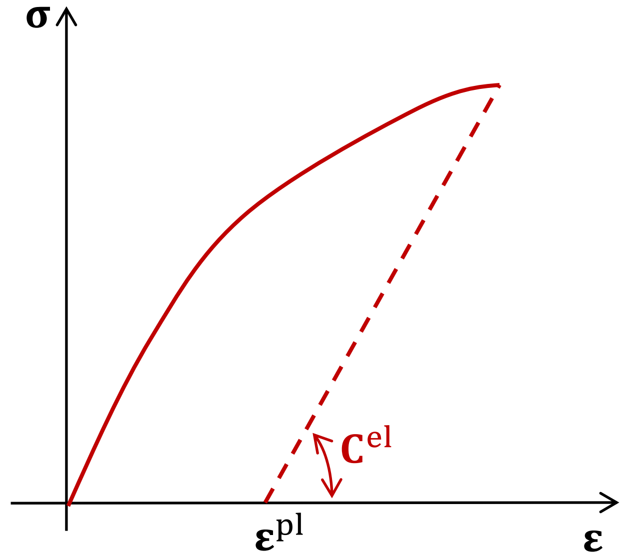

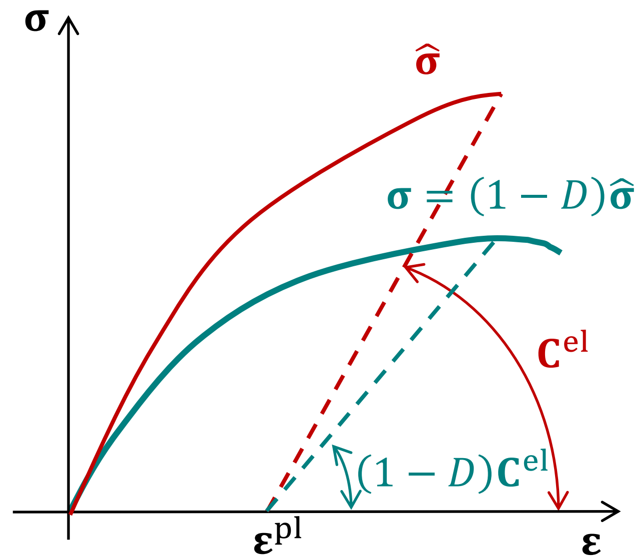

- Laminate studies
  - Bulk material law
    - Non-local damage-enhanced MFH
    - Intra-laminar failure
    - Account for anisotropy
  - Interface
    - DG/Cohesive zone model
    - Inter-laminar failure

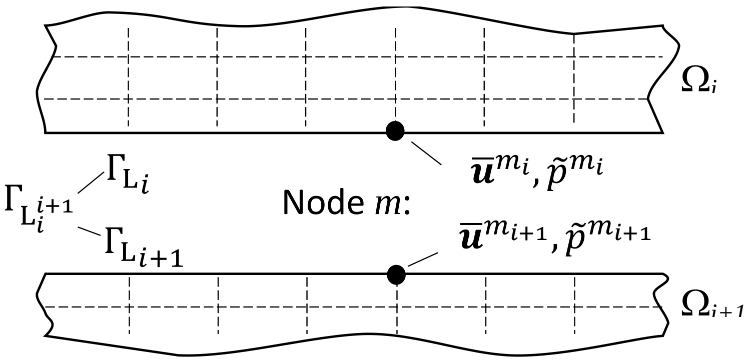

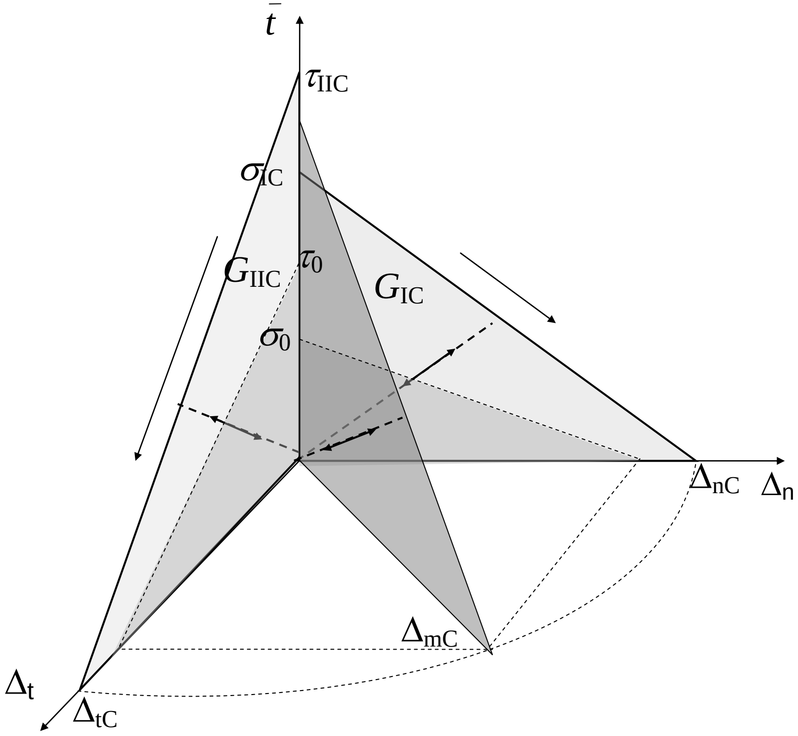

Beginning

Non-Local Damage Mean-Field-Homogenization

- $[45^o{}_4 / -45^o{}_4]_S$- open hole laminate (epoxy- with 60% UD CF)

Intra-laminar failure along fiber directions

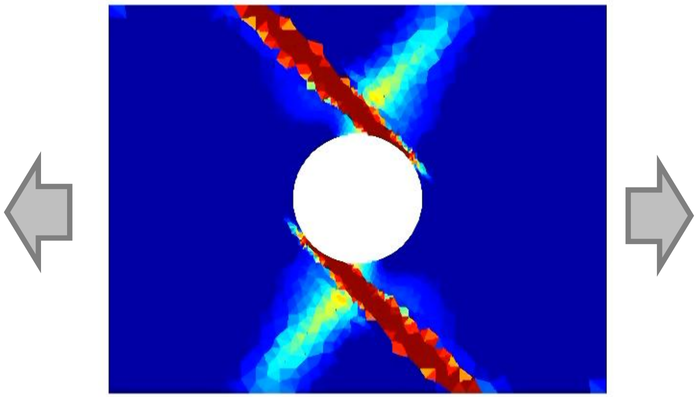

-45º-ply

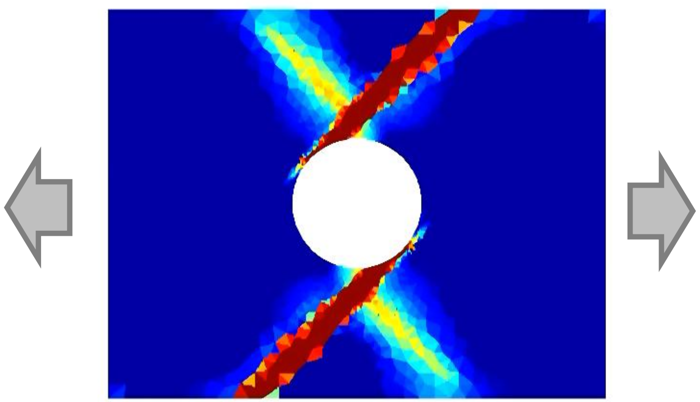

45º-ply

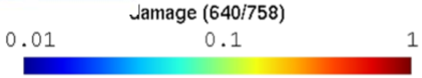

Inter-laminar failure matches experimental results

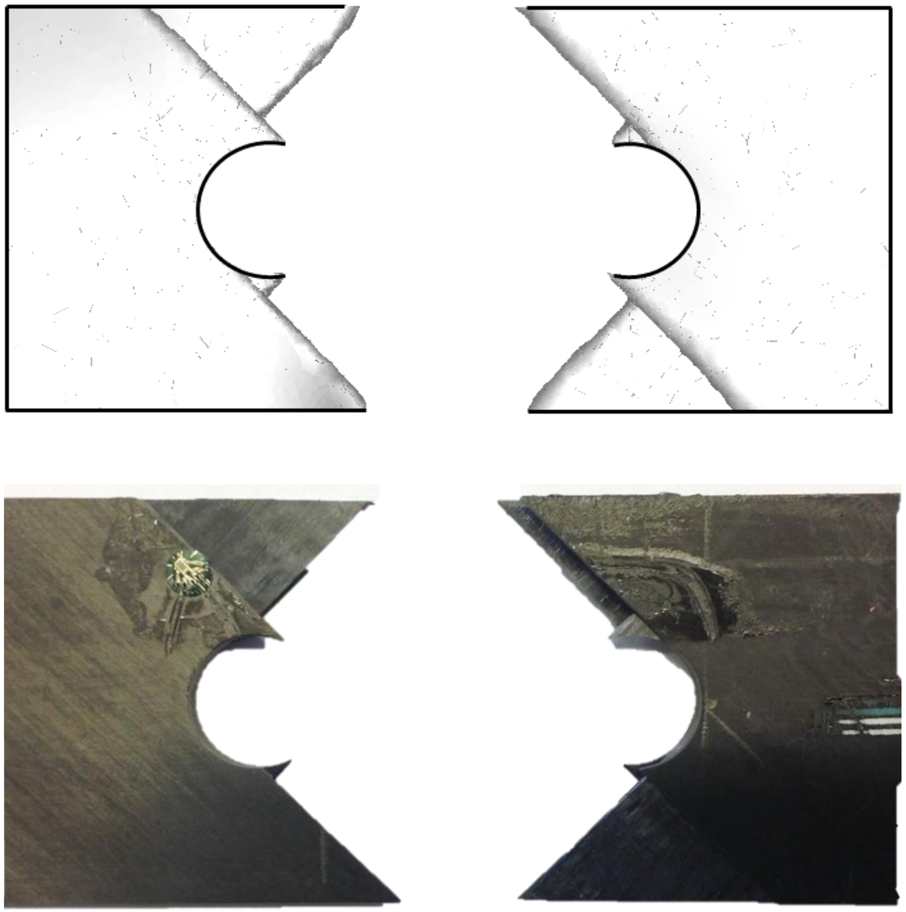

Non-Local Damage Mean-Field-Homogenization

- [90° / 45° / -45° / 90° / 0°]$_S$- open hole laminate
  - Intra-laminar failure along fiber directions (experiments: IMDEA Materials)

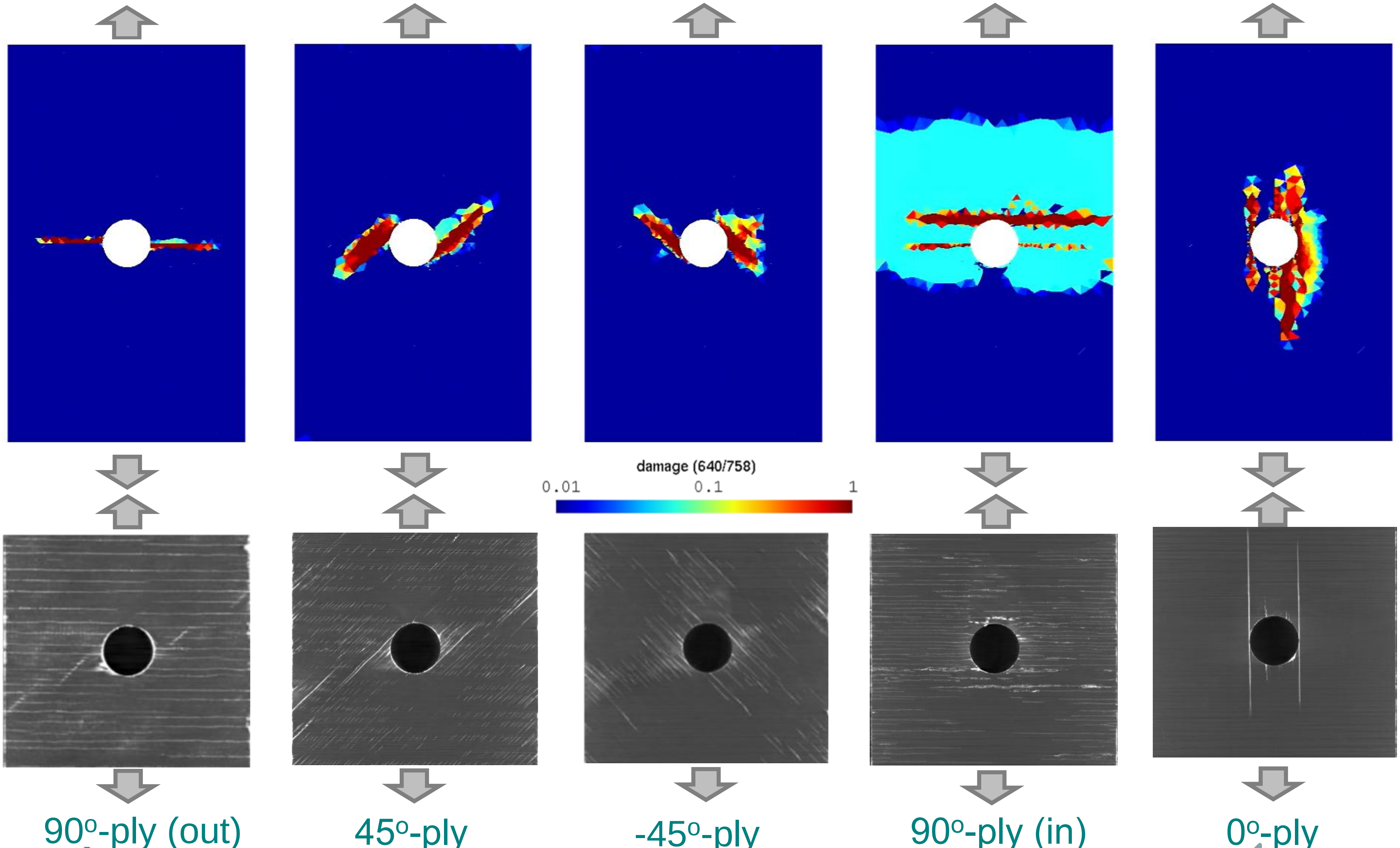

Non-Local Damage Mean-Field-Homogenization

- $[90^o / 45^o / -45^o / 90^o / 0^o]_S$- open hole laminate
  - Inter-laminar failure compared to experimental results (experiments: IMDEA Materials)

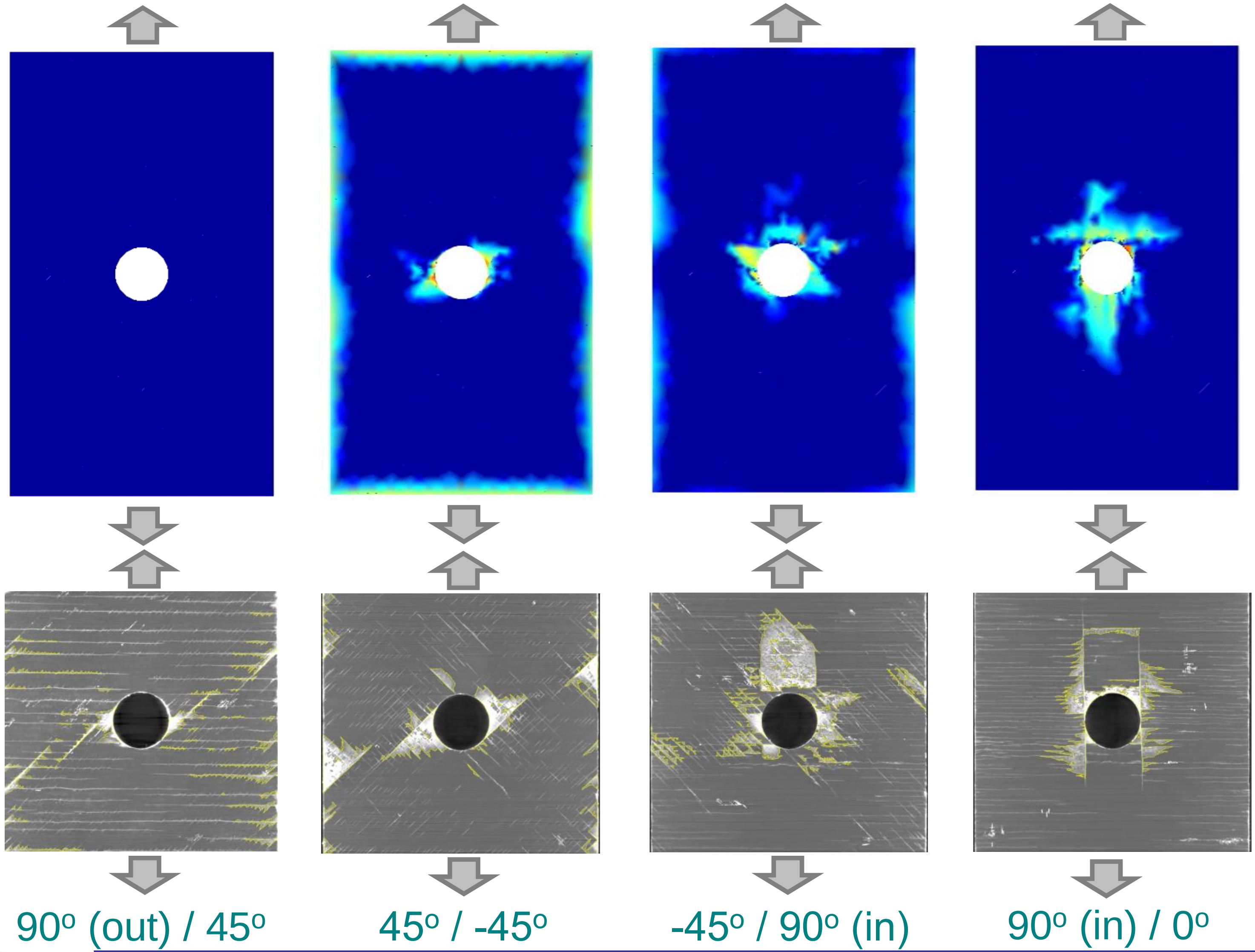

Non-Local Damage Mean-Field-Homogenization

- SIMUCOMP ERA-NET project
  - e-Xstream, CENAERO, ULiège (Belgium), IMDEA Materials (Spain), CRP Henri-Tudor (Luxemburg)
- Publications (doi)
  - 10.1016/j.compstruct.2015.02.070
  - 10.1016/j.ijsolstr.2013.07.022
  - 10.1016/j.ijplas.2013.06.006
  - 10.1016/j.cma.2012.04.011
  - 10.1007/978-1-4614-4553-1_13

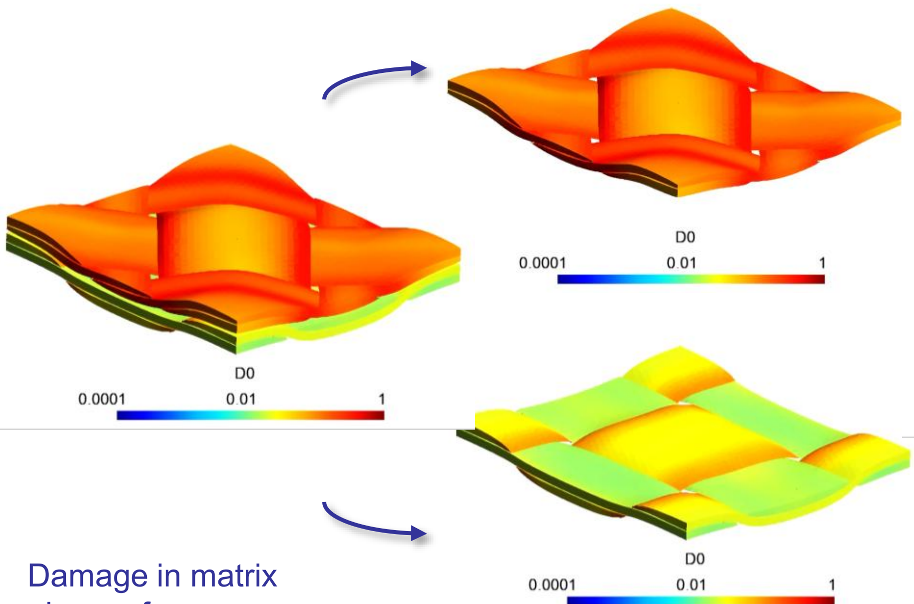

Damage in matrix phase of yarns

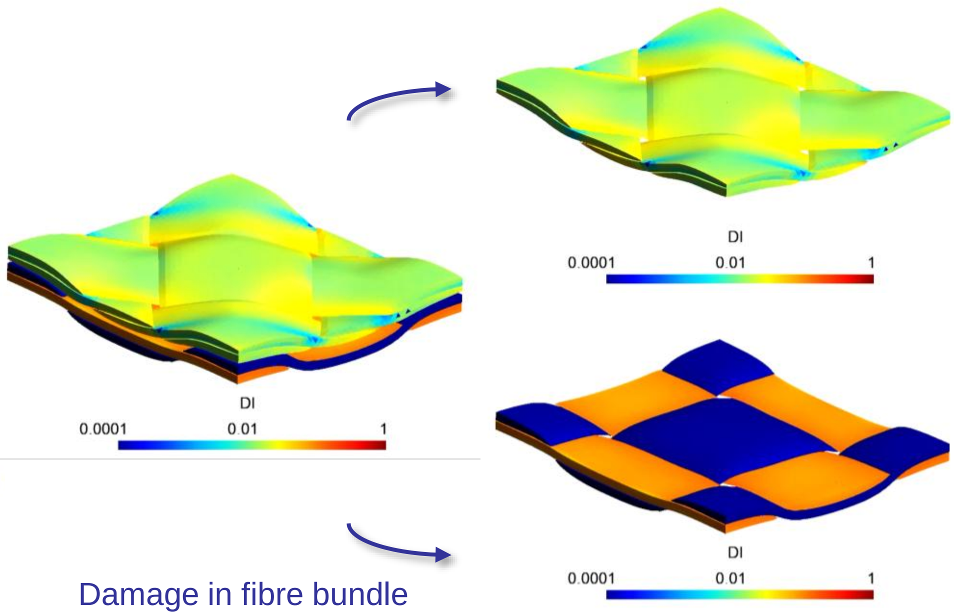

Damage in fibre bundle phase of yarns

Non-Local Damage & Phase-Field Enhanced Mean-Field-Homogenization

The research has been funded by the Walloon Region under the agreement no.7911-VISCOS in the context of the 21st SKYWIN call.

- Probabilistic damage model of fibre bundle
  - Failure probability for one fibre of length L at stress σ

$$P(\sigma, L) = 1.0 - \exp\left\{-\left(\frac{L}{L_0}\right)^{\alpha}\left(\frac{\sigma}{\sigma_0}\right)^{m}\right\}$$

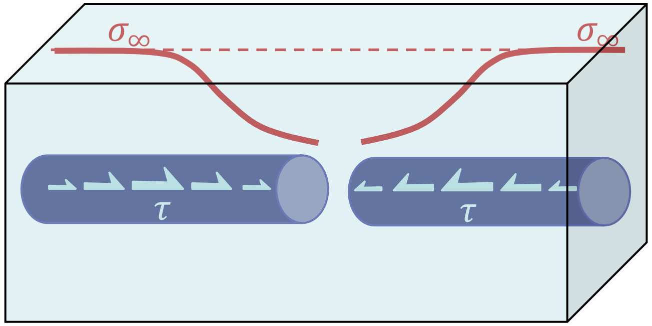

  - Damage of bundle: failure of k fibres of a bundle of N fibres

$$\left.\begin{aligned} D &= \frac{k}{N} \\ \hat{\sigma} &= \frac{\sigma}{(1-D)} \end{aligned}\right\} \Rightarrow \left\{\begin{aligned} &P(D|\hat{\sigma}, L) \approx N\left(p, \frac{p(1-p)}{N}\right) \\ &p = P(\hat{\sigma}\,; L) \end{aligned}\right.$$

  - Length effect

$$\left.\begin{aligned} \sigma(x) &= \sigma_\infty\left(1 - \exp\left(-\frac{|x|}{cl}\right)\right)^n \\ \tau &= \frac{r}{2}\frac{\mathrm{d}\sigma}{\mathrm{d}x} \end{aligned}\right\} \Rightarrow \left\{\begin{aligned} &L \text{ such that} \\ &\sigma(L) = 0.99\,\sigma_\infty \end{aligned}\right.$$

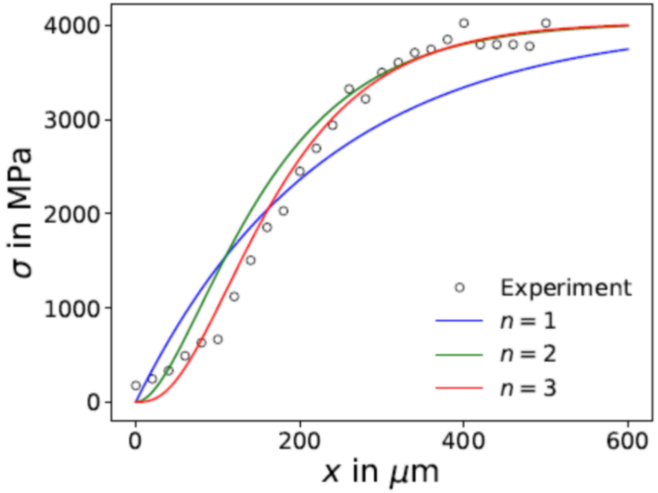

- Phase-field damage model of fibre bundle
  - Stress σ build up from failure

$$\sigma(x) = \sigma_\infty \left(1 - \exp\left(-\frac{|x|}{cl}\right)\right)^n$$

  - Definition of an auxiliary damage variable

$$d_\mathrm{I}(x) = \exp\left(-\frac{|x|}{cl}\right) \Rightarrow D_\mathrm{I}(x) = 1.0 - [1 - d_\mathrm{I}(x)]^n$$

  - Auxiliary governing equation in terms of fracture energy G_{IC}

$$d_\mathrm{I} - cl^2\nabla^2 d_I - \frac{cl}{G_{IC}} = -\frac{cl}{G_{Ic}}\frac{\partial \psi_\mathrm{I}^+}{\partial d_\mathrm{I}}$$

  - Material law

$$\psi(\boldsymbol{\varepsilon}, D_\mathrm{I}) = \frac{1}{2}\varepsilon : \mathbb{C}_\mathrm{I}^{\mathrm{el\ D}}(D_\mathrm{I}) \Rightarrow \boldsymbol{\sigma} = \frac{\partial \psi}{\partial \boldsymbol{\varepsilon}}$$

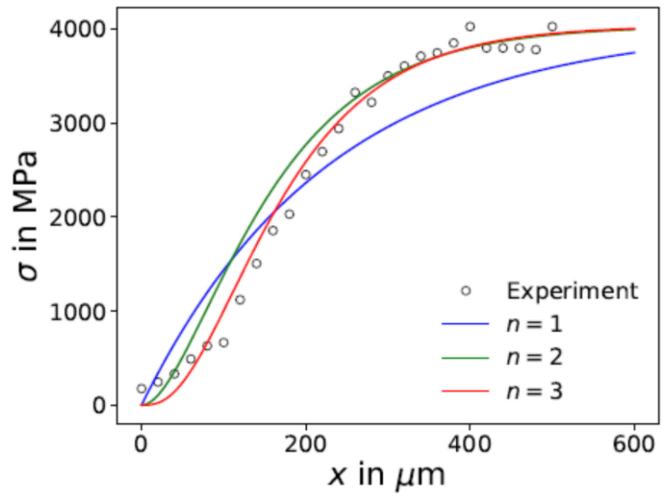

- Damage transverse isotropic model
  - Material law

$$\psi(\boldsymbol{\varepsilon}, D_{\mathrm{I}}) = \frac{1}{2}\varepsilon : \mathbb{C}_{\mathrm{I}}^{\mathrm{el\,D}}(D_{\mathrm{I}}) \Rightarrow \boldsymbol{\sigma} = \frac{\partial \psi}{\partial \boldsymbol{\varepsilon}}$$

$$\begin{cases} \nu_{\mathrm{I}}^{\mathrm{LT\,D}} = (1 - D_{\mathrm{I}})\nu_{\mathrm{I}}^{\mathrm{LT}} \\ E_{\mathrm{I}}^{\mathrm{L\,D}} = (1 - D_{\mathrm{I}})E_{\mathrm{I}}^{\mathrm{L}} \end{cases}$$

$$\Rightarrow \mathbb{C}_{\mathrm{I}}^{\mathrm{LCC}} = \mathbb{C}_{\mathrm{I}}^{\mathrm{el\,D}} = \begin{bmatrix} \begin{matrix} \frac{E_{\mathrm{I}}^{\mathrm{T}}\left(1-\nu_{\mathrm{I}}^{\mathrm{LT\,D}}\nu_{\mathrm{I}}^{\mathrm{TL}}\right)}{\Delta^{\mathrm{D}}} & \frac{E_{\mathrm{I}}^{\mathrm{T}}\left(\nu_{\mathrm{I}}^{\mathrm{TT}}+\nu_{\mathrm{I}}^{\mathrm{LT\,D}}\nu_{\mathrm{I}}^{\mathrm{TL}}\right)}{\Delta^{\mathrm{D}}} & \frac{E_{\mathrm{I}}^{\mathrm{T}}\left(\nu_{\mathrm{I}}^{\mathrm{LT\,D}}+\nu_{\mathrm{I}}^{\mathrm{TT}}\nu_{\mathrm{I}}^{\mathrm{LT\,D}}\right)}{\Delta^{\mathrm{D}}} \\ \mathrm{Sim} & \Delta^{\mathrm{D}} & \frac{E_{\mathrm{I}}^{\mathrm{T}}\left(\nu_{\mathrm{I}}^{\mathrm{LT}\,D}+\nu_{\mathrm{I}}^{\mathrm{TT}}\nu_{\mathrm{I}}^{\mathrm{LT\,D}}\right)}{\Delta} \\ \mathrm{Sim} & \mathrm{Sim} & \frac{E_{\mathrm{I}}^{\mathrm{L\,D}}\left(1-\nu_{\mathrm{I}}^{\mathrm{TT}}\nu_{\mathrm{I}}^{\mathrm{TT}}\right)}{\Delta^{\mathrm{D}}} \end{matrix} & 0 \\ 0 & \begin{matrix} 2\mu_{\mathrm{I}}^{\mathrm{LT}} & 0 & 0 \\ 0 & 2\mu_{\mathrm{I}}^{\mathrm{LT}} & 0 \\ 0 & 0 & \frac{E_{\mathrm{I}}^{\mathrm{T}}}{1+\nu_{\mathrm{I}}^{\mathrm{TT}}} \end{matrix} \end{bmatrix}$$

Non-Local Damage & Phase-Field Mean-Field-Homogenization

- Matrix damage model for MFH
  - Lemaitre Chaboche

$$\dot{D}_{0}= \left(\frac{\psi}{S_0}\right)^{s_0}\dot{\chi}, \text{ for } (\chi - p_{C0})\dot{\chi} > 0$$

$$\psi = \frac{1}{2}\boldsymbol{\varepsilon}:\mathbb{C}_0^{\mathrm{el}}:\boldsymbol{\varepsilon}$$

  - Saturated damage

$$D_0 = D_{\max_0}\left(\frac{1}{1+\exp(-\beta_0(\chi-p_{c0}))} - \frac{1}{1+\exp(\beta_0 p_{c0})}\right)\frac{1}{1-\frac{1}{1+\exp(\beta_0 p_{c0})}},$$

$$\text{for } \dot{\chi} > 0.$$

  - Anisotropic non-local form

$$\begin{cases} \chi = \max\limits_{t}\ \tilde{p}_0(t) \\ \tilde{p}_0 - \nabla\cdot\left(\boldsymbol{c}_g\cdot\nabla\tilde{p}_0\right) = p_0 \end{cases}$$

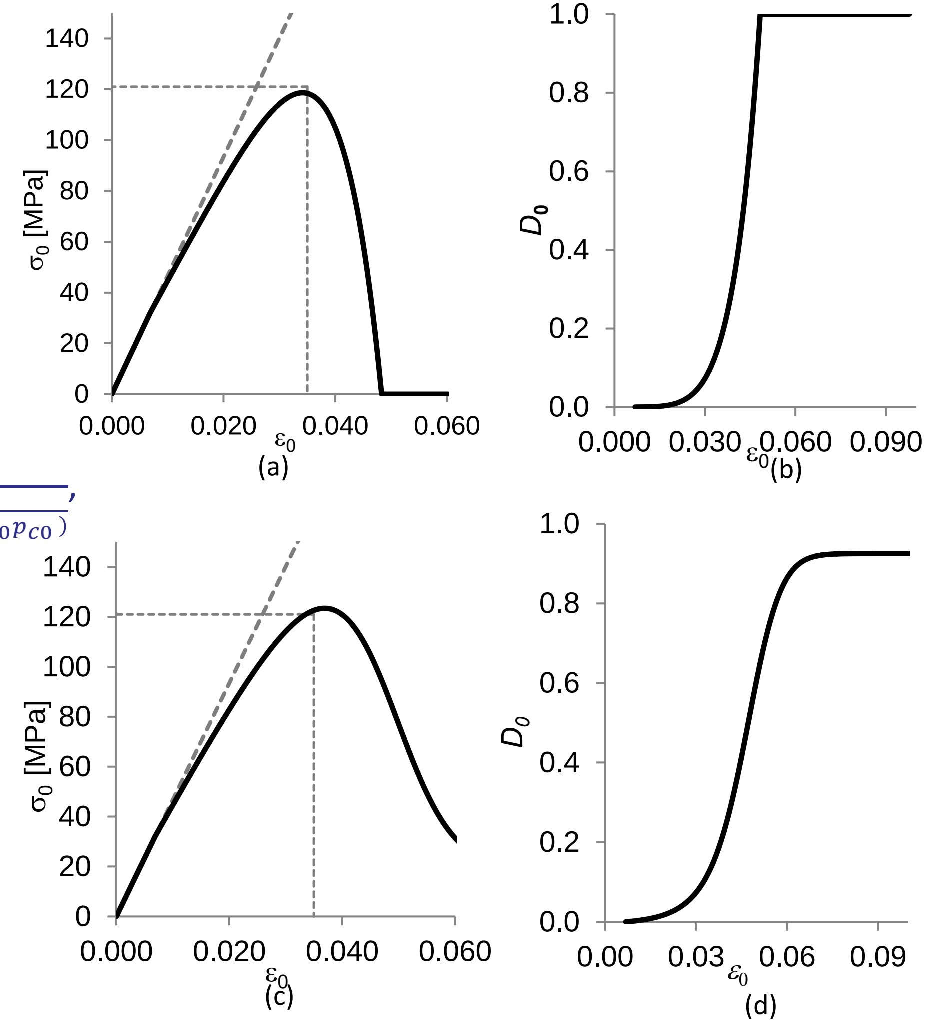

- MFH with matrix and fibre bundle damage models
  - Incremental-secant MFH
    - Unloading step

$$\Delta\boldsymbol{\sigma}_0 = -\mathbb{C}_0^{\text{el D}} : \Delta\boldsymbol{\varepsilon}_0^{\text{unload}}$$

$$\Delta\boldsymbol{\sigma}_{\text{I}} = -\mathbb{C}_{\text{I}}^{\text{el D}} : \Delta\boldsymbol{\varepsilon}_{\text{I}}^{\text{unload}}$$

$$\Delta\boldsymbol{\varepsilon}_{\text{I}}^{\text{unload}} = \mathbb{B}^{\epsilon}\left(\text{I}, \mathbb{C}_0^{\text{elD}}, \mathbb{C}_{\text{I}}^{\text{elD}}\right) : \Delta\boldsymbol{\varepsilon}_0^{\text{unload}}$$

    - Followed by reloading

$$\Delta\boldsymbol{\varepsilon}_{\text{I}}^{\text{r}} = \mathbf{B}^{\varepsilon}\left(\text{I}, \mathbb{C}_0^{\text{SD}}, \mathbb{C}_{\text{I}}^{\text{Sr}}\right) : \Delta\boldsymbol{\varepsilon}_0^{\text{r}}$$

$$\Delta\boldsymbol{\varepsilon}_{\text{I/0}}^{\text{r}} = \Delta\boldsymbol{\varepsilon}_{\text{I/0}} + \Delta\boldsymbol{\varepsilon}_{\text{I/0}}^{\text{unload}}$$

$$\begin{cases} \Delta\boldsymbol{\varepsilon}_{\text{I}}^{\text{r}} > \mathbf{0} \\ \Delta\boldsymbol{\varepsilon}_{\text{I}} < \mathbf{0} \end{cases}$$

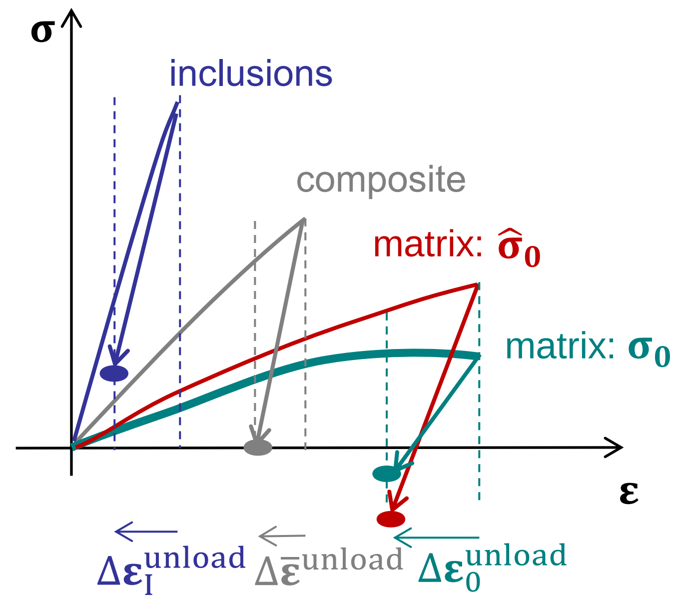

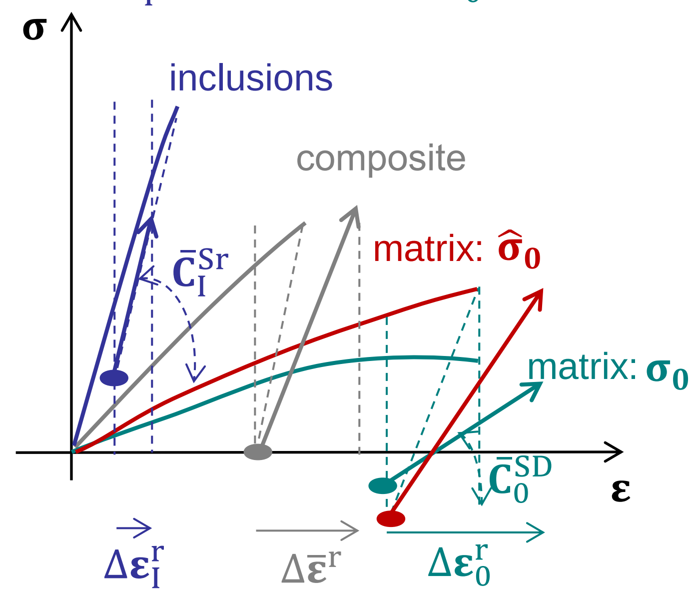

- MFH with matrix and fibre bundle damage models
  - Incremental-secant MFH
    - Damage in matrix

$$\begin{cases} \hat{\boldsymbol{\sigma}}_0 - \hat{\boldsymbol{\sigma}}_0^{\mathrm{res}} = \bar{\mathbb{C}}_0^{\mathrm{S}} : \Delta\boldsymbol{\varepsilon}_0^{\mathrm{r}} \\ \text{or } \hat{\boldsymbol{\sigma}}_0 = \bar{\mathbb{C}}_0^{\mathrm{S0}} : \Delta\boldsymbol{\varepsilon}_0^{\mathrm{r}} \\ \bar{\mathbb{C}}_0^{\mathrm{LCC}} = \bar{\mathbb{C}}_0^{\mathrm{SD}} = (1 - D_0)\bar{\mathbb{C}}_0^{\mathrm{S}} \end{cases}$$

    - Damage in Fibre bundle

$$\begin{cases} \hat{\boldsymbol{\sigma}}_{\mathrm{I}} - \hat{\boldsymbol{\sigma}}_{\mathrm{I}}^{\mathrm{res}} = \bar{\mathbb{C}}_{\mathrm{I}}^{\mathrm{S}} : \Delta\boldsymbol{\varepsilon}_{I}^{\mathrm{r}} \\ \bar{\mathbb{C}}_{\mathrm{I}}^{\mathrm{LCC}} = \bar{\mathbb{C}}_{\mathrm{I}}^{\mathrm{SD}} = \bar{\mathbb{C}}_{\mathrm{I}}^{\mathrm{el\,D}}(D_{\mathrm{I}}) \end{cases}$$

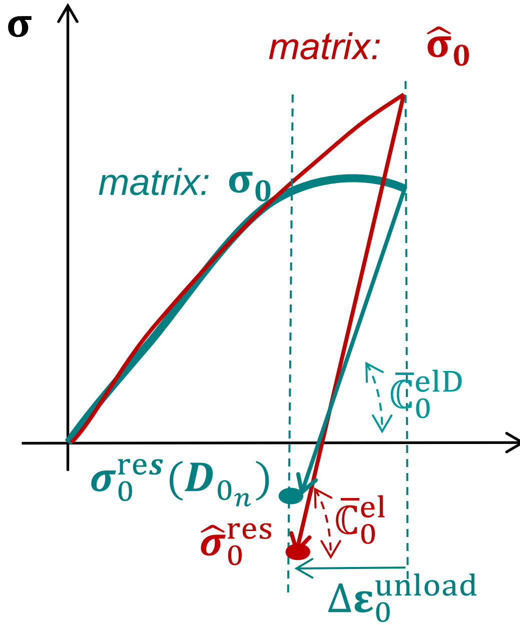

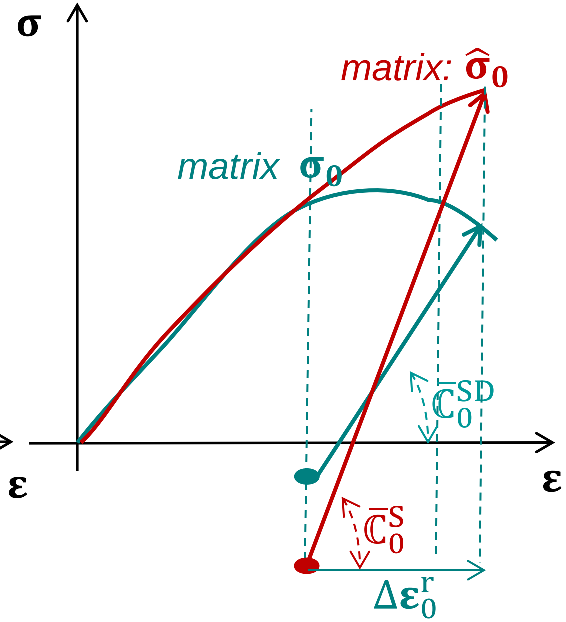

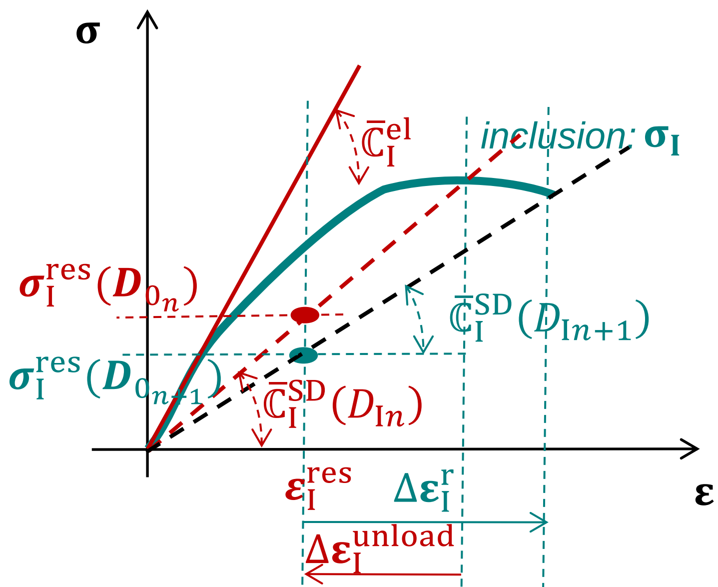

Beginning

Non-Local Damage & Phase-Field Mean-Field-Homogenization

- Test of Phase-Field formulation
  - Axial loading on composite

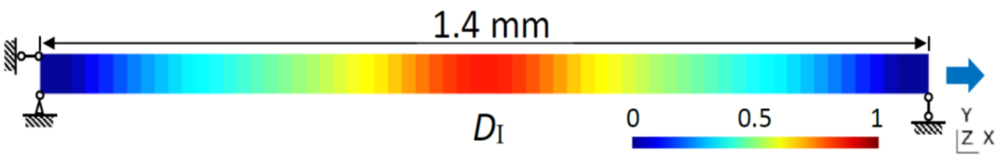

(a) Damage in fibres, configuration 1

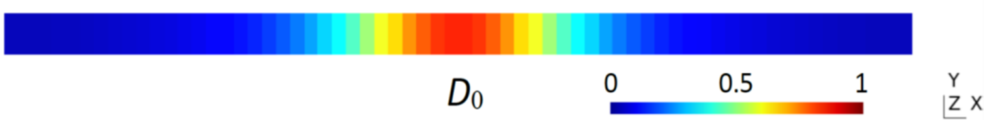

(b) Damage in matrix, configuration 1

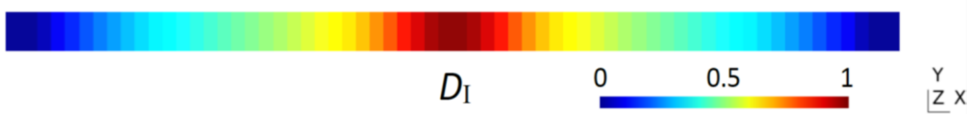

(c) Damage in fibres, configuration 2

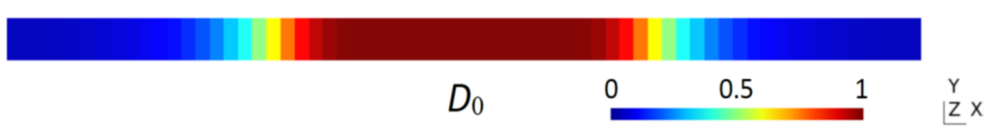

(d) Damage in matrix, configuration 2

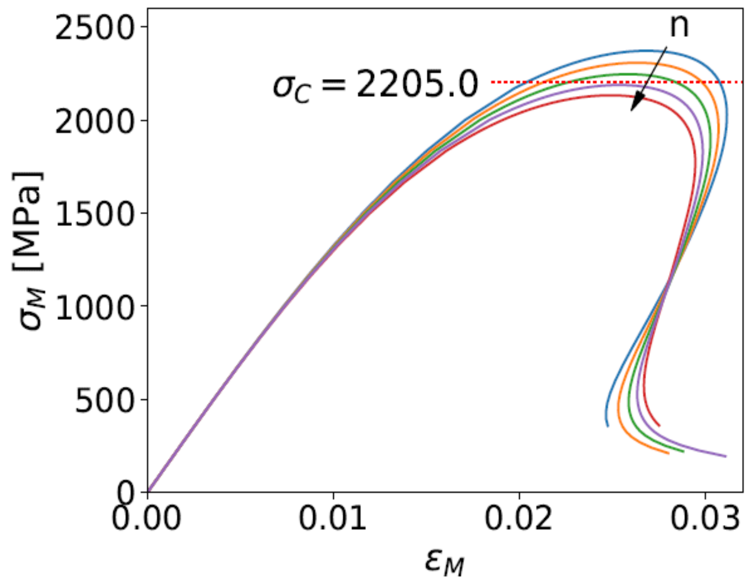

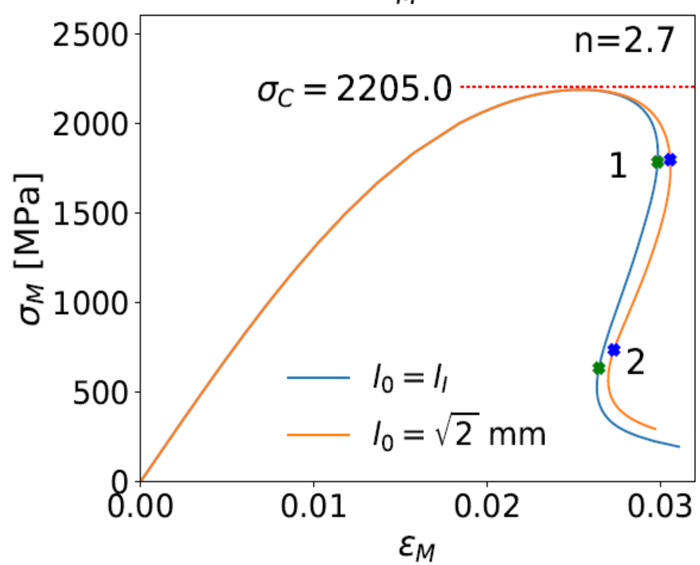

Non-Local Damage & Phase-Field Mean-Field-Homogenization

- Laminate study
  - AS4/8552 – Notched Specimen

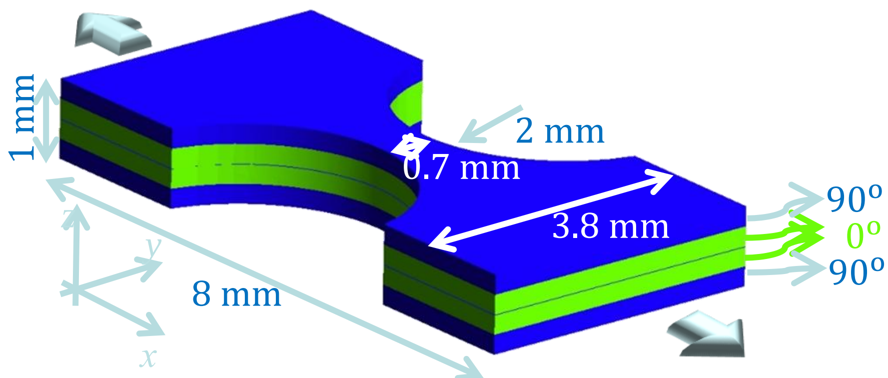

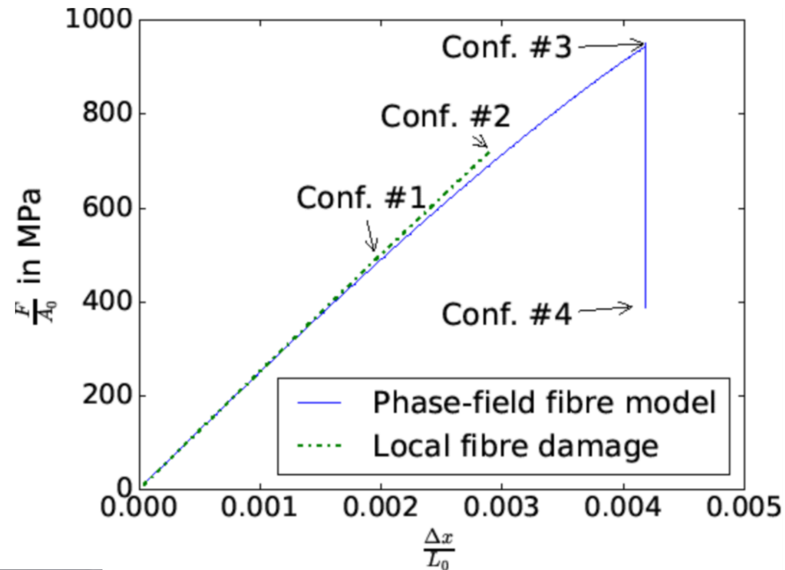

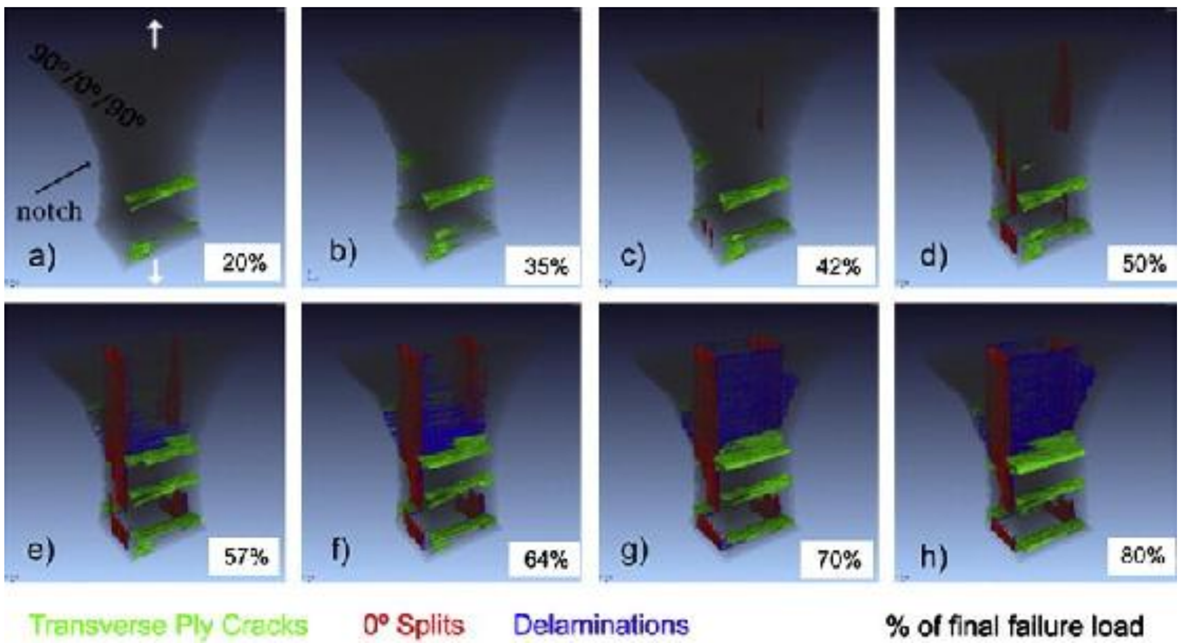

Composites Science and Technology, 71/12, A.E. Scott and M. Mavrogordato and P. Wright and I. Sinclair and S.M. Spearing, In situ fibre fracture measurement in carbonepoxy laminates using high resolution computed tomography, 1471-1477, 2011

Non-Local Damage & Phase-Field Mean-Field-Homogenization

- Laminate study
  - AS4/8552 – Notched Specimen: Configuration 1

Local fibre damage | *Phase-field fibre damage*

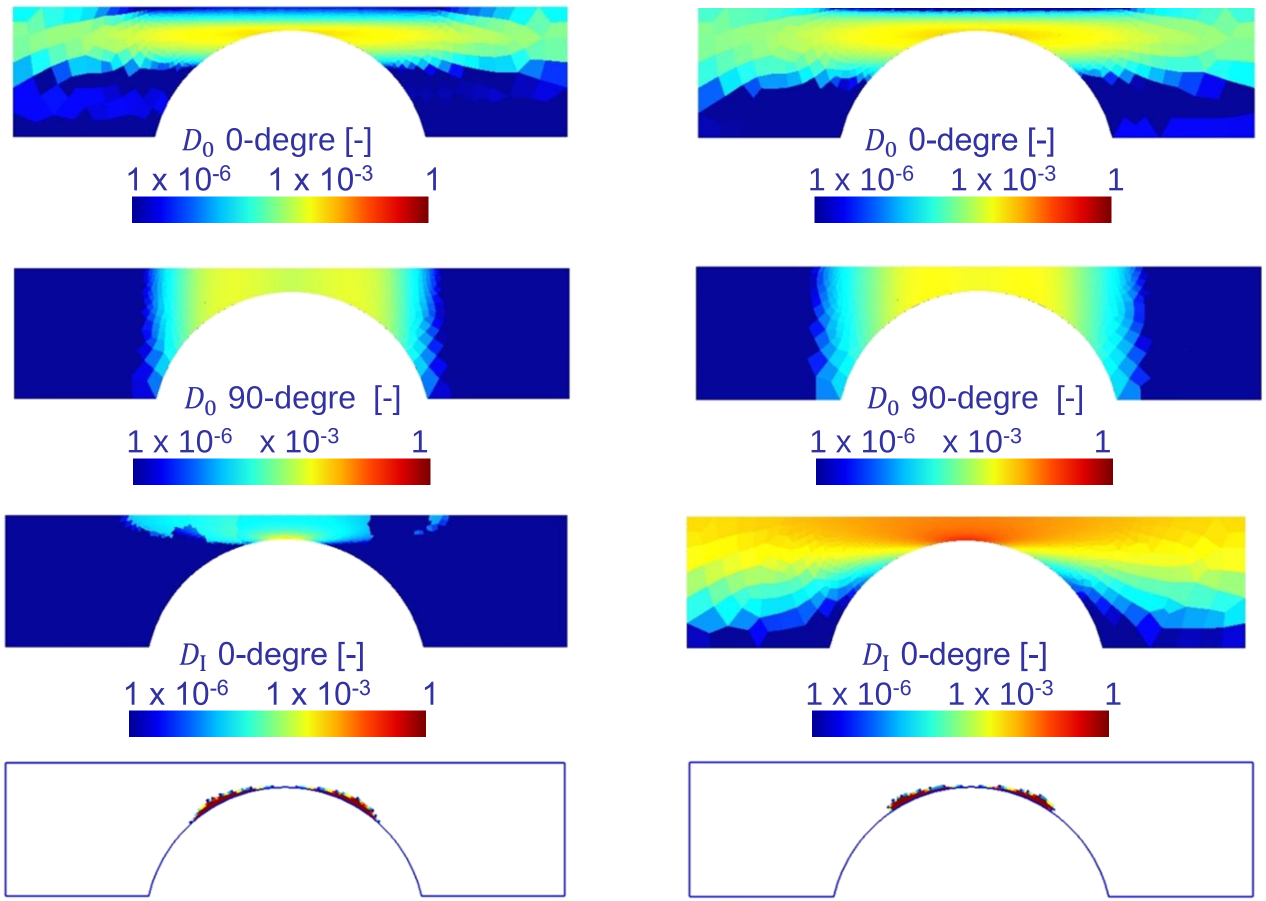

Active delamination | Active delamination

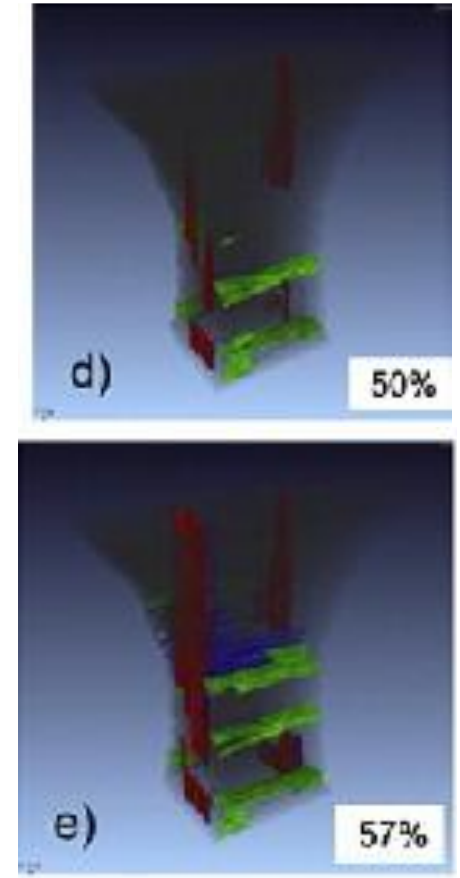

Composites Science and Technology, 71/12, A.E. Scott and M. Mavrogordato and P. Wright and I. Sinclair and S.M. Spearing, In situ fibre fracture measurement in carbonepoxy laminates using high resolution computed tomography, 1471-1477, 2011

Non-Local Damage & Phase-Field Mean-Field-Homogenization

- Laminate study
  - AS4/8552 – Notched Specimen: Configuration 2

Local fibre damage

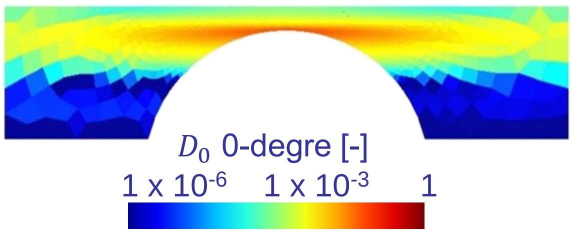

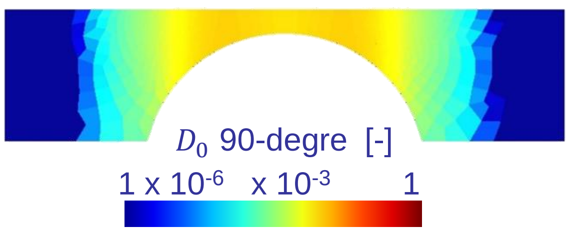

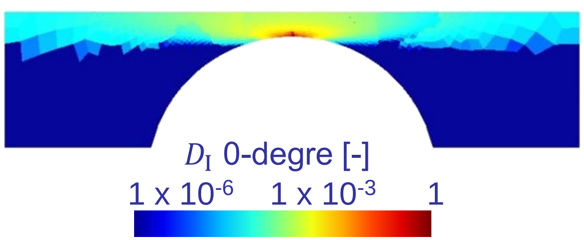

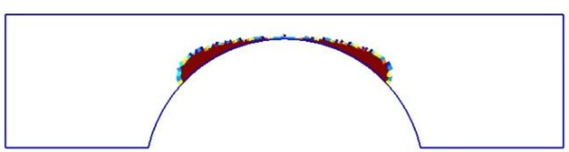

Active delamination

Phase-field fibre damage

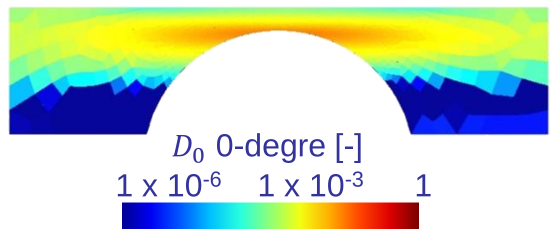

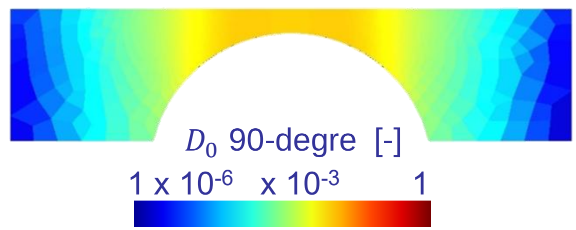

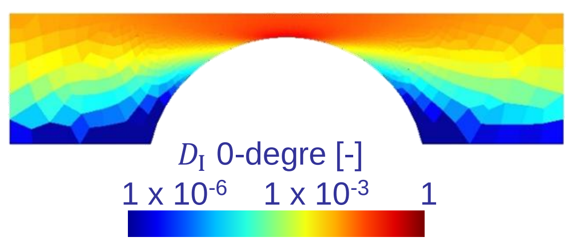

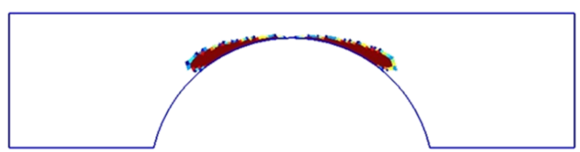

Active delamination

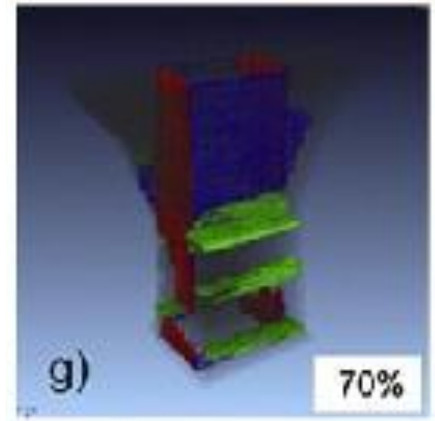

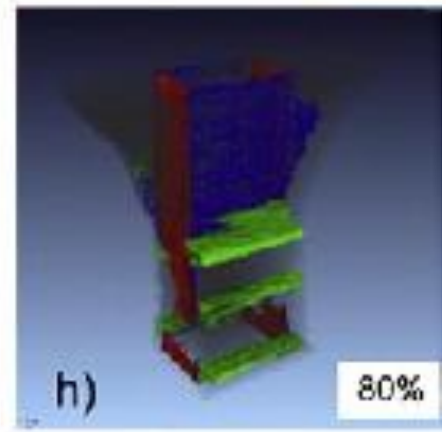

Composites Science and Technology, 71/12, A.E. Scott and M. Mavrogordato and P. Wright and I. Sinclair and S.M. Spearing, In situ fibre fracture measurement in carbonepoxy laminates using high resolution computed tomography, 1471-1477, 2011

Non-Local Damage & Phase-Field Mean-Field-Homogenization

- Laminate study
  - AS4/8552 – Notched Specimen: Configuration 3 & Configuration 4

Phase-field fibre damage, #3

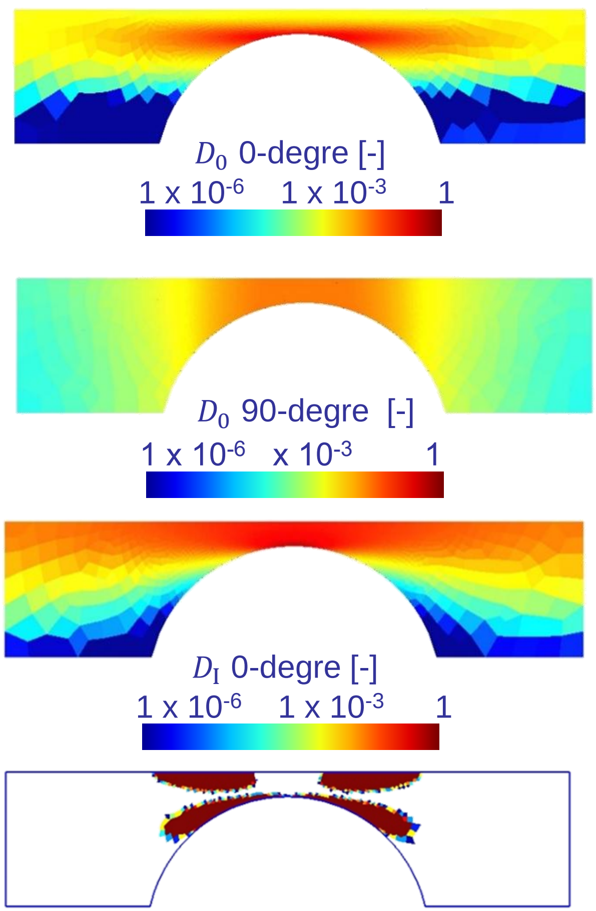

Active delamination

Phase-field fibre damage, #4

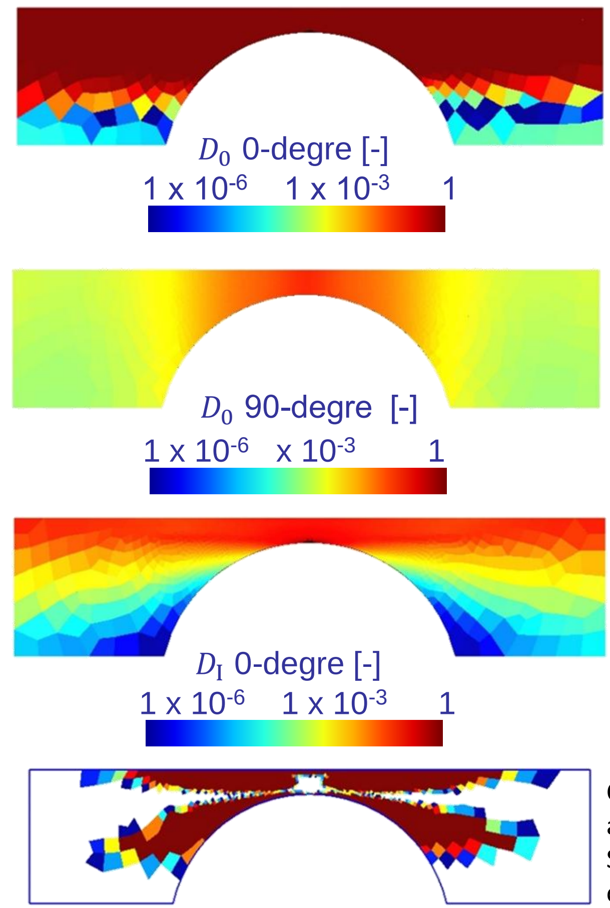

Active delamination

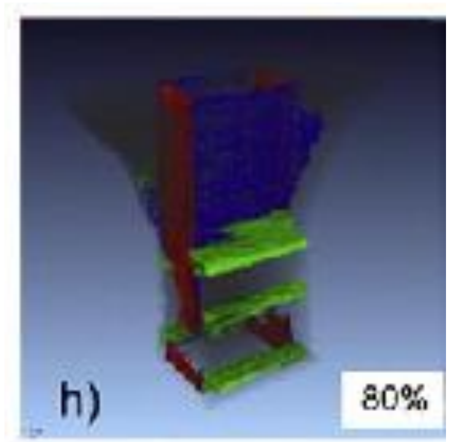

Composites Science and Technology, 71/12, A.E. Scott and M. Mavrogordato and P. Wright and I. Sinclair and S.M. Spearing, In situ fibre fracture measurement in carbonepoxy laminates using high resolution computed tomography, 1471-1477, 2011

- Laminate study
  - AS4/8552 – Notched Specimen

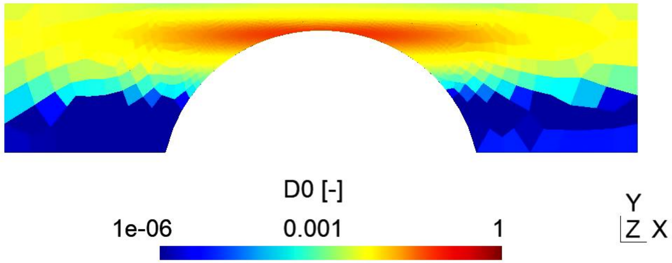

D_0 0-degre [-]

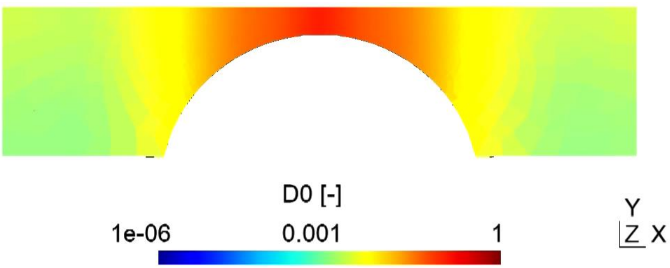

D_0 90-degre [-]

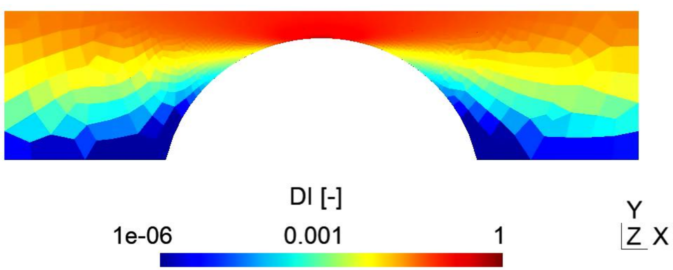

D_I 0-degre [-]

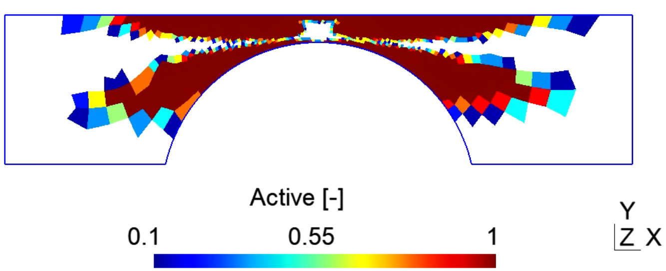

Active delamination

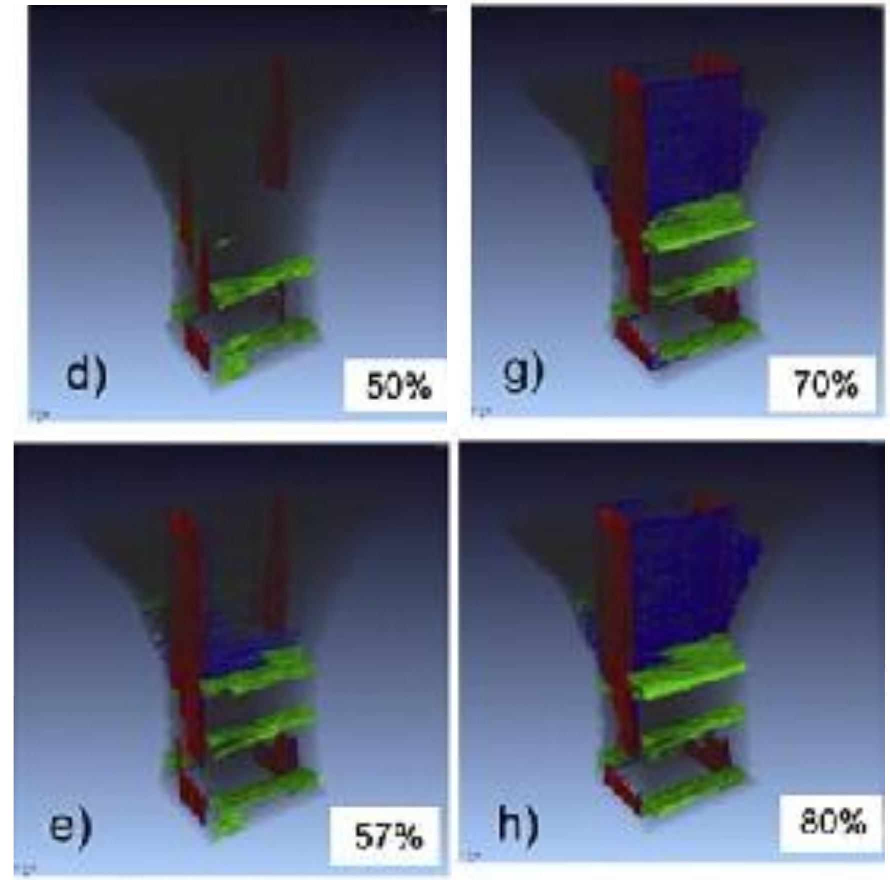

Composites Science and Technology, 71/12, A.E. Scott and M. Mavrogordato and P. Wright and I. Sinclair and S.M. Spearing, In situ fibre fracture measurement in carbonepoxy laminates using high resolution computed tomography, 1471-1477, 2011

Non-Local Damage & Phase-Field Mean-Field-Homogenization

- Geometry
  - Yarns:
    - Non-local damage & Phase-field MFH following yarn direction
  - Matrix
    - Non-local damage

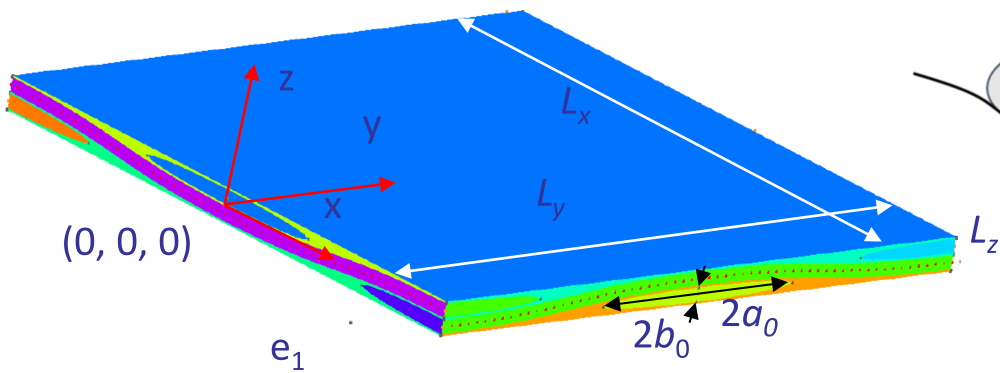

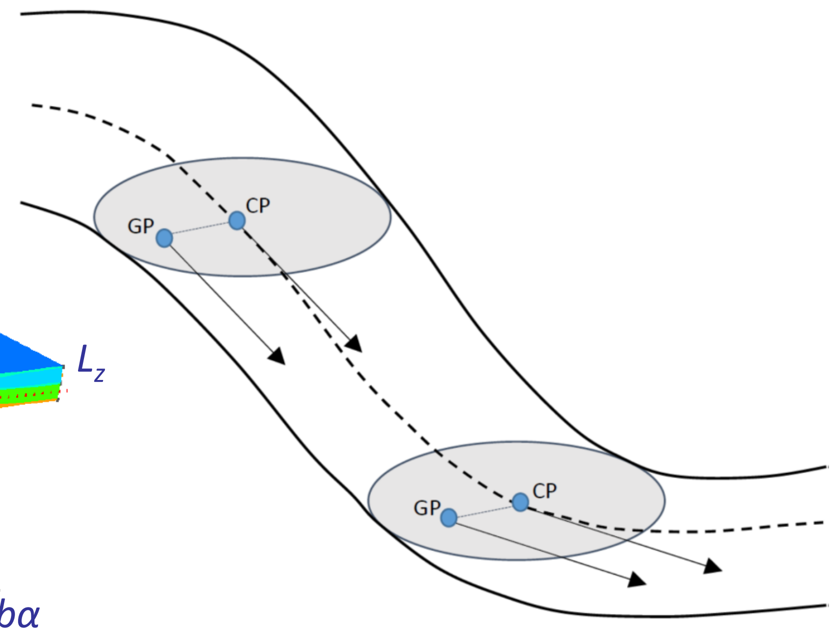

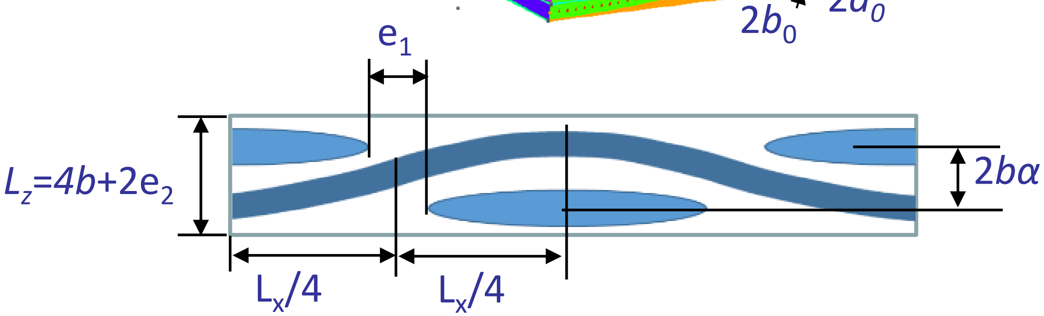

$$z = b\left[\frac{2}{1+e^{-\frac{l}{2}\left(2x-\frac{L_x}{2}\right)}} - 1\right]$$

Non-Local Damage & Phase-Field Mean-Field-Homogenization

- Damage distribution for uniaxial loading
  - Yarns:
    - Non-local damage & Phase-field MFH following yarn direction
  - Matrix
    - Non-local damage

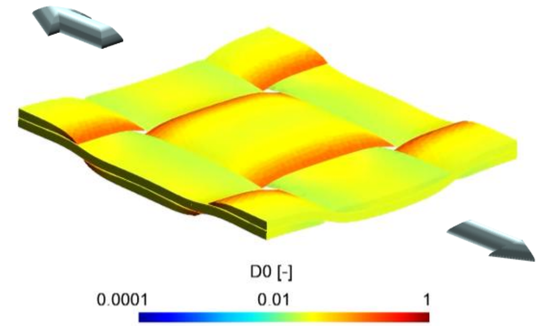

Damage in matrix phase out of yarns

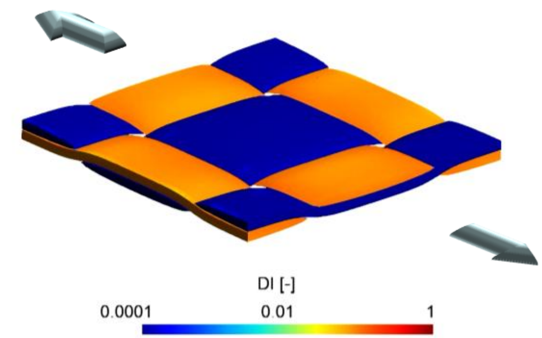

Damage in fibre bundle phase of yarns

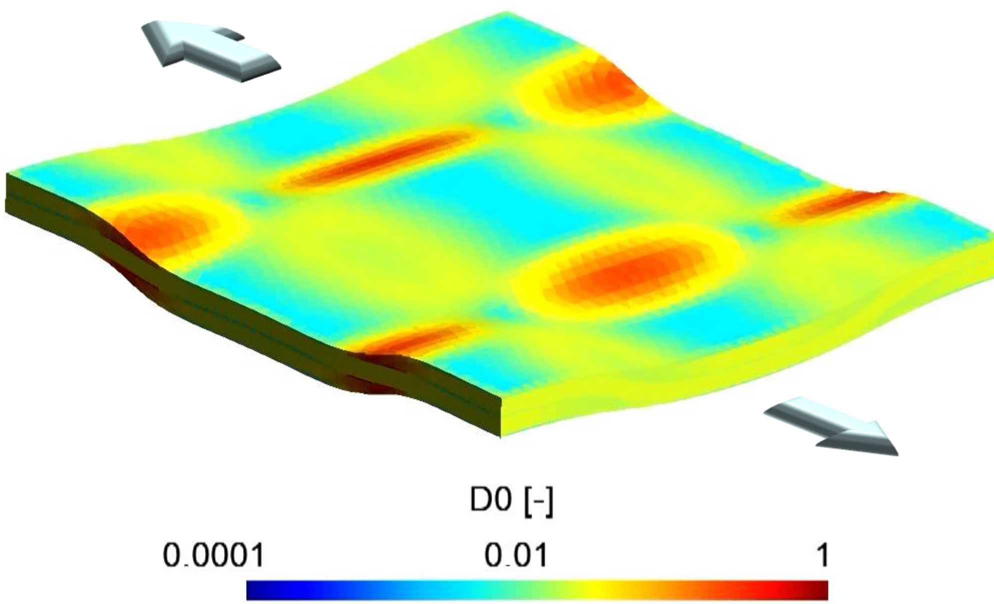

Damage in matrix (in & out of yarns)

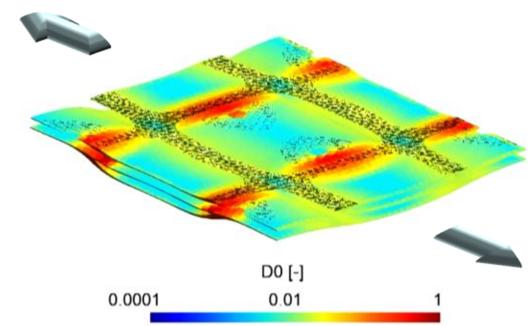

Damage in matrix phase of yarns

Non-Local Damage & Phase-Field Mean-Field-Homogenization

- Effect of boundary conditions
  - Side faces periodic and upper/lower faces flat (MBC/KUBC) vs. full PBC

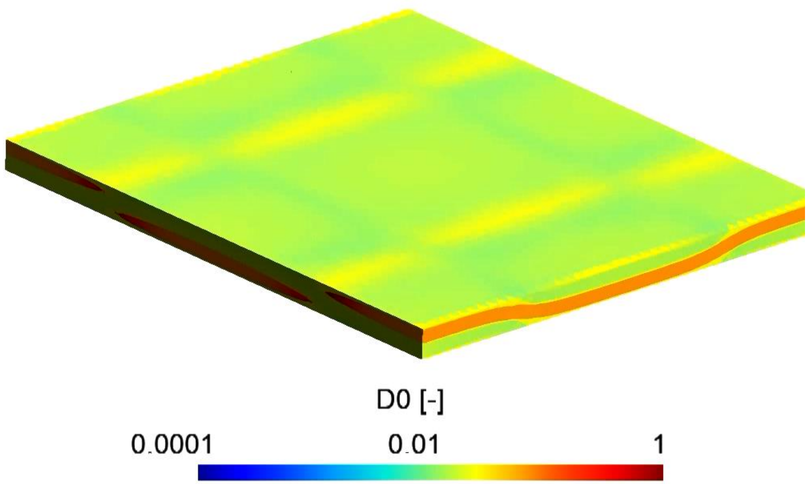

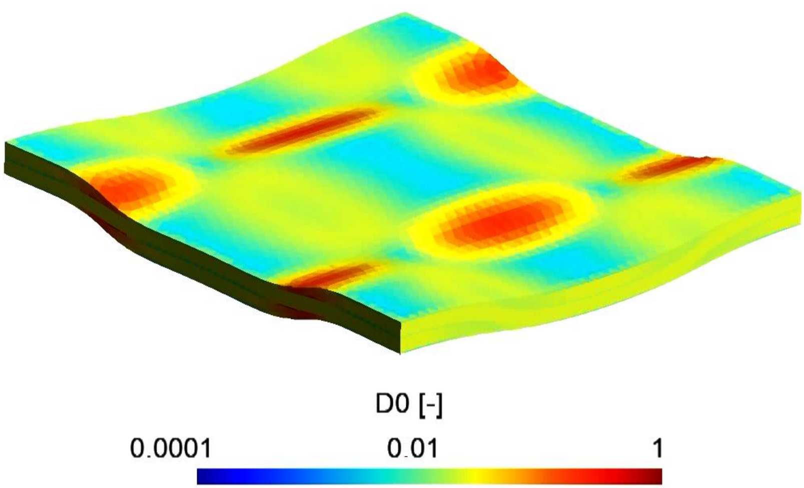

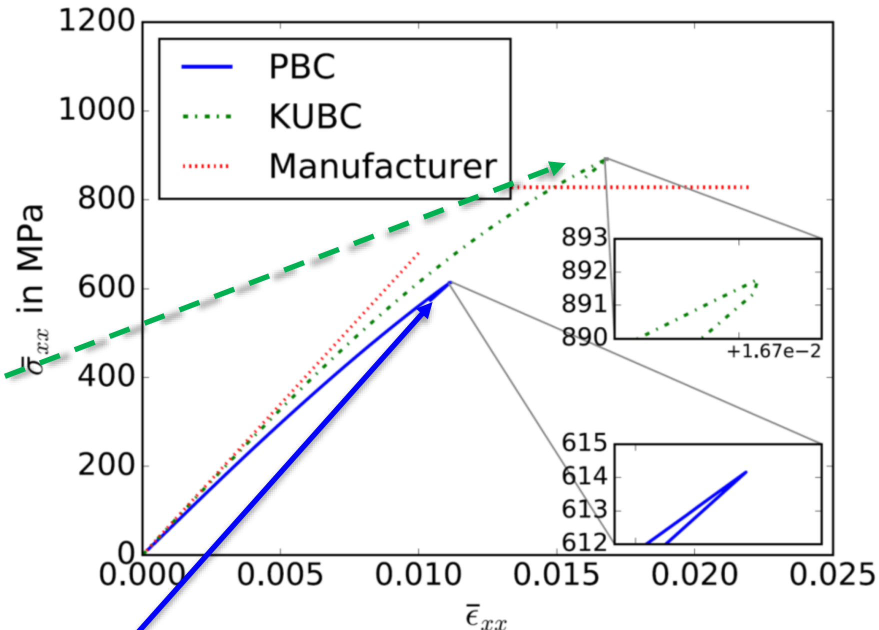

Non-Local Damage & Phase-Field Mean-Field-Homogenization

- Effect of boundary conditions
  - 2-ply layout with full periodic BC

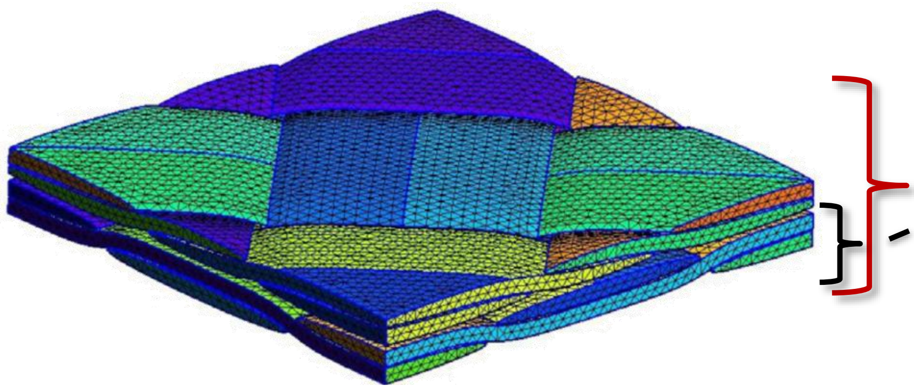

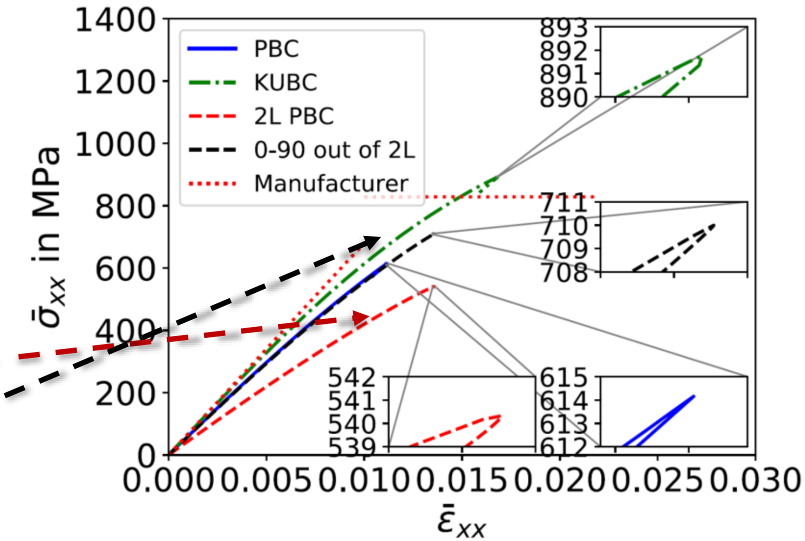

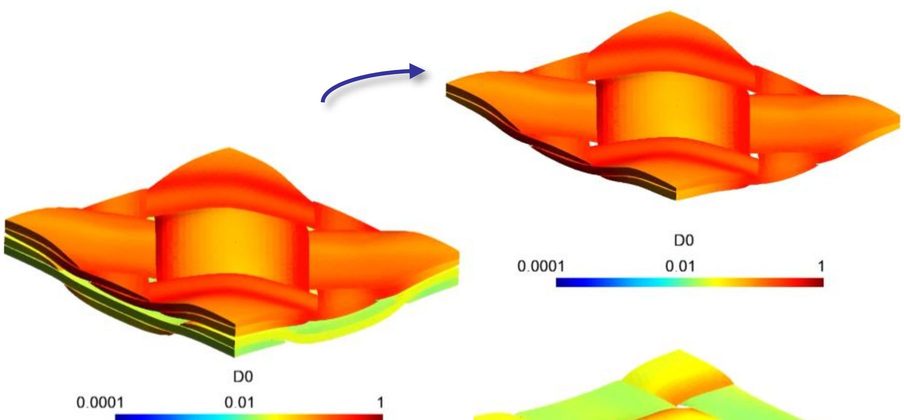

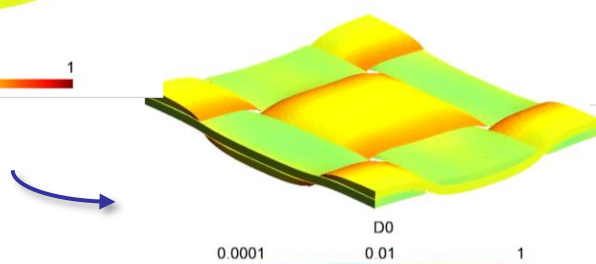

Damage in matrix phase of yarns

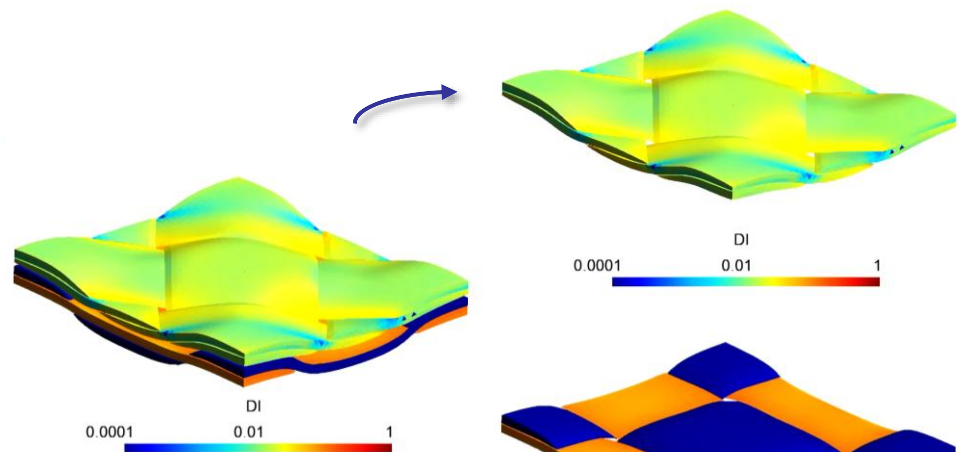

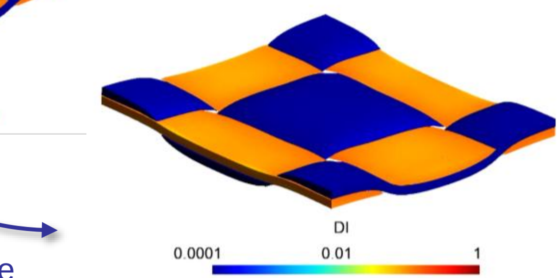

Damage in fibre bundle phase of yarns

Non-Local Damage & Phase-Field Mean-Field-Homogenization

- VISCOS project, 21st Call of Skywin
  - SONACA S.A., e-Xstream (Hexagon S.A.), Isomatex S.A., UCL, ULiege
- Publications (doi)
  - 10.1016/j.compstruc.2021.106650
  - 10.1016/j.compstruct.2021.114270
  - 10.1016/j.compstruct.2021.114058
    - Open data

Boundary conditions and tangent operator in multi-physics computational homogenization

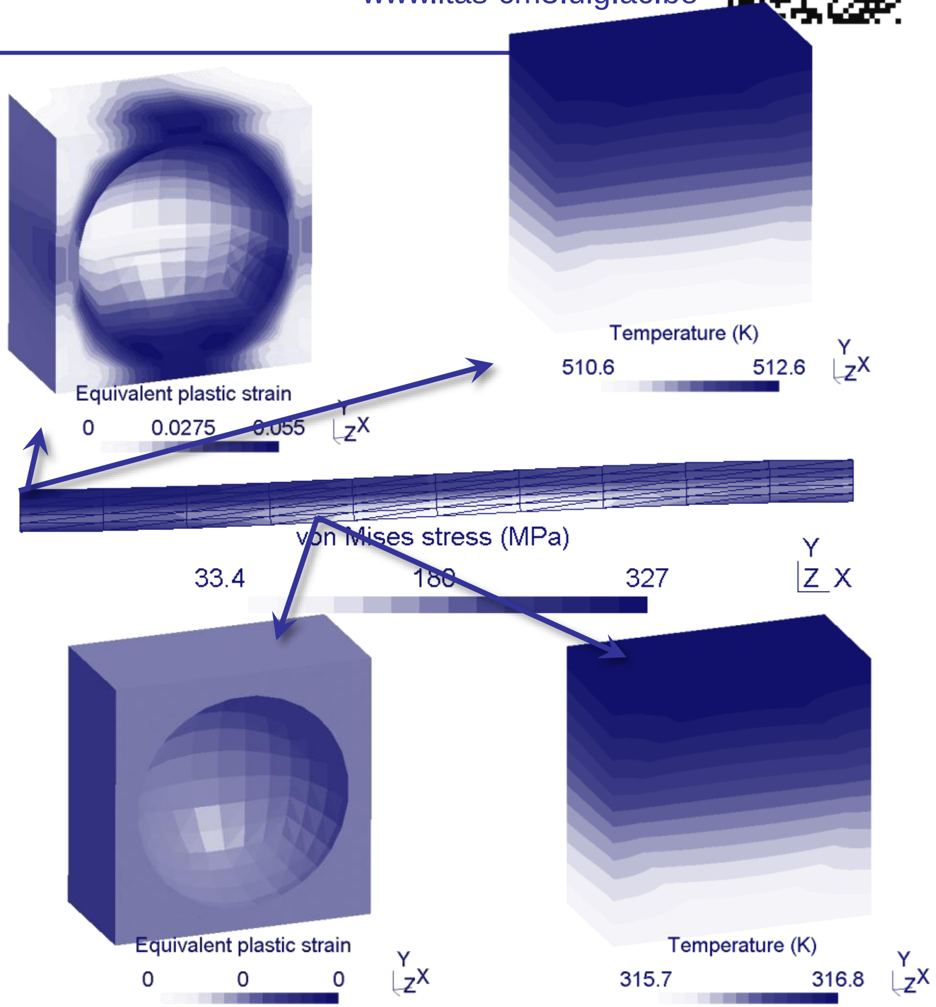

ARC 09/14-02 BRIDGING - From imaging to geometrical modelling of complex micro structured materials: Bridging computational engineering and material science
The authors gratefully acknowledge the financial support from F.R.S-F.N.R.S. under the project number PDR T.1015.14

- Multi-scale modeling
  - 2 problems are solved concurrently
    - The macro-scale problem
    - The meso-scale problem (on a meso-scale Volume Element)

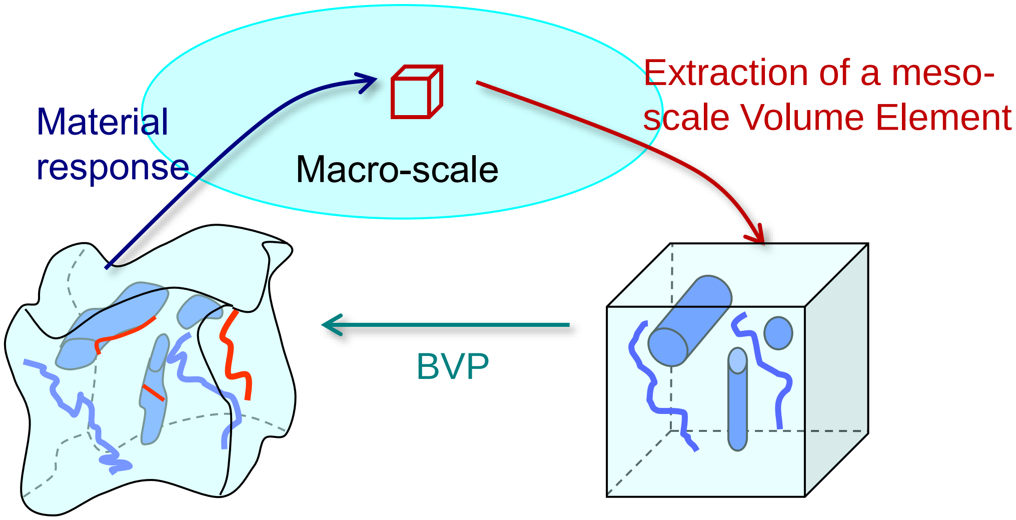

- Length-scales separation

$$L_{\text{macro}} >> L_{\text{VE}} >> L_{\text{micro}}$$

For accuracy: Size of the meso-scale volume element smaller than the characteristic length of the macro-scale loading

To be statistically representative: Size of the meso-scale volume element larger than the characteristic length of the micro-structure

Boundary conditions and tangent operator in FE^2

- Generalized multi-physics representation
  - Strong form $\mathcal{P} \cdot \nabla_0 = 0$
  - Fully-coupled constitutive law $\mathcal{P} = \mathcal{P}\left(\mathcal{X}^{C}, \mathcal{F}; \mathcal{Z}\right)$
    - $\mathcal{F}$: generalized deformation gradient, $\mathcal{X}^{C}$: fields appearing in the constitutive relations
    - $\mathcal{Z}$: internal variables
    - Tangent operators $\mathcal{L} = \frac{\partial \mathcal{P}}{\partial \mathcal{F}}$ & $\mathcal{J} = \frac{\partial \mathcal{P}}{\partial \mathcal{X}^{C}}$ but also $\mathcal{Y}_{\mathcal{F}} = \frac{\partial \mathcal{Z}}{\partial \mathcal{F}}$ & $\mathcal{Y}_{\mathcal{X}^{C}} = \frac{\partial \mathcal{Z}}{\partial \mathcal{X}^{C}}$
- Two-scale procedure

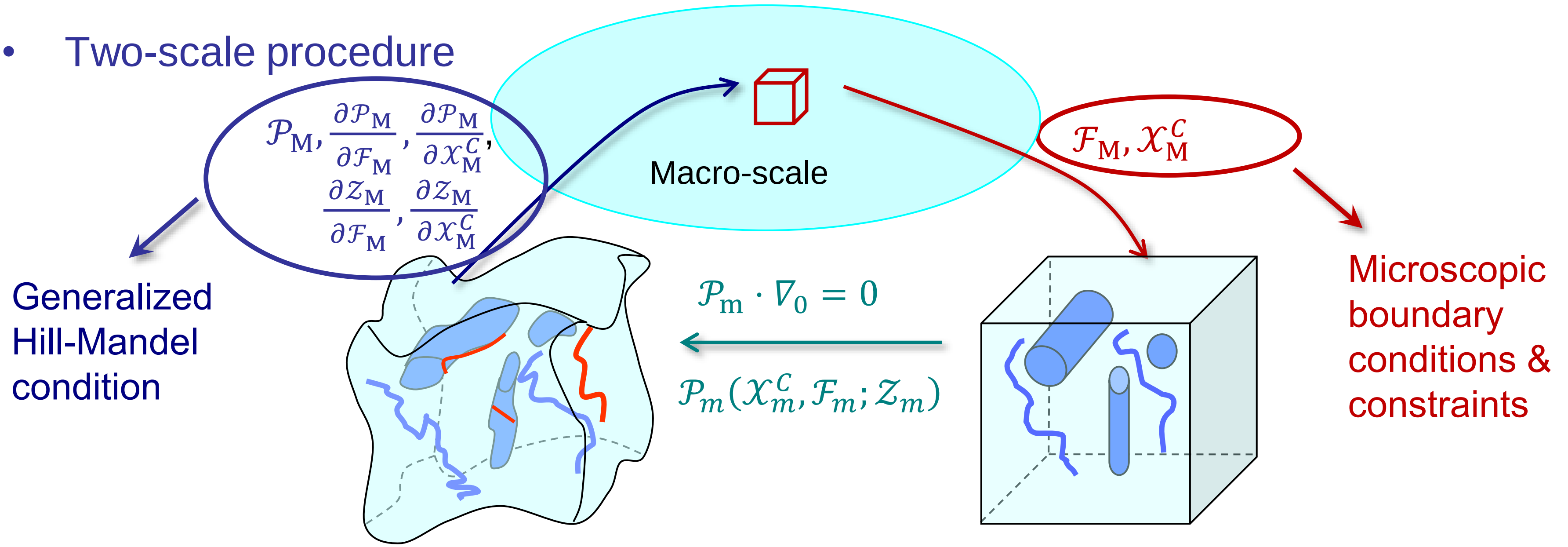

Boundary conditions and tangent operator in FE^2

- Generalized microscopic boundary conditions
  - Arbitrary field k kinematics: $\mathcal{X}_{\mathrm{m}}^{k} = \mathcal{X}_{\mathrm{M}}^{k} + \mathcal{F}_{\mathrm{M}}^{k} \cdot \mathrm{X}_{\mathrm{m}} + \mathcal{W}_{\mathrm{m}}^{k}$

Fluctuation

  - Constrained field k equivalence: $\int_{\omega_0} C_m^k \mathcal{X}_{\mathrm{m}}^{C^k} \, d\omega = \int_{\omega_0} C_m^k d\omega \, \mathcal{X}_{\mathrm{M}}^{C^k}$
  - E.g. periodic boundary conditions

Define an interpolant map

$$\mathbb{S}^i = \sum \mathbb{N}_k^i(\boldsymbol{X}_m) a_k^i$$

Substitute fluctuation fields

$$W_m^k(\boldsymbol{X}_m^+) = \mathbb{S}^i(\boldsymbol{X}_m^-) = W_m^k(\boldsymbol{X}_m^-)$$

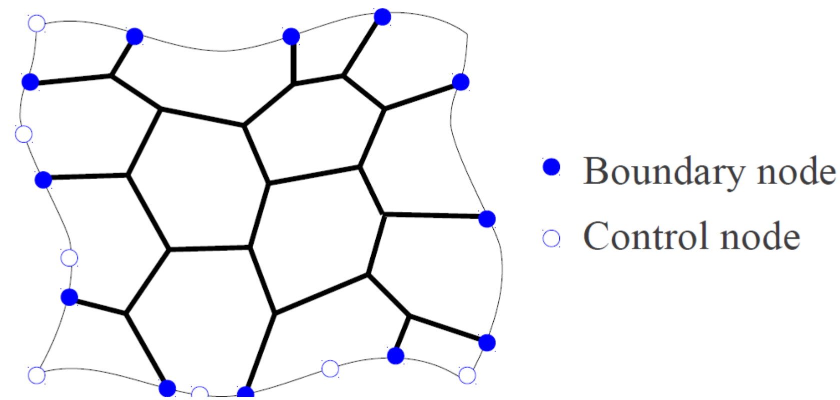

- Microscale BVP
  - Weak formulation

$$\begin{cases} \mathcal{P}_{\mathrm{m}} \cdot \nabla_0 = 0 \qquad \text{with} \;\; \mathcal{P}_m(\mathcal{X}_m^C, \mathcal{F}_m; \mathcal{Z}_m) \\ \mathcal{X}_{\mathrm{m}}^k = \mathcal{X}_{\mathrm{M}}^k + \mathcal{F}_{\mathrm{M}}^k \cdot \mathrm{X}_{\mathrm{m}} + \mathcal{W}_{\mathrm{m}}^k \\ \int_{\omega_0} C_m^k \mathcal{X}_{\mathrm{m}}^{C\,k}\, d\omega = \int_{\omega_0} C_m^k d\omega\, \mathcal{X}_{\mathrm{M}}^{C\,k} \end{cases}$$

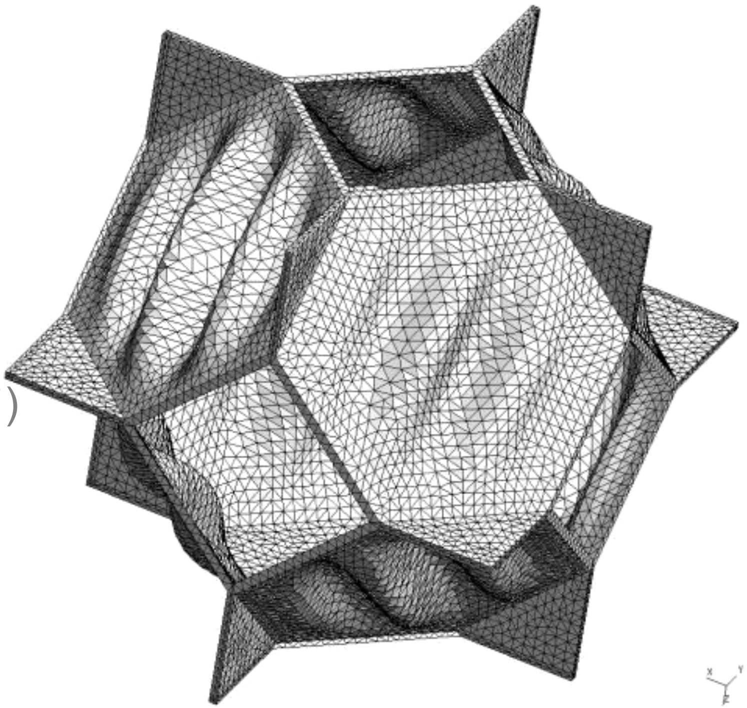

  - Weak finite element constrained form ($\omega_0 = \cup_e \omega^e$)

$$\begin{cases} \mathbf{f}_{\mathrm{m}}(\boldsymbol{\mathcal{U}}_m) - \mathbf{C}^{\mathrm{T}} \boldsymbol{\lambda} = 0 \\ \mathbf{C}\boldsymbol{\mathcal{U}}_m - \mathbf{S} \begin{bmatrix} \mathcal{F}_{\mathrm{M}} \\ \mathcal{X}_{\mathrm{M}}^C \end{bmatrix} = 0 \end{cases}$$

  - System linearization

$$\begin{cases} \mathbf{Q}^{\mathrm{T}} \dfrac{\partial \mathbf{f}_{\mathrm{m}}}{\partial \boldsymbol{\mathcal{U}}_m} \mathbf{Q} \delta \boldsymbol{\mathcal{U}}_m + \mathbf{r} - \mathbf{Q}^{\mathrm{T}} \dfrac{\partial \mathbf{f}_{\mathrm{m}}}{\partial \boldsymbol{\mathcal{U}}_m} \mathbf{C}^{\mathrm{T}} \left(\mathbf{C}\mathbf{C}^{\mathrm{T}}\right)^{-\mathbf{1}} \left(\mathbf{r}_{\boldsymbol{c}} - \mathbf{S} \begin{bmatrix} \delta\mathcal{F}_{\mathrm{M}} \\ \delta\mathcal{X}_{\mathrm{M}}^C \end{bmatrix} \right) = 0 \\ \mathbf{C}\delta\boldsymbol{\mathcal{U}}_m + \mathbf{r}_{\mathrm{c}} - \mathbf{S} \begin{bmatrix} \delta\mathcal{F}_{\mathrm{M}} \\ \delta\mathcal{X}_{\mathrm{M}}^C \end{bmatrix} = 0 \qquad \& \qquad \mathbf{Q} = \mathbf{I} - \mathbf{C}^{\mathrm{T}}\left(\mathbf{C}\mathbf{C}^{\mathrm{T}}\right)^{-\mathbf{1}}\mathbf{C} \end{cases}$$

- Multi-scale resolution
  - System linearization

$$\begin{cases} \mathbf{Q}^{\mathrm{T}} \dfrac{\partial \mathbf{f}_{\mathrm{m}}}{\partial \boldsymbol{\mathcal{U}}_m} \mathbf{Q} \delta \boldsymbol{\mathcal{U}}_m + \mathbf{Q}^{\mathrm{T}} \mathbf{r} - \mathbf{Q}^{\mathrm{T}} \dfrac{\partial \mathbf{f}_{\mathrm{m}}}{\partial \boldsymbol{\mathcal{U}}_m} \mathbf{C}^{\mathrm{T}} \left(\mathbf{C}\mathbf{C}^{\mathrm{T}}\right)^{-1} \left(\mathbf{r}_c - \mathbf{S} \begin{bmatrix} \delta \mathcal{F}_{\mathrm{M}} \\ \delta \mathcal{X}_{\mathrm{M}}^{C} \end{bmatrix} \right) = 0 \\ \mathbf{C} \delta \boldsymbol{\mathcal{U}}_m + \mathbf{r}_{\mathrm{c}} - \mathbf{S} \begin{bmatrix} \delta \mathcal{F}_{\mathrm{M}} \\ \delta \mathcal{X}_{\mathrm{M}}^{C} \end{bmatrix} = 0 \qquad \& \qquad \mathbf{Q} = \mathbf{I} - \mathbf{C}^{\mathrm{T}} \left(\mathbf{C}\mathbf{C}^{\mathrm{T}}\right)^{-1} \mathbf{C} \end{cases}$$

  - FEM resolution: $\delta \mathcal{F}_{\mathrm{M}} = \delta \mathcal{X}_{\mathrm{M}}^{C} = 0$

$$\delta \boldsymbol{\mathcal{U}}_m = -\widetilde{\mathbf{K}}^{-1} \left(\mathbf{Q}^{\mathrm{T}} \mathbf{r} + \left(\mathbf{C}^{\mathrm{T}} - \mathbf{Q}^{\mathrm{T}} \frac{\partial \mathbf{f}_{\mathrm{m}}}{\partial \boldsymbol{\mathcal{U}}_m} \mathbf{C}^{\mathrm{T}} \left(\mathbf{C}\mathbf{C}^{\mathrm{T}}\right)^{-1} \right) \mathbf{r}_c \right)$$

Only one matrix to factorize

$$\widetilde{\mathbf{K}} = \mathbf{C}^{\mathrm{T}} \mathbf{C} + \mathbf{Q}^{\mathrm{T}} \frac{\partial \mathbf{f}_{\mathrm{m}}}{\partial \boldsymbol{\mathcal{U}}_m} \mathbf{Q}$$

  - Constraints effect: $\mathbf{r} = \mathbf{r}_c = 0$

$$\frac{\partial \boldsymbol{\mathcal{U}}_m}{\partial \left[\mathcal{F}_{\mathrm{M}} \quad \mathcal{X}_{\mathrm{M}}^{C} \right]^{T}} = \widetilde{\mathbf{K}}^{-1} \left(\mathbf{C}^{\mathrm{T}} - \mathbf{Q}^{\mathrm{T}} \frac{\partial \mathbf{f}_{\mathrm{m}}}{\partial \boldsymbol{\mathcal{U}}_m} \mathbf{C}^{\mathrm{T}} \left(\mathbf{C}\mathbf{C}^{\mathrm{T}}\right)^{-1} \right) \mathbf{S}$$

  - Macro-scale operators at low cost

$$\begin{bmatrix} \dfrac{\partial \mathcal{P}_{\mathrm{M}}}{\partial \mathcal{F}_{\mathrm{M}}} & \dfrac{\partial \mathcal{P}_{\mathrm{M}}}{\partial \mathcal{X}_{\mathrm{M}}^{C}} \\ \dfrac{\partial \mathcal{Z}_{\mathrm{M}}}{\partial \mathcal{F}_{\mathrm{M}}} & \dfrac{\partial \mathcal{Z}_{\mathrm{M}}}{\partial \mathcal{X}_{\mathrm{M}}^{C}} \end{bmatrix} = \left(\bigwedge_{\omega^e} \frac{1}{V(\omega_0)} \int_{\omega_0^e} \begin{bmatrix} \dfrac{\partial \mathcal{P}_{\mathrm{m}}}{\partial \mathcal{F}_{\mathrm{m}}} \mathbf{B}^e & \dfrac{\partial \mathcal{P}_{\mathrm{m}}}{\partial \mathcal{X}_{\mathrm{m}}^{C}} \mathbf{N}^e \\ \dfrac{\partial \mathcal{Z}_{\mathrm{m}}}{\partial \mathcal{F}_{\mathrm{m}}} \mathbf{B}^e & \dfrac{\partial \mathcal{Z}_{\mathrm{m}}}{\partial \mathcal{X}_{\mathrm{m}}^{C}} \mathbf{N}^e \end{bmatrix} d\omega \right) \frac{\partial \boldsymbol{\mathcal{U}}_m}{\partial \left[\mathcal{F}_{\mathrm{M}} \quad \mathcal{X}_{\mathrm{M}}^{C} \right]^{T}}$$

- Thermo-elasto-plasticity

$$\begin{cases} \mathbf{P}_\mathrm{M} \cdot \boldsymbol{\nabla}_0 = 0 \\ \rho_\mathrm{M} C_{v\mathrm{M}} \dot{\vartheta}_\mathrm{M} - \mathcal{D}_\mathrm{M} + \mathbf{q}_\mathrm{M} \cdot \boldsymbol{\nabla}_0 = 0 \end{cases}$$

$$\begin{cases} \mathbf{P}_\mathrm{M} = \dfrac{1}{V(\omega_0)} \displaystyle\int_{\omega_0} \mathbf{P}_\mathrm{m} d\omega \\ \boldsymbol{q}_\mathrm{M} = \dfrac{1}{V(\omega_0)} \displaystyle\int_{\omega_0} \boldsymbol{q}_\mathrm{m} d\omega \\ \rho_\mathrm{M} C_{v\mathrm{M}} = \dfrac{1}{V(\omega_0)} \displaystyle\int \rho_\mathrm{m} C_{v\mathrm{m}} d\omega \\ \mathcal{D}_\mathrm{M} = \dfrac{1}{V(\omega_0)} \displaystyle\int \mathcal{D}_\mathrm{m} d\omega \\ \quad \& \\ \dfrac{\partial \mathbf{P}_\mathrm{M}}{\partial \mathbf{F}_\mathrm{M}}, \dfrac{\partial \mathbf{P}_\mathrm{M}}{\partial \vartheta_\mathrm{M}}, \dfrac{\partial \mathbf{P}_\mathrm{M}}{\partial \boldsymbol{\nabla}_0 \vartheta_\mathrm{M}}, \\ \dfrac{\partial \mathbf{q}_\mathrm{M}}{\partial \mathbf{F}_\mathrm{M}}, \dfrac{\partial \mathbf{q}_\mathrm{M}}{\partial \vartheta_\mathrm{M}}, \dfrac{\partial \mathbf{q}_\mathrm{M}}{\partial \boldsymbol{\nabla}_0 \vartheta_\mathrm{M}}, \\ \dfrac{\partial \mathcal{D}_\mathrm{M}}{\partial \mathbf{F}_\mathrm{M}}, \dfrac{\partial \mathcal{D}_\mathrm{M}}{\partial \vartheta_\mathrm{M}}, \dfrac{\partial \mathcal{D}_\mathrm{M}}{\partial \boldsymbol{\nabla}_0 \vartheta_\mathrm{M}} \end{cases}$$

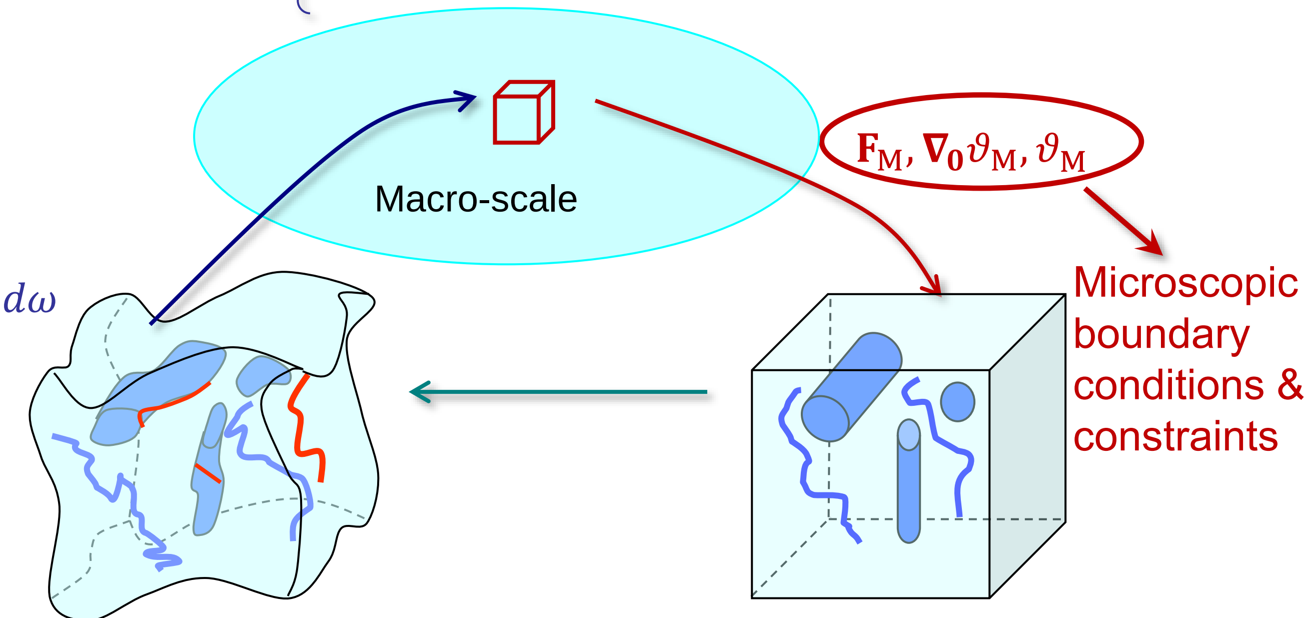

$$\begin{cases} \mathbf{P}_\mathrm{m} = \mathbf{P}_\mathrm{m}\left(\mathbf{F}_\mathrm{m}, \boldsymbol{\nabla}_0 \vartheta_\mathrm{m}, \vartheta_\mathrm{m}; p, \mathbf{F}_\mathrm{m}^\mathbf{p}\right) \\ \mathbf{q}_\mathrm{m} = \mathbf{q}_\mathrm{m}\left(\mathbf{F}_\mathrm{m}, \boldsymbol{\nabla}_0 \vartheta_\mathrm{m}, \vartheta_\mathrm{m}; p, \mathbf{F}_\mathrm{m}^\mathbf{p}\right) \\ \mathcal{D}_\mathrm{m} = \beta \dot{p} \tau + \vartheta \dfrac{\partial \dot{W}^\mathrm{el}}{\partial \vartheta} \\ \mathbf{P}_\mathrm{m} \cdot \boldsymbol{\nabla}_0 = 0 \\ \mathbf{q}_\mathrm{m} \cdot \boldsymbol{\nabla}_0 = 0 \end{cases}$$

- Thermo-elasto-plasticity
  - Thermal-softening hardening
    $\tau = (\sigma_0 + Hp)(1 - \omega_T(T - T_0))$

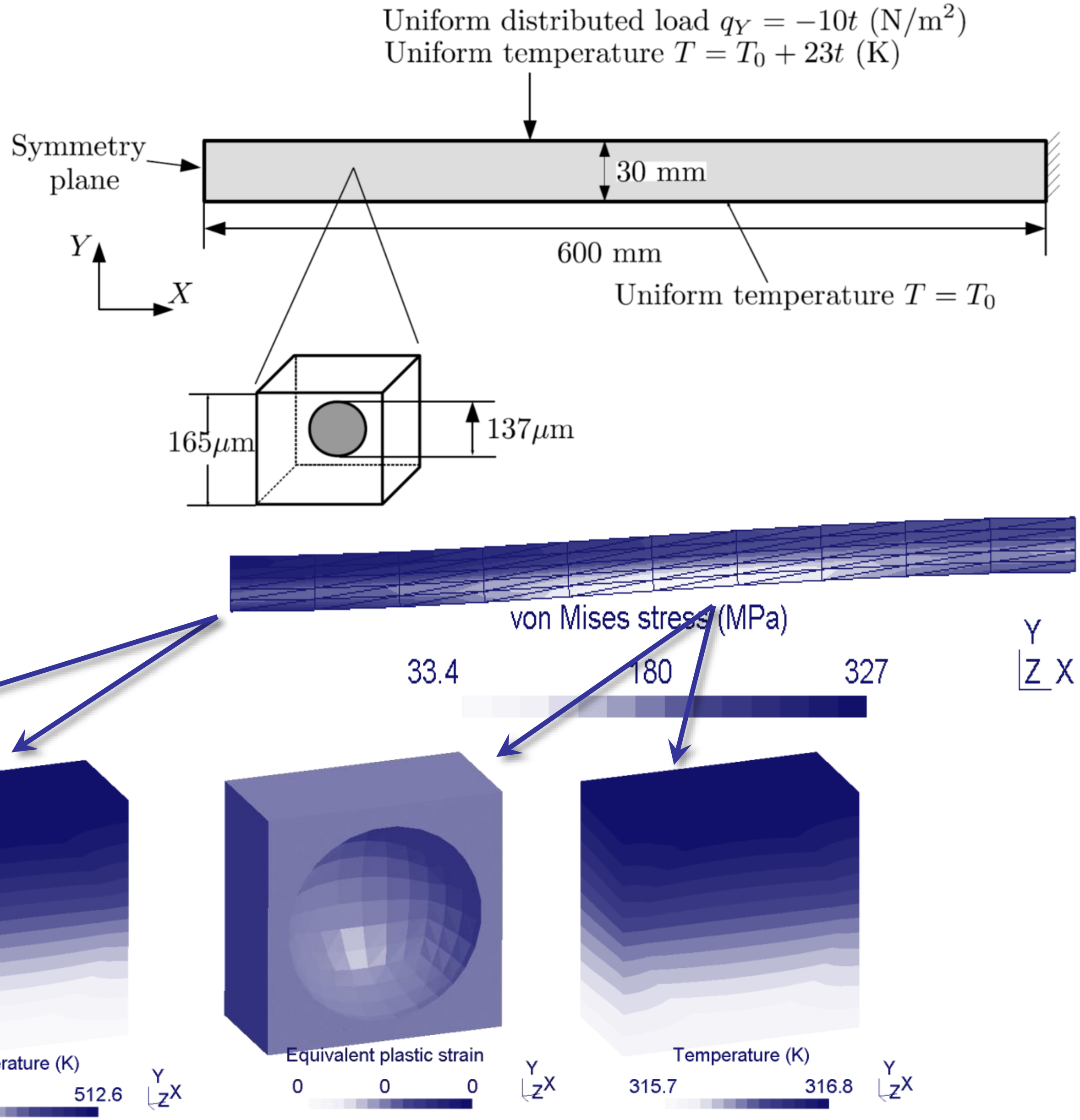

Beginning

Boundary conditions and tangent operator in FE^2

- BRIDGING ARC project (Periodic boundary conditions)
  - ULiège, Applied Sciences (A&M, EEI, ICD)
  - ULiège, Sciences (CERM)

- PDR T.1015.14 project (MFH with second-order moments)
  - ULiège, UCL (Belgium)

- Publications
  - 10.1007/s00466-016-1358-z
  - 10.1016/j.commatsci.2011.10.017

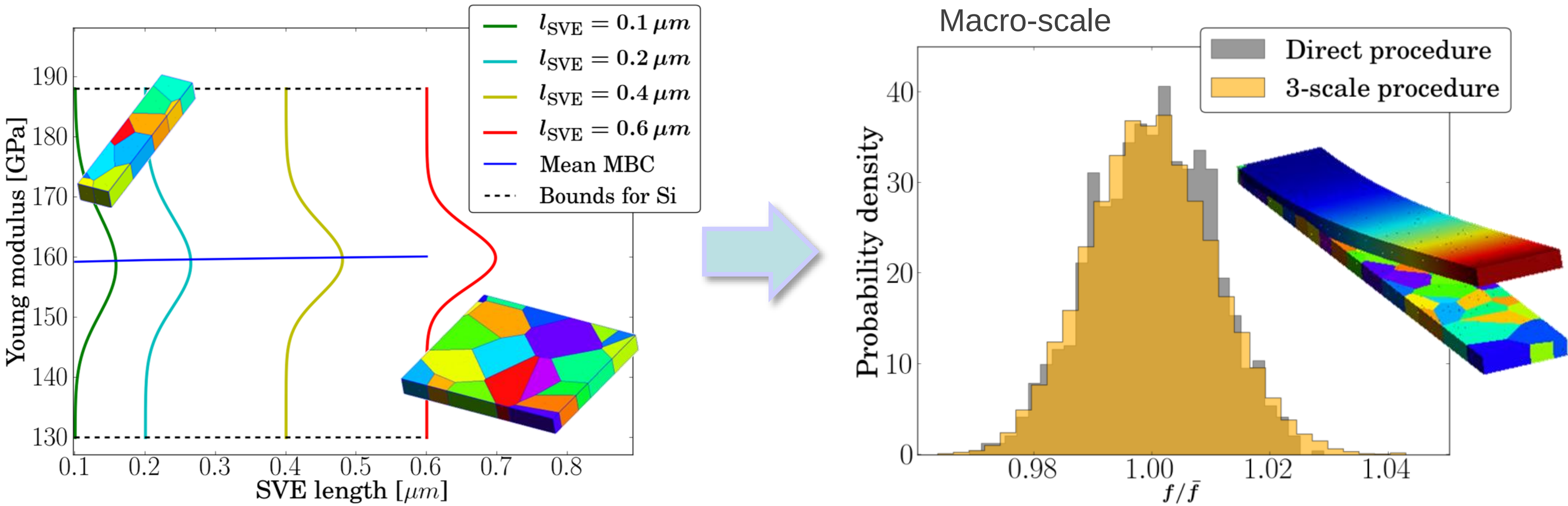

Stochastic 3-Scale Models for Polycrystalline Materials

3SMVIB: The research has been funded by the Walloon Region under the agreement no 1117477 (CT-INT 2011-11-14) in the context of the ERA-NET MNT framework.

- Multi-scale modeling
  - 2 problems are solved concurrently
    - The macro-scale problem
    - The meso-scale problem (on a meso-scale Volume Element)

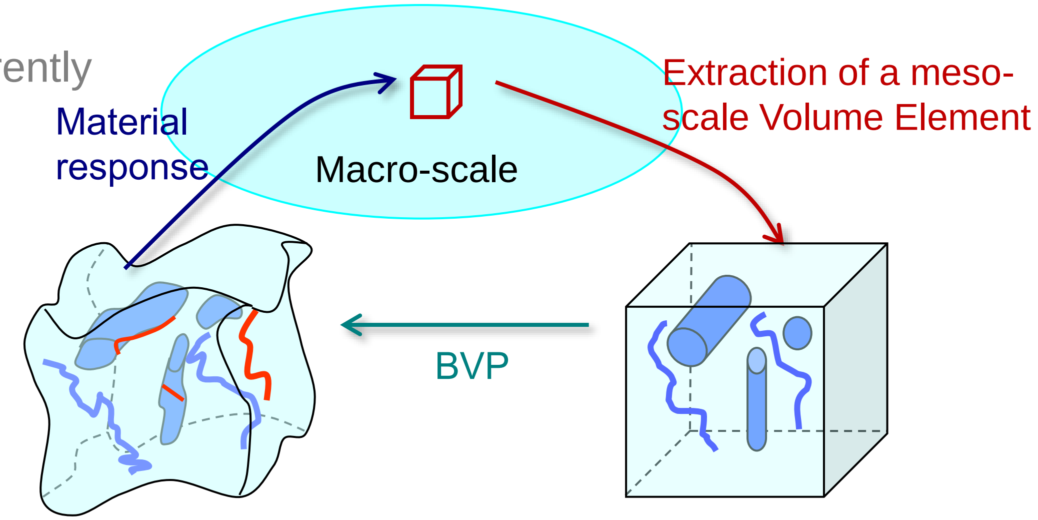

- For structures not several orders larger than the micro-structure size

$$L_{macro} >> L_{VE} >\sim L_{micro}$$

For accuracy: Size of the meso-scale volume element smaller than the characteristic length of the macro-scale loading

Meso-scale volume element no longer statistically representative:

- **Stochastic Volume Elements**

Stochastic 3-Scale Models

- Key idea

Micro-scale	Meso-scale	Macro-scale
➢ Samples of stochastic volume elements ➢ Random microstructure	➢ Intermediate scale ➢ The distribution of the material property $\mathbb{P}(C)$ is defined	➢ Uncertainty quantification of the macro-scale quantity ➢ Quantity of interest distribution $\mathbb{P}(Q)$

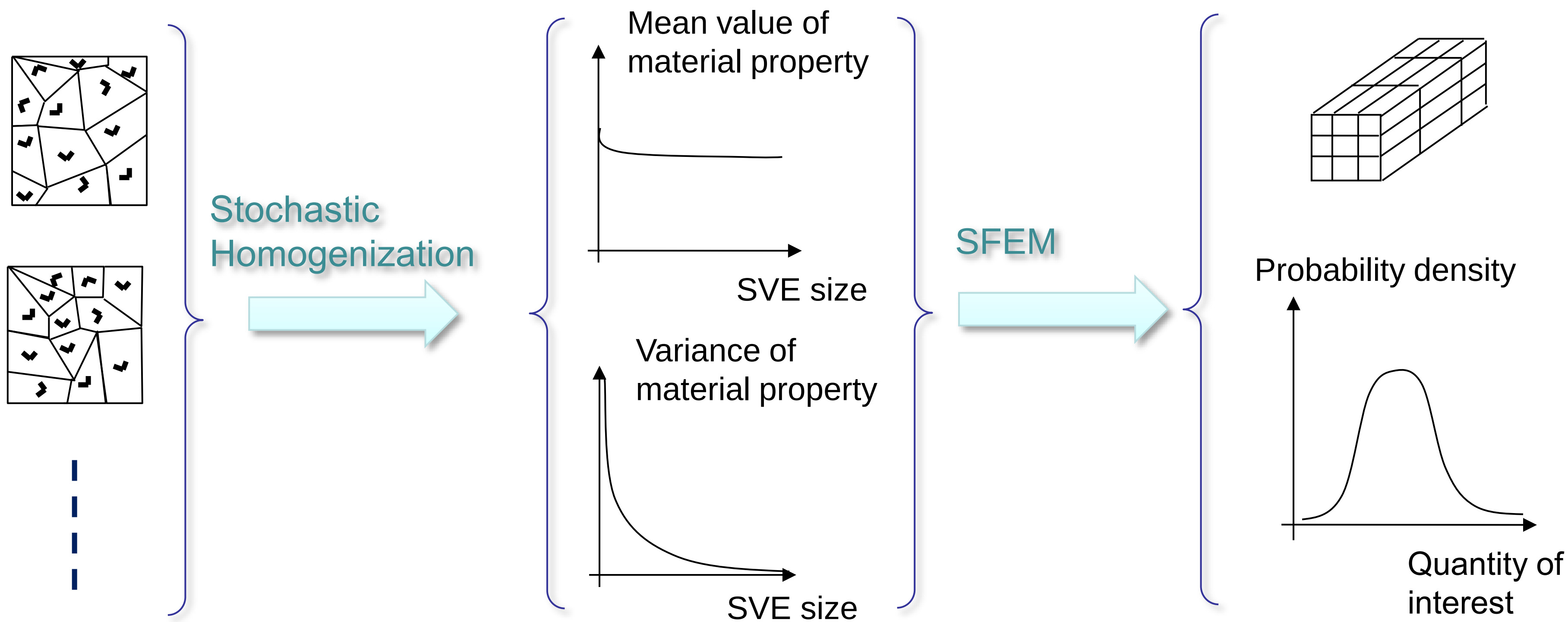

- Material structure: grain orientation distribution
  - Grain orientation by XRD (X-ray Diffraction) measurements on 2 µm-thick poly-silicon films

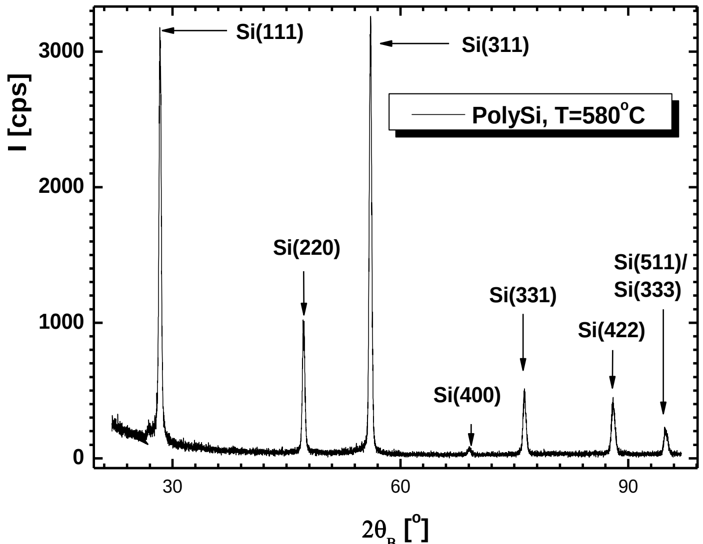

Deposition temperature: 580 °C

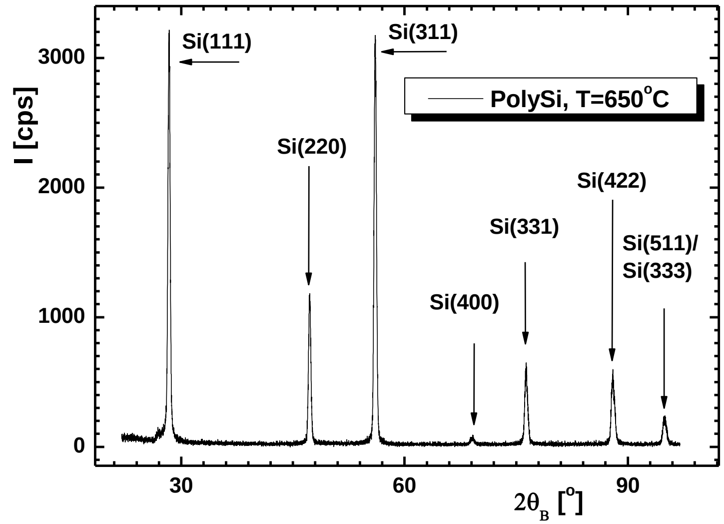

Deposition temperature: 630 °C

Deposition temperature [°C]	580	610	630	650
<111> [%]	12.57	19.96	12.88	11.72
<220> [%]	7.19	13.67	7.96	7.59
<311> [%]	42.83	28.83	39.08	38.47
<400> [%]	4.28	5.54	3.13	3.93
<331> [%]	17.97	18.14	21.32	20.45
<422> [%]	15.15	13.86	15.63	17.84

XRD images provided by IMT Bucharest, Rodica Voicu, Angela Baracu, Raluca Muller

- Application to polycrystalline materials: The micro-scale to meso-scale transition
  - Stochastic homogenization

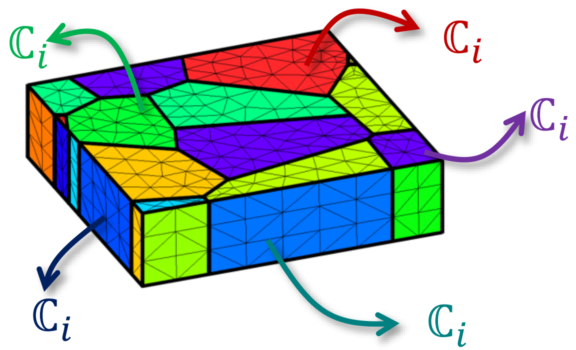

$$\boldsymbol{\sigma}_{m^i} = \mathbb{C}_i : \boldsymbol{\epsilon}_{m^i} \quad , \forall i$$

Stochastic Homogenization

$$\boldsymbol{\sigma}_M = \mathbb{C}_M : \boldsymbol{\epsilon}_M$$

Samples of the meso-scale homogenized elasticity tensors

  - Homogenized Young's modulus distribution

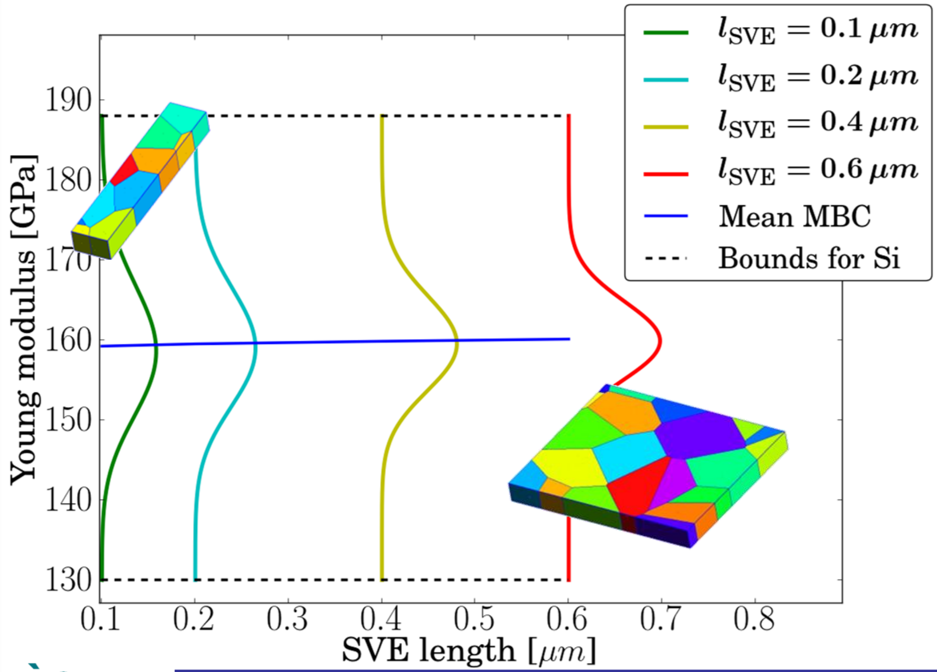

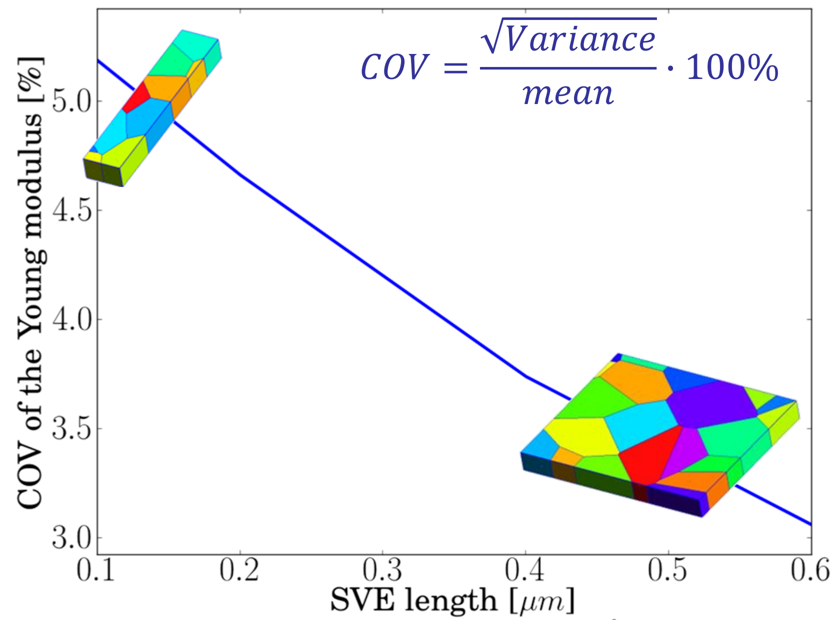

- Application to polycrystalline materials: The meso-scale spatial correlation
  - Use of the window technique

$$R_{\mathbb{C}}^{(rs)}(\boldsymbol{\tau}) = \frac{\mathbb{E}\left[\left(\mathbb{C}^{(r)}(\boldsymbol{x}) - \mathbb{E}\left(\mathbb{C}^{(r)}\right)\right)\left(\mathbb{C}^{(s)}(\boldsymbol{x}+\boldsymbol{\tau}) - \mathbb{E}\left(\mathbb{C}^{(s)}\right)\right)\right]}{\sqrt{\mathbb{E}\left[\left(\mathbb{C}^{(r)} - \mathbb{E}\left(\mathbb{C}^{(r)}\right)\right)^2\right]\mathbb{E}\left[\left(\mathbb{C}^{(s)} - \mathbb{E}\left(\mathbb{C}^{(s)}\right)\right)^2\right]}}$$

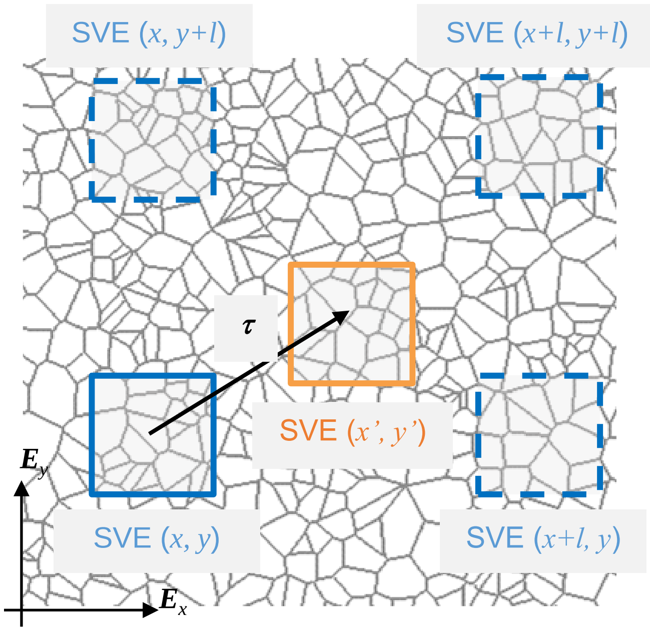

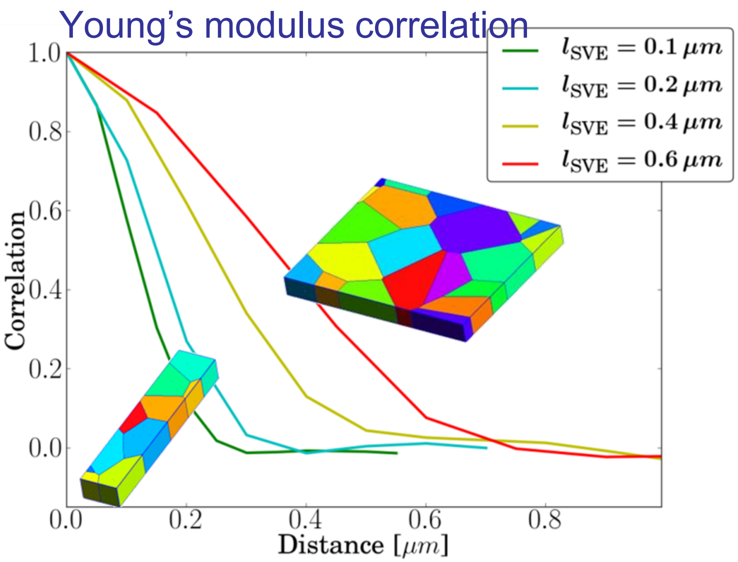

  - Definition of the correlation length $L_{\mathbb{C}}^{(rs)} = \frac{\int_{-\infty}^{\infty} R_{\mathbb{C}}^{(rs)}}{R_{\mathbb{C}}^{(rs)}(0)}$

- Application to polycrystalline materials: The meso-scale random field
  - Accounts for the meso-scale distribution & spatial correlation

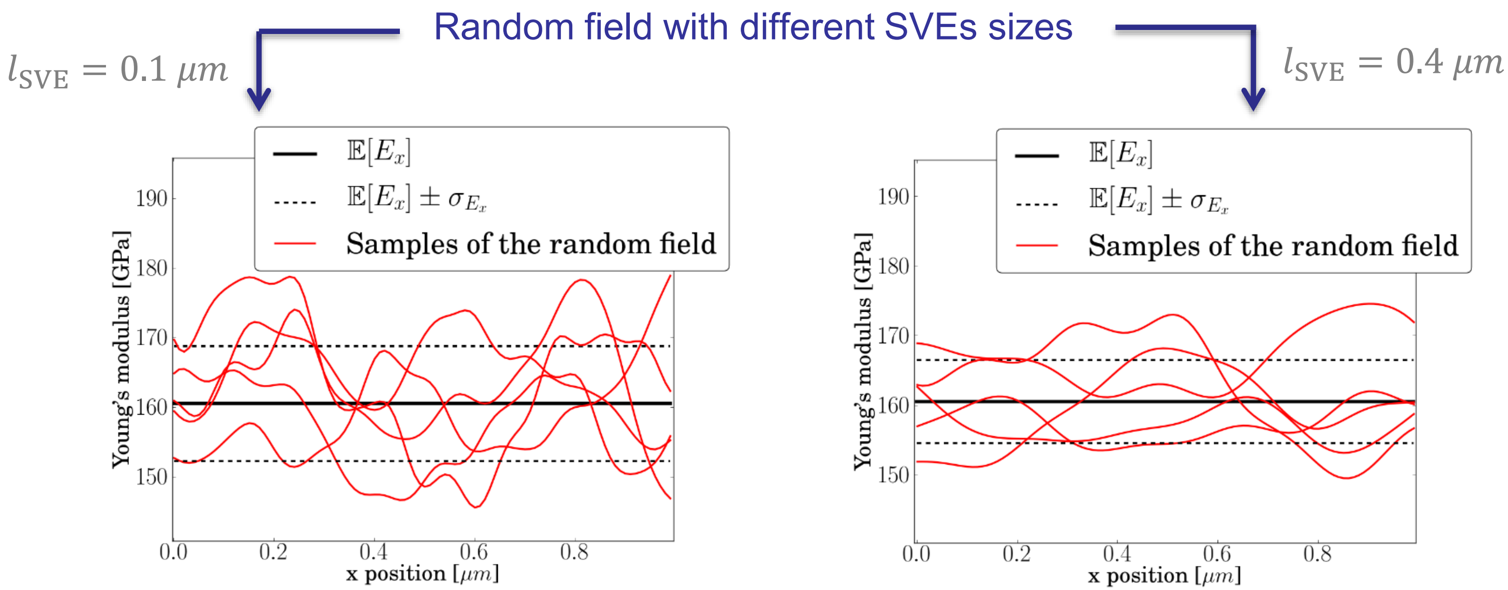

  - Needs to be generated using a stochastic model

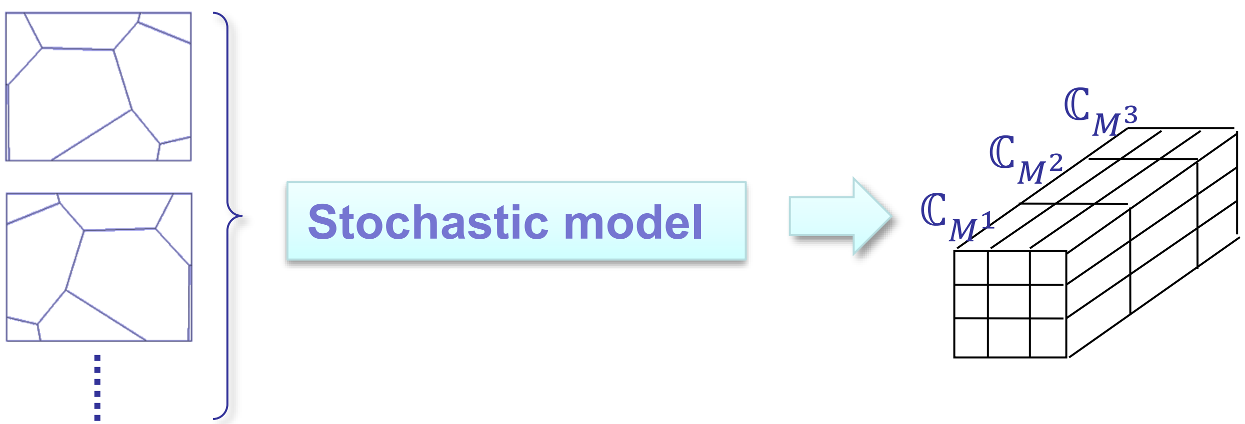

- Stochastic model of Gaussian meso-scale random fields
  - Define the homogenous zero-mean random field $\mathcal{A}'(\boldsymbol{x},\boldsymbol{\theta})$
    - Elasticity tensor $\mathbb{C}_\mathrm{M}(x,\theta)$ (matrix form $\boldsymbol{C}_M$) is bounded

$$\boldsymbol{\varepsilon}:(\mathbb{C}_\mathrm{M}-\mathbb{C}_\mathrm{L}):\boldsymbol{\varepsilon}>0 \qquad \forall\boldsymbol{\varepsilon}$$

    - Use a Cholesky decomposition

$$\boldsymbol{C}_\mathrm{M}(\boldsymbol{x},\boldsymbol{\theta})=\boldsymbol{C}_\mathrm{L}+\left(\bar{\mathcal{A}}+\mathcal{A}'(\boldsymbol{x},\boldsymbol{\theta})\right)^T\left(\bar{\mathcal{A}}+\mathcal{A}'(\boldsymbol{x},\boldsymbol{\theta})\right)$$

  - Evaluate the covariance function

$$\tilde{R}^{(rs)}_{\mathcal{A}'}(\boldsymbol{\tau})=\sigma_{\mathcal{A}'(r)}\sigma_{\mathcal{A}'(s)}R^{(rs)}_{\mathcal{A}'}(\boldsymbol{\tau}) = \mathbb{E}\left[\left(\mathcal{A}'^{(r)}(\boldsymbol{x})\right)\left(\mathcal{A}'^{(s)}(\boldsymbol{x}+\boldsymbol{\tau})\right)\right]$$

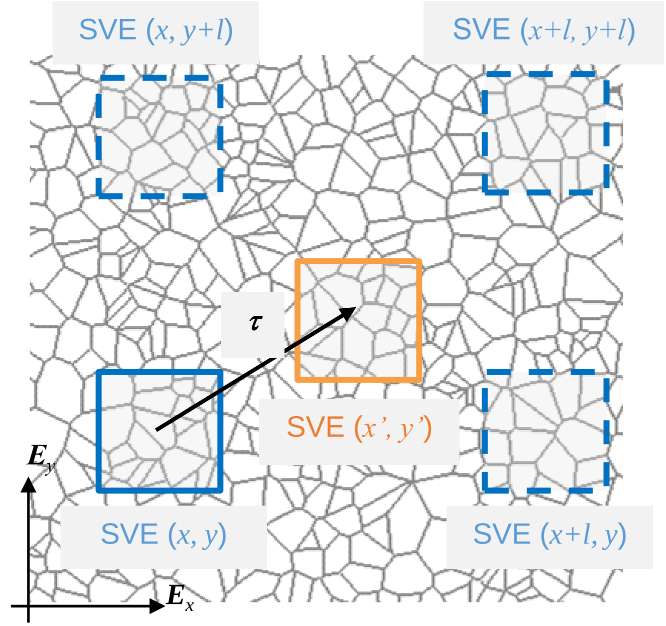

  - Evaluate the spectral density matrix from periodized zero-padded matrix $\tilde{\boldsymbol{R}}^{\mathrm{P}}_{\mathcal{V}'}(\boldsymbol{\tau})$

$$\boldsymbol{S}^{(rs)}_{\mathcal{A}'}\left[\boldsymbol{\omega}^{(\boldsymbol{m})}\right]=\sum_n \tilde{R}^{\mathrm{P}}_{\mathcal{A}'}{}^{(rs)}\left[\boldsymbol{\tau}^{(\boldsymbol{n})}\right]e^{-2\pi i\boldsymbol{\tau}^{(n)}\cdot\boldsymbol{\omega}^{(\boldsymbol{m})}} \;\&\; \boldsymbol{S}_{\mathcal{A}'}\left[\boldsymbol{\omega}^{(\boldsymbol{m})}\right]=\boldsymbol{H}_{\mathcal{A}'}\left[\boldsymbol{\omega}^{(\boldsymbol{m})}\right]\boldsymbol{H}^*_{\mathcal{A}'}\left[\boldsymbol{\omega}^{(\boldsymbol{m})}\right]$$

  - Generate a Gaussian random field $\mathcal{A}'(\boldsymbol{x},\boldsymbol{\theta})$

$$\mathcal{A}'^{(r)}(\boldsymbol{x},\boldsymbol{\theta})=\sqrt{2\Delta\omega}\,\Re\left(\sum_s\sum_{\boldsymbol{m}}\boldsymbol{H}^{(rs)}_{\mathcal{A}'}\left[\boldsymbol{\omega}^{(\boldsymbol{m})}\right]\eta^{(s,\boldsymbol{m})}\,e^{2\pi i\left(\boldsymbol{x}\cdot\boldsymbol{\omega}^{(\boldsymbol{m})}+\boldsymbol{\theta}^{(s,\boldsymbol{m})}\right)}\right)$$

- Stochastic model of non-Gaussian meso-scale random fields
  - Start from micro-sampling of the stochastic homogenization
    - The continuous form of the targeted PSD function

$$\boldsymbol{S}^{\mathrm{T}^{(rs)}}(\boldsymbol{\omega}) = \boldsymbol{\Delta\tau} \boldsymbol{S}_{\mathcal{V}'}^{(rs)}\left[\boldsymbol{\omega}^{(m)}\right] = \boldsymbol{\Delta\tau} \sum_{n} \widetilde{R}^{\mathrm{P}}_{\boldsymbol{\mathcal{A}}'}{}^{(rs)}\left[\boldsymbol{\tau}^{(n)}\right] e^{-2\pi i \boldsymbol{\tau}^{(n)} \cdot \boldsymbol{\omega}^{(m)}}$$

    - The targeted marginal distribution density function $\boldsymbol{F}^{\mathrm{NG}(\boldsymbol{r})}$ of the random variable $\boldsymbol{\mathcal{A}}'^{(\boldsymbol{r})}$
    - A marginal Gaussian distribution $\boldsymbol{F}^{G(\boldsymbol{r})}$ of zero-mean and targeted variance $\boldsymbol{\sigma}_{\boldsymbol{\mathcal{A}}'^{(\boldsymbol{r})}}$
  - Iterate

Generate Gaussian random vector $\boldsymbol{\mathcal{A}}'^{\mathrm{G}}(\boldsymbol{x})$ from $\boldsymbol{S}^{(rs)}(\boldsymbol{\omega})$

Map $\boldsymbol{\mathcal{A}}'^{G}(\boldsymbol{x})$ to a non-Gaussian field:

$$\boldsymbol{\mathcal{A}}'^{\mathrm{NG}^{(\boldsymbol{r})}}(\boldsymbol{x}) = \boldsymbol{F}^{\mathrm{NG}(\boldsymbol{r})^{-1}}\left(\boldsymbol{F}^{\mathrm{G}(\boldsymbol{r})}\left(\boldsymbol{\mathcal{A}}'^{\mathrm{G}^{(\boldsymbol{r})}}(\boldsymbol{x})\right)\right)$$

Evaluate the PSD $\boldsymbol{S}^{\mathrm{NG}^{(rs)}}(\boldsymbol{\omega})$ of $\boldsymbol{\mathcal{V}}^{\mathrm{NG}}(\boldsymbol{x})$

$\boldsymbol{S}^{\mathrm{NG}^{(rs)}} \simeq \boldsymbol{S}^{\mathrm{T}^{(rs)}}$?

No

$$\boldsymbol{S}^{(rs)}(\boldsymbol{\omega}) \leftarrow \boldsymbol{S}^{(rs)}(\boldsymbol{\omega}) \frac{\boldsymbol{S}^{\mathrm{T}^{(rr)}}(\boldsymbol{\omega})\boldsymbol{S}^{\mathrm{T}^{(ss)}}(\boldsymbol{\omega})}{\boldsymbol{S}^{\mathrm{NG}^{(rr)}}(\boldsymbol{\omega})\boldsymbol{S}^{\mathrm{NG}^{(ss)}}(\boldsymbol{\omega})}$$

- The meso-scale stochastic model
  - Application to film deposited at 610 ºC:
  - Comparison between micro-samples and generated fields

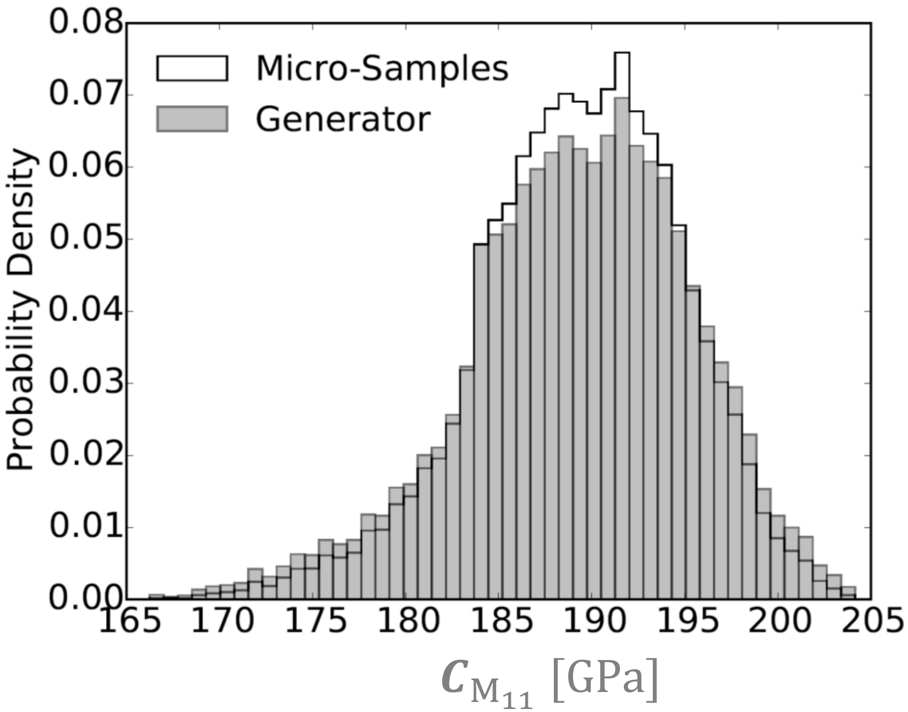

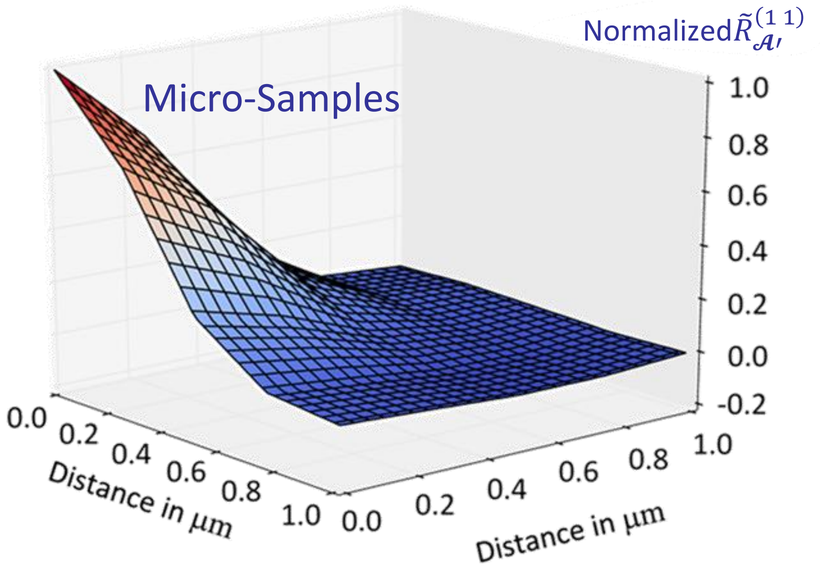

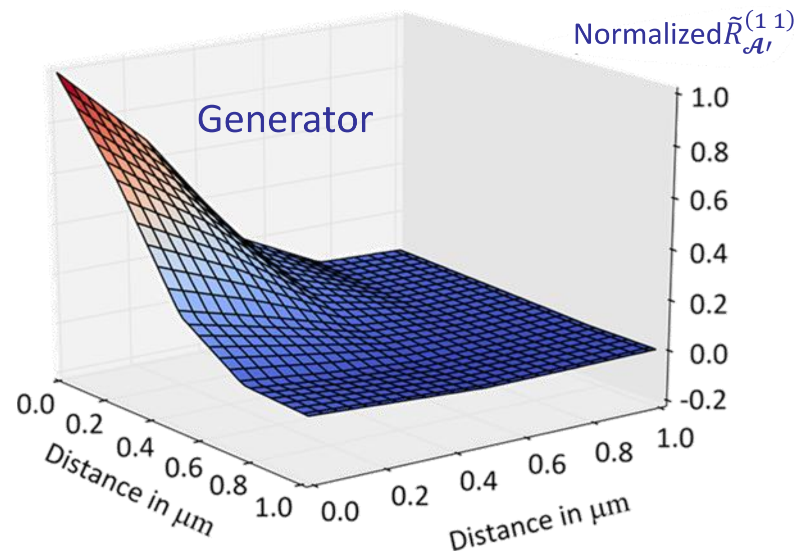

- Application to polycrystalline materials: The meso-scale to macro-scale transition
  - Convergence in terms of $\alpha = \frac{l_{\mathbb{C}}}{l_{\text{mesh}}}$, the correlation length and macro-mesh ratio
  - The results converge
    - With the mesh size for all the SVE sizes
    - Toward the direct Monte Carlo simulations results

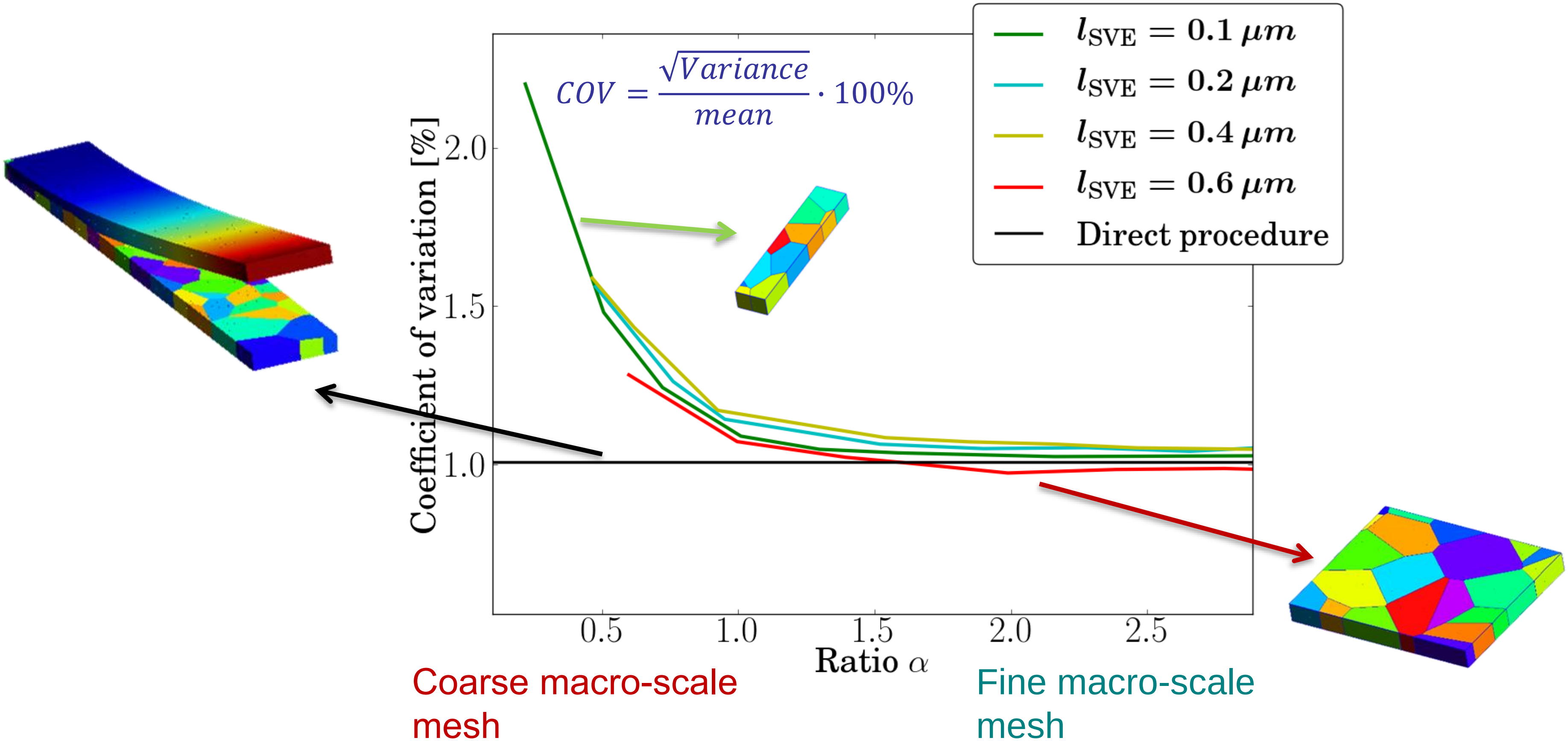

- Application to polycrystalline materials: The meso-scale to macro-scale transition
  - Comparison with direct Monte Carlo simulations

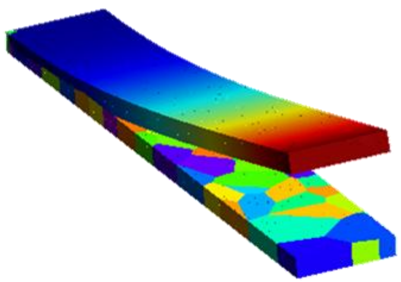

Relative difference in the mean: 0.57 %

Eigen frequency

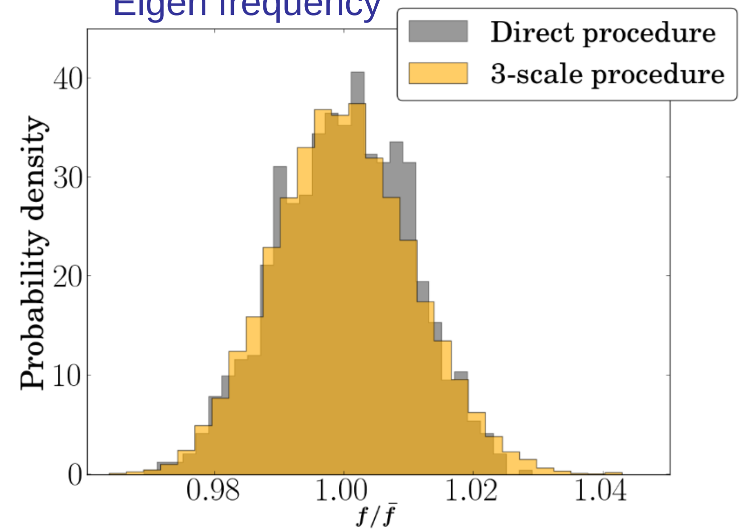

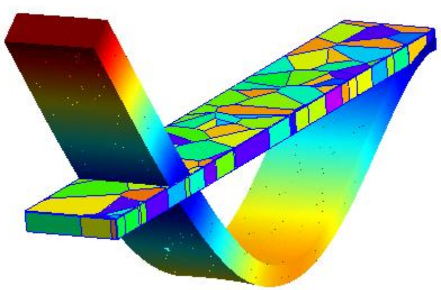

Relative difference in the mean: 0.44 %

Eigen frequency

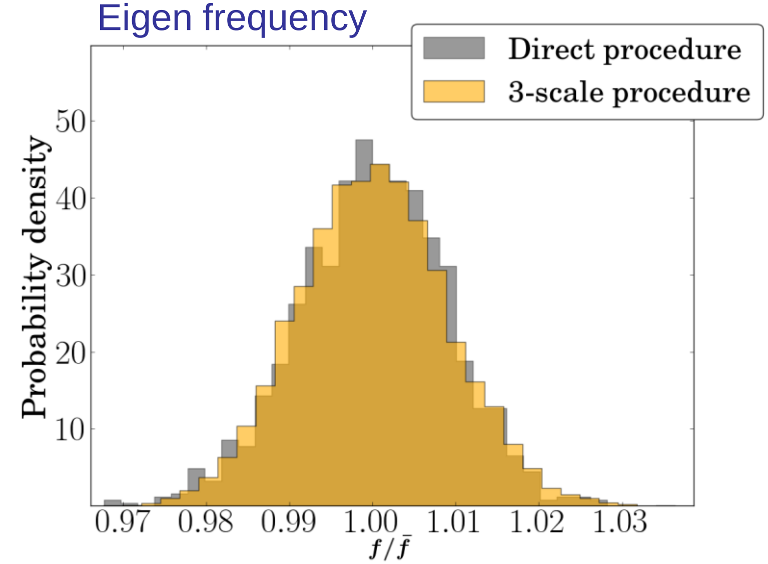

- Thermo-mechanical homogenization
  - Down-scaling

$$\begin{cases} \boldsymbol{\varepsilon}_{\mathrm{M}} = \dfrac{1}{V(\omega)} \displaystyle\int_{\omega} \boldsymbol{\varepsilon}_{\mathrm{m}} d\omega \\ \nabla_{\mathrm{M}} \vartheta_{\mathrm{M}} = \dfrac{1}{V(\omega)} \displaystyle\int_{\omega} \nabla_{\mathrm{m}} \vartheta_{\mathrm{m}} d\omega \\ \vartheta_{\mathrm{M}} = \dfrac{1}{V(\omega)} \displaystyle\int_{\omega} \dfrac{\rho_{\mathrm{m}} C_{v\mathrm{m}}}{\rho_{\mathrm{M}} C_{v\mathrm{M}}} \vartheta_{\mathrm{m}} d\omega \end{cases}$$

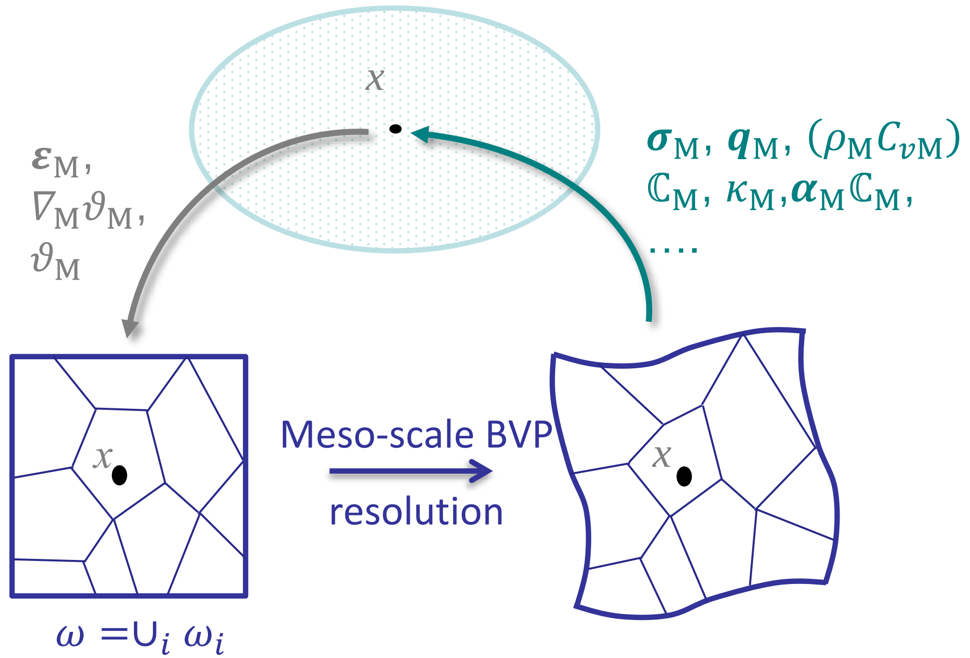

  - Up-scaling

$$\begin{cases} \boldsymbol{\sigma}_{\mathrm{M}} = \dfrac{1}{V(\omega)} \displaystyle\int_{\omega} \boldsymbol{\sigma}_{\mathrm{m}} d\omega \\ \boldsymbol{q}_{\mathrm{M}} = \dfrac{1}{V(\omega)} \displaystyle\int_{\omega} \boldsymbol{q}_{\mathrm{m}} d\omega \\ \rho_{\mathrm{M}} C_{v\mathrm{M}} = \dfrac{1}{V(\omega)} \displaystyle\int \rho_{\mathrm{m}} C_{v\mathrm{m}} dV \end{cases} \longrightarrow \begin{cases} \mathbb{C}_{\mathrm{M}} = \dfrac{\partial \boldsymbol{\sigma}_{\mathrm{M}}}{\partial \boldsymbol{u}_{\mathrm{M}} \otimes \boldsymbol{\nabla}_{\mathrm{M}}} \quad \& \quad \boldsymbol{\alpha}_{\mathrm{M}} : \mathbb{C}_{\mathrm{M}} = -\dfrac{\partial \boldsymbol{\sigma}_{\mathrm{M}}}{\partial \vartheta_{\mathrm{M}}} \\ \boldsymbol{\kappa}_{\mathrm{M}} = -\dfrac{\partial \boldsymbol{q}_{\mathrm{M}}}{\partial \nabla_{\mathrm{M}} \vartheta_{\mathrm{M}}} \end{cases}$$

  - Consistency → Satisfied by periodic boundary conditions

Stochastic 3-Scale Models

- Quality factor
  - Micro-resonators
    - Temperature changes with compression/traction
    - Energy dissipation

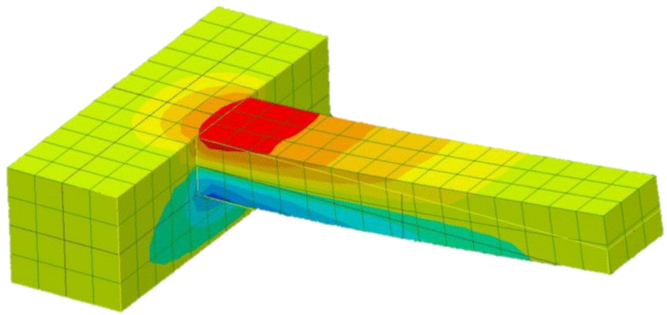

  - Eigen values problem
    - Governing equations

$$\begin{bmatrix} \mathbf{M} & \mathbf{0} \\ \mathbf{0} & \mathbf{0} \end{bmatrix} \begin{bmatrix} \ddot{\mathbf{u}} \\ \ddot{\boldsymbol{\vartheta}} \end{bmatrix} + \begin{bmatrix} \mathbf{0} & \mathbf{0} \\ \mathbf{D}_{\mathrm{u}\vartheta}(\boldsymbol{\theta}) & \mathbf{D}_{\vartheta\vartheta} \end{bmatrix} \begin{bmatrix} \dot{\mathbf{u}} \\ \dot{\boldsymbol{\vartheta}} \end{bmatrix} + \begin{bmatrix} \mathbf{K}_{\mathrm{uu}}(\boldsymbol{\theta}) & \mathbf{K}_{\mathrm{u}\vartheta}(\boldsymbol{\theta}) \\ \mathbf{0} & \mathbf{K}_{\vartheta\vartheta}(\boldsymbol{\theta}) \end{bmatrix} \begin{bmatrix} \mathbf{u} \\ \boldsymbol{\vartheta} \end{bmatrix} = \begin{bmatrix} \boldsymbol{F}_{\mathrm{u}} \\ \boldsymbol{F}_{\vartheta} \end{bmatrix}$$

    - Free vibrating problem

$$\begin{bmatrix} \mathbf{u}(t) \\ \boldsymbol{\vartheta}(t) \end{bmatrix} = \begin{bmatrix} \mathbf{u}_0 \\ \boldsymbol{\vartheta}_0 \end{bmatrix} e^{i\omega t}$$

$$\begin{bmatrix} -\mathbf{K}_{\mathrm{uu}}(\boldsymbol{\theta}) & -\mathbf{K}_{\mathrm{u}\vartheta}(\boldsymbol{\theta}) & \mathbf{0} \\ \mathbf{0} & -\mathbf{K}_{\vartheta\vartheta}(\boldsymbol{\theta}) & \mathbf{0} \\ \mathbf{0} & \mathbf{0} & \mathbf{I} \end{bmatrix} \begin{bmatrix} \mathbf{u} \\ \boldsymbol{\vartheta} \\ \dot{\mathbf{u}} \end{bmatrix} = i\omega \begin{bmatrix} \mathbf{0} & \mathbf{0} & \mathbf{M} \\ \mathbf{D}_{\vartheta\mathrm{u}}(\boldsymbol{\theta}) & \mathbf{D}_{\vartheta\vartheta} & \mathbf{0} \\ \mathbf{I} & \mathbf{0} & \mathbf{0} \end{bmatrix} \begin{bmatrix} \mathbf{u} \\ \boldsymbol{\vartheta} \\ \dot{\mathbf{u}} \end{bmatrix}$$

  - Quality factor
    - From the dissipated energy per cycle
    - $Q^{-1} = \dfrac{2|\mathfrak{I}\omega\,|}{\sqrt{(\mathfrak{I}\omega)^2 + (\mathfrak{R}\omega)^2}}$

- Application of the 3-Scale method to extract the quality factor distribution
  - 3D models readily available
  - The effect of the anchor can be studied

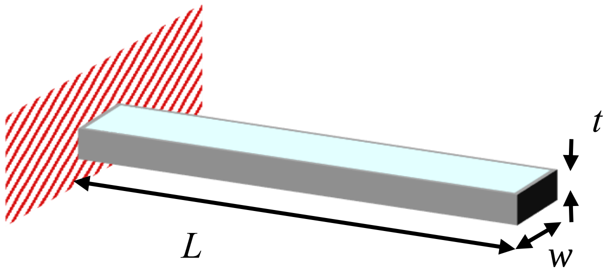

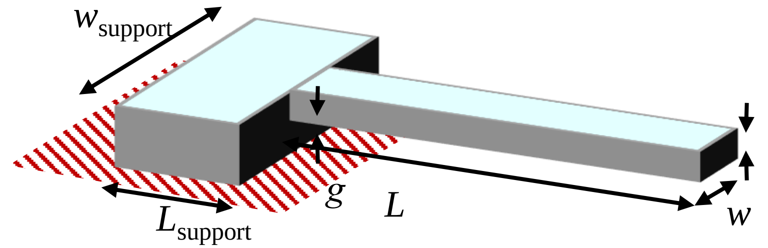

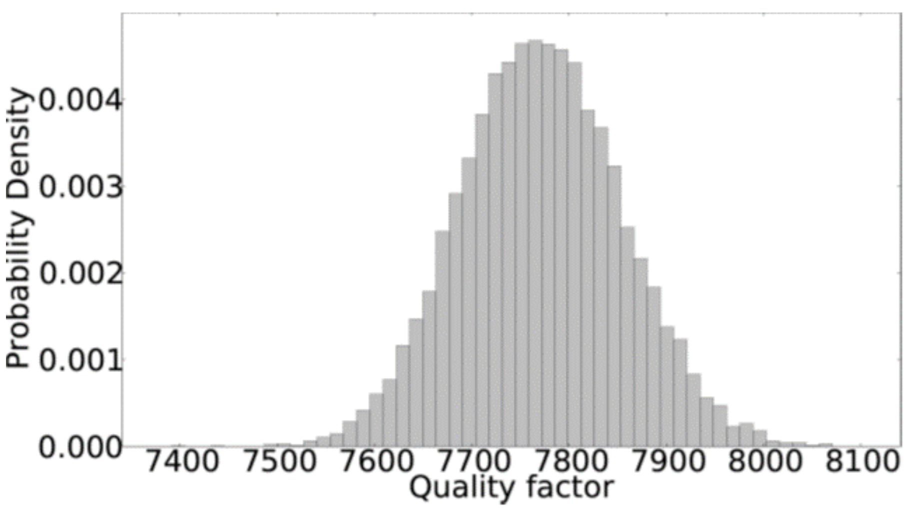

15 x 3 x 2 μm^3-beam,

deposited at 610 ºC

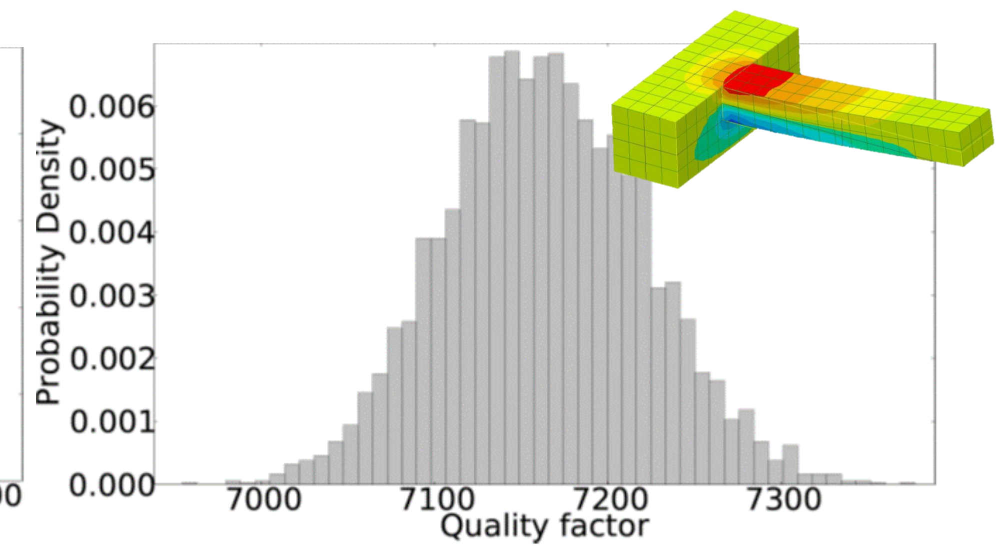

15 x 3 x 2 μm^3-beam & anchor,

deposited at 610 ºC

- Surface topology: asperity distribution
  - Upper surface topology by AFM (Atomic Force Microscope) measurements on 2 µm-thick poly-silicon films

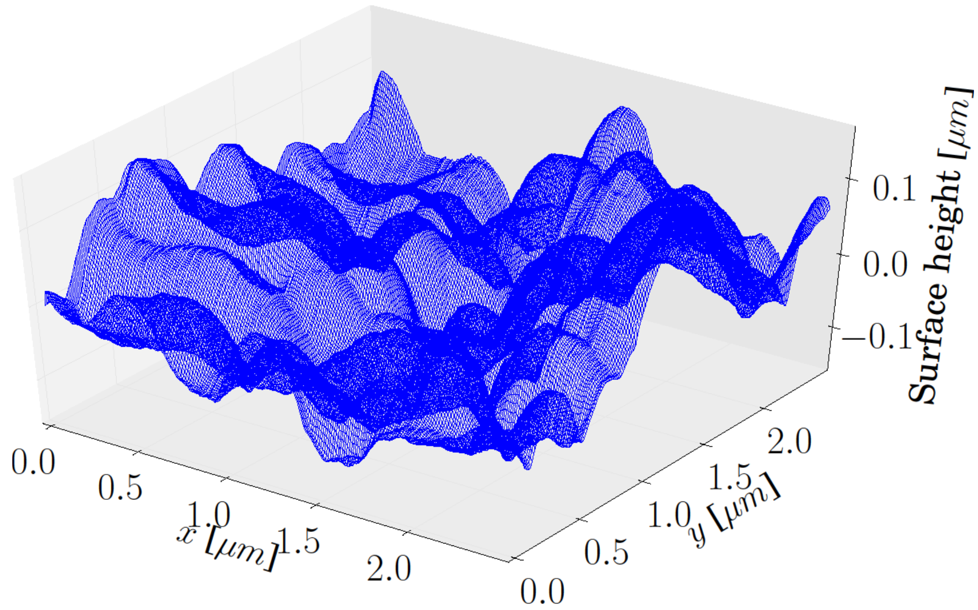

Deposition temperature [°C]	580	610	630	650
Std deviation [nm]	35.6	60.3	90.7	88.3

AFM data provided by IMT Bucharest, Rodica Voicu, Angela Baracu, Raluca Muller

- Accounting for roughness
  - Second-order homogenization

$$\begin{cases} \tilde{\boldsymbol{n}}_{\mathrm{M}} = \mathbb{C}_{\mathrm{M}_1} : \boldsymbol{\varepsilon}_{\mathrm{M}} + \mathbb{C}_{\mathrm{M}_2} : \boldsymbol{\kappa}_{\mathrm{M}} \\ \tilde{\boldsymbol{m}}_{\mathrm{M}} = \mathbb{C}_{\mathrm{M}_3} : \boldsymbol{\varepsilon}_{\mathrm{M}} + \mathbb{C}_{\mathrm{M}_4} : \boldsymbol{\kappa}_{\mathrm{M}} \end{cases}$$

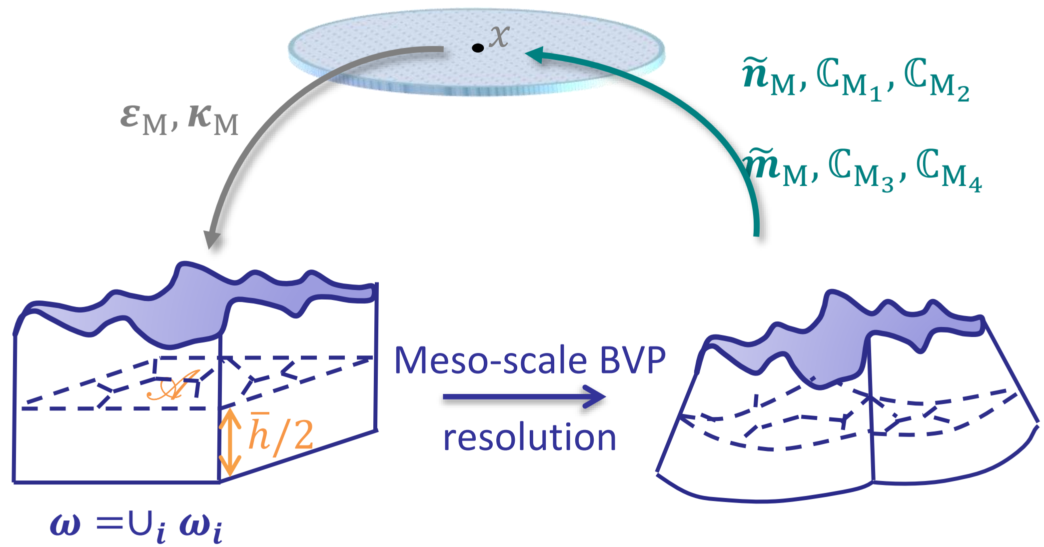

  - Stochastic homogenization
    - Several SVE realizations
    - For each SVE $\omega_j = \cup_i \omega_i$
    - The density per unit area is now non-constant

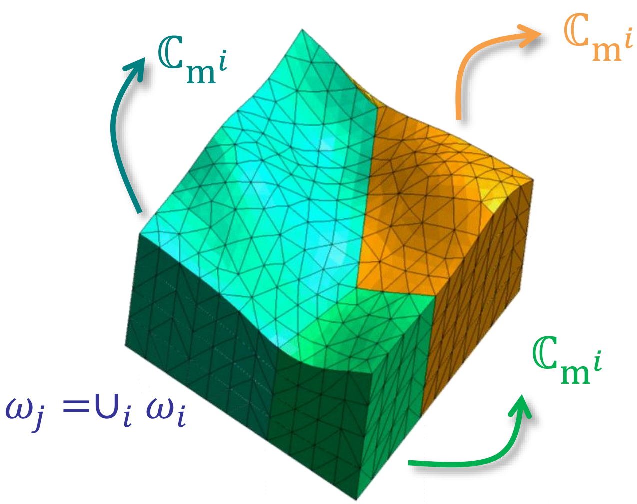

$\mathbb{C}_{\mathrm{m}^i}\ \forall i \longrightarrow \mathbb{C}_{\mathrm{M}_1^j}, \mathbb{C}_{\mathrm{M}_2^j}, \mathbb{C}_{\mathrm{M}_3^j}, \mathbb{C}_{\mathrm{M}_4^j} \longrightarrow \mathrm{U}_{\mathrm{M}^j}$

Computational homogenization

$\bar{\boldsymbol{\rho}}_{\mathrm{M}^j}$

Samples of the meso-scale homogenized elasticity matrix U_{M} & density $\bar{\boldsymbol{\rho}}_{\mathrm{M}}$

Stochastic 3-Scale Models

- Accounting for roughness
  - Cantilever of 8 x 3 x t $\mu\mathrm{m}^3$ deposited at 610 ºC

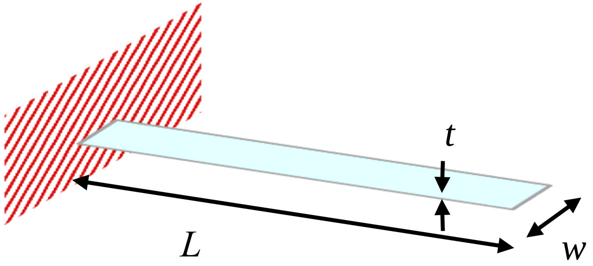

Flat SVEs (no roughness) - F

Rough SVEs (Polysilicon film deposited at 610 ºC) - R

Grain orientation following XRD measurements – Si_{pref}

Grain orientation uniformly distributed – Si_{uni}

Reference isotropic material – Iso

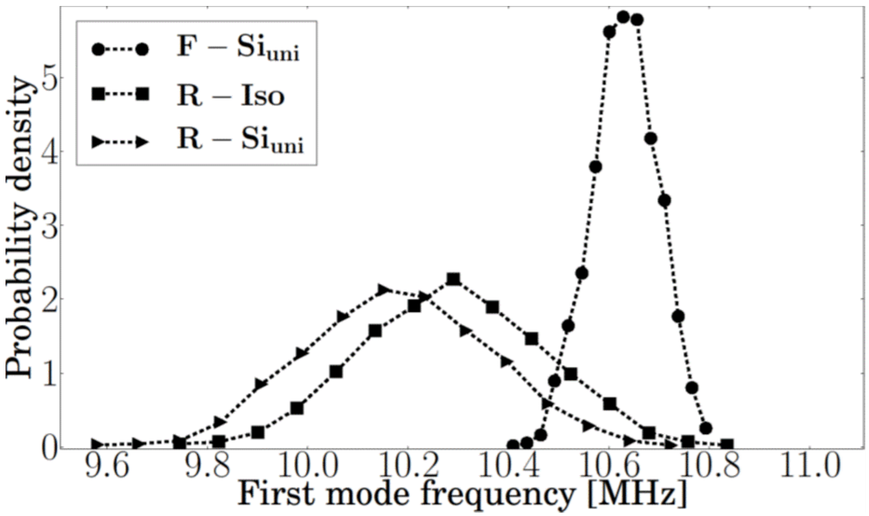

Roughness effect is the most important for 8 x 3 x 0.5 $\mu\mathrm{m}^3$ cantilevers

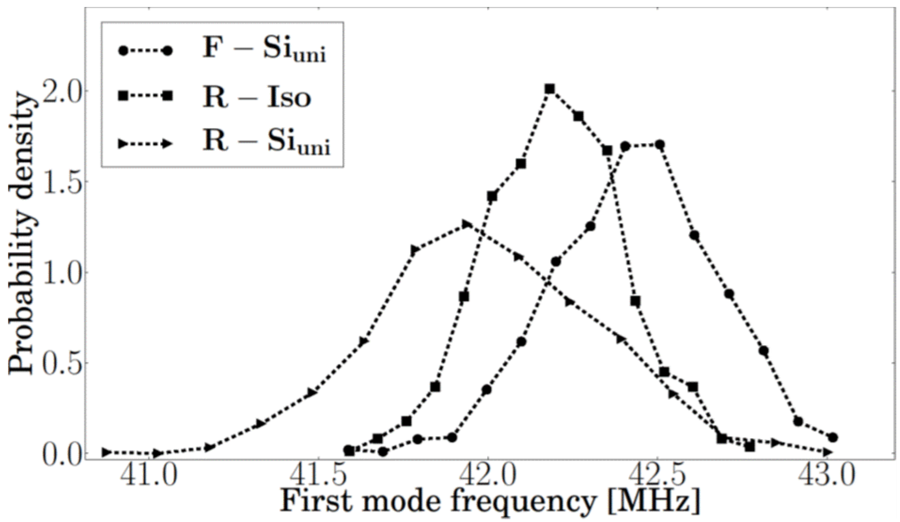

Roughness effect is of same importance as orientation for 8 x 3 x 2 $\mu\mathrm{m}^3$ cantilevers

- Application to robust design
  - Determination of probabilistic meso-scale properties
  - Propagate uncertainties to higher scale
  - Vibro-meter sensors:
    - Uncertainties in resonance frequency / Q factor

- 3SMVIB MNT.ERA-NET project
  - Open-Engineering, V2i, ULiège (Belgium)
  - Polit. Warszawska (Poland)
  - IMT, Univ. Cluj-Napoca (Romania)

- Publications (doi)
  - 10.1002/nme.5452
  - 10.1016/j.cma.2016.07.042
  - 10.1016/j.cma.2015.05.019

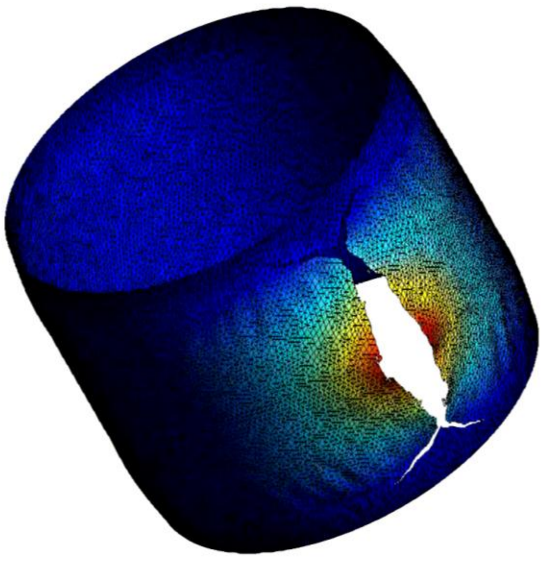

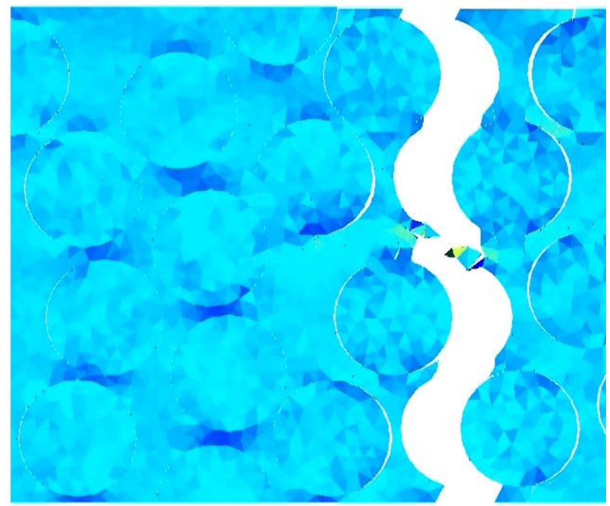

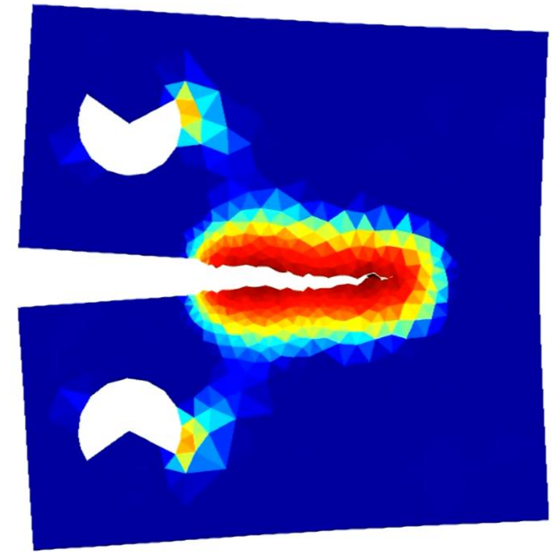

DG-Based (Multi-Scale) Fracture

The research has been funded by the Belgian National Fund for Education at the Research in Industry and Farming.
SIMUCOMP The research has been funded by the Walloon Region under the agreement no 1017232 (CT-EUC 2010-10-12) in the context of the ERA-NET +, Matera + framework.
The research has been funded by the Walloon Region under the agreement no.7581-MRIPF in the context of the 16th MECATECH call.

DG-Based Fracture

- Hybrid DG/cohesive law formulation
  - Discontinuous Galerkin method
    - Finite-element discretization
    - Same **discontinuous** polynomial approximations for the
      - **Test** functions φ_h and
      - **Trial** functions $\delta\varphi$
  - Can easily be combined with a cohesive law for fracture analyses
    - Interface elements already exist
    - Easy to shift from un-fractured to fractured states
    - Remains accurate before fracture onset (DG formulation)
    - Efficient // implementation
- Publications (doi)
  - [10.1016/j.cma.2010.08.014](10.1016/j.cma.2010.08.014)

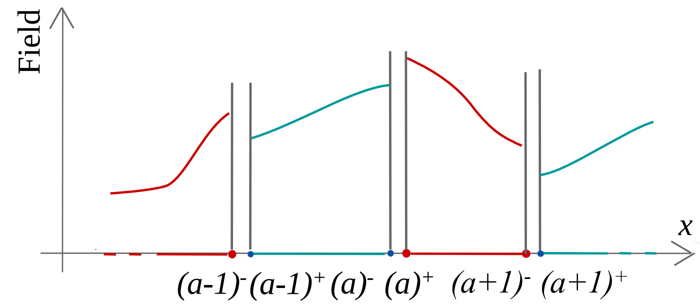

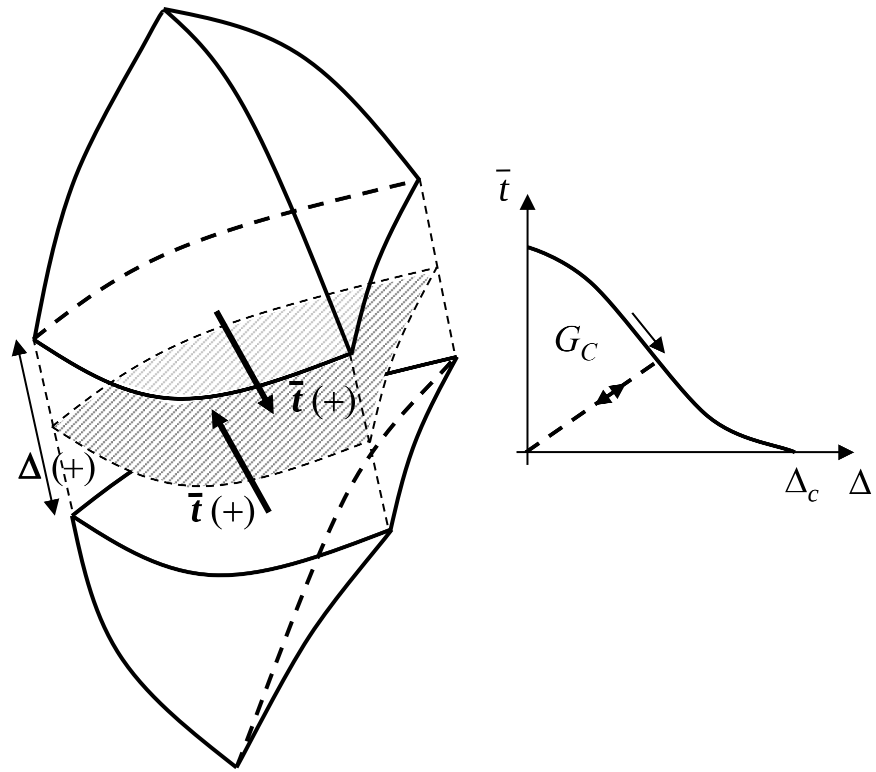

DG-Based Multi-Scale Fracture

- Multi-scale modeling
  - 2 problems are solved concurrently
    - The macro-scale problem
    - The meso-scale problem
      (on a meso-scale
      Volume Element)

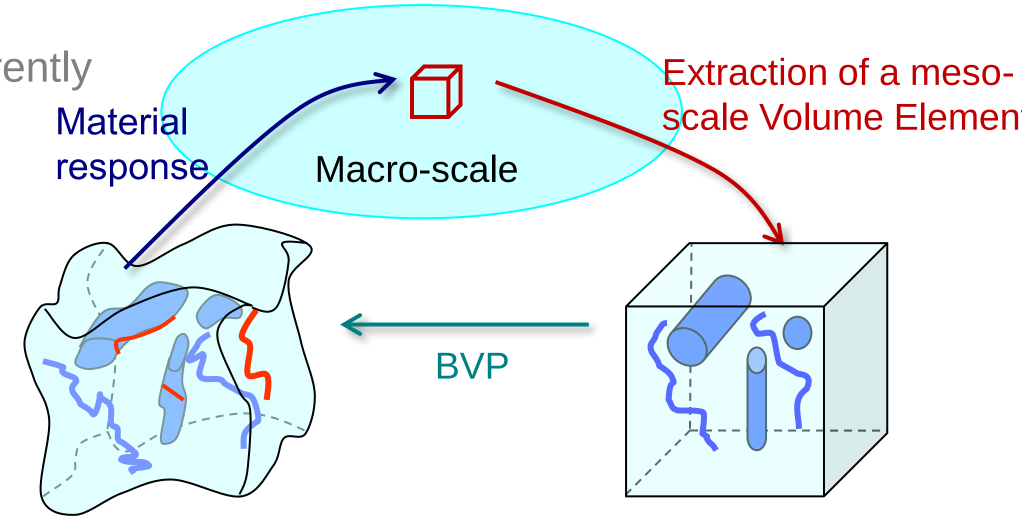

- For meso-scale volume elements embedding crack propagation

$L_{\text{macro}} >> L_{\text{VE}} \ ? \ L_{\text{micro}}$

For accuracy: Size of the meso-scale volume element smaller than the characteristic length of the macro-scale loading

The crack induces a loss of statistical representativeness
- **Should recover consistency lost due to the discontinuity**

DG-Based Multi-Scale Fracture

- Micro-Meso fracture model for intra-laminar failure
  - Epoxy-CF (60%), transverse loading
  - 3 stages captured

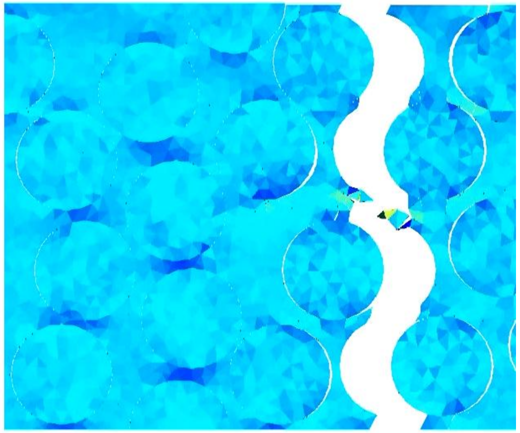

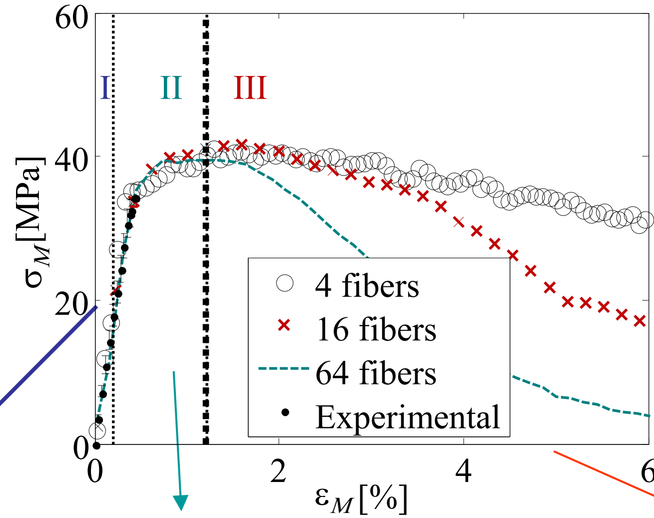

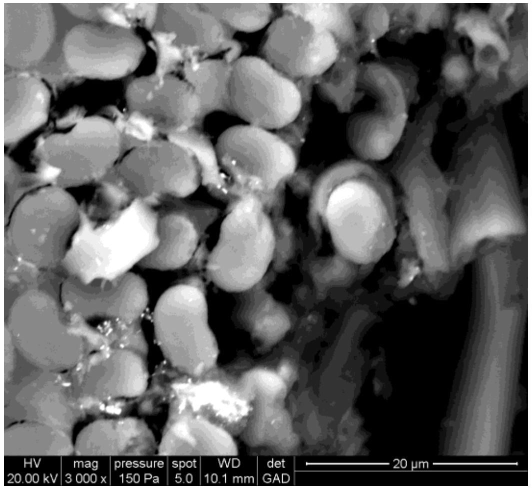

Elastic response

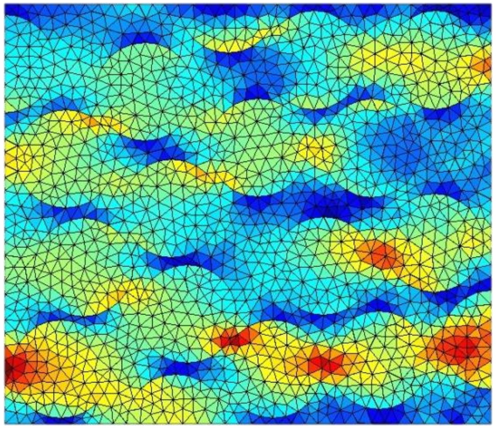

Damage due to debonding

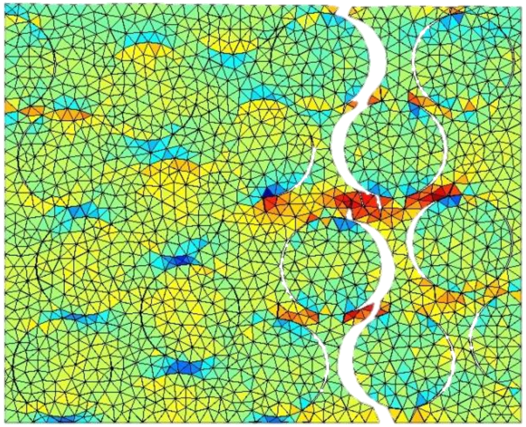

Meso-crack

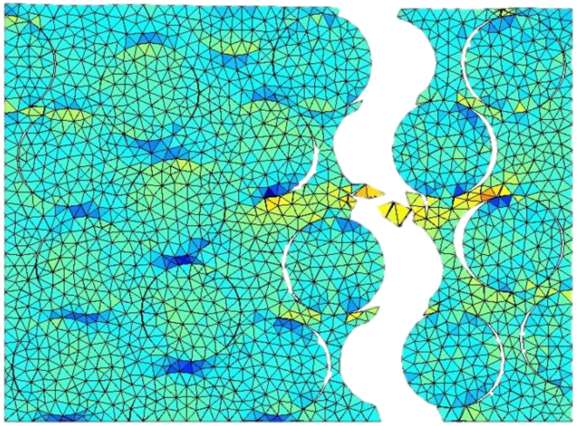

- Micro-Meso fracture model for intra-laminar failure (2)
  - Scale transition after softening onset
    - Should not depend on the RVE size
    - Extraction of the meso-scale TSL ($\bar{t}_M$ vs. Δ_M)

[Verhoosel et al., IJNME 2010]

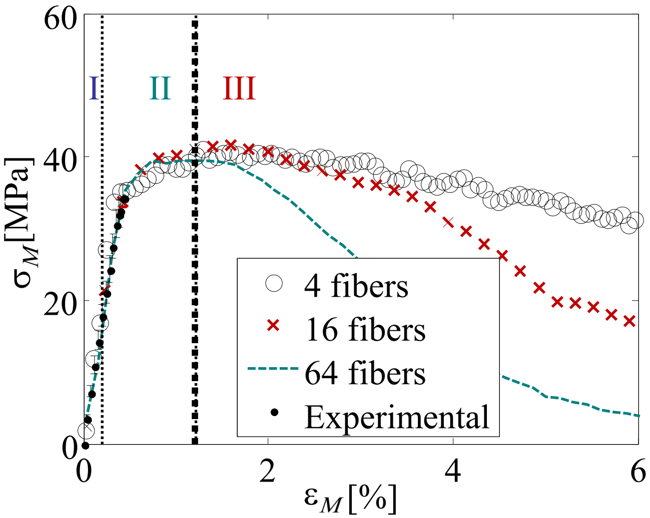

$$\delta\bar{t}_M = \boldsymbol{\delta\sigma_M} \cdot \boldsymbol{e_X}$$

$$\delta\boldsymbol{\Delta}_M = \delta\boldsymbol{u}^m - L_{\text{cell}}\boldsymbol{C_M}^{-1}:\boldsymbol{e_X} \otimes \boldsymbol{e_X} \cdot \boldsymbol{\delta\bar{t}}_M$$

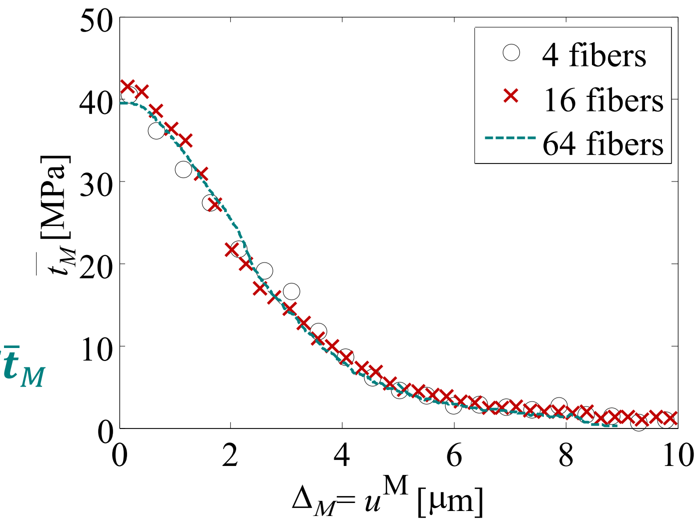

- SIMUCOMP ERA-NET project
  - e-Xstream, CENAERO, ULiège (Belgium)
  - IMDEA Materials (Spain)
  - CRP Henri-Tudor (Luxemburg)
- Publication (doi)
  - 10.1016/j.engfracmech.2013.03.018

DG-Based Dynamic Fracture

- Fracture of thin structures

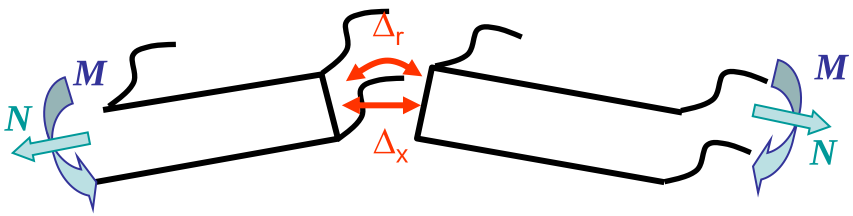

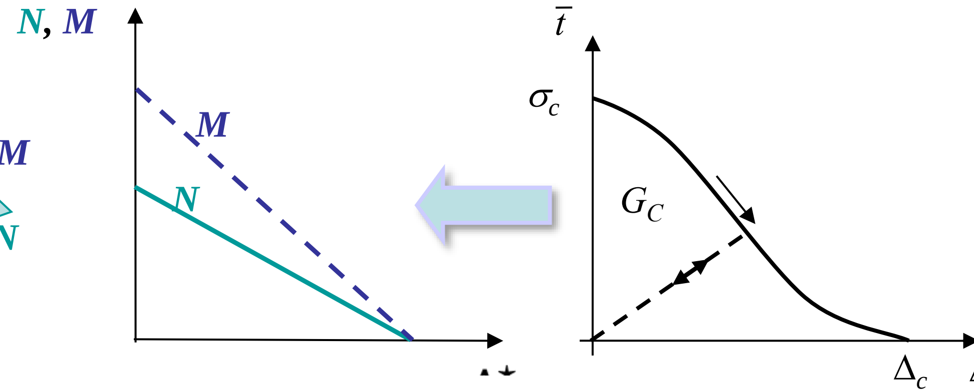

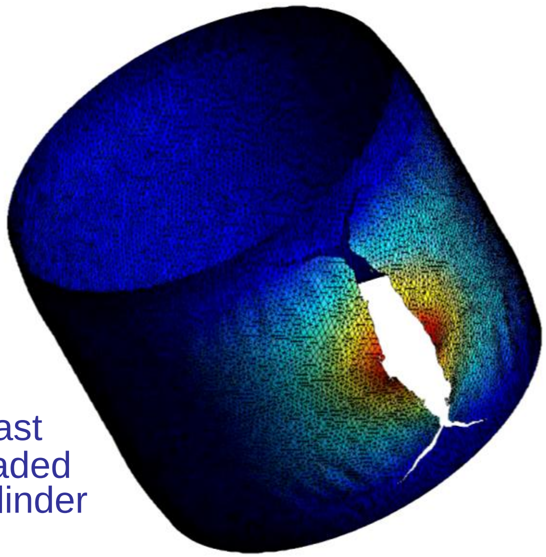

Blast loaded cylinder

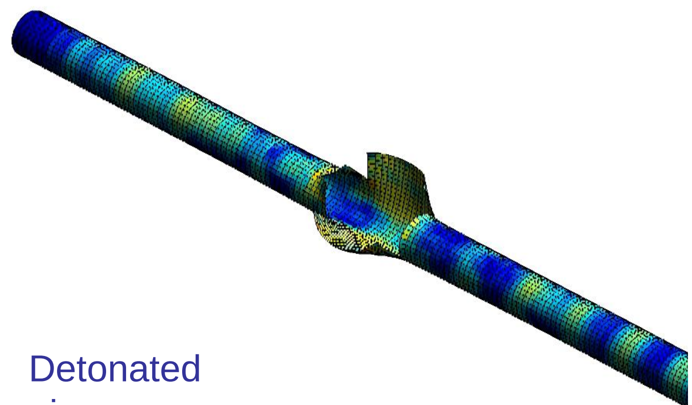

Detonated pipe

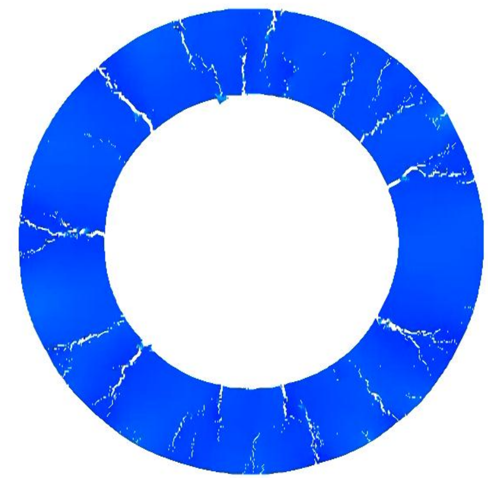

Fragmented disk

- FNRS-FRIA fellowship
- Publications (doi)
  - [10.1002/nme.4381](10.1002/nme.4381)
  - [10.1007/s10704-012-9748-5](10.1007/s10704-012-9748-5)
  - [10.1016/j.cma.2011.07.008](10.1016/j.cma.2011.07.008)
  - [10.1002/nme.3008](10.1002/nme.3008)

DG-Based elastic damage to crack transition

- Capture triaxiality effects: Cohesive Band Model (CBM)
  - Introduction of a uniform band of given thickness h_b [Remmers et al. 2013]

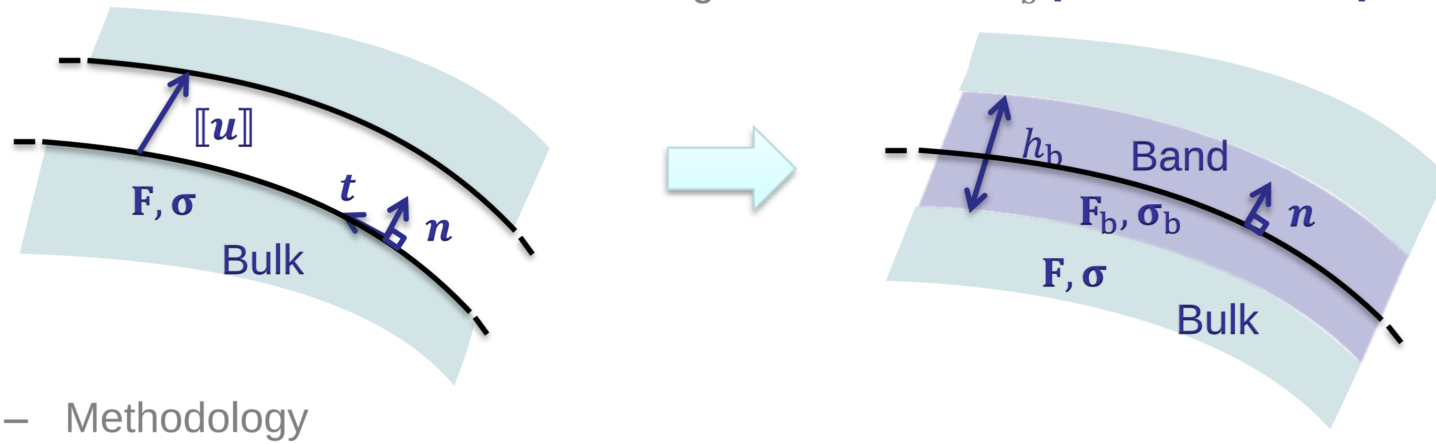

  - Methodology
    1. Bulk stress $\boldsymbol{\sigma}$ using non-local damage law
    2. Compute a “band” deformation gradient

$$\mathbf{F}_\mathrm{b} = \mathbf{F} + \frac{[\![\boldsymbol{u}]\!] \otimes \boldsymbol{N}}{h_\mathrm{b}} + \frac{1}{2} \boldsymbol{\nabla}_T [\![\boldsymbol{u}]\!]$$

    3. Band stress $\boldsymbol{\sigma}_\mathrm{b}$ using the (local) damage law
    4. Recover traction forces $\boldsymbol{t}([\![\boldsymbol{u}]\!], \mathbf{F}) = \boldsymbol{\sigma}_\mathrm{b} . \boldsymbol{n}$

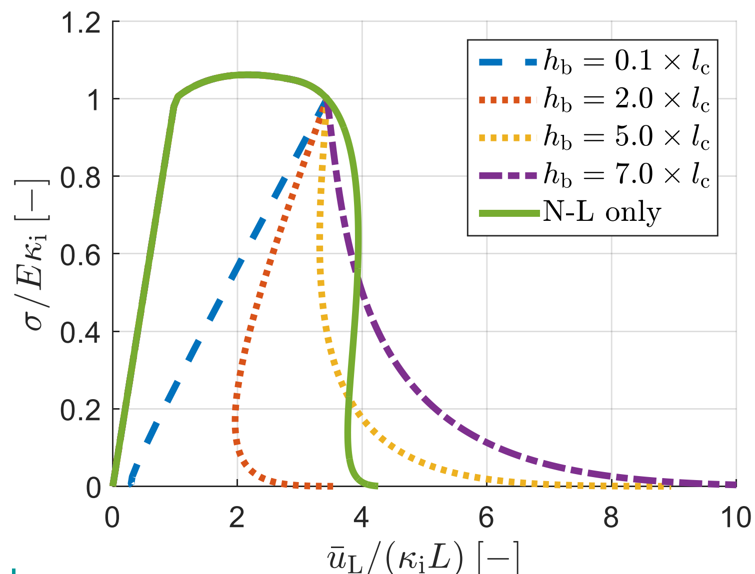

  - The cohesive band thickness
    - Evaluated to ensure energy consistency
    - Same dissipated energy as with a damage model

- Slit plate

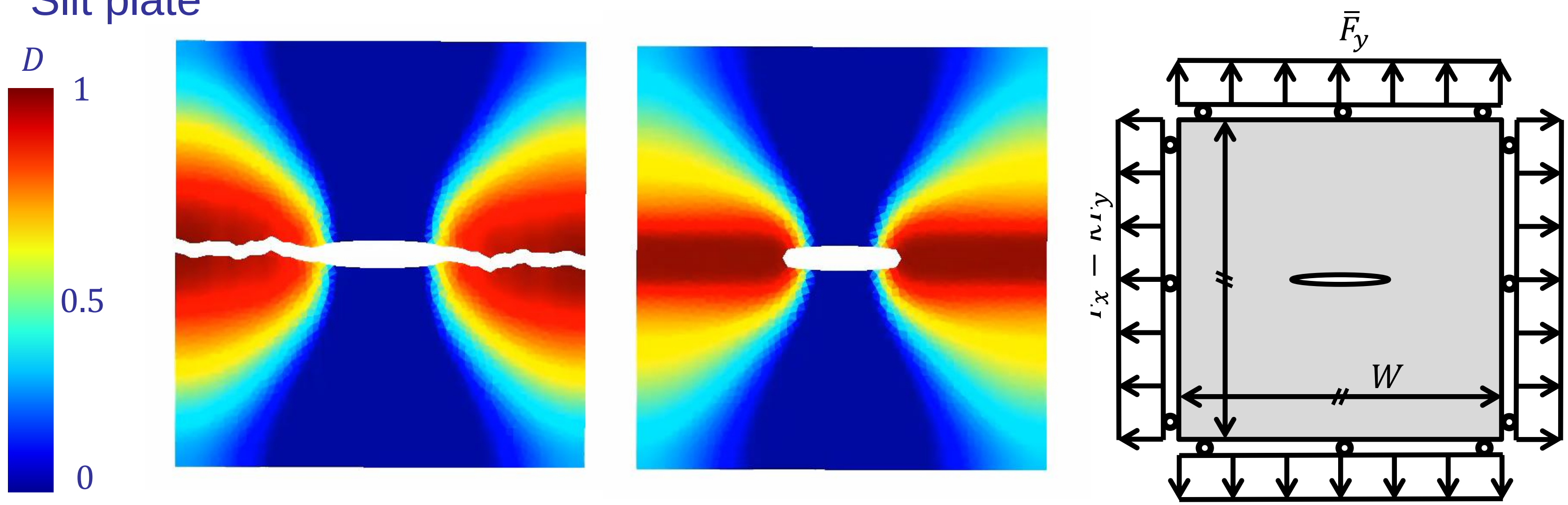

Non-Local+ CBM

Non-Local

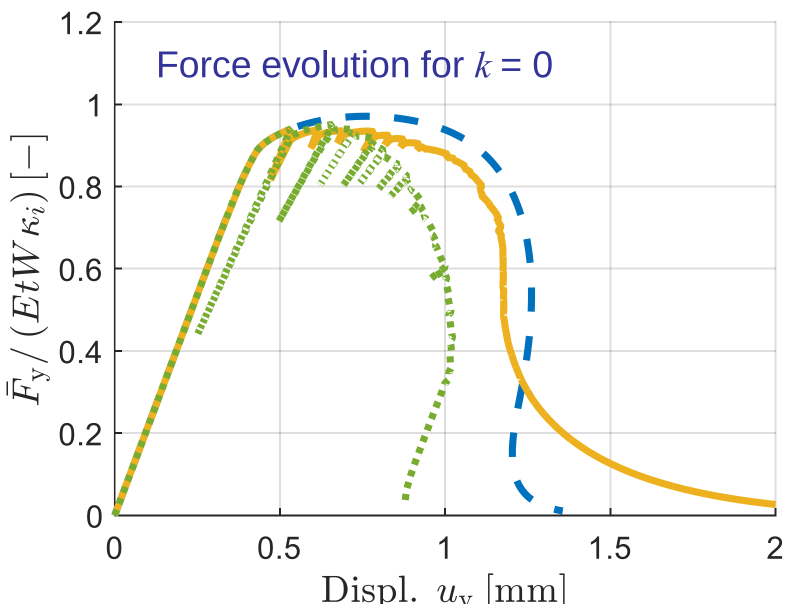

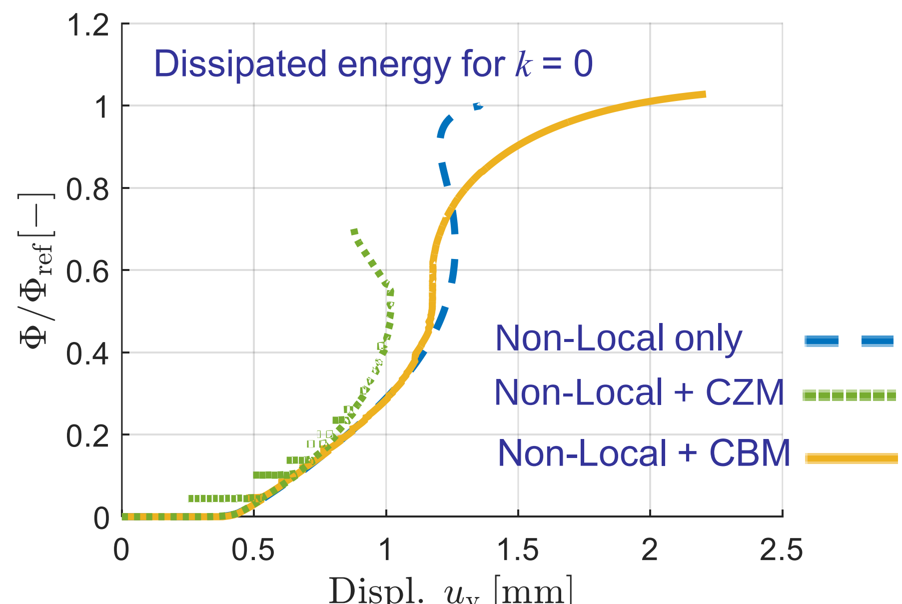

DG-Based elastic damage to crack transition

- Slit plate
  - Triaxiality effect through ratio k

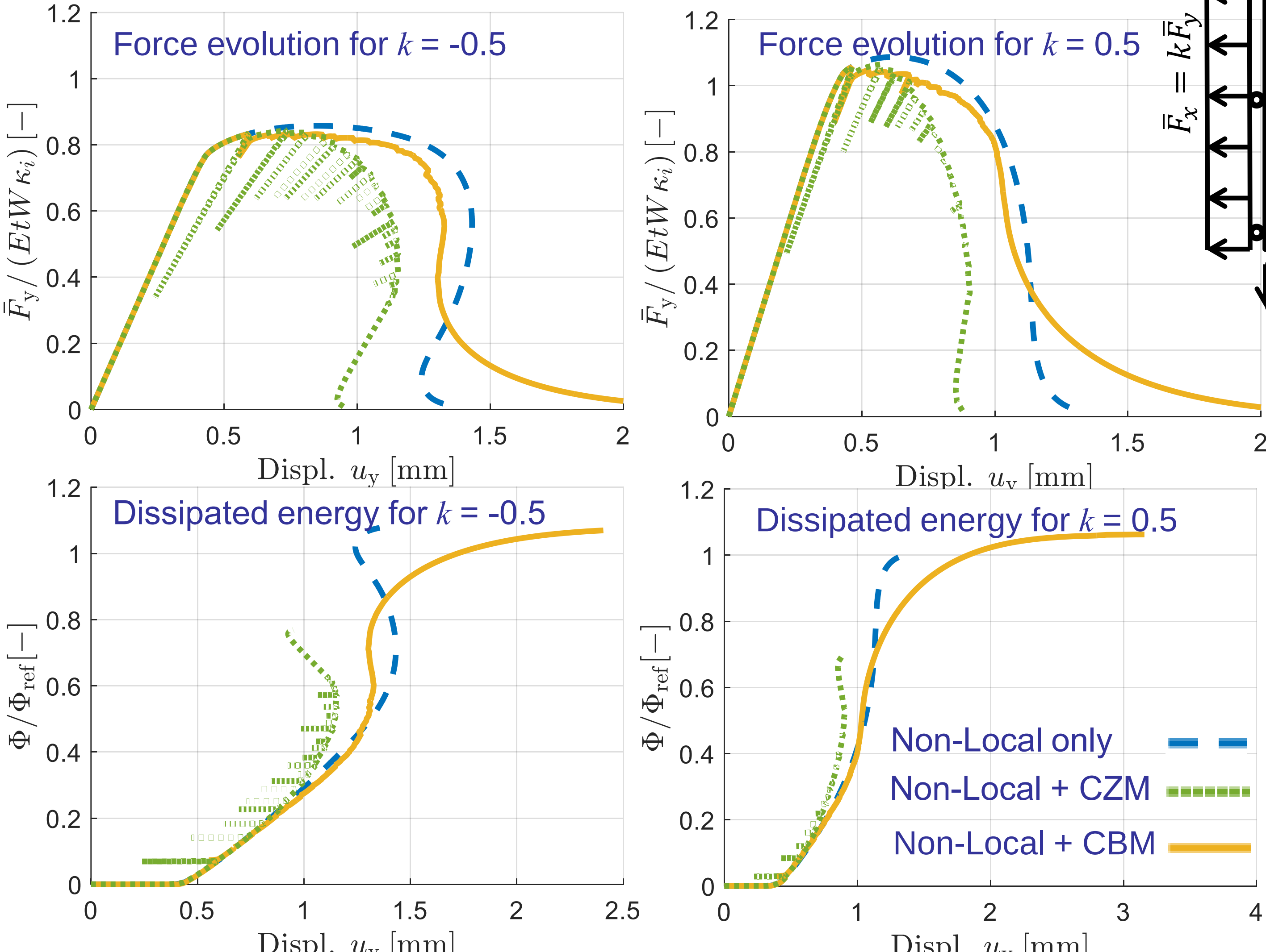

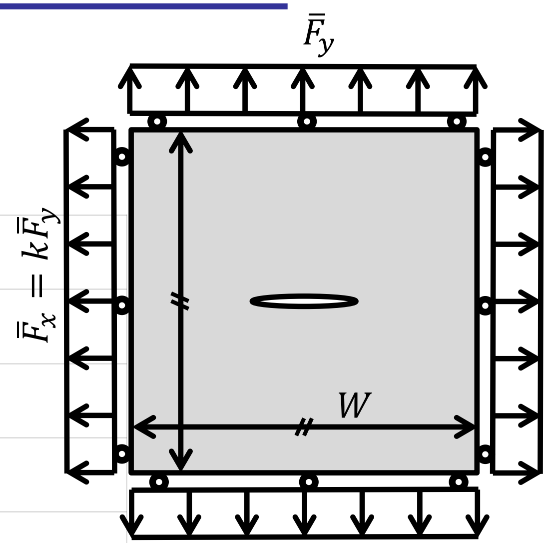

Beginning

DG-Based elastic damage to crack transition

- Comparison with phase field
  - Single edge notched specimen [Miehe et al. 2010]
    - Calibration of damage and CBM parameters with 1D case [Leclerc et al. 2018]

Non-local model | Cohesive band model | Force-displacement curve

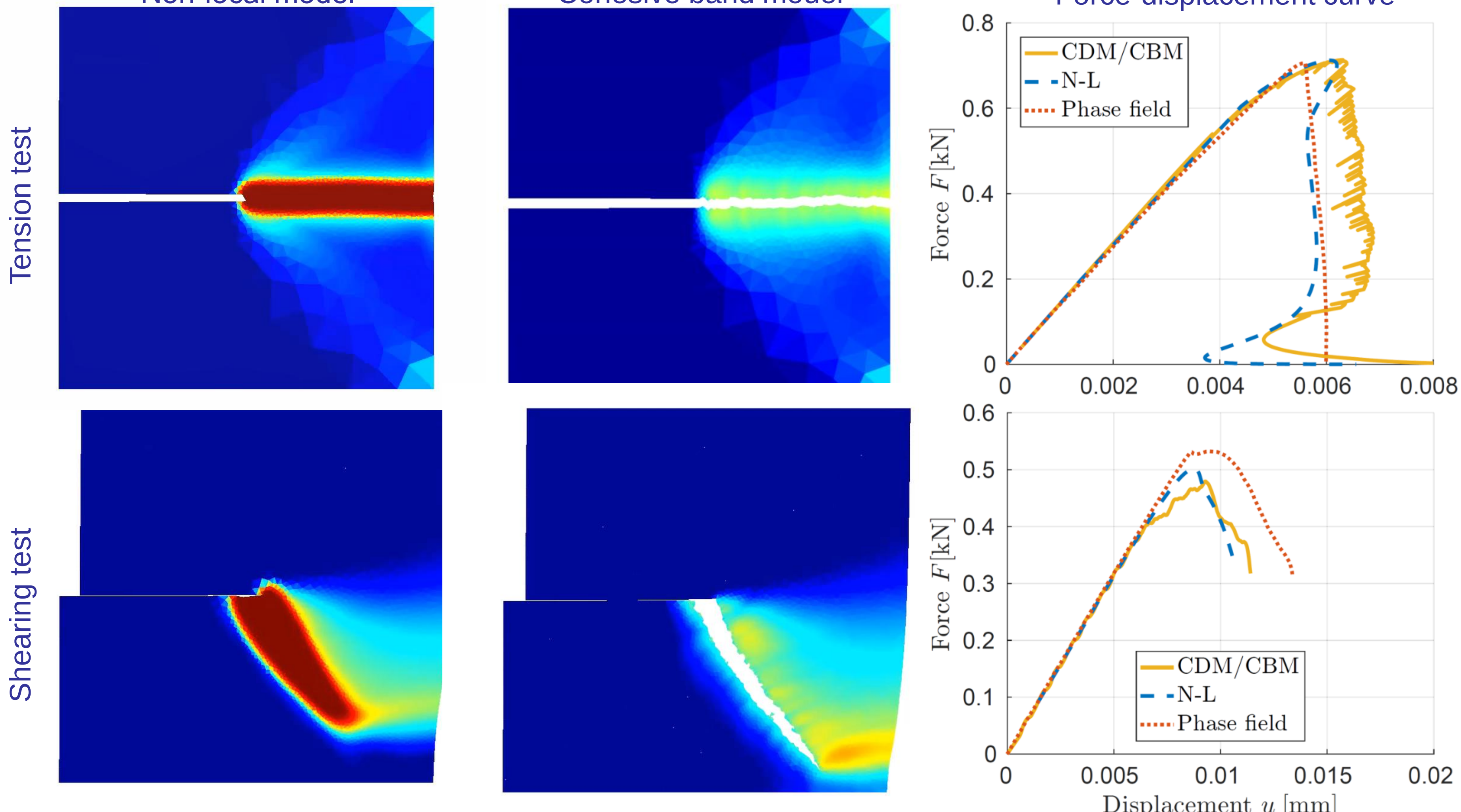

DG-Based elastic damage to crack transition

- Compact Tension Specimen:
  - Non-Local damage law combined to cohesive band model improves accuracy

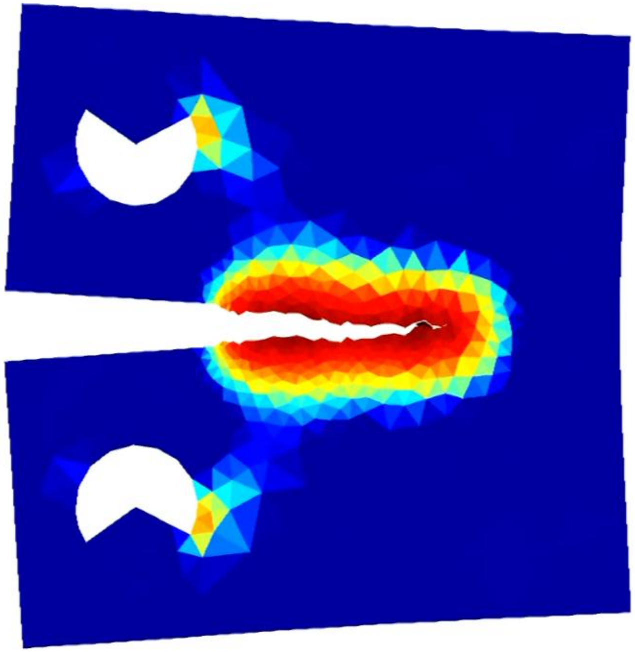

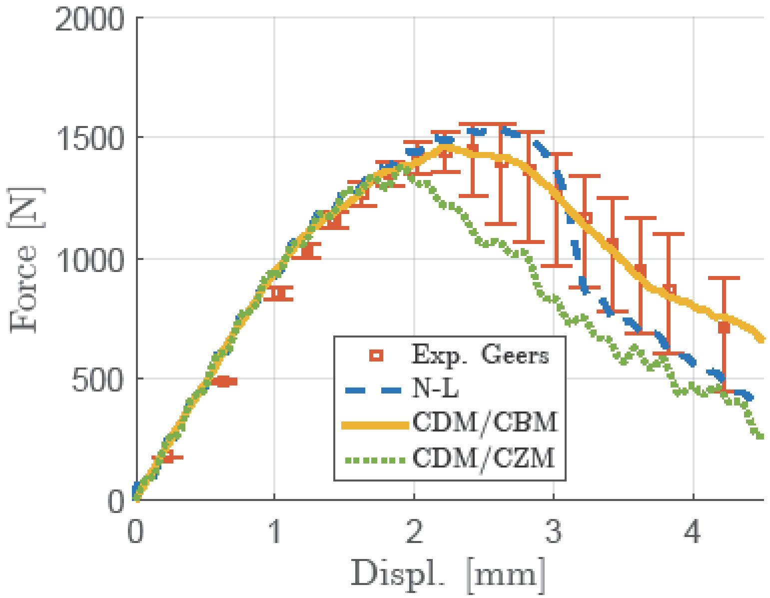

- MRIPF MECATECH project
  - GDTech, UCL, FZ, MECAR, Capital People (Belgium)
- Publication (doi)
  - [10.1002/nme.5618](https://doi.org/10.1002/nme.5618)
  - [10.1016/j.cma.2014.06.031](https://doi.org/10.1016/j.cma.2014.06.031)

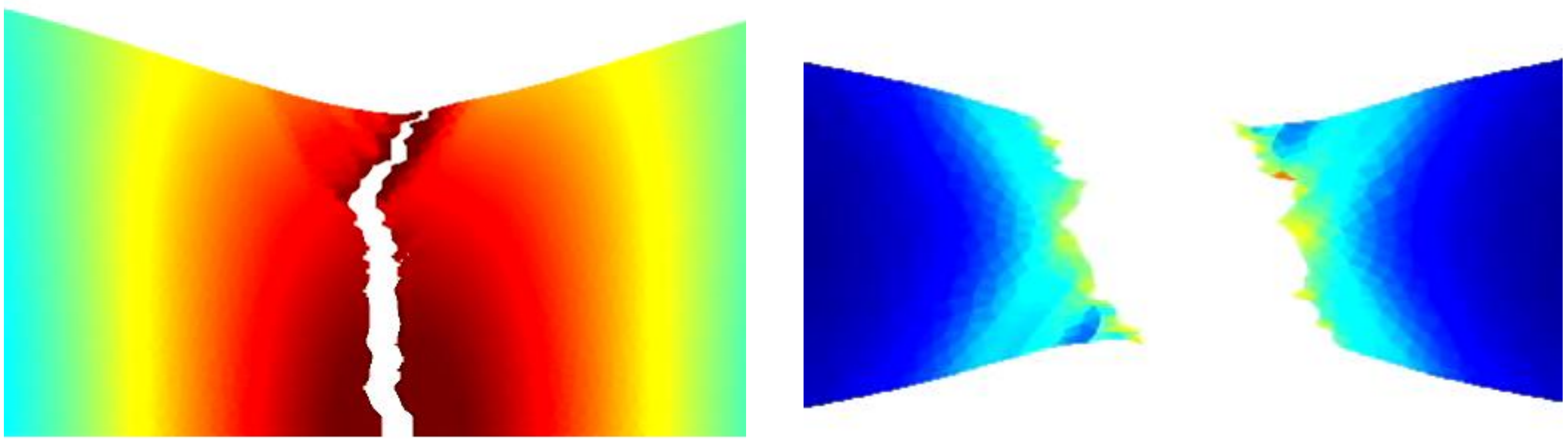

Non-local Gurson damage model to crack transition

The research has been funded by the Walloon Region under the agreement no.7581-MRIPF in the context of the 16th MECATECH call.

Non-local Gurson damage model to crack transition

- Objective:
  - To develop high fidelity numerical methods for ductile failure

- Numerical approach:
  - Combination of 2 complementary methods in a single finite element framework:
    - continuous (damage model)

      + transition to
    - discontinuous (cohesive band model including triaxiality / strain rate effects)

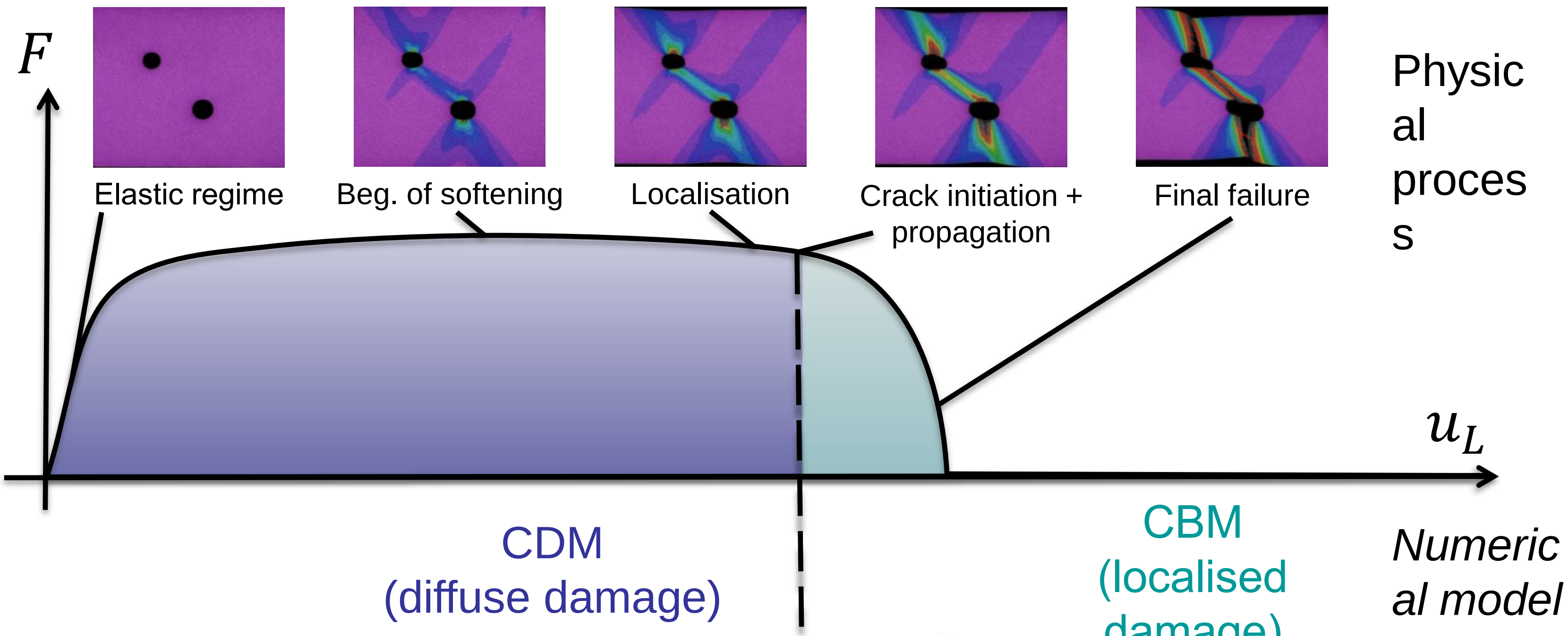

- Material changes represented via internal variables
  - Constitutive law $\boldsymbol{\sigma}\big(\boldsymbol{\varepsilon};\boldsymbol{Z}(t')\big)$
    - Internal variables $\boldsymbol{Z}(t')$
  - Different models
    - Lemaitre-Chaboche (degraded properties)
    - Gurson model (yield surface in terms of porosity f)

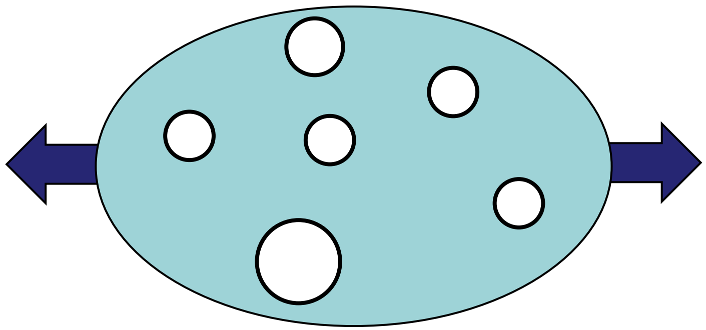

- Model implementation:
  - Local form
    - Mesh dependency
  - Requires non-local form [Bažant 1988]
    - Introduction of characteristic length l_c
    - Weighted average: $\tilde{Z}(\boldsymbol{x}) = \int_{V_C} W(\boldsymbol{y};\boldsymbol{x},l_c)\; Z(\mathbf{y})d\boldsymbol{y}$
  - Implicit form [Peerlings et al. 1998]
    - New degrees of freedom: $\tilde{Z}$
    - New Helmholtz-type equations: $\tilde{Z} - l_c^2\,\Delta\tilde{Z} = Z$

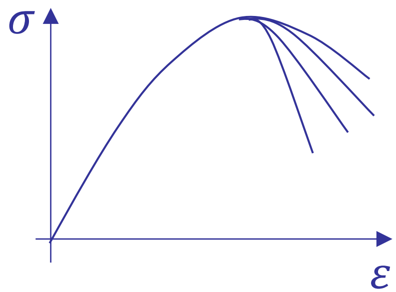

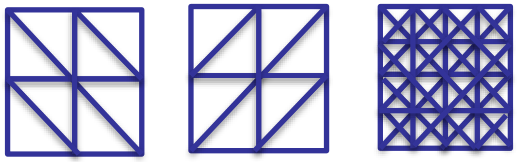

The numerical results change without convergence

Non-local Gurson damage model to crack transition

- Hyperelastic-based formulation
  - Multiplicative decomposition
    $\mathbf{F} = \mathbf{F}^{\mathrm{e}} \cdot \mathbf{F}^{\mathrm{p}}, \quad \mathbf{C}^{\mathrm{e}} = \mathbf{F}^{\mathrm{e}^T} \cdot \mathbf{F}^{\mathrm{e}}, \quad J^{e} = \det(\mathbf{F}^{\mathrm{e}})$
  - Stress tensor definition
    - Elastic potential $\psi(\mathbf{C}^{\mathrm{e}})$
    - First Piola-Kirchhoff stress tensor

      $$\mathbf{P} = 2\mathbf{F}^{\mathrm{e}} \cdot \frac{\partial \psi(\mathbf{C}^{\mathrm{e}})}{\partial \mathbf{C}^{\mathrm{e}}} \cdot \mathbf{F}^{\mathrm{p}^{-T}}$$

    - Kirchhoff stress tensors
      - In current configuration

        $$\boldsymbol{\kappa} = \mathbf{P} \cdot \mathbf{F}^{T} = 2\mathbf{F}^{\mathrm{e}} \cdot \frac{\partial \psi(\mathbf{C}^{\mathrm{e}})}{\partial \mathbf{C}^{\mathrm{e}}} \cdot \mathbf{F}^{\mathrm{e}^T}$$

      - In co-rotational space

        $$\boldsymbol{\tau} = \mathbf{C}^{\mathrm{e}} \cdot \mathbf{F}^{\mathrm{e}^{-1}} \cdot \boldsymbol{\kappa} \cdot \mathbf{F}^{\mathrm{e}^{-T}} = 2\mathbf{C}^{\mathrm{e}} \cdot \frac{\partial \psi(\mathbf{C}^{\mathrm{e}})}{\partial \mathbf{C}^{\mathrm{e}}}$$

- Logarithmic deformation
  - Elastic potential ψ:

    $$\psi(\mathbf{C}^{\mathrm{e}}) = \frac{K}{2} \ln^2(J^{e}) + \frac{G}{4} (\ln(\mathbf{C}^{\mathrm{e}}))^{\mathrm{dev}} : (\ln(\mathbf{C}^{\mathrm{e}}))^{\mathrm{dev}}$$

  - Stress tensor in co-rotational space

    $$\boldsymbol{\tau} = \underbrace{K \ln(J^{e})}_{p}\, \mathbf{I} + G (\ln(\mathbf{C}^{\mathrm{e}}))^{\mathrm{dev}}$$

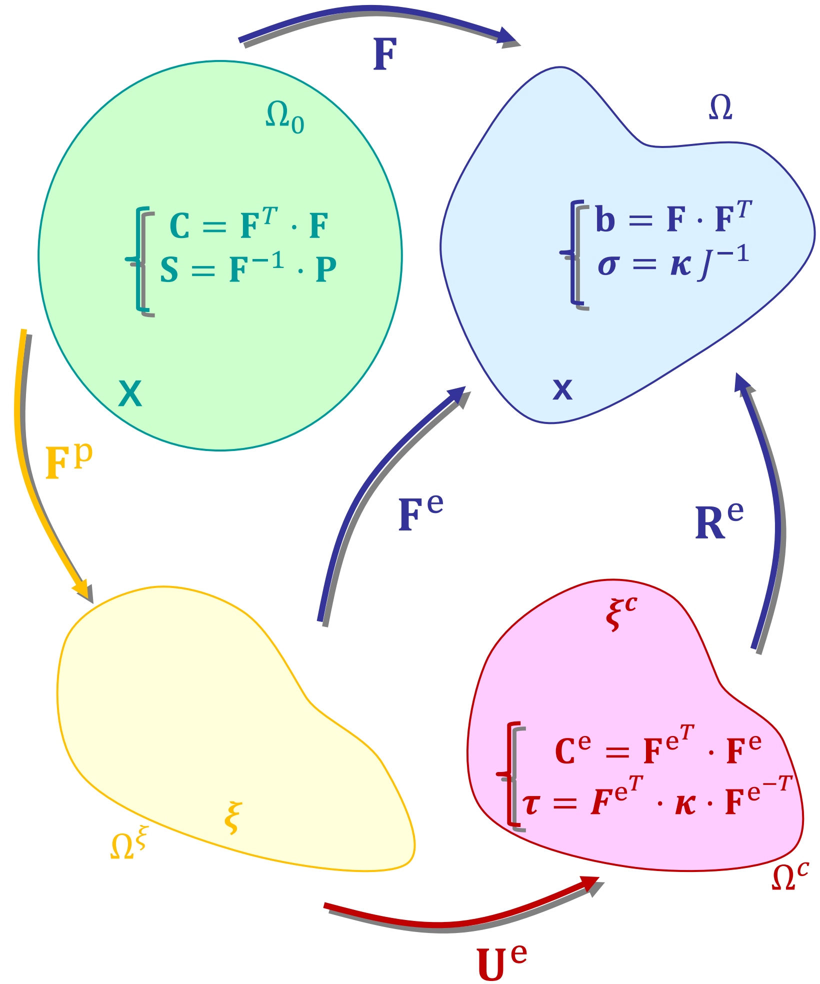

Non-local Gurson damage model to crack transition

- Porous plasticity (or Gurson) approach
  - Competition between 2 plastic modes:

Growth mode: Gurson model

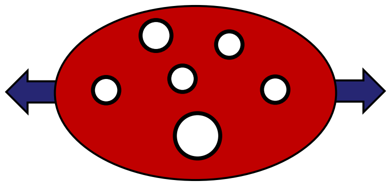

$$\phi_{\mathrm{G}} = \frac{\tau_{\mathrm{eq}}^2}{\tau_{\mathrm{Y}}^2} + 2q_1\tilde{f}\cosh\left(\frac{q_2 p}{2\tau_{\mathrm{Y}}}\right) - 1 - q_3^2\tilde{f}^2 \leq 0$$

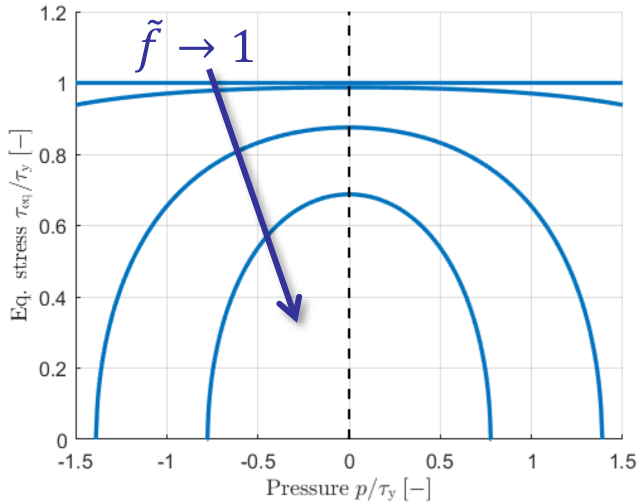

vs

Coalescence mode: Thomason model

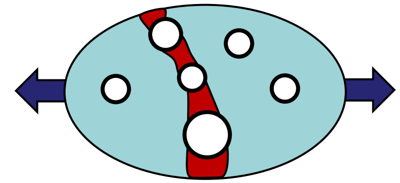

$$\phi_{\mathrm{T}} = \frac{2}{3}\tau_{\mathrm{eq}} + |p| - C_{\mathrm{T}}^{f}(\chi)\tau_{\mathrm{Y}} \leq 0$$

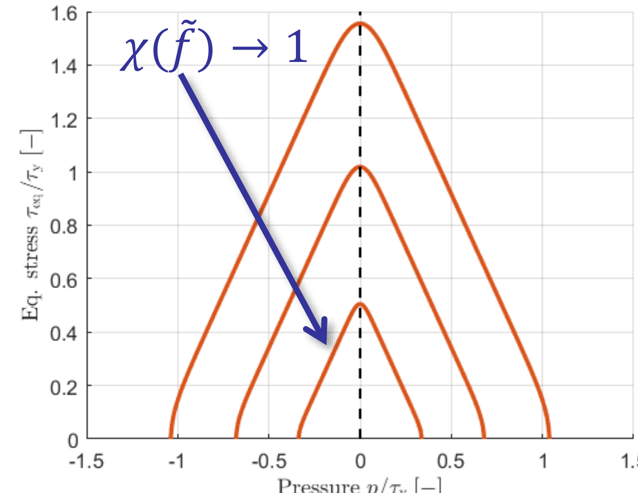

- Hybrid DG model: use of a Cohesive Band Model (CBM)
  - Principles
    - Substitute TSL of CZM by the behavior of a uniform band of thickness h_{b} [Remmers et al. 2013]

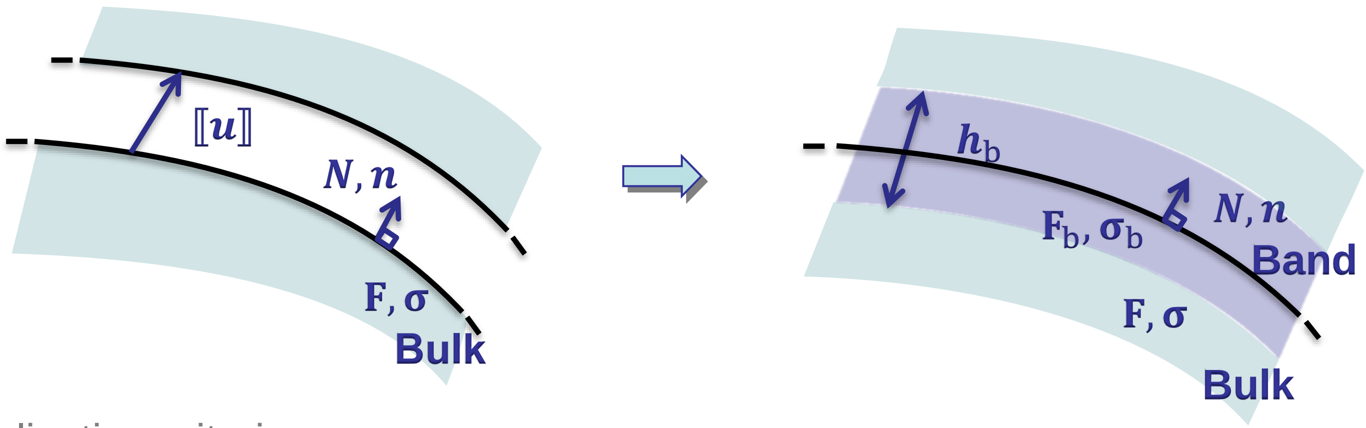

  - Localization criterion
    - Thomason: $\boldsymbol{N} \cdot \boldsymbol{\tau} \cdot \boldsymbol{N} - C_I^f \tau_y \geq 0$
  - Methodology [Leclerc et al. 2018]
    1. Compute a band strain tensor $\mathbf{F}_{\mathrm{b}} = \mathbf{F} + \frac{[\![\boldsymbol{u}]\!] \otimes \boldsymbol{N}}{h_b} + \frac{1}{2} \boldsymbol{\nabla}_T [\![\boldsymbol{u}]\!]$
    2. Compute a band stress tensor $\boldsymbol{\sigma}_{\mathrm{b}}\left(\mathbf{F}_{\mathrm{b}}; Z(\tau)\right)$ using the same CDM as bulk elements
    3. Recover a surface traction $\boldsymbol{t}([\![\boldsymbol{u}]\!], \mathbf{F}) = \boldsymbol{\sigma}_{\mathrm{b}} . \boldsymbol{n}$
  - What is the effect of h_{b} (band thickness)
    - Recover the fracture energy

Non-local Gurson damage model to crack transition

- Comparison with literature [Huespe2012,Besson2003]

Slanted plane strain specimen

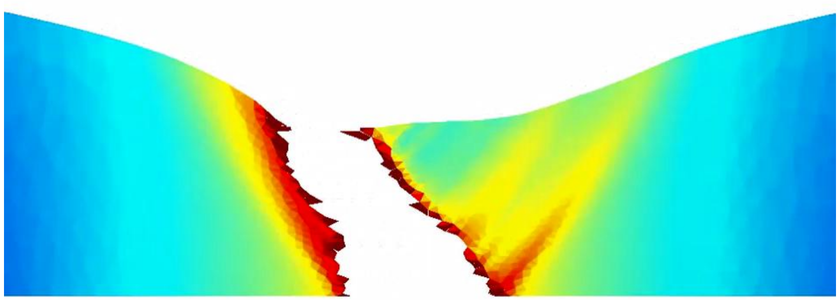

Cup-cone in round bar

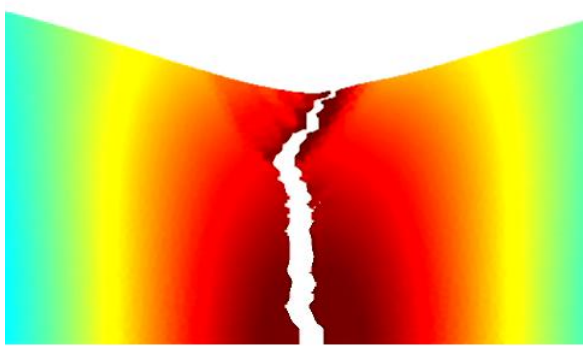

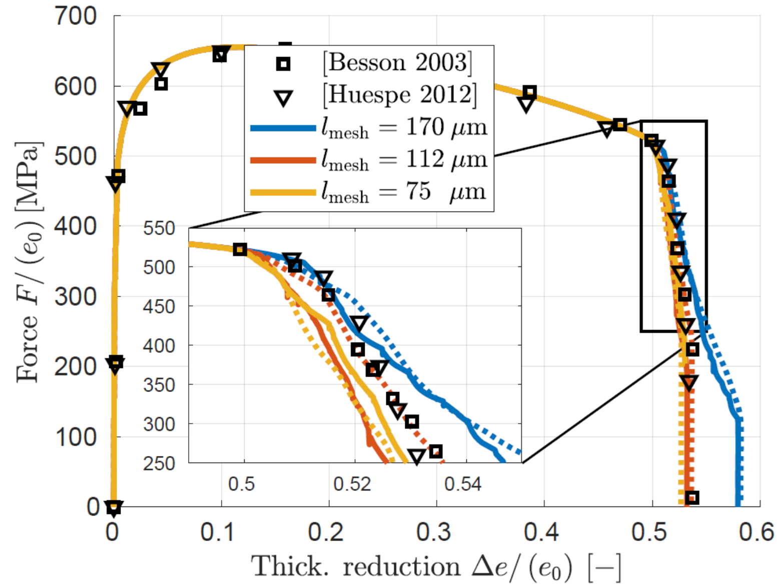

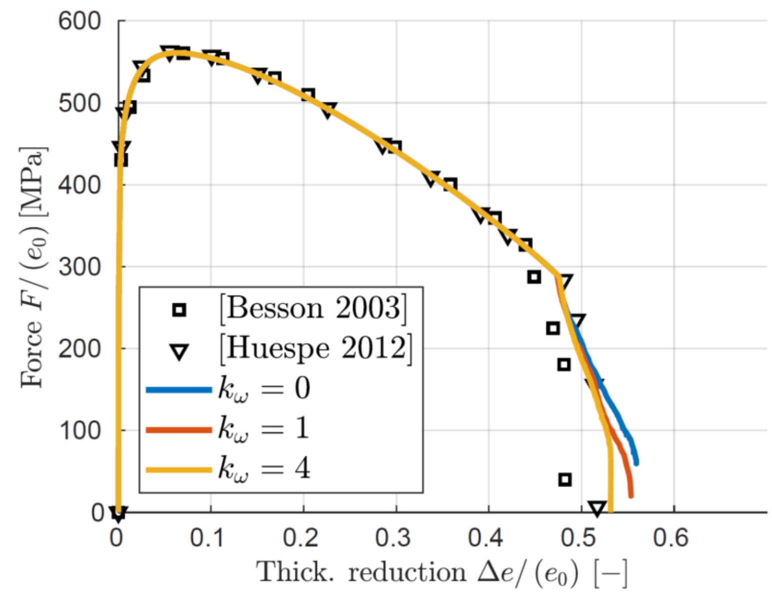

Non-local Gurson damage model to crack transition

- Grooved plate

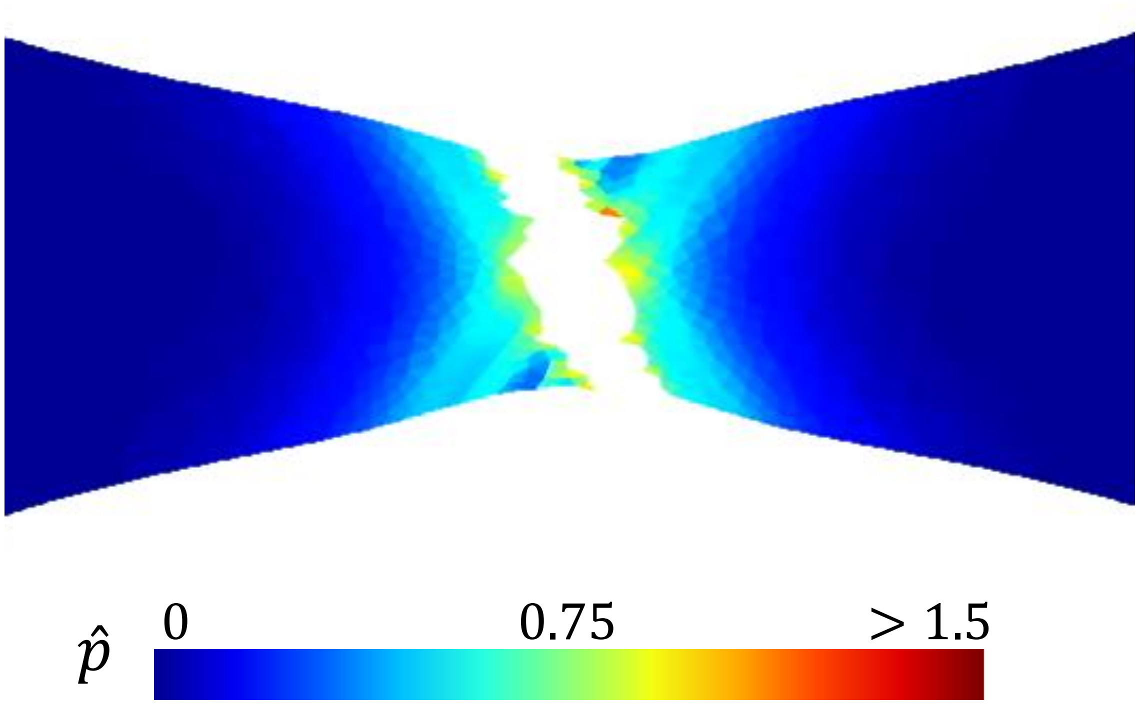

- MRIPF MECATECH project
  - GDTech, UCL, FZ, MECAR, Capital People (Belgium)
- Publication (doi)
  - 10.1002/nme.5618
  - 10.1016/j.ijplas.2019.11.010

Computational & Multiscale Mechanics of Materials

CM3

www.ltas-cm3.ulg.ac.be

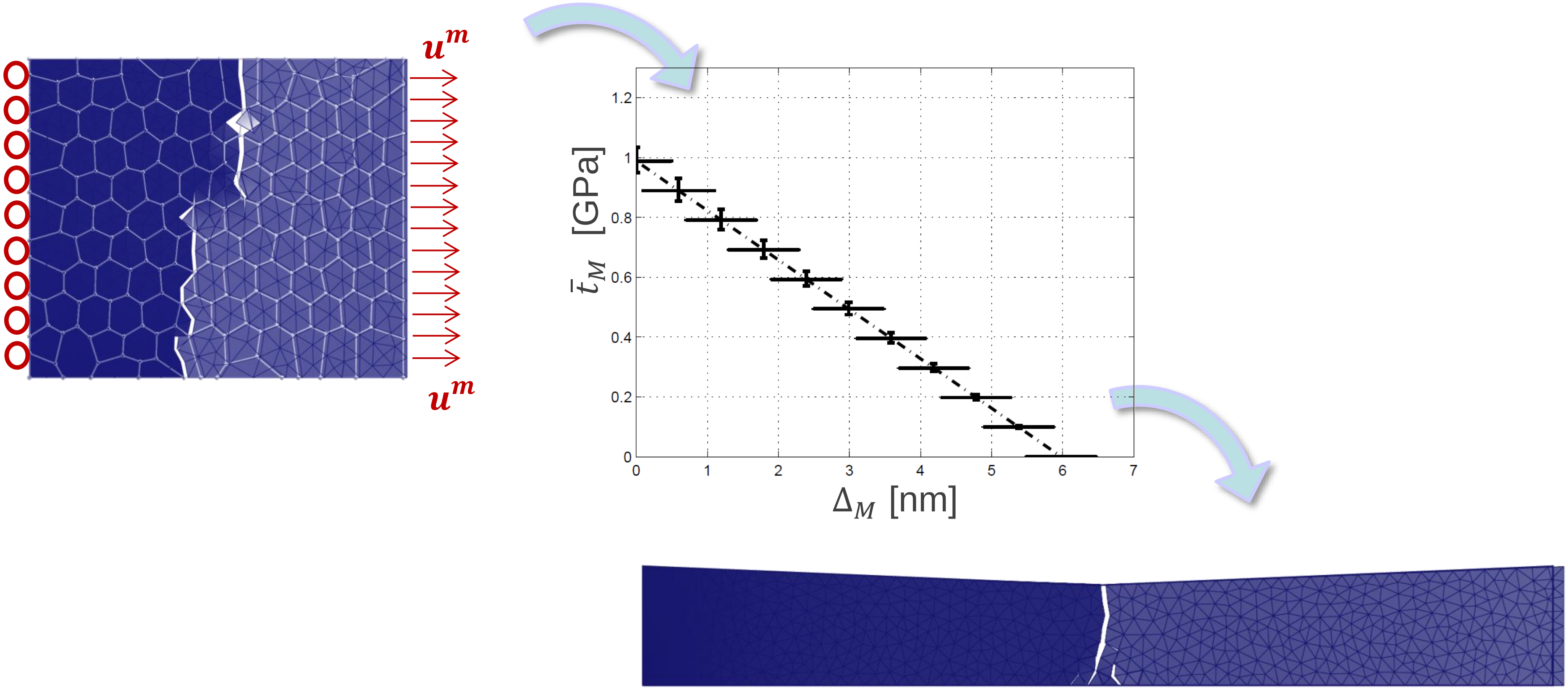

Stochastic Multi-Scale Fracture of Polycrystalline Films

Robust design of MEMS: Financial support from F. R. S. - F. N. R. S. under the project number FRFC 2.4508.11

LIÈGE université

- Multi-scale modeling
  - 2 problems are solved concurrently
    - The macro-scale problem
    - The meso-scale problem
      (on a meso-scale
      Volume Element)

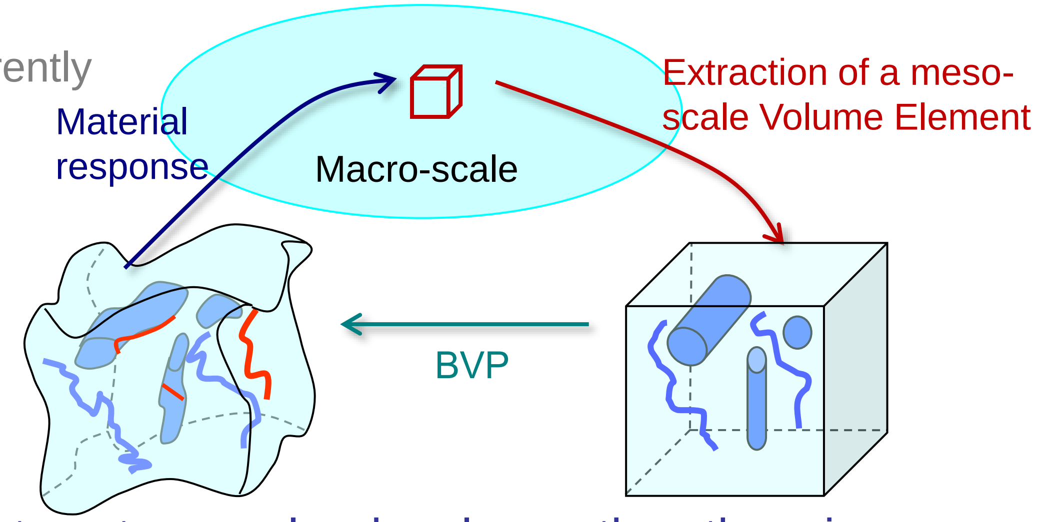

- For meso-scale volume elements not several orders larger than the micro-structure size and embedding crack propagations

$$L_{\text{macro}} >> L_{\text{VE}} \sim ?\ L_{\text{micro}}$$

For accuracy: Size of the meso-scale volume element smaller than the characteristic length of the macro-scale loading

Meso-scale volume element no longer statistically representative:
- **Stochastic Volume Elements**
- **Should recover consistency lost due to the discontinuity**

- Micro-scale model: Silicon crystal
  - Different fracture strengths and critical energy release rates

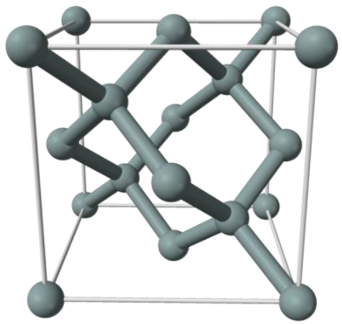

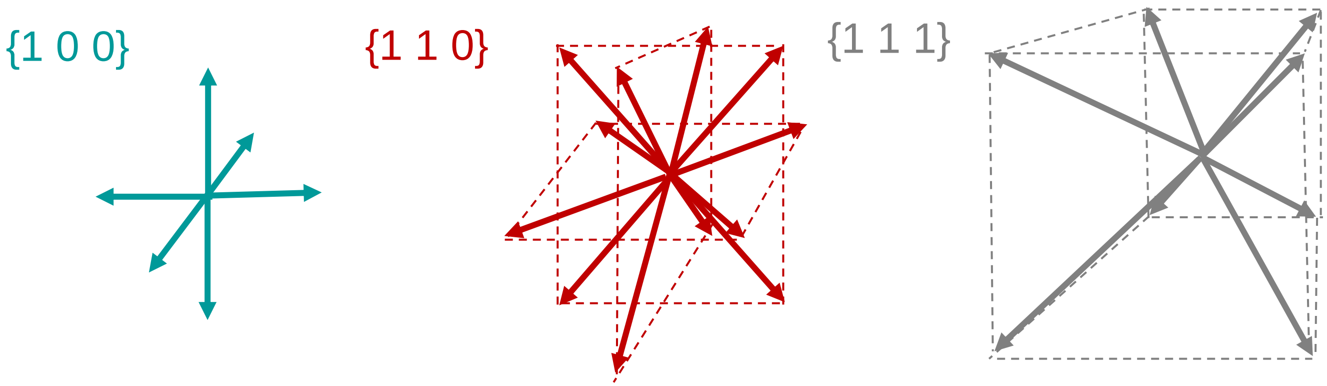

  - Define a “continuous” strength mapping

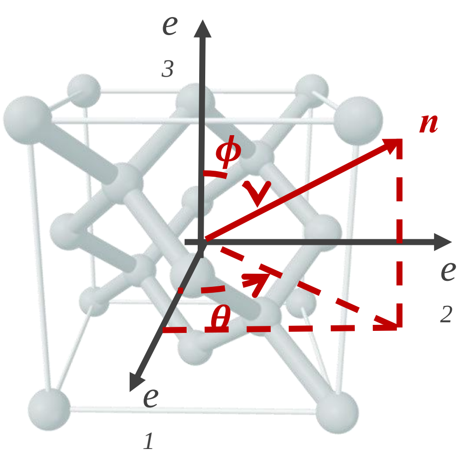

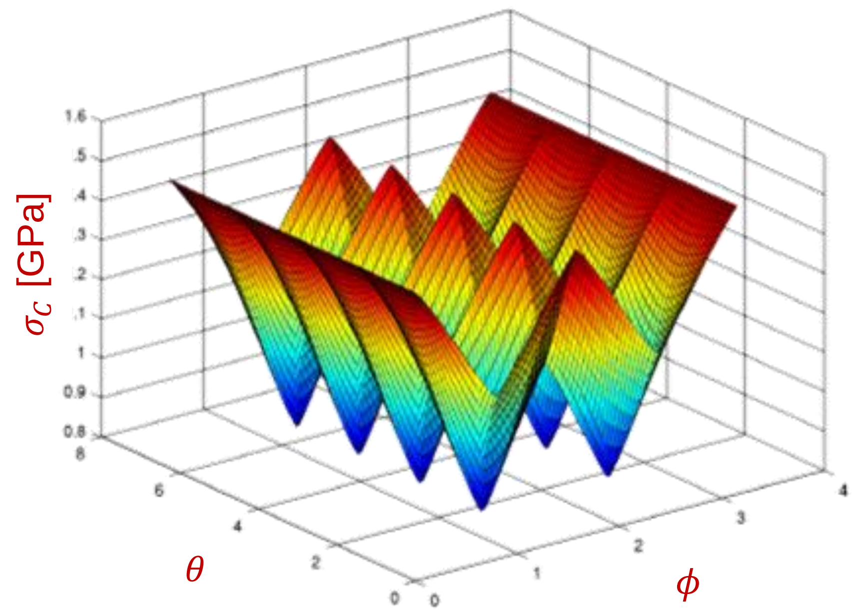

Stochastic Multi-Scale Fracture of Polycrystalline Films

- Micro-scale model: Polycrsytalline films
  - Discontinuous Galerkin method
  - Extrinsic cohesive law
  - Intra/Inter granular fracture
  - Accounts for interface orientation

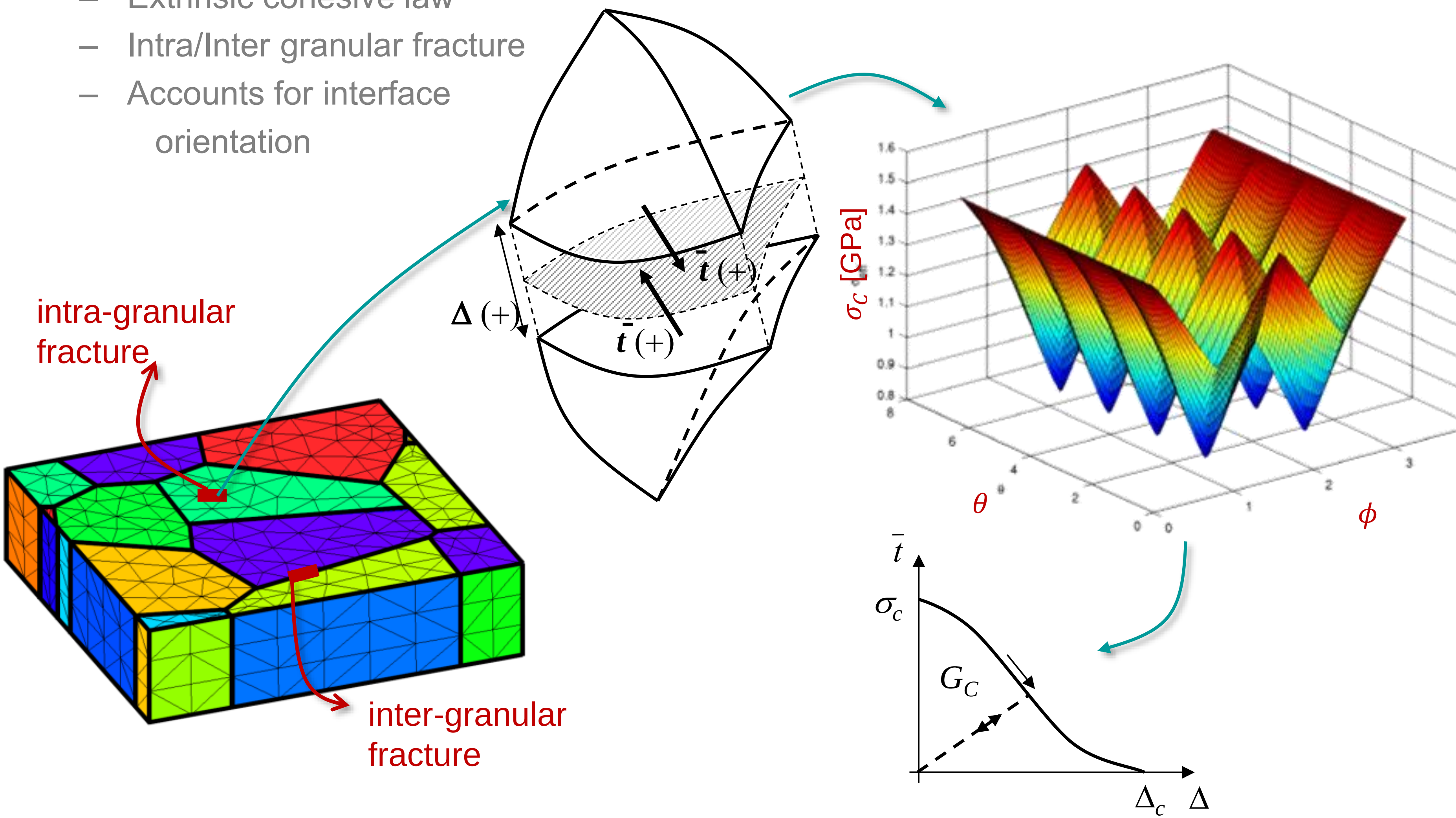

Stochastic Multi-Scale Fracture of Polycrystalline Films

- Stochastic micro-scale to meso-scale model
  - Several SVE realizations (random grain orientation)
  - Extraction of consistent meso-scale cohesive laws
    - $\bar{t}_M$ vs. Δ_M
    - for each SVE sample
  - Resulting meso-scale cohesive law distribution

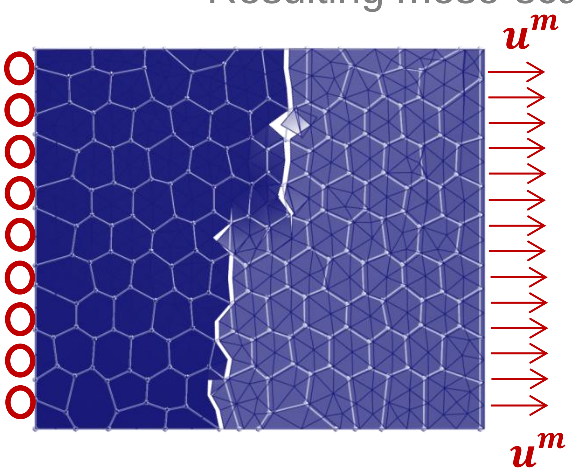

$$\delta \bar{\boldsymbol{t}}_M = \boldsymbol{\delta\sigma_M} \cdot \boldsymbol{e}_X$$

$$\delta \boldsymbol{\Delta}_M = \delta \boldsymbol{u}^m - L_{\text{cell}} \boldsymbol{C_M}^{-1} : \boldsymbol{e}_X \otimes \boldsymbol{e}_X \cdot \boldsymbol{\delta \bar{t}}_M$$

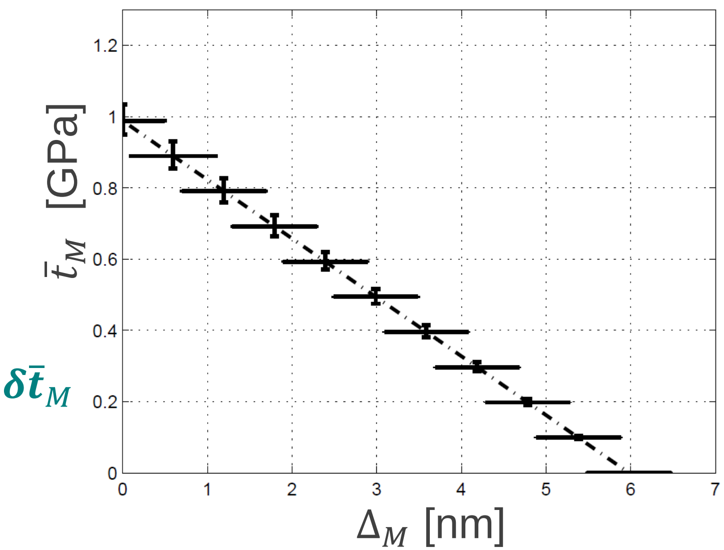

Stochastic Multi-Scale Fracture of Polycrystalline Films

- Macro-scale simulation
  - Finite element model non-conforming to the grains
  - Use homogenized (random) meso-scale cohesive laws as input

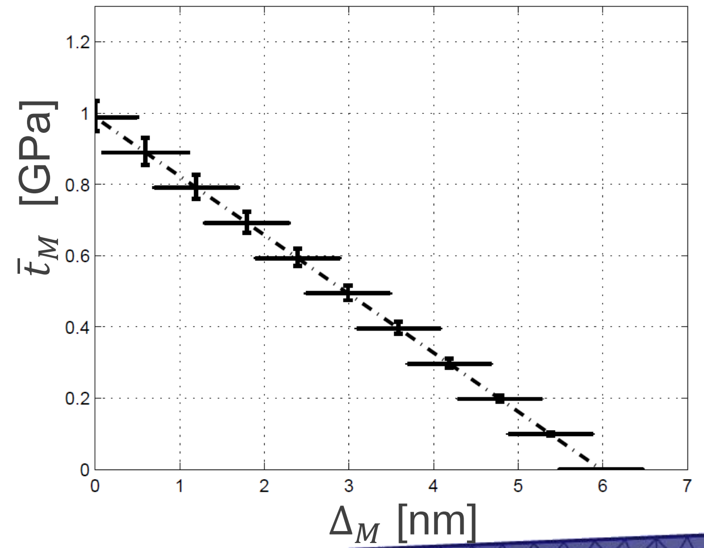

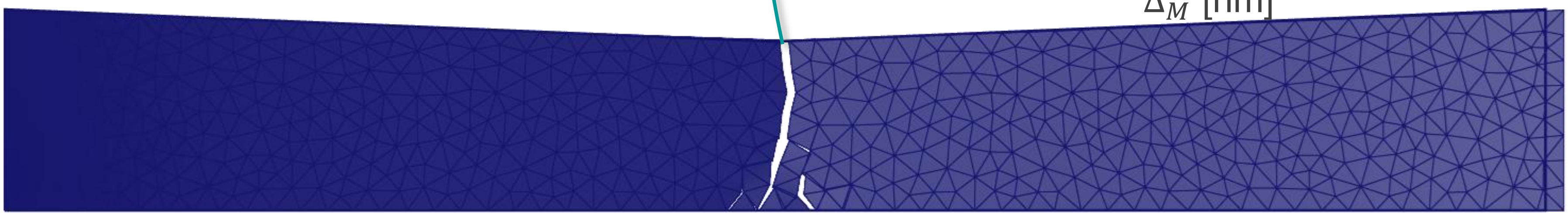

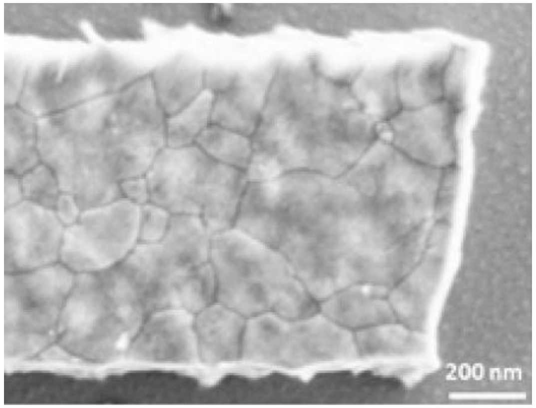

- Collaboration for experiments
  - UcL (T. Pardoen, J.-P Raskin)

- Publications
  - 10.1007/s00466-014-1083-4

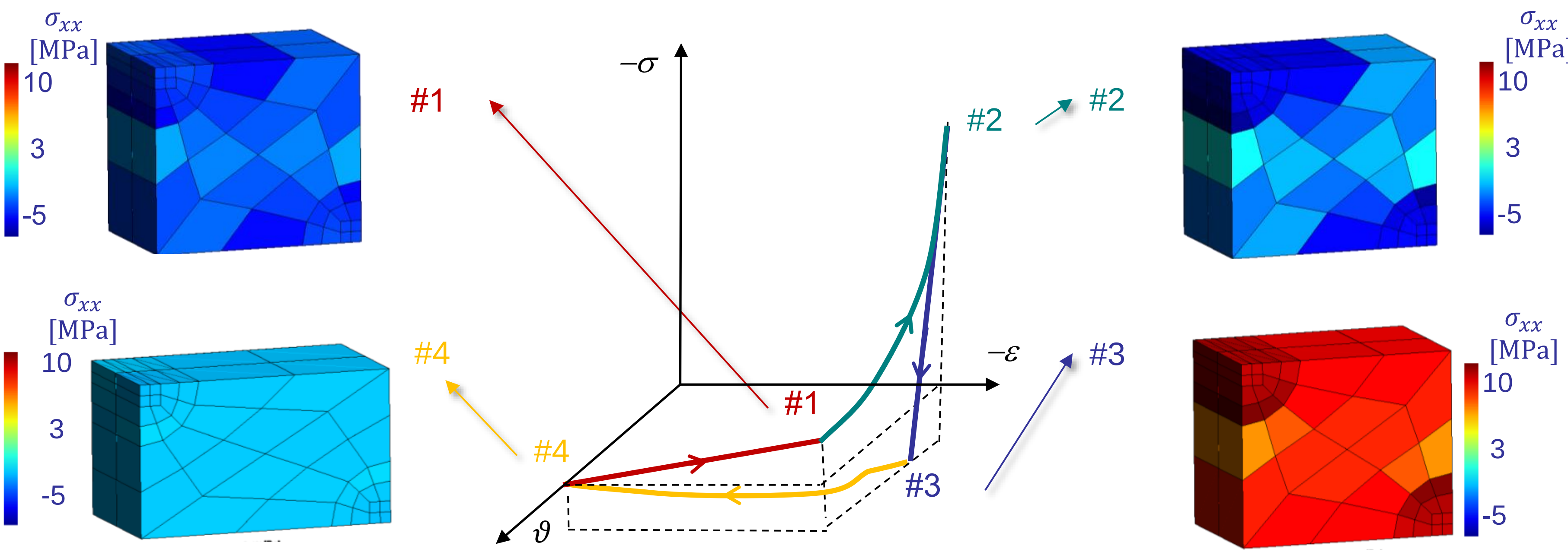

Smart Composite Materials

This project has been funded with support of the European Commission under the grant number 2012-2624/001-001-EM. This publication reflects the view only of the author, and the Commission cannot be held responsible for any use which may be made of the information contained therein.

- Electro-thermo-mechanical coupling
  - Finite field variation formulation
  - Strong coupling

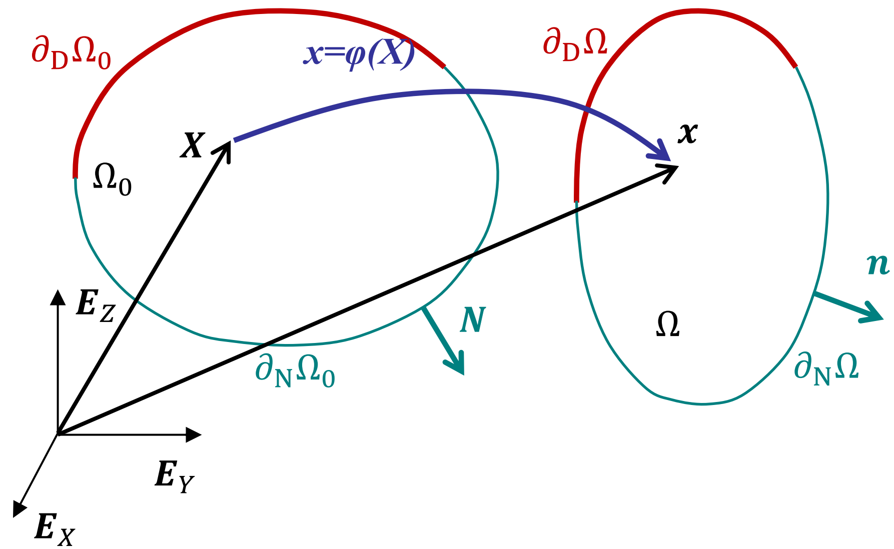

Conservation of electric charge	Conservation of energy	Conservation of momentum balance
$\mathbf{J}_e \cdot \boldsymbol{\nabla}_0 = 0$ $\mathbf{J}_e = \mathbf{J}_e(\mathbf{F}, \boldsymbol{\nabla}_0 V, V, \boldsymbol{\nabla}_0 \vartheta, \vartheta; \boldsymbol{Z})$	$\rho C_v \dot{\vartheta} - \mathcal{D} + \mathbf{J}_y \cdot \boldsymbol{\nabla}_0 = 0$ $\mathbf{J}_y = \mathbf{q} + V\mathbf{J}_e$ $\mathbf{q} = \mathbf{q}(\mathbf{F}, V, \boldsymbol{\nabla}_0 \vartheta, \vartheta; \boldsymbol{Z})$	$\mathbf{P} \cdot \boldsymbol{\nabla}_0 = 0$ $\mathbf{P} = \mathbf{P}(\mathbf{F}, \vartheta; \boldsymbol{Z})$ $\mathcal{D} = \beta \dot{p} \tau + \vartheta \frac{\partial \dot{W}^{\mathrm{el}}}{\partial \vartheta}$

- Two-way electro-thermal coupling
  - Seebeck coefficient α
  - Finite strain conductivities $\mathbf{K}(V,\vartheta) = \mathbf{F}^{-1}\cdot\mathbf{k}(V,\vartheta)\cdot\mathbf{F}^{-T}J$ & $\mathbf{L}(V,\vartheta) = \mathbf{F}^{-1}\cdot\mathbf{l}(V,\vartheta)\cdot\mathbf{F}^{-T}J$

$$\begin{pmatrix}\mathbf{J}_e\\ \mathbf{J}_y\end{pmatrix} = \begin{pmatrix}\mathbf{L}(V,\vartheta) & \alpha\mathbf{L}(V,\vartheta)\\ V\mathbf{L}(V,\vartheta)+\alpha T\mathbf{L}(V,\vartheta) & \mathbf{K}(V,\vartheta)+\alpha V\mathbf{L}(V,\vartheta)+\alpha^2 T\mathbf{L}(V,\vartheta)\end{pmatrix}\begin{pmatrix}-\boldsymbol{\nabla}_0 V\\ -\boldsymbol{\nabla}_0\vartheta\end{pmatrix}$$

Non energetically conjugated

[Liu IJES, 2012]

Change of variables

$$\begin{cases} f_V = -\dfrac{V}{\vartheta}\\ f_\vartheta = \dfrac{1}{\vartheta}\end{cases}$$

$$\begin{pmatrix}\mathbf{J}_e\\ \mathbf{J}_y\end{pmatrix} = \mathbf{Z}(\mathbf{F}, f_V, f_\vartheta)\begin{pmatrix}\boldsymbol{\nabla}_0 f_V\\ \boldsymbol{\nabla}_0 f_\vartheta\end{pmatrix}$$

  - The coefficients matrix $\mathbf{Z}(\mathbf{F}, f_V, f_\vartheta)$ is symmetric and definite positive

- Thermo-mechanical shape memory polymer
  - Deformations above glass transition temperature ϑ_g (1)
  - Fixed once cooled down below ϑ_g (2 & 3)
  - Recovery once heated up (4)

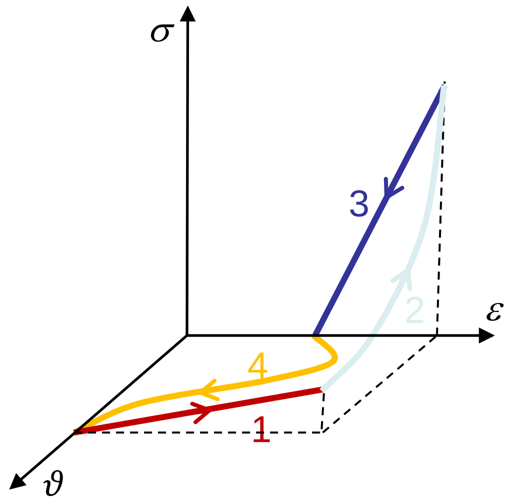

- Elasto-visco-plastic model constitutive behavior
  - Different mechanisms (α)
    - Multiplicative decomposition

      $\mathbf{F}^{(\alpha)} = \mathbf{F}^{\mathrm{e}(\alpha)} \mathbf{F}^{\mathrm{p}(\alpha)}$
    - Free energy

      $$\psi = \sum_{\alpha} \psi^{(\alpha)} \left(\mathbf{C}^{\mathrm{e}(\alpha)}, \vartheta \right)$$
    - Thermo-visco-plasticity

      $$\tau^{(\alpha)} = \mathcal{T} \left(\mathbf{C}^{\mathrm{e}(\alpha)}, \mathbf{F}^{\mathrm{p}(\alpha)}, \dot{p}^{(\alpha)}, \vartheta, \xi^{(\alpha)} \right)$$
  - Stress and dissipation

$$\begin{cases} \mathbf{P} = \mathbf{P}\left(\mathbf{F}, \vartheta ; \mathbf{F}^{\mathrm{p}(\alpha)}, p^{(\alpha)}, \xi^{(\alpha)} \right) \\ \mathcal{D} = \beta \dot{p}^{(\alpha)} \tau^{(\alpha)} \end{cases}$$

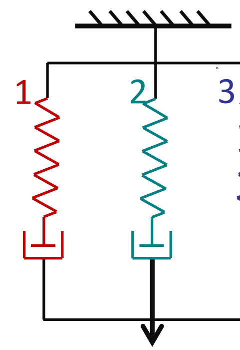

Intermolecular bonds/crosslink stretching

Moclecular resistance

[V. Srivastav et. al, 2010]

- Elasto-visco-plastic behavior of thermo-mechanical shape memory polymer

Refs. by [V. Srivastav et. al, 2010]

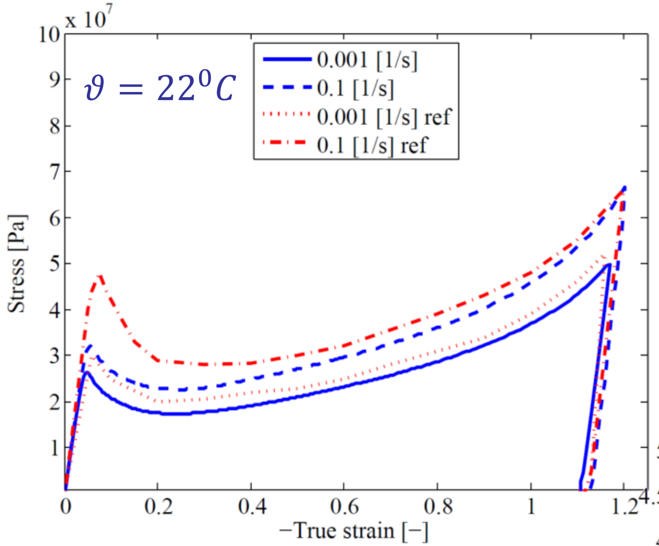

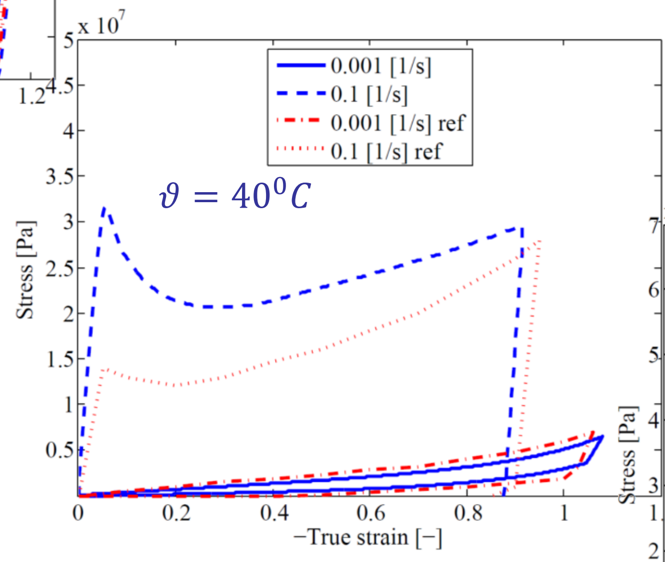

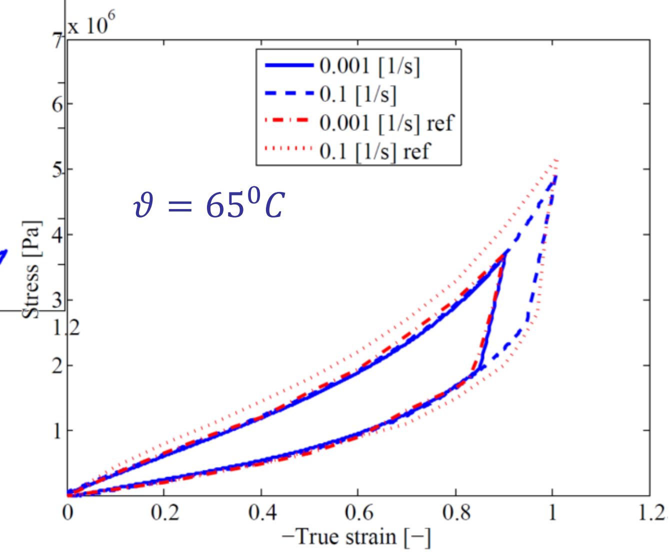

- Recovery of a shape memory composite unit cell
  - Carbon Fiber reinforced SMP
  - Shape memory effect triggered by Joule effect
  - Test with compressive force recovery:
    - #1: Compression deformation obtained above ϑ_g
    - #2: Fixation of the deformation above ϑ_g
    - #3: Reheat above ϑ_g at constant deformation:
      → recovery force, the cell wants to expend
    - #4: Release deformation/stress
      → recovery force vanishes

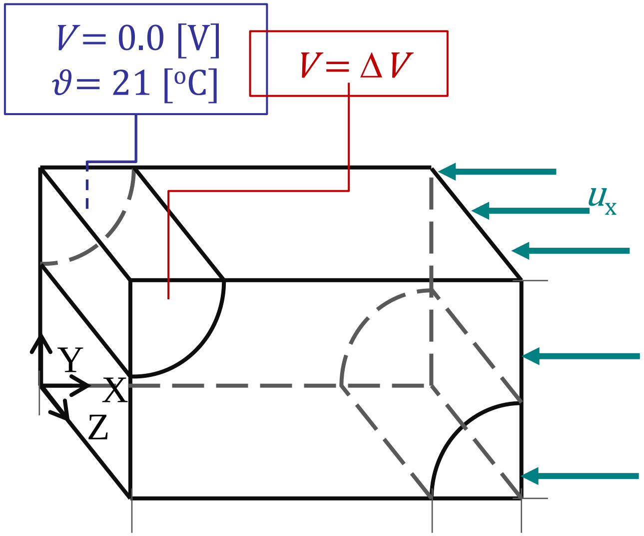

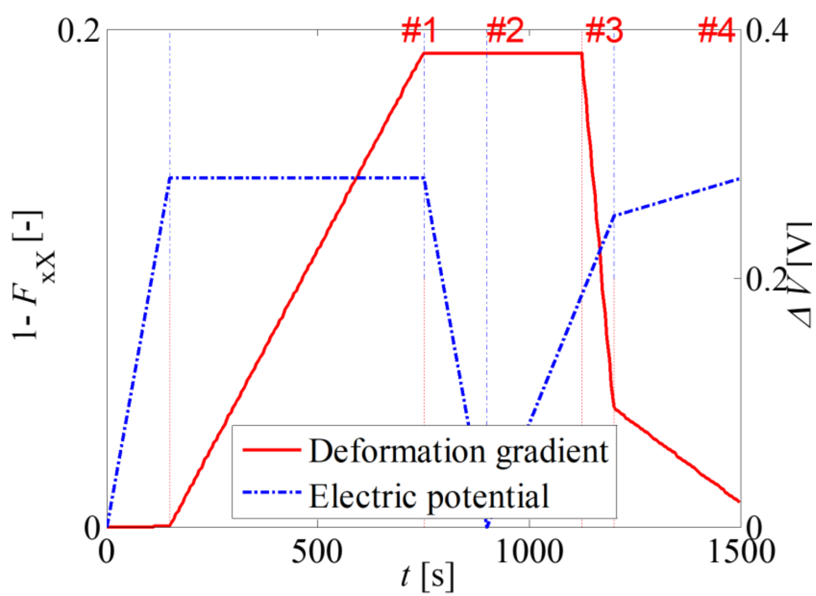

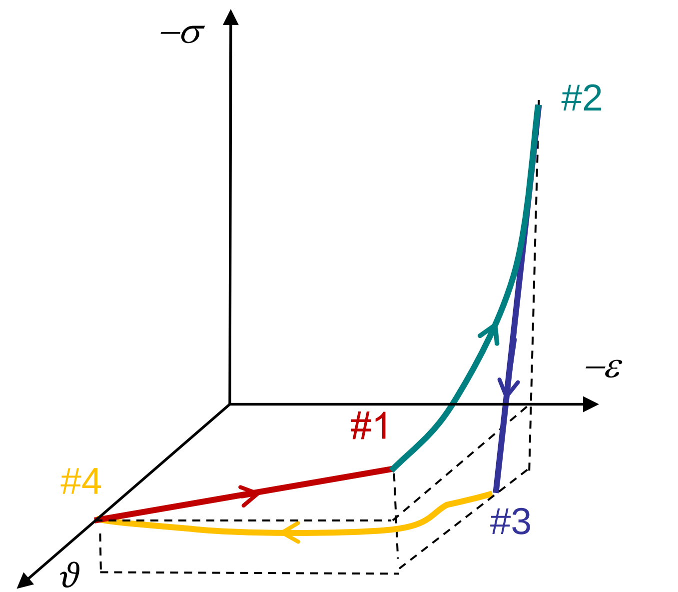

- Recovery of a shape memory composite unit cell
  - Carbon Fiber reinforced SMP
  - Triggered by Joule effecy

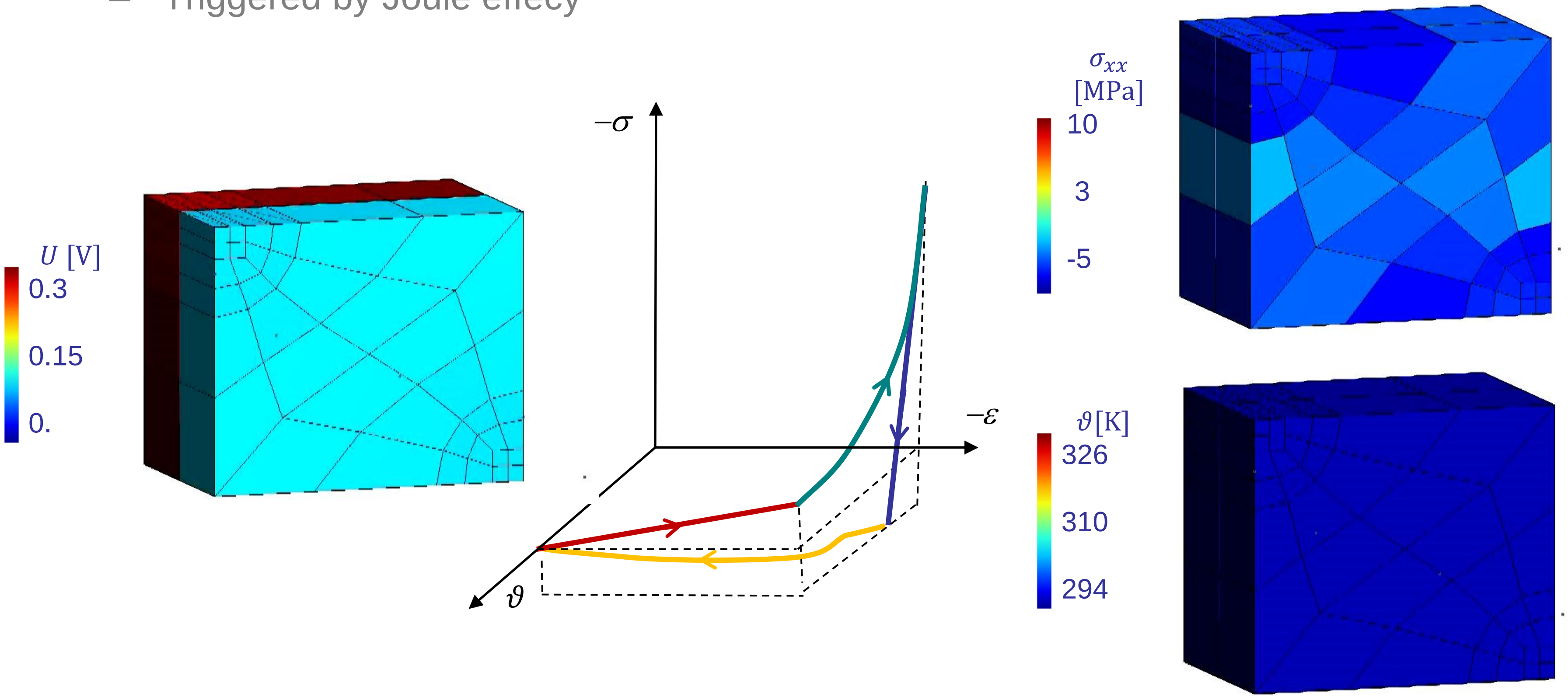

- Discontinuous Galerkin implementation
  - Finite-element discretization
  - Same **discontinuous** polynomial approximations for the
    - **Test** functions φ_h and
    - **Trial** functions $\delta\varphi$
  - Extended to non-linear electro-thermo-mechanical coupling

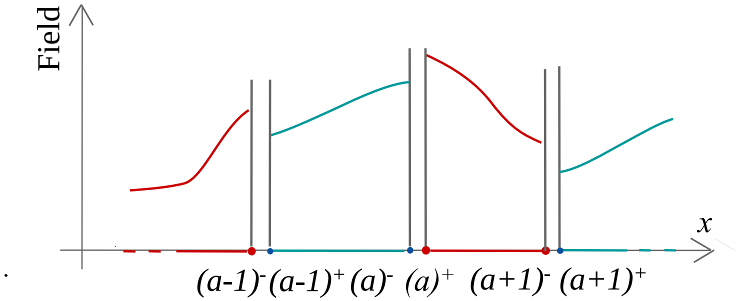

- Publication (doi)
  - 10.1007/s11012-017-0743-9
  - 10.1016/j.jcp.2017.07.028

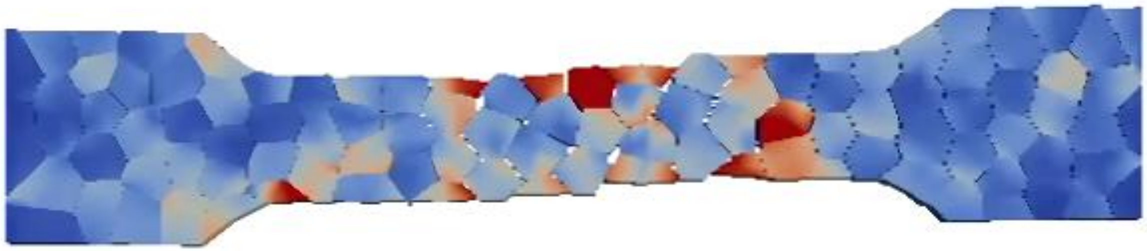

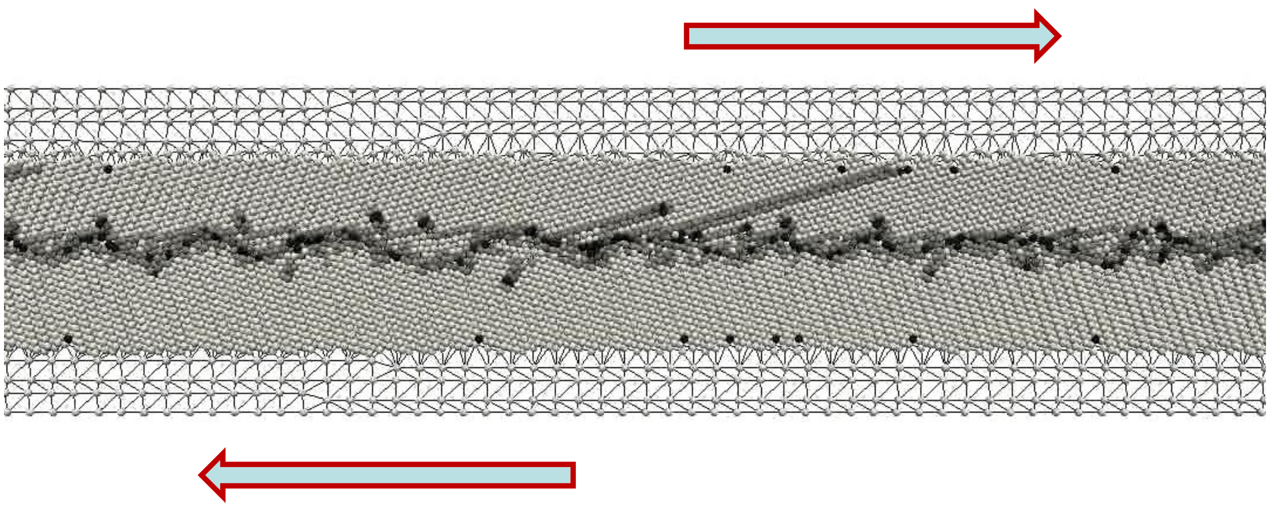

Multi-Scale Modeling of Nano-Crystal Grain Boundary Sliding

Multi-Scale Modeling of Nano-Crystal Grain Boundary Sliding

- 2-scale framework
  - Macro-scale: Finite Elements
  - Micro-scale: Quasi-Continuum

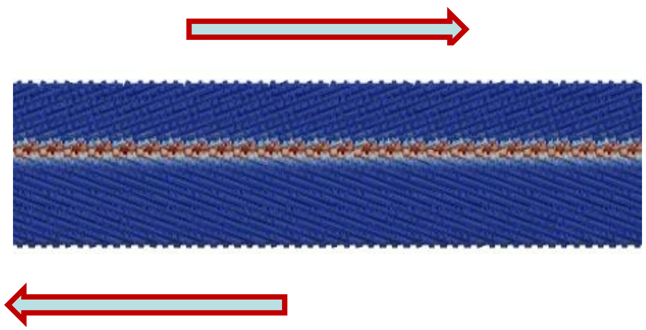

Grain-boundary sliding/opening characterization

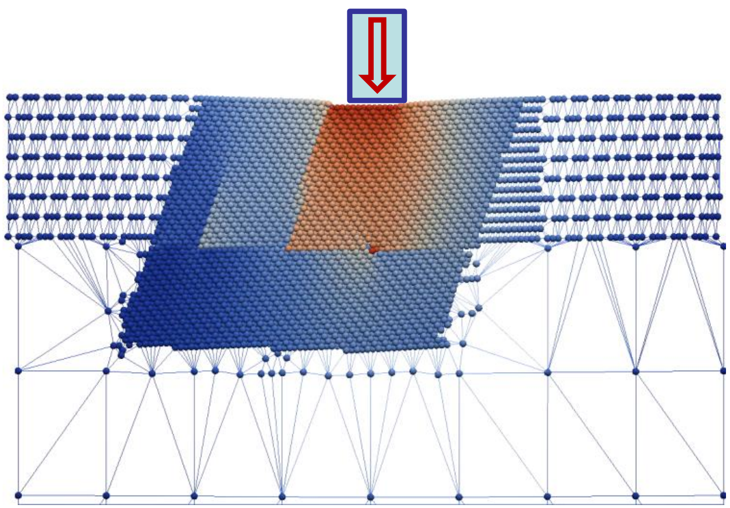

Crystal plasticity characterization by nano-indentation

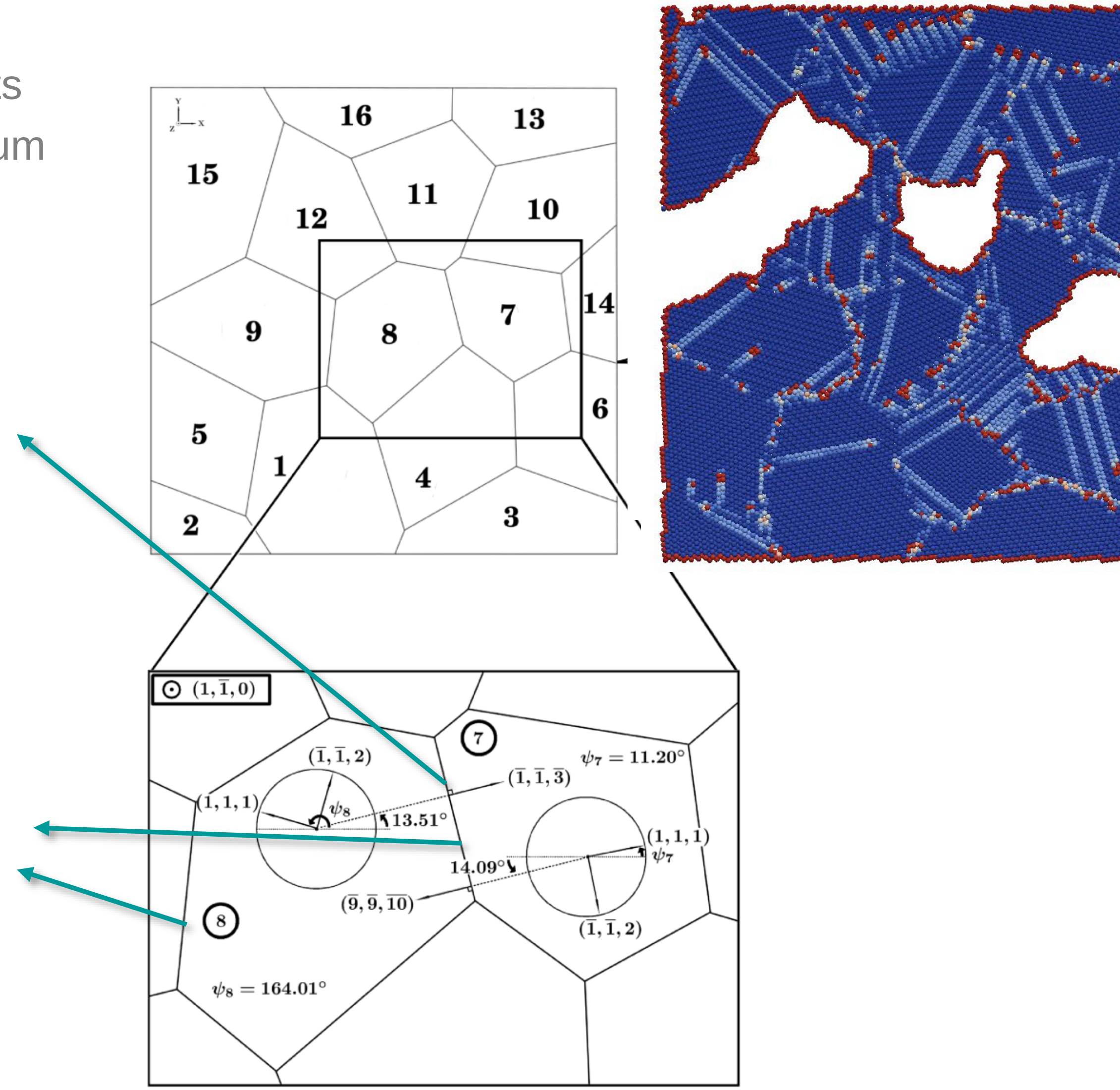

Multi-Scale Modeling of Nano-Crystal Grain Boundary Sliding

- Grain size effect
  - Competition between inter-intra granular

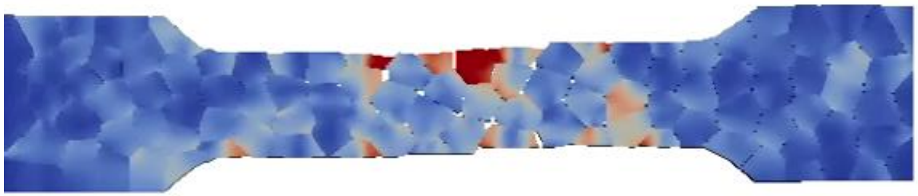

Grain size: 6.56 nm

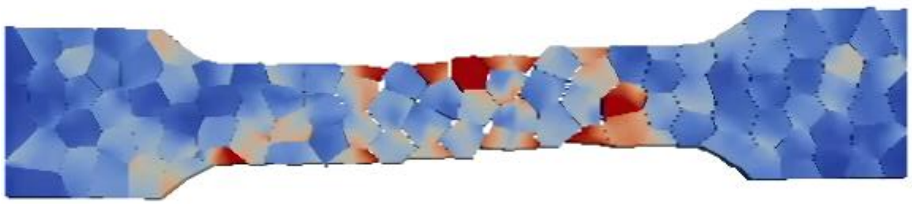

Grain size: 3.28 nm

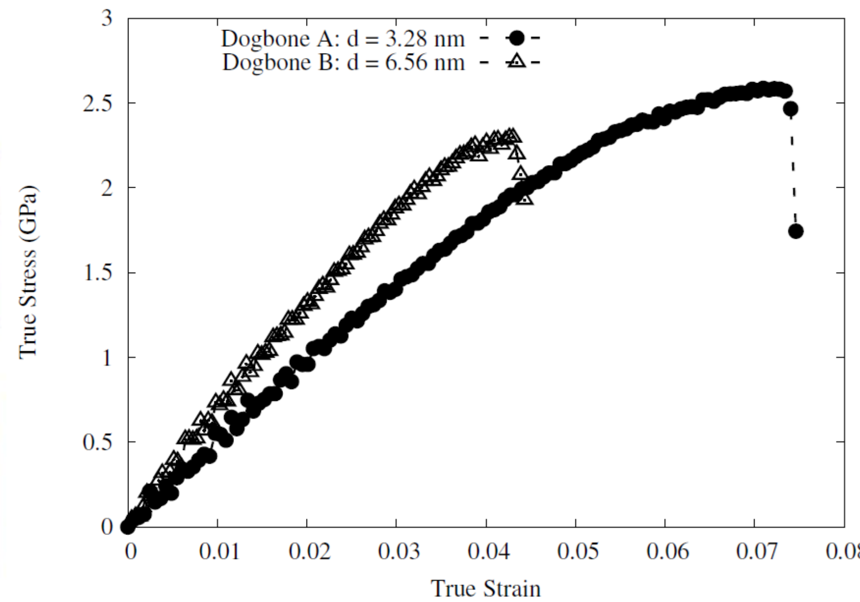

- Effect of nano-voids in the grain boundaries
  - Different deformation mechanism
  - Lower yield stress
- Collaboration
  - EC Nantes, Univ. of Vermont, Oxford
- Publications
  - 10.1016/j.commatsci.2014.03.070
  - 10.1016/j.actamat.2013.10.056
  - 10.1016/j.jmps.2013.04.009

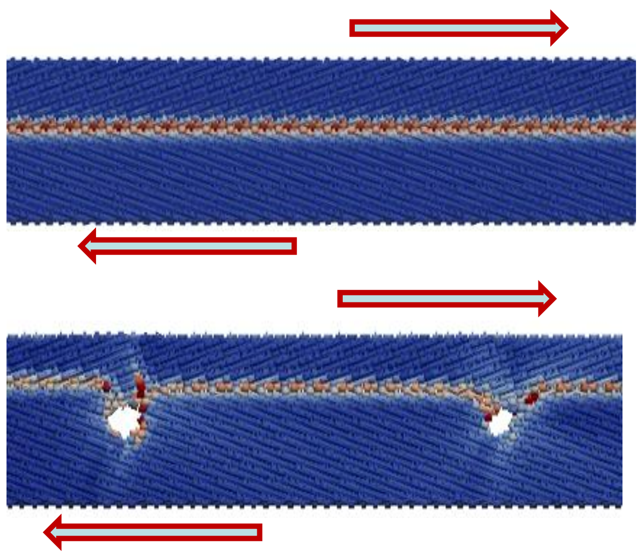

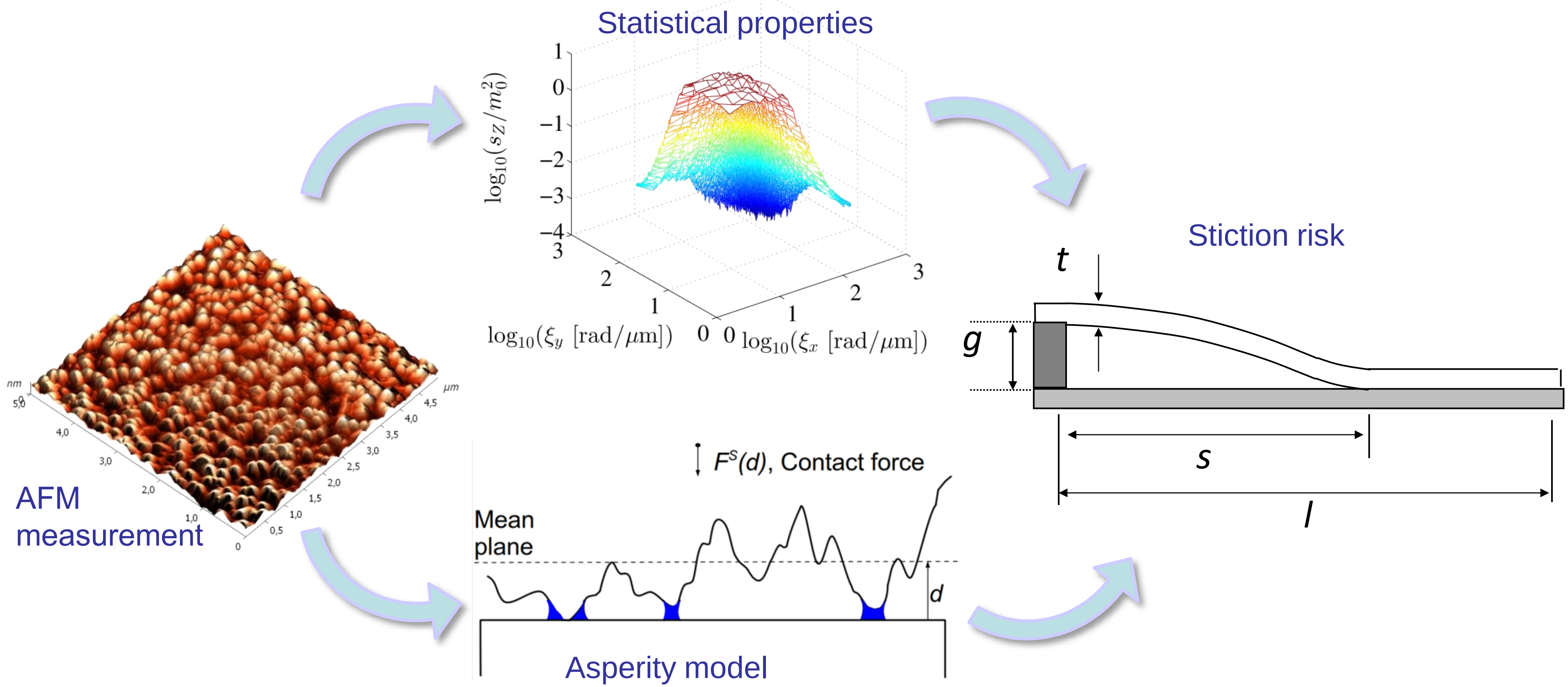

Stochastic Multi-Scale Model to Predict MEMS Stiction

3SMVIB: The research has been funded by the Walloon Region under the agreement no 1117477 (CT-INT 2011-11-14) in the context of the ERA-NET MNT framework.
The research has been funded by the Belgian National Fund for Education at the Research in Industry and Farming.

Stochastic Multi-Scale Model to Predict MEMS Stiction

- Stiction (adhesion of MEMS)
  - Different physics at the different scales
  - Elastic or Elasto-plastic behaviors
  - Due to van der Waals (dry environment) and/or capillary (humid environment) forces

- Requires surfaces topology knowledge (AFM measures)
  - Subject to uncertainties

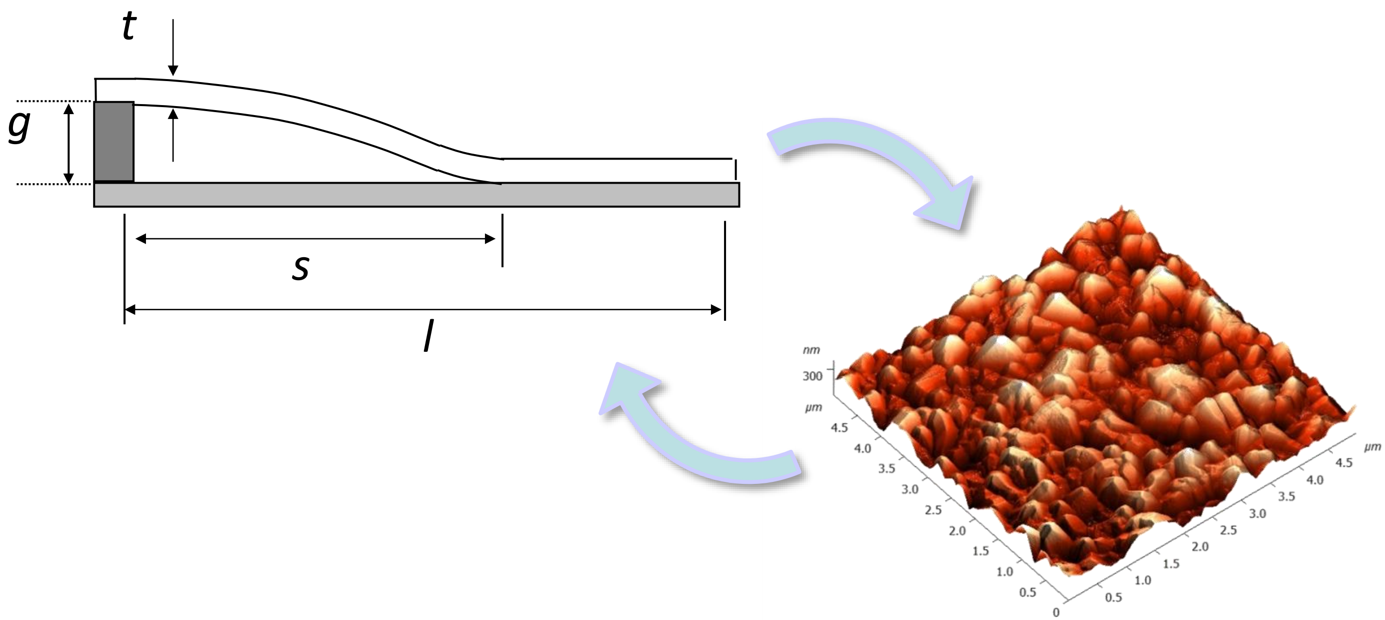

Stochastic Multi-Scale Model to Predict MEMS Stiction

- Deterministic multi-scale models for van der Waals forces
  - Extraction of meso-scale adhesive-forces
  - Using statistical representations of the rough surface (average solution)
  - Account for induced elasto-plasticity (cyclic loading)

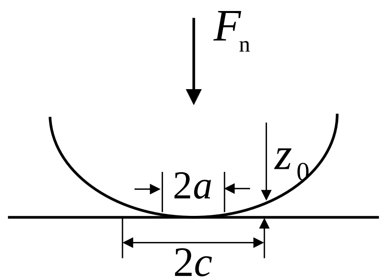

van der Waals/Hertz forces at the asperity level

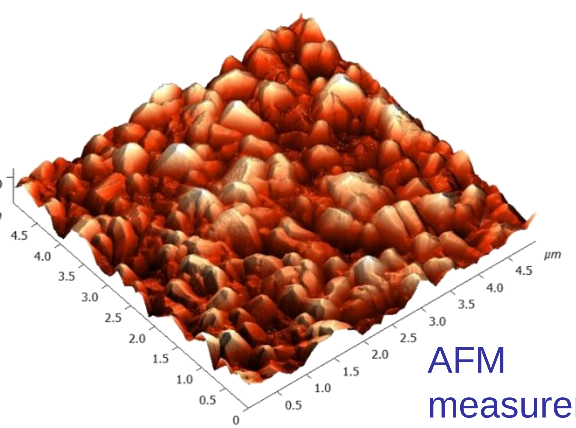

AFM measurement

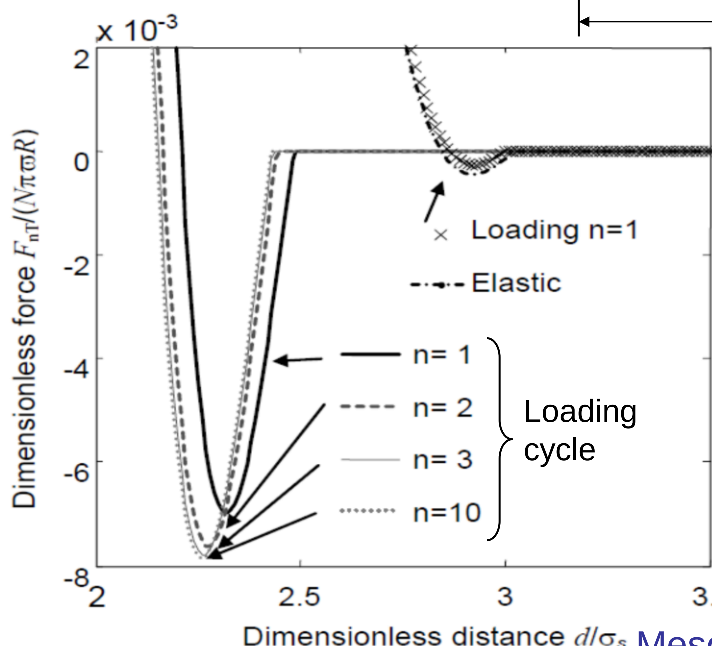

Meso-scale adhesive forces in terms of loading cycle

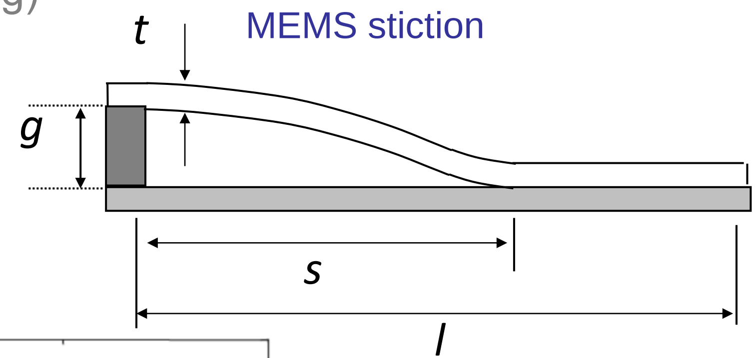

- New multi-scale models with capillary effect
  - Extraction of meso-scale adhesive-forces from a single surface measurement
  - Depends on the surface sample measurement location
  - Motivates the development of a stochastic multi-scale method

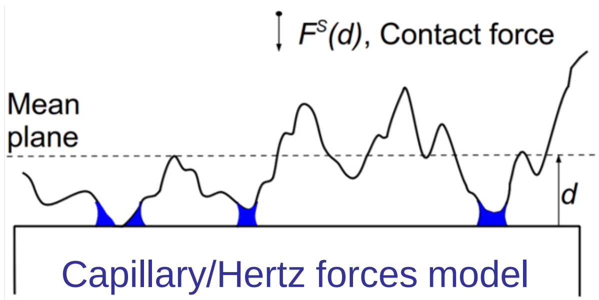

Capillary/Hertz forces model

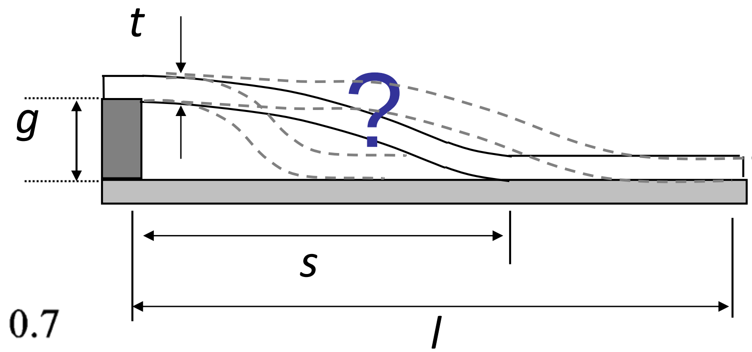

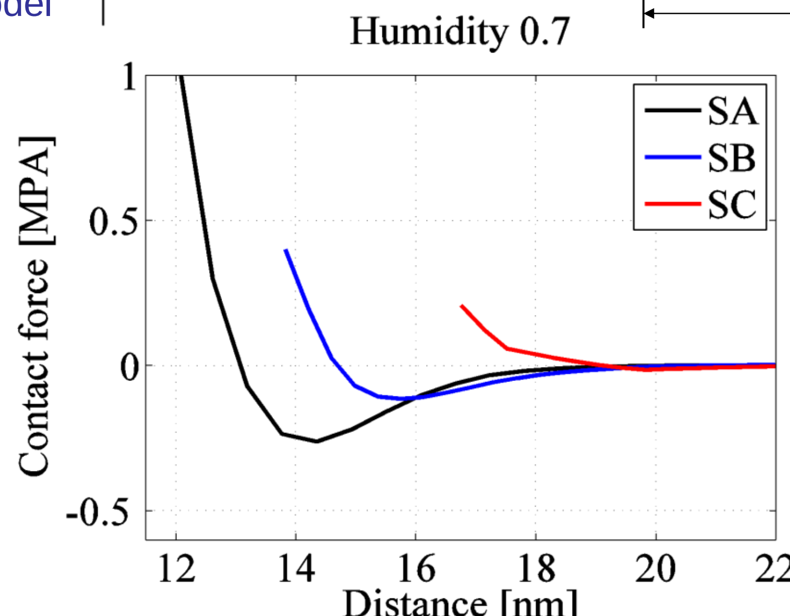

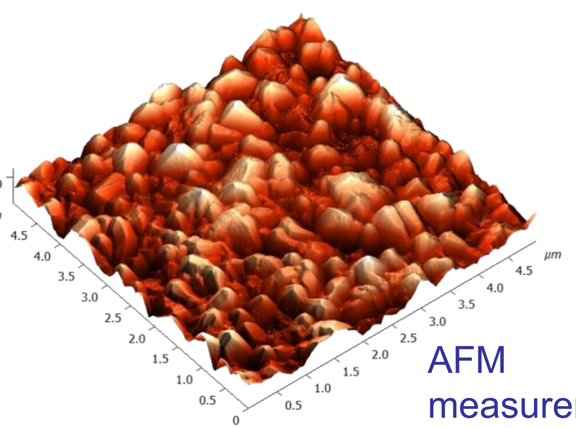

AFM measurement

Meso-scale adhesive forces in terms of surface sample

- Stochastic multi-scale model: From the AFM to virtual surfaces

Enforce statistical moments with maximum entropy method

$$m_i = \int_R z^i \mathrm{p}_Z(z)\, dz$$

$$\mathrm{p}_Z = \arg\max - \int_R \mathrm{p}_Z(z)\ \ln(\mathrm{p}_Z(z))\, dz$$

Evaluate PSD from covariance

$$\tilde{R}(\boldsymbol{\tau}) = \mathbb{E}[z(\boldsymbol{x}), z(\boldsymbol{x}+\boldsymbol{\tau})]$$

$$S_Z(\boldsymbol{\tau}) = \int_{R^2} \exp(-i\boldsymbol{\zeta}\cdot\boldsymbol{\tau})\tilde{R}_Z(\boldsymbol{\tau})d\boldsymbol{\zeta}$$

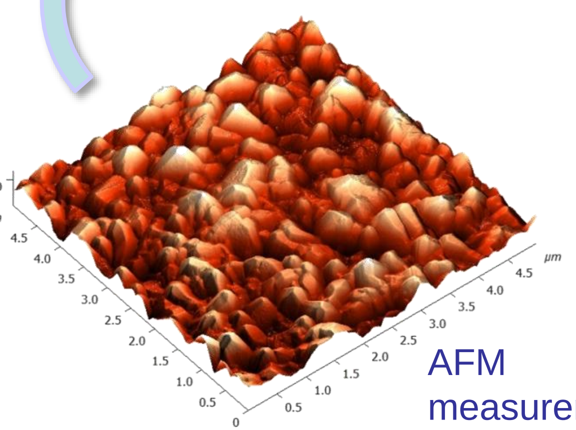

AFM measurement

Height Probability Density Function

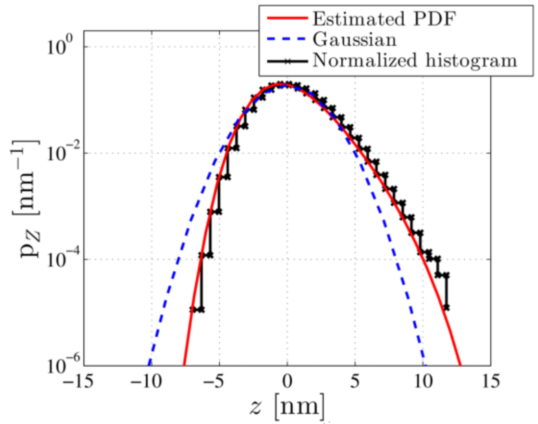

Power spectrum density

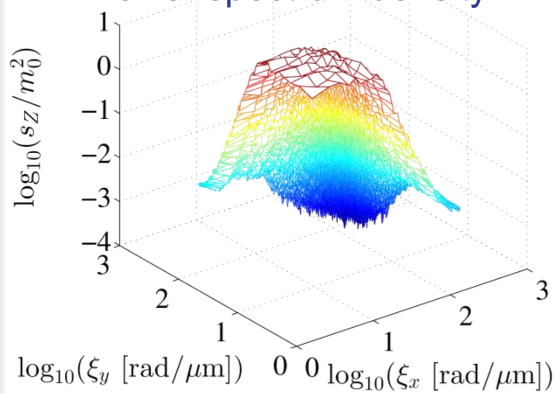

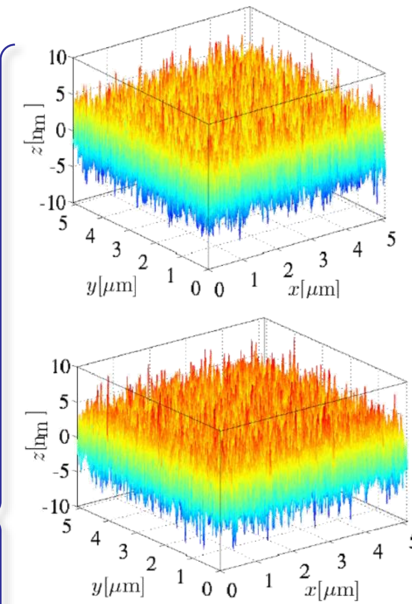

Generated non-Gaussian surface samples

Stochastic Multi-Scale Model to Predict MEMS Stiction

- Stochastic multi-scale model: Evaluate meso-scale surface forces

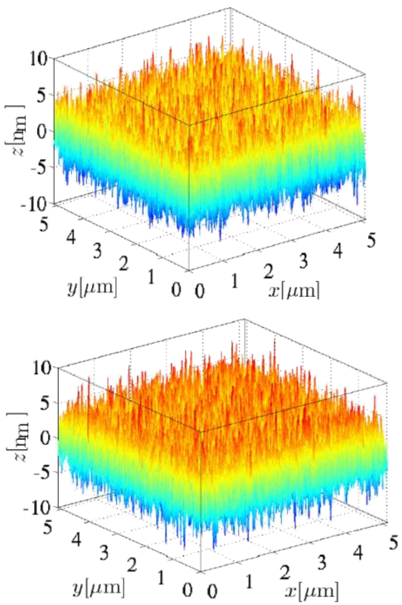

Generated non-Gaussian surface samples

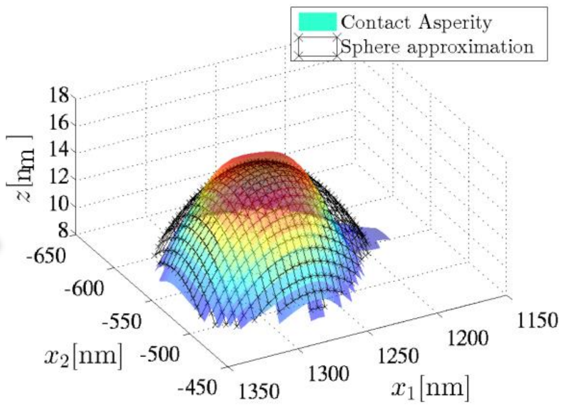

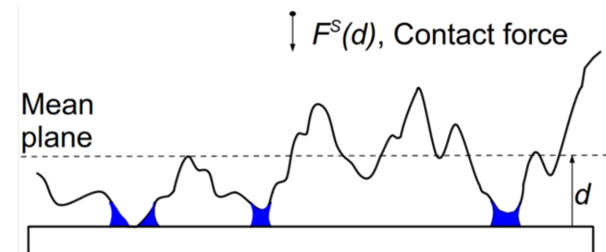

Capillary/Hertz forces model

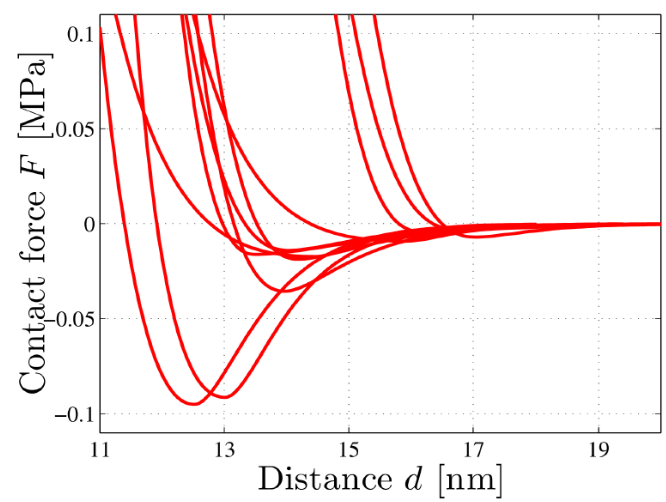

Computed meso-scale adhesive forces

- Stochastic multi-scale model: Stochastic model of meso-scale adhesion forces

Definition of parameter vector $\boldsymbol{v}$

$$\bar{f}(\bar{d}) = \Phi(\bar{d}, \boldsymbol{v})$$

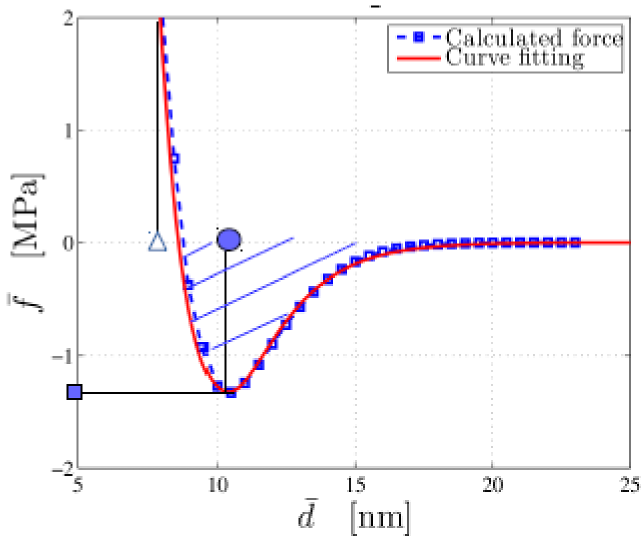

Enforce physical constraints

$$\boldsymbol{v}^{(i)} \rightarrow \boldsymbol{q}^{(i)}$$

Principal component analysis from covariance matrix $[\tilde{R}_Q]$ of vectors $\boldsymbol{q}^{(i)}$

$$\boldsymbol{\eta}^T = (\boldsymbol{q} - \overline{\boldsymbol{q}})^T [A][\lambda]^{-1/2}$$

Polynomial chaos expansion

$$\boldsymbol{\eta}^{\mathrm{PC}} = \sum c_\alpha \Psi_\alpha(\boldsymbol{\xi})$$

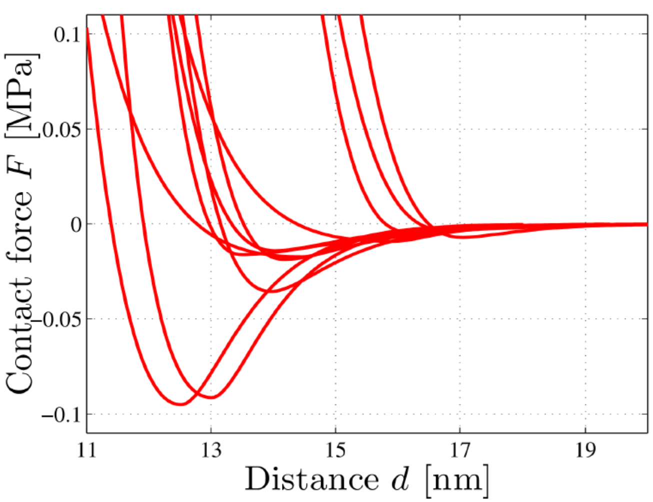

Computed meso-scale adhesive forces

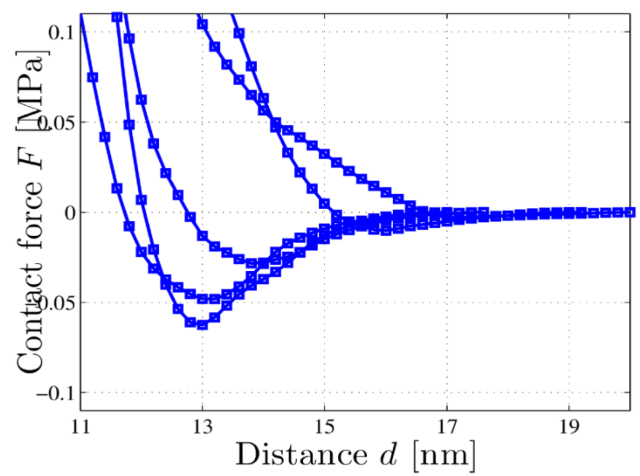

Generated adhesive forces

- Stochastic multi-scale model: Stochastic MEMS stiction analyzes

Stochastic finite elements (random contact law variable)

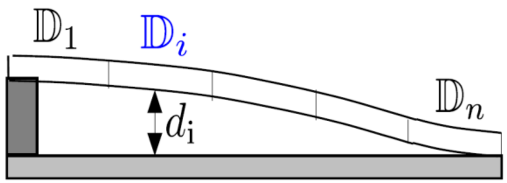

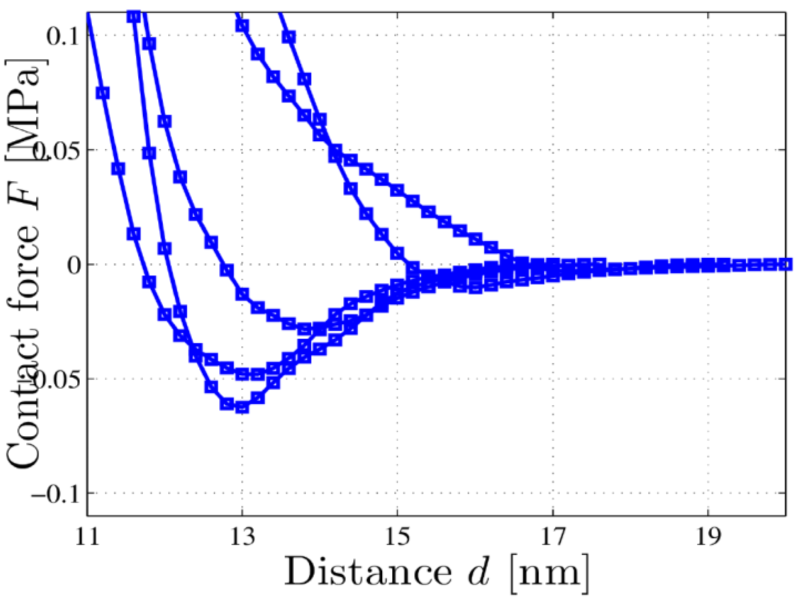

Generated meso-scale adhesive forces

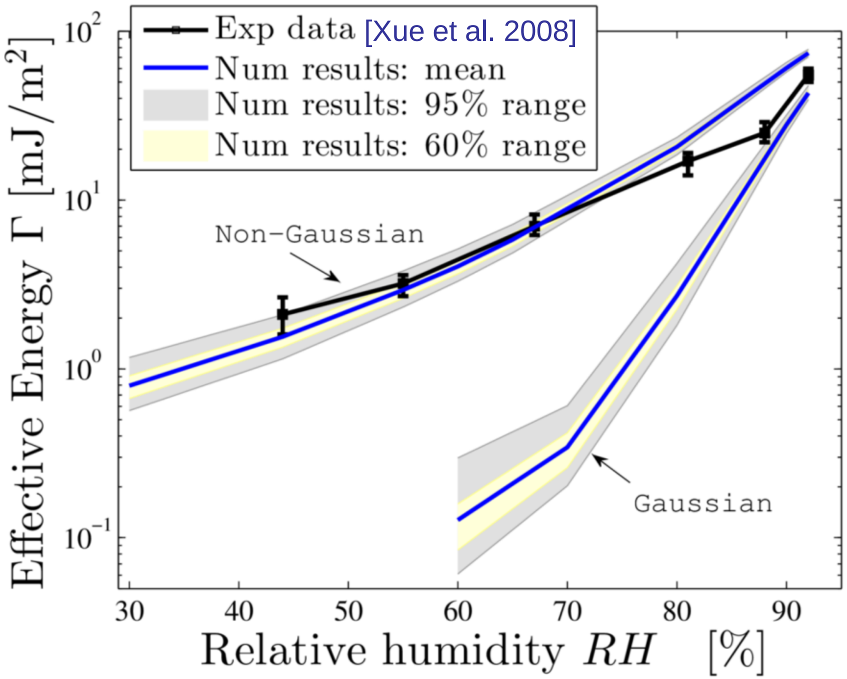

Stiction risk

Stochastic Multi-Scale Model to Predict MEMS Stiction

- Application to robust design
  - Determination of probabilistic meso-scale properties
  - Propagate uncertainties to higher scale
  - Vibro-meter sensors:
    - Uncertainties in stiction risk

- 3SMVIB MNT.ERA-NET project
  - Open-Engineering, V2i, ULiège (Belgium)
  - Polit. Warszawska (Poland)
  - IMT, Univ. Cluj-Napoca (Romania)

- FNRS-FRIA fellowship

- Publications (doi)
  - 10.1109/JMEMS.2018.2797133
  - 10.1016/j.triboint.2016.10.007
  - 10.1007/978-3-319-42228-2_1
  - 10.1016/j.cam.2015.02.022
  - 10.1016/j.triboint.2012.08.003
  - 10.1007/978-1-4614-4436-7_11
  - 10.1109/JMEMS.2011.2153823
  - 10.1063/1.3260248